DEEP-WATER PROCESSES AND FACIES MODELS: IMPLICATIONS FOR SANDSTONE PETROLEUM RESERVOIRS

HANDBOOK OF PETROLEUM EXPLORATION AND PRODUCTION
5

Series Editor
JOHN CUBITT

Previous volumes in this series:

DEEP-WATER PROCESSES AND FACIES MODELS: IMPLICATIONS FOR SANDSTONE PETROLEUM RESERVOIRS

HANDBOOK OF PETROLEUM EXPLORATION AND PRODUCTION
5

Dr. G. SHANMUGAM
Department of Earth and Environmental Sciences
The University of Texas at Arlington
Arlington, Texas
U.S.A.

For information on all Elsevier publications
visit our website at books.elsevier.com

Dedicated to the memories of three geologic pioneers of the 20th century:

John Essington Sanders (1926–1999)
Ph.D., Yale University, 1953
(Differentiated turbidity currents from debris flows)

Francis Parker Shepard (1897–1985)
Ph.D., University of Chicago, 1922
(Documented tidal currents in submarine canyons)

Charles Davis Hollister (1936–1999)
Ph.D., Columbia University, 1967
(Documented contour currents)

This Page Intentionally Left Blank

Contents

This Page Intentionally Left Blank

Acknowledgements

This Page Intentionally Left Blank

Preface

The principal goal of this book is to link deep-water process sedimentology with petroleum geology in an attempt to understand sand distribution, sandbody geometry, and reservoir quality of sandstone petroleum reservoirs. My 22 years of the petroleum-industry experience (1978–2000) with Mobil Oil Corporation (now ExxonMobil) has provided me an opportunity to accomplish the stated goal.

A textbook is essentially a comprehensive compilation of consensus derived from synthesis of published studies. However, such an orthodox approach is untenable for this book because of a lack of consensus even on the basic definition of turbidity currents and their deposits. Furthermore, different researchers tend to interpret the origin of the same deep-water bed differently. To overcome these obstacles, I have relied mainly on my own observations and interpretations of sediments and sedimentary rocks from 35 case studies of modern and ancient deep-water systems worldwide. I have transformed this rock-based experience into a practical handbook.

This book is intended for a wide range of knowledge levels. The first half of the book (Chapters 1, 2, 3, 4, 5, and 6) is aimed at undergraduate-level students. The second half of the book (Chapters 7, 8, 9, 10, 11, and 12) is suitable for graduate-level students and professional petroleum geoscientists. In practice, however, both students and petroleum geoscientists should benefit from the entire book.

Because this book has been written mostly with the student in mind, bulleted or numbered format is frequently used to highlight key points and to break the monotony of long text. To convince the reader of major points that I am trying to instill, the book is illustrated with 282 figures. A CD-ROM with color photographs and images is included. The book contains 908 references that include 55 self-citations.

This book is a milestone of my arduous but fruitful journey of the rocks that began in 1962. Although I have been gathering information on deep-water sedimentation since 1974, this book was written over a span of 14 months (April 2004–May 2005). Critical comments and suggestions from students and professionals would be beneficial for further discourse.

G. Shanmugam
E-mail: shanshanmugam@aol.com
June 6, 2005

This Page Intentionally Left Blank

Chapter 1

Introduction and process sedimentology

1.1 Introduction

> '*Despite an august history of 150 years, sedimentology as a science has advanced most rapidly since about 1950. This rapid advance resulted from a change of sedimentology as a pure to an applied science. Economic incentives, particularly in the exploration for petroleum, spurred prodigious expansion and rapid advances in sedimentology. Major oil companies began to realize that sedimentology was the key to success in exploration. Recognition of the enormous value of sedimentology as a key to the discovery of stratigraphic traps represented a turning point in the history of the science.*'
>
> (Friedman, 1998, p. 172)

Over 1200 oil and gas fields are known from deep-water systems (Stow and Mayall, 2000). The petroleum industry is increasingly moving exploration into the deep-water realm to meet the growing demand for oil and gas. There is no shortage of deep-water discoveries. During 1970–1998, 33 billion barrels of oil equivalent (BBOE) were added to the oil reserves from 29 giant deep-water discoveries (Pettingill, 1998). During January 2000–May 2004 alone, 4.5 BBOE (a 40% increase over the total BOE discovered during 1974–1999) were added to the deep-water reserves of the Gulf of Mexico (Richardson et al., 2004). And yet, much is uncertain about deep-water reservoirs in terms of their depositional origin and reservoir potential. For example:

- To address sedimentological problems associated with deep-water reservoirs, an SEPM-sponsored debate entitled *Processes of deep-water clastic sedimentation and their reservoir implications: what can we predict?* was held at the 1997 AAPG Annual Convention in Dallas, Texas. The moderator was H. E. Clifton, and the panelists were A. H. Bouma, J. E. Damuth, D. R. Lowe, G. Parker, and G. Shanmugam. The debate did not resolve the problems.
- Weimer et al. (2000a, p. 453) summarized the results of a joint EAGE/AAPG (Almeira, Spain, October 1998) research conference entitled *Developing and managing turbidite reservoirs: case histories and experiences* as follows: '*A repeated*

message at the conference was that there is more complexity than anticipated in turbidite reservoirs, contrary to many people's expectations.'

- Loizou (2004) concluded that one of the key reasons for exploration failures has been flawed geologic concepts. This conclusion was based on an analysis of all 147 exploration wells drilled along the U.K. Atlantic Margin since 1972.

To produce hydrocarbons economically, a proper understanding of the reservoir is a prerequisite. To meet this challenge successfully, petroleum geologists, petrophysicists, and engineers must have a good working knowledge of deep-water processes and their implications for sandstone reservoirs. But there are no books that focus on the linkage between deep-water processes sedimentology and petroleum geology. Published books and thematic volumes on deep-water sedimentation, for example, can be broadly grouped into two categories: (1) those that deal with depositional processes of modern and ancient deep-water systems, but not with subsurface petroleum reservoirs (e.g., Bouma et al., 1985; Pickering et al., 1989; Mutti, 1992); and (2) those that deal with deep-water petroleum reservoirs, but not with detailed process sedimentology (e.g., Weimer et al., 1994, 2000b).

1.1.1 Scope of this book

The primary purpose of this book is to make a link between deep-water process sedimentology and petroleum geology. Specific objectives are:

- To explain the principles and procedures of process sedimentology in petroleum geology.
- To trace the history of research on deep-water systems and to provide a philosophical retrospective on genetic nomenclature (Chapter 2).
- To provide a cutting edge overview of relevant deep-water processes and to catalog reasonable criteria for interpreting their deposits (Chapters 3 and 4).
- To discuss the importance of deep-water sand injections and to critically evaluate the role of tsunamis on deep-water sedimentation (Chapter 5).
- To document the variability of modern deep-water systems and their importance for reconstructing ancient environments (Chapter 6).
- To critically evaluate process-related problems and to dispel conceptual and nomenclatural myths surrounding turbidity currents and their deposits (Chapter 7).
- To demonstrate that the turbidite facies model and conventional fan models of sedimentology and sequence stratigraphy are obsolete (Chapters 8, 9, and 10).
- To review tectonic and eustatic controls of deep-water sedimentation (Chapter 11).
- To summarize implications of deep-water processes and environments for understanding sandstone petroleum reservoirs in terms of their spatial distribution, dimensions, geometry, and quality (Chapter 12).

1.1.2 Deep-water environments

Twenhofel (1932, p. 865) defined *bathyal* environments as that portion of the sea bottom between depths of 100 fathoms (600 ft or 183 m) and 1000 fathoms (6000 ft or 1830 m). The term *deep-water* is used here to include both marine and lacustrine settings. In modern oceans, the term refers to continental slope, rise, and basin environments that occur seaward of the shelf break at about 200 m water depths. In the Gulf of Mexico, the threshold that separates shallow water from deep water ranges from 200 to 457 m (Richardson et al., 2004). On the continental margin off northwestern Africa, the shelf break is found invariably at 100–110 m (Seibold and Hinz, 1974).

In the petroleum industry, the term deep-water is used to convey two different meanings: (1) most geologists would use the term to convey the deep-water depositional origin of a buried reservoir, even if the drilling for this reservoir commences from the shelf (e.g., Fig. 1.1, Well A); and (2) drilling engineers would use the term to denote the deep-water drilling depths, even if the buried
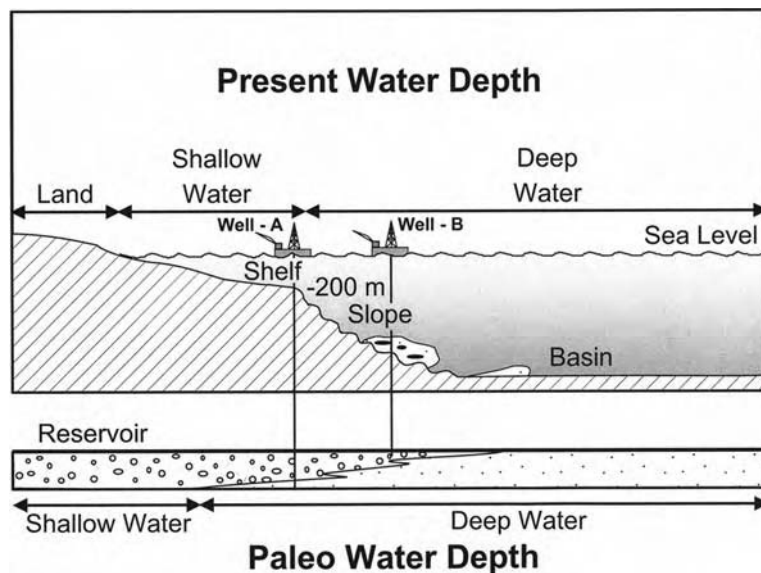
Fig. 1.1. The term 'deep-water' refers to bathyal water depths (> 200 m) that occur seaward of the continental shelf break on the slope and basin settings. In petroleum exploration and production, the term deep-water is used with two different meanings. First, geologists use the term to denote deep-water depositional origin of the reservoir, even if the drilling for this reservoir commences from shallow-water shelf (e.g., Well A). Second, drilling engineers use the term to denote deep-water drilling depths (e.g., Well B), even if the target reservoir is of shallow-water origin. Gravel symbol = reservoirs of shallow-water origin. Sand symbol = reservoirs of deep-water origin. (After Shanmugam (2000a). Reproduced with permission from Elsevier.)

reservoir is of shallow-water deposition (Fig. 1.1, Well B). This practice could cause a communication breakdown between a geologist and an engineer.

1.1.3 Deep-water systems

Deep-water systems have been portrayed conventionally by a simple submarine fan deposited by turbidity currents (Fig. 1.2). This is despite whether they are fan-shaped in morphology or not, and whether they are deposited by turbidity currents or not. However, a critical evaluation of deep-marine sedimentary systems revealed that they are quite complex. This book presents a pragmatic view that deep-water systems are complex and that they are populated with multiple processes and products (Fig. 1.3).

My skepticism about the dominance of turbidites in deep-water systems began to take root when I started describing cores and outcrops in great detail worldwide (Fig. 1.4). An epiphany had occurred in 1990 when I began describing cores from the North Sea (Fig. 1.5). Since then, I have realized that deep-water systems are extremely complex and variable, reflecting mostly chaos at the scale of
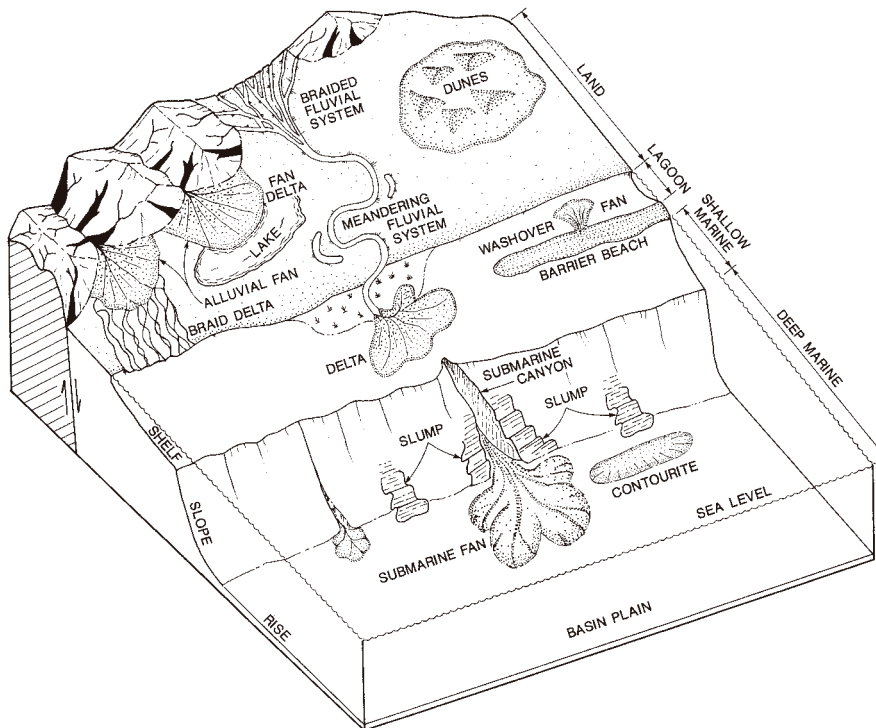
Fig. 1.2. Conventional model of deep-marine systems showing a submarine fan formed by turbidity currents. Such a simple model is no longer realistic. See Fig. 1.3 for a complex deep-water system.
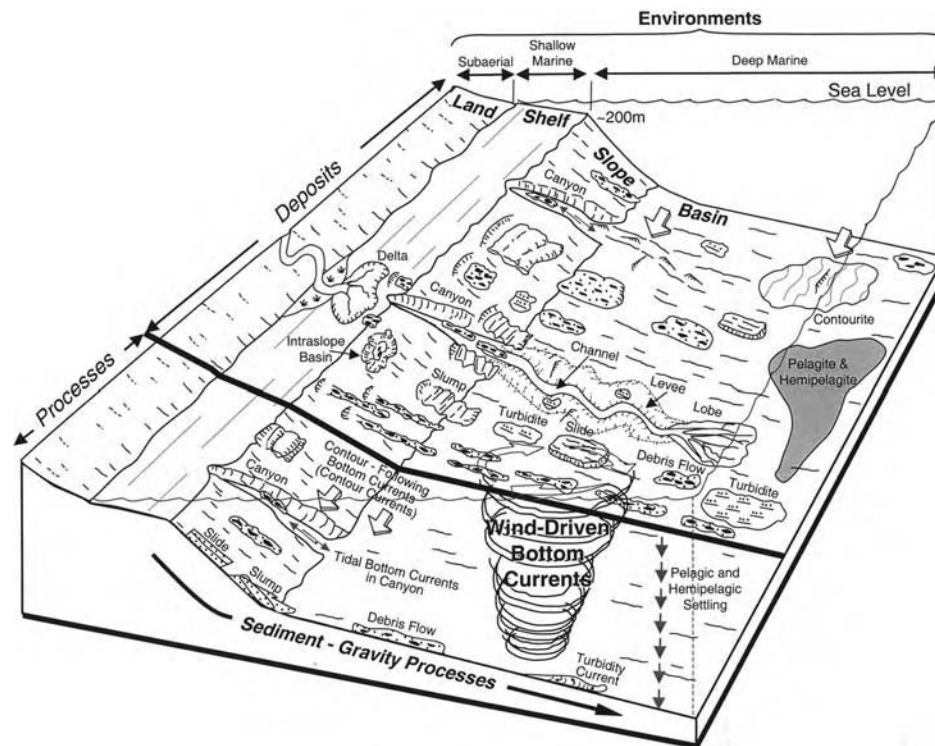
Fig. 1.3. Schematic diagram showing complex deep-marine sedimentary environments occurring at water depths deeper than 200 m (shelf-slope break). In general, shallow-marine (shelf) environments are characterized by tides and waves, whereas deep-marine (slope and basin) environments are characterized by mass movements (i.e., slides, slumps, and debris flows), bottom currents, and pelagic/hemipelagic deposition. Turbidity currents may be common in basinal settings. Submarine canyons are unique because the shelf-slope break does not control processes within the canyon; both tidal currents and mass flows operate within canyons (see Chapter 4). Note up- and down- tidal bottom currents in submarine canyons (opposing arrows). Along-slope movement of contour-following bottom currents and circular motion of wind-driven bottom currents are important processes outside of the canyon. (After Shanmugam (2003). Reproduced with permission from Elsevier.)

Fig. 1.4. Location map of cores and outcrops that I have used in detailed description of deep-water siliciclastic sediments and sedimentary rocks worldwide.

depositional units (Fig. 1.5). This epiphany was due to my exposure to remarkably complicated deep-water massive sands. The origin of massive sands, although controversial (Stow, 1992; Shanmugam, 1992a; Parize et al., 1999; Stow et al., 1999; Stow and Johansson, 2000), is of economic importance. This is because major petroleum-producing reservoirs in the North Sea, Norwegian Sea, Nigeria, Equatorial Guinea, California, and Gulf of Mexico are massive sands.

1.1.4 Database

This book is based on 35 case studies of deep-water systems that include many petroleum-producing massive sands worldwide. The constancy in all these case studies was that I, as the principal investigator, described these sediments and sedimentary rocks. Description was carried out at a scale of 1:20 to 1:50, totaling more than 30000 ft (9145 m), during the past 30 years (1974–2004). These modern and ancient deep-water systems include (Fig. 1.4):

(1) **Mississippi Fan,** Quaternary, DSDP Leg 96 core, Gulf of Mexico, U.S.
(2) **Green Canyon,** late Pliocene, conventional core, Gulf of Mexico, U.S.
(3) **Garden Banks,** middle Pleistocene, conventional core, Gulf of Mexico, U.S.
(4) **Ewing Bank 826,** Pliocene-Pleistocene, conventional core, Gulf of Mexico, U.S.
(5) **South Marsh Island,** late Pliocene, conventional core, Gulf of Mexico, U.S.
(6) **South Timbalier,** middle Pleistocene, conventional core, Gulf of Mexico, U.S.
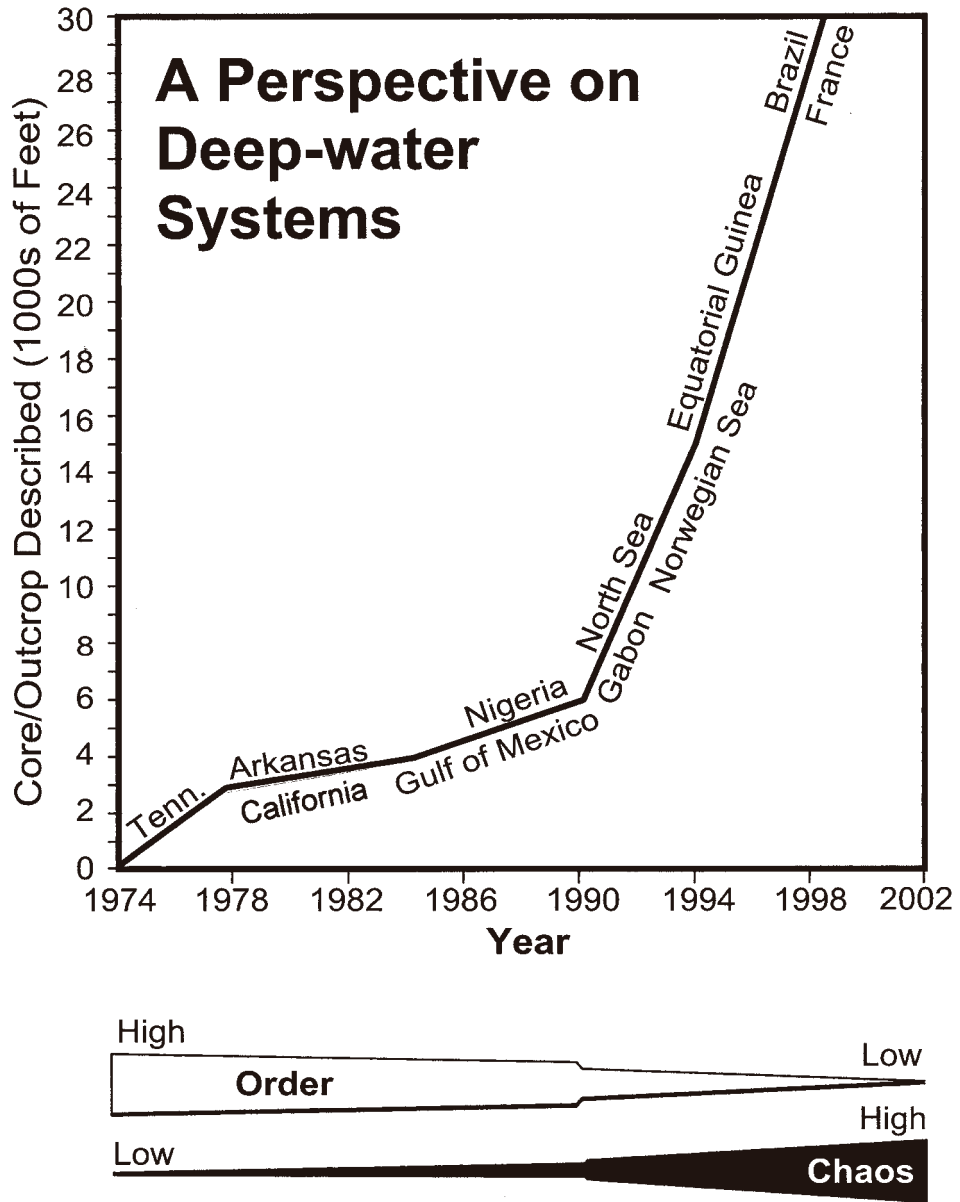
Fig. 1.5. *Top:* **Graph showing the total thickness of intervals of deep-water core and outcrop that I have described from 1974 to 2002 totaling 30000 ft (9144 m).** *Bottom:* **Bars showing my changing perspectives from one of order and simplicity (1974–1990) to one of chaos and complexity (1990–2002). Note that an epiphany had occurred in 1990 when I began describing cores, composed of deep-water massive sands, from North Sea reservoirs. (After Shanmugam (2000a). Reproduced with permission from Elsevier.)**

  (7) **High Island,** late Pliocene, conventional core, Gulf of Mexico, U.S.
  (8) **East Breaks,** late Pliocene-Holocene, conventional and piston cores, Gulf of Mexico, U.S.
  (9) **Midway Sunset Field,** upper Miocene, conventional core, onshore California, U.S.
 (10) **Jackfork Group,** Pennsylvanian, outcrop, Ouachita Mountains, Arkansas, and Oklahoma, U.S.
 (11) **Sevier Basin,** Middle Ordovician, outcrop, Southern Appalachians, Tennessee, U.S.
 (12) **Lagoa Parda Field,** lower Eocene, conventional core, Espirito Santo Basin, onshore Brazil
 (13) **Fazenda Alegre Field,** upper Cretaceous, conventional core, Espirito Santo Basin, onshore Brazil
 (14) **Cangoá Field,** upper Eocene, conventional core, Espirito Santo Basin, offshore Brazil
 (15) **Peroá Field,** lower Eocene to upper Oligocene, conventional core, Espirito Santo Basin, offshore Brazil
 (16) **Marlim Field,** Oligocene, conventional core, Campos Basin, offshore Brazil
 (17) **Marimba Field,** upper Cretaceous, conventional core, Campos Basin, offshore Brazil
 (18) **Roncador Field,** upper Cretaceous, conventional core, Campos Basin, offshore Brazil
 (19) **Frigg Field,** lower Eocene, conventional core, Norwegian North Sea
 (20) **Harding Field** (formerly Forth Field), lower Eocene, conventional core, U.K. North Sea
 (21) **Alba Field,** Eocene, conventional core, U.K. North Sea
 (22) **Fyne Field,** Eocene, conventional core, U.K. North Sea
 (23) **Gannet Field,** Paleocene, conventional core, U.K. North Sea
 (24) **Andrew Field,** Paleocene, conventional core, U.K. North Sea
 (25) **Gryphon Field,** upper Paleocene–lower Eocene, conventional core, U.K. North Sea
 (26) **Faeroe area,** Paleocene, conventional core, west of the Shetland Islands, U.K. Atlantic Margin
 (27) **Foinaven Field,** Paleocene, conventional core, west of the Shetland Islands, U.K. Atlantic Margin
 (28) **Mid-Norway region,** Cretaceous, conventional core, Norwegian Sea
 (29) **Agat region,** Cretaceous, conventional core, Norwegian North Sea
 (30) **Annot Sandstone,** Eocene-Oligocene, outcrop, Maritime Alps, SE France
 (31) **Edop Field,** Pliocene, conventional core, offshore Nigeria
 (32) **Zafiro Field,** Pliocene, conventional core, offshore Equatorial Guinea
 (33) **Opalo Field,** Pliocene, conventional core, offshore Equatorial Guinea
 (34) **Melania Formation,** lower Cretaceous, conventional core, offshore Gabon
 (35) **Krishna-Godavari,** Pliocene, conventional core, offshore southeastern India.

Personal knowledge gained from this robust data set has allowed me to be consistent in process interpretations.

1.2 Process sedimentology

Sedimentology is the scientific study of sediments (unconsolidated) and sedimentary rocks (consolidated) in terms of their description, classification, origin, and diagenesis. It is concerned with physical, chemical, and biological processes and products. *Physical sedimentology* involves processes and products of (1) weathering, (2) erosion, (3) transportation, (4) deposition, and (5) compaction of siliciclastic particles. Reading (1986a) suggested four steps for reconstructing ancient environments: (1) description of the rocks; (2) interpretation of processes; (3) establishment of vertical and lateral facies relationships; and (4) use of modern analogs. Friedman et al. (1992) discussed principles of process sedimentology.

1.2.1 Definition

Process sedimentology (aptly 'depositional process sedimentology'), a subdiscipline of physical sedimentology, is concerned with the detailed bed-by-bed description of siliciclastic sedimentary rocks for establishing the link between the deposit and the physics of the depositional process. It is the foundation for reconstructing ancient depositional environments and for understanding sandstone reservoir potential (Fig. 1.6).

1.2.2 Knowledge

(1) To practice process sedimentology, a certain level of basic knowledge in geology, physics, chemistry, mathematics, zoology, and botany is required.
(2) Undergraduate students must have had basic courses in sedimentology and stratigraphy, and a geology field camp.
(3) According to Brush (1965, p. 23), a combined knowledge of basic *physics*, *soil mechanics*, and *fluid mechanics* is essential for interpreting the mechanics of various fluid–sediment–gravity processes. These three disciplines were a part of my curriculum.
(4) *Fluid mechnics* is the study of the properties and behavior of fluids. Ludwig Prandtl, a German Engineer who conceived the boundary layer concept (Prandtl, 1904) and contributed to our understanding of *turbulence* theory (Prandtl, 1925 and 1926), is considered to be one of the founders of modern fluid mechanics (Oswatitsch and Wieyhardt, 1987; Kundu and Cohen, 2002). *Fluid dynamics,* the study of fluids (liquids and gases) in motion (Prandtl, 1952; Shapiro, 1961), is a branch of fluid mechanics. Fluid dynamics has a number of subdisciplines, including *hydrodynamics* (liquids in motion) and *aerodynamics* (gases in motion). In this book, we are concerned

Well

Slide

Slump

Sandy Debris Flow

Turbidite

- **Dimension**
- **Geometry**
- **Reservoir Property**
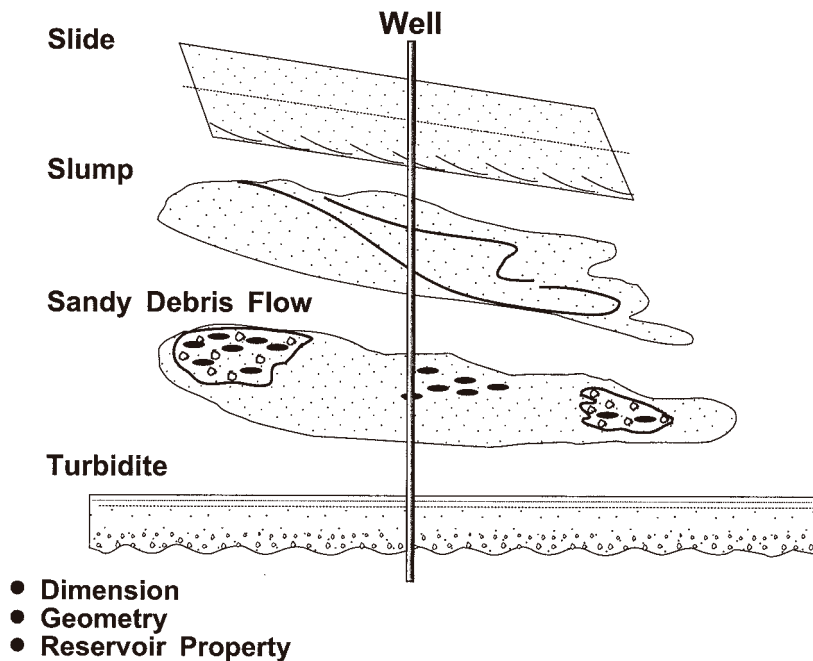
Fig. 1.6. A conceptual diagram showing the importance of process sedimentology. By knowing the process of origin, one might be able to predict the nature of sandbody dimension, geometry, and reservoir property away from the well bore.

with hydrodynamics. A *fluid* is defined as a material that flows (Van Wazer et al., 1963). A *flow* is defined as the continuous, irreversible deformation of sediment–water mixture that occurs in response to applied stress (Pierson and Costa, 1987). A gallery of fluid motion, archived by the American Institute of Physics (2004), is a good preamble to a novice. Geological application of fluid mechanics has been discussed by several researchers (e.g., Sanders, 1963; Allen, 1970, 1985a; Friedman and Sanders, 1978; Middleton and Wilcock, 1994; Hsü, 2004).

(5) The greater the number of deep-water rocks one describes in detail worldwide, the better the appreciation one develops for deep-water process sedimentology.

1.2.3 Methodology

Although basic methods of describing the rocks have been well established by the geologic pioneers long ago (e.g., Lahee, 1923; Twenhofel, 1932, his Chapter VIII; Krumbein and Sloss, 1963), these procedures have been compromised over the years. Furthermore, description of conventional core for the petroleum industry involves some special techniques. Thus the philosophy and methodology of core description are reiterated here.
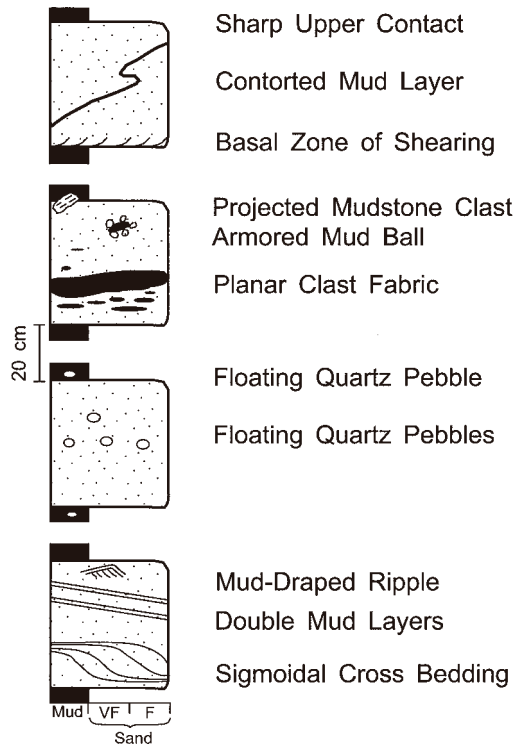
Fig. 1.7. Diagrams showing small-scale sedimentary features in the rocks that form the foundation of process sedimentology.

(1) <u>Be accurate, be precise, and be consistent in describing the rocks</u>.
(2) <u>Make direct observations on the core (and on the outcrop)</u>. Required information for interpreting fluid rheology, flow state, and sediment-support mechanism can be obtained only by examining the rocks directly for the presence of intricate small-scale sedimentary features (Fig. 1.7). Extracting details from the rocks is a tedious and time-consuming endeavor and there are no short-cut approaches.
(3) <u>Use slabbed cores</u>. Unslabbed cores are prone to cause misleading observations.
(4) <u>Clean the core (and outcrop) surface</u>. Before describing cores that have been in storage for a long period of time, scrape the surface with a knife and expose the fresh rock surface. Otherwise, surface chemical alteration and fungus growth can mimic sedimentary features. Weathered outcrops also need cleaning to expose the fresh rock surface.
(5) <u>Wet the slabbed core surface</u>. Wetting the core surface with a sponge or washing the entire core section tends to reveal subtle sedimentary features. Use these procedures only for consolidated sandstone intervals, not for unconsolidated sands.

(6) Be mindful of poor core recovery in unconsolidated sand. Carefully deter-
mine missing core intervals.

(7) Calibrate core depth with log depth for each cored section.

(8) Be mindful of artificial core disturbance. Poor handling of cores of semi-
consolidated or unconsolidated sediment may result in artificial contortion
of sediment layers. Failure to recognize this problem would result in an
erroneous description and related misinterpretation. This problem can be
remedied by comparing the core with core photograph taken immediately
after slabbing.

(9) Begin description at the stratigraphic bottom (oldest) and move upward to
the top (youngest).

(10) Describe the core (and outcrop) at a scale of 1:20 or in greater detail.
Details are the underpinning of process sedimentology. Detailed megas-
copic and microscopic examinations of both the resinated 1/3 slabs and
unresinated 2/3 cuts of cores should be carried out to insure complete cov-
erage.

(11) Maintain an objective distinction between observation and interpretation.

(12) Avoid using facies models during description (Chapter 8). The purpose of
describing sedimentary rocks is to seek the truth about their depositional
origin, not to validate an existing facies model (e.g., the Bouma Sequence).

(13) Plot details on sedimentological logs during description (Fig. 1.8). Avoid
the method of describing the rocks in the field using a field notebook and
then transferring details onto sedimentological logs later in the office.

(14) Identify depositional contacts. Establish bottom and top contacts of each
depositional unit.

(15) Use expanded grain-size scale on sedimentological logs (Fig. 1.8).
Expanded scale allows sandy intervals to be accentuated (protruded) in
comparison to muddy intervals (Fig. 1.9). Expanded scale is vital during
calibration of wireline logs with sedimentological logs. Use Wentworth-
size classes on the abscissa using either millimeter or phi scale (see Folk,
1968; Carver, 1971). Standard class divisions are: mud (< 0.0625 mm),
very fine sand (0.0625–0.125 mm), fine sand (0.125–0.25 mm), medium
sand (0.25–0.50 mm), coarse sand (0.50–1.0 mm), very coarse sand
(1.0–2.0 mm), and gravel (> 2.0 mm). If necessary, gravel grade can be further
subdivided into granule (2–4 mm), pebble (4–64 mm), cobble (64–256 mm),
and boulder (> 256 mm). Standard practice is to plot average grain size
with additional remarks on maximum grain size.

(16) Document grain-size scale as part of graphic lithologic columns. Graphic
lithologic column and grain-size column should be combined and docu-
mented as a single column. In other words, grain-size scale should be the
abscissa for lithologic columns (Fig. 1.9). A separate column for grain-size
plot, independent of lithologic column, is inefficient for communicating
nature of grading (Fig. 1.10). For example, ODP (Ocean Drilling Program)

Fig. 1.8. Sedimentological log sheet with expanded grain-size scale for core and outcrop description. Note expanded grain-size scale in which each size class is given enough space for plotting grain-size variations accurately. K.B. = Kelly Bushing. K.B. is the journal-box insert in the rotary table of a rotary drilling rig and its upper surface is the zero-depth reference for wireline logs and other downhole measurements. Comments column = use this space for core-related details, such as, (1) type of hole (e.g., straight *versus* deviated), (2) type of core liner (e.g., fiberglass), (3) type of core impregnation (e.g., resin), (4) diameter of core barrel, (5) core recovery (%), (6) type of core storage (e.g., frozen *versus* room temperature), (7) type of cut examined (e.g., 1/3 *versus* 2/3), (8) core-log shift, (9) oil staining, (10) fossils, (11) structural complications, (12) fractures, and (13) sample locations. Suggested logging scale is 1:20. Scale can be modified to suit individual's needs based on the degree of detail desired, total thickness of core to be described, and the time available. Suggested scale for each vertical division on the log is 2 ft or 0.5 m. An enlarged version of this log (11 × 17 inch size paper) is recommended.

Fig. 1.9. A graphic sedimentological column with expanded grain-size scale in the abscissa showing quantitative distribution of facies. Laminated mud facies = 6 ft (18%). Massive sand facies = 34 ft (50%). Normally graded sand facies = 11 ft (32%). Note sandy intervals are protruded in comparison to muddy intervals. C = Coaly fragments, ... = normally graded beds, solid black lines through massive sand represent internal glide planes. Zafiro Field, Pliocene, Equatorial Guinea (see Chapter 6).
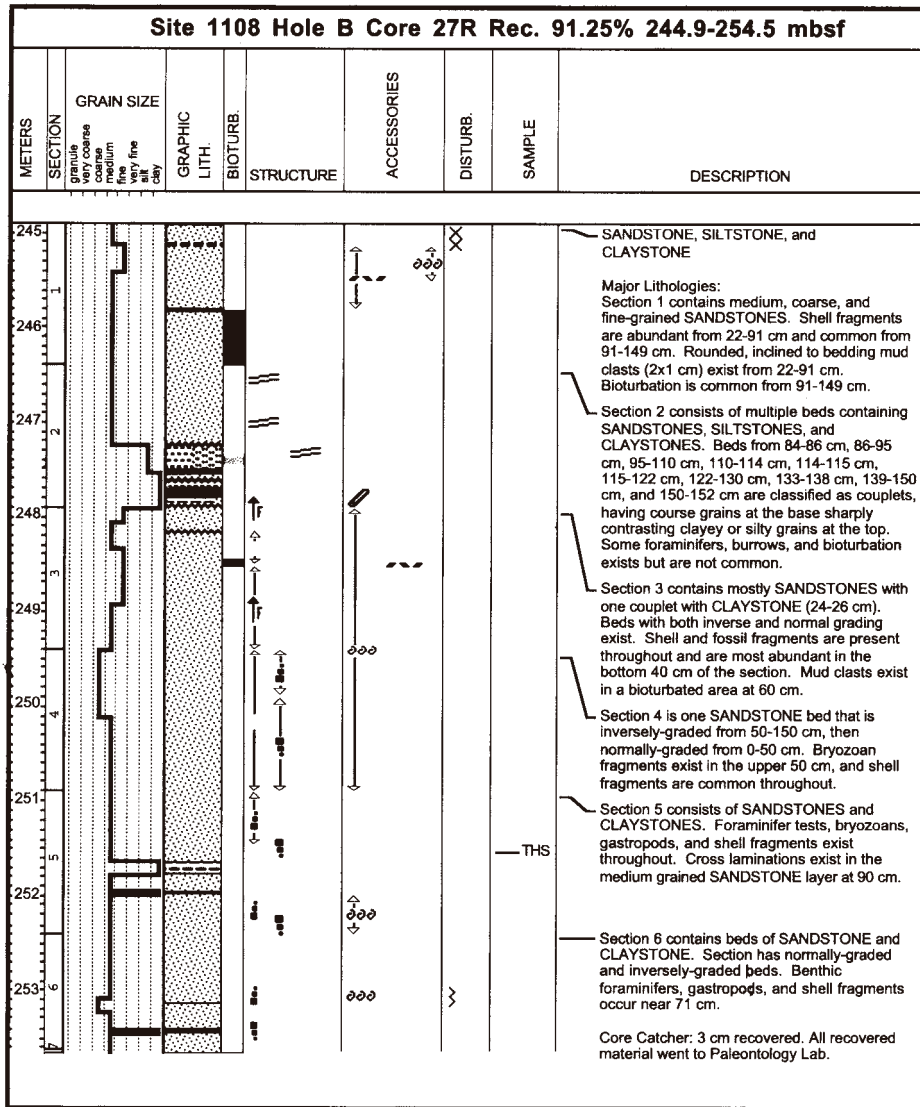
Fig. 1.10. A published graphic sedimentological log. Section 6 at the bottom is described as having normally graded and inversely graded beds. However, it is unclear from the graphic column the exact stratigraphic positions of lower and upper contacts of graded beds. Note that the graphic lithology column does not show protruded sandy intervals (compare with Fig. 1.9). These problems can be alleviated by combining graphic column with grain-size column and by using an expanded grain-size scale. Note that expanded grain-size column in Fig. 1.9 is nearly four times wider than the grain-size scale in this figure. Mbsf = meters below sea floor. (Credit: Core Description Section, ODP Leg 180, Site 1108 (Taylor et al., 2000).)

Leg 180 Initial Reports published a separate grain-size column for Site 1108 (Taylor et al., 2000). For Section 6 of Site 1108 (Fig. 1.10), the description reads, '*Section has normally-graded and inversely-graded beds*.' However, it is not obvious from the graphic column the nature of grading trends. In contrast, a graphic lithologic column combined with expanded grain-size scale shows not only the nature of graded beds but also the exact position of graded bed contacts (Fig. 1.9).

(17) <u>Record primary (i.e., depositional) sedimentary structures</u>. Be familiar with basic sedimentary structures and their origin (e.g., Pettijohn and Potter, 1964; Middleton, 1965; Middleton and Bouma, 1973; Middleton and Southard, 1977; Reineck and Singh, 1980; Allen, 1984; Collinson and Thompson, 1982; Harms et. al., 1982). In addition to depositional structures, record post-depositional features.

(18) <u>Record position and fabric of outsize grains, dense grains, and mudstone clasts</u>.

(19) <u>Identify reservoir facies in cores:</u> This involves integration of basic reservoir lithologies (e.g., usually gravel and sand), measured reservoir properties (e.g., porosity and permeability), and wireline-log properties for a given cored interval. This also requires visual estimation of sand percent for a given interval (see Fig. 1.8). Because each reservoir facies is linked to its depositional environment, one can understand its three-dimensional geometry and connectivity. Pay special attention to grain size and sorting because texture influences porosity and permeability (Beard and Weyl, 1973). While describing cores, record changes in framework composition, cement, matrix, oil shows (Swanson, 1981), and porosity types (Shanmugam, 1985). A petrographic microscope, thin sections, UV light source, and measured core porosity and permeability data are necessary for establishing reservoir facies.

(20) <u>Document sedimentary features with sketches and photographs</u>. If a feature is unfamiliar or too complex to classify, sketch it in detail and describe it objectively. Photographs of core and outcrop are the permanent record because core and outcrop are liable to undergo deterioration with time.

(21) <u>Use appropriate timing for core photography</u>. The timing of core photography is critical. Ideally, cores should be photographed immediately after they are slabbed and cleaned. Cores must be clearly marked with core depths. After photography is completed, cores should be preserved with solvent coating resin (e.g., mixture of acetone and resin) for long-term storage.

(22) <u>Use a professional scale</u>. Use of coins, lens caps, hammers, tooth brushes, hats, and human beings as scale in photographs can be confusing for documenting small-scale features.

(23) <u>Use X-radiography for massive sand intervals</u>. This technique may be helpful for resolving subtle amalgamation surfaces, internal contorted layering, and buried clasts. Formation MicroImager (FMI) may also be useful.

(24) Quantify geological data (Sorby, 1908; Griffiths, 1960). Quantification is vital for demonstrating the relative importance of depositional processes through time (Fig. 1.9).

1.2.4 Interpretation

 (1) Interpret each bed in terms of the physics of the flow. Only through bed-by-bed interpretation, an accurate quantification of facies can be made.
 (2) Apply James Hutton's (1788) principle of *Uniformitarianism* (Chapter 6). Emphasize modern analogs for interpreting ancient systems.
 (3) Apply Johannes Walther's (1894) Law (i.e., vertical disposition of depositional facies, without erosional breaks, represents their lateral disposition of depositional environments) with restraints. This is because of frequent occurrences of internal erosional events and glide planes in mass movements.
 (4) Apply experimental results for interpreting processes (Allen, 1985a).
 (5) Discern and discriminate published process interpretations. Carefully evaluate each publication in terms of its data for sufficiency, relevancy, and credibility. Avoid publications that promote model-driven process interpretations.
 (6) Curb any compromising of process interpretations for the sake of consensus (Chapter 7).
 (7) Avoid using triggering mechanisms for classifying depositional processes (Chapter 5).
 (8) Avoid using seismic geometry for interpreting depositional processes of ancient systems (Chapter 10).
 (9) Avoid using wireline-log motifs for interpreting depositional processes (Chapter 10).
 (10) Avoid using geometry of deep-water sandbodies as evidence for interpreting depositional processes. For example, one may infer sheet-like sandbodies by correlating wireline-log motifs, and then argue that these inferred sheet sands are evidence for *turbidite lobes*. Sand geometries may be inferred from processes, but not *vice versa* (see Chapter 10).
 (11) Interpret processes in a regional geologic context.
 (12) Reconstruct depositional environments based on process sedimentology.
 (13) Infer sand distribution, sandbody geometry, and reservoir quality based on process sedimentology (Fig. 1.6).

1.3 Synopsis

In accomplishing the goal of this book, which is to link process sedimentology with petroleum geology, sound principles of fluid mechanics, aspects of mass-transport processes, results of laboratory experiments, study of modern systems, and detailed examination of core and outcrop of ancient systems are used.

This Page Intentionally Left Blank

Chapter 2

History of deep-water research (1885–2005)

2.1 Introduction

The objective of this chapter is to trace the general trend of deep-water research during the past 120 years, since the first recognition of density currents in Swiss lakes in 1885.

2.2 History

The following list consists of pioneering studies, milestones, review articles, and significant events, but by no means a complete bibliography:

2.2.1 Period: 1885–1949

- First description of density currents in Swiss Lakes (Forel, 1885, 1887)
- 1872: The birth of modern deep-sea exploration by the voyage of *H.M.S. Challenger* (December 21, 1872–May 24, 1876) organized by the Royal Society of London and the Royal Navy (Murray and Renard, 1891)
- The conventional idea of tranquil deep-sea realm receiving only pelagic clays (Murray and Renard, 1891)
- Introduction of the concept of hyperpycnal and hypopycnal flows (Forel, 1892)
- Documentation of cable breaks by submarine avalanches along the submarine canyon axis (Milne, 1897)
- 1903: Establishment of an independent biological research laboratory that became Scripps Institution of Oceanography in 1912 as part of the University of California, La Jolla, California (F. P. Shepard's research institution)
- Discussion of theory of turbulence in fluid mechanics (Prandtl, 1925, 1926)
- First recognition of sequence of structures, which would later become the 'Bouma Sequence' (Sheldon, 1928)
- 1930: Establishment of Woods Hole Oceanographic Institution, Woods Hole, Massachusetts (C. D. Hollister's research institution)

- Recognition of a sequence of structures with five divisions, which would later become the 'Bouma Sequence' (Signorini, 1936)
- Documentation of deep bottom currents in the Atlantic Ocean (Wust, 1936)
- A hypothesis on the deep-water origin of graded facies (Bailey, 1936)
- A hypothesis on the origin of submarine canyons through erosion by density currents (Daly, 1936)
- Documentation of currents in submarine canyons (Stetson, 1936; Shepard et al., 1939)
- First experiments on density currents to test Daly's hypothesis (Kuenen, 1937)
- Documentation of density currents in Lake Mead (Grover and Howard, 1938)
- Introduction of the term *turbidity current* (Johnson, 1938)
- Description of graded sand in deep-sea cores (Bramlette and Bradley, 1940)
- Connection between tsunamis and origin of submarine canyons (Bucher, 1940)
- A hypothesis on the origin of chaotic sediments by tsunamis (Bailey, 1940)
- Density currents as agents for transporting sediments (Bell, 1942)
- Mass movements on natural slopes (Ward, 1945)
- Presentation of important papers on deep-water processes by Kuenen, Migliorini, and Shepard at the 18th International Geological Congress in London (U.K.): the initiation of the first deep-water paradigm (1948).

2.2.2 Period: 1950–1959

- First experiments on turbidity currents of high density (Kuenen, 1950a)
- First explanation of origin of graded bedding by turbidity currents: the foundation of the turbidite paradigm (Kuenen and Migliorini, 1950)
- Introduction of criteria for recognition of slope deposits (Rich, 1950)
- Recognition of transported shallow water fauna in deep-water sequences (Natland and Kuenen, 1951)
- Documentation of mass movements in heads of modern submarine canyons (Shepard, 1951)
- Association of ancient debrites and slides with turbidites (Doreen, 1951)
- Documentation of cable breaks by Grand Banks slumps (Heezen and Ewing, 1952; Heezen and Drake, 1964)
- Documentation of turbidites from modern oceans (Heezen and Ewing, 1952; Ericson et al., 1952)
- The link between soil mechanics and mass movements (Skempton, 1953)
- Introduction of the concept of dispersive pressure by colliding grains in high-concentration dispersions, which would later be termed 'grain flows' (Bagnold, 1954)
- First detailed account of modern submarine fans off California (Menard, 1955)
- Recognition of a lower laminar *inertia* region (grain flows) and an upper turbulent *viscous* region (turbidity currents) in experimental density–stratified flows (Bagnold, 1956)

- Introduction of the term *turbidite* for the deposit of a turbidity current (Kuenen, 1957)
- Recognition of the importance of detrital mud matrix in turbidite sandstone (Pettijohn, 1957)
- Debris-flow origin of pebbly mudstone (Crowell, 1957)
- First comprehensive classification of landslides (Varnes, 1958, 1978)
- Introduction of the term *fluxoturbidites* for deposits of sand avalanches (Kuenen, 1958; Dzulynski et al., 1959)
- Classification of canyon-fan systems *versus* slope-apron systems (Gorsline and Emery, 1959)
- Critique of the concept of turbidity currents (Ten Haaf, 1959a)
- Tectonic control of deep-sea sedimentation in continental margins (Drake et al., 1959)
- Recognition of high-concentration granular wedge at the base of a depositing turbidity current, which would later be termed a 'traction carpet' (Hsü, 1959).

2.2.3 Period: 1960–1969

- Recognition of high silt and clay content (13.5–34.5%) in turbidite sandstone (Sullwold, 1960)
- Emphasis on hydrocarbon reservoirs of turbidite origin (Sullwold, 1961)
- Introduction of the first vertical facies model of turbidites, which has become known as the *Bouma Sequence* (Bouma, 1962)
- Distinction between along-slope bottom currents and down-slope turbidity currents (Murphy and Schlanger, 1962)
- A detailed outcrop study of the Ordovician Martinsburg flysch in the central Appalachians (McBride, 1962a)
- Introduction of the term *traction carpet* for flowing-grain layers at the base of a depositing turbidity current (Dzulynski and Sanders, 1962)
- Introduction of the concept of 'auto-suspension' of transported sediment in turbidity currents (Bagnold, 1962)
- Diagenetic origin of mud matrix in greywacke (Cummins, 1962)
- First classification of gravity flows based on fluid rheology (Dott, 1963)
- Interpretation of fluid mechanics from sedimentary structures: the foundation of process sedimentology (Sanders, 1963)
- The importance of slumps, debris flows, grain flows, and liquefied flows in the origin of the Annot Sandstone, SE France (Stanley, 1963)
- First collection of papers on turbidite research (Bouma and Brouwer, 1964)
- 1964: Formation of the Joint Oceanographic Institutions for Deep Earth Sampling (JOIDES), composed of a group of four U.S. academic institutions: (1) Scripps Institution of Oceanography of the University of California at San Diego; (2) Lamont Geological Observatory of Columbia University (now Lamont-Doherty Earth Observatory); (3) Woods Hole Oceanographic

Institution; and (4) Institute of Marine Sciences of University of Miami (now Rosenstiel School of Marine and Atmospheric Science), for mapping of the global seafloor and deep-water drilling and coring (Source: Keir Becker, Chairman, JOIDES Science and Operations Committees; E-mail communication, 21 June, 2004)

- Description of deep-water sedimentary structures in Pliocene Pico Formation, California (Crowell, 1964)
- Photographic documentation of sole marks (Pettijohn and Potter, 1964)
- Importance of bottom currents in redistributing sediments in modern oceans (Hubert, 1964)
- A study of modern Zaire (formerly the Congo) submarine canyon, West Africa (Heezen et al., 1964)
- A book on sedimentary features of flysch (Dzulynski and Walton, 1965)
- First collection of papers on process sedimentology based on an SEPM symposium held in Toronto, Canada on May 18, 1964 (Middleton, 1965)
- Hydrodynamic interpretation of the 'Bouma Sequence', based on comparison with traction structures produced in experimental alluvial channels (Harms and Fahnestock, 1965; Walker, 1965)
- First clear differentiation of *turbulent* turbidity currents from *laminar* debris flows (Sanders, 1965)
- First documentation of nepheloid layers in deep water (Ewing and Thorndike, 1965)
- Use of vertical profile in environmental interpretation in physical sedimentology (Visher, 1965)
- First interpretation of deep-water bottom currents in the Pennsylvanian Ouachita flysch, Arkansas and Oklahoma (Klein, 1966)
- First flume experiments to understand body and head dynamics of turbidity currents (Middleton, 1966)
- Compilation of data on modern submarine canyons and valleys worldwide (Shepard and Dill, 1966)
- Recognition of a tight meander of the Monterey Canyon, offshore California (Shepard, 1966)
- 1966: Initiation of the first phase of the Deep Sea Drilling Project (DSDP) by signing the contract between the National Science Foundation and The Regents, University of California (Scripps Institution of Oceanography at the University of California, San Diego). Global Marine, Inc. performed the actual drilling and coring in 1966. Uniform Resource Locator (URL): http://www-odp.tamu.edu/glomar.html (accessed June 19, 2004)
- Recognition of parallel-to-slope thermohaline bottom currents in the deep sea and the introduction of the term *contour current* (Heezen, Hollister and Ruddiman, 1966; Hollister, 1967)

- Introduction of the term *contourite* for the deposit of a contour current (Hollister, 1967)
- Introduction of the terms *gravitite* for deposits of debris flows and *tractionite* for deposits of traction bottom currents (Natland, 1967)
- Discussion of sequence of structures in turbidites (Walton, 1967)
- Recognition of dish structures in turbidites (Wentworth, 1967)
- Recognition of bathymetric zonation using trace fossils (Seilacher, 1967)
- Documentation of paleocurrent patterns in the Ouachita flysch, Pennsylvanian, Oklahoma (Briggs and Cline, 1967)
- Interpretation of grain-flow deposits, California (Stauffer, 1967)
- Detailed description of a mid-sized modern submarine fan off Oregon (Nelson, 1968)
- A review of tsunamis (Coleman, 1968)
- 1968: the discovery of first deep-water Pardner Field in the Gulf of Mexico (Richardson et al., 2004)
- 1968: Initiation of the Deep Sea Drilling Project (DSDP) with the drillship *Glomar Challenger*, which drilled in a maximum water depth of 7044 m and penetrated 1741 m beneath ocean floor, for confirming the hypothesis of sea-floor spreading. Uniform Resource Locator (URL): http://www-odp.tamu.edu/glomar.html (accessed June 19, 2004)
- A detailed outcrop description of the Middle Ordovician flysch, Canada (Enos, 1969)
- First major critique of processes and products associated with the concept of turbidity currents (Van der Lingen, 1969).

2.2.4 Period: 1970–1979

- Introduction of the first model for modern submarine fans including the suprafan-lobe concept (Normark, 1970)
- A detailed outcrop study of the Pennsylvanian Ouachita flysch, Oklahoma (Cline, 1970)
- Documentation of large mass-transport deposits (slumps) on the modern Mississippi Fan, Gulf of Mexico (Walker and Massingill, 1970)
- Documentation of deep-water trace fossils in the Ouachita flysch, Pennsylvanian, Oklahoma (Chamberlain, 1971)
- A book on sea-floor features documented by underwater photographs (Heezen and Hollister, 1971)
- Bengal Fan: First detailed seismic study of the architecture, growth patterns, and sedimentation processes of the world's largest modern deep-sea fan, Bay of Bengal (Curray and Moore, 1971)
- Theoretical aspects of hydraulic jumps in turbidity currents (Komar, 1971)

- Criteria for recognition of deposits of coarse-grained high-concentration fluids (Fisher, 1971)
- Documentation of fine-grained deep-water carbonate turbidites in Monte Antola Flysch of Italy (Scholle, 1971)
- Documentation of modern slumps on continental slopes of 1–4° (Lewis, 1971)
- Introduction of first depositional lobe model for ancient submarine fans (Mutti and Ghibaudo, 1972)
- First channel-lobe submarine fan model based on outcrop studies in Italy and Spain (Mutti and Ricci Lucchi, 1972)
- Origin of laminated mudstone by turbidity currents (Piper, 1972)
- Navy Fan, offshore California: Sedimentation processes, architecture, and growth pattern of a small modern deep-sea fan on an active continental margin based on seismic and sediment cores (Normark and Piper, 1972)
- First major experiments on subaqueous debris flows (Hampton, 1972)
- Sidescan-sonar map of parts of floor of Santa Barbara Channel, California (Sanders, 1973)
- Origin of structureless deep-water conglomerates by liquefaction (Hendry, 1973)
- A collection of papers on *Evolving concepts in sedimentology* based on a conference held at the Johns Hopkins University in January 1971 to honor the distinguished contributions of the late Professor Francis Pettijohn (Ginsburg, 1973)
- An historical account of the turbidite paradigm (Walker, 1973)
- First collection of lecture notes on deep-water processes and facies models based on a Pacific Section SEPM Short Course given in Anaheim, California on May 12, 1973 (Middleton and Bouma, 1973)
- First classification of sediment-gravity flows based on sediment-support mechanisms (Middleton and Hampton, 1973)
- Experiments on decrease in scour rate of freshly deposited muds (Karcz and Shanmugam, 1974)
- Compilation of properties of submarine canyons (Whitaker, 1974)
- Distinction between turbiditic and non-turbiditic mudstone (Hesse, 1975)
- Documentation of water-escape structures (Lowe, 1975)
- First discussion of the concept of *sandy debris flows* with low clay content (Hampton, 1975)
- A classification of laminar-mass flow into *grain flow* with water as interstitial fluid and *slurry flow* with water–mud slurry as interstitial fluid (Carter, 1975)
- Amazon Fan, Equatorial Atlantic Ocean: Detailed seismic study of the architecture, growth patterns, and sedimentation processes of a large modern deep-sea fan (Damuth and Kumar, 1975)
- First turbidite facies scheme for interpreting deposits of submarine fans and the detached lobe concept of submarine fans (Mutti and Ricci Lucchi, 1975)
- The use of modern Bengal Fan as an analog for the Pennsylvanian Ouachita flysch in Oklahoma and Arkansas (Graham et al., 1975)

- Depositional cycles in turbidites (Ricci Lucchi, 1975)
- Distribution of large slides and debris flows on modern continental margins (Embley, 1976; Jacobi, 1976)
- Suspended sediment transport at the shelf margin (Pierce, 1976)
- Facies geometry of turbidite reservoirs, lower Pliocene, Ventura Field, California (Hsü, 1977)
- A collection of papers on deep-water carbonate environments (Cook and Enos, 1977)
- First seismic stratigraphic models for sedimentation on passive continental margins (Vail et al., 1977)
- First side-scan sonar surveys of modern submarine canyons, channels, and slope features (Belderson and Kenyon, 1976; Coleman and Garrison, 1977)
- Documentation of a large submarine slump, SE Africa (Dingle, 1977)
- A general submarine fan model with an emphasis on stratigraphic traps for hydrocarbon exploration (Walker, 1978)
- A collection of papers on submarine canyons, fans, and trenches (Stanley and Kelling, 1978)
- A collection of papers on continental slopes (Doyle and Pilkey, 1979)
- A vertical facies model for fine-grained turbidites (Piper, 1978)
- Detailed seismic study of the architecture, growth patterns, and sedimentation processes of a large modern deep-sea fan–Mississippi Fan (Moore et al., 1978)
- Tectonics and sedimentation of the Sevier Shale Basin, Middle Ordovician, Tennessee (Shanmugam, 1978)
- A model for deposits of fine-grained debris flows, Middle Ordovician, Tennessee (Shanmugam and Benedict, 1978)
- Tectonic significance of distal turbidites, Middle Ordovician, Tennessee (Shanmugam and Walker, 1978)
- Documentation of up- and down-bottom currents, induced by tidal forces, in submarine canyons (Shepard and Marshall, 1978; Shepard et al., 1979)
- A field trip guidebook for *AAPG Deep-water clastic reservoir school* held during May 14–18, 1979 in Ventura, California (Nilsen, 1979)
- Petrology of the modern Bengal Fan, Bay of Bengal (Ingersoll and Suczek, 1979)
- Dipmeter and wireline-log motifs of submarine channels and lobes (Selley, 1979)
- Distinction between fine-grained turbidites and contourites (Stow, 1979)
- A review of modern and ancient contourites (Stow and Lovell, 1979)
- A classification of sediment-gravity flows based on rheology and sediment-support mechanism (Lowe, 1979)
- Mounded seismic geometry of petroleum-producing Frigg Fan, lower Eocene, Frigg Field, North Sea (Heritier et al., 1979)
- A review of mass movement processes (Nardin et al., 1979)
- Documentation of mass movements on ancient carbonate slopes (Cook, 1979)

- Sizes of submarine slides (Woodcock, 1979)
- 1979: The year of first commercial production from the deep-water Cognac Field (312 m water depth) in the Gulf of Mexico (Table 2.1) (Richardson et al., 2004). Depending on water depths, different types of deep-water development systems are used in the Gulf of Mexico (Fig. 2.1):
  (1) *Fixed Platform (FP)* consists of a jacket with a deck placed on top. It is used for water depths up to 1500 ft (457 m).

Table 2.1 Selected productive deep-water projects in the Gulf of Mexico (Richardson et al., 2004)

Year of First Production	Field or Project	Operator	Block	Water Depth in ft (m)	System Type*** (See Fig. 2.1)
1979	Cognac*	Shell	MC 194	1023 (312 m)	Fixed Platform
1984	Lena	ExxonMobil	MC 280	1000 (305 m)	Compliant Tower
1989	Bullwinkle	Shell	GC 65	1353 (412 m)	Fixed Platform
1994	Auger	Shell	GB 426	2860 (872 m)	TLP
1996	Mars	Shell	MC 807	2933 (894 m)	TLP/Subsea
1996	Popeye	Shell	GC 116	2000 610 m)	Subsea
1997	Ram-Powell	Shell	VK 956	3216 (980 m)	TLP
1997	Troika	BP	GC 200	2721 (829 m)	Subsea
1999	Genesis	ChevronTexaco	GC 205	2590 (789 m)	Spar
2000	Conger	Amarada Hess	GB 215	1500 (457 m)	Subsea
2000	Diana	ExxonMobil	EB 945	4500 (1372 m)	Subsea
2000	Hoover	ExxonMobil	AC 25	4825 (1471 m)	Spar
2000	Europa	Shell	MC 935	3870 (1180 m)	Subsea
2001	Nile	BP	VK 914	3535 (1077 m)	Subsea
2001	Typhoon	ChevronTexaco	GC 237	2679 (817 m)	TLP
2002	Boomvang	Kerr McGee	EB 643	3650 (1113 m)	Spar
2002	Camden Hills	Marathon	MC 348	7216 (2199 m)	Subsea
2002	King Kong	Mariner	GC 472	3980 (1213 m)	Subsea
2002	King's Peak	BP	DC 133	6845 (2086 m)	Subsea
2003	Falcon	Pioneer	EB 579	3638 (1109 m)	Subsea
2003	Herschell/Na Kika	Shell	MC 520	6739 (2054 m)	FPS/Subsea
2003	Matterhorn	TotalFinaElf	MC 243	2850 (869 m)	TLP
2003	Pardner**	Anadarko	MC 401	1139 (347 m)	Subsea

*First commercial production from a deep-water field in the Gulf of Mexico.
**First deep-water field discovery (1968) in the Gulf of Mexico.
***System Type: TLP = Tension Leg Platform; FPS = Floating Production System.
Blocks
AC = Alaminos Canyon
DC = DeSoto Canyon
EB = East Breaks
GB = Garden Banks
GC = Green Canyon
MC = Mississippi Canyon
VK = Viosca Knoll
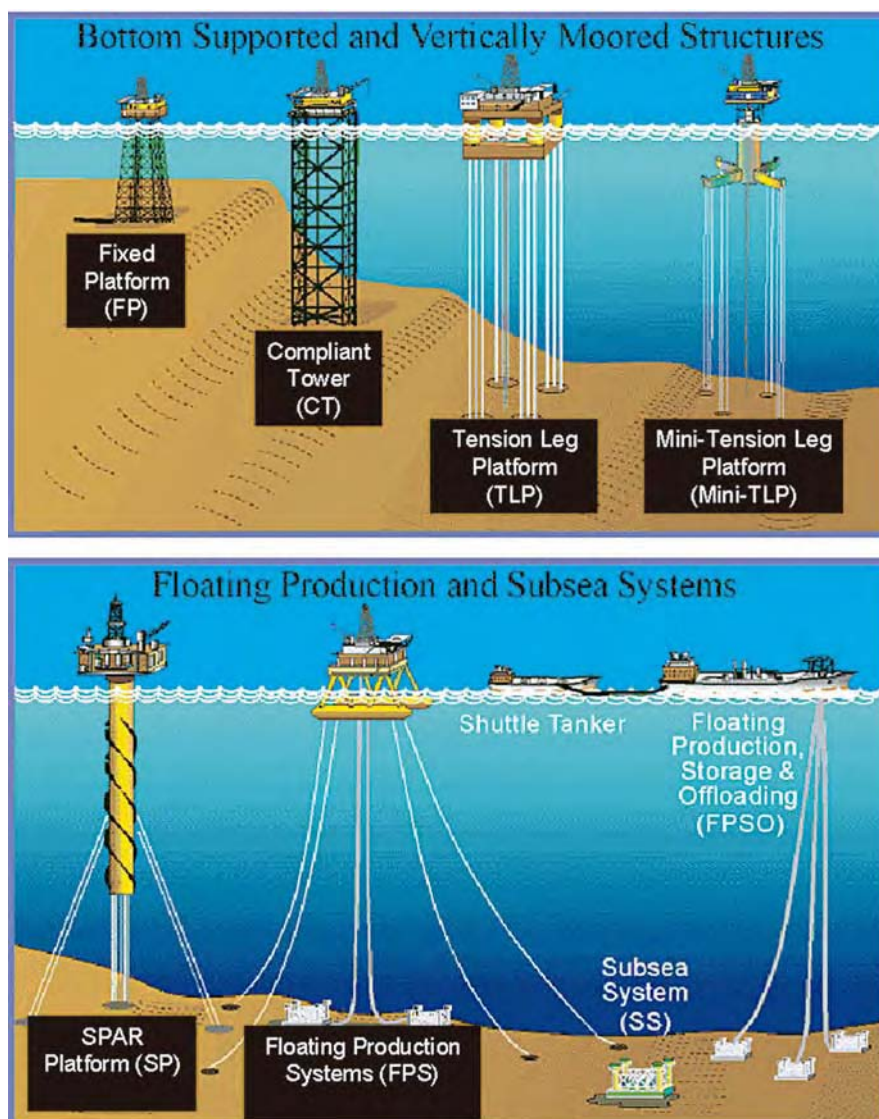
Fig. 2.1. **Types of deep-water development systems in the Gulf of Mexico.** *Fixed Platform (FP)* **is used for water depths up to 1500 ft (457 m).** *Compliant Tower (CT)* **is used for water depths between 1000 and 2000 ft (305–610 m).** *Tension Leg Platform (TLP)* **is used for water depths approaching 4000 ft (1220 m).** *Mini-Tension Leg Platform (Mini-TLP)* **is a low-cost platform developed for production of smaller deep-water reserves that would be uneconomic to produce using conventional TLP.** *SPAR Platform (SP)* **is used for water depths up to 3000 ft (914 m) and can be extended its use to water depths as great as 7500 ft (2286 m).** *Floating Production System (FPS)* **is used for water depths ranging from 600 ft (183 m) to 7500 ft (2286 m).** *Subsea System (SS)* **is used for water depths greater than 5000 ft (1524 m). See Table 2.1 for examples of producing fields from the deep-water of Gulf of Mexico. (After Richardson et al. (2004). Credit: U.S. Department of the Interior, Minerals Management Service, Gulf of Mexico Region.)**

(2) *Compliant Tower (CT)* consists of a narrow, flexible tower and a piled foundation that can support a conventional deck. It is used for water depths between 1000 and 2000 ft (305–610 m).

(3) *Tension Leg Platform (TLP)* consists of a floating structure held in place by vertical, tensioned tendons connected to the sea floor by pile-secured templates. It is used for water depths approaching 4000 ft (1220 m).

(4) *Mini-Tension Leg Platform (Mini-TLP)* is a low-cost platform developed for production of smaller deep-water reserves that would be uneconomic to produce using conventional TLP.

(5) *SPAR Platform (SP)* consists of a large diameter single vertical cylinder supporting a deck. It is used for water depths up to 3000 ft (914 m) and can be extended to water depths as great as 7500 ft (2286 m).

(6) *Floating Production System (FPS)* consists of a semi-submersible unit equipped with drilling and production equipment and anchored in place with wire rope and chain, or dynamically positioned using rotating thrusters. It is used for water depths ranging from 600 ft (183 m) to 7500 ft (2286 m).

(7) *Subsea System (SS)* ranges from a single subsea well producing to a nearby platform, FPS, or TLP to multiple wells producing through a manifold and pipeline system to a distant production facility. It is used for water depths greater than 5000 ft (1524 m).

2.2.5 Period: 1980–1989

- A review of deep-water sedimentologic models (Gorsline, 1980)
- Origin of inverse grading in muddy debrites (Naylor, 1980)
- Sand-layer geometry of modern basin-floor turbidites (Pilkey et al., 1980)
- Rhythms in fine-grained turbidites, Middle Ordovician, Tennessee (Shanmugam, 1980)
- A vertical facies model for fine-grained turbidites (Stow and Shanmugam, 1980)
- Debate over submarine-fan concepts (Nilsen, 1980)
- Excursion guidebook for some Italian Basins prepared for the 2nd IAS European Regional Meeting. Bologna, Italy (Ricci Lucchi, 1981)
- A collection of papers on DSDP (Deep Sea Drilling Project) (Warme et al., 1981)
- A compilation of turbidites from DSDP (Kelts and Arthur, 1981)
- Documentation of large mass-transport deposits on the modern Amazon Fan, Equatorial Atlantic (Damuth and Embley, 1981)
- A review of GLORIA (Geological Long Range Inclined Asdic, where Asdic is an acronym for sonar) side-scan sonar survey (Laughton, 1981)
- A review of origin of submarine canyons (Shepard, 1981)
- A review of petroleum source beds of deep-marine origin (Kvenvolden, 1981)
- A review of debris flow (Takahashi, 1981)

- A review of gravity currents in the laboratory, atmosphere, and ocean (Simpson, 1982)
- Compilation of data in support of eustatic control of turbidites and winnowed turbidites (Shanmugam and Moiola, 1982)
- Analogous tectonic evolution of Ordovician foredeep basins in the Southern and Central Appalachians (Shanmugam and Lash, 1982)
- Recognition of 'fluvial-like' meandering pattern in the Wilmington Canyon (Stubblefield et al., 1982)
- A collection of AAPG papers on deep-water models for stratigraphic traps (Tillman and Ali, 1982)
- Deep-water facies in subduction complexes (Underwood and Bachman, 1982)
- A facies model for deposits of high-density turbidity currents (Lowe, 1982)
- A review of sedimentology of submarine fans (Howell and Normark, 1982)
- 1982: First COMFAN (COMmittee on FANs) Meeting, Pittsburgh, Pennsylvania: Realization of complexity of modern and ancient submarine fans and that no general model is applicable to describe all deep-water systems (Bouma, 1983/1984).
- Recognition of four types of flow transformations in sediment-gravity flows (Fisher, 1983)
- A collection of papers on the shelfbreak processes and facies (Stanley and Moore, 1983)
- Hydrocarbon-bearing sands of depositional lobe origin, lower Pliocene, Italy (Casnedi, 1983)
- Modern Storegga Slide, offshore Norway (Bugge, 1983)
- Fan *versus* non-fan model (Chan and Dott, 1983)
- Concept of flow stripping by turbidity currents (Piper and Normark, 1983)
- 1983: DSDP Leg 96 – First coring of a modern submarine fan (Mississippi Fan), Gulf of Mexico (Bouma, Coleman et al., 1985)
- Theoretical classification of processes between cohesive and cohesionless debris flows (Shultz, 1984)
- Discussion of debris-flow dynamics in subaerial environments (Costa and Williams, 1984)
- A review of debris flows (Johnson, 1984)
- A review of mechanics of rapid granular flows (Savage, 1984)
- Short course notes on modern and ancient deep-sea fan sedimentation (Nelson and Nilsen, 1984)
- A collection of papers on fine-grained turbidites (Stow and Piper, 1984)
- Deep-sea depositional models for fine-grained organic-carbon-rich sediment (Arthur et al., 1984)
- Compilation of data in support of eustatic control of calciclastic turbidites (Shanmugam and Moiola, 1984)
- HEBBLE (High-Energy Benthic Boundary Layer Experiment) project, North Atlantic (Hollister and McCave, 1984)

- 1984: Replacement of the Deep Sea Drilling Project (DSDP) by the Ocean Drilling Program (ODP). Source: 'Brief history of the Ocean Drilling Program' in ODP Highlights by Chris Harrison, Chairman, JOIDES Executive Committee. Uniform Resource Locator (URL): http://joides.rsmas.miami.edu/files/ODP_Highlights.pdf (accessed June 19, 2004)
- Subaqueous slope failures in fjords (Syvitski, 1985)
- Discussion of behavior of turbidity currents (Allen, 1985b)
- 1985: Replacement of the *Glomar Challenger* (DSDP) by the *JOIDES Resolution* (ODP), a 143 m long and 21 m wide drilling vessel. *JOIDES Resolution,* with its rig capabilities to suspend as much as 9150 m of drill pipe to an ocean depth as great as 8235 m, has allowed participation of larger scientific parties, a larger laboratory and technical capability, and drilling operations in hostile oceans. Uniform Resource Locator (URL): http://www-dp.tamu.edu/shiphist.html (accessed June 19, 2004)
- Three types of turbidite systems based on lobe types and sea level control (Mutti, 1985)
- Provenance of modern deep-sea sands (Valloni, 1985)
- Submarine-ramp model, an alternative to submarine-fan model (Heller and Dickinson, 1985)
- First critique of the turbidite facies scheme used for interpreting submarine-fan environments (Shanmugam et al., 1985a)
- First critique of the detached lobe model of submarine fans (Shanmugam and Moiola, 1985)
- First model on seismic expression of submarine fans in a sequence-stratigraphic framework (Mitchum, 1985)
- A classification of deep-water facies (Pickering et al., 1986)
- A model for geometry of gully-fill sands and related sand injections, upper Jurassic, East Greenland (Surlyk, 1987)
- Introduction of basin-floor fan and slope fan models in a sequence-stratigraphic framework (Vail, 1987)
- Comparison of modern and ancient turbidite systems (Mutti and Normark, 1987)
- Mass wasting features on the continental slope, Northwest Europe (Kenyon, 1987)
- Second COMFAN Meeting, Parma, Italy, 1988
- Discovery of highly meandering distributary channels on modern deep-sea fans during GLORIA side-scan sonar survey of the Amazon Fan, Equatorial Atlantic (Damuth et al., 1988)
- First comprehensive review of modern and ancient submarine fans (Shanmugam and Moiola, 1988)
- Origin of duplex like structures in submarine fan channels by slumping, Ouachita Mountains, Arkansas (Shanmugam et al., 1988c)
- Experiments on high-density turbidity currents (Postma et al., 1988)

- Modern examples of sediment drifts, Argentine Basin, South Atlantic (Klaus and Ledbetter, 1988)
- Discussion of mechanisms of high concentration sediment-gravity flows, based on flume study and on field study of the Annot Sandstone, SE France (Oakeshott, 1989)
- A textbook on deep-marine environments (Pickering et al., 1989)
- A critique of the 'Bouma Sequence' (Hsü, 1989).

2.2.6 Period: 1990–1999

- A collection of papers based on a Pacific Section SEPM Short Course *Deep-Marine Sedimentation: Depositional models and case histories in hydrocarbon exploration & development* given in San Francisco, California on June 3, 1990 (Brown et al., 1990)
- Historical perspectives and evolution in the studies of deep-marine deposition (Brown, 1990)
- A review of deep-marine facies models (Shanmugam, 1990)
- A review of rapid granular flows (Campbell, 1990)
- A review of sediment movement on steep delta slopes (Nemec, 1990)
- First study of a modern fan – Mississippi Fan – using standard industry multi-fold seismic data in a sequence-stratigraphic framework (Weimer, 1990)
- A collection of papers on seismic expression of submarine fans (Weimer and Link, 1991)
- Sequence-stratigraphic models for deep-water systems (Vail et al., 1991)
- A critical review of submarine fan lobe concepts (Shanmugam and Moiola, 1991)
- A tribute to Francis Parker Shepard (1897–1985) (Rusnak, 1991)
- A collection of papers in marine geology in honor of Francis Parker Shepard (Osborne, 1991)
- Abandonment of Normark's (1970) suprafan lobe concept by Normark (1991)
- Abandonment of Walker's (1978) general submarine fan model by Walker (1992a)
- Abandonment of general submarine fan model by Mutti (1992)
- A photographic book on turbidite sandstones (Mutti, 1992)
- Reinterpretation of deep-water massive sands as sandy debrites in the North Sea (Shanmugam, 1992a)
- A review of submarine canyons (Shanmugam, 1992b)
- Dendritic channel patterns at the terminus of the Mississippi Fan, Gulf of Mexico (Twichell et al., 1992)
- A review of turbidity currents and their deposits (Middleton, 1993)
- A review of deep-sea contourites (Hollister, 1993)
- Documentation of giant ancient sandy slides, Antarctica (Macdonald et al., 1993)
- Documentation of hydrocarbon-bearing reservoirs in bottom-current reworked sands, Plio-Pleistocene, Gulf of Mexico (Shanmugam et al., 1993a,b)

- Documentation of deep-water reservoir sands of slump and debris flow origin, Norwegian North Sea (Shanmugam et al., 1994)
- A classification of turbidite fan models based on grain size and feeder system (Reading and Richards, 1994)
- A collection of papers on deformation of sediments (Maltman, 1994)
- A collection of papers on submarine fans and turbidite systems that include petroleum-producing reservoirs (Weimer et al., 1994)
- 1994: A collection of papers on contourites based on a symposium held at the 14th International Sedimentological Congress in Recife, Brazil in August 1994, which was also the *Third International Workshop on Bottom Currents and Contourites* (Stow and Faugerès, 1998)
- 1994: ODP Leg 155 (1994) – First systematic, continuous deep coring of stratigraphic and seismic units, architecture, and sediment facies of the Amazon Fan (Flood et al., 1995)
- A collection of papers on reservoir characterization of deep-water clastic systems (Hartley and Prosser, 1995)
- Reinterpretation of classic turbidites of the Pennsylvanian Jackfork Group in Arkansas and Oklahoma as deposits of sandy debris flows (Shanmugam and Moiola, 1995)
- Documentation of hydrocarbon-producing Pliocene sands of slump and debris flow origin in the Edop Field, offshore Nigeria (Shanmugam et al., 1995b; Shanmugam, 1997c)
- A critique of the basin-floor fan concept in a sequence-stratigraphic framework (Shanmugam et al., 1995a, 1996)
- An atlas of architectural style in turbidite systems (Pickering et al., 1995)
- A book on submarine channels (Clark and Pickering, 1996)
- A study of U.S. Continental slopes (Pratson and Haxby, 1996)
- First paper to question the basic tenet of high-density turbidity currents (Shanmugam, 1996a); this was the most cited article in modern sedimentary research according to Science Citation Index (Racki, 2002, 2003)
- Perception versus reality in deep-water exploration (Shanmugam, 1996b)
- A collection of papers on 'event' beds (Einsele et al., 1996)
- A collection of papers from a symposium in honor of Professor Gerard V. Middleton held at the Annual Meeting of the Geological Society of America, Northeastern Section, Buffalo, New York in March 1996 (Cheel and Leckie, 1997)
- Long runout distances of modern submarine slides (Hampton et al., 1996)
- A classification of debris-flow deposits (Coussot and Meunier, 1996)
- Documentation of slump and debris-flow dominated deep-water reservoirs using conventional core from the Zafiro Field, Equatorial Guinea (Famakinwa et al., 1996)
- Documentation of cores from the Northwest European Hydrocarbon Province (Oakman et al., 1997)

- A debate entitled *Processes of deep-water clastic sedimentation and their reservoir implications: what can we predict?* was held at the 1997 AAPG/SEPM Convention in Dallas, Texas.
- A critique of the Bouma Sequence and the turbidite mind set (Shanmugam, 1997a)
- A critique of the application of parasequence concept to deep-water systems (Shanmugam, 1997b)
- History behind dispelling the myth of sea-floor tranquility (Friedman and Sanders, 1997)
- A review of petroleum exploration in deep-water deposits (Sanders and Friedman, 1997)
- A review of physics of debris flows (Iverson, 1997)
- Documentation of tongue-like debris flows on the glaciated Norwegian-Barents Sea continental margin (Elverhoi et al., 1997)
- First experiments on subaqueous sandy debris flows with low clay content (Marr et al., 1997, 2001)
- Turbidite channel-levee complexes in submarine canyons in Brazil (Bruhn and Walker, 1997)
- First experiments documenting hydroplaning of subaqueous debris flows (Mohrig et al., 1998)
- Modern tidal rhythmites in a deep-water estuary (Cowan et al., 1998)
- A review of fossil contourites (Stow et al., 1998)
- A review of slope and base-of-slope systems (Galloway, 1998)
- A book on turbidite systems of SE France (Pickering and Hilton, 1998)
- A book on dimensions and geometries of deep-water systems (Shanmugam, 1998)
- 1998: A joint EAGE/AAPG research conference entitled *Developing and managing turbidite reservoirs: case histories and experiences* was held in Almeira, Spain in October 1998 (Weimer et al., 2000a)
- Reserves from 40 giant (> 500 million barrels oil equivalent) deep-water clastic reservoirs (Pettingill, 1998)
- A defense of facies models (Miall, 1999).

2.2.7 Period: 2000–May 2005

- A collection of papers presented at *Geoscience 98*, Keele (U.K.) at a Special Symposium entitled *Deep-water sedimentary systems: new models for the 21st Century* (Stow and Mayall, 2000)
- 2000: A *Workshop on the Prediction of Underwater Landslide and Slump Occurrence and Tsunami Hazards off of Southern California* was held during 10–11 March at the University of Southern California (Tappin, 2004)
- A special volume on fine-grained turbidites (Bouma and Stone, 2000)
- A review of deep-water massive sands (Stow and Johansson, 2000)

- A critical review of 50 Years (1950s–1990s) of the turbidite paradigm (Shanmugam, 2000a)
- A tribute to John Essington Sanders (1926–1999)*,* a geologic pioneer (Friedman, 2000)
- A presentation entitled '*John E. Sanders and the turbidite controversy*' at a '*Conference on the History of Geologic Pioneers,*' held at Rensselaer Center of Applied Geology, Troy, New York (Shanmugam, 2000b)
- A review of sandy submarine fans (Piper and Normark, 2001)
- A collection of papers on seismites, seismo-turbidites, and tsunamites (Shiki et al., 2000)
- A collection of papers on particulate gravity currents (McCaffrey et al., 2001)
- Sandy submarine braidplains as potential reservoir facies (Hesse et al., 2001)
- A collection of papers on deep-water reservoirs of the world (Weimer et al., 2001)
- Intrastratal deformation layers (Kawakami and Kawamura, 2002)
- Transition from debris flow to hyperconcentrated flow (Sohn et al., 2002)
- A review of bathymetric surveys of underwater landslides in Hawaii (Moore and Clague, 2002)
- A collection of 30 papers on modern and ancient contourite systems (Stow et al., 2002)
- A tribute to Charles Davis Hollister (1936–1999), the father of 'contourites' (McCave, 2002)
- 2002: A collection of papers based on a workshop entitled *Turbidites: models and problems* that was held during May 21–25, 2002 at the University of Parma, Italy (Mutti et al., 2003a)
- Dispelling of ten turbidite myths (Shanmugam, 2002a)
- Debate over inverse grading in turbidites (Shanmugam, 2002b)
- Online *Encyclopedia* article on deep-marine sediments (Shanmugam, 2002c)
- Online *Encyclopedia* article on submarine canyons (Shanmugam, 2002d)
- A keynote address on '*Deep-water processes and turbidite facies models: a paradigm shift*' (Shanmugam, 2002e)
- Documentation of deep-marine tidal bottom currents and their reworked sands in submarine canyons (Shanmugam, 2003)
- 2003: Initiation of the Integrated Ocean Drilling Program (IODP) to conduct basic research into the history of the ocean basins and the overall nature of the crust beneath the seafloor. Uniform Resource Locator (URL): http://www.oceandrilling.org/ (accessed June 19, 2004)
- Link between deltaic and turbiditic sedimentation (Mutti et al., 2003b)
- Stratigraphic process-response model for submarine channels in Permian Brushy Canyon outcrops (Gardner et al., 2003)
- Generation of turbidity current from submarine debris flows and slides in laboratory experiments (Mohrig and Marr, 2003)

- A critique of the classification of sediment-gravity flows (Dasgupta, 2003)
- A collection of papers based on the 1st International Symposium on *Submarine Mass Movements and Their Consequences* (Locat and Mienert, 2003)

  Significant projects on submarine mass movements:

(1) ADFEX (Arctic Delta Failure Experiment): 1989–1992
(2) GLORIA (Geological Long Range Inclined Asdic), a sidescan survey of U.S. Exclusive Economic Zone: 1984–1991
(3) STEAM (Sediment Transport on European Atlantic Margins): 1993–1996
(4) ENAM II (European North Atlantic Margin): 1996–1999
(5) STRATAFORM (STRATA FORmation on the Margins): 1995–2001
(6) Seabed Slope Process in Deep Water Continental Margin (Northwest Gulf of Mexico): 1996–2004
(7) COSTA (Continental Slope Stability): 2000–2004.

- Flow transformation in particulate gravity currents (Waltham, 2004)
- An overview of sedimentology in deep water exploration in the Gulf of Mexico with the belief that all deep-water reservoirs are turbidites (Abegg, 2004)
- Surging *versus* continuous turbidity currents in experiments (Lamb et al., 2004)
- An acknowledgement of complex deep-water environments and the limitations of simple facies models (Walker, 2004)
- A special volume on *COSTA – continental slope stability: major aims and topics* (Mienert, 2004)
- Discovery of sinuous Cap Timiris Canyon, offshore Mauritania (Krastel et al., 2004)
- A keynote address on '*Modern deep-water environments and their implications for sandstone petroleum reservoirs*' (Shanmugam, 2004)
- A collection of papers based on a symposium on '*Tsunamis*' that was held in Nice in the framework of the joint assembly of the three international bodies on Earth Sciences, i.e., the EGS (European Geophysical Society), the AGU (American Geophysical Union), and the EUG (European Union of Geosciences) during April 6–11, 2003 (Pelinovsky and Tinti, 2005)
- An integrated study for the safe development of a deep-water gas field (Ormen Lange) within the Storegga Slide Complex, NE Atlantic continental margin (Solheim et al., 2005)
- A review of sand injectites as an emerging global play in deep-water clastic environments (Hurst et al., 2005)
- A review of ancient sand-rich submarine fans (Mattern, 2005)
- Fluid mechanics and rheology of dense suspensions (Stickel and Powell, 2005).

2.3 Scientific revolutions

Kuhn (1962) argued that science is not a steady, cumulative acquisition of knowledge as portrayed in the textbooks. Instead, it is a series of peaceful interludes punctuated by intellectually violent revolutions. In these revolutions, one conceptual world view is replaced by another more complex view. Kuhn (1996, p. 84–85) wrote that

'*The transition from a paradigm in crisis to a new one from which a new tradition of normal science can emerge is far from a cumulative process, one achieved by an articulation or extension of the old paradigm. Rather it is reconstruction of the field from new fundamentals, a reconstruction that changes some of the field's most elementary theoretical generalizations as well as many of its paradigm methods and applications.*'

Kuhn's stages of scientific development may be grouped into five steps: (1) early random observations; (2) first paradigm; (3) crisis; (4) revolution; and (5) normal science or new paradigm (Fig. 2.2). Once the final step or normal science is achieved (i.e., the new paradigm); however, scientists enjoy a sense of confidence as well as comfort. This comfort often leads to complacency. The normal science is influential in: (1) forcing scientists to force-fit nature into preconceived models of the paradigm; (2) encouraging scientists to ignore data or observations that do not fit the basic principles of the paradigm; (3) discouraging scientists from inventing new theories; and (4) making scientists intolerant of new theories invented by others (Kuhn, 1996, p. 24). There are ample examples of such influences on deep-water research (see Chapters 8, 9, and 10).
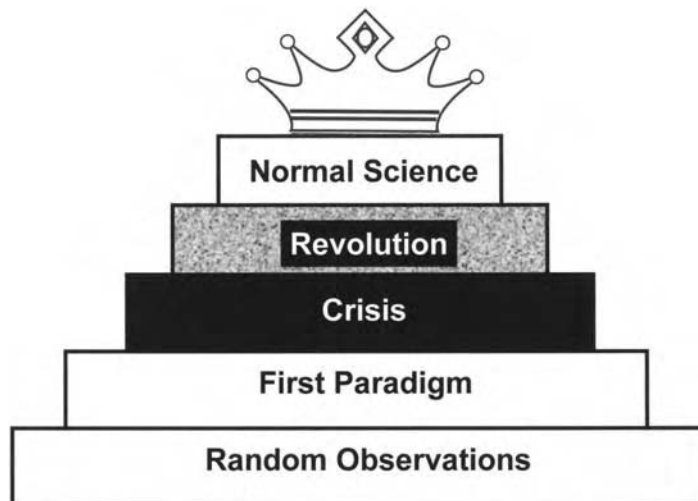
Fig. 2.2. A depiction of Kuhn's (1996) stages of scientific development.

The year 1872, when the Royal Society of London and the Royal Navy organized the voyage of *H.M.S. Challenger* (1872–1876), marked the birth of modern deep-sea exploration (Murray and Renard, 1891). In terms of Kuhn's scientific stages, deep-water research conducted during the period of 1872–1948 represents the first stage of 'early random observations.' The year 1948 may be considered to mark the advent of the 'first paradigm' (i.e., the turbidite paradigm). At the 18th International Geological Congress held in London (U.K.) in 1948, C. I. Migliorini discussed the formation of graded bedding by density currents; Francis P. Shepard showed underwater photographs of steep, massive walls of submarine canyons; and Philip H. Kuenen discussed the erosive potential of high-density currents in creating submarine canyons. Until 1950, when Kuenen and Migliorini (1950) published their seminal paper '*Turbidity currents as a cause of graded bedding,*' the geologic community generally believed that the deep sea was a tranquil realm free of current activity where only mud accumulated slowly from pelagic settling (see review by Friedman and Sanders, 1997). Since 1950, the deposition of turbidite sands in deep-water environments has gained global acceptance (Fig. 2.3). Today (2005), however, the turbidite paradigm has gone to the other extreme. Now we believe that virtually all deep-water sands are 'turbidites' deposited on submarine fans. During a period of just 55 years, geologists went from a state of caution to a state of complacency regarding turbidity currents and their deposits.

Although Walker (1973) and Stow (1985) believed that the normal science stage in deep-water research was achieved in 1950 and 1983, respectively, my view is that deep-water research is still in a crisis mode (Fig. 2.4). This crisis started when the importance of deep-water bottom currents was realized in the late 1960s. In the 1980s, fundamental questions were raised regarding the Bouma Sequence, fan models, and turbidite facies schemes. The 1990s were a period of re-evaluation and abandonment of fan models, debate over the concept of high-density turbidity currents, experiments on sandy debris flows, reinterpretation of deep-water massive turbidite sands as sandy debrites, and skepticism over the use of seismic geometries for interpreting depositional processes.

Throughout history, the geologic community has been known for its intolerance of new observations and theories (Shanmugam, 1986). A well-known example is the long-standing objection to the concept of long-runout landslides. This objection was based on the conventional wisdom that the runout distance of a landslide equals its vertical fall distance. Although there are many documented cases of landslides (e.g., submarine slides in Hawaii with more than 200 km of runout distances, see Hampton et al., 1996) with long-runout distances (up to 100 times their vertical fall) and high speeds (up to 200 miles or 320 km/h), the geologic community rejected mechanisms that attempted to explain landslides that travel so far and so fast. There are at least 20 published theories that explain this mechanical paradox. Some of these examples are: (1) lubrication by liquefied
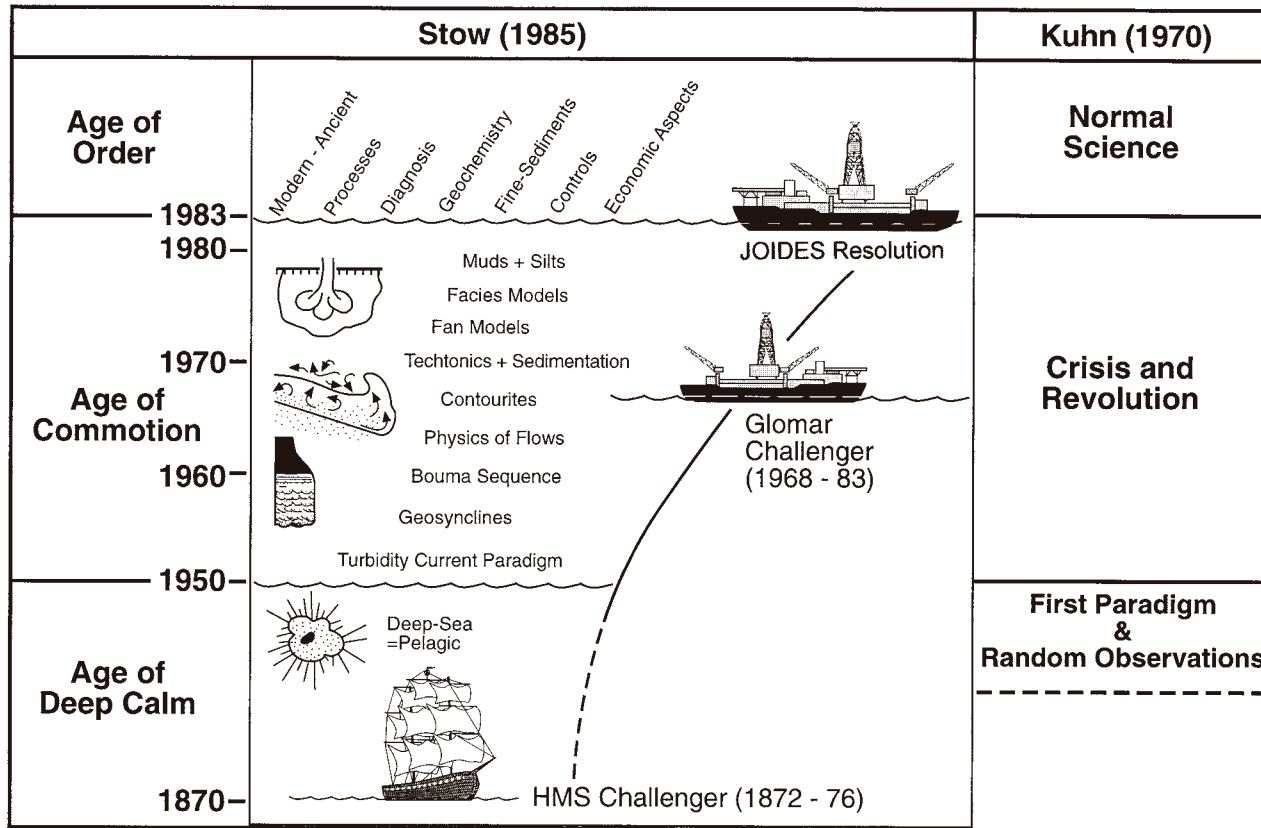
Fig. 2.3. Stow's (1985) Stages of deep-water research. Kuhn's (1970) stages are shown for comparison. (Modified after Stow (1985). Reproduced with permission from the Geological Society of London.)
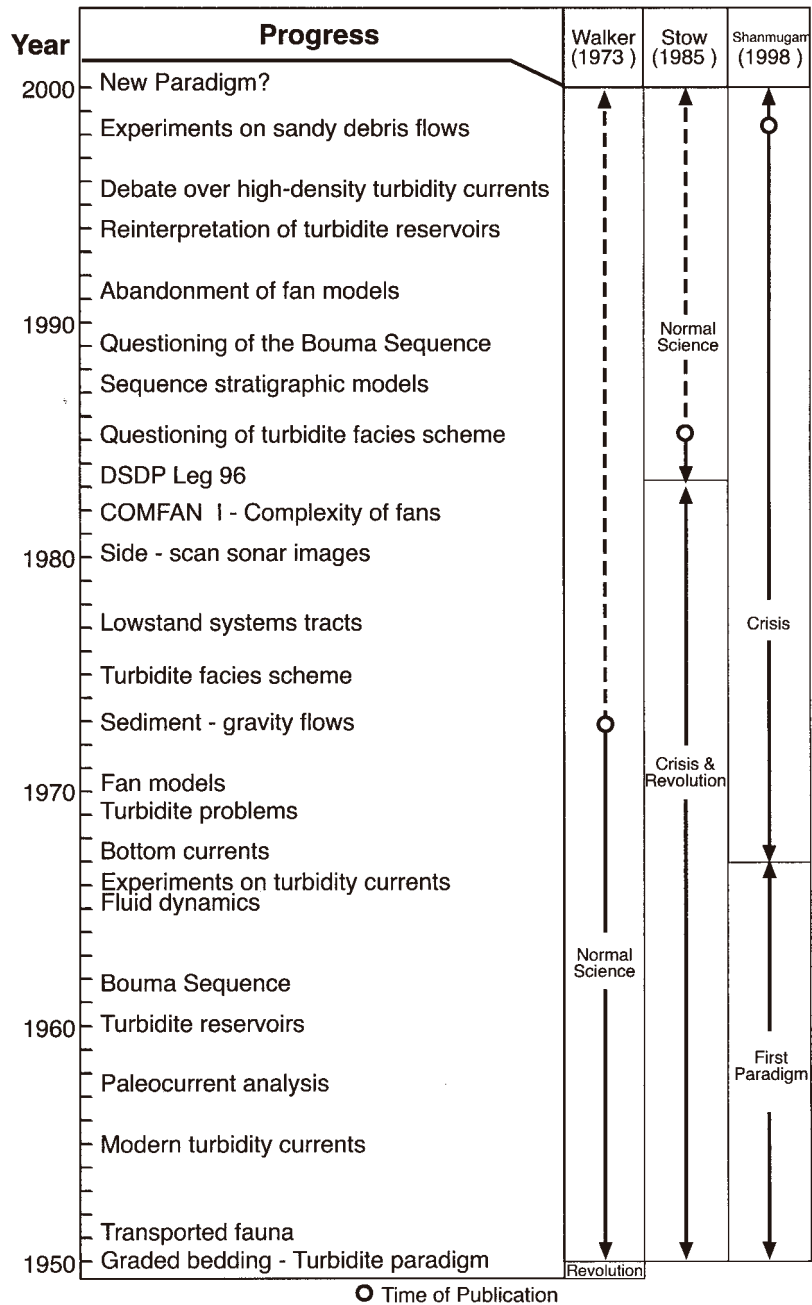
Fig. 2.4. **Differing perspectives on stages of deep-water research. Walker (1973) and Stow (1985) believed that the normal science stage was achieved in 1950 and 1983, respectively. However, I contend that we are still in a crisis mode. (After Shanmugam (2000a). Reproduced with permission from Elsevier.)**

saturated soil entrained during transport (Buss and Heim, 1881; Hungr and Evans, 2004); (2) cushion of compressed air beneath the slide (Shreve, 1968); (3) fluidization by dust dispersions (Hsü, 1975); (4) spontaneous reduction of friction angle at high rates of shearing (Scheidegger, 1975; Campbell, 1989); and (5) acoustic fluidization (Melosh, 1979). A major turning point on this mind set occurred on May 18, 1980 when the eruption of Mount St. Helens in the U.S. generated impressive long runout landslides that were captured on videotapes (see The Learning Channel, 1997). The lesson learned here was that we should not simply reject a new observation or theory because of a lack of precedents. By design, new observations and theories cannot have precedents.

Perhaps, the best known example is the rejection of Alfred Wegener's theory of 'continental drift' by the geologic community in the early part of the twentieth century. This was because there were no established mechanisms to explain the 'drifting continents.' Sir Edward Bullard (1975, p. 5) offered the most insightful answer to the question 'why the geologic community rejected Wegener's theory for so long?'

'*It is easy to see why there was such strong opposition to Wegener in the 1920s and 1930s. If weak or fallacious arguments are mixed with strong ones, it is natural for opponents to refute the former and to believe that the whole position has been refuted. There is always a strong inclination for a body of professionals to oppose an unorthodox view. Such a group has a considerable investment in orthodoxy: they have learned to interpret a large body of data in terms of the old view, and they have prepared lectures and perhaps written books with the old background. To think the whole subject through again when one is no longer young is not easy and involves admitting a partial misspent youth. Further, if one endeavors to change one's views in midcareer, one may be wrong and be shown to have adopted a specious novelty and tried to overthrow a well-founded view that one has oneself helped to build up. Clearly it is more prudent to keep quiet, to be a moderate defender of orthodoxy, or to maintain that all is doubtful, sit on the fence, and wait in statesmanlike ambiguity for more data (my own line till 1959).*'

The geologic community did reverse its position on this issue when paleomagnetic evidence derived from polar-wandering studies (Runcorn, 1962) and sea-floor magnetic anomalies (Vine and Mathews, 1963) began to provide irrefutable evidence of continental drift and sea-floor spreading.

Sir Bullard's (1975) humorous analysis is quite fitting to the issues of the turbidite paradigm. Considering the monumental efforts that went into promoting turbidite systems and submarine fans in the form of journal articles, books, research symposiums, short courses, core workshops, and field trips, it is no surprise that many in the geologic community, especially in the petroleum industry, vehemently oppose any critique of the turbidite paradigm. However, once the emotional response over the critique subsides, the intellect will prevail.

Although science is dynamic, changes in scientific concepts are not always swift. Just over 500 years ago, it was still believed that the Earth was at the center of the universe as proposed by Ptolemy in the second century A.D. It took nearly 1500 years to prove that the Earth was not at the center of the universe by the works of Copernicus, Galilei, and Newton (Kuhn, 1996; Filkin, 1997). For his scientific conviction that the Earth rotates around the Sun, Galileo Galilei was wrongly convicted on a charge of heresy and he spent the rest of his life under house arrest until his death on January 8, 1642. Hopefully, we can resolve the deep-water problems in a shorter time span and without any house arrest!

2.4 A Philosophical retrospective

2.4.1 Genetic nomenclature

Geologic literature is inundated with genetic nomenclatures. A genetic nomenclature, by design, has a built-in interpretation of process of origin. The tradition of genetic nomenclature in sedimentary geology began with the introduction of the term *turbidite* for a deposit of a turbidity current in deep-water environments (Kuenen, 1957). Kuenen and Migliorini (1950, p. 99) and Kuenen (1967, p. 212) suggested that normal grading of a turbidite bed was a consequence of deposition from a single waning turbidity current. The AGI *Glossary of Geology* (Bates and Jackson, 1980, p. 269) also explained the origin of normal grading by '*deposition from a single short-lived turbidity current*'. The linkage between a turbidite bed and its origin by a single process is the foundation of genetic nomenclature. Although turbidity currents and their deposits have served as the impetus for the proliferation of genetic nomenclature, turbidity currents themselves have become the subject of controversy (see Chapter 7). Nevertheless, flow behaviors of turbidity currents and debris flows have been reasonably well established (Sanders, 1965; Hampton, 1972).

In order for a genetic term to succeed: (1) it must be based on sound fluid dynamic *principles;* and (2) its *usage* must be accurate (relying on sedimentological description), precise (referring to a single process), and consistent (requiring a steady and a uniform application). Natural amalgamated deposits, however, are often the result of multiple processes. They exhibit a complex array of features. To maintain the integrity of a genetic term, however, researchers are often forced to de-emphasize features that are too 'complex' to meet the requirements of a particular process-based genetic term. If one chooses to classify a deposit using a genetic term, no matter how complex the deposit may be, the basic tenet (i.e., the built-in process interpretation) of the genetic term must be maintained. A prudent approach to classify complex deposits would be to follow principles of process sedimentology.

A constraint that all genetic nomenclatures must face is the changing scientific concepts with time. Science is not a steady, cumulative acquisition of knowledge

as portrayed in the textbooks (Kuhn, 1962). Instead, it is a series of peaceful inter-ludes punctuated by intellectually violent revolutions. In emphasizing the impact of these scientific revolutions, Kuhn (1996, p. 111) articulated '*What were ducks in the scientist's world before the revolution are rabbits afterwards.*' Because geologic concepts and interpretations change with time, the definitive quality of genetic nomenclature encounters problems.

An attribute of genetic nomenclatures is that they usually end with '-ite' (Table 2.2). This practice is more cosmetic than scientific in purpose. There are genetic terms that do not follow this practice. Examples are *flysch* for turbidites (Hsü, 1970) and *olistostrome* for debrites (Flores, 1955).

2.4.2 Kinds of problems

Genetic nomenclatures have been used not only for sedimentary features, but also for igneous, metamorphic, tectonic, and meteorite-impact features (Table 2.2). Problems related to genetic nomenclatures may be grouped into six kinds in geology:

2.4.2.1 Misrepresentation of flow behavior

As a practice, the name should directly reveal the nature of the flow behavior (e.g., turbidite for deposit of turbidity current). However, this is not the case in many instances:

- The term *contourite* represents current orientation (Hollister, 1967), not the flow behavior.
- The term *unifite* represents texture (i.e., ungraded mud) (Feldhausen et al., 1981), not the flow behavior.
- The term *aeolianite* represents the God (i.e., Aeolius) (Bates and Jackson, 1980), not the flow behavior.
- The term *meanderite* represents river sinuosity (Shanmugam, 1984), not the flow behavior.

2.4.2.2 Multiple processes for a single term

As a rule, a genetic term must represent a single process. Gani (2004), however, proposed the term *densite* for deposits of multiple processes (i.e., high-density turbidity current, sandy debris flow, slurry flow, concentrated density flow, lique-fied flow, and fluidized flow).

Natland (1967) originally coined the term *gravitite* for deposits of debris flows. Lisitsyn (1986), however, redefined the term *gravitite* for multiple processes and products that include submerged landslides, slumps, mud torents, slurry flows, fluxoturbidites, dynamictites, single argillites, low and high density turbidity

Table 2.2 Lexicon of selected genetic terms ending with '-ite' (Modified after Shanmugam (2006))

Genetic terms	Comments (This study)	References*
Aeolianite	Represents the Aeolius (the god of the winds), not flow behavior	Sayles (1931); Bates and Jackson (1980)
Anastomosite	Implies river type, not flow behavior	Shanmugam (1984)
Atypical turbidite	Multiple processes (slumps, debris flows, and sand flows, not turbidity current)	Stanley et al. (1978)
Braidite	Implies river type, not flow behavior	Shanmugam (1984)
Contourite	Implies current orientation, not flow behavior	Hollister (1967)
Debrite	Plastic debris flow	Pluenneke (1976)
Densite	Implies multiple processes, not a single process	Gani (2004)
Diamictite	Pebbly mudstone; implies no genetic (glacial) connotation	Flint et al. (1960)
Fluxoturbidite	Complex origin (sand avalanche?), not turbidity current	Dzulynski et al. (1959)
Grainite	Implies grains, not flow behavior	Khvorova (1978)
Gravitite	Implies sediment gravity, not flow behavior	Natland (1967)
Gravite	Implies multiple processes, not a single process	Gani (2004)
Hemipelagite	Hemipelagic settling	Arrhenius (1963)
Hemiturbidite	Muddy turbidity current	Stow et al. (1990)
High-concentration sandy turbidite	Implies sandy debris flow, not turbidity current	Abreu et al. (2003)
Homogenite	Implies uniform grain size (ungraded mud), not flow behavior	Kastens and Cita (1981)
Hyperpycnite	Implies relative flow density, not flow behavior	Mulder et al. (2002)
Impactite**	Impacts by meteorite	Stöffler and Grieve (2003)
Injectite**	Injection in igneous, sedimentary, and metamorphic rocks, not flow behavior	Vivas et al. (1988)
Interpretite	A spoof on genetic terms!	Davies (1997)
Meanderite	Implies river type, not flow behavior	Shanmugam (1984)
Megaturbidite	Implies debris flow, not turbidity current	Labaume et al. (1987)
Pelagite	Pelagic settling	Arrhenius (1963)
Rhythmite	Implies no genetic (turbidite) connotation	Bramlette (1946)
Seismite**	Seismic shocks	Iqbaluddin (1978)
Seismoturbidite	Implies mass flow, not turbidity current	Mutti et al. (1984)
Suspensite	Suspension settling	Lisitsyn (1986)
Tectonite	Tectonically deformed rocks	Turner and Weiss (1963)
Tempestite	Implies multiple processes, not a single process	Ager (1974)
Tidalite	Deposition from tidal currents	Klein (1971, 1998)
Tillite	Pebbly mudstone; implies no genetic (glacial) connotation	Harland et al. (1966)
Tractionite	Traction deposition by bottom current	Natland (1967)
Tsunamite	Multiple processes, not a single process	Gong-Yiming (1988)
Turbidite	Implies turbulent turbidity current	Kuenen (1957)
Undaturbidite	No discernible meaning	Rizzini and Passega (1964)
Unifite	Implies grain size (ungraded mud), not flow behavior	Feldhausen et al. (1981); Stanley (1981)
Winnowite	Winnowing action of bottom current.	Shanmugam and Moiola (1982).

*References include those that introduced the term, used the term early, or considered appropriate.
**Unrelated to depositional processes.

currents, and contourites. Surprisingly, Lisitsyn (1986) did not cite the reference of Natland (1967) who coined the term.

2.4.2.3 Two genetic terms for a single origin
As a rule, a genetic term must represent a single origin. The term *tectonite* was first used for a tectonic origin of a rock with deformation features (Turner and Weiss, 1963). Later, the term *seismite* was used for earthquake-induced deformation features (Einsele et al., 1996, p. 2). The distinction between tectonics and earthquakes is fallacious because earthquakes are integral parts of tectonic activities.

2.4.2.4 Misuse of established nomenclature
As a rule, the term turbidites must be used only for deposits of turbidity currents (Sanders, 1965). However, Nakajima and Kanai (2000, p. 3) misused the term *turbidites* for deposits of submarine slumps. Mutti et al. (1999, p. 19) misused the term *turbidites* for deposits of all sediment-gravity flows that include grain flows, debris flows, fluidized flows, and turbidity currents.

2.4.2.5 Nomenclature without sound principles
The term *fluxoturbidites* was introduced by Dzulynski et al. (1959). The origin of these deposits is unclear. These deposits appear to represent sand avalanches, slumps, and other mass movements. Hsü (1989, p. 85), after investigating the meaning of the term fluxoturbidites, concluded that, '… *this is another case when a geologist wanted to hide his ignorance behind an exotic name*.'

The term *undaturbidite* was introduced by Rizzini and Passega (1964, p. 71). This deposit was thought to be formed from a suspension induced by violent storms. It was considered to represent an intermediate type between *tempestite* and *turbidite*. The problem is that the concept of 'tempestite' itself was ill-defined.

The term *tempestite* was first coined by Gilbert Kelling for storm-generated shelf sandstones (Brenchley, 1985), but the first published reference is by Ager (1974). Johnson and Baldwin (1996, p. 249) acknowledged that '*The hydrodynamic interpretation of modern shelf storm deposits is difficult because it has never been possible to correlate precisely the physical processes accompanying major storms and processes acting on the sea bed. Processes proposed include: (i) storm waves; (ii) wind-driven currents; (iii) storm waves combined with ebbing tidal currents; (iv) storm-surge ebb currents; (v) rip currents; (vi) tsunamis; and (vii) density currents*.' This statement implies that tsunami is a storm-related process; however, storms and tsunamis are two genetically unrelated phenomena. Storms, for example, are caused by changes in meteorological (climate and weather) conditions, whereas tsunamis are caused by undersea seismic activity as well as by extraterrestrial (meteorite) impacts on the sea surface. There is no geological reason for these two phenomena to occur concurrently. Furthermore, storm is not a single process. Therefore, the genetic term 'tempestite' falters in principle.

In emphasizing the difficulties of interpreting storm deposits, Morton (1988, p. 8) stated, '*The sedimentologic consequences of great storms are still debated because we almost always lack direct evidence linking the observed depositional features with extremely rare meteorologic events that have poorly defined characteristics other than the implied condition of equaling or exceeding storms of historical record.*'

The term *tsunamite* was used for deposits of tsunamis (Gong-Yiming, 1988). Direct evidence for depositional mechanics of tsunamis, however, is lacking. Although the rapid velocities of tsunami waves allow them to transport sediment ranging in size from mud to boulders, the mechanics of tsunami waves and related sediment transport have never been adequately modeled (Dawson and Shi, 2000). Attempts to simulate the movement of large boulders by tsunamis have encountered difficulties in simulating the effects of bottom friction on boulders of different shapes and densities (Noji et al., 1993). To date, no one has ever established the link between tsunami as a process and its deposit. Without the process-product linkage, the genetic term 'tsunamite' is meaningless for process interpretations (see Chapter 5).

2.4.2.6 Different levels of usage

A lingering problem in geology has been the usage of a single word whose meaning would change depending upon the level (sense) in which it is being used. Examples are:

- The term *ophiolite* was introduced to denote serpentinized mafic and ultramafic rocks ranging from spilite and basalt to gabbro and periodotite (Steinmann, 1905; see Wood, 1974). It was later used both as an *assemblage* term ('Steinmann Trinity') to emphasize its association with pillow lavas and radiolarian cherts (Hess, 1955), and as a *tectonic* term to represent oceanic mantle and crust (Dewey and Bird, 1970).
- The term *mélange* was introduced as a mapable rock unit by Greenly (1919). But it was later used as a genetic term to represent both *sedimentary mélange* or olistostrome (Hsü, 1974, p. 325) and *tectonic mélange* (Raymond, 1975, p. 8).
- The term *flysch* was introduced as an informal rock-stratigraphic unit (Studer, 1827). But it was later used not only as a descriptive term (*greywacke*) but also as an interpretive (*turbidite*) term (Hsü, 1970). In the 1960s, 'flysch', 'greywacke,' and 'turbidite' were used as synonymous terms.
- The term *greywacke* was first introduced as a descriptive term in 1789 (see Bates and Jackson, 1980), but was later used as an interpretive (*turbidite*) term (Pettijohn, 1957, p. 313).
- The term *facies* is being used as: (1) a *descriptive* term (e.g., sandstone facies); (2) an *interpretive process-product* term (e.g., turbidite facies); and (3) an *interpretive environmental* term (e.g., fluvial facies). Reading (1986b, p. 4) discouraged the usage of the term 'fluvial facies' for implying 'fluvial environment.'

He preferred to use the term facies only for the products of an environment, not for the environment (setting) itself.

• The term *tsunamite* is being used at two different interpretive levels (*sedimentological vs. historical*) (see Chapter 5). Customarily, researchers tend to place more emphasis on historical data than on sedimentological data for classifying deposits as products of tsunamis (Cita and Aloisi, 2000). This is troubling because the history can establish only the occurrence of a tsunami as a phenomenon; it cannot establish the physics of the flow. As a consequence, the term 'tsunamite' is the only word in the lexicon of geology that can represent a multitude of deposits or rocks that include turbidite, debrite, tempestite, fluxoturbidite, undaturbidite, seismite, seismoturbidite, gravitite, gravite, densite, tractionite, hyperpycnite, tidalite, unifite, homogenite, and injectite.

  Since the term 'greywacke' was first introduced in 1789, geologists have shown a remarkable tolerance for words with multiple meanings (e.g., flysch and greywacke) and for words with no discernible meanings (e.g., fluxoturbidite and undaturbidite). However, once in a while someone like R. L. Folk comes along and puts an end to this dialectal nonsense. Folk (1968, p. 125), following McBride (1962b), abandoned the term 'greywacke' by stating that he, '…*has discarded the term 'greywacke' from any seat in a quantitative, mineralogically-oriented classification of sandstones.*' The term greywacke is seldom used now. In short, genetic terms have caused more confusion than clarity in communicating fluid dynamics of depositional processes.

2.5 Synopsis

Despite the progress made in terms of gathering marine geological data, core and outcrop studies, theoretical understanding, and flume experiments during the past 120 years (1885–2005), our understanding of deep-water processes is still incomplete.

Chapter 3

Gravity-driven processes

3.1 Introduction

The objective of this chapter is to explain basic types and mechanics of gravity-driven processes and to provide criteria for interpreting processes in the rock record. This should minimize the two problems that students commonly face in dealing with deep-water gravity-driven processes: (1) controversy surrounding the meaning of a particular process in terms of its physical behavior; and (2) disagreements on criteria for recognizing deposit of that particular process. Readers who wish to explore the details of controversies surrounding deep-water processes should refer to Chapter 7.

Gravity-driven processes, such as slides, slumps, debris flows, and turbidity currents (Fig. 3.1), are important agents for transporting sediments downslope into deep-marine environments. Shelf-edge sediment failures, which are commonly responsible for generating gravity-driven processes, are triggered initially by one or more of the following external and internal causes:

- Eustatic changes in sea level (Daly, 1936)
- Submarine volcanic activity (Milne, 1897)
- Earthquakes, such as the 1929 Grand Banks tremor off U.S. east coast and Canada (Heezen and Ewing, 1952)
- Salt movements in intraslope basins, Gulf of Mexico (Tripsanas et al., 2004)
- Glacial loading on the Scotian margin, North Atlantic (Mosher et al., 2004)
- Oversteepening of submarine slope near the mouth of the Magdalena River, Colombia (Heezen, 1956)
- High sedimentation in the Mississippi delta-front setting, Gulf of Mexico (Coleman and Prior, 1982)
- Tsunamis (Gutenberg, 1939)
- Storm waves (Henkel, 1970)
- Biologic erosion of submarine canyon walls (Warme et al., 1978; Shepard, 1981)
- Generation of gas (Dill, 1964).
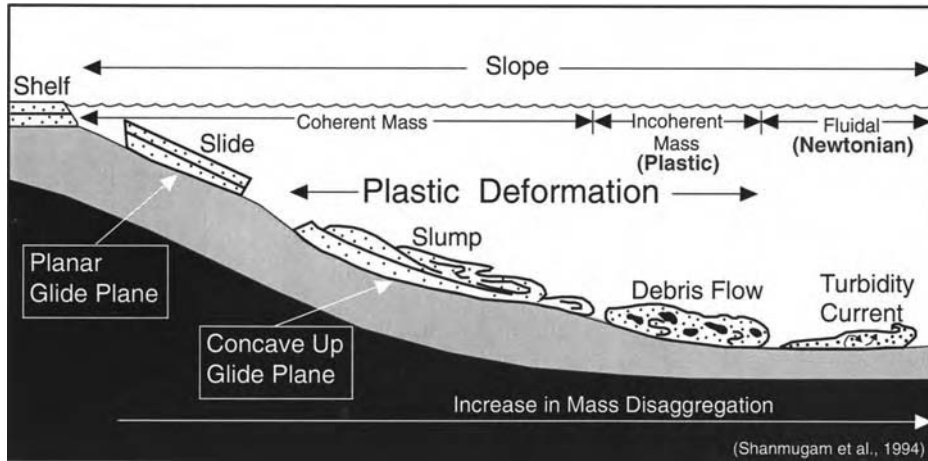
Fig. 3.1. Schematic diagram showing four common types of gravity-driven processes that transport sediment into deep-water environments. A *slide* represents a coherent translational mass transport of a block or strata on a planar glide plane (shear surface) without internal deformation. A slide may be transformed into a *slump*, which represents a coherent rotational mass transport of a block or strata on a concave-up glide plane (shear surface) with internal deformation. Upon addition of fluid during downslope movement, slumped material may transform into a *debris flow*, which transports sediment as an incoherent body in which inter-granular movements predominate over shear-surface movements. A debris flow behaves as a plastic flow with strength. As fluid content increases in a laminar debris flow, the flow may evolve into a Newtonian *turbidity current*. Not all turbidity currents, however, evolve from debris flows. Some turbidity currents may evolve directly from sediment failures. Turbidity currents can develop near the shelf edge, on the slope, and in distal basinal settings. (After Shanmugam et al. (1994). Reprinted by permission of the American Association of Petroleum Geologists whose permission is required for further use.)

Gravity-driven processes in deep-water environments, based partly on Varnes (1958, 1978), Dott (1963), Sanders (1965), Middleton and Hampton (1973), Dingle (1977), Lowe (1982), Lee et al. (1993), Shanmugam et al. (1994), and Shanmugam and Moiola (1995), are broadly classified into two types: (1) mass transport and (2) sediment flows (Table 3.1). This is not a new classification, but rather a scheme that attempts to utilize existing concepts and terminologies for interpreting common downslope processes.

3.2 Mass-transport processes

Mass transport is a general term used for the failure, dislodgement, and down-slope movement of sediment under the influence of gravity in both subaerial and subaqueous environments. Mass-transport processes, also known as mass

Table 3.1 A classification of subaqueous gravity-driven processes

Major type	Nature of moving material	Nature of movement	Sediment concentration (volume %)	Fluid rheology and flow state	Depositional process
Mass transport (also known as mass movement, mass wasting, or landslide)	Coherent mass without internal deformation	Translational motion between stable ground and moving mass			Slide
	Coherent mass with internal deformation	Rotational motion between stable ground and moving mass	Not applicable	Not applicable	Slump
Sediment flow (in cases, mass transport)	Incoherent body (sediment-water slurry)	Movement of sediment-water slurry *en masse*	High 25–95% (Shanmugam, 2000a)	Plastic rheology and laminar state	Debris flow (mass flow)
Sediment flow	Incoherent body (water-supported particles in suspension)	Movement of individual particles within the flow	Low 1–23% (Middleton, 1967)	Newtonian rheology and turbulent state	Turbidity current

movements, mass wasting, or landslides, have been classified in various ways using different terminologies (e.g., Ward, 1945; Varnes, 1958, 1978; Dingle, 1977; Lee et al., 1993; Hampton et al., 1996). Although these classifications are useful, problems emerge when we try to apply them to both seismic data and to outcrop data. We cannot always interpret mechanisms of emplacement by using morphological features seen on seismic data. However, sedimentological features seen in core and outcrop allow such a possibility. Mass-transport processes are composed mainly of slides and slumps.

3.2.1 Slides

A slide is a coherent mass of sediment that moves along a planar glide plane and shows no internal deformation (Fig. 3.1). Slides represent translational movement. Submarine slides can travel hundreds of kilometers (Fig. 3.2). For example, the runout distance of Nuuanu Slide, offshore Hawaii, is 230 km (Normark et al., 1993). Long-runout distances of 50–100 km for slides are common (Hampton et al., 1996). Submarine slides are common in fjords because the submerged sides of glacial valleys are steep and because the rate of sedimentation is high due to sediment-laden rivers that drain glaciers into fjords (Lee et al., 1993). The term 'slide' is used for both a process and a deposit.
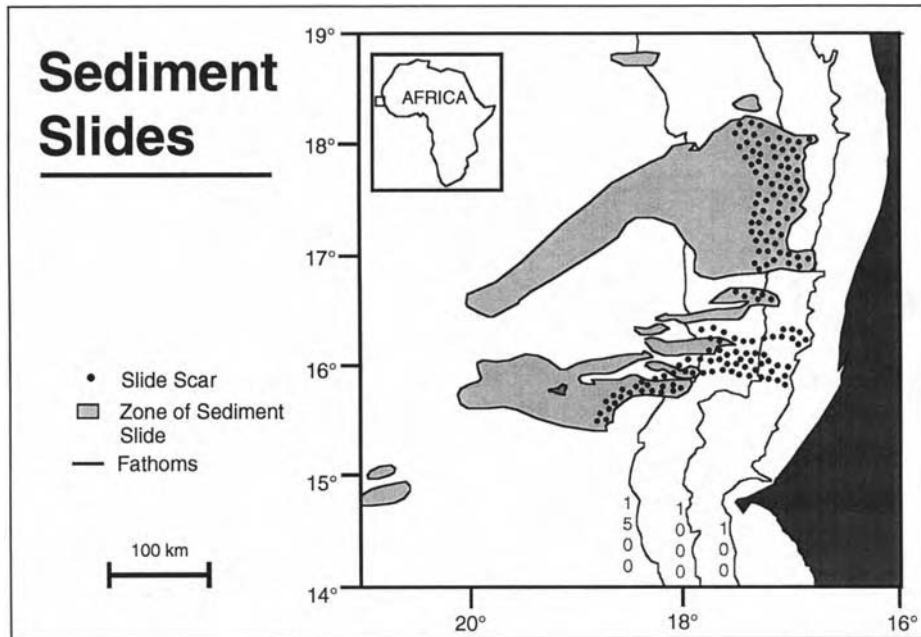
Fig. 3.2. Long-distance transport of detached slide blocks from the shelf edge (~ 100 fathoms = 600 ft = 183 m); offshore northwestern Africa. Note two slide blocks near the 15° latitude marker have traveled nearly 300 km from the shelf edge (i.e., 100-fathom contour). (After Jacobi (1976). Reproduced with permission from Elsevier.)

General characteristics of each facies listed below should be used to interpret only depositional mechanisms, not transportational mechanisms (see Chapter 7). General characteristics of slide deposits are:

- Gravel to mud lithofacies
- 100s of km long (Fig. 3.2)
- Transported shallow-water blocks encased in deep-water strata (Twenhofel, 1932, p. 740)
- Primary basal glide plane (Fig. 3.3A)
- Basal zone of shearing (Fig. 3.3B)
- Secondary internal glide planes (Fig. 3.3A)
- Upslope areas with tensional faults
- Occur on slopes of 1–4° (Booth et al., 1993)
- Transformation of slides into debris flows in frontal zone (Fig. 3.4)
- Associated clastic injections (Fig. 3.3)
- Sheet-like geometry (Fig. 3.4)
- Large-scale slides may be recognized in high-resolution seismic profiles of modern systems
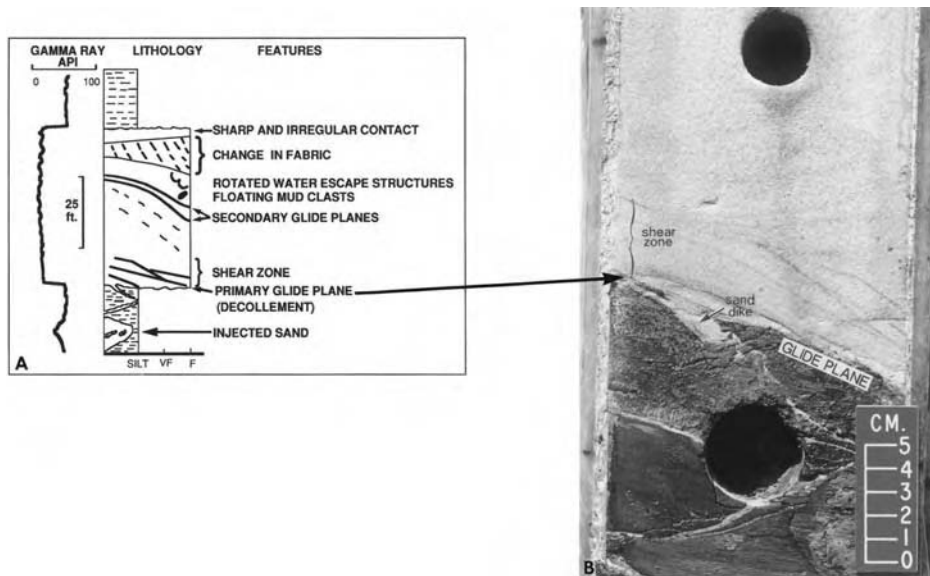
Fig. 3.3. (*A*) **Sketch of a cored interval showing blocky wireline log motif of a sandy slide/slump unit.** (*B*) **Core photograph showing basal contact (arrow) that is interpreted as a primary glide plane (a decollement). Note a sand dike (i.e., injectite) at the base of shear zone. Eocene, North Sea.**

Fig. 3.4. Photograph showing downslope mass transport of subaerial landslides in step-like segments. Mechanics of subaerial and submarine landslides are nearly the same. Note transformation of slide into debris flows with angular clasts in the frontal zone (bottom left). Tree in the center is about 3 m tall. Near Gubbio, Italy.

- Common in areas of tectonic activity, earthquakes, steep gradients, salt move-
  ments, and rapid sedimentation.

On the modern Norwegian continental margin, large mass-transport deposits
occur on the northern and southern flanks of the Voring Plateau (Bugge 1983;
Jansen et al. 1987). The Storegga Slide (offshore Norway), for example, has a maxi-
mum thickness of 430 m and a length of more than 800 km. The Storegga Slide on
the southern flank of the plateau exhibits mounded seismic patterns in sparker pro-
files and the core is composed primarily of debrites (Bugge 1983; Jansen et al.,
1987). The slide was triggered by earthquakes (Bugge 1983; Jansen et al., 1987).

3.2.2 Slumps

A slump is a coherent mass of sediment that moves on a concave-up glide plane and
undergoes rotational movements causing internal deformation (Fig. 3.1). In prac-
tice, distinguishing slides from slumps can be difficult. The term 'slump' is used for
both a process and a deposit. General characteristics of slump deposits are:

- Gravel to mud lithofacies
- Basal zone of shearing (Fig. 3.3)
- Upslope areas with tensional faults (Fig. 3.5)
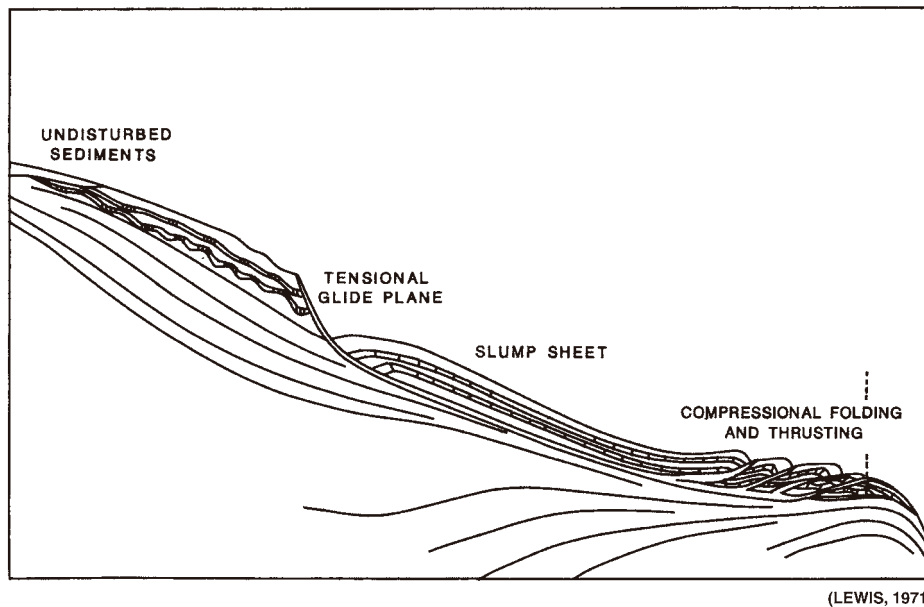
(LEWIS, 1971)

**Fig. 3.5. Sketch of a modern submarine slump sheet showing tensional glide plane in the
upslope detachment area and compressional folding and thrusting in the downdip frontal
zone. (After Lewis (1971). Reproduced with permission from Blackwell.)**

- Downslope edges with compressional folding (Fig. 3.5) or thrusting (i.e., toe thrusts)
- Slump folds overlain by undeformed strata at outcrop scale (Fig. 3.6)
- Contorted layers interbedded with uncontorted layers at core scale (Fig. 3.7)
- Irregular upper contact

Fig. 3.6. Outcrop photograph showing slump-folded heterolithic facies overlain by undeformed deep-water sandstone. Eocene, La Jolla, California.

Fig. 3.7. Core photograph showing alternation of contorted and uncontorted siltstone (light color) and claystone (dark color) layers of slump origin. Paleocene, North Sea.

- Chaotic bedding in heterolithic facies
- Steeply dipping and truncated layers (Fig. 3.8)
- Associated sand injections (Fig. 3.8)
- Lenticular to sheet-like geometry with irregular thickness
- Contorted bedding has been recognized in Formation MicroImager (FMI) (Hansen and Fett, 2000; their Fig. 11)
- Large-scale modern slumps may be recognized as chaotic facies in high-resolution seismic profiles.

3.2.3 Flow slide, debris slide, debris avalanche, and creep

The term *flow slide* has been used for high-velocity subaerial processes that could be considered a transitional type between slumps and debris flows (Shreve, 1968; Rouse, 1984). A slow-moving mass that breaks up into smaller
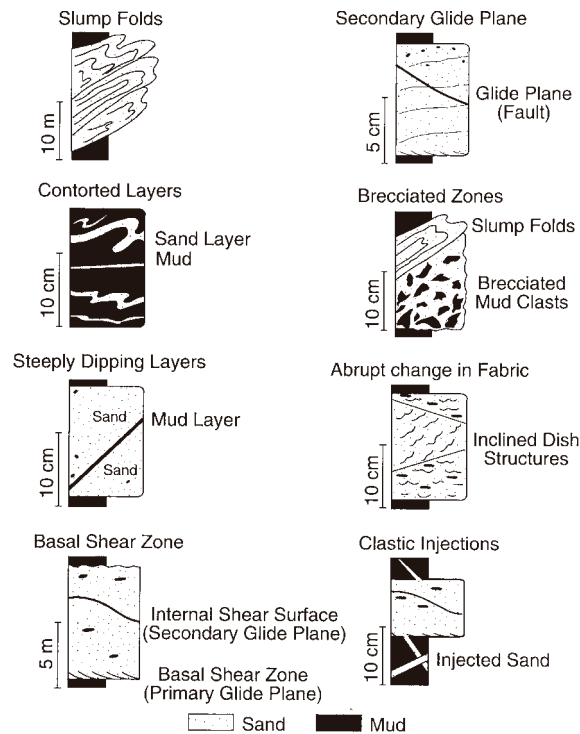
Fig. 3.8. Summary of features associated with slump deposits observed in cores.

blocks as it advances is called *debris slide*, whereas a fast-moving mass that breaks up into smaller blocks as it advances is called *debris avalanche* (Varnes, 1978). Catastrophic (fast-moving) debris flows are called *sturzstrom* (Hsü, 2004). The term *creep* refers to a slow-moving mass movement. These velocity-based terms are subjective because the distinction between a 'fast-moving' and a 'slow-moving' flow has not been defined using a precise velocity value. Furthermore, there are no reliable criteria to establish absolute velocities of ancient flows in the rock record. Thus these terms are not practical in process sedimentology.

3.3 Sediment flows

Middleton and Hampton (1973) distinguished sediment-gravity flows from fluid-gravity flows. In a *fluid-gravity flow* (e.g., river currents and some deep-ocean currents), fluid is directly driven by gravity, whereas in a *sediment-gravity flow*,

the interstitial fluid is driven by the grains moving downslope under the influence of gravity. Furthermore, Middleton and Hampton classified sediment-gravity flows into four types based on sediment-support mechanisms. They are: (1) *turbidity current* with turbulence; (2) *fluidized sediment flow* with upward moving intergranular flow; (3) *grain flow* with grain interaction (i.e., dispersive pressure); and (4) *debris flow* with matrix strength.

Dasgupta (2003, p. 278) debunked the classification of sediment-gravity flows with the following statement: '*Driving of interstitial fluid by the moving particle, the essential criterion (by definition) for a flow to be identified as a sediment gravity flow, does not take place in any of the flow types originally classified as sediment gravity flows.*'

Dasgupta argued that in turbidity currents, grains are suspended by turbulent viscosity of the fluid, and therefore the fluid is driving the flow, not the sediment. In fluidized flows, the enhanced pore-fluid pressure controls the flow, not the sediment. In grain flows, the interstitial fluid is the same as the ambient fluid, and therefore, the concept fails. In debris flows, the sediment-fluid mixture moves *en masse*, and therefore, the concept of sediment moving the fluid suffers.

In this book, the general term *sediment flows* of Middleton and Hampton is used for grain flows, debris flows, and turbidity currents. Fluidized flows are not important mechanisms for transporting sediment in deep-water environments (see Chapter 5).

3.3.1 Rheology of fluids

The *rheology* of fluids, an important property that distinguishes debris flows from turbidity currents, can be expressed as a relationship between applied shear stress and rate of shear strain (Fig. 3.9). Newtonian fluids (i.e., fluids with no inherent strength), like water, will begin to deform the moment shear stress is applied, and the deformation is linear. In contrast, some naturally occurring materials (i.e., fluids with strength) will not deform until their yield stress has been exceeded (Fig. 3.9); once their yield stress is exceeded, deformation is linear. Such materials (e.g., wet concrete) with strength are considered to be Bingham plastics (Fig. 3.9). For flows that exhibit plastic rheology, the term 'plastic flows' is appropriate. Using rheology as the basis, deep-water sediment flows are divided into two broad groups, namely, (1) *Newtonian* flows and (2) *plastic* flows. The Newtonian flows represent turbidity currents and plastic flows represent debris flows. This is analogous to the classification originally proposed by Dott (1963).

The rheology of a sediment–water mixture is governed mainly by sediment concentration and to a lesser extent by grain size and the physical and chemical properties of transported solids (Pierson and Costa, 1987, p. 4). A compilation of
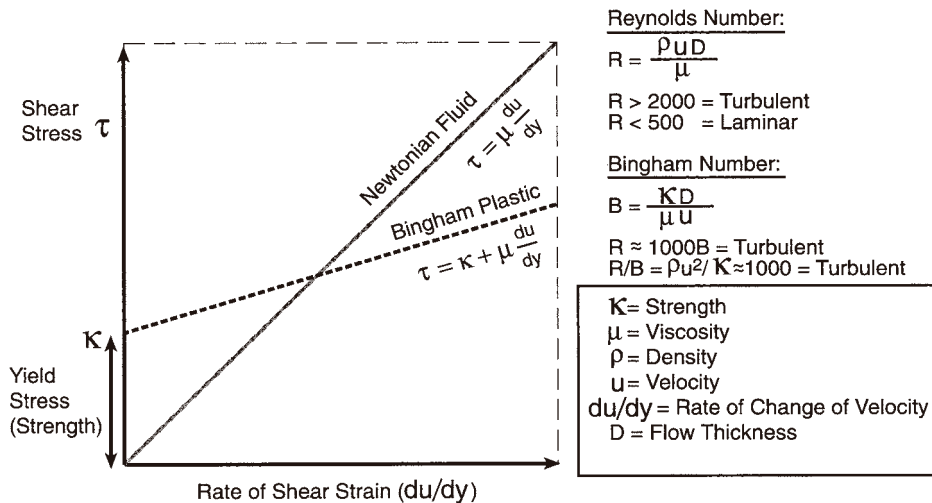
Fig. 3.9. Rheology (stress-strain relationships) of Newtonian fluids and Bingham plastics. Graph shows that the fundamental rheological difference between debris flows (Bingham plastics) and turbidity currents (Newtonian fluids) is that debris flows exhibit strength, whereas turbidity currents do not. (Compiled from several sources (Dott, 1963; Enos, 1977; Pierson and Costa, 1987; Phillips and Davies, 1991; Middleton and Wilcock, 1994). After Shanmugam (1997a). Reproduced with permission from Elsevier.)

published sediment concentration values of various flow types shows that the boundary between Newtonian and plastic flows occurs at about 20–25% by volume (Fig. 3.10). In this rheological classification, *high-density turbidity currents* are not meaningful because their sediment concentration values represent both Newtonian and plastic flows (Fig. 3.10).

3.3.2 Laminar *versus* turbulent flows

In addition to fluid rheology, flow state is used in distinguishing laminar debris flows from turbulent turbidity currents (Table 3.1). The difference between laminar and turbulent flows was demonstrated in 1883 by Osborne Reynolds, an Irish engineer, by injecting a thin stream of dye into the flow of water through a glass tube. At low rates of flow, the dye stream traveled in a straight path. This regular motion of fluid in parallel layers, without macroscopic mixing across the layers, is called a *laminar flow*. At higher flow rates, the dye stream broke up into chaotic eddies. Such an irregular fluid motion, with macroscopic mixing across the layers, is called a *turbulent flow*. The change from laminar to turbulent flow occurs at a critical *Reynolds number* (the ratio between inertia and viscous forces) of about 2000 (Fig. 3.9). The phenomena of turbulence, however, is a complex and controversial topic. In commenting on the contentious issue of turbulence,
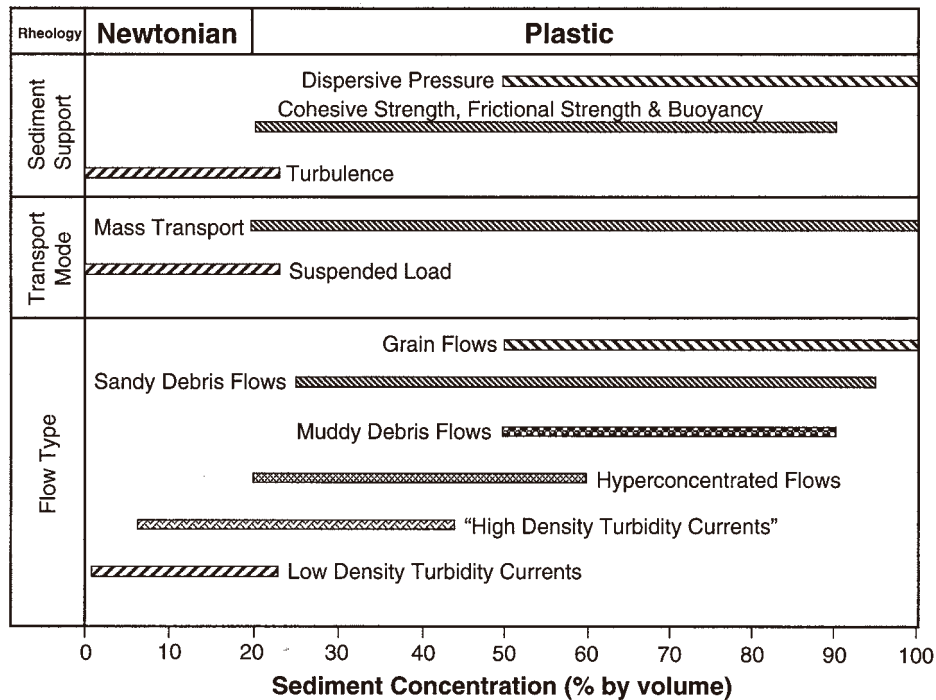
Fig. 3.10. Classification of gravity-driven sediment flows, based on fluid rheology, into *Newtonian* and *plastic* types. Turbidity currents are Newtonian flows, whereas all mass flows (muddy debris flows, sandy debris flows, and grain flows) are plastic flows. Turbidity currents occur only as subaqueous flows, whereas debris flows and grain flows can occur both as subaerial and as subaqueous flows. Sediment concentration is the most important property in controlling fluid rheology. High-density turbidity currents are not meaningful in this rheological classification because their sediment concentration values represent both Newtonian and plastic flows. High-density turbidity currents are included here solely for purposes of discussion. Also, for purposes of comparison, subaerial flows (river currents and hyperconcentrated flows) are considered. Published values of sediment concentration by volume% are: (1) river currents (1–5%; e.g., Galay, 1987), (2) low-density turbidity currents (1–23%; e.g., Middleton, 1967, 1993), (3) high-density turbidity currents (6–44%; Kuenen, 1966; Middleton, 1967), (4) hyperconcentrated flows (20–60%; Pierson and Costa, 1987), (5) muddy debris flows (50–90%; Coussot and Muenier, 1996), (6) sandy debris flows (25–95%; Shanmugam, 1997a; which was partly based on reinterpretations of various processes that exhibit plastic rheology in papers by Middleton, 1966, 1967; Wallis, 1969; Lowe, 1982; Shultz, 1984), (7) grain flows (50–100%; partly based on Rodine and Johnson, 1976; Shultz, 1984; Pierson and Costa, 1987). (After Shanmugam (2000a). Reproduced with permission from Elsevier.)

Lesieur (1987) stated, '*It is even difficult to agree on what exactly is the problem to be solved.*' The problem is that turbulent flows are characterized by many properties that include (Kundu and Cohen, 2002):

(1) Randomness (irregular, chaotic, and unpredictable)
(2) Nonlinearity

(3) Diffusivity
(4) Vorticity
(5) Dissipation.

It is beyond the scope of this book to address these complex properties of turbulence.

3.3.3 Plastic debris flows

Debris flow is a sediment flow with plastic rheology and laminar state from which deposition occurs through freezing en masse.

Johnson (1970) favored a Bingham plastic rheological model for debris flows. Although rheology is a complex parameter and is difficult to measure accurately (Phillips and Davies, 1991), it is a useful parameter for distinguishing turbidity currents from debris flows. Although most debris flows move as incoherent material, some plastic flows may be transitional in behavior between coherent mass movements and incoherent sediment flows. Marr et al. (2001), for example, generated strong, moderate, and weak debris flows in flume experiments. In these experiments, strongly coherent debris flows are analogous to coherent mass-transport processes. Some modern debris flows have been classified as mass movements (e.g., Embley and Jacobi, 1986) and as slides (e.g., Rothwell et al., 1991; Elverhoi et al., 1997). Debris flows are typically laminar in state (Hampton, 1972, p. 791).

The term 'debris flow' is used for both a process and a deposit. An early usage of the term 'debrite' for deposits of debris flows was in an unpublished M. S. thesis by Pluenneke (1976), but a published reference is by Stow (1984). The term *olistostrome*, coined by Flores (1955), is used for debrites with huge exotic blocks. Since the introduction of the term 'turbidite' for deposits of turbidity currents by Kuenen (1957), genetic terms ending with 'ite' have proliferated. However, not all of these terms are meaningful in terms of communicating depositional processes (Table 2.2). Problems with genetic terms are discussed in Chapter 2.

General characteristics of muddy and sandy debrites (Fisher, 1971; Hampton, 1972, 1975; Middleton and Hampton, 1973; Enos, 1977; Shanmugam and Benedict, 1978; Shanmugam et al., 1994, 1995a; Shanmugam, 1996a) are:

- Gravel to mud lithofacies
- Floating or rafted mudstone clasts near the tops of beds in muddy matrix (Fig. 3.11)
- Planar clast fabric in muddy matrix (Fig. 3.11A)
- Projected clasts in mudstone (Fig. 3.11B)
- Brecciated mudstone clasts in sandy matrix
- Rafted large-sized clasts in sandy matrix (Fig. 3.12)
- Planar clast fabric in sandy matrix (Fig. 3.12)
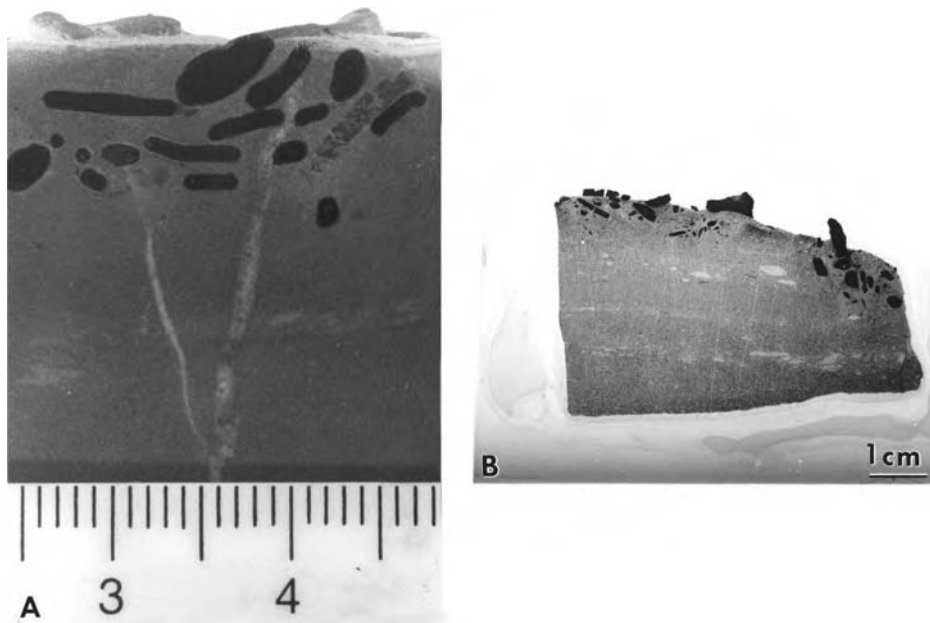
Fig. 3.11. (*A*) **Photograph of a polished slab showing planar clast fabric (i.e., long axis is aligned parallel to bedding surface) indicative of laminar flow. Scale in centimeter. (*B*) Photograph of an entire thin section showing projected mudstone clasts suggesting freezing of flow in laminar state. Middle Ordovician, Tennessee. (After Shanmugam and Benedict (1978). Reproduced with permission from SEPM.)**

- Inverse grading of rock fragments
- Inverse grading, normal grading, inverse to normal grading, and no grading of matrix
- Floating quartz granules in sandy matrix (Fig. 3.13)
- Inverse grading of granules in sand
- Pockets of gravels
- Irregular, sharp upper contacts and lateral pinch-out geometries
- Side-by-side occurrence of garnet granules (density: 3.5–4.3) and quartz granules (density: 2.65)
- Lenticular to sheet-like geometry.

These features are useful for interpreting debrites in cores and outcrops; however, they cannot be recognized in seismic profiles or wireline logs. Debrites with floating clasts have been recognized in Formation MicroImager (FMI) (Hansen and Fett, 2000; their Fig. 10). Bathymetric survey of modern deep-water environments using high-resolution multibeam-mapping system has revealed debris fields on the Monterey Fan, offshore California (Gardner et al., 1996).
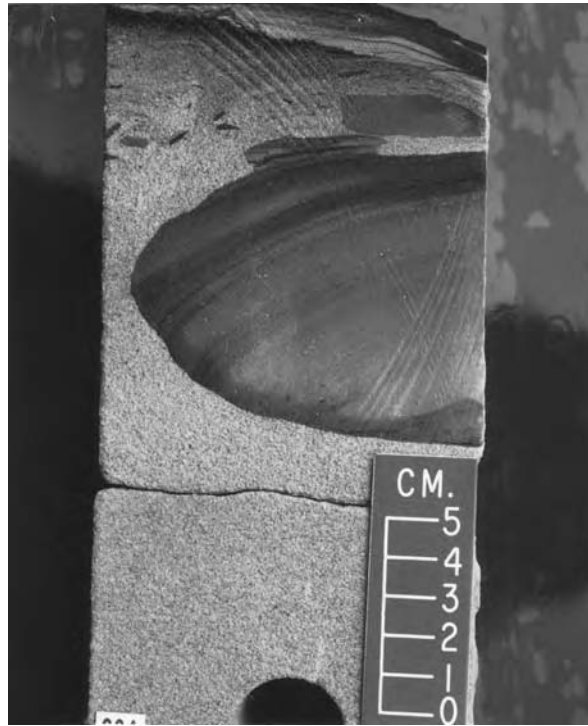
Fig. 3.12. Core photograph of massive fine-grained sandstone showing floating mudstone clasts of different sizes with planar clast fabric near the sharp and irregular upper contact. Note a thin rippled siltstone unit above the massive sandstone. Paleocene, North Sea.

3.3.4 Experimental sandy debris flows

The concept of sandy debris flows was first introduced by Hampton (1975). Sandy debris flows are defined on the basis of (1) plastic rheology (Fig. 3.10); (2) multiple sediment-support mechanisms (cohesive strength, frictional strength, hindered settling, and buoyancy), (3) mass-transport mode; (4) more than 25–30% sand and gravel; (5) 25–95% sediment (gravel, sand, and mud) concentration by volume; and (6) variable clay content (as low as 0.5% by weight). Rheology is more important than grain-size distribution in controlling sandy debris flows. Sandy debris flows could develop in slurries of any grain size (very fine sand to gravel), any sorting (poor to well), any clay content (low to high), and any modality (unimodal and bimodal) (Shanmugam, 1996a, 1997a, 2000a).

Theoretically, grain flows (i.e., cohesionless debris flows) and muddy debris flows (i.e., cohesive debris flows) may be considered to be two end members of

Fig. 3.13. Core photograph showing floating quartz granules (arrow) in fine-grained sand implying flow strength. Eocene, North Sea.

plastic flows (Fig. 3.14). Sandy debris flows are considered to represent an intermediate position between grain flows (with frictional strength) and muddy debris flows (with cohesive strength) (Shanmugam, 1997a). An advantage of this concept is that it requires neither the steep slopes necessary for grain flows nor the high matrix content necessary for cohesive debris flows.

One of the main criticisms leveled against the concept of sandy debris flows was the flawed notion that all debris flows must have high clay content in order to provide the necessary strength (e.g., D'Agostino and Jordan, 1997). Although Hampton (1975) noted that as little as 2% clay is sufficient to provide the strength for sandy debris flows, Costa and Williams (1984) described a number of mud-poor debris flows in which mud constituted less than 2 per cent of the debris flow.

To verify the concept of sandy debris flows with low clay content, experiments were conducted on subaqueous sandy debris flows at St. Anthony Falls Laboratory of the University of Minnesota (Marr et al., 1997, 2001; Shanmugam, 2000a). The experimental flume used was 10 m in length, 30 cm in width, and 80 cm in depth (Fig. 3.15). The flume was fitted with three different slopes: 4.6, 1.1, and 0° to observe changes in deposition at points of slope change. These slope angles are analogous to those of modern continental slope, rise, and abyssal plain.
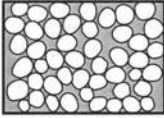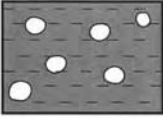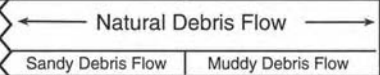
Fig. 3.14. Theoretical *versus* natural debris flows. Theoretically, grain flows (i.e., cohesionless debris flows) and muddy debris flows (i.e., cohesive debris flows) are considered to be two end members of rheological debris flows (Lowe, 1979). Following Lowe (1979), the rheological term 'plastic' is used for both grain flows (frictional strength) and muddy debris flows (cohesive strength). Sandy debris flows, not studied before in experiments, are considered to represent an intermediate position between the end-member types. Multiple sediment support mechanisms are proposed for sandy debris flows. An advantage of this concept is that it requires neither the steep slopes required for grain flows nor the high matrix content necessary for cohesive debris flows. (After Shanmugam (1997a). Reproduced with permission from Elsevier.)
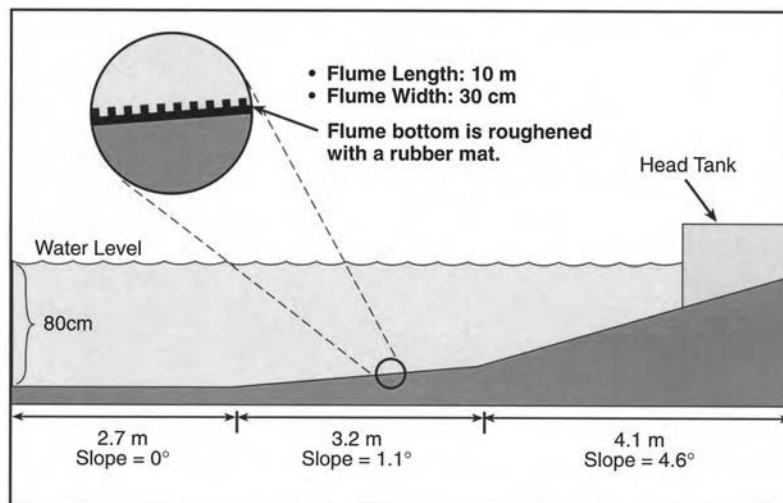
Fig. 3.15. Dimensions of the flume used in sandy debris flow experiments. (After Shanmugam (2000a). Reproduced with permission from Elsevier.)

Sediment slurries were composed of silica sand (120 μm size), clay (bentonite or kaolinite), coal slag (same bulk density as silica sand: 2.6 g/cm^3), and water. Coal slag of 500 μm size (coarse sand) was used as a tracer material to establish flow behavior and depositional pattern of coarse-grained grains in comparison to very fine-grained sandy matrix. Sandy debris flows were generated with bentonite clay content as low as 0.5% by weight or with kaolinite clay as low as 5% by weight. Sandy debris flows were also generated using medium-grained sand (300 μm size) with bentonite clay content as low as 1.5% by weight or kaolinite clay as low as 5% by weight.

On the basis of experimental sandy debris flows, the following general observations, comments, and inferences have been made (Shanmugam, 2000a):

(1) Sandy debris flows are a viable mechanism for transporting and depositing sand in subaqueous environments.

(2) Sandy debris flows can travel long distances on gentle slopes of less than 1°.

(3) Contrary to popular belief, sandy debris flows do not require high clay content. A clay content as low as 0.5% is sufficient to generate sandy debris flows. However, without at least 0.5% of clay, debris flows will not develop. In the complete absence of clay, the sand–water slurry either becomes a short-lived grain flow or a short-lived turbidity current.

(4) Sandy debris flows are developed from slurries of both bimodal and unimodal grain-size distribution.

(5) The ratio of water to clay and the types of clay determined the flow behavior. For example, by maintaining a constant amount of kaolinite at 15% by weight, and by increasing the water content to 25, 30, and 40% by weight, three different types of sandy debris flows (i.e., strong, moderate, and weak) were generated (Fig. 3.16). The increase in water reflects a decrease in fluid strength. The significance of this observation is that changes in water content alone can make a difference in the flow behavior without changing clay content. Thus the amount of clay in the deposit is not always a useful criterion for interpreting the nature of flow. Primary sedimentary features are more reliable for interpreting flow behavior than clay content. Deposits of sandy debris flows with low clay content (e.g., 0.5%) are potential candidates for misinterpretation as deposits of high-density turbidity currents or grain flows.

(6) Strong debris flows developed thick fronts with well-defined body, whereas weak debris flows developed poorly defined body (Fig. 3.17).

(7) Weak flows developed thick turbulent suspension (i.e., turbidity current) on top (Fig. 3.18A), whereas strong flows did not (Fig. 3.18B). Strong flows also showed well developed snouts (Fig. 3.18B).

(8) Subaqueous debris flows developed hydroplaning (Fig. 3.19), whereas subaerial debris flows did not (Mohrig et al., 1998). Experimental studies of subaqueous debris flows have shown that hydroplaning can dramatically reduce
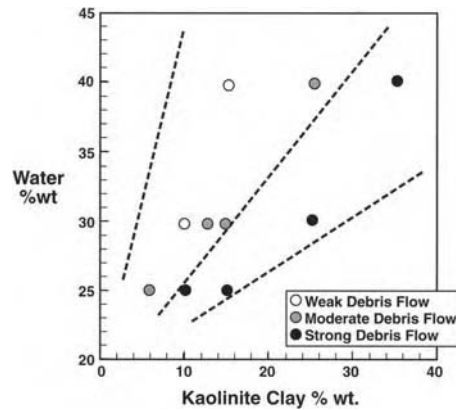
Fig. 3.16. Plot showing the control of flow strength (strong, moderate, and weak) in experimental sandy debris flows by water and clay content. An increase in clay content or a decrease in water content would result in stronger debris flows; see text for details. (After Shanmugam (2000a). Reproduced with permission from Elsevier.)
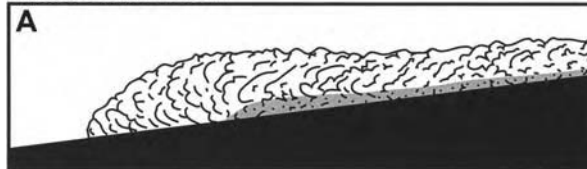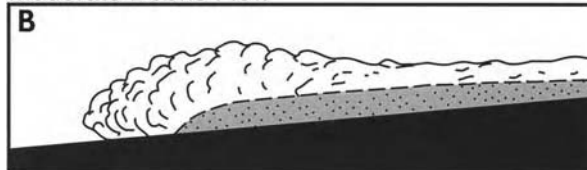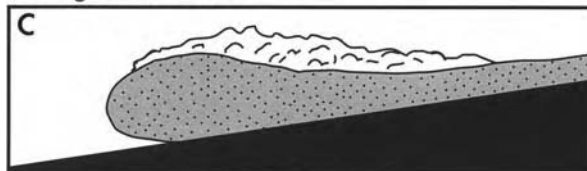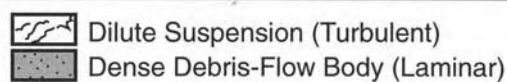
Fig. 3.17. Weak, moderate, and strong types of sandy debris flows and their properties. (After Shanmugam (2002a). Reproduced with permission from Elsevier.)
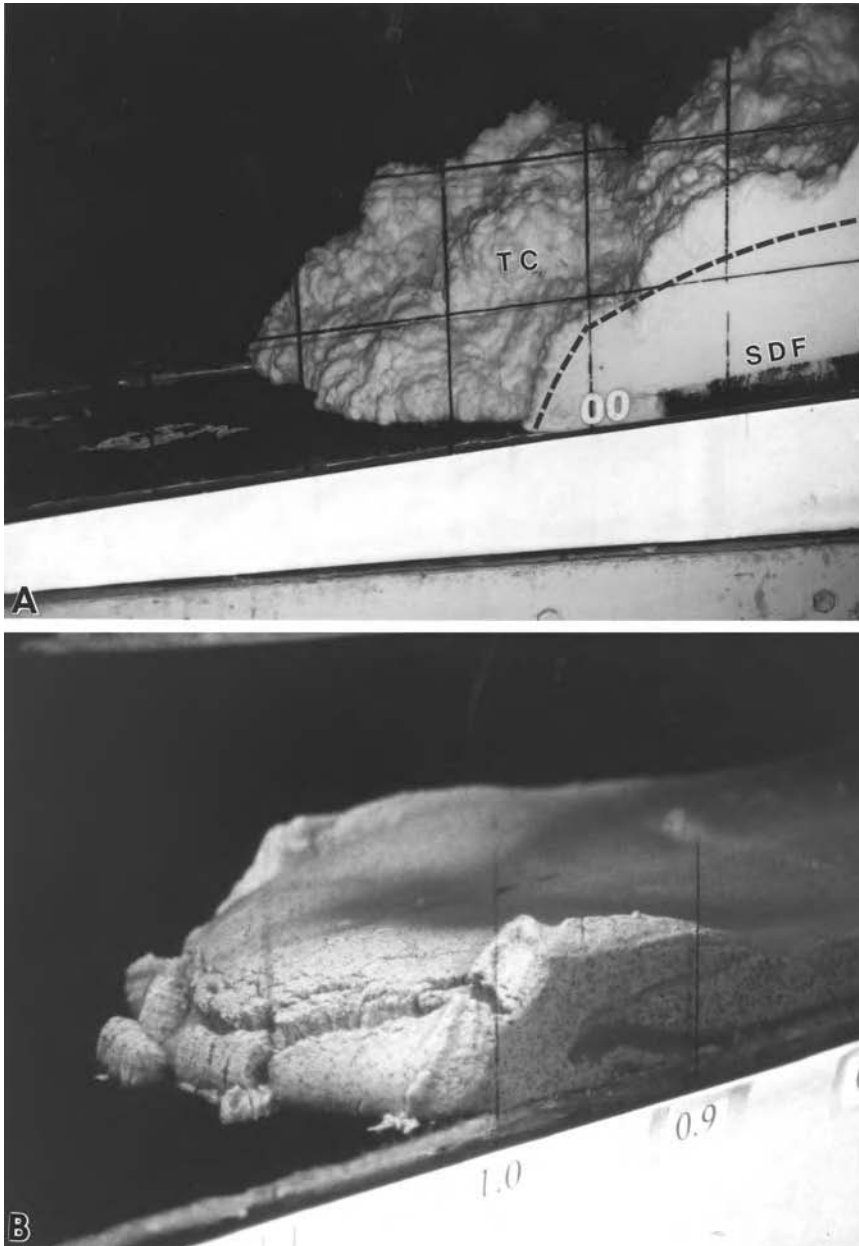
Fig. 3.18. (*A*) Side view of flume tank showing weak debris flows with well-developed turbulent clouds (TC) on top of sandy debris flows (SDF). Dashed line marks the boundary between laminar debris flow and turbulent turbidity current. Such density-stratified flows may be erroneously classified as high-density turbidity currents (see Chapter 7). (*B*) Side view of flume tank showing strong debris flows with well-developed snout. Note absence of turbulent suspension on top. Also note irregular upper surface caused by sudden freezing of the flow. Deformation in the front suggests strongly coherent character of flow, which may be called a slump. Horizontal distance between the 0.9 and 1.0 markers is 10 cm.
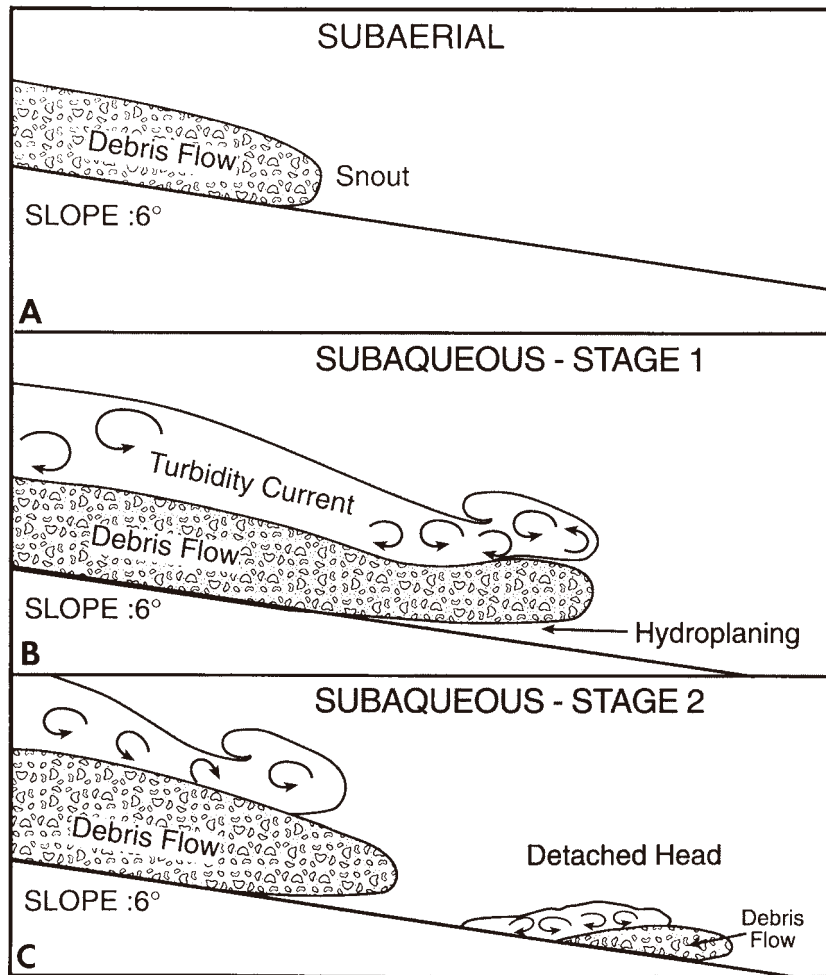
Fig. 3.19. Three profiles of experimental debris flows. (*A*) Slow-moving subaerial debris flow without hydroplaning. (*B*) Fast-moving subaqueous debris flow with hydroplaning (arrow) beneath the head of debris flow. (*C*) Fast-moving subaqueous debris flow with detached head. Note turbulent flows above subaqueous debris flows. Based on experiments of Mohrig et al. (1998). (After Shanmugam (2002a). Reproduced with permission from Elsevier.)

the bed drag, and thus increase head velocity. This explains why subaqueous debris flows can travel fast and afar on gentle slopes.

(9) Water-escape structures (dishes and pillars) have been observed in experimental sandy debris flows. Dish structures in experimental sandy debris flows formed in three stages, namely: (1) hydroplaning; (2) water entrapment (Fig. 3.20A); and (3) water escape (Fig. 3.21). During the hydroplaning stage, water penetrates underneath the plastic flow layer (Fig. 3.21, Stage 1). When the deposit begins
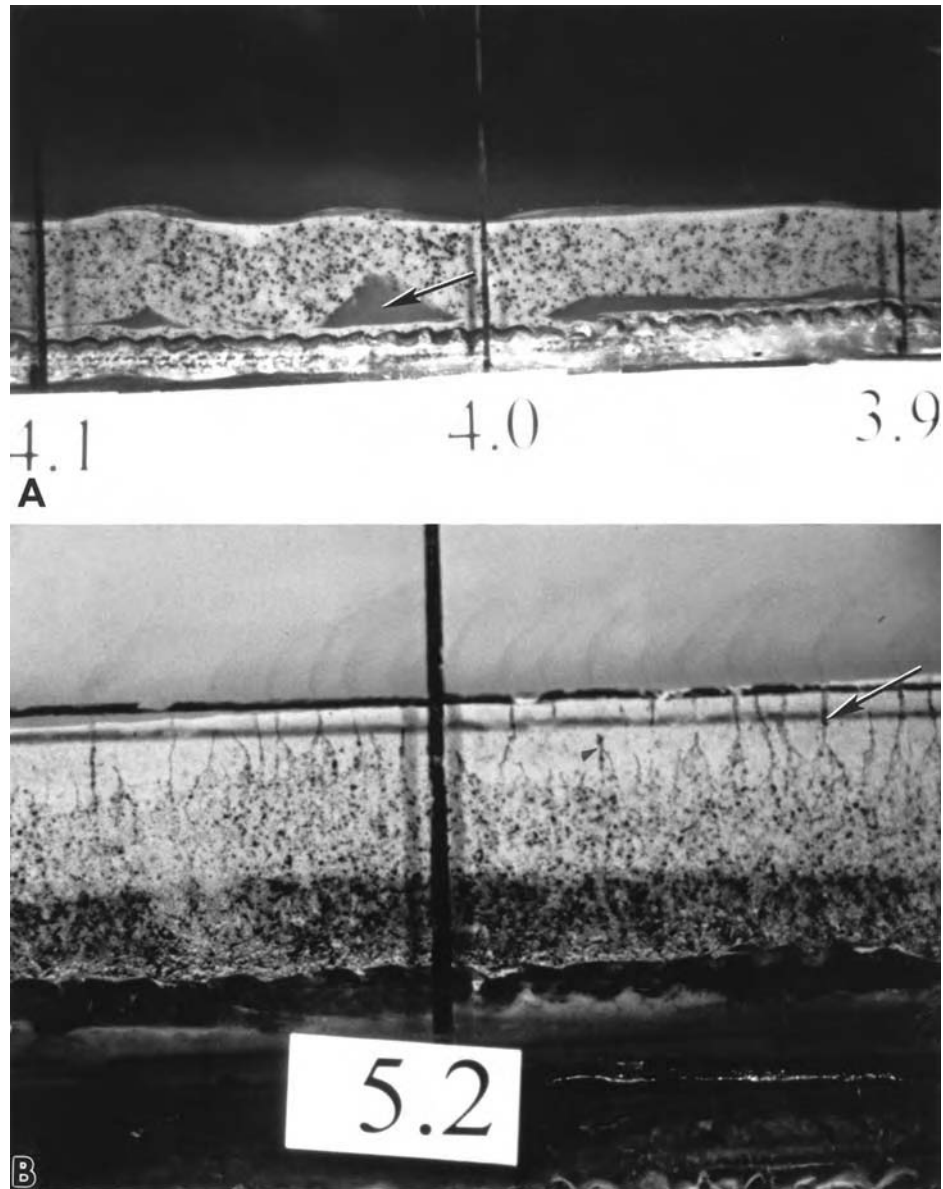
Fig. 3.20. (*A*) **Side view of flume tank showing sandy debris flows with water entrapment (arrow) beneath a debris-flow layer (i.e., Stage 2 in Fig. 3.21). The trapped water would escape when the sandy debris flow layer begins to settle toward the flume floor, causing sand volcanoes. Horizontal distance between the 4.0 and 4.1 markers is 10 cm. Flow direction is from right to left. (*B*) Side view of flume tank showing sandy debris flows with vertical pipes (arrow) created by escaping water. Note that the amount of coal slag gradually decreases upward, which represents coarse-tail normal grading. Width of photo is approximately 10 cm. Flow direction is from right to left.**
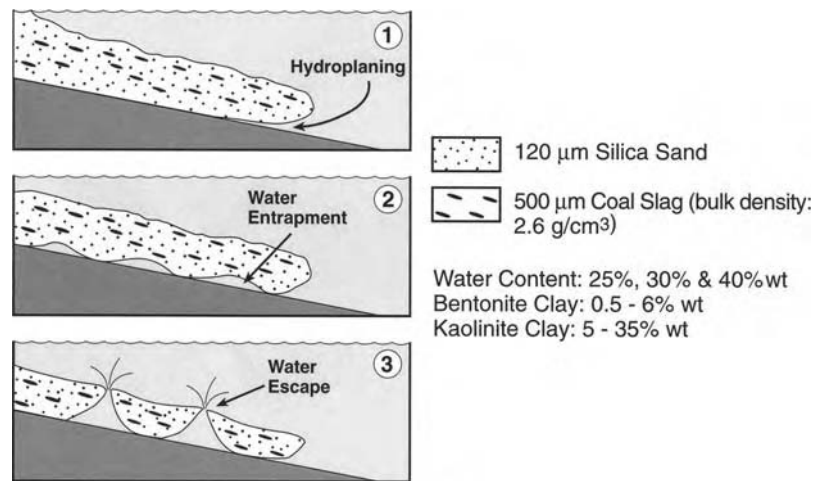
Fig. 3.21. Diagram showing stages of development of water-escape structures in sandy debris flows: (1) hydroplaning, (2) water entrapment in cavities (see Fig. 3.20A), and (3) water escape. Deposition of debris-flow layer squeezes the water in the cavities causing it to escape upward, resulting in sand volcanoes, dish structures, and vertical pipes. Diagram is based on direct observations of experiments as well as observations of videotapes of experiments. (After Shanmugam (2000a). Reproduced with permission from Elsevier.)

to settle, water gets trapped in cavities underneath the bed (Fig. 3.21, Stage 2). Finally, further settling of sediment causes the trapped water to escape by bursting open the top of the cavity, resulting in a sand volcano. A fully developed volcano would form a dish-shaped basal surface (Fig. 3.21, Stage 3), which would eventually mimic dish structures in the rock record. Water escape also results in vertical pipes or pillars (Fig. 3.20B). Water-escape structures in deep-water sands were previously used as evidence for deposition from liquefied flows and high-density turbidity currents (Lowe, 1975, 1982). Our experiments suggest that water-escape structures are common in subaqueous sandy debris flows with hydroplaning. Perhaps, the presence of water-escape structures in sandy debris flows may be used to infer hydroplaning in the rock record. The origin of dish structures and pillars is commonly ascribed to liquefaction and fluidization (see Chapter 5).

(10) Both normal grading (Fig. 3.22A) and inverse grading (Fig. 3.22B) developed in sandy debris flows. Coarse-tail normal grading was observed only in weak and moderate debris flows (Fig. 3.20B). Settling of coarser grains occurs from suspension through hindered settling after the flow had stopped. This settling of grains from a non-turbulent (i.e., laminar) flow after a flow had halted is different from settling of grains that may occur from a turbulent turbidity current even during transport.
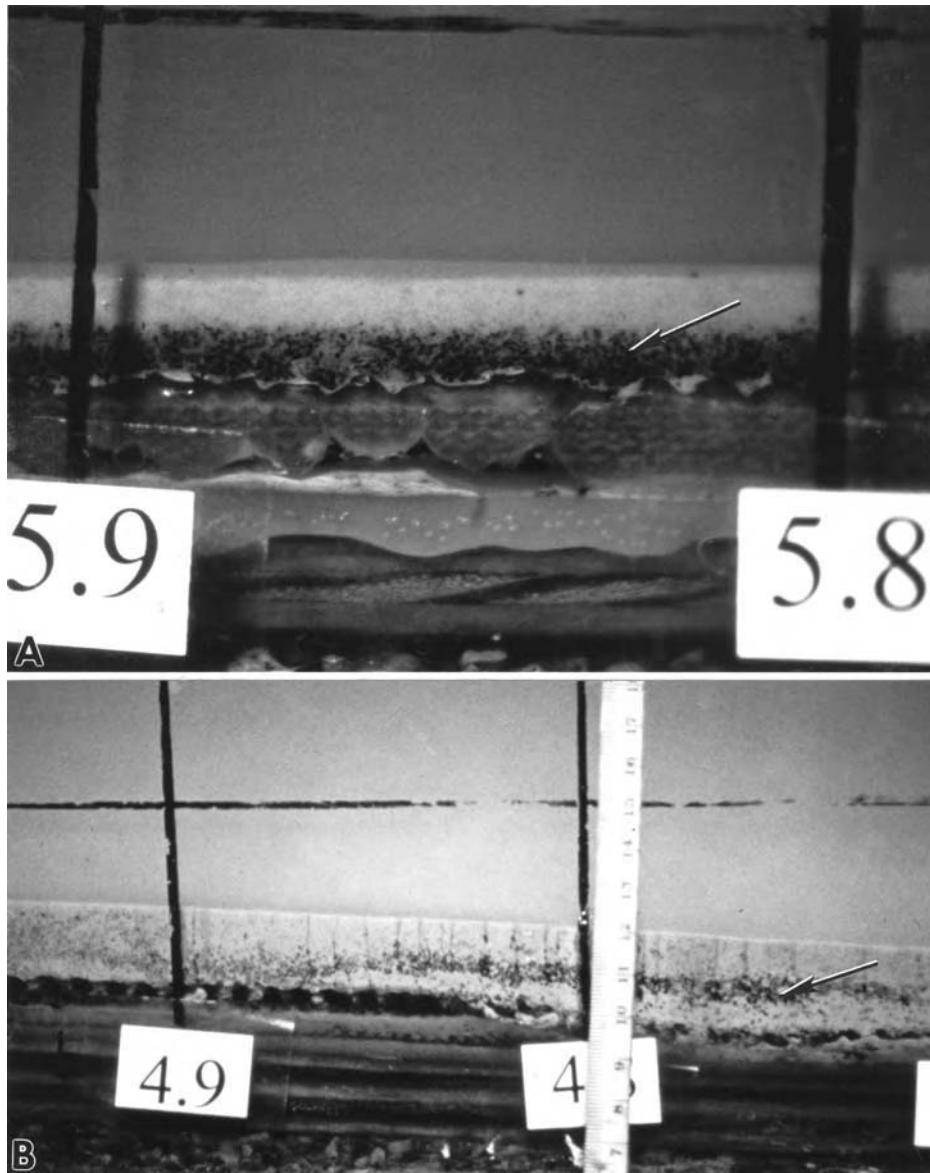
Fig. 3.22. (*A*) Side view of flume tank showing normal grading in sandy debris flows with concentration of coarser coal slag at the bottom (arrow). In the rock record, this could be misinterpreted as a turbidite. Normal grading has been reported from muddy debris flows as well (Vallance and Scott, 1997). Horizontal distance between the 5.8 and 5.9 markers is 10 cm. Flow direction is from right to left. Note smooth upper surface due to settling of sediment. (*B*) Side view of flume tank showing sandy debris flows with a middle layer of coal slag (arrow) in a sandy debrite unit (white). The sandy debrite unit is composed of a basal inversely graded layer; an upper normally graded layer, separated by a middle coal slag layer. Horizontal distance between the 4.8 and 4.9 markers is 10 cm. Flow direction is from right to left.

(11) In the rock record, sandy debrites with normal grading may be misinterpreted as turbidites. However, normally graded sandy debrites can be distinguished from normally graded sandy turbidites by associated features. For example, floating clasts and granules are common in normally graded debrites, whereas floating clasts and granules are unlikely to be present in true turbidites.

(12) In experiments using 300 μm size silica sand and 5 wt.% kaolinite, sandy debrites developed not only a normal grading, but also a relatively clean basal sand layer. This clean basal sand layer is attributed to sudden settling of sand grains coupled with upward migration of mud due to elutriation (Fig. 3.23). In experiments, debris flows commonly undergo flow transformation and generate turbidity currents on their top (Hampton, 1972). Surface and elutriation flow transformations are commonly responsible for transferring mud from underlying debris flows into overlying turbidity currents (Fig. 3.23). Such a mechanism has important implications for developing alternative deep-water depositional models. This is because the conventional wisdom dictates that only turbidites form mud-poor reservoir sands. Our experiments, however, have shown that sandy debris flows are capable of forming clean, mud-poor sands (see Chapter 12).
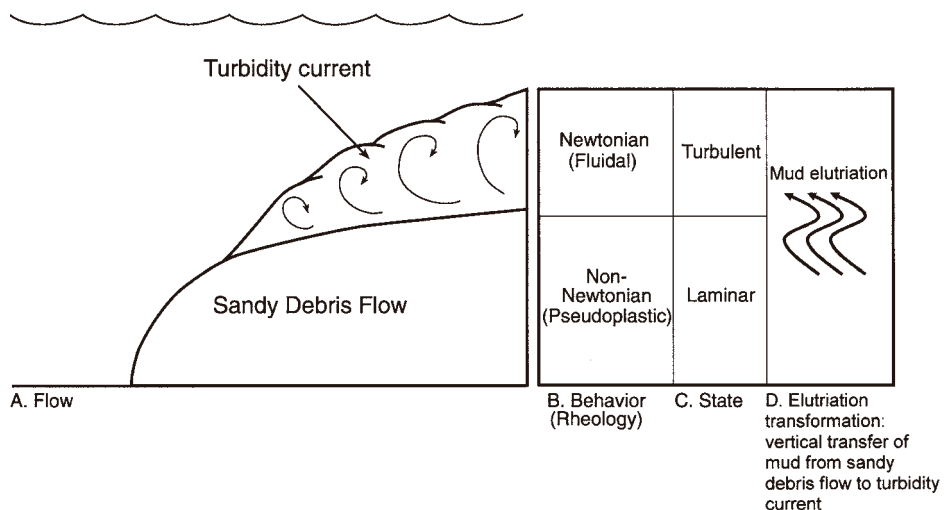
Fig. 3.23. (*A*) **Origin of turbidity currents from mud derived from underlying debris flows due to flow transformation (Based on experiments of Hampton, 1972).** (*B*) **Non-Newtonian rheology of lower debris flows and Newtonian rheology of upper turbidity currents.** (*C*) **Laminar state of lower debris flows and turbulent state of upper turbidity currents.** (*D*) **Curved vertical arrows showing elutriation of mud from lower debris flows to upper turbidity currents. (Based on concept of Fisher, 1983.)**

(13) Massive sands emplaced by sandy debris flows often exhibit random distri-
      bution of coal slag (coarse sand) throughout the bed composed of very fine-
      grained sand (Fig. 3.24A). This is analogous to floating granules in sandstone.
      Such massive sands in the rock record are potential candidates for misinter-
      pretation as deposits of high-density turbidity currents (see Chapter 7).

(14) Internal layers in sandy debrites were developed by post-depositional
      movement along failure planes (or secondary glide planes) during remobi-
      lization (Fig. 3.24A). In the rock record, such layers could be misidentified
      as parallel lamination, resulting in an erroneous process interpretation
      (i.e., traction).

(15) Imbricate slices developed when the front of a flow froze, and the body of
      the same flow broke away from the front end and overrode the front as suc-
      cessive thrust slices (Fig. 3.24B). Imbricate slices suggest compression.
      Large-scale compressional ridges have been reported from a modern sub-
      marine 'flow slide' in a fjord, British Columbia (Prior et al., 1982). Such
      ridges have been reported from modern glacial deposits as well (Fig. 3.25).
      Imbricate slices (duplex-like structures) have also been reported from the
      subaerial Blackhawk landslide (Shreve, 1968). The origin of duplex-like
      structures (i.e., imbricate slices) in the Pennsylvanian Jackfork Group,
      Ouachita Mountains, has been attributed to synsedimentary slumping
      (Shanmugam et al., 1988c; see Chapter 9). Such debris flows may be clas-
      sified both as mass transport and as sediment flows because of their transi-
      tional behavior.

(16) Strong flows commonly generated irregular upper surfaces by freezing
      (Fig. 3.26).

(17) Freezing of a strong flow developed an irregular snout in the front of the
      flow (Fig. 3.27A).

(18) During remobilization, frontal parts of sandy debris flows detached them-
      selves from the main body and started to move ahead (outrun) of the main
      body as isolated blocks (Fig. 3.27B). Such isolated (outrunner) blocks are
      evidence of tensional movement. Large bodies of isolated muddy debris
      flows and slumps have been reported from modern oceans (Embley, 1976;
      Embley and Jacobi, 1977; Embley, 1980).

In summary, sandy debris flows have developed a variety of sedimentological
features (Fig. 3.28). Some of these features may be misinterpreted as deposits
of turbidity currents (e.g., normal grading), or even as tectonic features
(e.g., duplex structures). Because of the complexity of the features of sandy
debris flows, there are no simple vertical facies models for deposits of sandy
debris flows. For the same reason, interpretation of sandy debris flows in the rock
record would require excruciatingly detailed observations of intricate sedimen-
tary features.
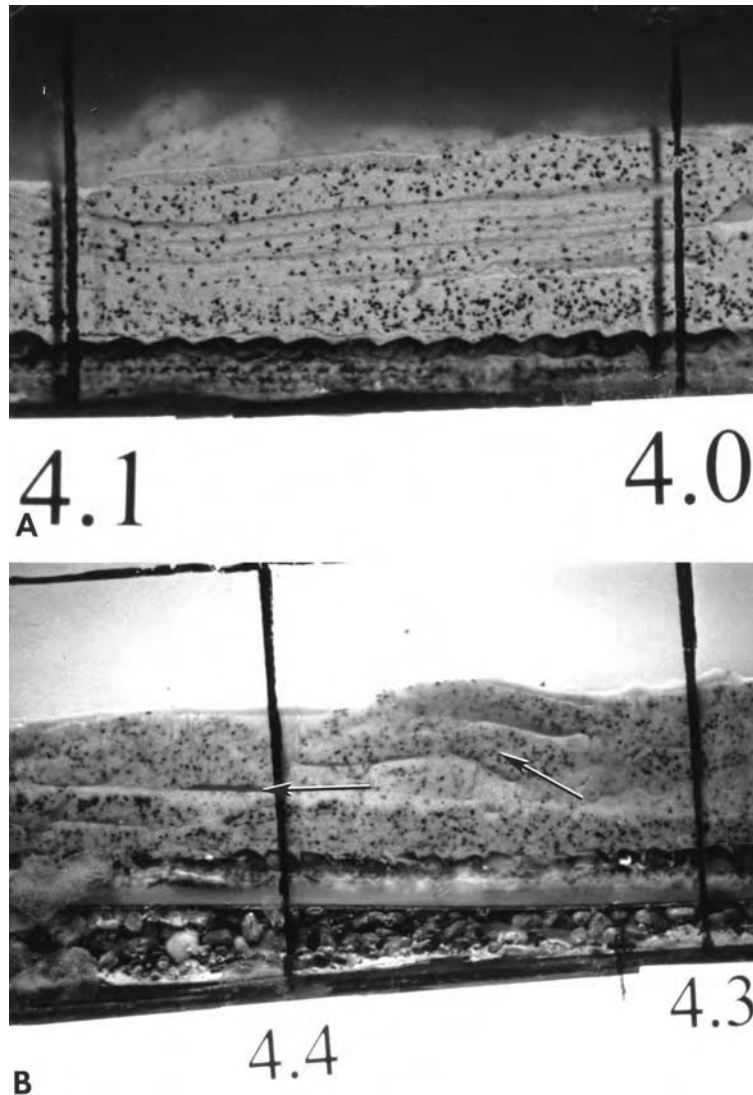
Fig. 3.24. (*A*) Side view of flume tank showing sandy debris flows with random distribution of 'floating' coal slag (black grains) in massive sand. Note internal layering that could be mistaken for parallel laminae (e.g., traction structures). Horizontal distance between the 4.0 and 4.1 markers is 10 cm. Flow direction is from right to left. (*B*) Side view of flume tank showing sandy debris flows with imbricate slices (inclined arrow). Such imbrications develop in sandy debris flows when the front of a flow freezes, the body of the flow breaks and thrusts over the slice in the front due to compression. Similar features (duplex-like structures) in the rock record have been ascribed to synsedimentary slumping (Shanmugam et al., 1988c). Note nearly horizontal or gently dipping internal layers (horizontal arrow). These layers are caused by post-depositional movement along failure planes (or secondary glide planes) during remobilization of flows. In the rock record, these horizontal layers could be misidentified as parallel lamination, which could result in erroneous interpretations of traction processes. Horizontal distance between the 4.3 and 4.4 markers is 10 cm. Flow direction is from right to left.
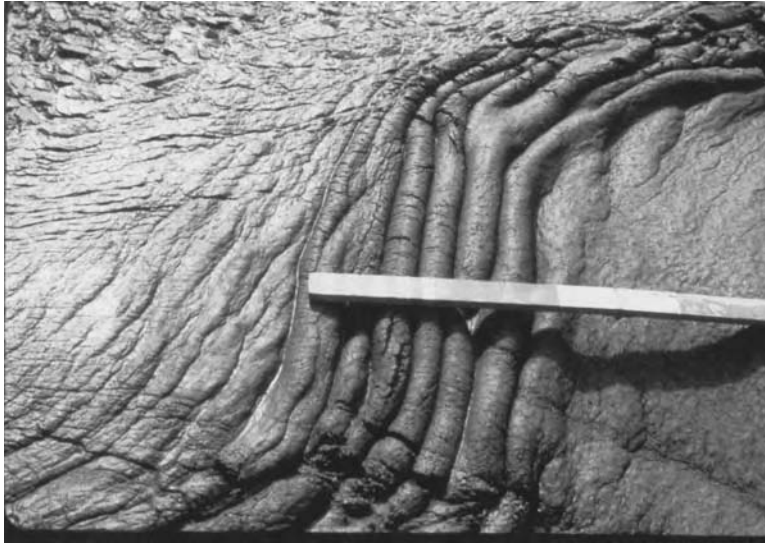
Fig. 3.25. Subaerial slurry flows (i.e., plastic debris flow with movement from left to right) showing development of synsedimentary folding in the frontal zone of Matanuska Glacier, Alaska (Lawson, 1981). This folding is analogous to the origin of imbricate slices in experiments on sandy debris flows (see Fig. 3.24B). Synsedimentary structures like this may be classified both as slumps and as debris flows. (Photo courtesy of G. D. Klein.)
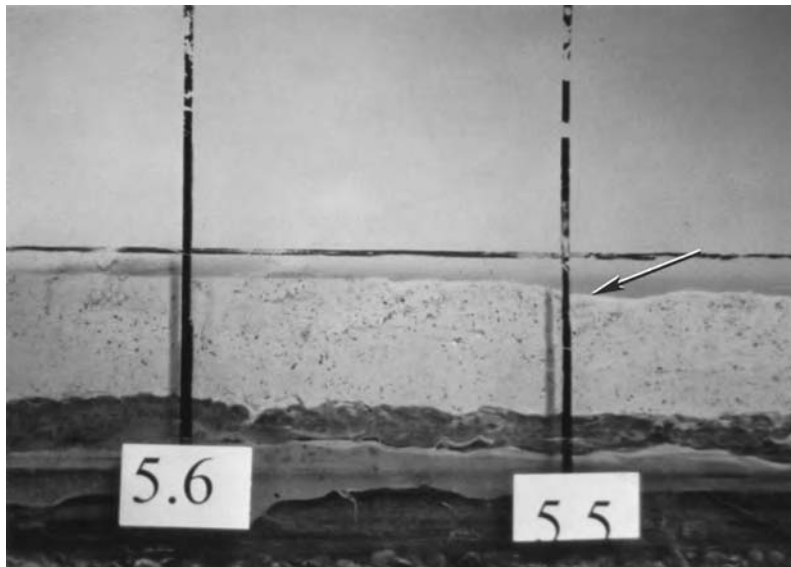
Fig. 3.26. Side view of flume tank showing sandy debris flows with irregular upper surface (arrow) due to sudden freezing of flow. Horizontal distance between the 5.5 and 5.6 markers is 10 cm. Flow direction is from right to left.
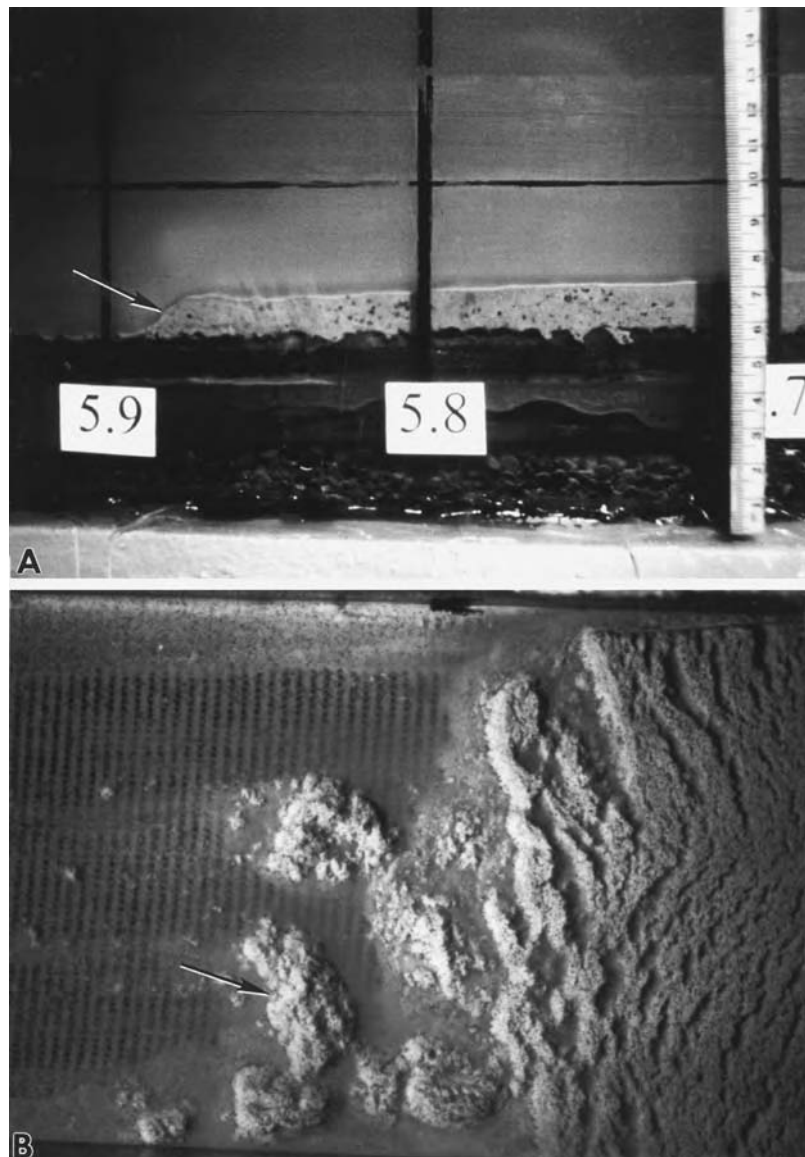
Fig. 3.27. (*A*) **Side view of flume tank showing sandy debris flow with a sharp and irregular snout (arrow), caused by freezing of the flow. Random distribution of coal slags is due to freezing of the flow with strength. Horizontal distance between the 5.8 and 5.9 markers is 10 cm. Flow direction is from right to left. (*B*) Map view of experimental sandy debris flows showing isolated blocks of sand bodies (arrow). These sandy debrite bodies slowly got detached from the main body by tension. Detachments may be explained by hydroplaning and related faster moving head with respect to the body. Width of photo is approximately 10 cm. Flow direction is from right to left. (After Shanmugam (2000a). Reproduced with permission from Elsevier.)**
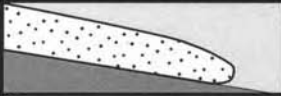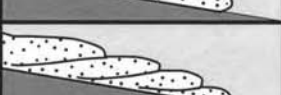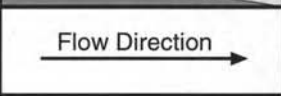
Features	Observation	Interpretation
	Sharp Upper Contact	Freezing of Flow and Plastic Rheology
	Irregular Upper Contact and Lateral Pinch-out Geometry	Freezing of Primary Relief and Plastic Rheology
	Irregular Front (Snout)	Freezing of Primary Relief and Plastic Rheology
	Non-Erosive Base and Water Entrapment (∠)	Laminar Flow and Hydroplaning
	Dish Structures and Water Entrapment (∠)	Hydroplaning and Water Escape
	Vertical Pipes	Hydroplaning and Water Escape
	Grain Segregation and Normal Grading	Grain Settling from Weak Flow
	Planar Fabric and Inverse Grading	Laminar Flow and Flow Strength
	Random Fabric	Flow Strength and Freezing of Flow
	Internal Layers	Mass Movement and Secondary Glide Planes
	Imbricate Slices	Mass Movement and Compression
	Isolated Blocks	Mass Movement and Tension
Flow Direction →	▦ 120 µm Silica Sand ▦ 500 µm Coal Slag (bulk density: 2.6 g/cm^3)	

Fig. 3.28.   Summary of features observed in experimental sandy debris flows. (After Shanmugam (2000a). Reproduced with permission from Elsevier.)

The importance of basin-filling by 'cohesionless debris flows' was emphasized by Syvitski and Farrow (1989, p. 30). These researchers described deposits of these sandy flows as:

'*They tend to contain structureless clean well-sorted sand with mixed grading, i.e., both reverse and normal grading. They may contain synsedimentary clasts and there appears to be little difference between the characteristics of a pebbly grain flow and a sandy debris flow deposit…*'

Sandy debrites have been interpreted to be the dominant depositional facies in several hydrocarbon-producing reservoirs composed of massive sands in the North Sea and Norwegian Sea (see Chapter 10).

3.3.5 Newtonian turbidity currents

Turbidity current is a sediment flow with Newtonian rheology and turbulent state in which sediment is supported by turbulence and from which deposition occurs through suspension settling.

Middleton and Hampton (1973) originally considered turbidity currents as mass flows. However, mass flows exhibit a distinctly different behavior than turbidity currents. Nardin et al. (1979, p. 63) defined mass flows as: '*Transport processes dominated by plastic behavior, where shear stress is distributed throughout the mass, are referred to as mass flows*.' Therefore, the term 'mass flows' is restricted only to plastic debris flows in this book (see Table 3.1), and the term does not include Newtonian turbidity currents. Unlike Martinsen (1994, his Fig. 5.1), who classified turbidity currents as *mass movements*, turbidity currents are not classified here as mass movements either (Table 3.1). Other conflicting definitions of turbidity currents are discussed in Chapter 7.

With increasing fluid content, plastic debris flows tend to become Newtonian turbidity currents (Fig. 3.1). However, not all turbidity currents evolve from debris flows. Some turbidity currents may evolve directly from sediment failures. Although turbidity currents may constitute a distal end member in basinal areas, they can occur in any part of the system (i.e., shelf edge, slope, and basin).

The evolutionary concept of turbidity currents can be summarized as follows:

(1) Density flows (Johnson, 1938, 1939)
(2) Underflows (Bell, 1942)
(3) Density flows with sediment in suspension that *includes* underlying laminar layer (Kuenen, 1951) (Fig. 3.29)
(4) Newtonian rheology (Dott, 1963)
(5) Sediment in turbulent suspension that *excludes* underlying laminar layer (Sanders, 1965) (Fig. 3.29)
(6) Waning flow (Sanders, 1965)
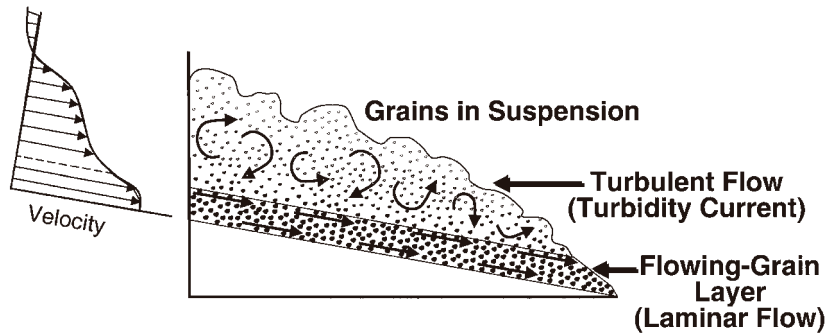
Fig. 3.29. A schematic profile through a density-stratified flow showing an upper turbulent turbidity current and a lower laminar flowing-grain layer. According to Sanders (1965, p. 218), only upper turbulent flows are turbidity currents and lower flowing-grain layers are not turbidity currents. Kuenen (1951) considered such density-stratified flows as high-density turbidity currents (see Chapter 7). Profile, based on experiments of Kuenen (1950a), was modified after Sanders (1965). (From Shanmugam (2002a). Reproduced with permission from Elsevier.)

(7) Sediment-support mechanism by turbulence (Middleton and Hampton, 1973) (Fig. 3.30)
(8) Surge-type events that do not attain hydrodynamic equilibrium (Allen, 1973)
(9) Unsteady and non-uniform flow (Allen, 1985b)
(10) '*Turbidity currents are thought to be unsteady, indeed catastrophic events, generated by sediment slumping on an oversteepened subaqueous slope.*' (Middleton, 1993, p. 91).

Fig. 3.30. A front view of an experimental turbidity current showing flow turbulence from bottom to top. Note the absence of a basal laminar layer. Experiments have shown that turbidity currents can and do occur as separate entity without an underlying high-concentration laminar flow. (Photograph from experiments by M. L. Natland. Photo courtesy of G. C. Brown.)

General characteristics of turbidites (i.e., deposits of turbidity currents) are:

- Fine-grained sand to mud
- Normal grading without complications (i.e., without floating clasts or granules). This is because velocity (*u*) decreases with time (*t*) in a waning flow (Fig. 3.31A). As a result, a waning flow would deposit coarse-grained material first followed by fine-grained material, causing a normal grading (Fig. 3.31B)
- Sharp or erosional basal contact (Fig. 3.32)
- Gradational upper contact (Fig. 3.32)
- Thin layers, commonly centimeters thick (Fig. 3.32)
- Sheet-like geometry in basinal settings (Fig. 3.33)
- Lenticular geometry may develop in channel-fill settings.

A conspicuous absence in the above list of characteristics is the Bouma Sequence. Problems in using the Bouma Sequence as a criterion for recognizing turbidites are discussed in Chapter 8. Although thick massive sands have been interpreted as high-density turbidites, such interpretations are problematic (see Chapter 7).

Classic examples of basin-plain turbidites, such as those exposed along the foreshore at Zumaya, Spain are usually in the range of 10 cm to 1 m in thickness (Fig. 3.33).

Laterally, they can be traced for several kilometers. Such extensive sheet-like turbidites deposited in the open oceans of Atlantic-type margins, however, are seldom preserved in the geologic record.

Deep-water deposits are often the result of complex interplay of several processes. Interpretation of Paleocene and Eocene reservoirs of deep-water origin
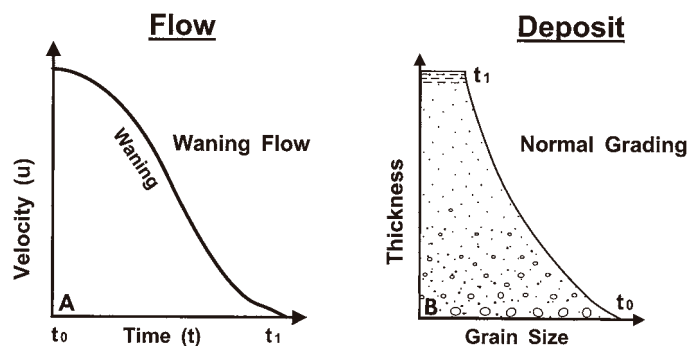
Fig. 3.31. (*A*) **Waning flow in which velocity (*u*) decreases with time (*t*). (*B*) Normal grading is the product of a waning flow from which deposition of coarser material is followed by finer material. Normal grading is the product of a single depositional event. Normal grading does not contain complex features, such as sudden vertical increase in grain size, floating granules or floating mudstone clasts (see Chapters 7 and 8).**
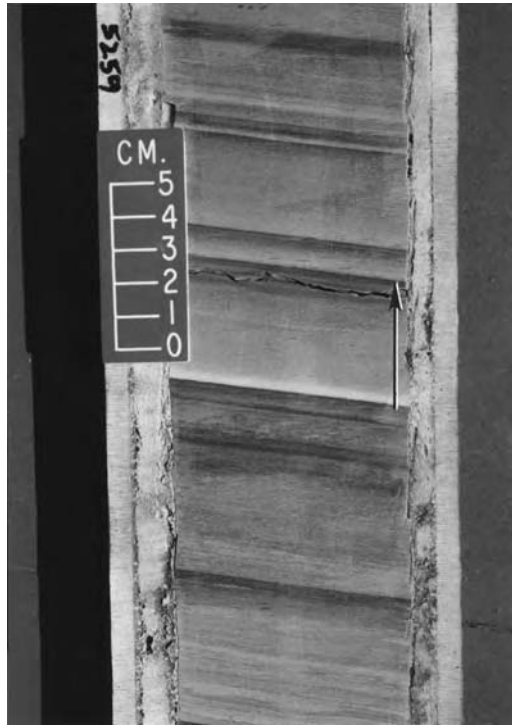
Fig. 3.32. Core photograph showing turbidite units with sharp basal contact, normal grading, and gradational upper contact. Arrow marks a normally graded unit with fine-grained sand at bottom (light color) grading into clay (dark color) near top. Zafiro Field, Pliocene, Equatorial Guinea (see Chapter 6).

in the North Sea suggests a variety of deep-water processes, namely slumps, sandy debris flows, turbidity currents, and bottom currents (Fig. 3.34).

3.3.6 Elusive turbidity currents

Shepard et al., (1979) believed that turbidity currents were common in modern submarine canyons; however, these researchers justified that turbidity currents could not be documented because of their high velocities. There is no geological reason why all turbidity currents should be such high-velocity flows that they invariably elude documentation. Like all other gravity-driven processes, turbidity currents should operate under a wide range of velocity conditions based on sediment concentration, sea-floor gradient, etc.

Shepard et al. (1979) attributed canyon currents with relatively low velocities (e.g., 25 cm/s) to tidal forces; but they inferred a turbidity current origin for a down-canyon current with a high velocity of 190 cm/s (i.e., 6.84 km/h) in the Scripps Canyon, offshore California. The problem with their inference is that

Fig. 3.33. Outcrop photograph showing thin-bedded turbidite sandstone with sheet-like geometry, lower Eocene, Zumaya, northern Spain.

turbidity currents are defined on the basis of Newtonian fluid rheology and turbulent flow state, not on flow velocity (e.g., Dott, 1963; Sanders, 1965; Middleton and Hampton, 1973; Shanmugam, 2000a). One cannot distinguish turbidity currents from debris flows based on flow velocity alone. Martinsen (1994, p.142), for example, reported rapid debris flows with a velocity of 500 km/h. The eruption of Colombia's Nevado del Ruiz volcano in 1985 triggered a subaerial mud flow that traveled at a speed of 320 km/h (The Learning Channel, 1997). Thus the flow with a 190 cm/s (i.e., 6.84 km/h) velocity in the Scripps Canyon could as well have been a debris flow.

Because turbidity currents are rapid surges with short duration (i.e., few hours), they tend to bypass submarine canyons quickly. Although Shepard et al. (1979) collected current-meter velocity data for a period of up to 30 days at a stretch; they were nevertheless unable to record the velocity of turbidity currents. The rarity of turbidity currents may explain why no one has ever photographed turbidity currents in modern submarine canyons. Unlike turbidity currents, photographic documentation of active slumps, grain flows, and sandy debris flows in modern submarine canyons is common (see Shepard and Dill, 1966; Shepard et al., 1969). Documented examples are:

(1) Observed occurrences of *slumps* in the head of Scripps Submarine Canyon that include one in 1959, three in 1961, two in 1962, and four in 1963 (Shepard and Dill, 1966, their Table 3)
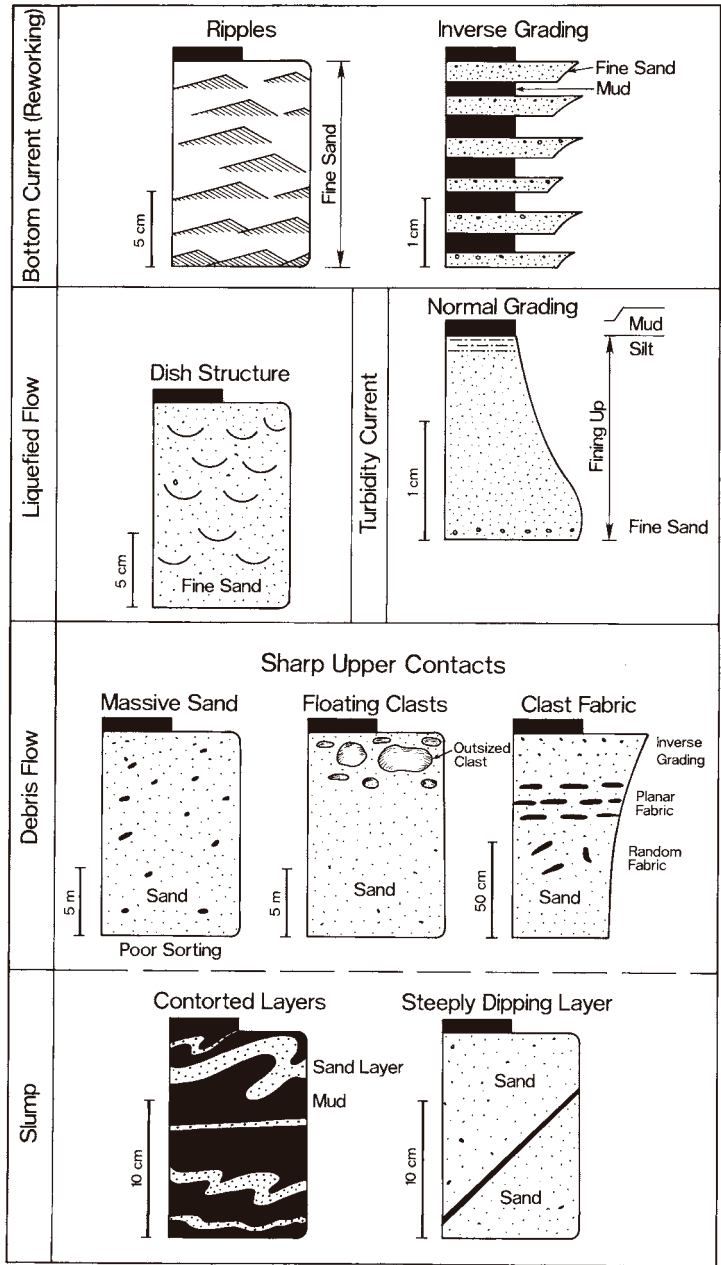
Fig. 3.34. Summary of depositional features observed in cores indicating a variety of depositional processes. Eocene and Paleocene, North Sea.

(2) Underwater photograph of sand fall (i.e., *grain flows*) in a gully (Shepard and Dill, 1966, their Fig. 55)

(3) Underwater photograph of rounded cobbles in sandy matrix (i.e., *sandy debris flows*) (Shepard and Dill, 1966, their Fig. 63)

(4) Underwater photograph of sand flows or *sandy debris flow*s (Shepard and Dill, 1966, their Fig. 139)

(5) Underwater photograph of sand flows or *sandy debris flows* near a small canyon mouth (Shepard and Dill, 1966, their Fig. 140).

Considering these photographic documentations of ubiquitous deep-water slumps, grain flows, and sandy debris flows, large-scale turbidity currents in modern canyons and oceans have remained a stealth phenomenon. The present-day highstand of sea level has often been used as an excuse for the absence of turbidity currents in modern oceans. Such excuses, however, do not hold true because sea level is only one of 11 causes that can trigger sediment failures and related gravity processes. Evidence for a true turbidity current event in modern deep-marine environments must come either from the direct measurement of the Reynolds Number or from videos or photographs that show a flow is indeed turbulent in state. In addition, it is essential to establish that the flow is a sediment-gravity flow and it exhibits the Newtonian rheology. To date, no one has documented true turbidity currents in modern deep-water environments by applying these criteria.

Khripounoff et al. (2003, p. 151) claimed '*Direct observation of intense turbidity current activity in the Zaire submarine valley at 4000 m water depth,*' but they did not provide evidence for the Newtonian rheology and turbulent state. The maximum measured velocity of 121.4 cm/s in the Zaire valley is not the proof of turbidity currents. Another such assertion was by Parsons et al. (2003, p. 839) who claimed, '*In fact, one of us (JDP) has personally observed (via an ROV) a dilute turbidity current associated with internal wave resuspension in the Eel Canyon.*' But the authors did not provide any information on the *Reynolds Number* of the resuspension. Nor did they explain whether the resuspension was a sediment-gravity flow or not. These details are critical because not all resuspensions transform into downslope turbidity currents. Previously, similar claims of recognition of 'turbidity currents' in modern environments were made using geophysical methods of remote acoustic detection (e.g., Hay et al., 1982). Such techniques are incapable of resolving the turbulent state or the Newtonian rheology of turbidity currents.

3.4 Synopsis

Slides, slumps, and sandy debris flows are important gravity-driven processes for transporting deep-water sand and gravel. Turbidity currents are Newtonian flows that do not have the strength to carry coarse-grained sand and gravel.

This Page Intentionally Left Blank

Chapter 4

Deep-water bottom currents

4.1 Introduction

The objective of this chapter is to explain basic types of deep-water bottom currents and to provide sedimentological criteria for interpreting their deposits in the rock record. Ocean currents may be broadly divided into (1) surface currents, (2) bottom currents, and (3) vertical currents. Wind-driven surface currents are an important source of bottom currents. Surface currents operate throughout the water column, from the sea surface to a depth of about 4000 m. Examples of this type are the Loop Current in the Gulf of Mexico (Pequegnat, 1972), and the Gulf Stream in the North Atlantic (Fuglister, 1951; Worthington, 1976). Ocean-surface currents are deflected to the right in the Northern Hemisphere and to the left in the Southern Hemisphere due to the Coriolis Force. An example is the Antarctic Circumpolar Current (Rebesco et al., 2002). Ocean-bottom currents are mainly driven by density differences caused by changes in temperature and salinity. Southard and Stanley (1976) distinguished five types of bottom currents at the shelf break. These currents are generated by (1) surface waves; (2) tidal forces; (3) wind forces; (4) thermohaline differences; and (5) internal waves. Although tsunami-related traction currents have been speculated in bathyal water depths (Yamazaki et al., 1989), mechanics of such currents have not been understood (see Shanmugam, 2006). Vertical-upwelling currents are caused either by surface waters moving away from each other or by surface waters moving offshore. Upwelling along the coast brings cold, nutrient-rich waters to the surface from below. Examples of surface currents associated with upwelling are the Guinea Current (Bakun, 1978) and the Agulhas Current (Walker, 1986). I have selected three types of deep-water bottom currents, namely (1) thermohaline-induced geostrophic bottom currents (i.e., contour currents), (2) wind-driven bottom currents, and (3) deep-marine tidal bottom currents for discussion here. Prior to discussing bottom currents, it is helpful to distinguish bottom currents from turbidity currents (Bouma and Hollister, 1973; Stow, 1979).

4.2 Bottom currents *versus* turbidity currents

Bottom currents and their deposits differ from turbidity currents and their deposits in the following respects (Shanmugam et al., 1993a; Shanmugam, 2000a, 2003):

• Bottom currents are driven by thermohaline, wind, or tidal forces, whereas turbidity currents are driven by sediment gravity
• Bottom currents may flow parallel to the strike of the regional slope, in circular motions (gyres) unrelated to the slope, and may flow up and down the submarine canyons, whereas turbidity currents always flow downslope
• Bottom currents may occur on the shelf, slope, and basinal environments, whereas turbidity currents are more common on the slope and basinal environments
• Bottom currents persist for long periods of time and can develop equilibrium conditions, whereas turbidity currents are episodic or surge-type events that fail to develop equilibrium conditions
• Bottom currents are free of sediment, and for this reason, they are termed as '*clear water currents*' (Bouma and Hollister, 1973, p. 82); whereas turbidity currents cannot exist without entrained sediment
• Bottom currents show oscillating energy conditions, whereas turbidity currents exhibit waning energy conditions
• Bottom currents transport sand primarily by traction (i.e., bed load movement by sliding, rolling, and saltation; Allen, 1984), whereas turbidity currents transport fine-grained sand and mud in suspension
• Traction structures (e.g., parallel and ripple laminae and cross beds) are common in bottom-current deposits, whereas normal grading is the norm in turbidites
• Bottom-current deposits exhibit sharp upper contacts, whereas turbidites show gradational upper contacts
• Bottom currents can result in well-sorted sand with good porosity and permeability because of reworking and winnowing away of mud, whereas turbidity currents do not form well-sorted sand. Turbidites are mud-rich facies (see Chapter 12).

4.3 Thermohaline-induced geostrophic bottom currents

Thermohaline-induced bottom currents are common in the world oceans. An example of such bottom currents is the Antarctic Bottom Water (AABW). AABW was first identified by Brennecke (1921) in the northwest corner of the Weddell Sea in the Antarctic region (Fig. 4.1). The origin of the AABW was attributed to the formation of ice from surface freezing over the Antarctic continental shelves. Ice forms when sea water experiences a concurrent increase in salinity and a decrease in temperature, which causes an increase in the density of cold-saline (i.e., *thermohaline*) water directly beneath the ice. This dense-water mass sinks and flows down the continental slope. It then spreads out to other parts of the ocean (Fig. 4.1).

WBUC = WESTERN BOUNDARY UNDERCURRENT
AABW = ANTARCTIC BOTTOM WATER
GSG = GULF STREAM GYRE
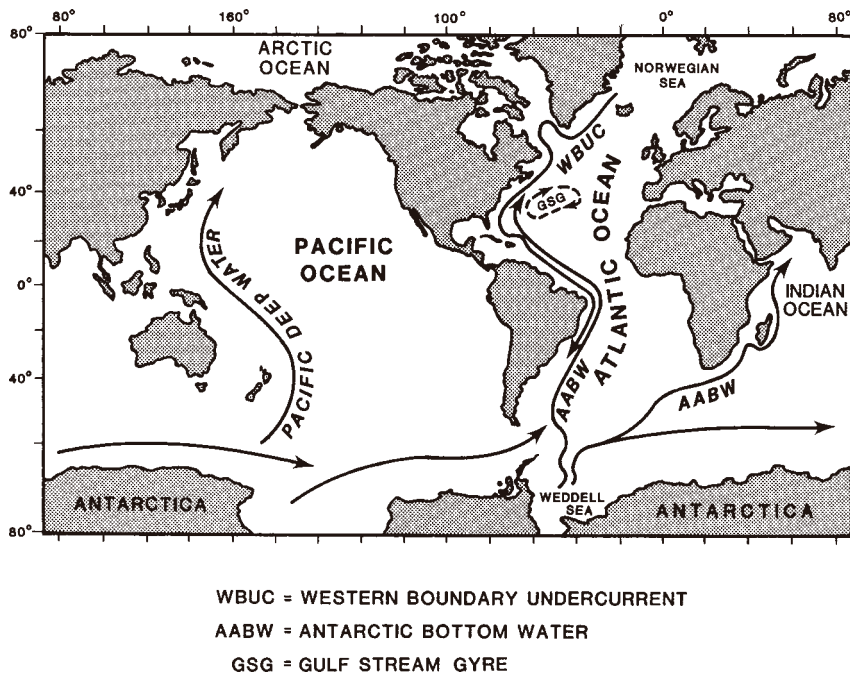
Fig. 4.1. Simplified circulation patterns of major thermohaline bottom currents (contour currents). Most contour currents originate from the Weddell Sea and from the Norwegian Sea. (Compiled from several sources (Wust, 1950; Stommel, 1958; Heezen and Hollister, 1971; Stow and Lovell, 1979).)

The Western Boundary Undercurrent (WBUC or WBU), the Arctic counterpart to AABW, originates as a cold dense water mass from the Norwegian Sea off Greenland (Worthington and Volkman, 1965). It flows along the western margin of the North Atlantic (Fig. 4.1). These thermohaline currents tend to flow parallel to the slope, that is, along the slope at right angle to downslope flowing gravity-induced currents (Fig. 4.2). The WBUC is deflected to the west as a result of the Coriolis force in the Northern Hemisphere. Because of its tendency to flow parallel to bathymetric contours, the WBUC is known as a *contour* current (Heezen et al., 1966). These currents are commonly known as *geostrophic* contour currents because they strike a balance between the Coriolis and the gravity forces.

Examples of bottom currents in various parts of the world's oceans and their acronyms are:

• **AABW**: Antarctic Bottom Water
• **ABW**: Arctic Bottom Water
• **AAIW**: Antarctic Intermediate Water (Brazilian margin)
• **ACC**: Antarctic Circumpolar Current (Antarctica)
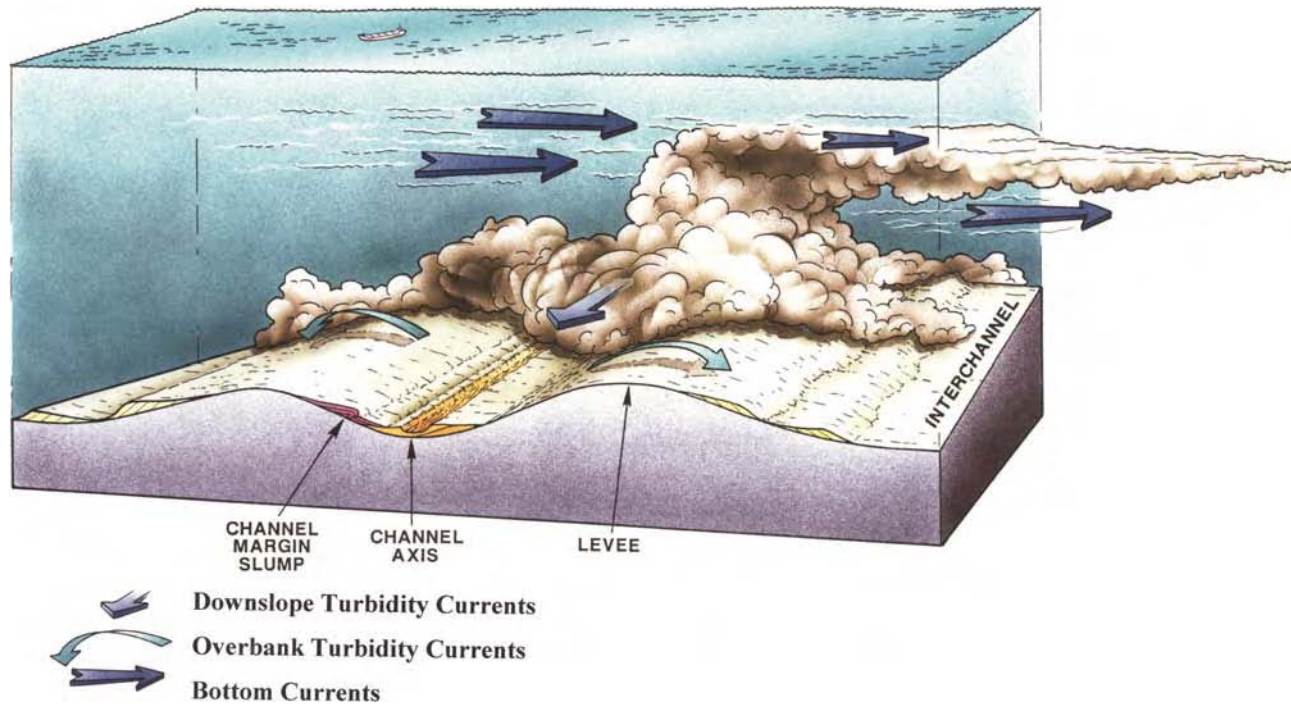
Fig. 4.2. A conceptual model showing spatial relationship between downslope turbidity currents and along-slope bottom currents (contour currents). (After Shanmugam et al. (1993a). Reprinted by permission of the American Association of Petroleum Geologists whose permission is required for further use.)

- **AW**: Atlantic Water (Mediterranean Sea)
- **BC**: Brazil Current
- **BICC**: Brazil Intermediate Counter Current
- **CDW or CPDW**: Circumpolar Deep Water (Antarctica)
- **LIW**: Levantine Intermediate Water (Mediterranean Sea)
- **MOW**: Mediterranean Outflow Water
- **MUC**: Mediterranean Undercurrent
- **NADW**: North Atlantic Deep Water
- **NPDW**: North Pacific Deep Water (Japan)
- **NSDW**: Norwegian Sea Deep Water
- **NSOW**: Norwegian Sea Overflow Water
- **SACW**: South Atlantic Central Water (Brazilian margin)
- **WBUC or WBU**: Western Boundary Undercurrent
- **WDW**: Warm Deep Water (Antarctica)
- **WSBW**: Weddell Sea Bottom Water (Antarctica).

4.3.1 Velocity

The speed of bottom currents can be several knots (1 knot = 51 cm/s). Measured velocities usually range from 1–20 cm/s (Hollister and Heezen, 1972); however, exceptionally strong, near-bottom currents with maximum velocities of up to 300 cm/s were recorded in the Straits of Gibraltar (Gonthier et al., 1984). Bottom-current velocities of 73 cm/s were measured at a water depth of 5000 m on the lower continental rise off Nova Scotia (Richardson et al., 1981). A summary of maximum current velocities of bottom-water masses in various parts of the world's oceans is given in Table 4.1.

Because of their high velocities, bottom currents in the deep sea are quite capable of erosion, transportation, and redeposition of fine to coarse sand. Regional erosional unconformities in the deep sea throughout thousands of square kilometers of sea floor have been attributed to erosion by bottom currents (Berggren and Hollister, 1977; Tucholke and Embley, 1984; Shanmugam, 1988).

4.3.2 Deposits

Deposits of deep-marine 'contour currents' have been termed *contourites* (Hollister, 1967). In deep-water environments, deposits of bottom currents that are dominated by traction structures have been classified as *tractionite* (Natland, 1967). In this book, the general term 'bottom-current-reworked sands' is used.

General characteristics of bottom-current reworked sands have been discussed by Hubert (1964), Hollister (1967), Hollister and Heezen (1972), Bouma and

Table 4.1 Maximum current velocities of bottom currents in the world's oceans

Study area	Depth (m)	Maximum current velocity (cm/s)
SE of Iceland, North Atlantic (Steele et al., 1962)	2100 slope	30
Greenland-Iceland-Faeroes Ridge, North Atlantic (Worthington and Volkman, 1965)	2000–3000	12
Faeroe Bank Channel, North Atlantic (Crease, 1965)	760	109
Faeroe-Shetland Channel, North Atlantic (Akhurst, 1991)	900	33
Straits of Gibraltor (Gonthier et al., 1984)	400–1400	300
Hebrides Slope, North Atlantic (Howe and Hmphrey, 1995)	403–468	48
Rise, Off Nova Scotia, North Atlantic (Richardson et al., 1981)	5000	73
Western North Atlantic (Wust, 1950)	2000–3000	17
Off Blake Plateau, North Atlantic (Swallow and Worthington, 1961)	3300–3500	20
Off Cape Cod, North Atlantic (Volkman, 1962)	10–3200	21.5
Antillean-Caribbean Basin (outer), North Atlantic (Wust, 1963)	4000–8000	10
Off Cape Hatteras, North Atlantic (Barrett, 1965)		21
West Bermuda Rise, North Atlantic (Knauss, 1965)	5200	17
Off North Carolina, North Atlantic (Rowe and Menzies, 1968)	1500–4000	25
Blake Bahama Outer Ridge, North Atlantic (Amos et al., 1971)	4300–5200	26
Rise, near Hatteras Canyon, North Atlantic (Rowe, 1971)		33
Rise, Off New England, North Atlantic (Zimmerman, 1971)	3000–5000	26.5
Greater Antilles Outer Ridge, North Atlantic (Tuholke et al., 1973)	5300–5800	20
Gulf of Mexico, Loop Current (Cooper et al. (1990))	100	204
Green Canyon 166 area, Gulf of Mexico. Drilling operations were temporarily suspended in August of 1989 because of high current velocities that reached 153 cm/s (Koch et al., 1991).	45	153
Upper slope. Offshore Brazil, Equatorial Atlantic (Viana et al., 1998)	200	300
Argentine Basin, Western South Atlantic (Ewing et al., 1971)		30
Tonga Trench and vicinity, Western South Pacific (Reid, 1969)	>4800	19
Samoan Passage, Western South Pacific (Hollister et al., 1974)		50
Carnegie Ridge, Eastern Equatorial Pacific (Lonsdale and Malfait, 1974)	1000–2000	>30
Trench, Ryukyu Trench, Japan (Tsuji, 1993)	340	51
Amirante Passage, Western Indian Ocean (Johnson and Damuth, 1979)	4000–4600	30
Scotia Ridge, Antarctic Circum Polar Current, Antarctica (Zenk, 1981)	3008	17*

*1-year vector averaged speed.

Hollister (1973), Unrug (1977), Stow and Lovell (1979), Lovell and Stow (1981), Shanmugam (1990, 2000a), and Ito (2002). These characteristics are:

- Fine-grained sand and silt
- Thin-bedded to laminated sand (usually less than 5 cm) associated with deep-marine mud
- Rhythmic occurrence of sand and mud layers
- Sharp to gradational bottom contacts
- Sharp, non-erosional, upper contacts
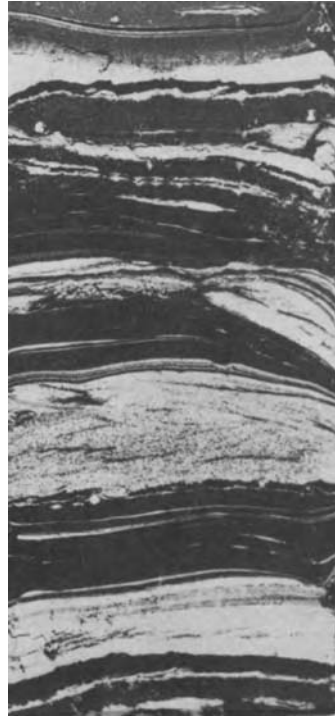
Fig. 4.3. Core photograph showing well sorted fine-grained sand and silt layers (light color) with interbedded mud layers (dark color). Note sand layers with sharp upper contacts, internal ripple-cross laminae, and mud offshoots. Also note lenticular nature of some sand layers. Pleistocene, continental rise off Georges Bank, Vema 18–374, 710 cm, water depth 4756 m. Width of core is about 6 cm. (After Hollister (1967, his Fig. VI-1, p. 208) and Bouma and Hollister (1973). Reproduced with permission from SEPM.)

- Well-sorted sand
- Low depositional mud matrix (clean sand) (Fig. 4.3)
- Inverse size grading (coarsening upward) at various scales
- Horizontal laminae
- Low-angle cross laminae
- Ripple-cross laminae (Fig. 4.3)
- Lenticular bedding or starved ripples (Fig. 4.3). Lenticular laminae of bottom-current origin have been reported from DSDP leg 28, Site 268, in Antarctica (Piper and Brisco, 1975).
- Mud-offshoots in ripples
- Mud-draped ripples
- Alternating traction and suspension structures.
- Flaser bedding
- Occurrence of sand layers with traction structures in discrete units.

No single criterion by itself is unique to bottom-current reworked facies. Although many of the above listed criteria can be attributed to processes other than bottom-current reworking; the association of several of the above criteria in a given deep-water example, along with the knowledge of regional depositional setting, greatly enhances the chance of recognizing bottom-current reworked facies. It may be difficult to establish that, a given example in the rock record was originated by contour-following thermohaline currents without establishing the paleo-water circulation pattern. Deposits in the rock record have been interpreted as contourites (Bouma and Hollister, 1973; Bein and Weiler, 1976).

4.3.3 Problematic contourite facies model

A general facies model for muddy and sandy contourites was proposed by Stow et al. (1998, 2002). This model was similar to that first proposed for the modern Faro Drift in the Gulf of Cadiz, south of Portugal (Gonthier et al., 1984). The model consists of a basal negatively (inversely) graded unit overlain by a positively (normally) graded unit (Fig. 4.4). The grain size varies vertically from mud at the bottom, through sandy silt in the middle, to mud at the top. Sand and silt comprise only 5% of the sediment. Bioturbation is ubiquitous throughout. Gonthier et al. (1984) attributed the vertical change in grain size (vertical increase followed by vertical decrease) to corresponding variations in current velocity (vertical increase followed by vertical decrease) associated with the deep Mediterranean outflow.

According to Stow et al. (1998), contourites are sediments that have been deposited or reworked by geostrophic bottom currents that follow bathymetric contours in water depths greater than 300 m. There are several problems with this contourite model:

(1) The general facies model does not include deposits of bottom currents induced by surface wind currents and tidal currents in submarine canyons that operate in water depths greater than 300 m.

(2) In dealing with ancient strata, it is not always possible to differentiate whether a bottom current that followed bathymetric contours or a bottom current that did not follow bathymetric contours, reworked the bed. This is because not all bottom currents follow bathymetric contours (e.g., the Loop Currents in the Gulf of Mexico, as discussed below). Therefore, a general contourite model is applicable only to ancient examples in which it can be demonstrated that geostrophic currents indeed followed bathymetric contours in paleo water depths in excess of 300 m.

(3) The term 'sandy' is used loosely for both quartz sands (i.e., clastic contourites of Stow et al., 1998) and biogenic sands (i.e., biogenic contourites of Stow et al., 1998) in the model. Quartz sands have a bulk density of 2.65 g/cm³,
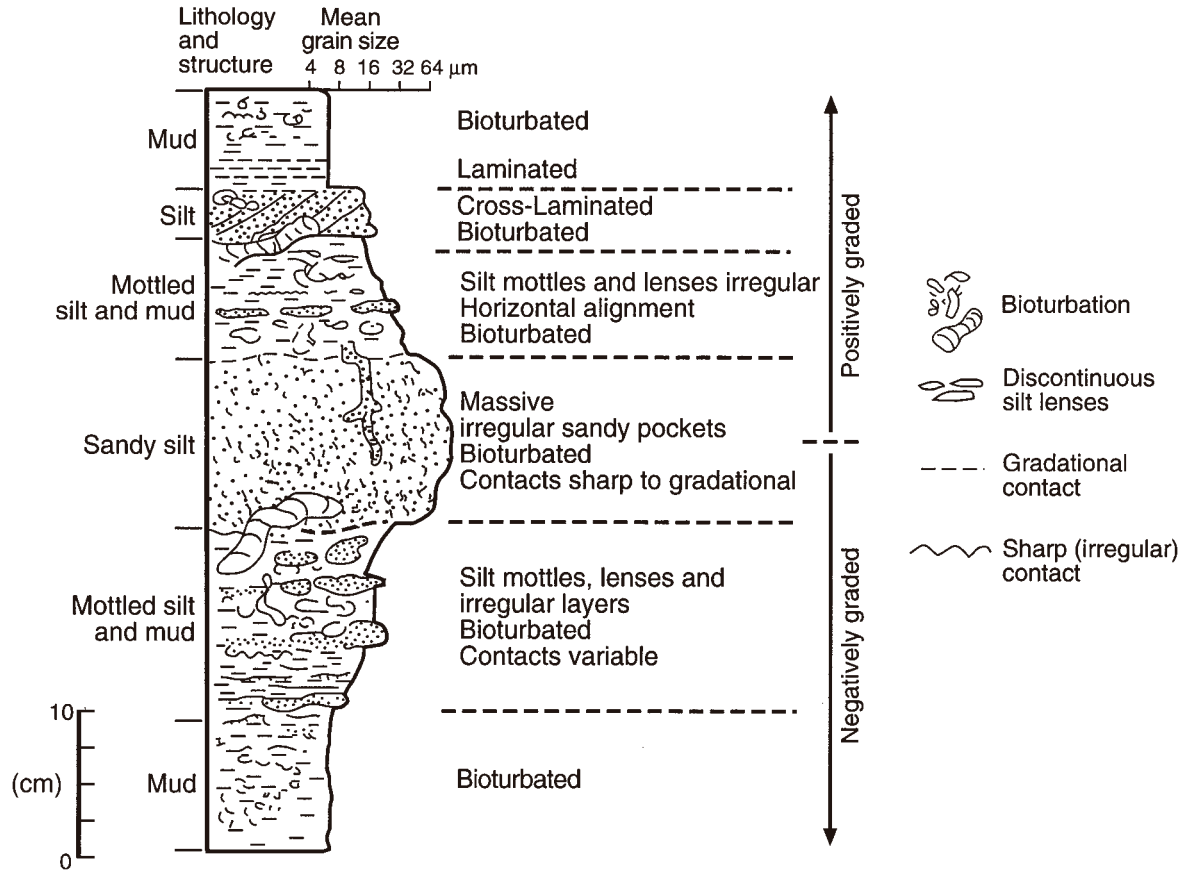
Fig. 4.4. Composite facies model for muddy and sandy contourites. Vertical grain- size variations and bioturbation, advocated by the model, are not unique to contourites. This general model for sandy contourites is based on an example (Faro Drift) that is 95% mud, and only 5% sand and silt (see Gonthier et al., 1984). (After Stow et al. (1998). Reproduced with permission from Elsevier.)

whereas biogenic sands (mostly foraminiferal calcitic grains) have a bulk density of 2.71 g/cm^3. More importantly, foraminiferal sands are globular in shape with hollow interiors, whereas, quartz grains are variable in shape with dense interiors. As a consequence, foraminiferal sands, generally float in water, in comparison to quartz sands, although calcite has a higher bulk density than quartz! Therefore, lumping both quartzitic and calcitic sands in the 'sandy contourites' category is hydrodynamically confusing.

(4) In the original Faro Drift example that served as the basis for the model, sands and silts comprise about 5% of the sediment (Gonthier et al., 1984). The composite contourite model is a general one for both muddy and sandy contourites (Stow et al., 1998). Thus a sandy contourite model, based on an example (the Faro Drift) composed of more than 95% mud, is misleading.

(5) In discussing the composite contourite facies model (Fig. 4.4), Stow et al. (1998, p. 14) stated that in deep-water drifts, '…*direct evidence of current influence is often meagre*.' It is ironic that a general model for 'contour currents' has neither strong direct evidence for currents nor evidence for currents that follow bathymetric contours. A facies model is designed to reveal something unique about a particular environment or process; but the contourite model does not reveal anything unique about contour currents.

(6) The model strongly suggests that bioturbation is characteristic of contourites (see also Lovell and Stow, 1981). This suggestion was based on the belief that active bottom currents would increase the oxygen concentration of the water mass (Chough and Hesse, 1985), and would thereby increase the activity by benthic organisms. Tucholke et al. (1985), however, suggested that the degree of preservation of bioturbation, is a function of bottom current intensity; strong bottom currents do not favor preservation of biogenic structures. There is nothing unique about bioturbated mud in deep-water sequences that suggests deposition from contour-following, deep geostrophic currents. Bioturbated mud in the deep sea is equally abundant in areas that are unaffected by contour currents. Even if bioturbation were prevalent in areas of contour currents, it would not directly reveal anything unique about contour currents. In the rock record, convincing cases of contourites without bioturbation have been documented (Dalrymple and Narbonne, 1996).

4.4 Wind-driven bottom currents

4.4.1 The Loop Current

The Loop Current in the eastern Gulf of Mexico is a wind-driven bottom current (Fig. 4.5). The Loop Current enters the Gulf of Mexico through the Yucatan Straight as the Yucatan Current; it then flows in a clockwise loop in the eastern Gulf as the Loop Current, and exits *via* the Florida Strait as the Florida Current

(NEUMANN AND PIERSON, 1966; NOWLIN, 1972; MULLINS et al, 1987)
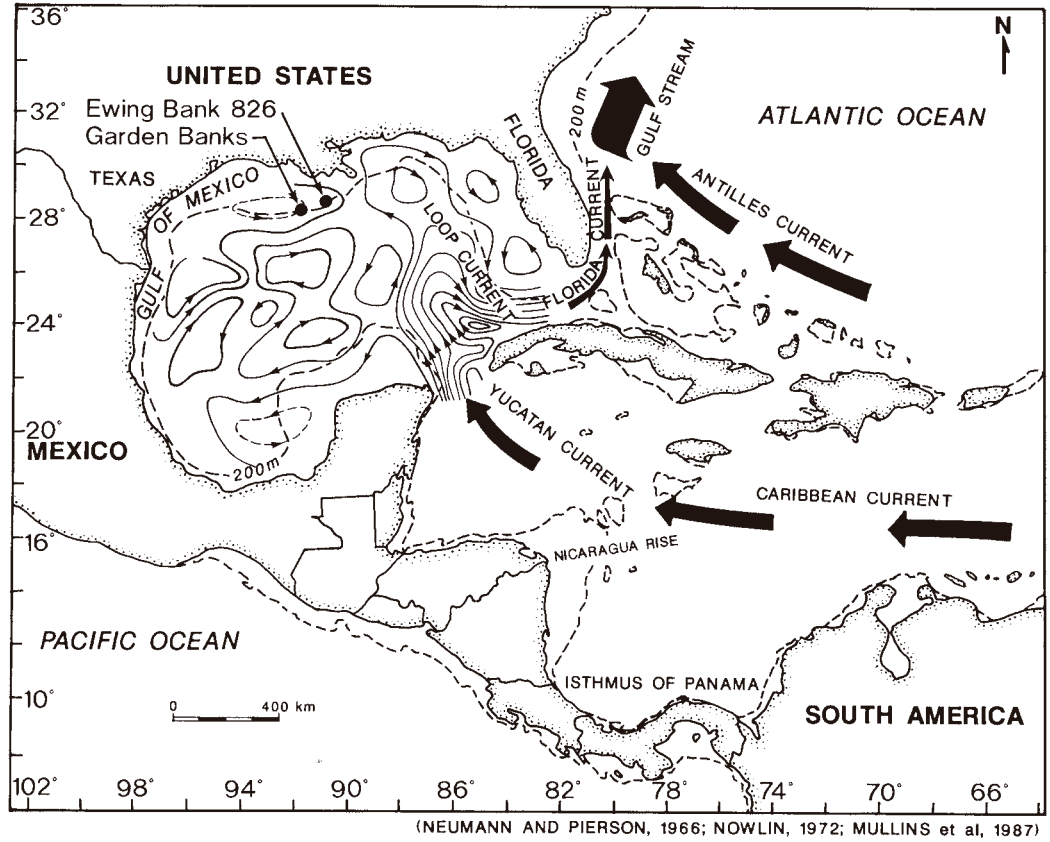
Fig. 4.5. Present circulation pattern of the Loop Current (after Neumann and Pierson, 1966; Nowlin, 1972; and Mullins et al., 1987). This wind-driven surface current is considered to be affecting the sea bottom (Pequegnat, 1972). Note the eddies detached from the Loop Current in the Ewing Bank area. (After Shanmugam et al. (1993a). Reprinted by permission of the American Association of Petroleum Geologists whose permission is required for further use.)

(Neumann and Pierson, 1966; Nowlin, 1972; and Mullins et al., 1987). Finally, this current merges with the Antilles Current to form the Gulf Stream. The Loop Current also propagates eddies into the north-central Gulf of Mexico where the Ewing Bank area, a case study used in this book, is located (Fig. 4.5).

4.4.2 Velocity

Velocities in eddies that have detached from the Loop Current have been recorded as high as 4 knots (204 cm/s) at a depth of 100 m (Cooper et al., 1990). The Loop Current and related eddies pose significant problems for deep-water drilling (Koch et al., 1991). For example, drilling operations in the Green Canyon 166 area were temporarily suspended in August of 1989 because of high current velocities that reached nearly 3 knots (153 cm/s) at a depth of 45 m, and 1 knot (51 cm/s) at a depth of 250 m. These intense bottom currents affect the ability of a drilling rig to hold station over a wellhead (Koch et al., 1991). In fact, the Minerals Management Service (MMS) of the U.S. Department of the Interior issued a safety alert to operating petroleum companies in the Gulf of Mexico stating,

'*You are advised of the possible existence of significant Gulf of Mexico (GOM) deepwater currents that could affect offshore operations and facility designs. The Minerals Management Service (MMS) has become aware of proprietary, site-specific measurements recorded over a 2-year period in Gulf of Mexico Outer Continental Shelf waters 6000 ft (1829 m) deep. Those measurements seem to indicate the presence of currents with velocities approaching one knot and which extend from a level 3000 ft (914 m) below the water surface down to the seafloor.*'

(Source: MMS Notice No. 180, March 4, 1999).

Current velocity measurements, bottom photographs, high-resolution seismic records, and GLORIA side-scan sonar records indicate that the Loop Current influences the sea floor at least periodically in the Gulf of Mexico (Pequegnat, 1972). Computed flow velocities of the Loop Current vary nearly from 100 cm/s at the sea surface to greater than 25 cm/s at 500 m water depth (Nowlin and Hubert, 1972). This high surface velocity suggests a wind-driven origin for these currents. Flow velocities measured using a current meter reach up to 19 cm/s at a depth of 3286 m (Pequegnat, 1972). Such currents are capable of reworking fine-grained sand on the sea floor. Deep-thermohaline-driven water masses cannot be responsible for reworking in this area because such water masses are unable to enter the Gulf of Mexico due to sea floor topographic barriers in the Caribbean basins (Fig. 4.6).

Current ripples, composed of sand at a depth of 3091 m on the sea floor, are a clear evidence of deep bottom-current activity in the Gulf of Mexico today (Pequegnat, 1972). These current ripples are draped by thin layers of mud called 'mud-offshoots' (Fig. 4.7).

The strong Loop Current/Gulf Stream circulation was created in the mid-Miocene due to closure of the Isthmus of Panama (Mullins et al., 1987). Furthermore, circulation of surface water masses may have been intensified
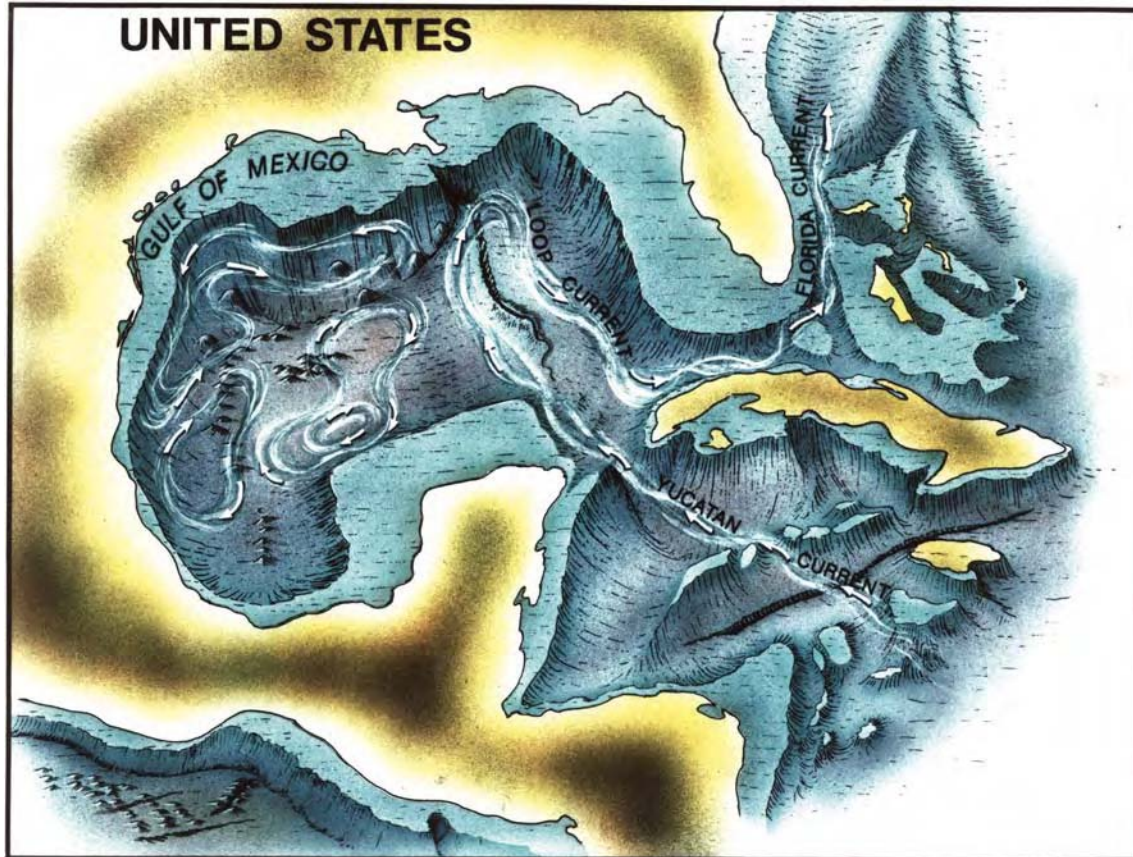
Fig. 4.6. A rendering of present-day sea-floor topography of the Gulf of Mexico showing the distribution of the Yucatan Current, the Loop Current, and the Florida Current. Deep-thermohaline-driven water masses are unable to enter the Gulf of Mexico from the Atlantic Ocean due to complex sea-floor topographic barriers in the Caribbean basins.
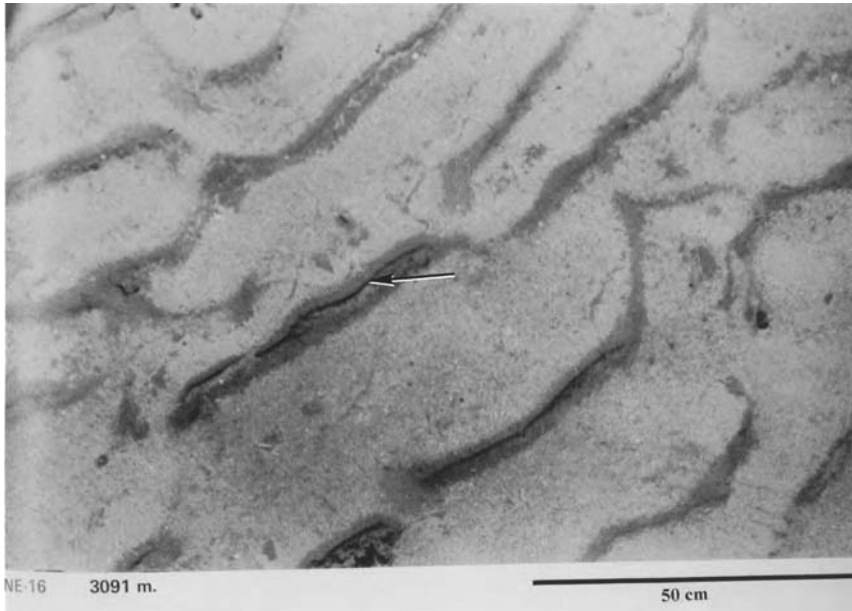
Fig. 4.7. **Under-sea photograph showing possible mud-draped (arrow) current ripples at 3091 m water depth in the Gulf of Mexico. Similar mud drapes may explain the origin of mud offshoots observed in the core (see Fig. 4.17). A current measuring nearly 18 cm/s was recorded on the day this photograph was taken. Current flow was from upper left to lower right. Bar scale is 50 cm. Alaminos Cruise 69-A-13, St.35. From Pequegnat (1972). (Reproduced with permission from Gulf Publishing Company.)**

during the glacial periods of the Plio-Pleistocene (Arrhenius, 1952). In the Gulf of Mexico, during the Pliocene and Pleistocene glacial lowstands, circulation of the Loop Current may have been much more vigorous than it is today, a time of interglacial highstand. Thus in the northern Gulf of Mexico intensified Loop Current circulation may have led to sustained and strong periods of current activity. In support of this hypothesis, Ewing Bank reservoirs show not only convincing evidence of bottom-current reworking but also a tendency to correlate with lowstands of sea level. In this respect, they are similar to other bottom-current reworked sands in the geologic record (Shanmugam and Moiola, 1982).

4.4.3 Ewing Bank Block 826 Field, Plio-Pleistocene, Gulf of Mexico

The Ewing Bank Block 826 Field is located nearly 100 km (62 miles) off the Louisiana coast in the Northern Gulf of Mexico (Fig. 4.8). It contains hydrocarbon-producing clastic reservoirs that were interpreted as deposits of deep-marine bottom currents (Shanmugam et al., 1993a, b, 1995c).
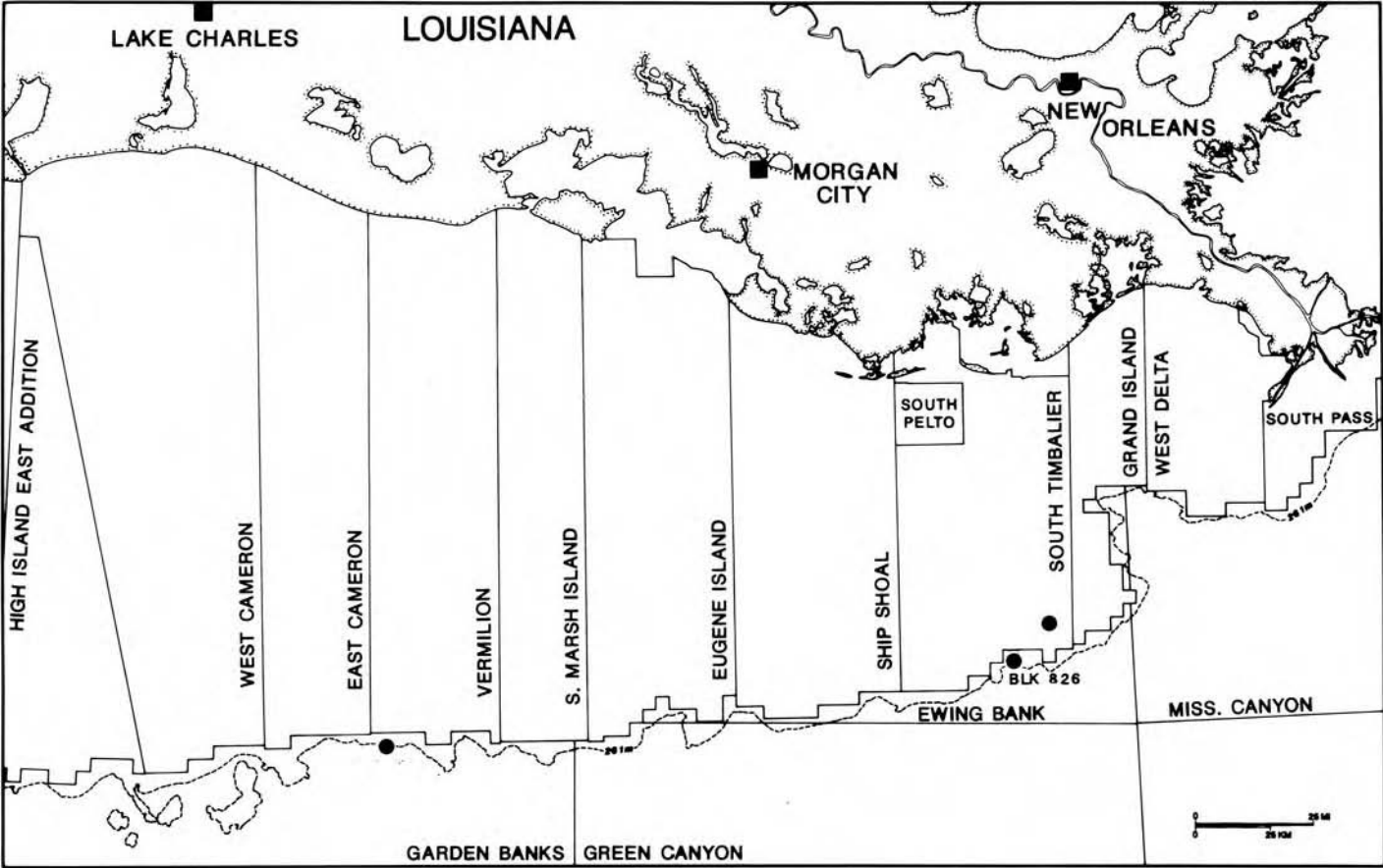
Fig. 4.8. Location map of the Ewing Bank and adjacent areas in the Northern Gulf of Mexico. Solid dots show locations of cores.

The Ewing Bank Block 826 Field was discovered in May, 1985. It lies approximately in 150 m (500 ft) of water along the 'flexure trend' (present-day outer shelf and upper continental slope). Cores from the Upper Pliocene reservoir sands (L-1 and N-1) and the Middle Pleistocene sequence are discussed here.

During 1985 and 1986, six wildcat and appraisal wells were drilled. Four cores (12 594.00–13 328.30 ft) (3839–4062 m) of Upper Pliocene age from Sohio's Ewing Bank 826, OCS-G-5800 Well No. 3, and two cores (13 360.00–13 416.70 ft) (4072–4089 m) from the Well No. 3ST (Sidetrack) were described. The No. 3 well is a straight hole in which log depths equal core depths. In the No. 3 sidetrack well, which is a deviated hole (about 30º deviation), the log depth is 13 ft (4 m) deeper than the core depth. During the coring operation, four inch conventional core barrel was used with a fiberglass liner. Cores were examined at the Petroleum Testing Service, Inc., Santa Fe Springs, California, where the cores were kept in frozen storage.

Sedimentary structures from the L-1 sand of the 3ST well, reveals three distinctly different depositional facies: a lower levee unit, a middle turbidite channel sand unit, and an upper bottom-current reworked sand unit (Fig. 4.9). The levee unit is characterized by slumped mud, the turbidite channel unit by normally graded sand, and the bottom-current reworked sand unit by current ripples and by sharp upper contacts.

The Ewing Bank cores exhibit the following features:

• Predominantly fine-grained sand and silt
• Thin-bedded to laminated sand (usually less than 5 cm) intercalated with deep-water mud (Fig. 4.10)
• Rhythmic sand and mud layers
• Numerous layers (50 or more per 1 m of core) (Fig. 4.10)
• Sharp (non-erosional) upper contacts (Fig. 4.10)
• Sharp to gradational bottom contacts
• Internal erosional surfaces (Fig. 4.11)
• External truncation surfaces (Fig. 4.12)
• Well-sorted sand and low depositional matrix
• Megascopic inverse size grading (Fig. 4.13)
• Microscopic inverse size grading (Fig. 4.14)
• Horizontal lamination and low-angle cross lamination (Fig. 4.10)
• Cross bedding (Figs. 4.11, 4.12)
• Lenticular bedding or starved ripples at core scale (Fig. 4.10)
• Current ripples with preserved crest or with eroded crest (Fig. 4.15)
• Ripple forms with curved bases (Fig. 4.15)
• Flaser bedding (Fig. 4.16)
• Mud-offshoots (Fig. 4.17)
• Occurrence of sand layers with traction structures in discrete units, but not as part of a vertical sequence of structures (Fig. 4.18).
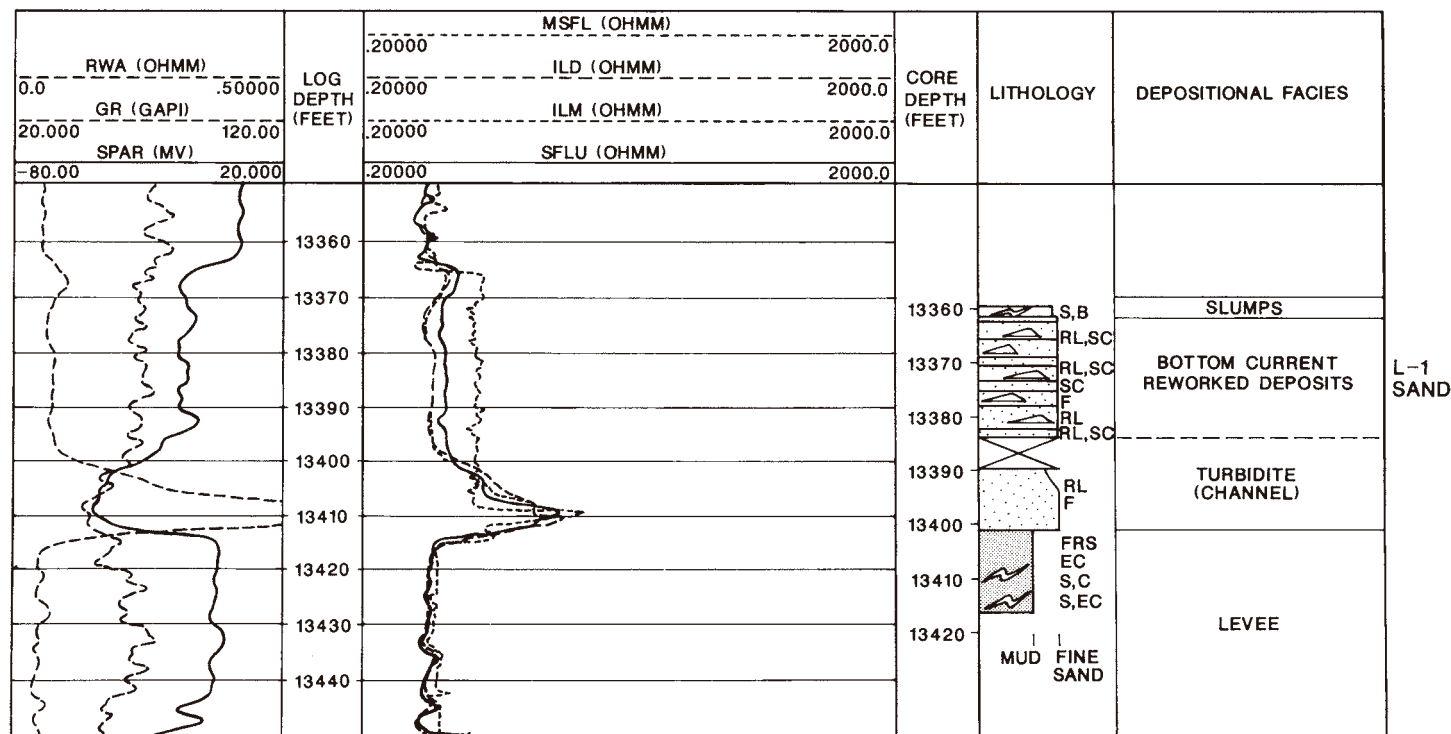
Fig. 4.9. Vertical distribution of levee, turbidite channel, and bottom-current reworked facies and their log motifs in the L-1 sand. Well No. 3ST (Sidetrack), Ewing Bank Block 826, Gulf of Mexico. S = slump, B = breccia, RL = ripple cross-laminae, SC = sharp upper contact, F = fault, FRS = fracture-fill sand, EC = erosional contact, C = calcareous. (After Shanmugam et al. (1993a). Reprinted by permission of the American Association of Petroleum Geologists whose permission is required for further use.)
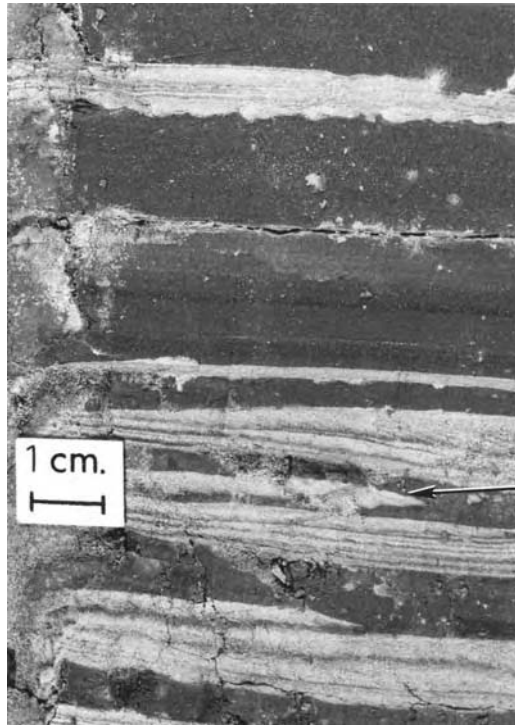
Fig. 4.10. Core photograph showing discrete thin sand layers with sharp upper contacts. Traction structures include horizontal laminae, starved ripples (arrow), and low-angle cross laminae (sand unit above arrow). Dip of cross laminae to the right suggests current flow was from left to right in this example. Note rhythmic occurrence of sand and mud layers. Middle Pleistocene, Gulf of Mexico. (After Shanmugam et al. (1993a). Reprinted by permission of the American Association of Petroleum Geologists whose permission is required for further use.)

Some of these traction structures are also observed in *contourite* deposits discussed before. Therefore, caution must be exercised in classifying a deposit as a 'contourite' based solely on traction structures without independent evidence for contour-following bottom currents in the area. Thus, a general term 'bottom-current reworked sand' is preferred.

In the Ewing Bank cores, ripple wavelengths of cross laminae ranges from 10 to 20 cm and amplitudes are less than 2 cm. The foreset thickness, in the range of 4 or 5 cm, suggests long, stable periods of bedload movement. Cross laminae and bedding are the strongest evidence for bottom-current-reworking. This is because avalanching and current traction is more likely to occur under 'clear-water' bottom currents than under sediment-charged turbidity currents. Also, sustained flow conditions, required for the formation of cross beds, are common in bottom currents, not in turbidity currents (see Chapter 7).
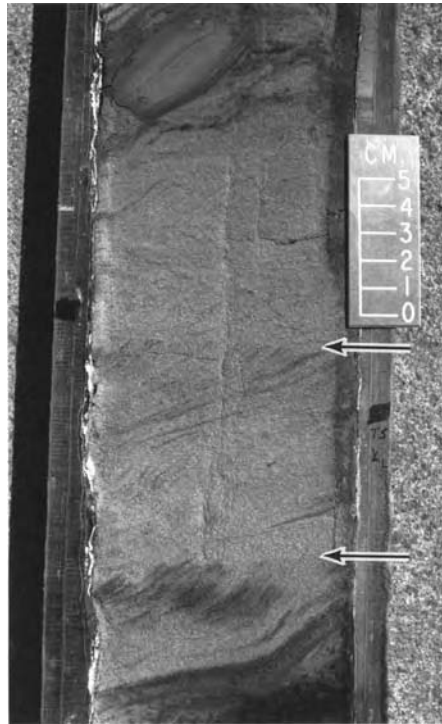
Fig. 4.11.   Core photograph showing cross-bedded sands with faint internal truncation surfaces (arrows). Beds dip to the left. Middle Pleistocene, Ewing Bank Block 826, Gulf of Mexico.

The erosional truncation surfaces (Fig. 4.11) or reactivation surfaces, which occur within cross-laminated units, reflect pulses of increased energy within bottom-currents. Such oscillating energy conditions of bottom currents have been measured over the HEBBLE (High-Energy Benthic Boundary Layer Experiment) site on the Nova Scotia continental rise (Hollister and McCave, 1984).

Ripples with curved bases (Fig. 4.15) are probably wave ripples that occur as part of a deep-water (upper bathyal) sequence. Conventionally, wave ripples are considered to be indicators of a shallow-water environment. One possible explanation for these features in deep water might be internal waves. Karl et al. (1986), for example, suggested that delivery of large volumes of fresh water and large quantities of sediment directly to the slope during periods of low sea level might enhance the propagation of high-frequency internal waves.

Most of the features discussed above are products of deposition by traction or combined traction and suspension (Fig. 4.18). These features are interpreted here as evidence for bottom-current reworking. Bottom-current reworked sands have also been recognized in the Pliocene and Pleistocene intraslope reservoirs in the
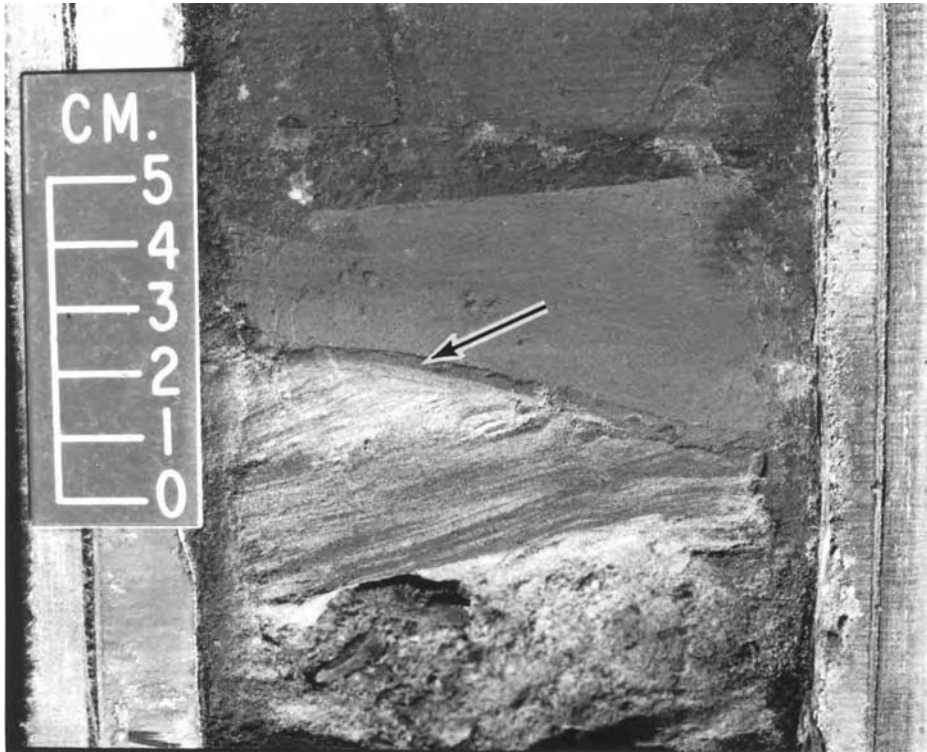
Fig. 4.12. Core photograph showing an erosional truncation surface (arrow) between cross-laminated sand unit and overlying mud unit. Upper Pliocene, Ewing Bank Block 826, Gulf of Mexico. (After Shanmugam et al. (1993a). Reprinted by permission of the American Association of Petroleum Geologists whose permission is required for further use.)

Garden Banks, South Timbalier, High Island A–474/A–499 (Anspach et al., 1989), and Green Canyon areas (Fig. 4.8) in the Gulf of Mexico. Other lines of evidence also suggest that bottom currents could have operated in the Gulf of Mexico during the Pleistocene and Holocene times. For example, cores from Site 614A of DSDP Leg 96 of latest Pleistocene age on the Mississippi Fan reveal evidence for bottom-current reworking in the form of sand layers with sharp upper contacts, inverse grading, and cross-laminae (Shanmugam et al., 1988a).

4.4.4 Ewing Bank depositional model

A depositional model has been proposed for the Ewing Bank Block 826 area (Fig. 4.19). This model includes interaction of three types of currents, namely, channelized turbidity currents, overbank turbidity currents, and bottom currents.
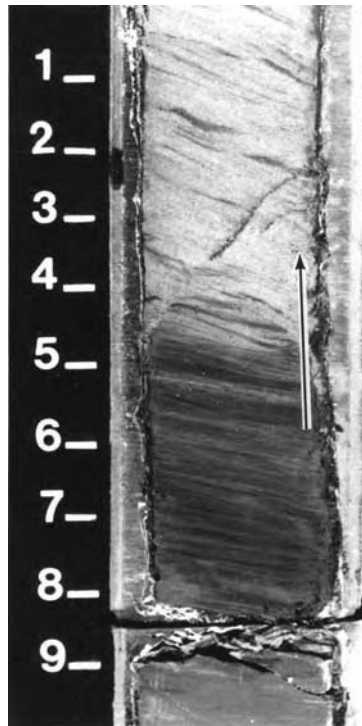
Fig. 4.13. Core photograph showing megascopic inverse size grading. Arrow shows the gradational nature of basal contact from mud (dark color) at the bottom to sand (light color) at the top. Each scale division is 3 cm. Middle Pleistocene, Gulf of Mexico. (After Shanmugam et al. (1993a). Reprinted by permission of the American Association of Petroleum Geologists whose permission is required for further use.)

The vertical facies association of the cored L-1 sand, composed of levee, turbidite channel, and bottom-current reworked sand in the 3ST well (Fig. 4.9), is the basis for their lateral disposition in the depositional model (Fig. 4.19). Although the model is not drawn to scale, the approximate position of the two wells, the relative depths of penetration into individual reservoir sands L-1 and N-1, and the cored intervals are illustrated in Figure 4.19. The model depicts the distribution of bottom-current reworked sands in interchannel slope area as a distinctly different facies from channel-levee facies.

In the proposed model, the lateral extent of sand bodies is based on both well and seismic data. In order to properly tie the Ewing Bank 826 No. 3 and No. 3ST wells to the 3-D seismic, two computer systems were used. A time-based cross-section along the deviated No. 3 well bore was created through MSAS, a VAX based Mobil software package on an Intergraph workstation. An arbitrary seismic
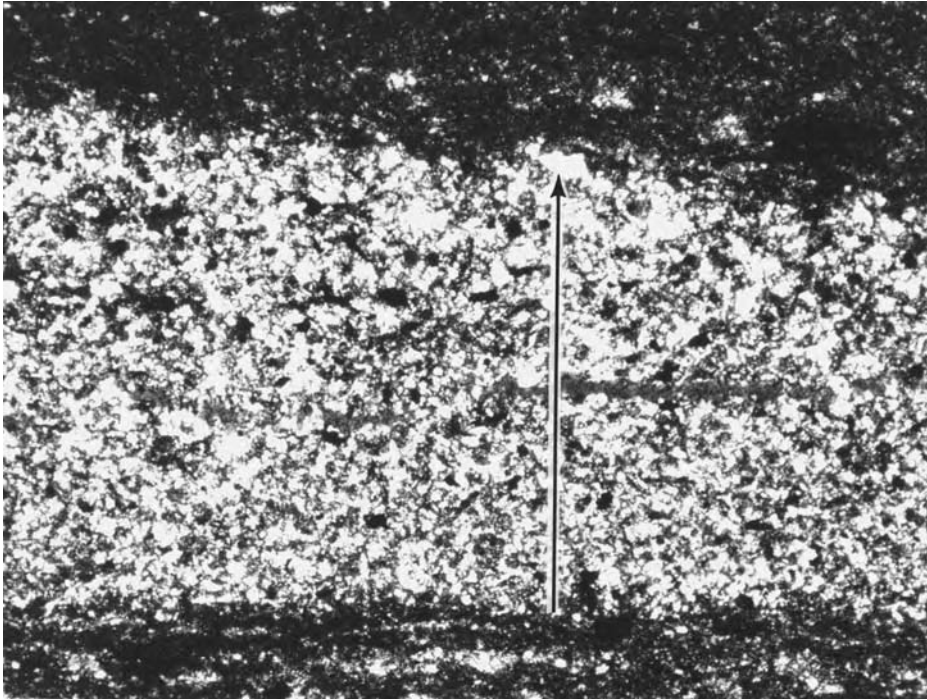
Fig. 4.14. Photomicrograph of a fine-grained sand layer (arrow) showing microscopic inverse size grading and sharp upper contact. Note largest quartz grain (tip of arrow) at the top of this 1 mm thick sand layer . Middle Pleistocene, Gulf of Mexico. (After Shanmugam et al. (1993a). Reprinted by permission of the American Association of Petroleum Geologists whose permission is required for further use.)

line was also created at the same scale and orientation using a LANDMARK workstation. Figure 4.20 is an overlay of the time-based cross-section on the scaled arbitrary line from northwest to southeast showing amplitudes related to the L-1 and N-1 sands.

Although not penetrated by the sidetrack well, the N-1 sand is traceable in seismic sections beneath the sidetrack well (Fig. 4.20). The eastward transition of N-1 sand from a bottom-current reworked facies into a channel/levee complex is schematic (see Fig. 4.19). In general, the transition zone between bottom-current reworked sand and turbidite channel sand is composed of fine-grained levee facies. This facies association and related reservoir heterogeneity is critical for field development of bottom-current reworked sand reservoirs. Importantly, there is no difference in seismic reflection patterns between reworked sand and turbidite channel sand (see Figs. 4.19 and 4.20).
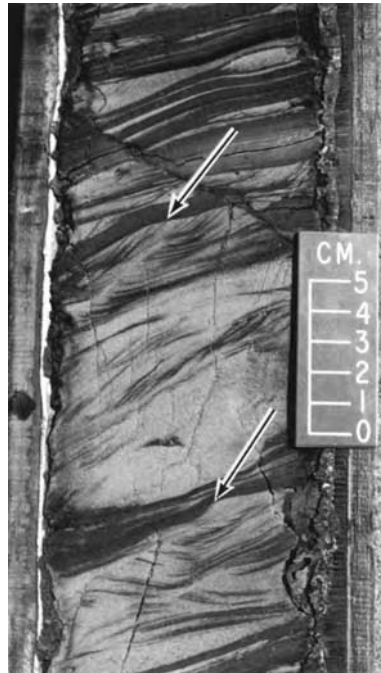
Fig. 4.15. Core photograph showing discrete sand units comprised of current ripples with variable dip directions suggesting multiple current directions. Preserved (lower arrow) and eroded (upper arrow) tops of ripples indicate variable energy conditions of the current. Ripples with curved bases probably indicate wave influence. Middle Pleistocene, Ewing Bank Block 826, Gulf of Mexico. (After Shanmugam et al. (1993a). Reprinted by permission of the American Association of Petroleum Geologists whose permission is required for further use.)

In the absence of core, one could misinterpret the L-1 sand, which shows continuous and parallel reflections in seismic profile (Fig. 4.20), as laterally continuous sheet-like turbidite sand representing the outer part of a submarine fan 'lobe' (Shanmugam and Moiola, 1991). The core information, however, suggests that the L-1 sand is composed of lower turbidite channel sand and an upper reworked sand (Fig. 4.19). Such a vertical facies association does not imply sheet-like sand bodies. This case study underscores the need to integrate core information with seismic facies analysis for developing realistic depositional models. It is also critical to understand the origin of sands from core before correlating these sands over long distances using wireline-log motifs. The sandbody geometry and reservoir quality of these bottom-current reworked sands are discussed in Chapter 12.
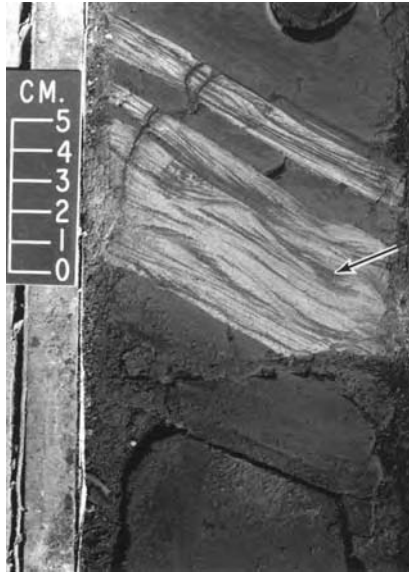
Fig. 4.16. Core photograph showing flaser bedding. Note the presence of mud in ripple troughs (arrow). Upper Pliocene, Ewing Bank Block 826, Gulf of Mexico. (After Shanmugam et al. (1993a). Reprinted by permission of the American Association of Petroleum Geologists whose permission is required for further use.)
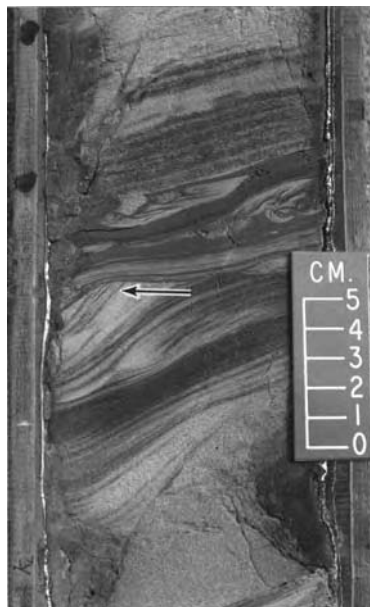
Fig. 4.17. Core photograph showing discrete sand units with current ripples and mud offshoots (arrow). Note sigmoidal configuration of ripples and truncated tops. Middle Pleistocene, Ewing Bank Block 826, Gulf of Mexico. (After Shanmugam et al. (1993a). Reprinted by permission of the American Association of Petroleum Geologists whose permission is required for further use.)

Mud Offshoots

Suspension
(Mud–Offshoot)

Traction

5 cm

Climbing-Ripple Cross-Bedding

Traction and
Suspension

5 cm

Flaser Bedding

Suspension
Traction

5 cm

Lenticular Bedding

Suspension

Traction

5 cm

Horizontal Bedding

Traction

5 cm

Rhythmic Bedding

Sharp Upper Contact

Traction
Suspension

1 cm

Cross-Bedding

Traction

Erosion

5 cm

Sharp Upper Contact

Sharp Upper Contact

Inverse Grading

Gradational
Lower Contact

10 cm

Fine Sand   Mud
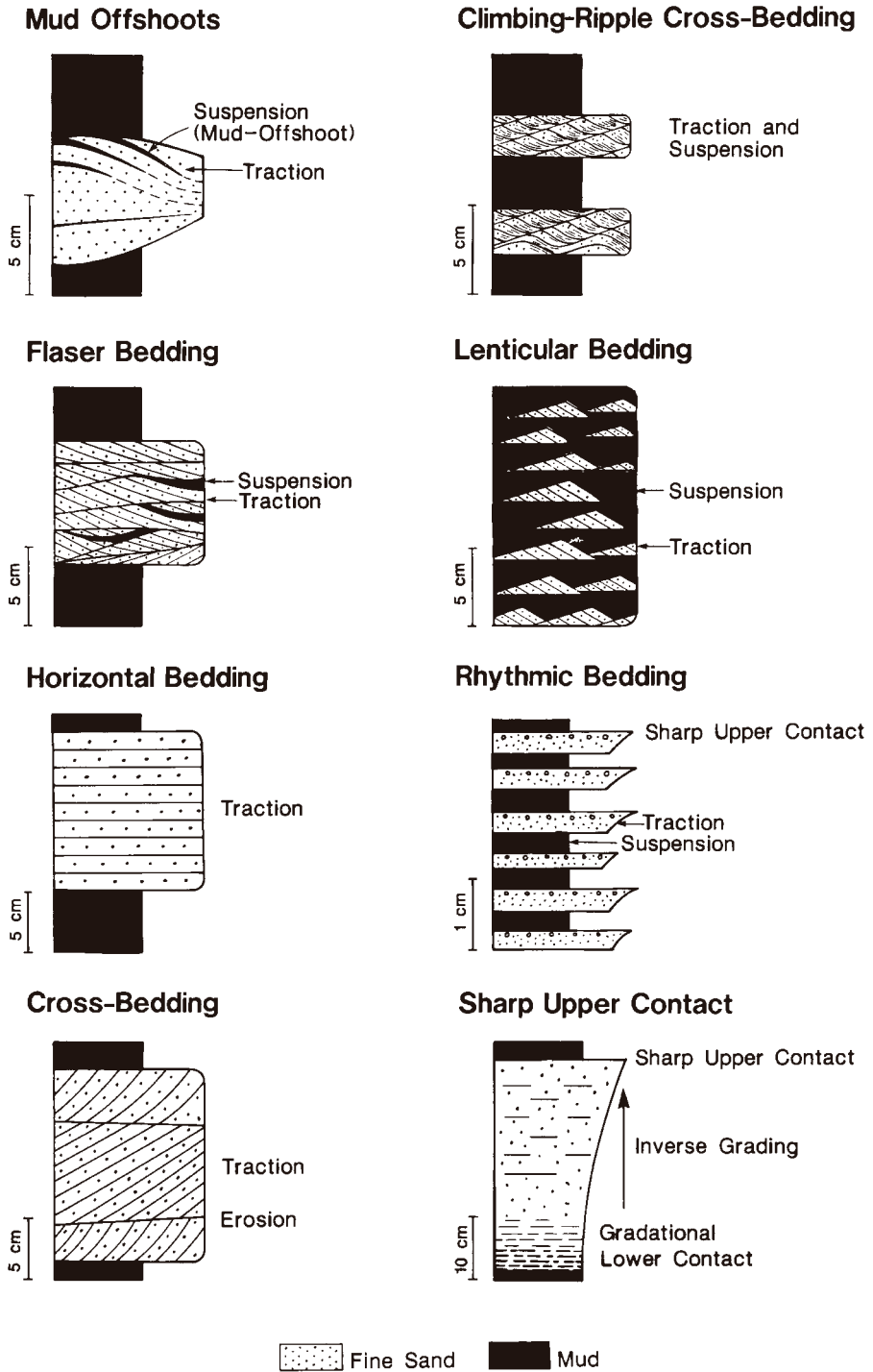
Fig. 4.18.   Summary of features indicative of deep-marine bottom-current reworking. (After Shanmugam et al. (1993b). Reproduced with permission from the Geological Society of America.)
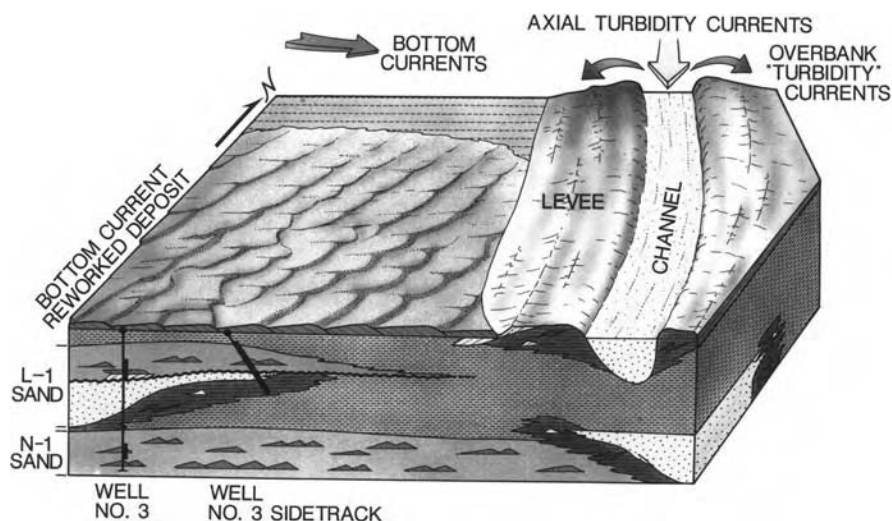
Fig. 4.19. A schematic depositional model for the Pliocene and Pleistocene sands in the Ewing Bank Block 826 area. Note that bottom-current reworked sands in the interchannel area constitute a distinctly different facies from channel-levee facies. Compare the position of No. 3, and No. 3ST wells in the model with their position in the seismic profile (Fig. 4.20). Cored intervals are shown by thick lines. (After Shanmugam et al. (1993a). Reprinted by permission of the American Association of Petroleum Geologists whose permission is required for further use.)
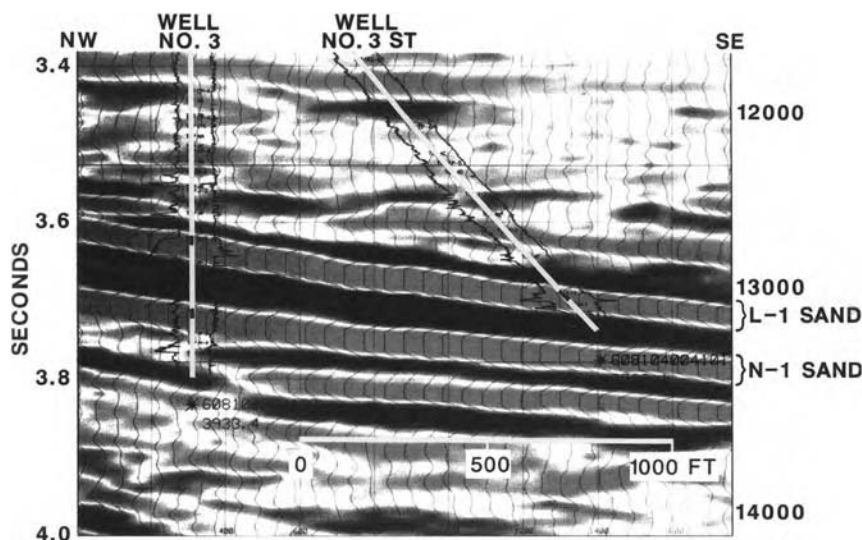
Fig. 4.20. A seismic profile showing position of cored wells through two sand units examined. Note continuous and parallel reflection patterns of the L-1 sand between the two wells. Although continuous and parallel reflection patterns may be interpreted to mean sheet-like sands, core from the L-1 sand shows a lower turbidite channel sand and an upper reworked sand (Fig. 4.19). (After Shanmugam et al. (1993a). Reprinted by permission of the American Association of Petroleum Geologists whose permission is required for further use.)

4.5 Deep-marine tidal bottom currents in submarine canyons

4.5.1 Background

Deep-marine tidal bottom currents in submarine canyons and in their vicinity are one of the best-studied and most extensively documented modern geologic processes (e.g., Shepard et al., 1969, 1979; Shepard, 1976; Beaulieu and Baldwin, 1998; Petruncio et al., 1998; Xu et al., 2002). In spite of this available knowledge, when interpreting deep-marine deposits we fail to make use of this great wealth of data on deep-marine tidal currents. Although the importance of tidal processes and their deposits in coastal and continental shelf (shallow marine) environments is well documented (e.g., Alexander et al., 1998); our understanding of deep-marine tidal deposits is still in its infancy.

Submarine canyons constitute an important and unique setting for focusing tidal energy in both shallow-marine (shelf equivalent) and deep-marine (slope equivalent) environments. This is because the shelf-slope break does not exist within submarine canyons and with increasing water depths canyons serve as a single environmental entity (Fig. 4.21). Therefore, the terms 'shelf' and 'slope'
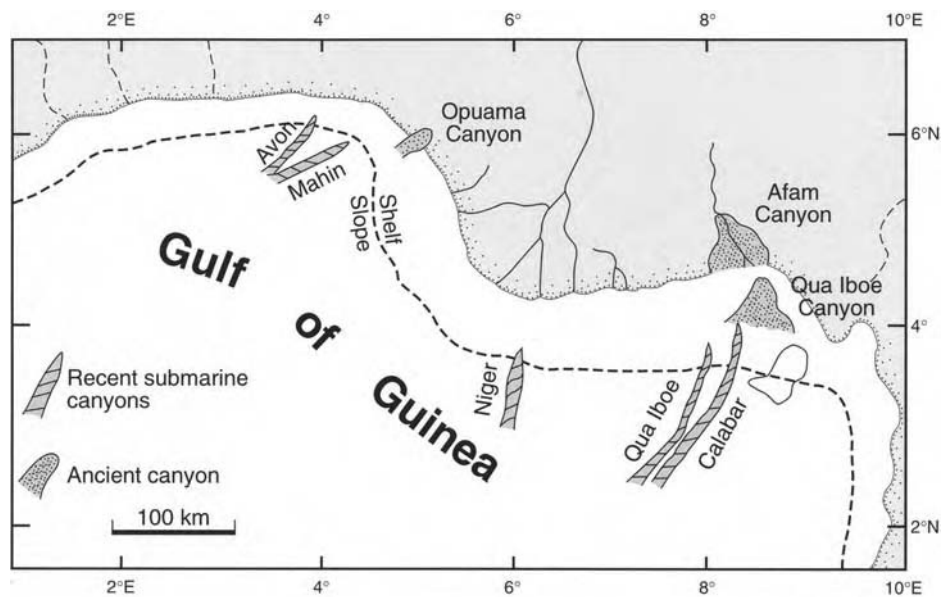
Fig. 4.21. Map showing location of modern and ancient submarine canyons in the Gulf of Guinea, West Africa. Outside submarine canyons, the shelf-slope break (dashed line) is not only an important physiographic boundary between shelf and slope, but also a major controlling factor of processes on the shelf (e.g., tides and waves) and on the slope (e.g., mass transport). However, within submarine canyons (e.g., recent Calabar Canyon), the shelf-slope break does not control processes. Map is modified after Petters (1984). (Reproduced with permission from Blackwell.)

are not meaningful for describing environments within the canyon. Outside of the canyon, however, the shelf-slope break is an important physiographic boundary between the two major submarine provinces, namely the shelf and the slope (Vanney and Stanley, 1983). The shelf-slope break exerts a major control over types of processes on the shelf and on the slope. In shelf settings tidal and wave processes are common, whereas in slope settings mass movements (e.g., slides, slumps, and debris flows) are common. Although continuous pelagic/hemipelagic deposition dominates on the continental slope most of the time, episodic mass flows and their deposits are volumetrically more important in the geologic record of slope deposits.

In areas, where the shelf-slope break is absent (i.e., ramp settings), sediment-transport processes from 'shallow-water' to 'deep-water' environments would be much more transitional and complicated. Inside submarine canyons, irrespective of whether a canyon is in a ramp or in a slope setting, sediment-transport processes would be similar. Shepard et al. (1979) convincingly documented the co-existence of mass flows and tidal currents within modern submarine canyons. Aspects of submarine canyons will be discussed further in Chapter 6.

Although the importance of tidal currents in modern submarine canyons has been known for decades (e.g., Shepard and Dill, 1966; Shepard, 1976), the petroleum industry has largely ignored the significance of tidal facies in deep-water exploration and production. During the past three decades, an understanding of deep-marine tidal bottom currents has been developed by synthesizing a great wealth of published information. This information includes direct observations from deep-diving vehicles, dredging from canyon floors, underwater photographs of canyon floors, photographs and X-radiographs of box cores, seismic profiles, current-velocity measurements (Shepard, 1976; Shepard and Dill, 1966; Shepard et al., 1969, 1979; Dill et al., 1975), and from study of conventional core and outcrop (Shanmugam, 2002a, 2003). Selected examples of studies that dealt with tidal processes and/or their deposits in modern and ancient deep-water environments are:

(1) Laird (1972) considered the presence of climbing ripples, alternation of parallel and cross laminae, and divergence of current directions as evidence for deep-water tidal bottom currents in the Devonian of New Zealand.
(2) Lonsdale and Malfait (1974) suggested that deep tidal bottom currents at a water depth of 2.65 km reworked foraminiferal sand into dune bed forms on the north flank of the Carnegie Ridge in the eastern equatorial Pacific. In discussing the origin of abyssal bedforms, discovered at water depths of 1.5–6 km in the Pacific and Atlantic Oceans, Lonsdale and Spiess (1977, p. 72) stated, '*Tidal currents are ubiquitous in the deep ocean, but their speeds and geological effectiveness are poorly understood.*'

(3)   Klein (1975) studied DSDP Leg 30 cores taken from Mesozoic and Tertiary sequences in the western equatorial Pacific. He suggested that small-scale sedimentary structures, such as current ripples, micro-cross laminae, clay drapes, flaser bedding, lenticular bedding, and parallel laminae, reflected alterna-ting traction and suspension deposition by tidal processes in deep-water environments.

(4)   Shepard et al. (1979) documented systematically that up-canyon and down-canyon currents closely correlated with timing of tides. In the Monterey Canyon, which is the largest submarine canyon on the California coast, the importance of tidal currents has been documented (Xu et al., 2002).

(5)   Skilbeck (1982) interpreted bipolar cross laminae and rhythmic clay drapes in the Carboniferous slope facies in New South Wales, Australia as deposits of deep-water tidal currents.

(6)   Galloway and Hobday (1983) summarized the geologic significance of deep-ocean tidal currents.

(7)   Hollister and Nowell (1991, p. 449) recognized the complexity of processes involved in generating benthic storm events in the High Energy Benthic Boundary Layer Experiment (HEBBLE). They stated, '*The magnitude of high-frequency fluctuations and vertical gradients also contained semi-diurnal periodicity*.' Woodgate and Fahrbach (1999) attributed benthic storms, with bottom-current velocity of 43 cm/s at a depth of 3340 m, in the Greenland Sea to semi-diurnal tide. Beaulieu and Baldwin (1998) recognized the importance of tidal currents in the benthic boundary layer at an abyssal station off central California. Thomsen et al. (2002) documented tidally modulated processes in the benthic boundary layer at the Iberian continental margin.

(8)   Mutti (1992, his Plate 1B) interpreted thin beds of rippled sandstone in submarine channel-fill sequences of the Permian Brushy Canyon Formation, Delaware Basin, West Texas, as bottom-current deposits. He noted that these beds are very similar to subtidal sandstone facies. In explaining the origin of traction structures by bottom currents in the Permian Brushy Canyon Formation, Texas, Harms (1974) clearly pointed out that these currents were not turbidity currents.

(9)   Tsuji (1993, his Fig. 7) reported maximum current velocity of 51 cm/s at a depth of 340 m on the slope in the Ryukyu Trench in Japan and showed a close relationship between current speeds and tidal oscillations.

(10) Taira and Teramoto (1985) reported deep-sea tidal currents as high as 40 cm/s in velocity at water depths of more than 2000 m in the Sagami and Suruga Troughs, Japan.

(11) Viana et al. (1998) reported the importance of semi-diurnal tides in the vicinity of the São Tomò canyon head in offshore Brazil.

(12) Cowan et al. (1998) documented tidal rhythmites of couplets from modern deep-water estuarine environments at 240 m water depth in Muir Inlet (Alaska), which is a macrotidal setting with a mean tidal range of 4.2 m. This documentation was the first to show neap-spring tidal cyclicity and sediment couplets in cores taken from modern deep-water estuarine environments.

(13) Egbert and Ray (2000) demonstrated that tidal dissipation occurs in the open ocean at abyssal depths by using satellite altimeter data from Topex/Poseidon.

(14) Shanmugam (2003) documented ancient examples of deep-marine tidal facies in Nigeria and France.

4.5.2 Tidal processes and their deposits

To understand deep-water tidal currents, first we need to review shallow-water tidal processes and their deposits. Basic principles of tides have been discussed in textbooks (e.g., Strahler and Strahler, 1974; Friedman and Sanders, 1978). Most coasts and continental shelves are subjected to semi-diurnal tides (i.e., rise and fall in sea level twice daily). Tidal currents are effective in transporting and depositing sand in estuaries. Here velocities commonly reach 150 cm/s (Reading and Collinson, 1996). Sedimentary features indicative of tidal processes in shallow-water environments (e.g., Reineck and Wunderlich, 1968; Klein, 1970; Visser, 1980; Terwindt, 1981; Allen, 1982; Banerjee, 1989; Nio and Yang, 1991; Dalrymple, 1992; Archer, 1998; Shanmugam et al., 2000) are:

- Heterolithic facies
- Double mud layers
- Thick (spring)-thin (neap) bundles
- Alternation of parallel and cross laminae
- Climbing ripples
- Rhythmic alternation of sandstone-shale couplets (tidal rhythmites)
- Cross-beds with mud-draped foresets
- Bidirectional (herringbone) cross bedding
- Sigmoidal cross bedding (i.e., full-vortex structures) with mud drapes and tangential basal contacts
- Reactivation surfaces
- Crinkled laminae
- Elongate mudstone clasts
- Flaser bedding
- Wavy bedding
- Lenticular bedding.

Most of these traction structures that develop in shallow-water estuaries also develop in deep-water canyons and channels with tidal currents.

4.5.3 Velocity of tidal currents in submarine canyons

Tidal currents are significant processes in many modern submarine canyons (Shepard et al., 1979). The interaction of the canyon topography with the tidal current is particularly important. In the modern Zaire (formerly the Congo) Canyon in West Africa (Fig. 4.22), the canyon head can be traced 25 km up the estuary on land (Heezen et al., 1964; Shepard and Emery, 1973; Droz et al., 1996). The deep Zaire Canyon is simply a deep-water extension of the Zaire estuary. The width and the relief of the canyon increase seaward from the estuary reaching a maximum width of 15 km and a maximum depth of 1300 m near the shelf break (Babonneau et al., 2002). The mean tidal range in the Zaire Canyon is 1.3 m (Shepard et al., 1979).

Even in submarine canyons that do not have up-dip estuaries the link between tides and canyon currents has been well established. Shepard et al. (1979) measured

Scale: 1° Latitude = 60 Nautical Miles (III km)
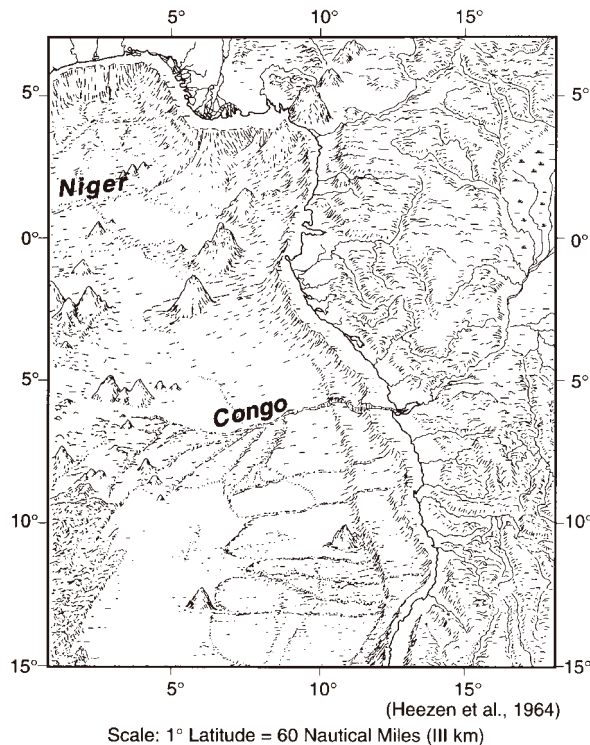
Fig. 4.22. Physiographic diagram showing the modern Zaire (formerly the Congo) and Niger submarine canyons, West Africa. The Zaire Canyon head can be traced for 25 km up the estuary on land. Diagram is simplified after Heezen et al. (1964). (Reprinted by permission of the American Association of Petroleum Geologists whose permission is required for further use.)
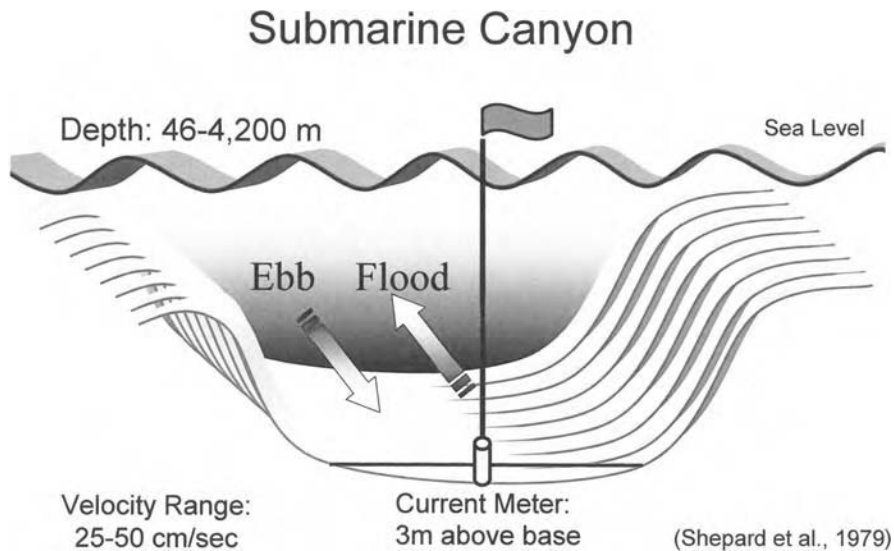
Submarine Canyon

Fig. 4.23. A conceptual diagram showing cross section of a submarine canyon with ebb and flood tidal currents (opposing arrows). Shepard et al. (1979) measured current velocities in 25 submarine canyons at water depths ranging from 46–4200 m by suspending current meters commonly 3 m above the sea bottom. Measured maximum velocities commonly range from 25–50 cm/s. (After Shanmugam (2003). Reproduced with permission from Elsevier.)

current velocities in 25 submarine canyons at water depths ranging from 46–4200 m by suspending current meters usually 3 m above the sea bottom (Fig. 4.23). These canyons include the Hydrographer, Hudson, Wilmington, Washington, Norfolk, Rio de la Plata, Christiansted, and Zaire in the Atlantic Ocean; and the Fraser, Monterey, Carmel, Hueneme, Santa Cruz, Santa Monica, Redondo, Newport, La Jolla/Scripps, San Lucas, Rio Balsas, and Hawaii canyons in the Pacific Ocean. Maximum velocities of up- and down-canyon currents commonly ranged from 25–50 cm/s (Table 4.2). Keller and Shepard (1978) reported velocities as high as 70–75 cm/s, velocities sufficient to transport even coarse-grained sand, from the Hydographer Canyon.

The following lines of evidence and reasoning suggest that bottom currents in submarine canyons are genetically related to tides:

(1) Because turbidity currents and other sediment-gravity flows almost always travel downslope, the up-canyon semidiurnal currents observed by Shepard et al. (1979) cannot be turbidity currents or other sediment-gravity flows. Although internal waves may travel upslope, they do not occur semidiurnally.

(2) Time-velocity plot of data obtained at a water depth of 448 m in the Hueneme Canyon, California shows an excellent correlation between the timing of up- and down-canyon currents and the timing of tides (Fig. 4.24).

Table 4.2 Selected examples of maximum velocities of up- and down-canyon currents measured at varying water depths by suspending current meters 3 m above sea bottom (Compiled from Shepard et al., 1979)

Water depth (m)	Submarine canyon and location	Mean tidal range (m)	Up-canyon current velocity (cm/s)	Down-canyon current velocity (cm/s)
348	Hydrographer, Atlantic,U.S.	1.6	39	52
375	La Jolla, Pacific, U.S.	2.5	19	18
400	Zaire (Congo), West Africa	1.3	22	13
448	Hueneme, Pacific, U.S.	2.4	32	32
458	Santa Monica, Pacific, U.S.	2.7	27	30
914	Wilmington, Atlantic, U.S.	1.8	20	21
1445	Monterey, Pacific, U.S.	2.0	30	30
1737	Kaulakahi, Pacific Islands	0.9	26	24
1904	Rio Balsas, Mexico	0.7	21	21
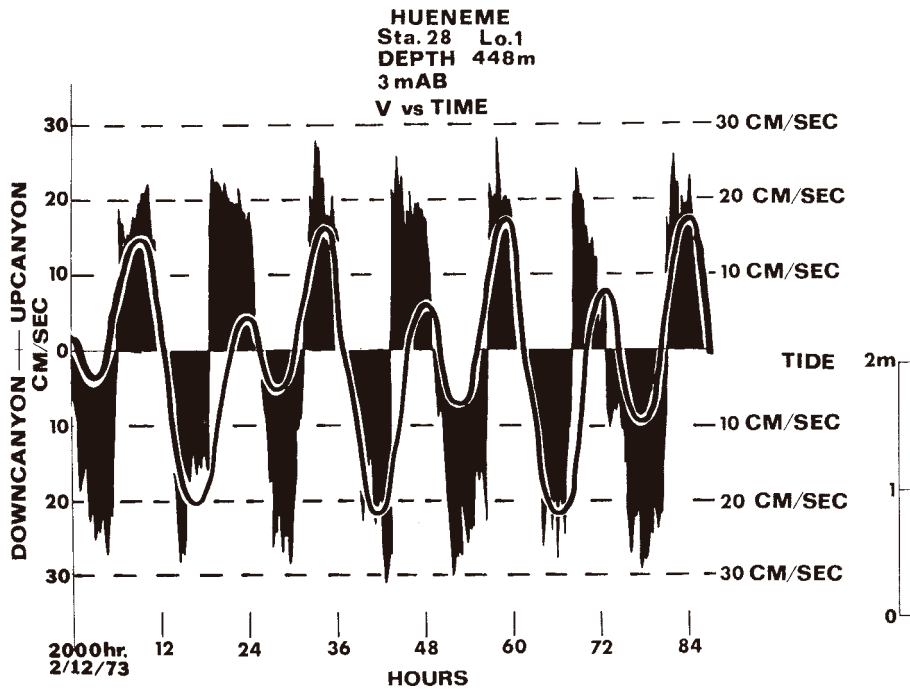
Fig. 4.24. Time-velocity plot from data obtained at 448 m in the Hueneme Canyon, California, showing excellent correlation between the timing of up- and down-canyon currents and the timing of tides obtained from tide tables (solid curve). 3 mAB = Velocity measurements were made 3 m above sea bottom. (Modified after Shepard et al. (1979). Reprinted by permission of the American Association of Petroleum Geologists whose permission is required for further use.)
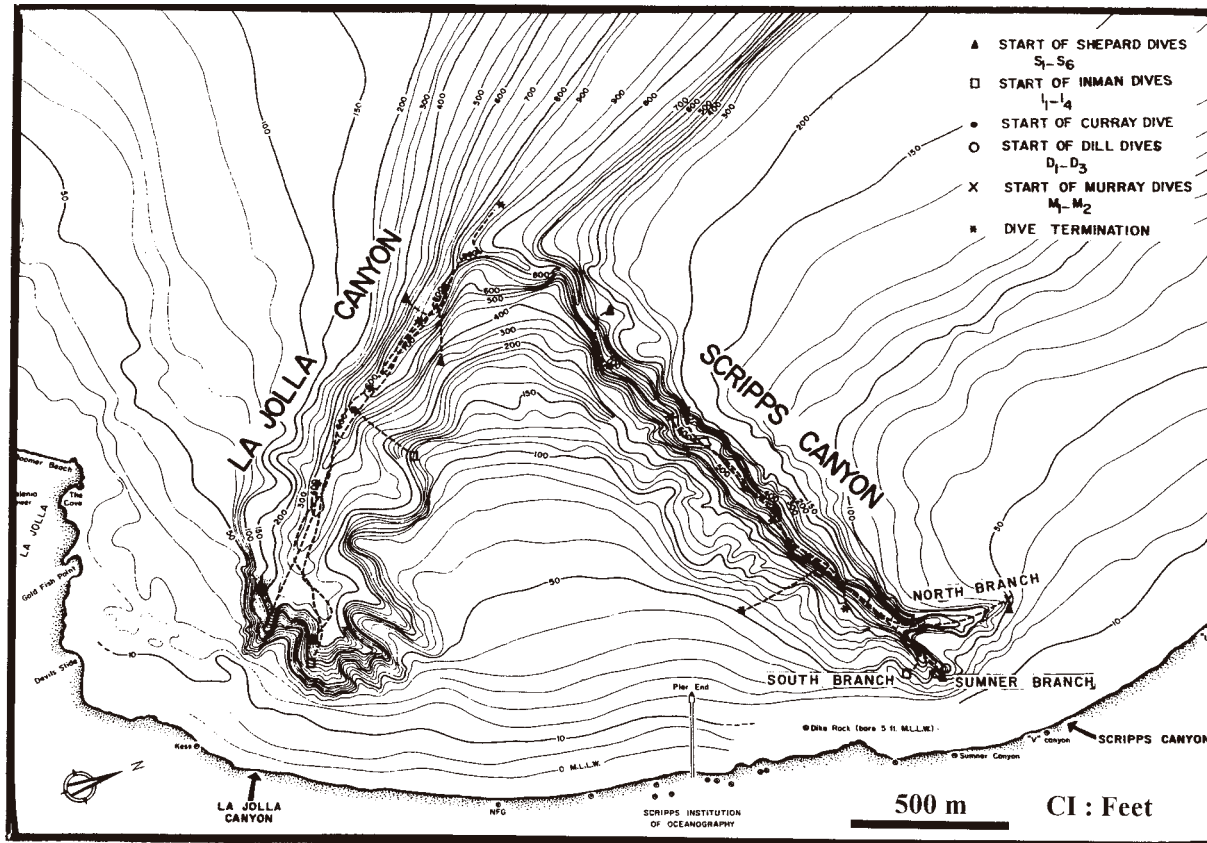
(Modified after Shepard et al., 1979)

Fig. 4.25. Map showing location of La Jolla and Scripps canyons, offshore California. (Modified after Shepard et al. (1979). Reprinted by permission of the American Association of Petroleum Geologists whose permission is required for further use.)

(3) Shepard and Emery (1973, their Fig. 10) documented, along floor of the Zaire Canyon at 400 m depth, up-canyon currents during rising tides and down-canyon currents during ebbing tides. Similar relationships exist in many other submarine canyons worldwide (Shepard et al., 1979).

In addition, canyon deposits contain signatures of tidal influence. Box core 1 taken from the La Jolla submarine canyon (Fig. 4.25) at a depth of 1039 m shows a basal massive division and an upper parallel and ripple-laminated division (Fig. 4.26A). Shepard et al. (1969, their Fig. 19A) originally described these divisions as Bouma Ta, Tb, and Tc divisions and interpreted them as turbidites. This is based on the notion that the experimental traction structures of Simons et al. (1965) are analogous to the natural structures of turbidites in the Bouma Sequence. However, there is a major disconnect between experimental structures and turbidite structures (see Chapters 7 and 8). The parallel laminated division in the La Jolla Canyon core has been redescribed as double mud layers because of their distinct mud couplets (Fig. 4.26A), and reinterpreted as deposits of tidal currents (Shanmugam, 2003). Visser (1980) first explained the origin of double mud layers by alternating ebb and flood tidal currents with extreme time-velocity asymmetry in shallow-water subtidal settings. The thick sand units reflect deposition during dominant tides, whereas the thin sand units are probably products of subordinate tides. Because tidal currents operate semidiurnally in the modern La Jolla Canyon (Shepard et al., 1969), it is meaningful to interpret the double mud layers observed in the box core 1 from the La Jolla Canyon as deposits of tidal currents (Fig. 4.26A). Shepard et al. (1969) did not consider a tidal origin for the La Jolla Canyon core perhaps because they published their paper prior to the publication of Visser (1980) who first linked double mud layers to tidal processes.

In the La Jolla Canyon core, one could argue that if each mud couplet represents deposition during a single tidal cycle, the few cycles preserved in the box core must represent only a short time interval. If so, what happened during all other tidal cycles? The answer lies in the depositional settings and related processes. In tidally influenced coastal and shelf settings, for example, tidal processes deposit sediment all the time without major interruptions. Therefore, depositional facies in coastal settings would represent a continuous record of tidal deposition. In contrast, mass movements (i.e., slides, slumps, avalanches, grain flows, and debris flows) in canyon settings are likely to interrupt tidal deposition.

4.5.4 Facies association in submarine canyons

Submarine canyons are not only unique for providing a protected environment for focusing tidal energy from shallow-marine estuaries to deep-marine canyons, but also prone for generating mass movements (e.g., slides, slumps, grain flows, and debris flows) due to failure of steep canyon walls. This facies association is evident in both modern and interpreted ancient examples (Table 4.3).
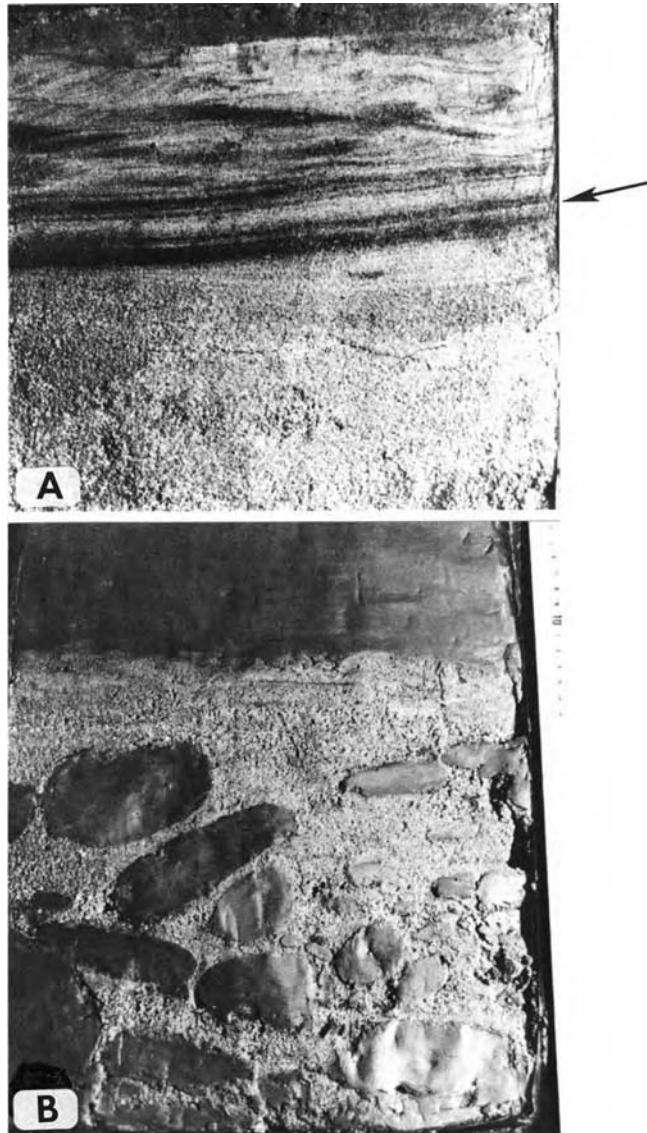
Fig. 4.26. (*A*) **Photograph of box core 1 taken from the La Jolla Canyon, offshore California, at a depth of 1039 m showing a basal massive division and upper parallel and ripple-laminated divisions. Shepard et al. (1969, their Fig. 19A) originally described these divisions as Ta, Tb and Tc divisions of the Bouma Sequence and interpreted them as turbidites. In this book, however, the parallel-laminated division is considered as double mud layers because of their distinct mud couplets (arrow). Double mud layers are interpreted here as deposits of tidal currents. (*B*) Photograph of box core 72 taken from the La Jolla Canyon at a depth of 1085 m showing floating mudstone clasts in sand. In this book, floating mudstone clasts in sand are interpreted as deposits of sandy debris flows. (From Shepard et al. (1969, their Fig. 21B). Reprinted by permission of the American Association of Petroleum Geologists whose permission is required for further use.)**

Table 4.3 Summary of examples showing a close association of tidal currents and mass flows and their deposits in modern and ancient submarine canyons. This table is based on published information on direct observations from deep-diving vehicles, underwater photographs of canyon floors, photographs and X-radiographs of box cores, current-meter data, seismic profiles, and study of conventional core and outcrop data. Note that two of the published cores (La Jolla) and outcrops (Annot) have been reinterpreted in this study. After Shanmugam (2003)

Modern and ancient submarine canyons	Tidal currents and their deposits	Mass movements* and their deposits
Modern La Jolla, Pacific, U.S.	Current reversal (Shepard et al., 1979; their Table 1) and double mud layers (Shepard et al., 1969, their Fig. 19A; This study)	Slide and debris flow (Shepard et al., 1969, their Figs. 9, 10 & 21B)
Modern Scripps, Pacific, U.S.	Current reversal (Shepard et al., 1979, their Table 1)	Slumps (Marshall, 1978)
Modern Monterey, Pacific, U.S.	Current reversal (Shepard et al., 1979, their Table 1)	Mass movements (Martin and Emery, 1967, p. 2281)
Modern Rio Balsas, Pacific, Mexico	Current reversal (Shepard et al., 1979, their Table 1)	Slumps (Dill et al. 1975)
Modern San Lucas, Pacific, Baja Mexico	Current reversal (Shepard et al., 1979, their Table 1)	Grain flow and sandy debris flow (Shepard and Dill, 1966, their Figs. 55 &139)
Modern Hudson, Atlantic, U.S.	Current reversal (Shepard et al., 1979, their Table 2)	Muddy debris flow (Shepard and Dill, 1966, their Fig. 74)
Modern Zaire (Congo), Atlantic, West Africa	Current reversal (Shepard et al., 1979, their Table 1)	Slumping (Shepard and Emery, 1973, their Fig. 7)
Modern Mera, Honshu, Japan	Tidal currents and sigmoid ripples (Shepard and Dill, 1966; see also Tsuji, 1993 for tidal currents with 51 cm/s velocity in the Ryukyu Trench to the south)	Breccia recovered from Dill, dredging (Shepard and 1966), which could be interpreted as deposits of mass flows
Pliocene Qua Iboe, Atlantic, West Africa	Double mud layers (This study)	Slumping and debris flow (This study)
Eocene-Oligocene Annot Sandstone, SE France (Outcrop study)	Double mud layers and sigmoid cross bedding (This study)	Slumping and debris flow (Stanley et al., 1978; their Fig. 8–3, This study)
Eocene Torrey, California (Outcrop study)	Rippled and cross-bedded facies (May et al., 1983)	Slides, sandy debris flows, grain flows (May et al., 1983).

*Mass movements include slides, slumps, grain flows, and debris flows, but not turbidity currents (see Dott, 1963).

4.5.5 Modern La Jolla Canyon, California

In the modern La Jolla Canyon in California, velocity measurements of tidal currents as well as photographic documentation of active slides and debris flows with angular blocks and cobbles on the canyon floor exist (see Shepard et al., 1969, their Figs. 6 and 9). As discussed earlier, box cores taken from the La Jolla canyon show evidence of deposition by both tidal currents (Fig. 4.26A) and sandy debris flows (Fig. 4.26B).

4.5.6 Torrey Canyon, Eocene, California

In strata of the Eocene Torrey Submarine Canyon exposed near San Diego, California, May et al. (1983) recognized a variety of mass-flow facies in association with tidal facies (Table 4.3). May et al. (1983, p. 324 and 325) attributed the coarse-grained facies in the basal Torrey Canyon unit to deposition from sandy debris flows, with a transition to turbidity currents or grain flows. Large blocks (10 m across) of mudstone that rest on the basal erosional surface represent mass flows, such as rock falls and slides. In addition, May et al. interpreted rippled and cross-bedded units as tidal facies.

4.5.7 Edop Field, Pliocene, offshore Nigeria

In the Niger Delta area of West Africa, five modern submarine canyons (Avon Mahin, Niger, Qua Iboe, and Calabar) have been recognized (Fig. 4.21). In the Calabar River, the tidal range is 2.8 m and tidal flows with reversible currents are common (Allen, 1965). In the Calabar estuary, maximum ebb current velocities range from 60–280 cm/s, and flood current velocities range from 30–150 cm/s. These velocities are strong enough to transport particles of sand and gravel grade. The Calabar estuary has a deep-water counterpart that cuts through sediments of the outer shelf and slope, forming the modern Calabar submarine canyon (Fig. 4.21). Thus as they do in the Zaire Canyon to the south (Fig. 4.22), tidal currents are likely to operate in the Calabar and Qua Iboe canyons.

The Edop Field (Fig. 4.27) is located in the ancient Qua Iboe Canyon (see Fig. 4.21). The Pliocene Intra Qua Iboe (IQI) reservoir in the Edop Field is a major hydrocarbon-producing siliciclastic reservoir (Fig. 4.28). Based on recognition of a 3–km wide erosional feature observed on a seismic time slice (Fig. 4.29), a submarine canyon or 'fairway' for the Edop reservoir has been documented (Shanmugam, 1997c, his Fig. 21).

A total of 3000 ft (875 m) of conventional core from six Mobil wells (Mobil 9A Sidetrack, 14D, 19B, 21D, 25C, and 31) from the Edop Field was described (Shanmugam et al., 1995b; and Shanmugam, 1997c). Sedimentological description of cores from 9A sidetrack, 25C, and 21D wells has resulted in seven interpreted depositional facies: (1) sandy slump/debris flow; (2) muddy slump/debris flow; (3) bottom-current reworking; (4) muddy turbidity currents; (5) pelagic/hemipelagic settling; (6) wave influence; and (7) tidal influence.

The bulk of the cored interval is interpreted to be deposits of sandy and muddy slumps and debris flows. The single most diagnostic property of these facies is their heterolithic composition with chaotic geometry and contorted bedding. Slump folds (Fig. 4.30), contorted bedding (Fig. 4.31), floating mudstone clasts (Fig. 4.32), glide planes (Fig. 4.33), planar clast fabric, and floating quartz granules are common and indicate deposition from slumps and debris flows.
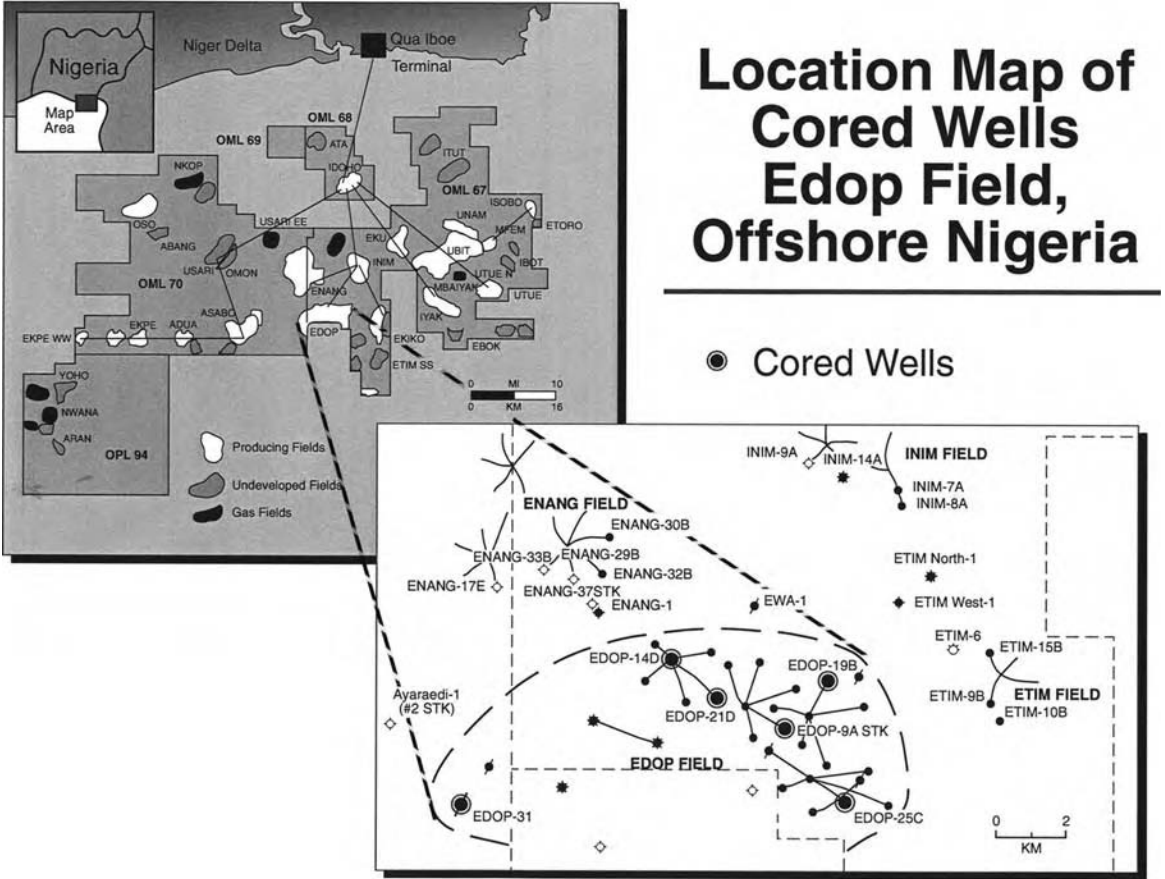
Fig. 4.27. Location map showing cored wells in the Edop Field, offshore Nigeria. (Modified after Shanmugam (1997c).)
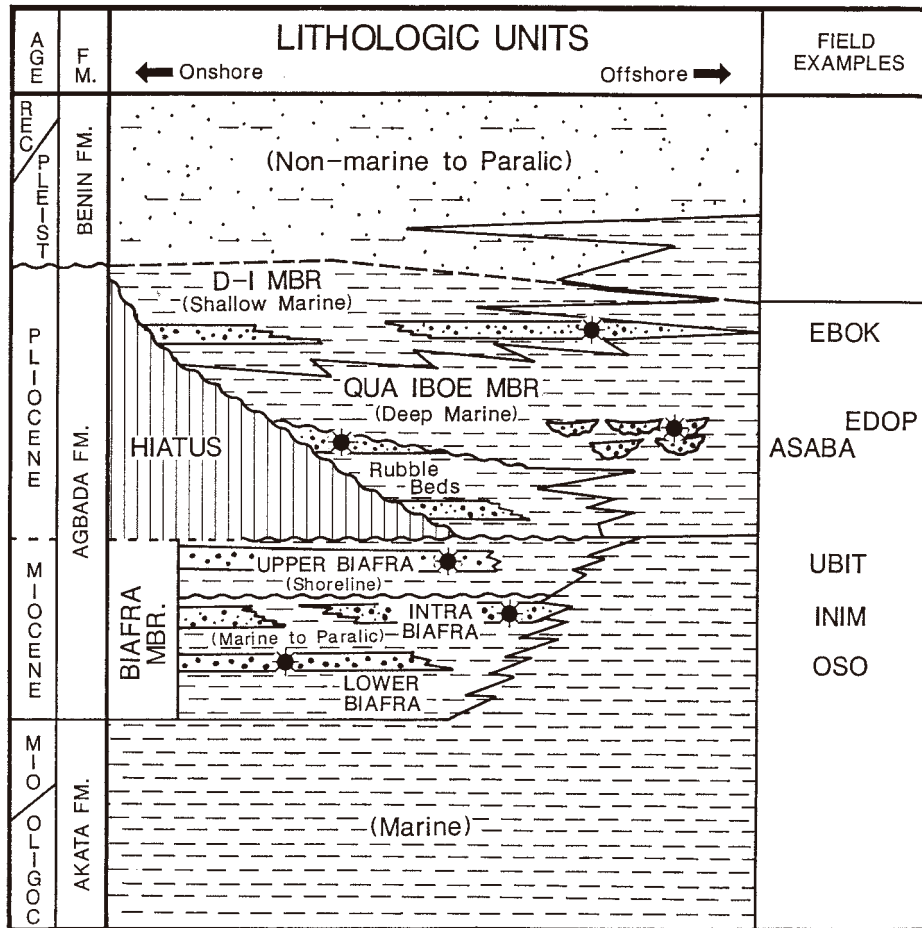
Fig. 4.28. Generalized stratigraphic column for the Edop Field area, offshore Nigeria. Intra Qua Iboe (IQI) Member is the principal reservoir in the Edop Field.

Some cored intervals are composed of fine to very fine sand with well-developed double mud layers (Fig. 4.34), mud-draped ripples (Fig. 4.35), and tidal rhythmites with thick and thin sand layers. These features have been interpreted as products of tidal currents.

Diurnal inequality and tidal cyclicity are considered to be diagnostic properties of clastic tidal deposits (de Boer et al., 1989; Kuecher et al., 1990; Nio and Yang, 1991). Most areas of the Earth experience semidiurnal (i.e., two tides per day) periodicity (de Boer et al., 1989). One key element of the tidal system is that alternating 'high' and 'low' peak current velocities are represented by alternating 'thick' and
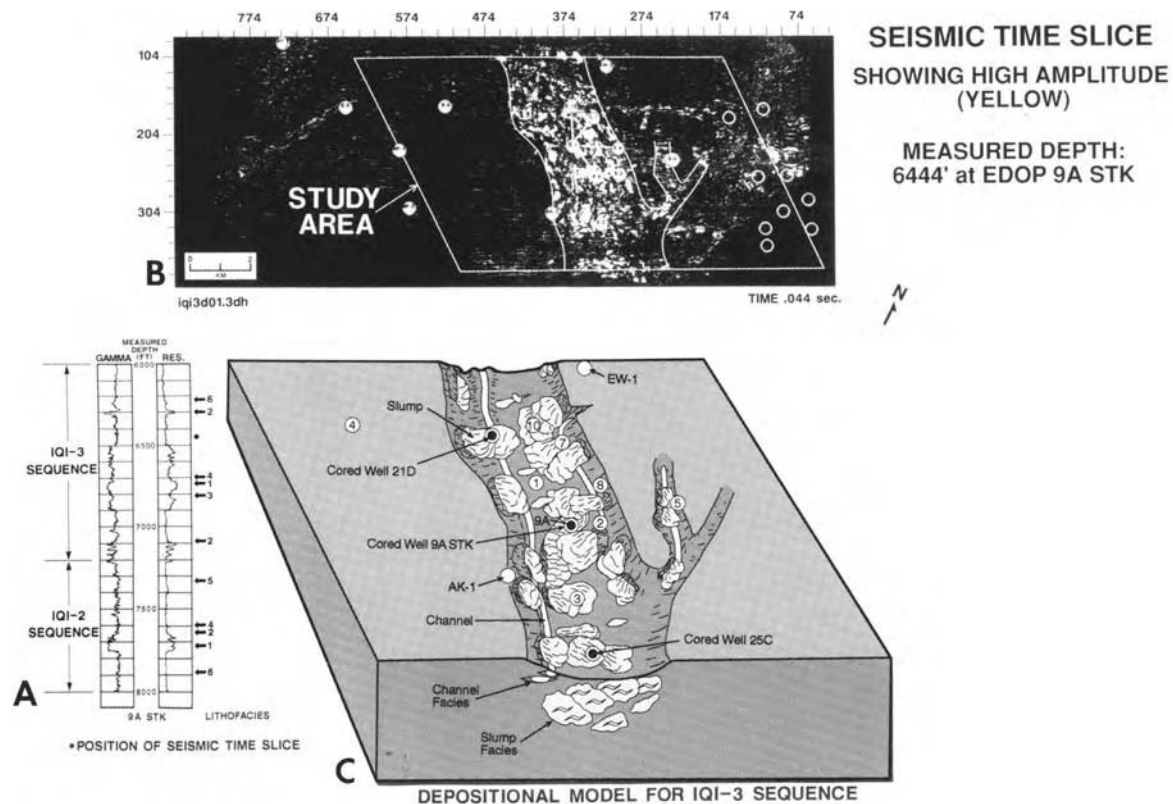
Fig. 4.29. Depositional model for the IQI-3 sequence in the Edop Field, offshore Nigeria, based on integration of wireline log, seismic time slice, and conventional core data. (*A*) Wireline logs of IQI-3 Sequence in the upper part of the cored interval (6000–7200 ft) (1829–2195 m) in the Mobil 9A Sidetrack well. Positions of lithofacies are shown by arrows. Facies 3 represents slumps. (*B*) Seismic time slice from the IQI-3 sequence. (*C*) Depositional model showing a submarine 'fairway' (i.e., canyon) filled with slump facies. High frequency events of sandy slumps and debris flows tend to fill the 'fairway' (i.e., canyon), causing thick amalgamated reservoir with good communication between sand beds. (Modified after Shanmugam (1997c).)
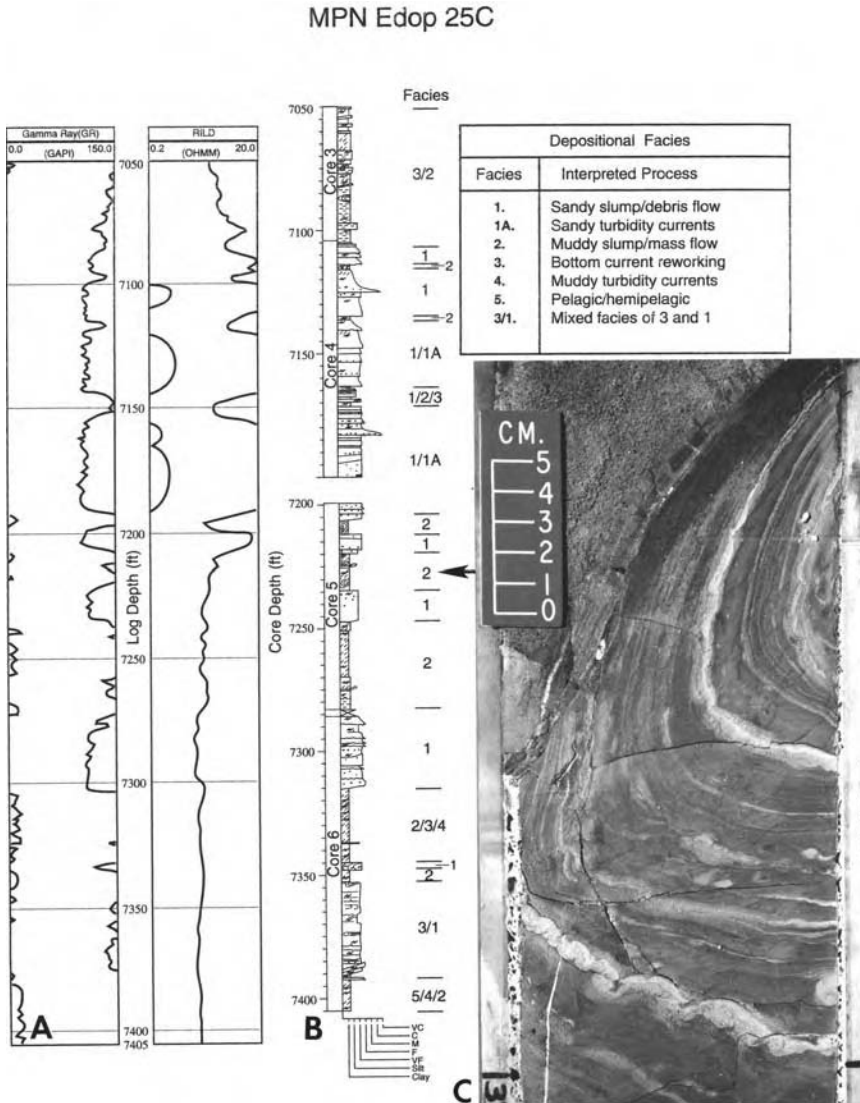
Fig. 4.30. (*A*) **Blocky wireline log motifs, IQI-3, Mobil 25C well, Edop Field, offshore Nigeria.**
(*B*) **Depth-tied sedimentological log. (*C*) Facies 2: Core photograph showing an asymmetrical**
slump fold in mudstone. 7232′ (2204 m) core depth. Arrow shows stratigraphic position of core
photograph. MPN = Mobil Producing Nigeria. (After Shanmugam (1997c).)

'thin' sand layers or bundles, respectively. This alternation of thick and thin sand
bundles reflects alternating ebb and flood episodes known as diurnal inequality
(de Boer et al., 1989). Thick-thin alternations of sand bundles, which are unique to
the tidal regime (de Boer et al., 1989), are evident in the Edop reservoir.
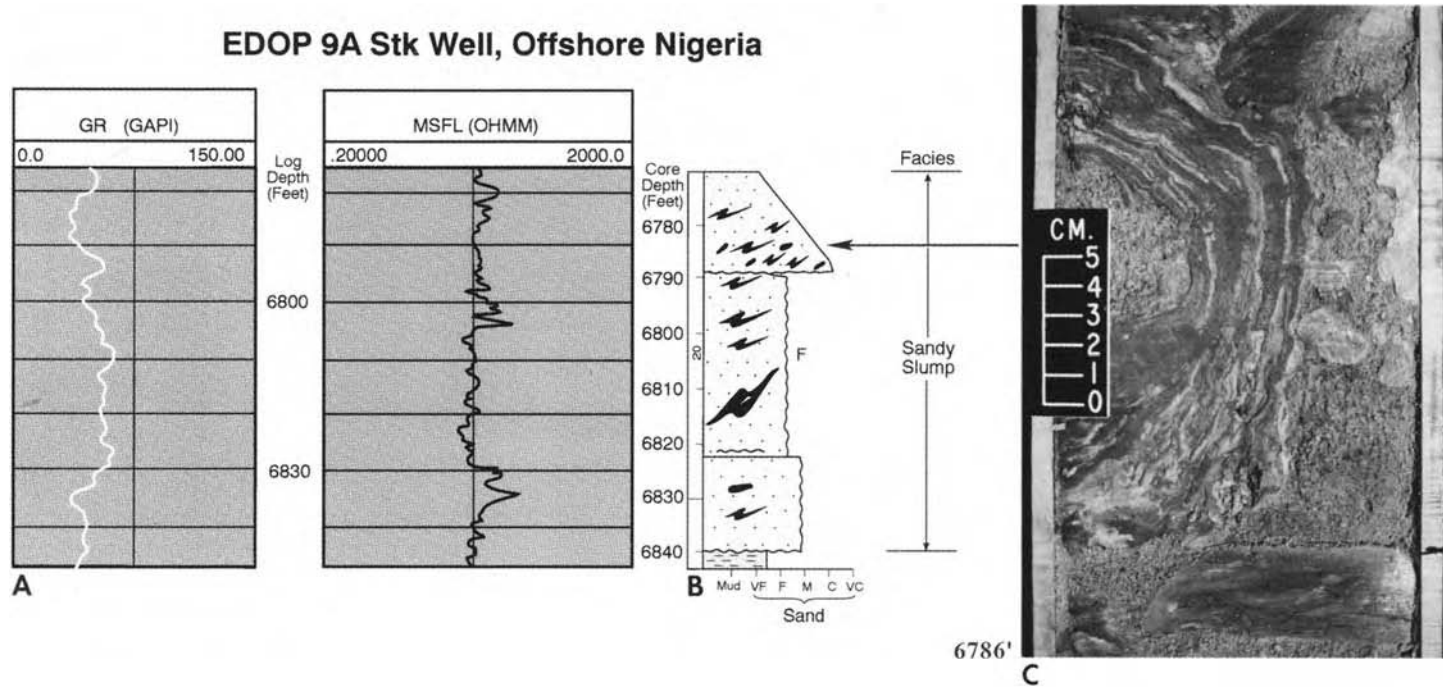
Fig. 4.31. (*A*) Serrated wireline log motif, IQI-3, Mobil 9A Sidetrack well, Edop Field, offshore Nigeria. (*B*) Depth-tied sedimentological log. (*C*) Sandy slump facies: Core photograph showing contorted sand with deformed mudstone layers. 6786′ (2069 m) core depth. Arrow shows stratigraphic position of core photograph. (After Shanmugam (1997c).)
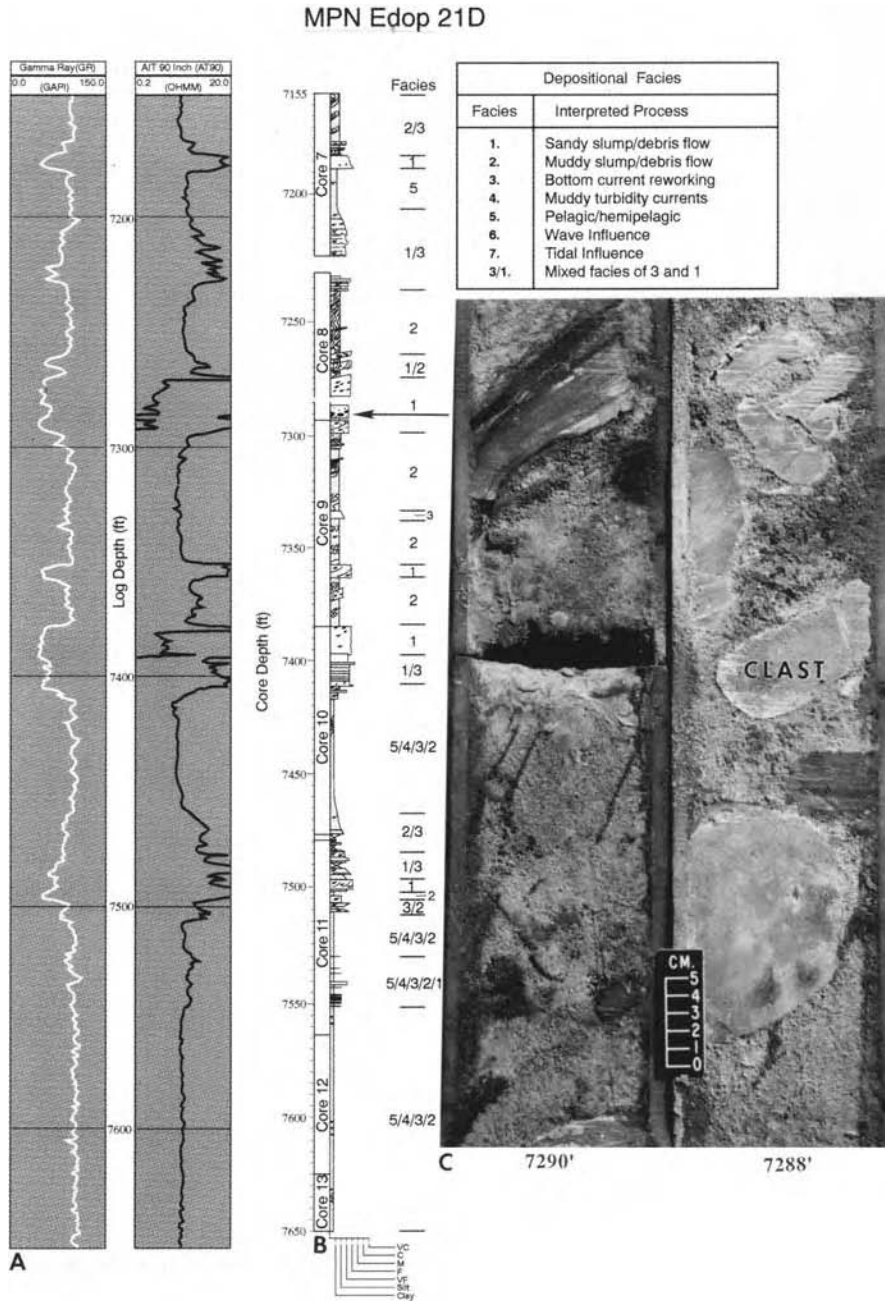
Fig. 4.32. (*A*) Coarsening-up, fining-up, and blocky wireline log motifs, IQI-3, Mobil 21D well, Edop Field, offshore Nigeria. (*B*) Depth-tied sedimentological log. (*C*) Facies 1: Core photograph showing floating mudstone clasts in fine-grained sand. 7286′–7290′ (2221–2222 m) core depth. Arrow shows stratigraphic position of core photograph. MPN = Mobil Producing Nigeria. (After Shanmugam (1997c).)

MPN Edop 25C
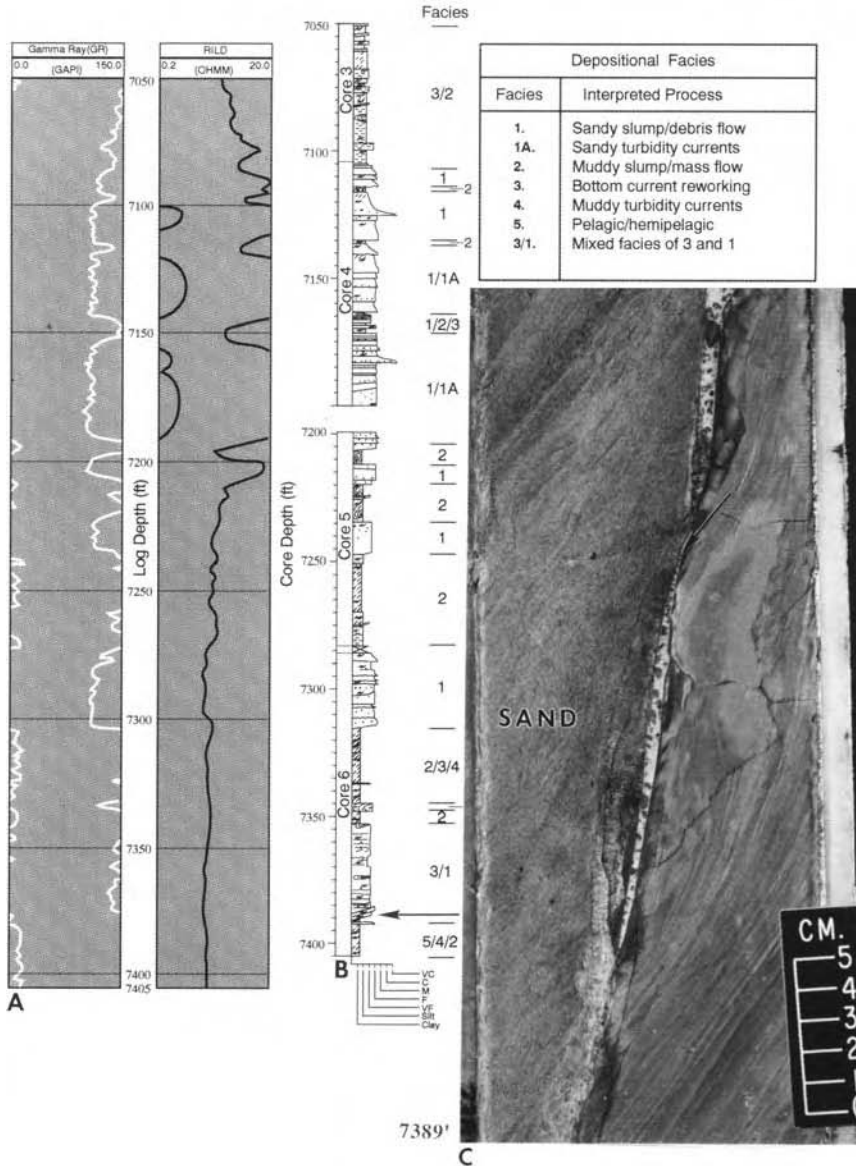
Fig. 4.33. (*A*) **Blocky wireline log motifs, IQI-3, Mobil 25C well, Edop Field, offshore Nigeria.** (*B*) **Depth-tied sedimentological log.** (*C*) **Facies 1: Core photograph showing sheared contact between overlying sand (left) and underlying mudstone. The steeply dipping (80°) contacts represent primary glide plane (arrow) of a major slump/slide sheet. Note the effects of shearing in the form of drag lamination in the underlying mudstone. 7389′ (2253 m) core depth. Arrow shows stratigraphic position of core photograph. MPN = Mobil Producing Nigeria. (After Shanmugam (1997c).)**
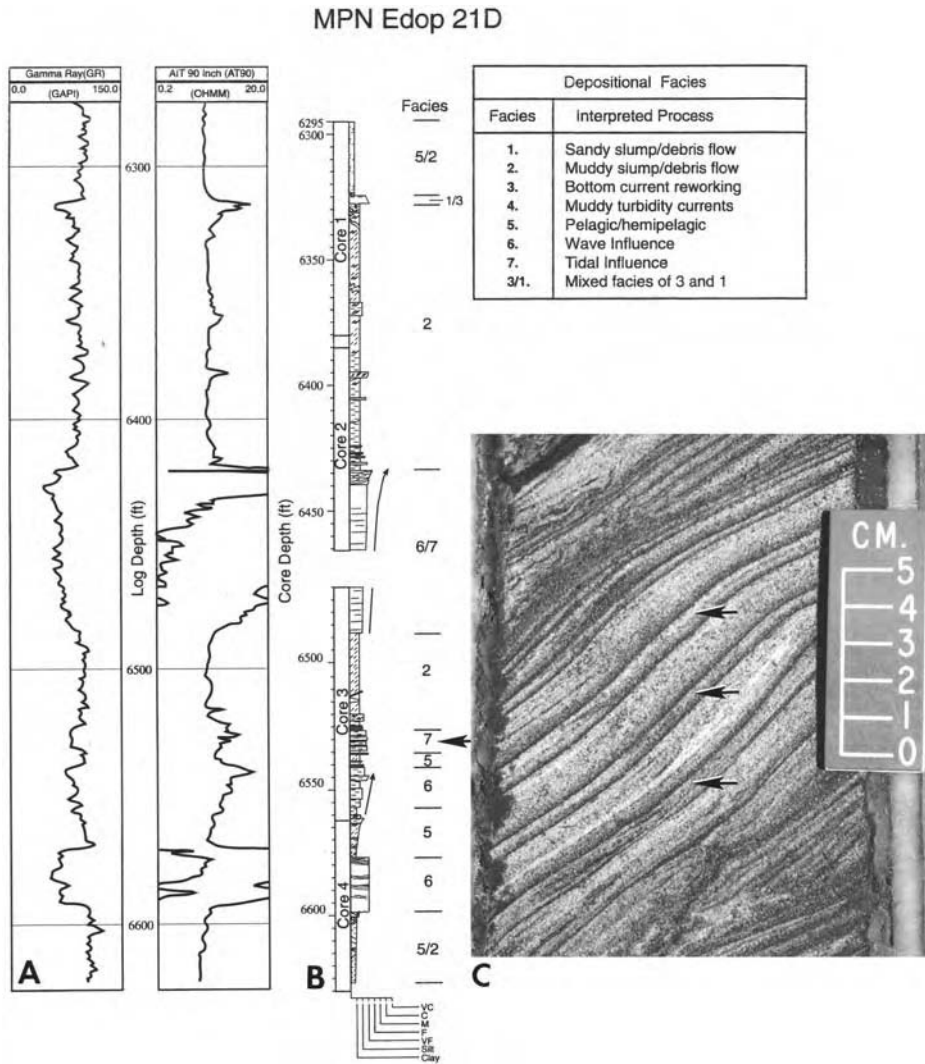
Fig. 4.34. (*A*) Wireline log motifs, Mobil 21D well, Edop Field, offshore Nigeria. (*B*) Depth-tied sedimentological log showing interpreted facies. (*C*) Facies 7: Core photograph showing double mud layers (three arrows). Arrow shows stratigraphic position of core photograph. Note close association of Facies 7 (tidal) and Facies 2 (muddy slumps/debris flows). (After Shanmugam (2003). Reproduced with permission from Elsevier.)

In addition to diurnal inequality, clastic tidal deposits also exhibit cyclicity (de Boer et al., 1989). Tidal units tend to thicken progressively to a maximum (spring tide), then thin to a minimum (neap tide), and then thicken to the next maximum (spring tide), resulting in a complete cycle every 14 days. Ideally,
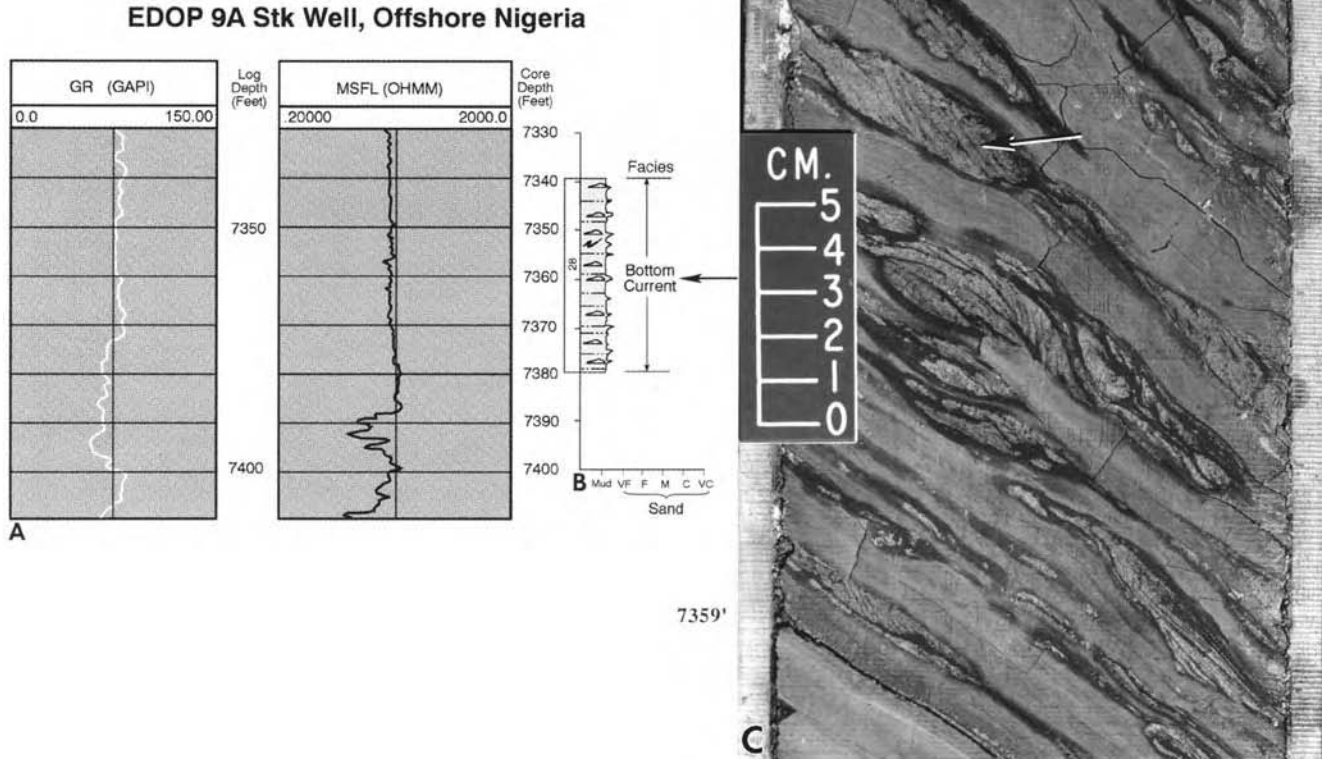
Fig. 4.35. (*A*) Serrated wireline log motif, IQI-2, Mobil 9A Sidetrack well, Edop Field, offshore Nigeria. (*B*) Depth-tied sedimentological log. (*C*) Bottom current reworked facies: Core photograph showing rippled lenticular sand with mud drapes (arrow). Lenticular sands are oil stained. 7359′ (2243 m) core depth. Arrow shows stratigraphic position of core photograph. (After Shanmugam (1997c).)
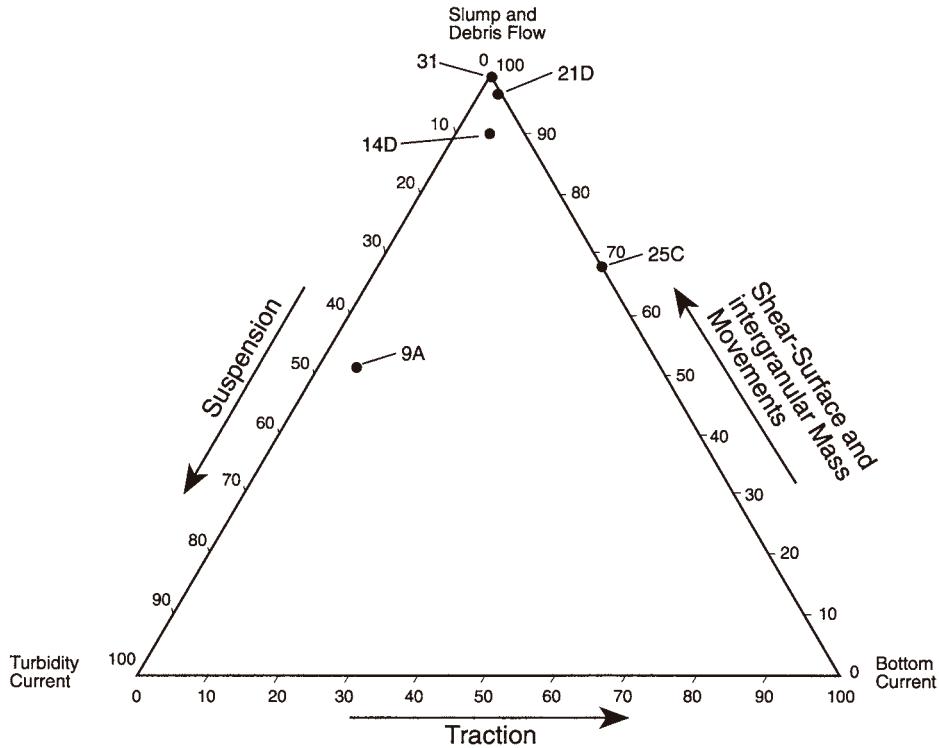
Fig. 4.36. Ternary diagram showing slump and debris flow dominated resedimented facies in the IQI-3 (Mobil 21D, 14D, 25C, 9A Sidetrack wells), and IQI-2 (Mobil 31 well) sequences, Edop Field area, offshore Nigeria. Note that Mobil 21D core contains both debrite and tidalite facies. (After Shanmugam (1997c).)

sediments deposited during 14 days should be composed of 28 sand bundles in a semidiurnal tidal regime (i.e., two tides a day), or 14 sand bundles in a diurnal tidal regime (i.e., one tide a day). In the Edop reservoir, there is evidence for tidal cyclicity in some sandstones. However, the exact number of sand-mud couplets is difficult to count because of synsedimentary faulting and limited amount of cores (Shanmugam, 1997c).

In the Edop reservoir (Fig. 4.36), the tidal facies (Facies 7) is closely interbedded with slump and debris flow facies (Facies 2). Tidal facies in association with slump and debrite facies in the ancient Qua Iboe Canyon is consistent with the facies association observed in other submarine canyons (Table 4.3).

4.5.8 The Annot Sandstone, Eocene–Oligocene, SE France

The Annot Sandstone (Eocene–Oligocene) in the French Maritime Alps, SE France is a well-studied deep-water system (Bouma, 1962; Stanley, 1975; Pickering and Hilton, 1998). The Annot Sandstone outcrops served as the foundation for developing

the first vertical turbidite facies model (Bouma, 1962). Problems with the turbidite facies model are addressed in Chapter 8.

Twelve units of the Annot Sandstone (Eocene–Oligocene) were measured along a road section in the Peira Cava area of the French Maritime Alps (Fig. 4.37). Units 2, 10, and 11 are selected for discussion here. Bouma (1962) originally interpreted these units as turbidites. However, these units have been reinterpreted as deposits of deep-marine tidal currents (Shanmugam, 2003).

Unit 2 is 10 m thick and it represents an amalgamated unit with multiple depositional events (Fig. 4.38A). Planes of abrupt decrease in grain size at 2 m, 2.2 m, and 8.4 m, and a change in sedimentary structures at 7 m suggest amalgamation surfaces within the unit (Fig. 4.38A). The lower interval of Unit 2 (0–2.75 m) is composed of contorted layers with pockets of gravel (Fig. 4.38C) and floating mudstone clasts, features suggestive of deposition from slumps and debris flows.

The upper interval of Unit 2 (2.75–10 m) is composed of a basal inverse grading, floating mudstone clasts, and armored mudstone balls with 3 mm quartz granules in the lower part (2.75–7 m) and double mud layers (Fig. 4.38B), mud draped ripples (Fig. 4.38B), and alternating parallel and rippled laminae in the upper part (7–10 m).

Using the Bouma's (1962) turbidite model, one could describe the upper interval (2.75–10 m) as being normally graded, and composed of Ta, Tb, Tc, Td, and Te divisions. They would be interpreted as turbidites. However, such a general description does not take into account the basal inverse grading, the floating mudstone clasts, and the floating armored mudstone balls. These features indicate deposition from plastic flows, not turbidity currents. In particular, waning turbidity currents can deposit only normal grading, not inverse grading (Sanders, 1965; Shanmugam, 2002a).

Our general tendency is to interpret normally graded beds, such as the upper interval (2.75–10 m) of Unit 2 (Fig. 4.38A), as a turbidite bed. However, such an interpretation is problematic for the following reasons: (1) an amalgamated unit represents multiple depositional events, whereas a turbidite bed represents a single depositional event (Kuenen, 1967); (2) inverse grading and mudstone balls represent mass-flow deposition (see Bagnold, 1954; Sanders, 1965); and (3) double mud layers represent tidal deposition. Furthermore, the presence of abundant mud drapes on traction structures suggests fluctuating energy conditions that are difficult to explain by a waning turbidity current. In short, Annot Unit 2 is composed of deposits of mass flows and tidal bottom currents.

Unit 10 is composed of interbedded sandstone and mudstone intervals. The sandstone interval exhibits sigmoidal cross bedding (Fig. 4.39B). Cross beds show mud-draped tangential toesets and fanning (i.e., thickening) of the foresets in fine- to coarse-grained sandstone. These structures in outcrop exhibit an overall sigmoidal shape, and hence are called *sigmoidal cross bedding*. Pickering and Hilton (1998) interpreted such cross beds as deposits of high-density turbidity currents. The concept of high-density turbidity currents is controversial (see Chapter 7).
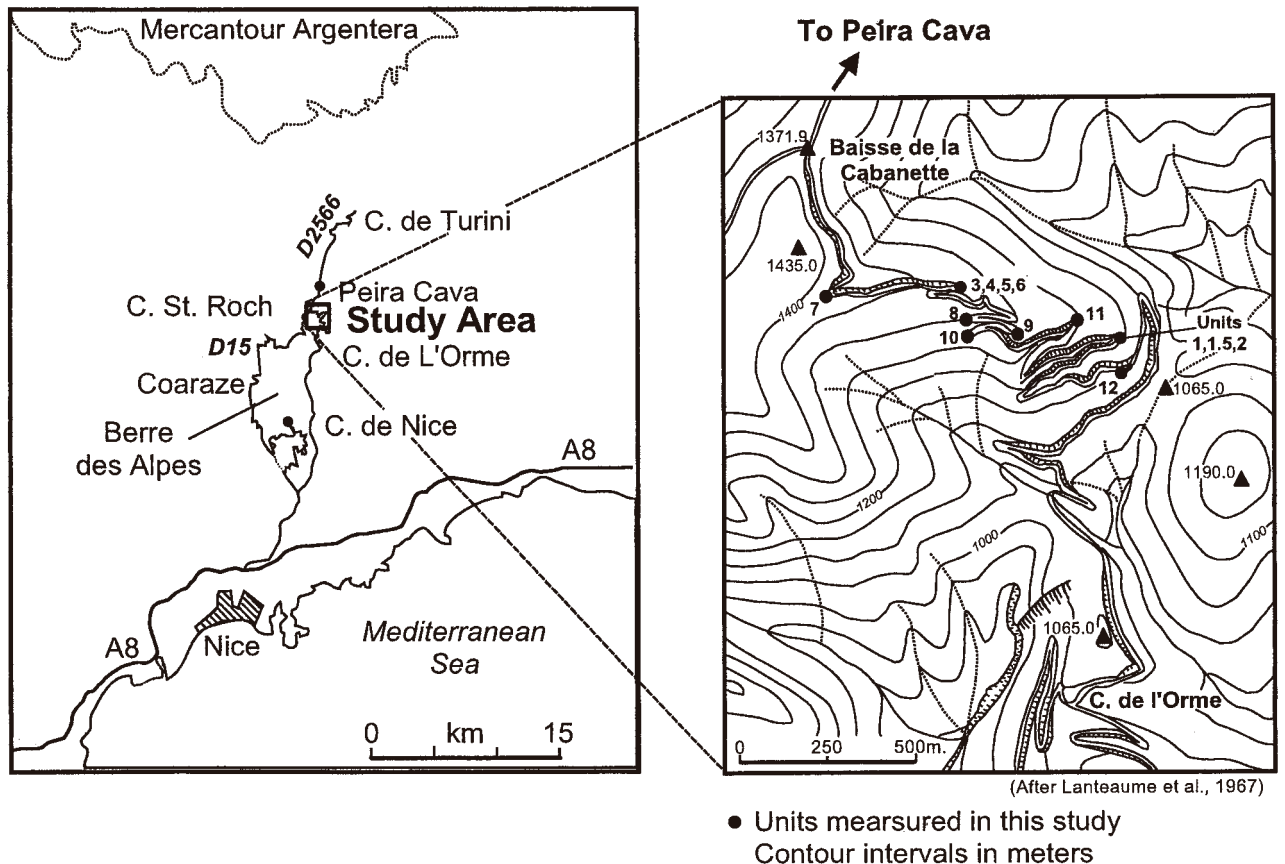
Fig. 4.37. Map showing location of Annot Sandstone (Eocene-Oligocene) units (solid dots) measured along a road section near Peira Cava, French Maritime Alps, north of Nice, southeastern France. Road section is partly based on Lanteaume et al. (1967). (After Shanmugam (2002a). Reproduced with permission from Elsevier.)
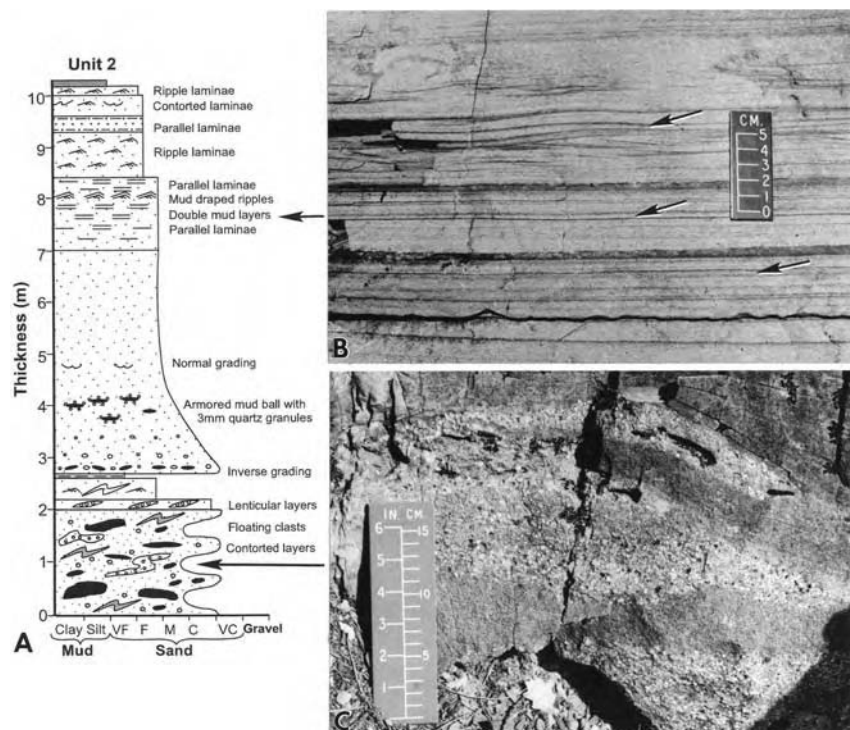
Fig. 4.38. (*A*) Sedimentological log of Annot unit 2 in which the lower interval (0–2.75 m) is composed of contorted layers with pockets of gravel and floating mudstone clasts. The upper interval (2.75–10 m) is composed of a lower part (2.75–7 m) with inverse grading and armored mudstone balls with 3 mm quartz granules, and normal grading, and an upper part (7–10 m) with a complex alternation of parallel laminae, double mud layers, mud draped ripples, parallel laminae, ripple laminae, parallel laminae, contorted laminae, and ripple laminae. Note abrupt decrease in grain size at 2 m, 2.2 m, and 8.4 m, and change in sedimentary structures at 7 m. These planes of abrupt decrease in grain size represent amalgamation surfaces within the unit. (*B*) Outcrop photograph of Annot Unit 2 showing double mud layers (three arrows). Note mud-draped ripples between upper and middle arrows. Left-pointing arrow shows stratigraphic position of photograph. (*C*) Outcrop photograph of Annot Unit 2 showing contorted layers with pockets of gravel in coarse-grained sandstone. Arrow shows stratigraphic position of photograph. (See Figure 4.37 for location of Annot unit 2.)
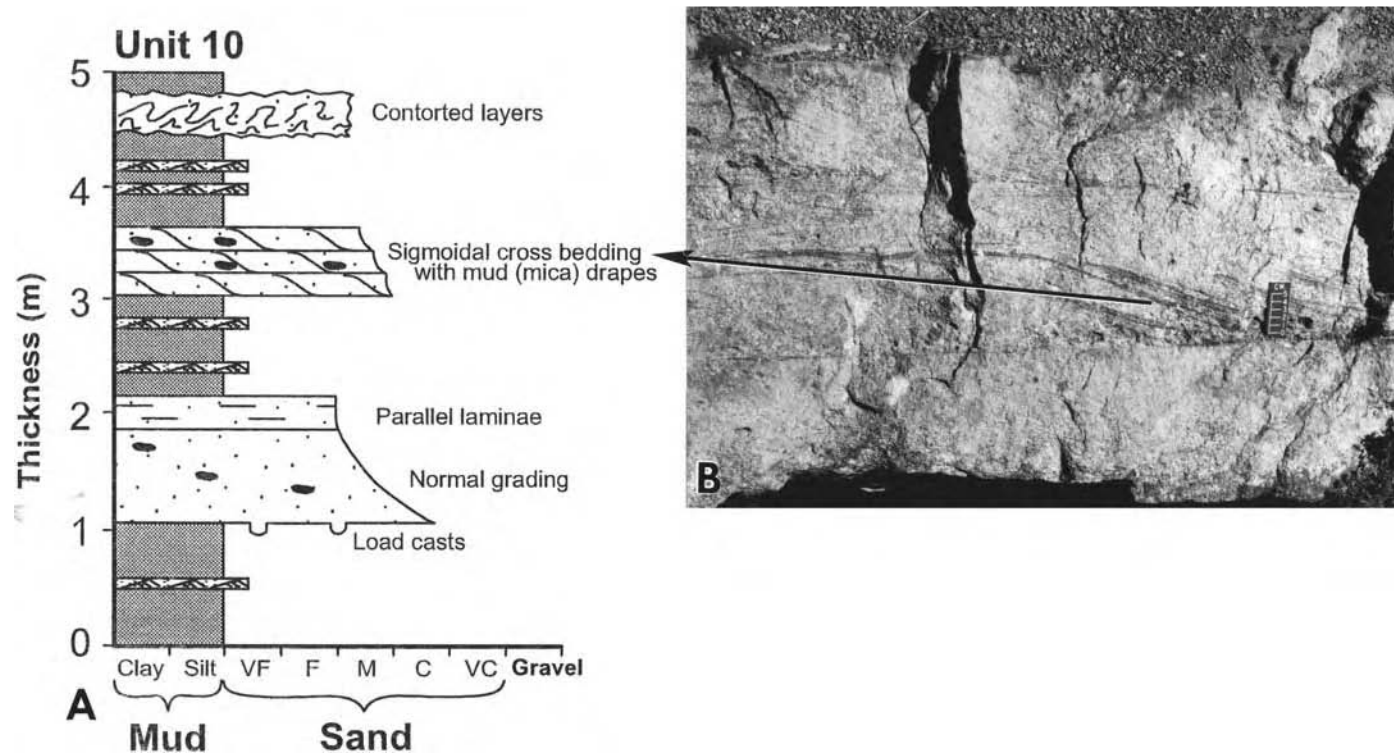
Fig. 4.39. (*A*) Sedimentological log of Annot Unit 10 showing three sets of sigmoidal cross bedding. Note contorted layers of a sandstone bed above (4.75 m) and a normally graded sandstone bed with clasts below (1–2 m). Note rippled sand beds in intervening mudstone intervals. (*B*) Outcrop photograph of Annot Unit 10 showing the middle set of sigmoidal cross bedding (arrow) with mud drapes (dark coloration). Note faint tangential lower contacts of the upper set. Lower set of sigmoidal cross bedding is poorly developed and thus is not obvious in the photograph. Rarely, mica has been observed along with mud. Arrow shows stratigraphic position of photograph. (See Figure 4.37 for location of Annot Unit 10.)

In sigmoidal cross bedding, tangential basal contacts, steeply dipping foresets, and fanning of the foresets may be equivalent to the full-vortex part of tidal bundles in shallow-water environments (Terwindt, 1981). Tidal bundles represent a lateral succession of cross-strata deposited in one event by the dominant tide (Terwindt, 1981). During Annot deposition, tidal currents were probably responsible for forming sigmoidal cross bedding in canyon or channel settings.

Tangential toesets are not unique to tidal deposits because these structures only indicate that the avalanche facies resulted from a combination of tractional and suspension fall-out processes. Such processes are common in other environments as well (e.g., fluvial and eolian). However, the deep-water origin of the Annot Sandstone has restricted our options to either turbidity currents or tidal currents. Under this constraint, tangential toesets can be explained better by tidal currents than by turbidity currents. This is because a genetic link between tangential cross bedding and tidal currents has been well established (Terwindt, 1981), whereas a link between tangential cross bedding and turbidity currents has not been documented. Lee et al. (2002) reported the generation of upslope-migrating antidunes by Froude-supercritical turbidity currents. However, the origin of sigmoidal cross bedding with mud drapes is difficult to explain by upslope-migrating antidune bedforms deposited by Froude-supercritical turbidity currents. Furthermore, no one has ever generated sigmoidal cross bedding with mud drapes by Froude-supercritical turbidity currents in flume experiments. Contorted layers at 4.75 m in Unit 10 (Fig. 4.39A), which suggests synsedimentary slumping, are evidence of a close association of tidal facies and mass flow facies.

In Unit 11 (Fig. 4.40), sigmoidal cross bedding shows tangential basal contacts (Fig. 4.40B). Bouma and Coleman (1985) interpreted these cross beds as lateral migratory channel-fill deposits by turbidity currents in sinuous submarine channels. Bouma and Coleman (1985) considered these submarine deposits to be analogous to fluvial point-bar deposits in subaerial environments. The problems in interpreting deep-water deposits using fluvial point-bar analogy are discussed in Chapter 7.

An inversely graded gravel layer underlies the sigmoidal cross bedding of Unit 11 (Fig. 4. 40). Inverse grading is typical of mass flow deposition (Bagnold, 1954; Sanders, 1965). In short, Units 2, 10, and 11 all exhibit a close association between tidal facies and mass flow facies.

Evidence for tidal current reworking in the Annot Sandstone is present not only in sandstone but also in mudstone. For example, Units 10 (Fig. 4.39) and 11 (Fig. 4.40) show tidal features both in sandstone (i.e., sigmoidal cross bedding) and in intervening mudstone intervals (i.e., mud draped ripples). However, the interruption of tidal deposition by mass flows (i.e., slumps, grain flows, and debris flows) is common in the Annot sandstone.

In referring to their study of tidal currents in submarine canyons, Shepard et al. (1979, p. 2) aptly stated, '*To petroleum geologists, eager to understand processes of sedimentation, this study would seem to be of paramount importance.*' Indeed,
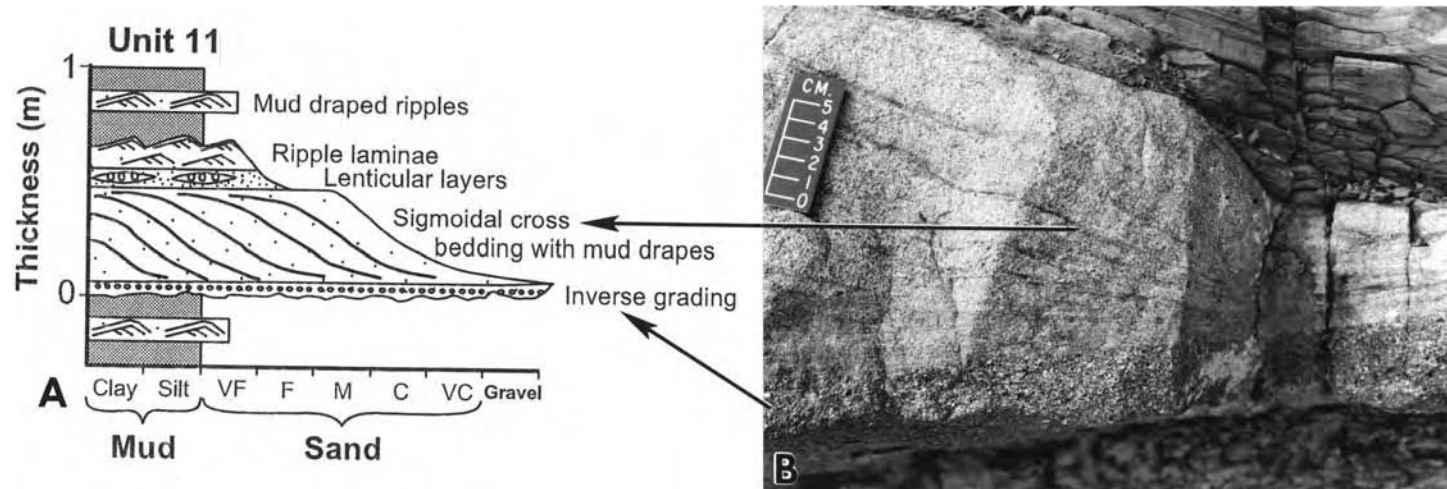
Fig. 4.40. (*A*) Sedimentological log of Annot Unit 11 showing sigmoidal cross bedding with mud drapes. Note underlying inverse grading of gravel layer. Note mud draped ripple beds in adjacent mudstone intervals. (*B*) Outcrop photograph of Annot Unit 11 showing sigmoidal cross bedding with tangential basal contacts. Upper arrow shows stratigraphic position of sigmoidal cross bedding and lower arrow shows stratigraphic position of inverse grading. (See Figure 4.37 for location of Annot Unit 11.)
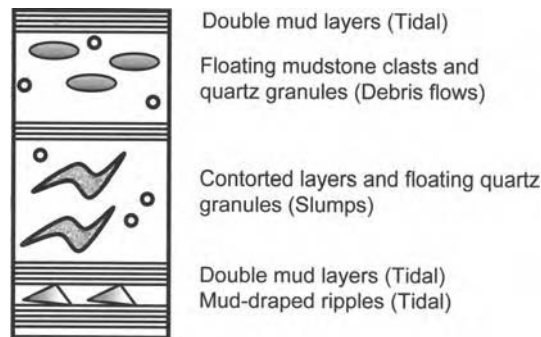
Fig. 4. 41. An ideal facies association showing interbedded occurrence of double mud layers (tidal origin), floating mudstone clasts and quartz granules (debris flow origin), double mud layers (tidal origin), contorted layers and floating quartz granules (slump origin), and double mud layers with mud-draped ripples (tidal origin). In the rock record, such a facies association may be used as evidence for deposition within submarine canyons. (After Shanmugam (2003). Reproduced with permission from Elsevier.)

recognition of tidal facies in deep-water sequences has important implications for reconstructing ancient environments. Deposits of tidal processes and mass movements (i.e., slides, slumps, grain flows, and debris flows) characterize fills of modern and ancient submarine canyons (Table 4.3). This complex facies association (Fig. 4.41), mimicking both 'shallow water' and 'deep water' deposits, is unique to canyon environments. Therefore, this facies association may be used as a criterion for recognizing submarine canyon settings in the rock record where erosional evidence for canyons is lacking. Because mass-movement facies (i.e., deposits of slides, slumps, and debris flows) can occur both inside and outside submarine canyons, the correct identification of tidal facies in deep-water sequences is extremely critical for establishing the canyon-facies association. The importance of tidal facies in understanding deep-water sand distribution in channel-mouth environments is discussed in Chapter 12.

4.6 Synopsis

Bottom currents (induced by thermohaline, wind, or tidal forces) are the primary cause of developing traction structures in deep-water sands. Bottom-current reworked sands are important petroleum reservoirs.

This Page Intentionally Left Blank

Chapter 5

Other processes and the phenomena of tsunamis

5.1 Introduction

The objective of this chapter is to discuss various other processes and phenomena that influence deep-water sedimentation either directly or indirectly. They are: (1) liquidization; (2) clastic injection; (3) mud diapirism; (4) sediment plumes; (5) wind transport; (6) ice rafting; (7) nepheloid layers; (8) volcanism; (9) pelagic and hemipelagic settling; and (10) tsunamis.

5.2 Liquidization

Allen (1984) used a general process term *liquidization* to describe mechanisms involving a change of state from solid-like to liquid-like (i.e., 'quick') in cohesionless grain mass. The two mechanisms of liquidization are liquefaction and fluidization.

Liquefaction occurs when loosely packed, well-sorted, granular material collapses totally as a consequence of increased pore-fluid pressure. This *in situ* disruption of the grain fabric, commonly a consequence of seismic shock, results in reduction of shear strength to merely nothing. Liquefaction involves neither influx of external fluids into the grain mass nor volume change. Lowe (1979, p. 76) defined a type of sediment-gravity flow known as *liquefied flow* in which '… *the sediment is not fully supported but is settling through its pore fluid, which is displaced upward*.' Unlike other sediment flows (debris flow and turbidity current), liquefied flow is an ineffective agent for transporting sediment downslope because it is primarily an *in situ* process. Thus liquefied flow is not considered here as a sediment flow.

Fluidization occurs when a 'quick' condition is achieved by forcing a fluid upward through the grain mass, until the immersed weight of the grains is balanced by the total fluid drag (Allen, 1984). Unlike liquefaction, fluidization requires influx of external fluid and its upward movement. In their classification

of sediment-gravity flows, Middleton and Hampton (1973, p. 2) defined *fluidized sediment flow* as a flow in which '…*the sediment is supported by the upward flow of fluid escaping from between the grains as the grains are settled out by gravity*…' Fluidized flow is also an ineffective agent for transporting sediment downslope. Thus it is not considered here as a sediment flow.

In deep-water slope and canyon environments, rapid deposition of well-sorted sand by sandy debris flows and slumps commonly results in syn- and post-depositional liquidization. Escape of fluids upward in rapidly deposited granular material tends to cause water-escape structures (Fig. 5.1). The escaping fluids tend to remove clay from a lower zone and accumulate it in an upper zone when the fluids encounter a low-permeability layer (Fig. 5.1). Such encounters redirect fluid movement from a vertical to a horizontal direction (Lowe and Lopiccolo, 1974). This redirection creates a color couplet with a light-colored (clay-depleted) lower layer and a dark-colored (clay-enriched) upper layer (Fig. 5.1). The orientation of color couplets may be used to determine the amount of upward push or to determine the amount of deformation a horizontal layer has suffered. The color couplets may also be used to determine the relative timing of various layers based on cross-cutting relationships (Fig. 5.1). Internal glide planes associated with slide deposits are potential candidates for forming color couplets.

5.3 Clastic injections

Clastic injections are both depositional and post-depositional in origin. They were reported by early researchers of the nineteenth century (Strangways, 1821; Murchison, 1827; Strickland, 1840; Darwin, 1846; Diller, 1890). Thus far, the origin of clastic injections has been primarily of academic interest, but lately it has received much attention from the petroleum industry (Purvis et al., 2002).

Concordant, commonly horizontal, clastic injections are called 'sedimentary sills.' Discordant, vertical to inclined, injections are called 'sedimentary dikes' (also spelled 'dykes'). Sand is commonly injected into a host mud, but mud injections into host sand and sand injection into host sand has also been observed. Clastic injections have been observed in many environments (e.g., fluvial, lacustrine, shallow-marine, deep-marine, etc.). The term *injectite* for injection features was used informally in the petroleum industry in the early 1980s (e.g., Mobil), but examples of published references are by Vivas et al. (1988) and by Macsotay et al. (1997, 2003). The term injectite is used in this book for injection features in igneous, sedimentary, and metamorphic rocks.

5.3.1 Injection features

Sand injectites are difficult to recognize in cores because they often resemble sandy debrites composed of massive sands and brecciated clasts. Injectites also mimic

Fig. 5.1. Core photograph showing water-escape dish structures by liquidization in fine-grained, well-sorted sand. The arrow shows a concave-up (dish structure) color couplet with left wing dipping at 45° from the core horizontal due to deformation. Note cross-cutting relationship between two dish structures in which an earlier formed dish structure (1) has been terminated by a later one (2). Eocene, North Sea.

passive fissure-fills called Neptunian dykes (Maltman, 1994, p. 28). Various features associated with deep-water sand injectites (Hiscott, 1979; Shanmugam et al., 1994; Dixon et al., 1995; Purvis et al., 2002; Duranti and Hurst, 2004) are:

- Large sand pillars with cross-cutting relationships (Fig. 5.2).
- Razor-sharp planar margins (Fig. 5.3). Caution must be exercised when applying this feature as a criterion for recognizing injectites because freezing of sandy debris flows can also result in sharp planar contacts.

Fig. 5.2. Core photograph showing a vertical pillar of sand (arrow) cutting across mudstone. Lower left is bottom and upper right is top. Pliocene, offshore Nigeria.

- Shear fractures confined to sandy intervals (Fig. 5.3).
- Discordant sills. Although sand sills are defined as concordant features, sills may terminate depositional laminae in mudstone host slightly and still be nearly concordant (Fig. 5.3).
- Crenulated margins of sand injections (Fig. 5.4).
- Indented margins of sand injections (Fig. 5.5).
- Pulverized matrix along the margins of sand injections (Fig. 5.6).
- Curved-up or curved-down fabric. Usually, a sand injectite drags along adjacent mud in the direction of penetration (Fig. 5.7).
- Over-steepened layers.
- Straight branching or offshoot (Fig. 5.8).
- Curved branching of sand injectite with offshoots in multiple directions (Fig. 5.9).

Fig. 5.3. Core photograph showing horizontal sandstone injection with razor-sharp margin into mudstone host. Note vertical shear fractures (arrow) within the sill. Also note termination of depositional laminae in mudstone above and below by the injection. Although sandstone sills are concordant features, they terminate depositional laminae (i.e., horizontal layers in mudstone) and thus qualifying to be discordant 'dikes' as well. Eocene, North Sea.

- Roof pendants and brecciated mudstone clasts (Fig. 5.10). Caution must be exercised in applying this line of evidence for recognizing clastic injections because angular mudstone clasts can occur in a variety of scenario: (1) debris cone (scree) and fault breccias (Crowell, 1961); (2) hydraulic fracturing in earthquake-affected areas (Obermeier, 1998); (3) brecciation of cohesive layers in laboratory experiments (Nichols, 1995); and (4) angular clasts formed by
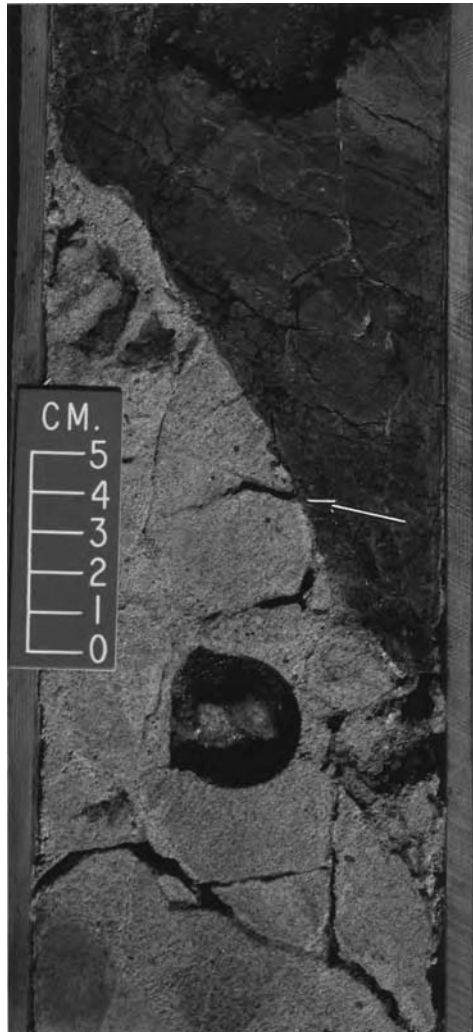
Fig. 5.4. Core photograph of a sandstone injection showing crenulated margin with mudstone host (arrow). Note chips of mudstone (dark color) inclusions near the top of scale. Eocene, North Sea.

breakage of slide into smaller fragments in frontal zones (Fig. 3.4). Therefore, not all breccias are indicative of clastic injection.

- <u>Sandstone-clast breccia</u>.
- <u>Massive or structureless sands</u>. Injected sands are considered to be massive (i.e., without stratification or other primary structures) by Duranti and Hurst (2004). Sands deposited in laboratory experiments by sandy debris flows are also

Fig. 5.5. Core photograph of a sandstone injection showing indented margin (arrow) with mudstone host. Note mudstone chips near the bottom of injected sandstone. Eocene, North Sea.

massive (Marr et al., 2001). Some sandy injectites may be massive, but not all massive sands are injectites.

- Ptygmatic folding due to compaction (Fig. 5.11).
- Lateral punch-out or tapered protrusion (Fig. 5.12).
- Blunt termination.
- Layering and normal grading (Fig. 5.13). A classic geologic case study of injectite is the Skaergaard intrusion, exposed along the central east Greenland

Fig. 5.6. Core photograph of a sandstone injection showing pulverized matrix at the margin with mudstone host (arrow) above. Note scattered mudstone chips near the top of injected sandstone. Eocene, North Sea.

coast, just above the Arctic Circle. It was emplaced, apparently as a single magma batch, into Archean basement gneisses and related rocks, and into Cretaceous sediments. The Skaergaard intrusion exhibits layering and normal grading (Union College Geology Department, 2005); and their origin has been controversial (Anderson et al., 1998).

Fig. 5.7. Core photograph of a sandstone injection showing downward drag of mudstone in the direction of penetration (arrow). Eocene, North Sea.

- Injected sand with cross bedding into host massive sand (Fig. 5.14).
- Small-scale injections with sand-filled microfractures in mudstone host (Fig. 5.15).
- Sandstone blobs in mudstone host (Fig. 5.16). Such features may be indicative of liquidized sand.
- Chickenwire structure. This structure has been observed in anhydrites (evaporites) as well.
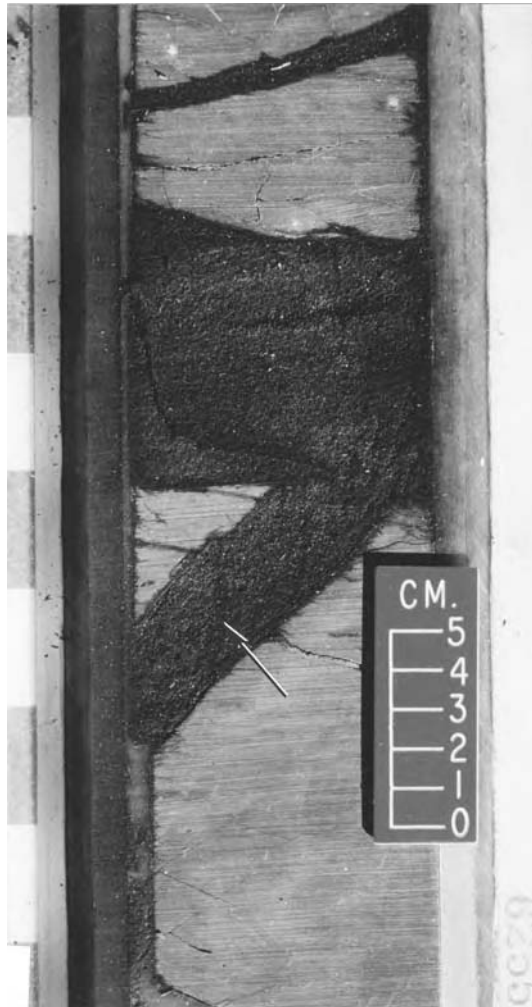
Fig. 5.8. Core photograph showing straight branching (offshoot) of a sand injectite (arrow). Dark–coloration of sand is due to oil staining. Eocene, North Sea.

- Seismic mounds. Although mounded seismic geometry has been reported for sands with clastic injections in the North Sea (Purvis et al., 2002; Duranti and Hurst, 2004), depositional geometries of slumps, slides, and debris flows also show mounded seismic geometry (Shanmugam et al., 1995a).

In summary, no single feature is unique to sand injectites. The only generality that can be made about clastic injections is that they resemble: (1) debrite; (2) slumps; (3) slides; (4) fault breccia; (5) massive sand; (6) graded turbidite sands; (7) cross-bedded sands; (8) layered sands; or (9) anhydrites.
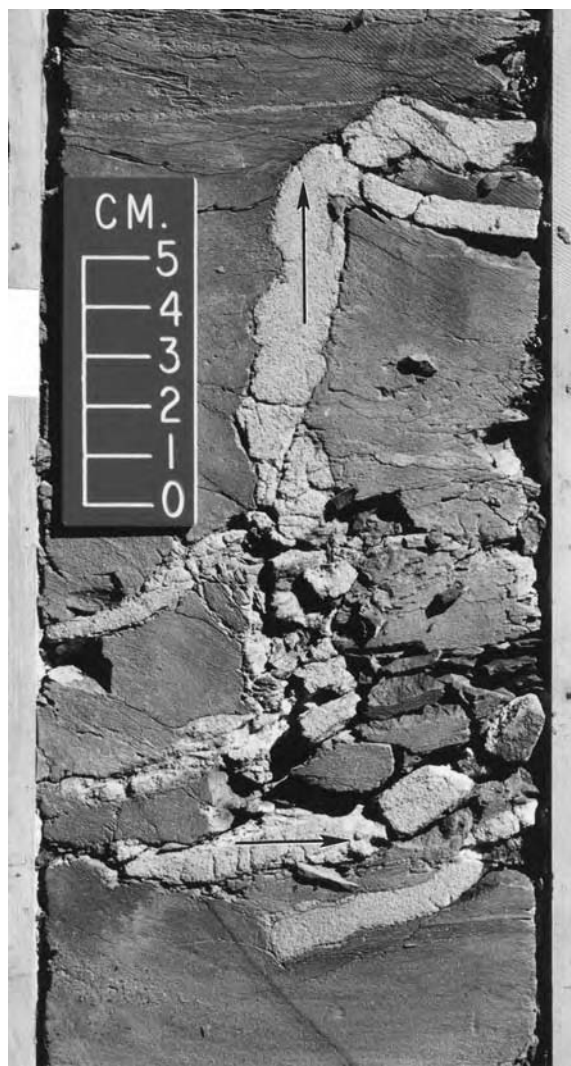
Fig. 5.9. Core photograph showing curved branching of sand injectite with offshoots in multiple directions. Note both dikes (vertical arrow) and sills (horizontal arrow). Eocene, North Sea.

5.3.2 Triggering mechanisms

General triggering mechanisms of injections are: (1) sedimentary slumping (Truswell, 1972); (2) sedimentary depositional loading (Hiscott, 1979; Surlyk, 1987; Shanmugam et al., 1994); (3) glacial loading (Le Heron and Etiene, 2005; Le Heron et al., 2005); (4) tectonic stress (Peterson, 1966); (5) seismicity-induced
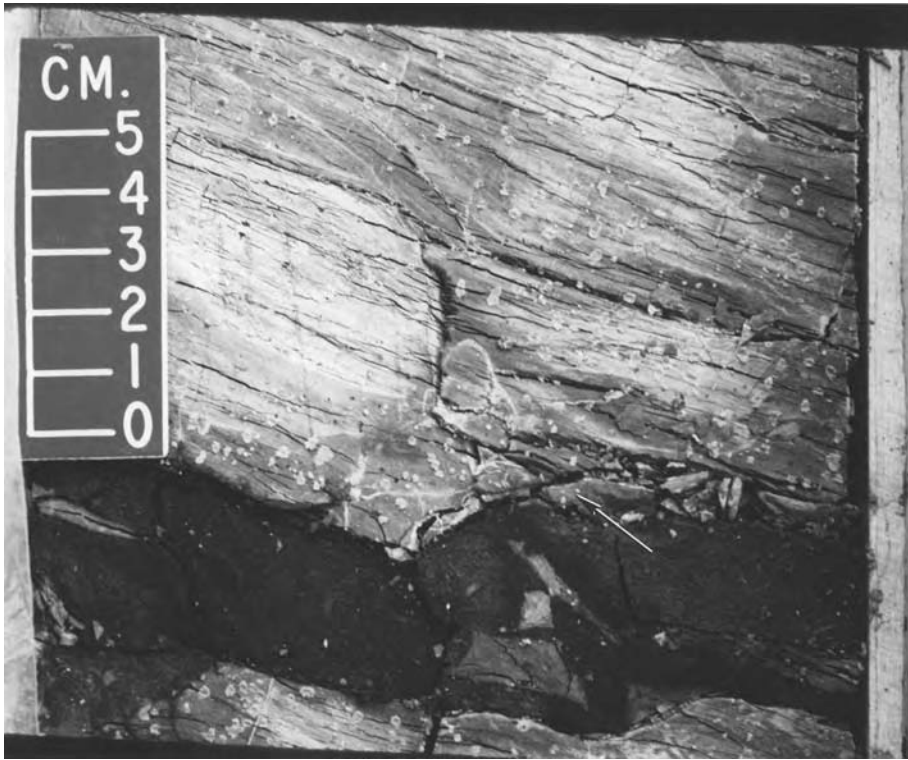
Fig. 5.10. Core photograph of a sand injectite showing roof pendants and mudstone chips (arrow) in a sill. Note mudstone clast breccia in oil-stained sand injectite near the bottom. Eocene, North Sea.

liquefaction (Obermeier, 1989); (6) igneous intrusion (Anderson et al., 1998); (7) vertical migration of fluid from within the basin (Brooke et al., 1995); and (8) impact origin (Srurkel and Ormö, 1997). According to Jolly and Lonergan (2002), seismicity and depositional processes are the two most commonly cited triggering mechanisms of clastic injections.

5.3.3 A model

Various models have been proposed for sand injections (e.g., Shanmugam et al., 1994; Duranti and Hurst, 2004). A model for sand injections, based on selected case studies (Shanmugam et al., 1994, 1995a; Shanmugam, 2002a), is discussed here. Core and outcrop examples suggest that deep-water sandstone injectites occur beneath thick units of sandy slumps and sandy debrites. Such a relationship suggests that clastic injections are genetically related to loading induced by
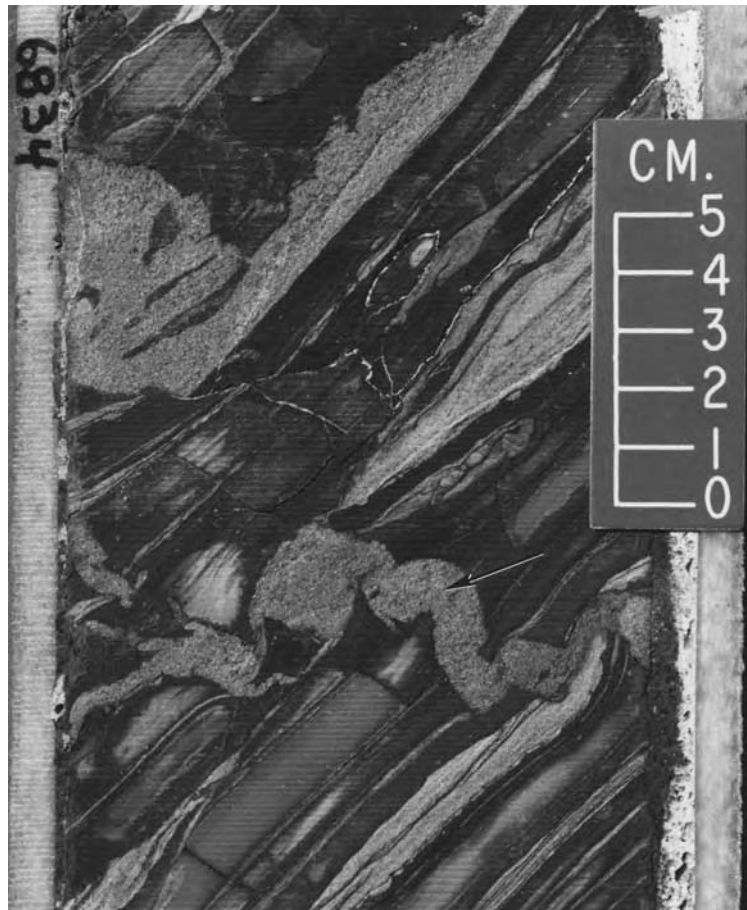
Fig. 5.11. Core photograph of a sandstone injectite showing ptygmatic folding of a dike due to compaction (arrow). Pliocene, offshore Nigeria.

slumping and mass flows. A model for injectite is proposed using the following five stages of development in deep-water environments:

(1) <u>Depositional stage</u>: Sediment failures on the upper slope deposit large pockets of sandy slumps, sandy slides, and sandy debrites.
(2) <u>Sealing stage</u>: Rapid burial of these sandy deposits by subsequent muddy deposits results in sealing of pockets of sand.
(3) <u>Overpressuring stage</u>: As subsequent slumps and slides travel over the buried and sealed sandbodies, loading and liquidization of the sand results. Sudden increase in stress related to slump-induced loading may cause extreme pore-fluid pressure to build up within the sand (i.e., overpressure).
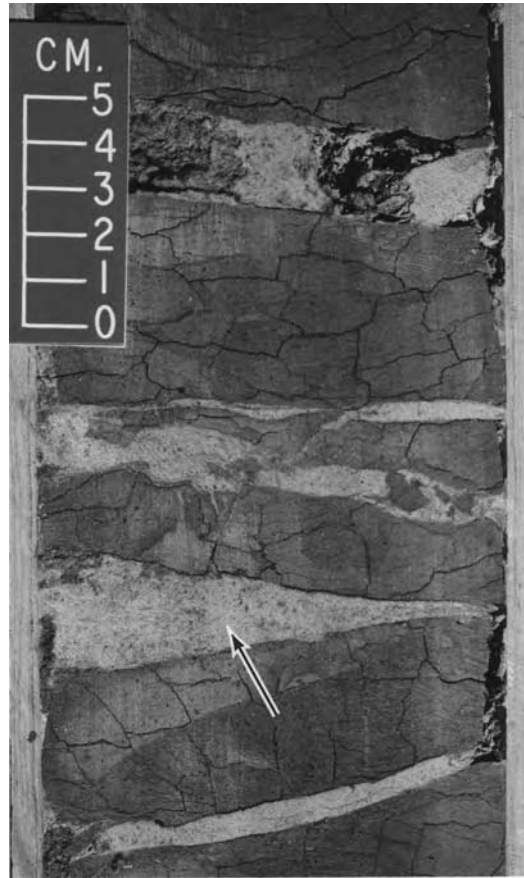
Fig. 5.12. Core photograph showing lateral pinch-out shape (arrow) of a sand injectite. Eocene, North Sea.

(4) <u>Fracturing stage</u>: Overpressuring causes dilation of the sand, which produces fractures or tension gashes within the sand as well as in the adjacent mud. These tension gashes effectively reduce the pressure of the pore fluid (Kimura et al., 1989).

(5) <u>Injection stage</u>: Liquidized sand is forcefully injected into those fractures in adjacent mudstone units that provide the most favorable pressure gradients (Fig. 5.17).

5.4 Mud diapirism

Mud diapirs in the continental slope off the Mississippi Delta have been well documented (Coleman and Prior, 1982). Sediment loading and rapid burial of cohesive
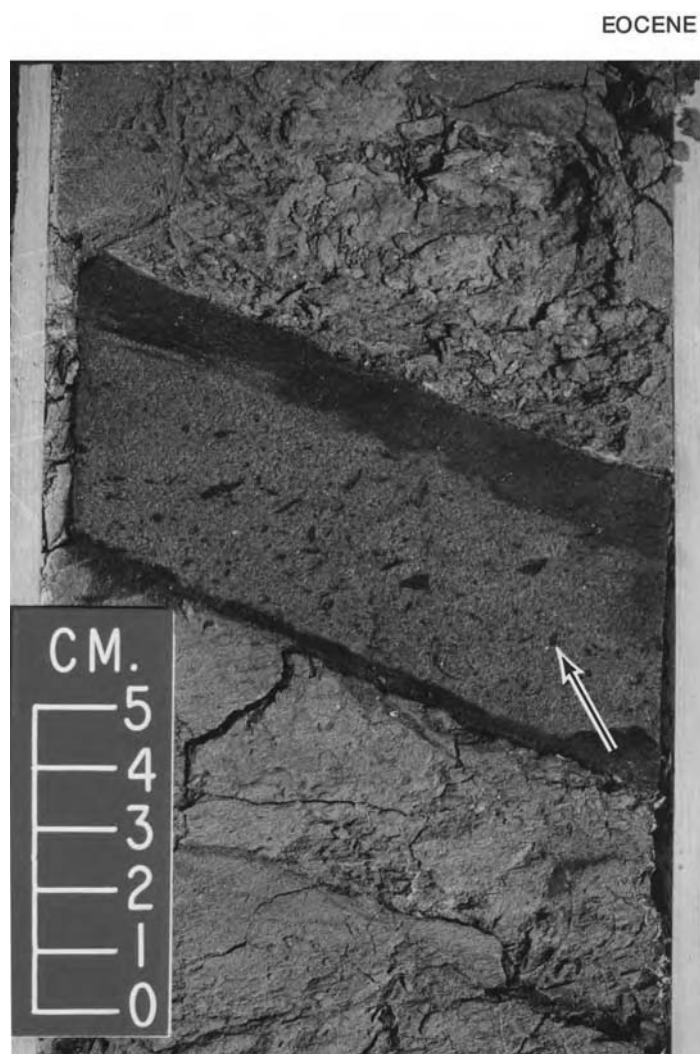
Fig. 5.13. Core photograph of a sandstone injectite showing internal layering. Note basal layer with mudstone clasts (arrow) and upper darker layer free of clasts. The basal layer is coarser than the upper layer, and thus it might be termed a 'normally grading.' Eocene, North Sea.

sediments commonly result in overpressuring. This leads to gravitational instability, which triggers vertical and lateral flowage of sediment. In areas of rapid sedimentation, mud diapirs or mud lumps are the most common type of sediment flowage and deformation. Aspects of sediment deformation have been discussed by Maltman (1994) and Collinson (1994).
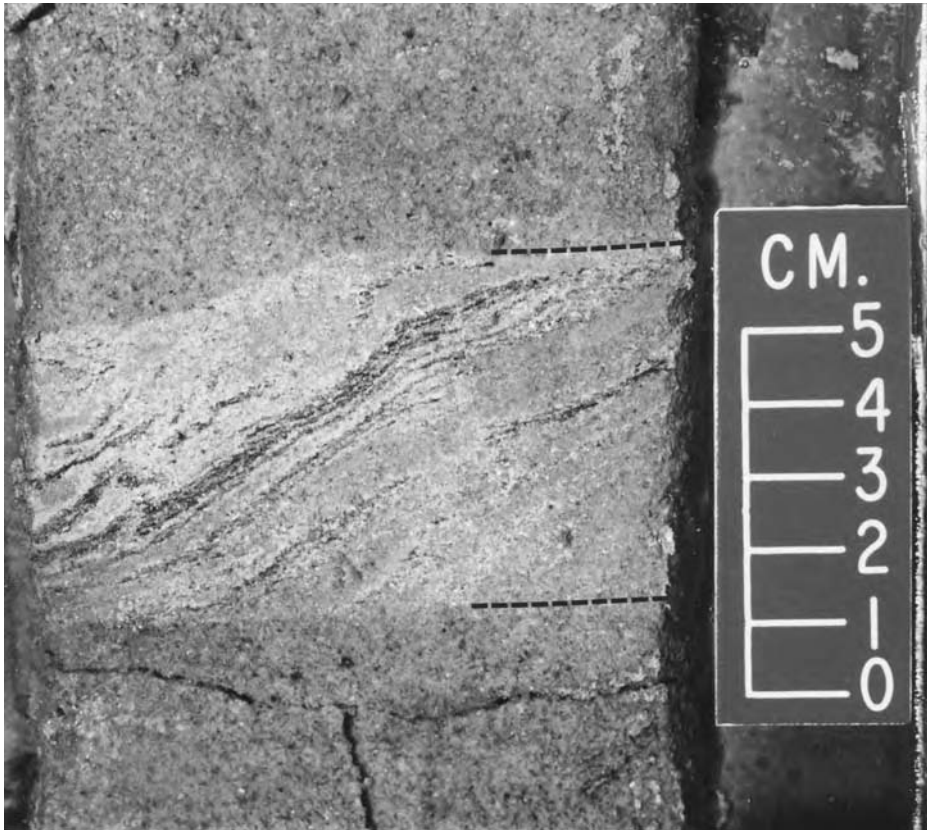
Fig. 5.14. Core photograph showing injection of cross-bedded sand (middle) into massive sand. Note distinct change in lithology revealed by a change in texture and coloration between the injected (cross bedded) and host (massive) sands. Dashed lines mark the upper and lower margins of the injected sand. Eocene, North Sea.

5.5 Sediment plumes, wind transport, ice rafting, nepheloid layers, and volcanism

In addition to primary gravity-driven processes, minor amount of sediment is also brought into deep-water environments by a variety of secondary processes (Boggs, 2001). They are:

(1) Fresh-water sediment plumes traveling across narrow shelves into deep-water slopes.

(2) Winds blowing silt and clay fractions from desert areas directly into deep-water environments. An example is plumes of eolian dust streaming over Namibia's Skeleton Coast into the waters of the South Atlantic Ocean (Fig. 5.18).

Fig. 5.15. Core photograph of small-scale injection features showing sand-filled microfractures in mudstone host. Note small-scale normal faults. Eocene, North Sea.

(3) Glacio-marine transport of rafted sediment (ranging in size from mud to gravel) by icebergs.
(4) Transport of fine sediment by nepheloid layers near the shelf break (Pierce, 1976).
(5) Transport of pyroclastic material from subaerial and submarine volcanism (Fisher and Schmincke, 1984).
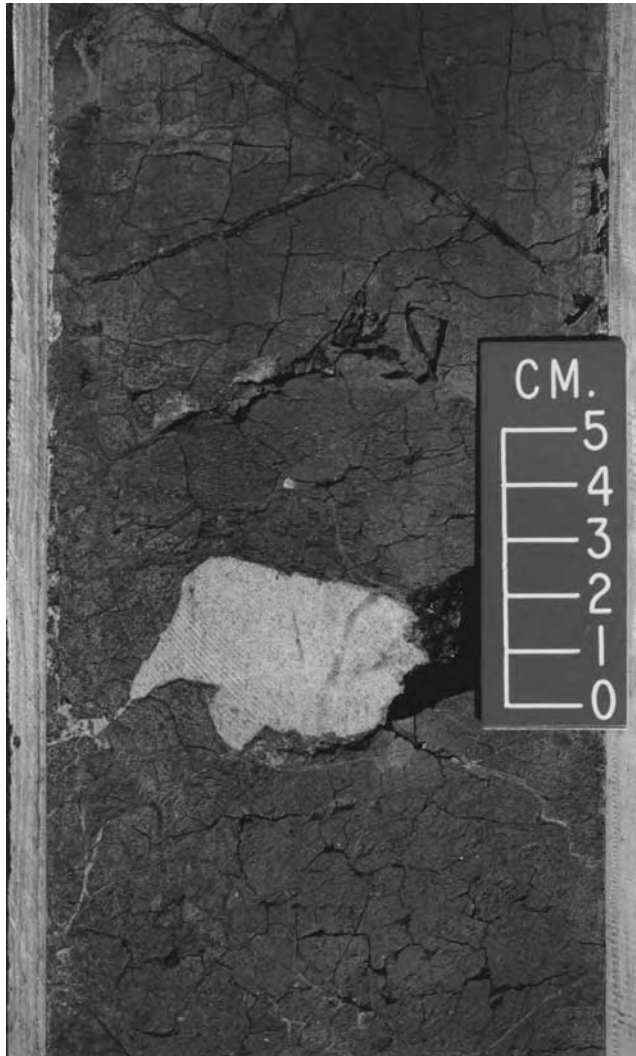
Fig. 5.16. Core photograph showing a sandstone blob injected into mudstone host. Such features may be interpreted to be injection of liquefied sand. Eocene, North Sea.

5.6 Pelagic and hemipelagic settling

Pelagic and hemipelagic processes generally refer to settling of mud fractions derived from the continents and from the shells of microfauna through the water column onto the entire deep-ocean floor (Fig. 1.3). Lisitsyn (1986) labeled pelagic and hemipelagic deposits as *suspensites*. The term *hemipelagites* refers to deposits of hemipelagic settling of deep-sea mud in which more than 25% of the
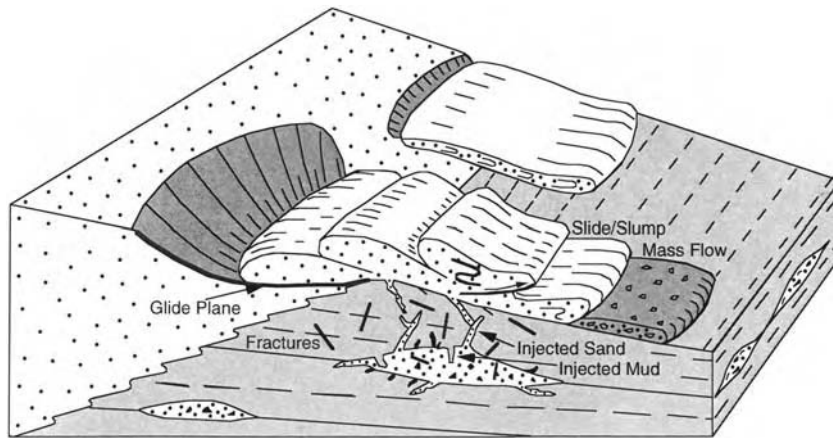
Fig. 5.17. A model for the origin of sandstone injectites. See text for details. After Shanmugam et al. (1994). Reprinted by permission of the American Association of Petroleum Geologists whose permission is required for further use.
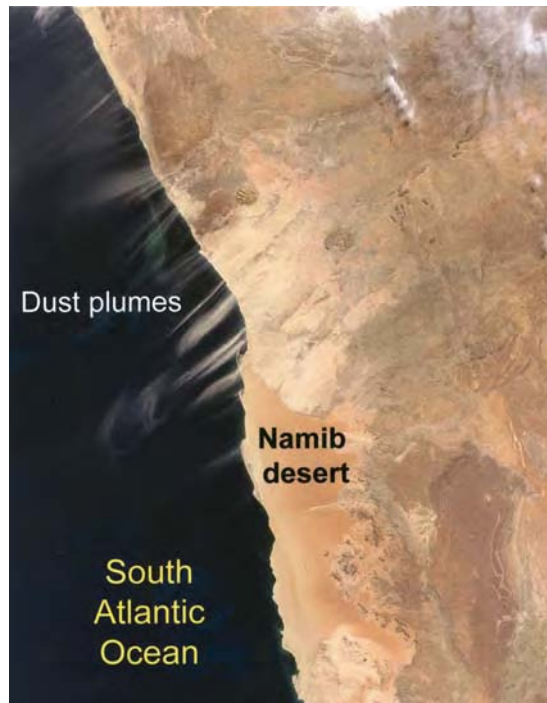
Fig. 5.18. Satellite image showing plumes of eolian dust streaming over Namibia's Skeleton Coast into the waters of the South Atlantic Ocean. Moderate Resolution Imaging Spectroradiometer (MODIS) from the Terra satellite on July 13, 2003. Credit: NASA's Visible Earth. Uniform Resource Locator (URL): http://visibleearth.nasa.gov/data/ev256/ ev25682_Namibia.A2003194.0905.1km.jpg (accessed August 20, 2004).

fraction coarser than 5 microns is of terrigenous, volcanogenic, and/or neritic origin. Although pelagic and hemipelagic muds accumulate throughout the entire deep-ocean floor, they are better preserved in parts of abyssal plains (Fig. 1.3). Rates of sedmentation vary from less than one mm per 1000 years to greater than 50 cm per 1000 years, with the highest rates on the upper continental margin.

General characteristics of pelagites and hemipelagites are:

- Mudstone lithofacies
- Parallel lamination
- Faint normal grading
- Bioturbation
- Deep-marine body fossils and trace fossils
- Sheet-like geometry conformable to underlying sea-floor topography (drape).

5.7 The phenomena of tsunamis

During the last decade (1995–2005), tsunami-related research has received much attention (Einsele et al., 1996; Shiki et al., 2000; Bryant, 2001; Tappin, 2004). However, the importance of tsunamis on deep-water sedimentation has never been addressed in detail in textbooks and edited volumes on sedimentology (e.g., Blatt et al., 1972; Pettijohn, 1975; Friedman and Sanders, 1978; Reineck and Singh, 1980; Leeder, 1982; Walker, 1984a; Pickering et al., 1989; Reading, 1996; Boggs, 2001).

Tsunami is a Japanese word that translates in English roughly into 'harbor wave' (tsu = harbor crossing and nami = wave). A tsunami is a water wave or series of waves, with long wavelengths and long periods, caused by an impulsive vertical displacement of the body of water by earthquakes (USGS, 2005), landslides (Tappin, 2004), volcanic explosions (van den Bergh, 2003), and extraterrestrial (meteorite) impacts (Simms, 2003). Tsunamis are random, unpredictable, non-meteorological phenomena that can occur in major water bodies anywhere on the globe at any time. Although tsunamis are commonly referred to as 'tidal wave,' this is a misnomer because tides represent the daily rise and fall of sea level under the extraterrestrial, gravitational influences of the moon and the sun on the rotating earth. Similarly, the term 'seismic sea wave' for tsunamis is misleading because it restricts the origin of tsunamis to earthquakes alone. Thus the Japanese word 'tsunami' (i.e., harbor wave) has been internationally adopted because it covers all forms of sea wave generation (NOAA, 2005a). When they reach the coast or an estuary, tsunami waves may mimic a rising or falling tide, a series of breaking normal sea waves, or a bore. Tsunami waves, composed of (1) sinusoidal, (2) Stokes, (3) solitary, (4) N-simple, (5) N-double, and (6) Mach-Stem types, have played a key role in shaping many coastal regions of the world (Bryant, 2001). According to a recent survey (Gusiakov, 2005), 688 tsunamis occurred in the

Table 5.1 Number of tsunamis and submarine earthquakes that occurred in the main tsunamigenic regions of the Pacific from 1901 to 2000. From Gusiakov (2005)

Regions	Number of tsunamis	Number of submarine earthquakes
Japan	123	255
South America	102	122
New Guinea–Solomon	86	130
Indonesia	68	86
Kuril–Kamchatka	68	150
Central America	62	112
New Zealand–Tonga	62	162
Philippines	55	73
Alaska–Aleutians	49	108
Hawaii	13	3
All Pacific	**688**	**1201**

tsunamigenic regions in the Pacific during 1901–2000 (Table 5.1). At this rate, nearly seven million tsunamis of varying magnitudes would occur per million years in the Pacific alone. Scheffers and Kelletat (2003) reported that at least 100 megatsunamis have occurred during the past 2000 years worldwide. Although the term 'megatsunami' is used informally for large tsunamis (e.g., those with wave heights > 40 m), there is no standard scientific definition.

Storm waves are meteorological phenomena. They are controlled by seasons and latitudes. Tropical cyclones (tropical storms, hurricanes, and typhoons) originate between 30°N and 20°S latitudes during summer months, and they travel from east to west (Gray, 1968). In contrast, extratropical cyclones are mid- to high-latitude winter storms that travel from west to east. Tropical storms have a sustained wind speed of 39–73 mph (63–118 km/h), whereas hurricanes and typhoons have a wind speed of greater than 74 mph (119 km/h). An estimated frequency of storms striking the U.S. Atlantic coastline ranges from 14 to 85 per year (Simpson and Lawrence, 1971).

Wind-generated normal surface waves are called 'sea waves' and they are complex (Komar, 1976). Tsunami waves and large wind-generated waves share the same characteristic in 'shallow water' where they both are considered 'long' waves. Normal sea waves, however, differ from tsunami waves in some important respects. *First,* small parcels of water associated with normal sea waves move in circular orbits (Harvey, 1976), whereas the orbits of water parcels of tsunami waves are elliptical. *Second,* sea-wave energy is focused near the sea surface, whereas tsunami-wave energy is concentrated below the sea surface. Although in both cases, the wave energy is carried in an indeterminate zone from the surface downward, the wind-generated waves may not carry their energy all the way to the deep ocean bottom. *Third,* unlike wind-generated sea waves, tsunamis with small wave amplitude and relatively long passage time are the reasons why sailors invariably fail to realize when a major tsunami wave passing under their ship. *Fourth,* no rapid withdrawal of sea water from the shoreline

occurs before normal sea waves, whereas prior to a tsunami the sea water recedes rapidly exposing the sea floor. Fifth, normal sea waves come and go without flooding over higher coastal areas, whereas most tsunami waves and major storm waves invariably flood over land areas.

5.7.1 The tsunamite problem

The term 'tsunamite' has been formally adopted in thematic special volumes (Shiki et al., 2000), printed journal articles (Michalik, 1997; Pratt, 2002; Simms, 2003), online *Encyclopedia* articles (Rodolfo, 2003), and other publications (Aschoff et al., 2001; and Barnett and Ettensohn, 2003). A 'GeoRef' database search has yielded Gong-Yiming (1988) as the earliest reference for the usage of the term 'tsunamite.' Yamazaki et al. (1989) used the term 'tsunamite' for tractive current-reworked conglomerates by tsunamis. Shiki and Yamazaki (1996, p. 177) defined 'tsunamites' as follows: '*We use the term tsunamites not only for sediments transported by the tsunami wave itself, but also for tsunami-induced current deposits. This usage is much the same as that of the term tempestites, which is used for storm-induced sediments.*' Like the term 'tempestite' for deposit of a storm, it makes sense to label deposit of a tsunami as 'tsunamite.' Unfortunately, this is where the simple logic ends on this matter.

   Although the term tsunamite appears to be a simple word with a straightforward meaning, a closer examination reveals a highly complex word with multiple and convoluted meanings. Furthermore, the meaning of the word changes drastically from one case to the next. The tsunamite problem is an amalgamation of issues at several levels. They are difficult to define precisely, but they can be described broadly as follows:

(1) The crux of the problem is concerned with reinterpretation of deep-water turbidites and debrites as tsunamites. Unlike turbidites that are interpreted on the basis of sedimentary features, tsunamites are interpreted on the basis of historical evidence. In interpreting deep-water muddy deposits as products of tsunamis using historical evidence, Cita and Aloisi (2000, p. 181) acknowledged that, '*No sedimentological characteristics peculiar to tsunamites are observed in the deep-sea homogenite of the eastern Mediterranean.*' The problem is that the term 'homogenite' is used here as a synonym for 'tsunamite.' The other problem is that the term 'homogenite' actually represents 'turbidite' (Cita and Aloisi, 2000, their Fig. 12). In other words: homogenite = tsunamite = turbidite. Similarly, debrite beds were reclassified as tsunamites (Barnett and Ettensohn, 2003). The reason for this nomenclatural overlap is that tsunamis are oceanographic phenomena of local to global magnitude. As a phenomenon, a tsunami can trigger a variety of processes, including turbidity currents and debris flows. Without realizing this, many turbidites and debrites have been reinterpreted as 'tsunamites,' causing nomenclatural congestion in the geologic literature.

(2) When a deposit is interpreted as a turbidite, the emphasis is focused solely on the process of deposition (turbidity current). On the other hand, when the same deposit is reinterpreted as a tsunamite, the focus shifts from a depositional process (turbidity current) to a triggering event (tsunami). As a result, useful information on depositional process is being replaced by ambiguous information on tsunami. The ambiguity comes from a plethora of processes (overwash surges, backwash, oscillatory flows, combined flows, slides, slumps, debris flows, and turbidity currents) that can be generated by tsunamis in a range of environments (lacustrine, coastal, shallow-marine, and deep-marine). As a result, virtually any sedimentary deposit in the geologic record could be reinterpreted as a tsunamite, so long as there is historical evidence. Such a reinterpretation undermines sedimentological progress that has been made over the past 50 years to distinguish specific depositional facies (e.g., turbidites *vs*. debrites). Thus the basic premise behind reinterpreting a deposit as a tsunamite is flawed.

(3) On a fundamental level, a prevailing notion is that deposition can occur directly from tsunami waves in deep-water environments. This is a conceptual problem. It may be attributed partly to a lack of synthesis of available data on the mechanics of sediment transport from shallow-water into deep-water environments during periods of violent storms and tsunamis.

The tsunamite problem is a blend of nomenclatural, interpretational, conceptual, and observational issues. Deposits of tsunamis have been interpreted from lacustrine (Bondevik et al. 1997), coastal (Whelan and Keating, 2004), shallow-marine (Bussert and Aberhan, 2004), and deep-marine environments (Kastens and Cita, 1981). The problem is that a plethora of sedimentary features, which include erosional unconformity of regional extent, boulder to mud lithofacies, matrix-rich conglomerate, breccia units, chaotic bedding, clastic injection, normally graded sand, inversely graded sand, floating mudstone clasts, hummocky cross stratification, trough cross stratification, wave ripple lamination, current ripple lamination, and antidune cross lamination, have been used for interpreting deposits of tsunamis (Table 5.2). These features suggest extreme variability in processes that include erosion, reworking, overwash surges, backwash, lower flow regime currents, upper flow regime currents, bidirectional tidal currents, oscillatory flows, storm-generated combined flows, liquefaction, fluidization, soft-sediment deformation, slides, slumps, freezing of boulders in debris flows, settling of sand from turbidity currents, and settling of mud from hemipelagic suspension clouds. Selected case studies are discussed below to demonstrate interpretational problems associated with tsunamites.

5.7.1.1 Tempestite versus tsunamite

There are major challenges in distinguishing tempestites from tsunamites (Young and Bryant, 1998). Cores of shoreface sediments off Fire Island, Long Island,

Table 5.2 **Examples of features associated with deposits of tsunamis**

Reference	Features
Coleman (1968)	Chaotic bedding
Ballance (1981)	Coconuts in 'turbidites'
Bourgeois et al. (1988)	Coarse-grained sandstone with mudstone clasts grades upward into wave-rippled sandstone
Moore and Moore (1988)	Inverse grading with basalt boulders (1.5 m diameter) and dune-like ridges in boulders (1 m high and 10 m apart)
Yamazaki et al. (1989)	Gravel clusters and imbrication
Shiki and Yamazaki (1996)	Antidune with chute and pool structure
Bondevik et al. (1997)	Erosional unconformity
Michalik (1997)	'Rope-ladder' texture (i.e., sigmoidal deformation)
Dawson and Shi (2000)	Floating boulders in sandy matrix and sheet geometry
Cita and Aloisi (2000)	Coarse fraction at the base of biogenic sandy unit (normal grading)
Rossetti et al. (2000)	Fine sandstone with swaley, trough, tabular, and hummocky cross stratification (HCS)
Bryant (2001)	Dune bedforms, imbricated boulder stacks, and cavitation features
Pratt (2002)	Earthquake-induced deformation structures, sporadic distribution of conglomerates, high degree of scouring, and angularity of intraclasts
Simms (2003)	Unit with HCS, which is underlain by seismites containing slump folds, microfaults, dikes, truncated top, etc.
van den Bergh et al. (2003)	Reworked shell fragments
Barnett and Ettensohn (2003)	Breccia with angular chert and dolostone clasts
Bussert and Aberhan (2004)	Inverse to normal grading and opposing current directions
Whelan and Keating (2004)	Gravel-size corals mixed with man-made items
Lawton et al. (2005)	Clast-supported textures, normally graded planar conglomerate-sandstone couplets, and upcurrent-dipping low-angle cross-laminae.

New York exhibited 2 m thick normally graded fine sand. This graded sand was attributed to waning stages of a storm (Kumar and Sanders, 1976). Based on historical data, this sand could be classified as *tempestite*. However, normally graded beds can also be deposited during overwash surges triggered by storms (Leatherman and Williams, 1977). These overwash beds could also be classified as tempestite. The problem is that in one case the term tempestite represents *shoreface* deposits, whereas in the other it represents *overwash* deposits.

In Papua New Guinea, deposits of the 1998 tsunami contain normally graded sand (Fig. 5.19), which is a *tsunamite*. Classification of these modern deposits, based on historical data, as tsunamite is not much of a challenge. However, classification of ancient graded sandstone, for which there is no historical data, as tsunamite would be a challenge. This is because tsunamite, tempestite, and turbidite all exhibit normal grading.

In explaining the origin of ancient hummocky cross stratification (HCS), Rossetti et al. (2000, p. 309) stated, '…*combined flows responsible for the genesis of these structures were formed by tsunami waves enhanced by tsunami-induced ebb currents and/or tidal currents.*' This tsunamite interpretation of HCS is problematic
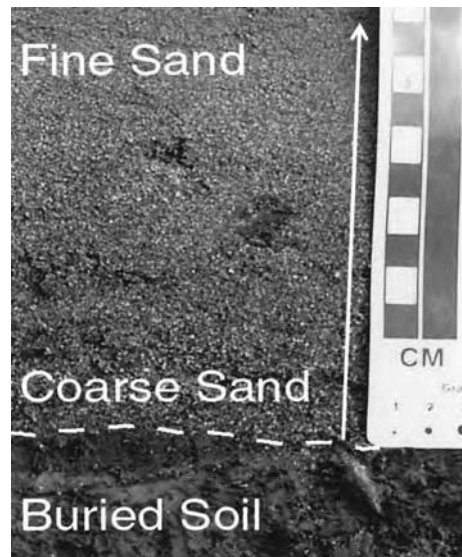
Fig. 5.19. Photograph showing a normally graded sandy unit (vertical arrow). Note erosional base (dashed line) between the sand and underlying brown muddy soil. This sand was related to the July 17, 1998 tsunami in Papua New Guinea. Thus the graded sand could be classified as a *tsunamite*. Sample location: Arop School Transect (Jaffe, 2005). (Credit: USGS and Jaffe (2005).)

because HCS has been traditionally considered as evidence for storm deposition (Harms et al., 1975). Thus HCS can represent both tsunamites and tempestites.

According to Michalik (1997, p. 221), '*Tsunamites are special type of tempestites.*' This implies that tsunamis and storms are genetically related. They are not (see Chapter 2). However, their deposits may be analogous. Clearly, the separation of tempestites from tsunamites is a semantic distinction without a sedimentologic difference.

5.7.1.2 Debrite versus tsunamite

The Middle Devonian Duffin Bed of New Albany Shale in southcentral Kentucky was originally interpreted as a debrite, but it was later reinterpreted as a tsunamite (Barnett and Ettensohn, 2003). Barnett and Ettensohn (2003, p. 602) acknowledged that '*Indisputable evidence for tsunamis is absent and will probably be difficult to identify in shallow-water, epicontinental settings, but an association of features and circumstances, especially evidence of coeval seismicity, can rule out more common alternatives and lend support for a tsunami model origin*.' The problem is that there is no indisputable evidence for tsunami as a process.

Michalik (1997, his Figs. 4.2, 4.3, and 4.8) used sigmoidal deformation features (i.e., 'rope-ladder texture') as the evidence for tsunami deposition in shallow-water

carbonate platforms. These deformation features are analogous to imbricate slices deposited by sandy debris flows in flume experiments (see Shanmugam, 2000a, his Fig. 18B) and to duplex-like structures formed by slumps in deep-water channels (Shanmugam et al., 1988c). Thus soft-sediment deformation is not unique to tsunami deposition.

In their study of the Maastrichtian conglomerates in northeastern Mexico, Aschoff et al. (2001) concluded that field and petrographic analyses show evidence for both debrite and tsunamite origin. The problem is that debrites and tsunamites are one and the same.

5.7.1.3 Turbidite (homogenite) versus tsunamite

The term *homogenite* was first coined for deep-sea tsunami deposits, composed of thick marly intervals with a normally graded sandy base, in the Mediterranean Sea (Kastens and Cita, 1981). Conventionally, such normally graded intervals would be interpreted as turbidites (Kuenen and Migliorini, 1950). However, Cita et al. (1996) opted for a tsunami origin based on historical evidence for volcanic eruptions that may have generated tsunami waves. As pointed out earlier, the term *homogenite*, which was used as a synonym for *tsunamite*, actually represents a *turbidite*! The great thickness and lack of lamination in these muddy units were used as evidence against a turbidite interpretation (Cita et al., 1982). Conventionally, deposits of turbidity currents have been recognized on the basis of evidence for Newtonian fluid rheology, turbulent flow state, and suspension settling (Dott, 1963; Sanders, 1965). Normal grading is a reliable criterion for interpreting turbidites (Kuenen and Migliorini, 1950). Bed thinness and lack of traction structures, such as parallel lamination, are not reliable criteria.

Although the term homogenite implies a homogeneous nature of sediment, these sediments are not homogeneous in texture. Cita et al. (1996, p. 155) indeed acknowledged that '*We keep the term "homogenite" which we do know is not well accepted by several orthodox sedimentologists for consistency with our previous works. The quotations indicate that the term has not to be considered as strictly referring to the homogeneous characteristics of the sediments, which indeed are not always and not entirely homogeneous. "Homogenite" is the sedimentary expression of a unique event, with a definite stratigraphic position.*' The problem is that the term 'homogenite' represents neither a homogeneous texture nor a direct deposition from tsunamis.

5.7.1.4 Seismite versus tsunamite

According to Einsele et al. (1996, p. 2), '*In-situ earthquake structures may be termed to as "seismites", including sand dikes, sand blows, and mud volcanoes…*' It is important to note that the origin of seismites does not involve sediment transport and deposition. The term seismite simply refers to deformation of existing sediment. Also, not all deformation structures in the rock record are induced by

seismic shocks. Although deep-water turbidites could be deposited from turbidity currents triggered by earthquakes, such as the 1929 'Grand Banks' earthquake (Piper et al., 1988), earthquakes themselves are not depositional processes. Seilacher (1984) emphasized that although seismites may exhibit deformation structures, independent verification of the seismic origin is still needed in every case.

In the Triassic of the United Kingdom, a seismite unit is overlain by a 'tsunamite' unit with hummocky cross-stratified and wave-ripped sandstone (Simms, 2003). But for the underlying 'seismite' unit, the overlying 'tsunamite' unit with hummocky cross stratification would otherwise be interpreted as a 'tempestite.' The problem here is the use of a genetic term (seismite), which is already an interpretive term, as the basis for another interpretation (tsunamite).

5.7.1.5 A solution

A solution is to only use descriptive sedimentary features as the basis of interpreting depositional processes and to label deposits based on depositional processes. This descriptive approach is necessary because sedimentary features represent flow conditions that prevailed during the final stages of deposition (Middleton and Hampton 1973; Postma, 1986). These depositional features, however, may not necessarily relate to the processes of transport (see Chapter 7). Similarly, depositional features are unrelated to triggering mechanisms of depositional processes (Einsele et al., 1996).

In classifying a deposit, it is irrelevant whether a given depositional process was triggered by earthquakes, tsunamis, meteorite impacts, or volcanic explosions. Otherwise, the same deposit would be classified differently by different researchers without regard for the physics of depositing flow. First, for example, a deposit with inverse grading, floating mudstone clasts, and planar clast fabric would be interpreted as a *debrite* strictly based on its sedimentary features that exhibit evidence for plastic fluid rheology, laminar flow state, and flow strength (Fisher, 1971; Hampton, 1972; Middleton and Hampton, 1973; Shanmugam, 1996a). Second, the same deposit could be interpreted as a *tsunamite* if it can be documented that debris flows were generated by tsunamis based on historical and circumstantial evidence. Third, the same deposit could also be interpreted as a *seismite* if it can be established that tsunamis, which generated the debris flows, were initially triggered by seismic activity.

The question remains how to classify deep-water deposits that may be related to tsunamis. A simple rule is to classify deep-water deposits as turbidites, debrites, contourites, or other types based on sedimentological criteria. Then, these deposits could be further characterized as 'tsunami-related turbidites,' or 'tsunami-related debrites.' Such a characterization would not only recognize the role of tsunamis, but also would preserve the integrity of process interpretation.

Since the earliest interpretation of fluvial processes by the Greek philosopher Herodotus (born 484 B.C.) (Miall, 1996), fluvial deposits have been interpreted

successfully over the past two millennia without the need for genetic terms, such as *braidite, meanderite,* or *anastomosite* (Shanmugam, 1984). Therefore, genetic (erudite) nomenclatures, such as tsunamite and tempestite, are not prerequisites for geologic interpretations.

5.7.2 Quantification of waves

To resolve the conceptual component of the tsunamite problem, physical aspects of tsunamis, storms, and waves must be quantified and compared, and the link between shallow-water processes and deep-water processes must be established.

5.7.2.1 Wave height
A wave height is the vertical distance between the highest point of a wave crest and a wave trough. However, there are a plethora of definitions of wave height (H) associated with tsunamis (Bryant, 2001). They are H at the source region, H above mean water level (sinusoidal), H at shore, and H at run-up point above present sea level. Run-up wave heights can be thirty times greater than the height of the open-ocean tsunami approaching the shore (Bryant, 2001, p. 98). As a tsunami wave leaves the point of origin (e.g., earthquake epicenter) in the open ocean and approaches the coast, its velocity decreases and wave height increases. Tsunami waves had raised the water level up to 41 m (Johnson, 1919). Based on recent studies, Papadopoulos and Kortekaas (2003) have compiled data on observed wave heights of landslide-generated tsunamis from published sources. These wave heights ranged from 1 to 524 m (Table 5.3). The 524 m height, observed at Lituya Bay in association with the 1958 Alaskan Earthquake (Miller, 1960), represented tsunami run-up height (Bryant, 2001). Wave heights of the 2004 Indian Ocean Tsunami reached up to 15 m (Wikipedia, the free encyclopedia, 2005). The coastline of Sumatra, near the fault boundary, received waves over 10 m tall, while those of Sri Lanka and Thailand received waves over 4 m (NOAA, 2005b). On the other side of the Indian Ocean, Somalia and the Seychelles were struck by waves approaching 4 m in height. Wave height measured from space, 2 hours after the earthquake, reached 60 cm near the east coast of India (Fig. 5.20). On July 17, 1998, a magnitude 7.0 earthquake generated a series of catastrophic tsunami waves that hit the north coast of Papua New Guinea (PNG). Tappin et al. (2001) attributed the PNG Tsunami to submarine slumps. Maximum water level of the PNG Tsunami reached up to 15 m near the Sissano Lagoon (Jaffe, 2005).

The Category 5 (i.e., hurricanes with wind speed > 249 km/h in the Saffir–Simpson Scale) Hurricane Camille hit the Mississippi Gulf Coast on 17th and 18th of August 1969. It had winds up to 94 m/s (338 km/h), a maximum wave height of 22 m, and a diameter of about 650 km (Morton, 1988). Swell, which represents smooth waves beyond the storm center, reaches wave height of 15 m (Shepard, 1973). Supertyphoon Tip in the Pacific Ocean (October 1979) had a

Table 5.3 Observational wave heights of landslide-generated tsunamis. Compiled from several sources (see Papadopoulos and Kortekaas, 2003)

Location of tsunami (Year)	Wave height (m)	Possible cause
Hammerås (1963)	1	slides in loose deposits
Nice (1979)	3	aseismic submarine slide
Eikesdalsvann (1966)	3	aseismic subaerial rock fall
Izmit (1999)	3	seismic coastal slide
Songevann (1935)	3	slides in loose deposits
Nordset (1956)	> 3	slides in loose deposits
Stegane (1948)	3–5?	rock fall
Sokkelvik (1959)	4	slides in loose deposits
Trondheim (1888)	4–5	slides in loose deposits
Kitimat (1975)	5	slides in loose deposits
Aegion (1963)	6	aseismic coastal slide
Skagway (1994)	9–11	slides in loose deposits
Fatu Hiva (1999)	10	aseismic subaerial rockslide
Ravnefjell (1950)	12–15	rock fall
Papua New Guinea (1998)	15	seismic submarine slide
Tjelle (1756)	38	rock fall
Loenvann (1905)	41	aseismic subaerial rock fall
Ravnefjell (1936)	> 49	rock fall
Tafjord (1934)	62	aseismic subaerial rockslide
Loenvann (1936)	74	aseismic subaerial rock fall
Rammerfjell (1731)	77	rock fall
Vaiont (1963)	100	rock fall
Lituya Bay (1958)	524*	seismic subaerial rock fall

*Represents maximum tsunami run-up height above mean sea level (Bryant, 2001, p. 23).

maximum wave height of 15 m and a peak wind velocity of 85 m/s (Dunnavan and Diercks, 1980). One of the highest wind-generated surface waves recorded was 34 m high (Komar, 1976, p. 78).

Allen (1970, p. 159), based on more than 40000 observations, quantified that 45% of normal sea waves are less than 1.2 m in height, 80% are less than 3.6 m high, and 10% exceed a height of 6 m. Allen (1984, p. 32), based on published data, estimated that wave heights would increase with increasing wind speed as follows:

- At a mean wind speed of 0 m/s, wave height would be 0 m.
- At a mean wind speed of 7.5 m/s, wave height would be 1.0 m.
- At a mean wind speed of 16.7 m/s, wave height would be 5.5 m.
- At a mean wind speed of 21.7 m/s, wave height would be 9.0 m.
- At a mean wind speed of 26.8 m/s, wave height would be > 14.0 m.

5.7.2.2 Wavelength
A wavelength is the horizontal distance between two successive wave crests. The wavelengths of tsunamis are hundreds of kilometers long. The Chilean
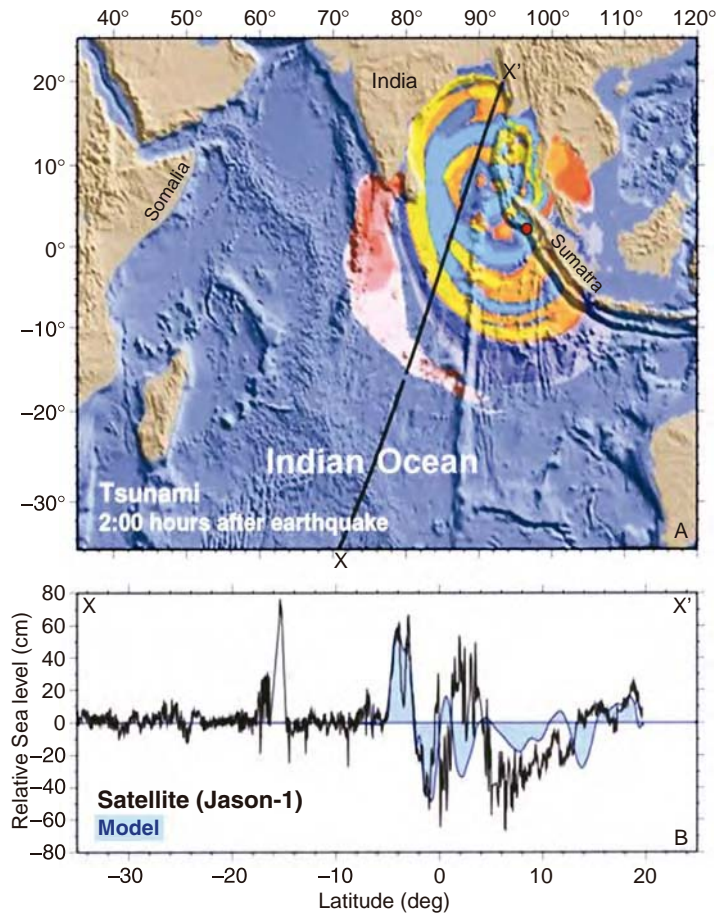
Fig. 5.20. (*A*) **Map showing propagating tsunami waves away from the epicenter (solid dot) of the 2004 Indian Ocean Earthquake on December 26, 2004. The epicenter was located 3.307°N 95.947°E off the west coast of Sumatra. Measurements of sea level were made from space using the Satellite (Jason-1) 2 h after the earthquake. (*B*) Plot of relative sea level along the transect X–X′ (see Fig. 5.20A for location). (Modified after NOAA (2005c).)**

tsunami of 1960 had a wavelength of about 500–800 km (Takahasi and Hatori, 1961). Wavelengths of storms vary from 15 to 75 m, and those of swells range from 300 to 900 m (Friedman and Sanders, 1978). Normal sea waves hitting a California beach have a wavelength of about 150 m (University of Washington, 2005).

5.7.2.3 *Wave period, speed, and duration*
A wave period is the time required for one wavelength to pass a fixed point. According to Bryant (2001, p. 27), tsunamis typically have wave periods of 100–2000 s (1.6–33 min), and this range is called the 'tsunami window.' Tsunamis with longer wave periods of 40–80 min were reported (Takahasi and

Hatori, 1961; their Table 4). In the Pacific Ocean, tsunamis had wave periods of 15–100 min (Apel, 1987).

In the U.S. Virgin Islands, wave periods associated with the 1989 Hurricane Hugo reached 13–16 s (Hubbard, 1992). Normal swells have wave periods of 6 to 14 s, whereas normal sea waves have short wave periods of about 9 s (Friedman and Sanders, 1978).

In the Pacific Ocean, typical wave speeds of tsunamis are 230 m/s (Apel, 1987). Waves of the 2004 Indian Ocean Tsunami traveled at up to 800 km/h (222 m/s) in the open ocean (NOAA, 2005a; USGS, 2005). Travel times of this tsunami ranged from minutes in Sumatra (close to epicenter) to 8 h in Somalia, Africa.

The time a storm takes to cross the continental shelf is called 'shelf duration' (Morton, 1988). Shelf duration was 12 h for the 1969 Hurricane Camille in the Gulf of Mexico and 48 h for the March 1962 storm in the U.S. Atlantic coast (Cooperman and Rosendal, 1962). The 1962 storm was particularly destructive because it lasted more than four spring high tides. In such cases, the potential for destruction increases considerably when the normal astronomical tide combines forces with abnormal meteorological storm events.

5.7.2.4 Sediment transport on the shelf

Aspects of sediment transport by nearshore processes, such as longshore and rip currents, were discussed by Komar (1976). Snedden et al. (1988) concluded that during fair-weather periods, winds cannot generate bottom-current flow sufficient in strength to transport fine sand beyond the shoreface region (i.e., water depths of 0–10 m). In an investigation of sediment transport on the San Pedro continental shelf off Southern California, measurements showed significant bedload transport caused by surface sea waves (maximum wave speeds 10–30 cm/s) at 22 m of water, but no such bedload transport was observed at 67 m of water near the shelfbreak (Karl et al., 1983).

In contrast to sea waves, storm waves can erode and transport sediment in deeper shelf environments at depths of 200 m (Komar et al., 1972). This is because *combined flows*, a combination of unidirectional and oscillatory currents, are powerful storm-generated agents of sediment transport on the shelf (Swift et al., 1986). Butman et al. (1979), using long-term measurements, documented that storm-induced currents were the most significant process in sediment transport on the mid-Atlantic continental shelf.

Tropical Storm Delta (September 3–5, 1973) in the Gulf of Mexico generated alongshore flows with velocities of 200 cm/s and offshore flows with velocities of 50–75 cm/s in 21 m of water (Forristall et al., 1977). A current meter, located 100 km east of the eye of the Hurricane Camille (Mississippi Gulf Coast) in 10 m water, measured near-bottom current velocities up to 160 cm/s (Murray, 1970). Major storms would create near-bottom velocities of about 500 cm/s in 20 m of water and 300 cm/s in 45 m of water (Morton, 1988). At these high velocities,

gravel-sized material would be eroded, transported, and deposited. Direct measurements of storm-related erosion of the shelf floor range from 1 to 2 m (Blumberg, 1964; Herbich, 1977). Both tsunamis (Einsele et al., 1996) and storms (Henkel, 1970) can cause shelf-edge sediment failures that can trigger slumps and sediment flows into deep-water environments.

5.7.2.5 Sediment tansport in submarine canyons

Submarine canyons serve as the physical link between shallow-water and deep-water environments for sediment transport (see Chapters 4 and 6). The origin of submarine canyons by tsunamis was first proposed by Bucher (1940). Chaotic sediments were attributed to deposition from tsunamis in submarine canyons (Bailey, 1940). The possible role of tsunamis in generating deep-water turbidity currents was first suggested by (Kuenen, 1950b) and later emphasized by Coleman (1968).

Tsunamis and storms influence sediment transport in submarine canyons associated with passive-margin and active-margin settings. The Redondo Canyon, for example, commences at a depth of 10 m near the shoreline (see Chapter 6). Such a scenario would allow for a quick transfer of sediment from shallow-water into deep-water environments. In the San Pedro Sea Valley (see Chapter 6), large debris blocks have been recognized as submarine landslides. Lee et al. (2003) suggested that these landslides may have triggered local tsunamis. The significance of this suggestion is that tsunamis can trigger submarine landslides, which in turn, can trigger tsunamis. Such mutual-triggering mechanisms can result in frequent sediment failures in deep-water environments during periods of tsunamis. The problem is that tsunami-generated landslides would not be any different from earthquake-generated landslides. So the volumetric significance of tsunamis–generated landslides may never be realized in the ancient rock record.

Inman et al. (1976) made simultaneous measurements of currents and pressure in the Scripps Submarine Canyon (La Jolla, California), and of winds, waves, and pressure over the adjacent shelf for several years. They measured the strongest down-canyon current at a speed of 190 cm/s at a depth of 44 m. This high-velocity sediment flow was recorded during the passage of a storm front on November 24, 1968 over La Jolla. In the Scripps Canyon, a large slump mass of about 10^5 m^3 in size was triggered by the May 1975 storm (Marshall, 1978). Coarse sand and cobbles up to 15 cm in diameter in micaceous sands were moving down the head of the Scripps Canyon (Shepard et al., 1969). These sands could be interpreted as deposits of sandy debris flows. Shepard et al., (1969, p. 411) attributed these sediment movement to the intensity of winter storms, which moved sediment from the beaches into the heads of the canyons. In addition to these mass movements, submarine canyons are subjected to daily deep-marine tidal currents. Maximum velocities of up- and down-canyon tidal currents commonly ranged from 25 to 50 cm/s (see Chapter 4). Studies showed that internal waves also move up and down submarine canyons (Shepard et al., 1979).

The first quantitative analysis of sediment transport caused by Hurricane Hugo, which passed over St. Croix in the U.S. Virgin Islands on September 17, 1989, in a submarine canyon was made by Hubbard (1992). Hugo had generated winds in excess of 110 knots (204 km/h) and waves 6–7 m in height. In the Salt River submarine canyon (> 100 m deep), a current meter measured net downcanyon currents reaching velocities of 2 m/s and oscillatory flows up to 4 m/s. Hugo had caused erosion of 2 m of sand in the Salt River Canyon at a depth of about 30 m. A minimum of 2 million kg of sediment were flushed down the Salt River Canyon into deep water. The transport rate associated with Hurricane Hugo was 11 orders of magnitude greater than that measured during fair-weather period.

A tsunami with 7–9 m wave height reached St. Croix on 18 November 1867 (Bryant 2001, p.16), but no quantitative data on sediment transport rate are available. In comparison to Hugo with 6–7 m wave height, it is reasonable to expect that the 1867 tsunami with 7–9 m wave height would have generated even higher transport rates in St. Croix. In the Salt River Canyon, much of the soft reef cover (e.g. sponges) had been eroded away by the power of the storm. Debris composed of palm fronds, trash, and pieces of boats found in the canyon were the evidence for storm-generated sediment flows (Hubbard 1992). Storm-induced sediment flows have also been reported in a submarine canyon off Bangladesh (Kudrass et al., 1998), in the Capbreton Canyon, Bay of Biscay in SW France (Mulder et al., 2001), and in the Eel Canyon, California (Puig et al., 2003), among others.

In summary, tsunamis and storms are two genetically unrelated phenomena. In spite of their differences in origin, both tsunamis and storms are remarkably similar in their physical power and in their ability to trigger sediment flows into deep-water environments. Submarine canyons play an important role for focusing sediment transport, but sediment transfer can also occur outside of the canyons.

5.7.3 Depositional model

Tsunami-related deposition in deep-water environments is broadly divided into four stages.

5.7.3.1 Triggering stage

Earthquakes (Fig. 5.21A), volcanic explosions, undersea landslides, and meteorite impacts can trigger displacement of the sea surface causing tsunami waves. The site of triggering mechanisms (i.e., earthquake epicenter, Fig. 5.21A) is unrelated to the ultimate site of deep-water deposition (Fig. 5.21B). In the case of the 2004 Indian Ocean Tsunami, for example, the site of tsunami origin was located in northern Sumatra, whereas the possible site of deep-water deposition would be on the continental slopes of the east coast of southern India (Fig. 5.20A). The tectonic setting of the east coast of India is analogous to the modern passive-margin setting of the U.S. Atlantic Margin with submarine canyons and gullies.
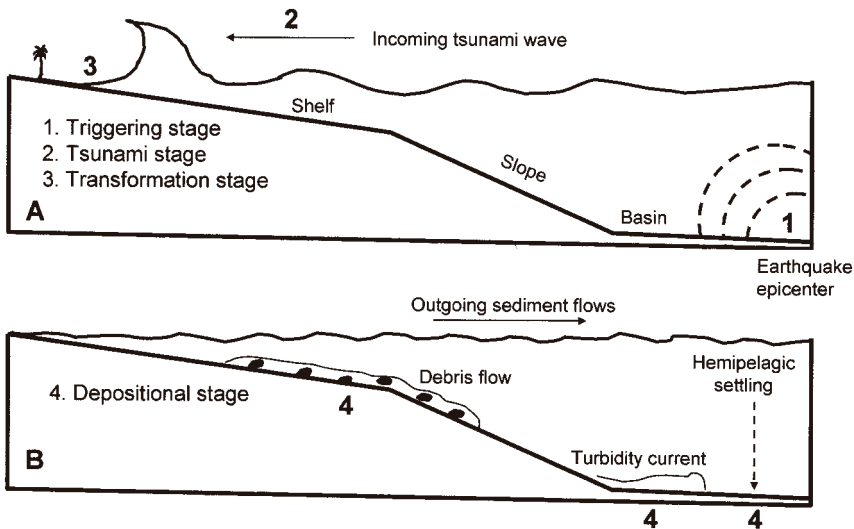
Fig. 5.21. Depositional model showing the link between tsunamis and deep-water deposition. (*A*) 1. *Triggering stage* in which earthquakes trigger tsunami waves. 2. *Tsunami stage* in which an incoming (up-run) tsunami wave increases in wave height as it approaches the coast. 3. *Transformation stage* in which an incoming tsunami wave erodes and incorporates sediment, and transforms into sediment flows. (*B*) 4. *Depositional stage* in which outgoing (backwash) sediment flows (i.e., debris flows and turbidity currents) deposit sediment in deep-water environments. Suspended mud created by tsunami-related events would be deposited *via* hemipelagic settling. (After Shanmugam (2006))

Submarine canyons and feeder channels, common on the east coast of India (Bastia, 2004, his Fig. 7A), are potential conduits for transporting sediment by tsunami-triggered sediment flows into the deep sea. This stage involves neither sediment transport nor deposition.

5.7.3.2 Tsunami stage

Tsunami waves carry energy traveling through the water, but these waves do not move the water. During this transient stage, velocity, wavelength, and wave height of an incoming (run-up) tsunami wave change with time, depth, and proximity to the coast. The incoming wave is depleted in entrained sediment. A theoretical analysis indicates that tsunami waves are unlikely to entrain sediment coarser than fine sand and silt in water depths greater than 200 m (Pickering et al., 1991). This stage is one of wave movement, and it does not involve sediment transport.

5.7.3.3 Transformation stage

As the tsunami wave approaches the coast, it tends to erode and incorporate sediment into the incoming wave. This sediment-entrainment process commences once there is significant frictional interaction with the sea bottom. This transformation occurs when waves of all kinds (i.e., normal sea waves, storm waves, or

tsunami waves) approach the coast. It is called *shoaling transformations* (Friedman and Sanders, 1978). The transformation is evident in numerous videos of the 2004 Indian Ocean Tsunami. The incoming ocean waters are clearly blue in color (implying sediment free), but these waters transform into brown in color near the coast because of their incorporation of sediment. The transformation to brown color is the result of the wave breaking, and the wave will break in different water depths according to its wavelength and sea-floor irregularities. The outgoing sediment-rich waters invariably carry a large amount of sediment and assorted debris. Such a transformation of tsunami waves into sediment-rich flows is somewhat analogous to gravity-flow transformation (Fisher, 1983). The outgoing sediment flows should no longer be considered as tsunami waves.

5.7.3.4 Depositional stage
The outgoing sediment flows would generate not only debris flows and turbidity currents, but also suspended clouds of mud resulting in hemipelagic settling (Fig. 5.21B). These sediment flows are the primary depositional processes in deep-water environments. In terms of depositional features, tsunami-generated debrites and turbidites would not be any different from earthquake-generated debrites and turbidites.

5.8 Synopsis

Recognition of sand injectites is vital for developing realistic reservoir models for producing petroleum. A popular myth is that tsunami waves can deposit sediment directly in deep-water environments. The reality is that tsunami-related deposition in the deep sea can commence only after the transformation of tsunami waves into sediment flows. These sediment flows already have established names (e.g., debris flow and turbidity current). Deposits of these processes are recognized on the basis of their sedimentary features. These deposits already have established names (e.g., debrite and turbidite). Thus the term tsunamite is obsolete. Considering the high frequency of tsunamis (Gusiakov, 2005), tsunami events can be important controlling factors of deep-water deposition similar to periods of falling sea levels (e.g., Shanmugam and Moiola, 1982).

This Page Intentionally Left Blank

Chapter 6

Depositional environments

6.1 Introduction

The objective of this chapter is to analyze modern deep-water systems for reconstructing ancient deep-water environments using the principle of *Uniformitarianism*. A depositional environment is a specific geomorphic setting with characteristic physical, chemical, and biological processes and their products. Modern deep-water depositional environments are discussed under six broad categories: (1) deep-lacustrine environments; (2) submarine slope environments; (3) submarine canyon and gully environments; (4) submarine fan environments; (5) submarine non-fan environments; and (6) submarine basin-plain environments. Selected ancient examples are discussed in demonstrating depositional similarities between modern and ancient systems. The term 'modern' is used here to refer to present-day deep-water systems that are still active or that have been active since the Quaternary period.

6.2 Deep-lacustrine environments

Deep-lacustrine environments are similar to deep-marine environments in terms of gravity-driven downslope processes and bottom currents. Deep and large lakes of the world were discussed by Herdendorf (1990). Some large lakes are remarkably deep with a maximum depth of 1637 m (Table 6.1). In continental rift basins, deep lakes originate during an early phase of rift history (Lambiase, 1990).

6.2.1 Modern Lake Baikal, South-Central Siberia

Lake Baikal is located in the central part of the tectonically active Baikal Rift Zone in South-Central Siberia. This lake, the world's deepest (1637 m), is 636 km long and 79 km wide. This voluminous lake (23000 km³) contains approximately 20% of the world-wide reserve of fresh water (salinity 0.76%) (Galaziy, 1993). Basin-fill deposits may be as old as late Cretaceous and up to 8000 m thick (Vanneste et al. 2001). The upper hundreds of meters of these deposits consist

Table 6.1 The world's deepest lakes. (Source: National Park Service, U.S. Department of the Interior. Uniform Resource Locator (URL): http://www.nps.gov/crla/brochures/deeplakes.htm (accessed June 15, 2004))

Rank	Lake	Location	Depth
1	Baikal*	Siberia, Russia	5369 ft (1636 m)
2	Tanganyika	Africa (Tanzania, Zaire & Zambia)	4708 ft (1435 m)
3	Caspian Sea	Iran and Russia	3104 ft (946 m)
4	Nyasa	Africa (Mozambique, Tanzania & Malawi)	2316 ft (706 m)
5	Issyk Kul	Kyrgizstan, Central Asia	2297 ft (700 m)
6	Great Slave	Northwest Territories, Canada	2015 ft (614 m)
7	Crater Lake	Oregon, U.S.A.	1943 ft (592 m)
8	Lake Tahoe*	California & Nevada, U.S.A.	1685 ft (514 m)
9	Lake Chelan	Washington, U.S.A.	1419 ft (433 m)
10	Great Bear	Northwest Territories, Canada	1356 ft (413 m)
11	Lake Superior	Canada & U.S.A.	1333 ft (406 m)
12	Titicaca	Peru	1214 ft (370 m)
13	Pend Oreille	Idaho, U.S.A.	1150 ft (351 m)

*Discussed in this book.

of alternations of interglacial diatomaceous muds and glacial turbidite layers (Nelson et al., 1998). Aspects of gas hydrate-bearing sediments in Lake Baikal were discussed by Vanneste et al. (2001).

6.2.2 Modern Lake Tahoe, California–Nevada border

Using high-resolution multibeam mapping system, a bathymetric survey of Lake Tahoe was made (Gardner et al., 2000). The lake has steep margins on the western (McKinney Bay), northern, and eastern sides, and a relatively gentle margin on the southern side (Fig. 6.1). The lake is characterized by a narrow, flat nearshore zone, a steep slope that plunges more than 400 m, and a flat lake floor. On the western margin of the lake, off McKinney Bay, the slope varies from 30 to > 70°. A major debris tongue, with a width of 7.5 km and a length of 9 km, occurs just immediately downdip of a scarp in the McKinney Bay area (Fig. 6.2). This debris tongue has a pronounced 5–m high arcuate toe. Downdip of the debris tongue, large debris blocks (1000 m long, 400 m wide, and 80 m high) are scattered on the flat lake floor. These blocks have been interpreted as part of a major debris avalanche. They were triggered by a failure on the western margin about 300 Ka. Also, coalescing of subaqueous debris cones (i.e., bajadas) has been observed (Gardner et al., 2000, their Fig. 8). These researchers stated, '*Sediment transport processes following the debris avalanche created a series of sinuous channels that funneled sediment across the hummocky reaches of the upper debris-avalanche field toward the center of the basin….*'

The channels are 100 m wide, 1–2 m deep, and more than 3.8 km long. The exact origin of these sinuous channels is unclear.
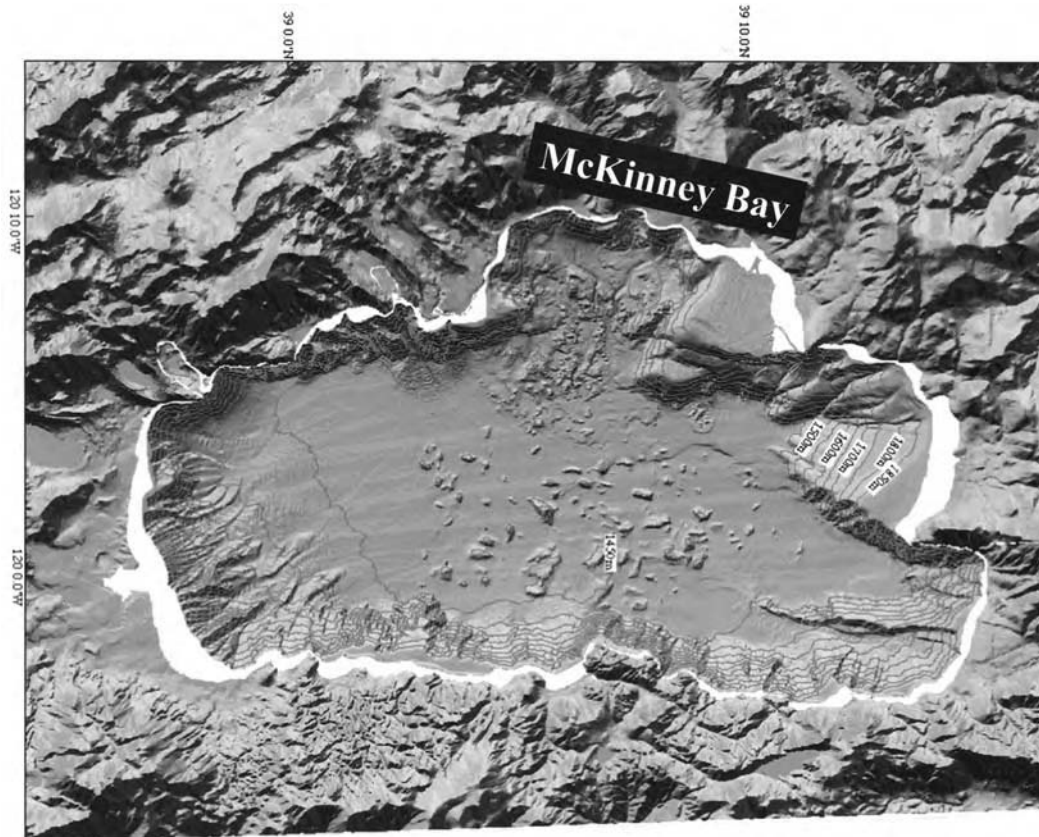
Fig. 6.1. Shaded-relief surface of Lake Tahoe (California-Nevada border) and surrounding land. Contour intervals (50 m) represent elevation above sea level. Maximum lake depth is about 450 m. White zone indicates nearshore environment. (After Gardner et al. (2000). Credit: U.S. Geological Survey. Uniform Resource Locator (URL): http://wrgis.wr.usgs.gov/dds/dds-55/pacmaps/lt_shd.htm (accessed June 15, 2004).)
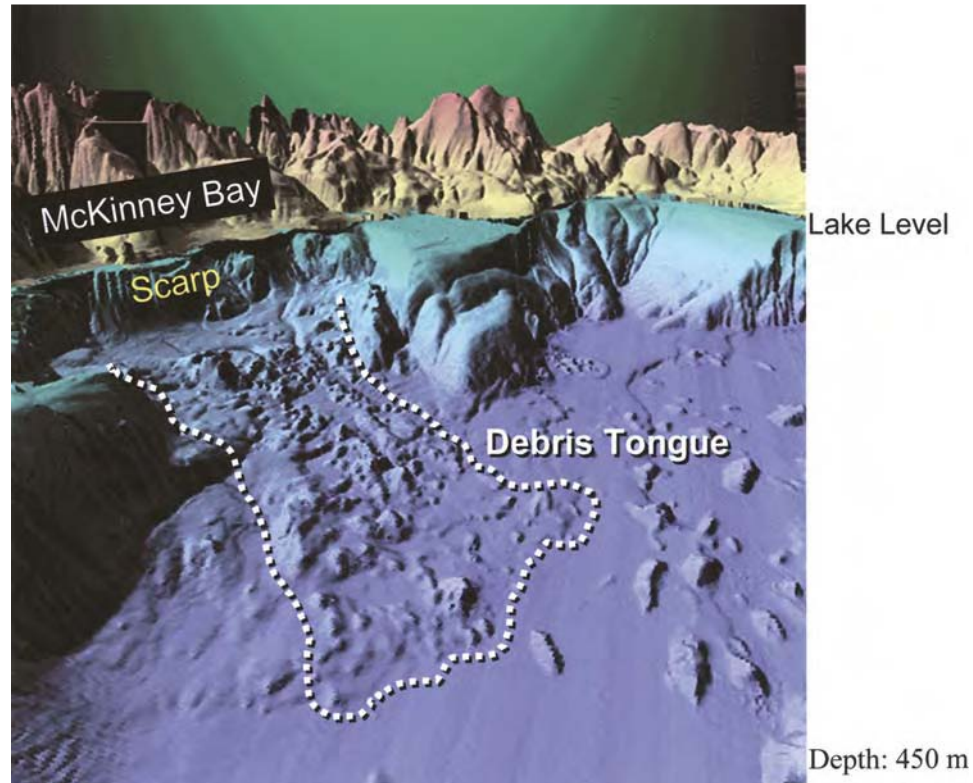
Fig. 6.2. Oblique view of western side of Lake Tahoe and surrounding mountains looking towards the northwest (California). Underwater section is in blue tones and land is in brown tones. View shows large failure on the western lake margin, off McKinney Bay. Debris tongue (dashed line) is 7.5 km wide and 9 km long. Thin distal area is about 15 m thick, large blocks within the debris tongue are up to 20 m high. Top of the failure is at about 1635 m and toe of the debris tongue is at 1434 m elevation above sea level. Vertical exaggeration is 5x. See Gardner et al. (2000) for details. (Credit: U.S. Geological Survey. Uniform Resource Locator (URL): http://wrgis.wr.usgs.gov/dds/dds-55/pacmaps/lt_persp.htm (accessed June 15, 2004).)

On the middle of the floor of the lake basin there are topographic mounds. These mounds, according to Hyne et al. (1973), are the result of mass wasting that occurred on the western margin off McKinney Bay. This mass wasting has been attributed to collapse of ice dams. The occurrence of deep-water mounds by mass wasting is of importance for developing deep-water exploration models. This is because basin-floor fans, formed by turbidites, are also considered to exhibit mounded geometry in seismic profiles (see Chapter 10).

6.2.3 Deep-lacustrine basin, Cretaceous, South Gabon

The Lucina Formation, offshore South Gabon, is composed of deep-water facies deposited in an early Cretaceous syn-rift lake (Smith, 1995). Deep-lacustrine sands in this basin constitute principal reservoirs in the Lucina and Lucina West Marine fields. Smith (1995, p. 201) recognized five depositional facies:

(1) Facies 1, composed of clean sandstone, was interpreted as '*En masse deposition from high-concentration cohesionless sediment gravity flows due to intergranular friction.*' This process is analogous to grain flows with plastic rheology (Fig. 3.10).
(2) Facies 2, composed of muddy sandstone, was interpreted as '*En masse deposition from high-concentration mud-rich sediment gravity flows.*' This process is analogous to sandy debris flows (Fig. 3.10).
(3) Facies 3, composed of massive siltstone, was interpreted as '*En masse deposition from high-concentration mud-rich sediment gravity flows.*' This process is analogous to muddy debris flows (Fig. 3.10).
(4) Facies 4, composed of thinly-bedded laminated sandstone, was interpreted as '*Suspension fallout from dilute turbidity currents followed by tractional reworking.*' This is analogous to both turbidity currents and bottom current reworking.
(5) Facies 5, composed of mudstone, was interpreted as '*Suspension fallout from dilute silt-mud turbidity currents.*' This is analogous to turbidity currents (see Chapter 3).

Smith (1995, his Fig. 8) interpreted these facies as channel-lobe turbidite packages and proposed a conventional submarine fan model. However, the term *en masse* implies sudden deposition of entire body of sediment by plastic flows, not settling of individual particles from Newtonian turbidity currents. In the conventional fan model, lobes are deposits of turbidity currents, not those of debris flows (see Chapter 9).

6.3 Submarine slope environments

Submarine slopes are considered to be that inclined part of the sea floor between the shelf-slope break and the basin floor (Fig. 1.3). Modern continental slopes

around the world average about 4° (Heezen et al., 1959), but slopes can range from less than 1° to greater than 40°. Slopes on active margins (e.g., California and Oregon) are relatively steeper than those on passive margins (e.g., Louisiana). Regional slopes off the United States are as follows (Pratson and Haxby, 1996):

(1) New Jersey–Maryland: 2.5°
(2) Florida: 4.4°
(3) Louisiana: 0.5°
(4) California: 1.8°
(5) Oregon: 2.0°

6.3.1 Modern Los Angeles Margin, California

Bathymetric survey of the Los Angeles Margin (Fig. 6.3), based on high-resolution multibeam mapping systems, shows:

  (1) Well-developed shelf, slope, and basin environments
  (2) Steep and eroded continental slope off the Palos Verdes Peninsula
  (3) Gullied upper slope
  (4) Major submarine canyons on the slope
  (5) Redondo Canyon with its canyon head at very shallow water (less than 10 m)
  (6) Sinuous Santa Monica and Redondo (Haner, 1971) submarine canyons
  (7) Braided Newport Canyon
  (8) Side-by-side occurrence of the sinuous San Gabriel canyon and braided Newport canyons near the shelf edge at steep gradients
  (9) Occurrence of mass-transport deposits at the toe of Redondo, San Gabriel, and Newport submarine canyons
(10) Large debris blocks in the San Pedro Sea Valley.

   Large debris blocks, seen on the basin floor, were shed off the walls of the San Pedro Sea Valley during underwater landslides (Gardner et al., 2002, their Figure 4). These debris fields extend up to 10 km beyond the base of the slope along the Palos Verdes Margin (Lee et al., 2003). Large-scale debris flows have been active on the slope and base-of-slope environments of the Los Angeles Margin.

6.3.2 Modern East Breaks area, Gulf of Mexico

In the northern Gulf of Mexico, the principal factors that controlled sea-floor topography in intraslope minibasins during the Tertiary were: (1) salt tectonics; (2) compression; and (3) strike slip along thin-skinned transfer zones (Apps et al., 1994). Among these factors, salt withdrawal and diapirism have been particularly important. These two factors have resulted in a sea-floor topography of the modern continental slope that is quite complex in terms of shape and relief (Fig. 6.4).
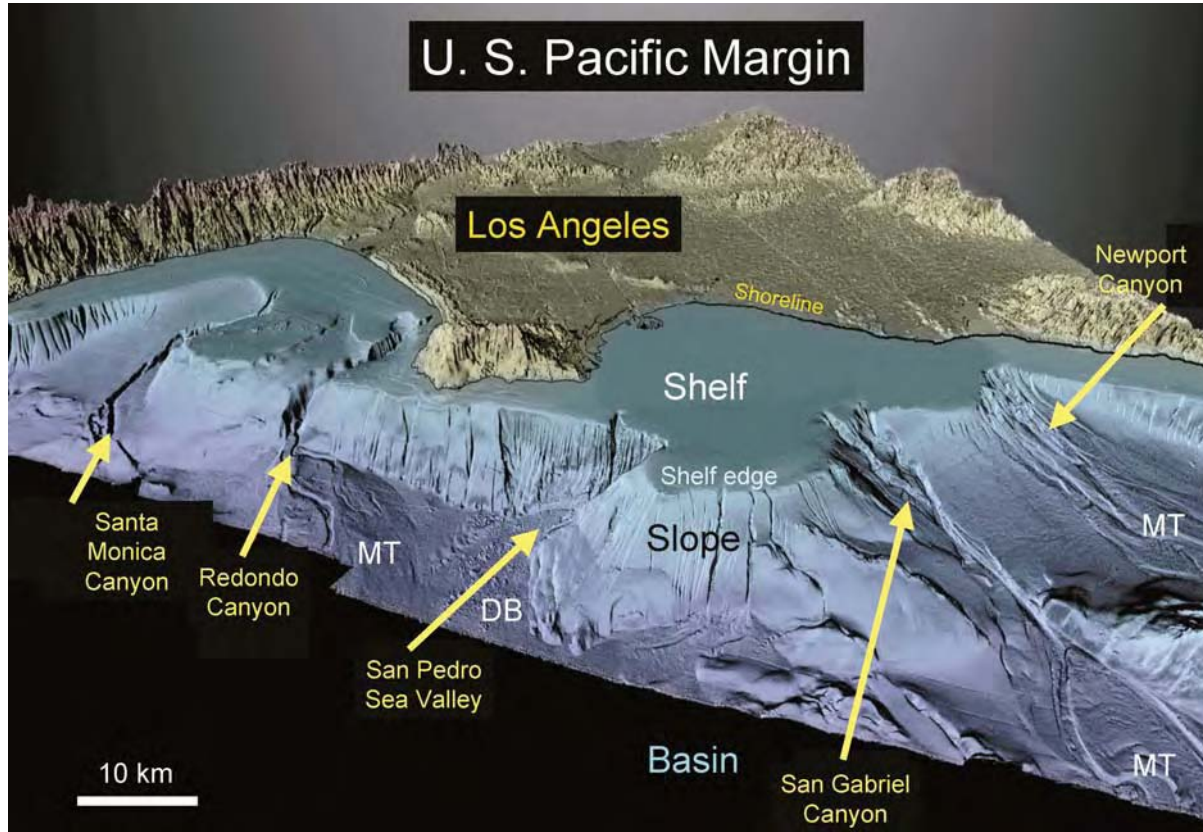
Fig. 6.3. **Perspective view of Los Angeles Margin bathymetry looking towards the northeast. The canyon head of the Redondo Canyon is at a water depth of 10 m near the shoreline. Note side-by-side occurrence of sinuous San Gabriel canyon and braided Newport canyons near the shelf edge at steep gradients. MT = Mass transport deposits. DB = debris blocks. Vertical exaggeration is 6x. (Credit: Gardner et al. (2002) and U.S. Geological Survey. Uniform Resource Locator (URL): http://wrgis.wr.usgs.gov/dds/dds-55/pacmaps/la_pers2.htm (accessed June 15, 2004).)**
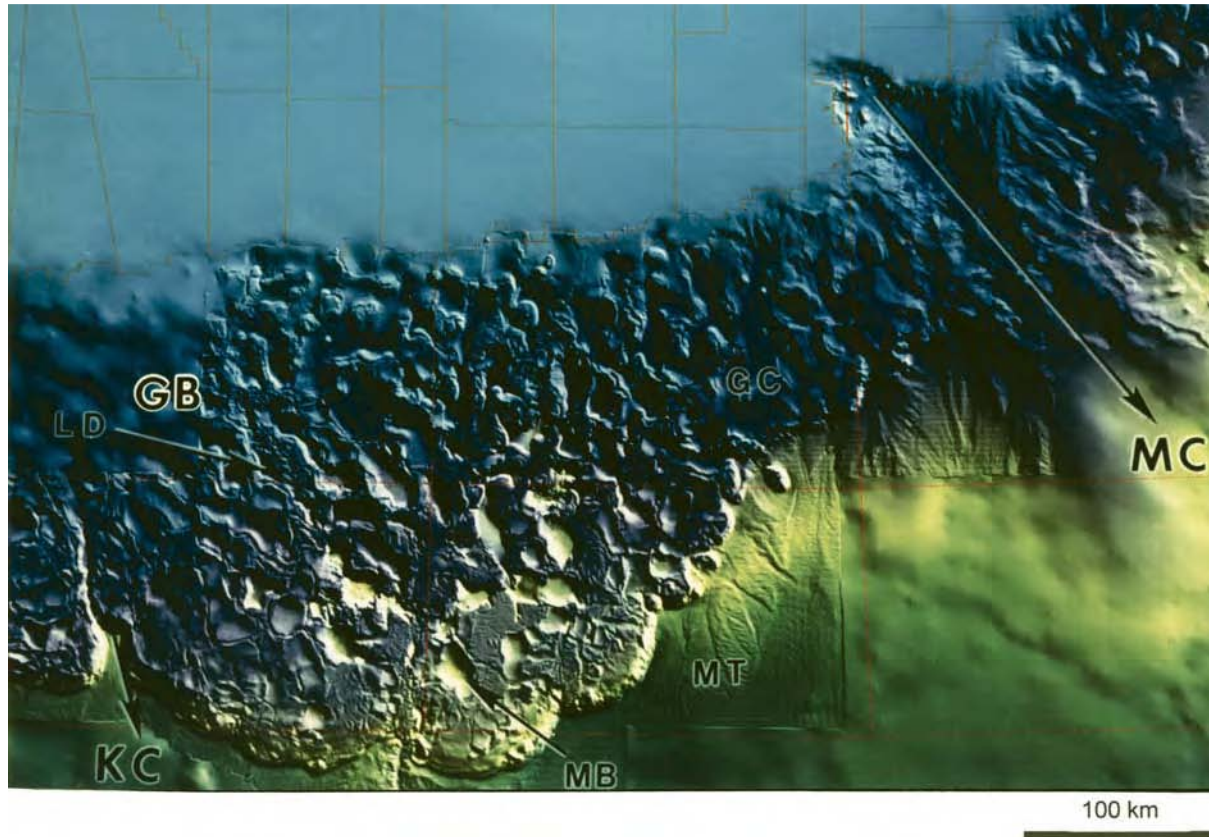
Fig. 6.4. 3-D perspective of modern Gulf of Mexico intraslope basins based on high-resolution bathymetric swath data. Note highly irregular sea-floor topography controlled by salt tectonics. Basins commonly range in width from 10 to 20 km. GB = Garden Banks area, GC = Green Canyon area, MT = Mass Transport (slide/slump/debris flow), MB = Mini Basin, LD = Linear Depression, MC = Mississippi Canyon, and KC = Keathley Canyon.

In addition to this complexity, a variety of depositional processes played a major role in controlling sand distribution in intraslope basins.

Piston cores taken during the Ida Green cruise, which covered East Breaks and Garden Banks blocks in the northern Gulf of Mexico (Fig. 6.5), were described for understanding the depositional origin and distribution of sand and mud. These cores are composed of Holocene–Pleistocene age sediments. The cores are composed of the following depositional facies (Table 6.2):

(1) Facies 1: contorted sand with mudstone clasts (sandy slumps and debris flows) (Fig. 6.6).
(2) Facies 2: contorted mud with mudstone clasts (muddy slumps, debris flows, and sand injections) (Fig. 6.7).
(3) Facies 3: laminated and rippled fine-grained sand (bottom current reworking) (Fig. 6.8).
(4) Facies 4: normally graded mud (muddy turbidity currents).
(5) Facies 5: laminated and bioturbated mud (pelagic and hemipelagic settling).

Deposits of muddy slump and debris flow and the pelagic/hemipelagic settling are the most dominant facies in the study area (Table 6.2). Deposits of sandy debris flow are present in the East Breaks, Alaminos Canyon, and Walker Ridge blocks (Table 6.2).

A major submarine mass-transport feature was recognized in the East Breaks area by Rothwell et al. (1991) and by McGregor et al. (1993). These authors labeled this feature as the 'East Breaks Slide' (Fig. 6.9A). This feature can be seen on high-resolution subbottom profiles (10–kHz) as a mounded geometry (Fig. 6.9B). It is up to 180 m thick, 3–24 km wide, and over 80 km long (Woodbury et al., 1978). The term 'slide' was used loosely for various gravity-driven processes, such as slides, slumps, and debris flows (Fig. 6.9).

In the East Breaks area, Rothwell et al. (1991) recognized two distinct debris tongues (west and east) (Fig. 6.10A). These features originated on the upper slope (200–1000 m) in front of a sandy shelf-margin delta, where the gradient is up to 3°, and were deposited in the middle slope position (1000–1500 m) where the gradient is 0.5°.

Core samples taken from the western tongue (core hole 14–6, Woodbury et al., 1978), show contorted bedding and irregular sand lenses indicative of deposition from debris flows and slumps (Fig. 6.10B). Such deposits would be classified as Facies 1 and 2 (discussed above). The tongue-like patterns of debris flows in the Gulf of Mexico are strikingly similar to those formed in flume experiments and those recognized on the Norwegian continental margin (see Chapter 12).

Sandy debrites, with a thickness of 2 m, have been recognized (Fig. 6.6). This is surprising because modern deep-water slope environments are generally considered to be a mud-rich realm because of the present highstand of sea level. Such sandy
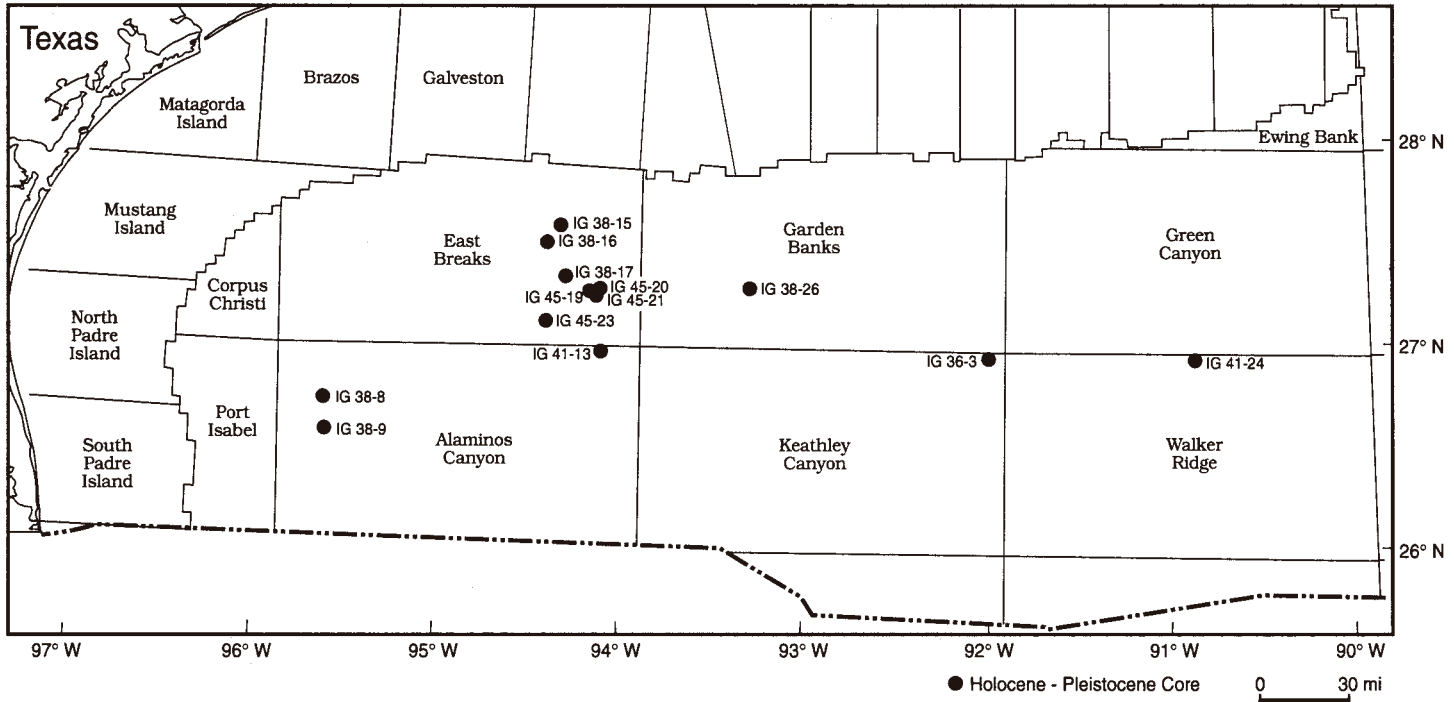
Fig. 6.5. Map showing location of piston cores (Holocene–Pleistocene), taken during the Ida Green Cruise (IG) under Shipboard Scientist W. E. Behrens (University of Texas at Austin), from the Gulf of Mexico. In June 1995, cores were described at the Ocean Drilling Program's Gulf Coast Repository in College Station, Texas.

Table 6.2 Distribution of facies in the cores taken during the Ida Green (IG) cruise, Holocene–Pleistocene, Gulf of Mexico

Cruise #	Core thickness (cm)	Facies 1 (%)	Facies 2 (%)	Facies 3 (%)	Facies 4 (%)	Facies 5 (%)	Mixed facies (%)
IG 38–15 (EB)	526	4	8			65	1/2/3/5:23
IG 38–16 (EB)	918		46			42	1/3/4/5:12
IG 38–17 (EB)	846		55			30	2/3/5:15
IG 45–19 (EB)	340		65			35	
IG 45–20 (EB)	363	61	39				
IG 45–21 (EB)	819		5			69	5/3:8 2/5/3:18
IG 45–23 (EB)	743		73			27	
IG 38–8 (AC)	387	34	7			47	3/5:12
IG 38–9 (AC)	442	25		2		73	
IG 41–13 (AC)	415		49			51	
IG 38–26 (GB)	666		100				
IG 36–3 (KC)	686		53				2/5:47
IG 41–24 (WR)	620	15	11			62	2/5:12

Blocks:
EB = East Breaks Block
AC = Alaminos Canyon Block
GB = Garden Banks Block
KC = Keathley Canyon Block
WR = Walker Ridge Block

intervals imply a potential for a sand-prone environment in intraslope basins even during periods of highstands.

6.3.3 Modern Beaumont Basin, Gulf of Mexico

Beaumont Basin, an intraslope basin (Fig. 6.11), is located on the northwest continental slope of the Gulf of Mexico at a depth of about 2000 m (Tripsanas et al., 2004). It is characterized by a nearly square shape (16 × 18 km), high relief (600–850 m), and steep gradients (4–14°). A 4.4 m long piston core (JPC–07) taken from the Beaumont Basin is composed of five facies (Tripsanas et al., 2004, their
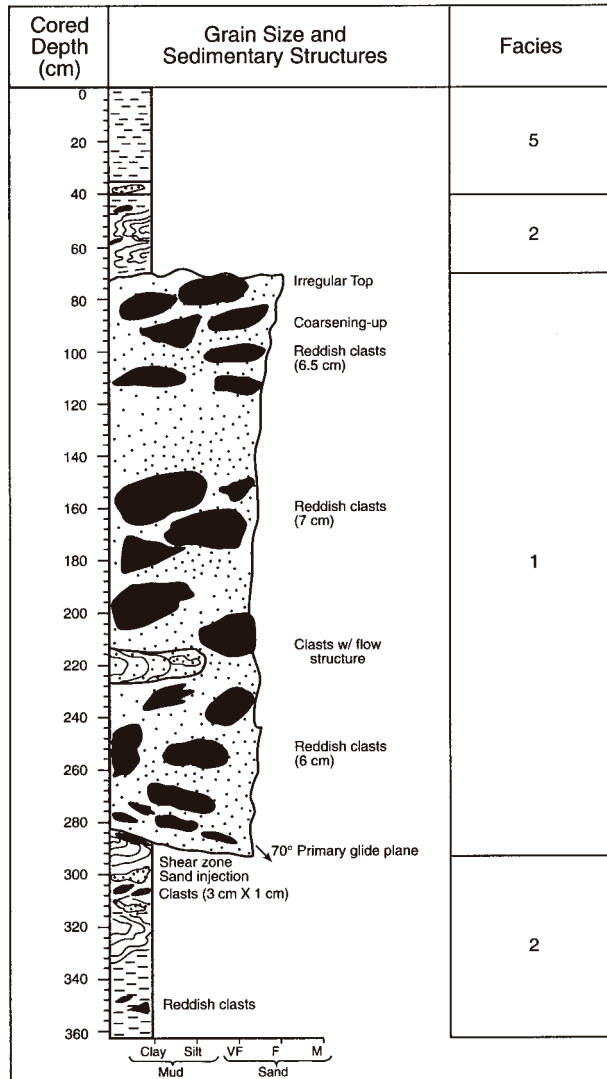
Fig. 6.6. Sedimentological log showing Facies 1, 2, and 5. Note thick interval of sand with floating mudstone clasts (Facies 1). IG 45–20, East Breaks area, Holocene–Pleistocene, Gulf of Mexico. Water depth: 1416 m. IG45 = Ida Green Cruise # 45. Facies 1: Deposits of sandy debris flow and slump. Facies 2: Deposits of muddy debris flow and slump. Facies 3: Deposits of bottom current reworking. Facies 4: Deposits of turbidity currents. Facies 5: Deposits of pelagic and hemipelagic settling. (See Fig. 6.5 for location map.)

Fig. 9, p. 813). I have quantified these facies. Accordingly, these facies in ascending order are: (1) debrite with big clasts and boulders (29%); (2) clast-dominated debrite (32%); (3) highly sheared plastic debrite (16%); (4) clast-dominated debrite (14%); and (5) turbidite (9%). In other words, this core is composed of 91% debrite and 9% turbidite facies. A 7.5–m long piston core (JPC–06)
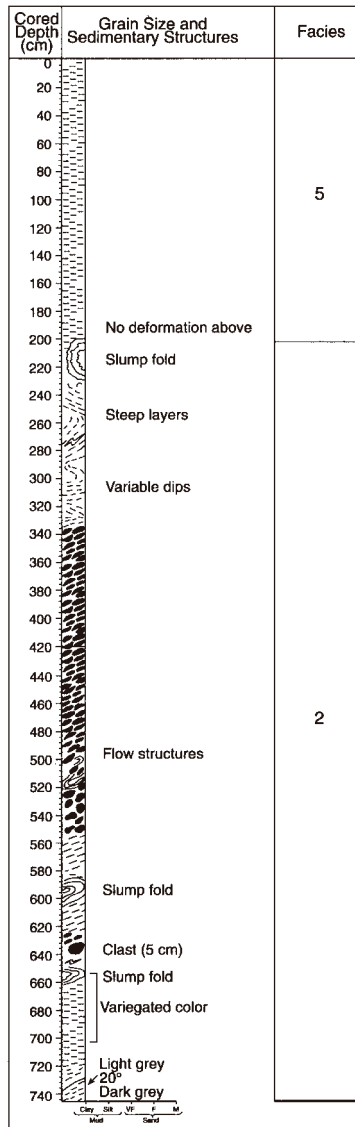
Fig. 6.7. Sedimentological log showing Facies 2 and 5. Note thick interval of contorted mud (Facies 2) and undeformed, laminated mud (Facies 5). IG 45–23, Holocene-Pleistocene, East Breaks area. Water depth: 1767 m. IG 45 = Ida Green Cruise # 45. (See Fig. 6.5 for location map and Fig. 6.6 for explanation of facies.)

from the basin is composed of 78% debrite and 22% hemipelagite (Tripsanas et al., 2004, their Fig. 9, p. 813). The abundance of slumps, slides, and debris flows in the Beaumont Basin has been attributed to the oversteepening of the flanks by the seaward mobilization of underlying salt masses (Tripsanas et al., 2004, p. 801).
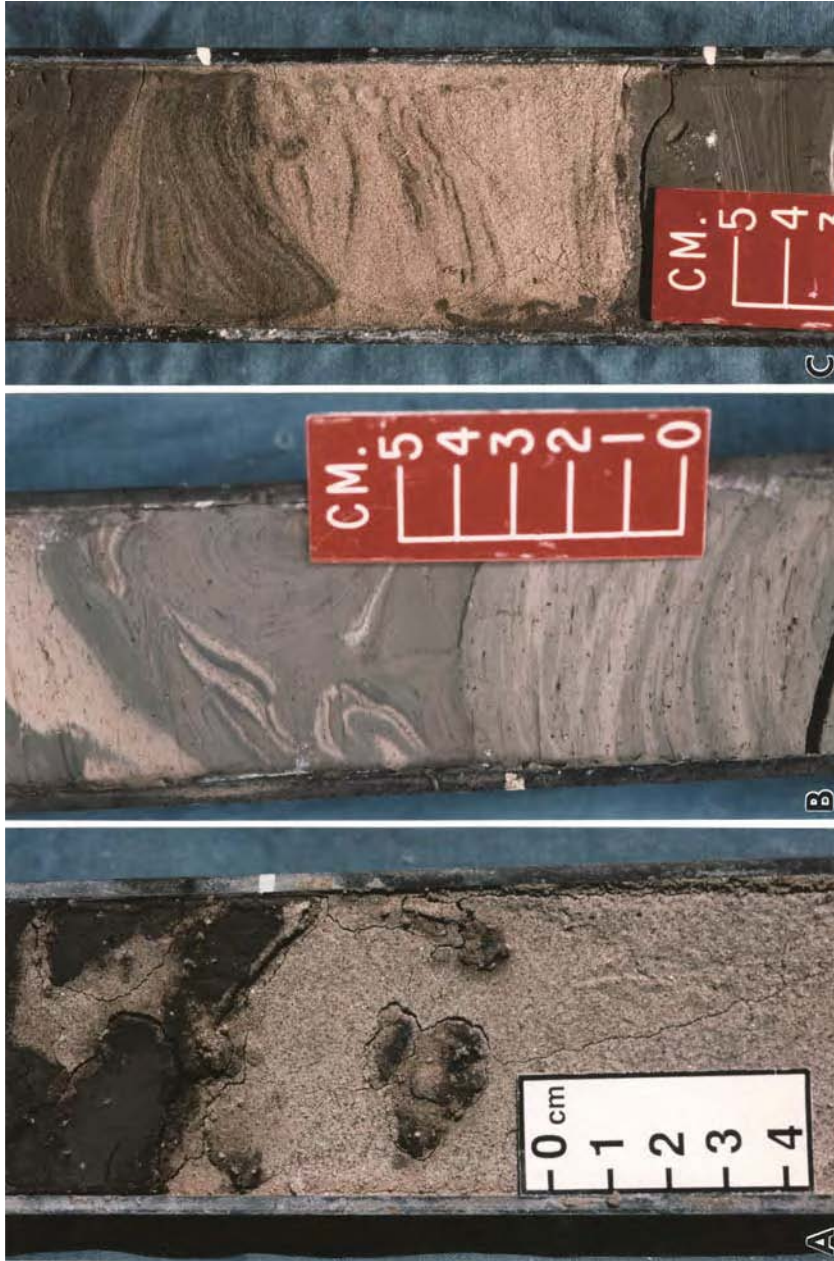
Fig. 6.8. (*A*) Core photograph showing floating mud clasts (black) in fine-grained sand (Facies 1), IG 45–20, 120 cm. (*B*) Core photograph showing contorted mud (Facies 2), IG 36–3, 430 cm. (*C*) Core photograph showing ripple laminae with some deformation in very fine-grained sand (Facies 3), IG 38–17, 260 cm. (See Fig. 6.5 for location map and Fig. 6.6 for explanation of facies. Photos by G. Shanmugam. Photos used with permission, GIB project, The University of Texas at Austin, Institute for Geophysics.)
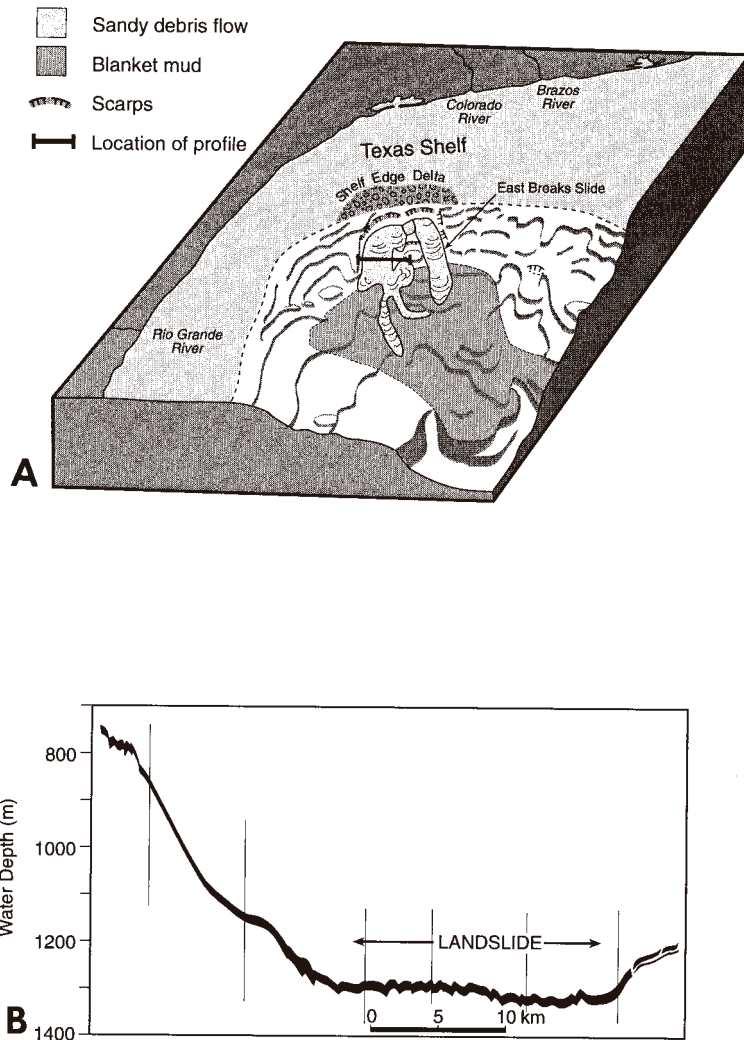
Fig. 6.9. (*A*) The 'East Breaks Slide' composed of sandy debris flows with tongue-like geometry, Gulf of Mexico. (*B*) High-resolution subbottom profile (10–kHz) of the western tongue (see location of profile in *A*) showing irregular and mounded geometry. Note the authors used the term 'landslide' for sandy debris flow. (After Rothwell et al. (1991). Reprinted by permission of the American Association of Petroleum Geologists whose permission is required for further use.)

6.3.4 Green Canyon 65 Field, Plio-Pleistocene, Gulf of Mexico

Green Canyon 65 Field (Bullwinkle Prospect) is located in a salt-withdrawal minibasin of Plio-Pleistocene age. Holman and Robertson (1994, their Fig. 10) proposed the conventional submarine fan model of Mutti and Ricci Lucchi (1972) for this reservoir. However, the Mutti-Ricci Lucchi fan model is designed
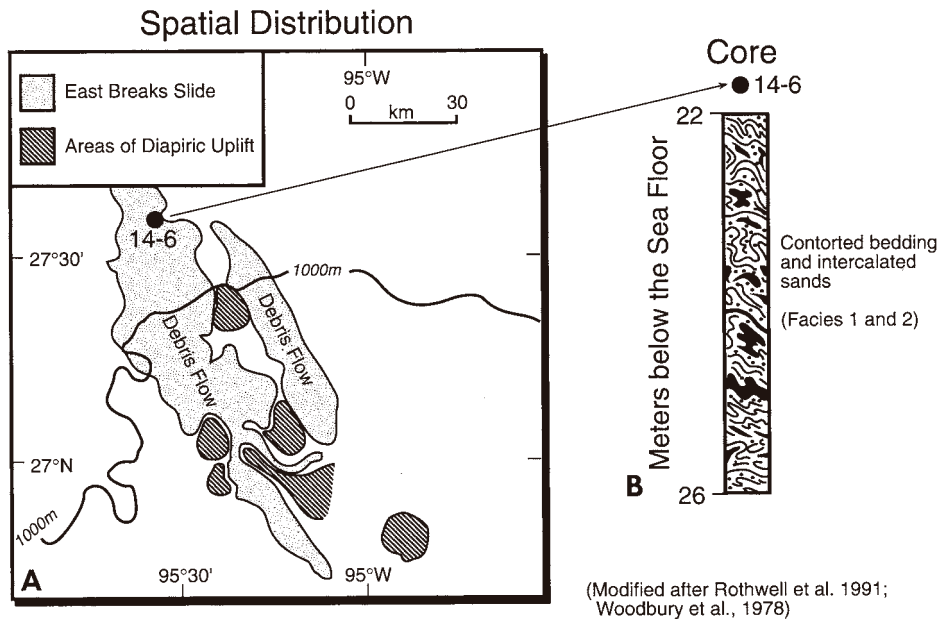
Spatial Distribution

(Modified after Rothwell et al. 1991;
 Woodbury et al., 1978)

Fig. 6.10. (*A*) Two debris-flow tongues of the 'East Breaks slide.' Modified after Rothwell et al. (1991). (*B*) Core taken from the western tongue is composed of contorted sand and mud (Facies 1 and 2). Note that the Ida Green Cruise cores also show Facies 1 and 2. Position of core 14–6 is shown by a solid dot on the western tongue. (See Fig. 6.6 for explanation of facies. From Woodbury et al. (1978). Reprinted by permission of the American Association of Petroleum Geologists whose permission is required for further use.)

for base-of-slope unconfined settings, not for salt-withdrawal intraslope mini-basins. More importantly, the conventional fan model is designed for turbidite-dominated systems, not debrite-dominated systems (see Chapter 9). In spite of convincing evidence for the dominance of slumps and debrites in the modern slope settings of the Gulf of Mexico (e.g., Woodbury et al., 1978; Rothwell et al., 1991; McGregor et al., 1993; Shanmugam and Zimbrick, 1996; Tripsanas et al., 2004), most exploration geoscientists continue to adopt turbidite fan models.

6.3.5 Auger Field, Miocene–Pliocene, Gulf of Mexico

The Auger Field is located in the Garden Banks 427, 470, and 471 blocks of the Gulf of Mexico. The distribution of Miocene–Pliocene reservoir sands in the Auger Field has been attributed to deposition from turbidity currents (McGee et al., 1994; Bilinski et al., 1995). McGee et al. (1994, their Fig. 8) proposed three reservoir types, namely, (1) amalgamated nonleveed channels deposited in shingles; (2) amalgamated sheet sands; and (3) layered sheet sands. These three types simply represent upper, middle, and lower fan environments in the conventional fan model.
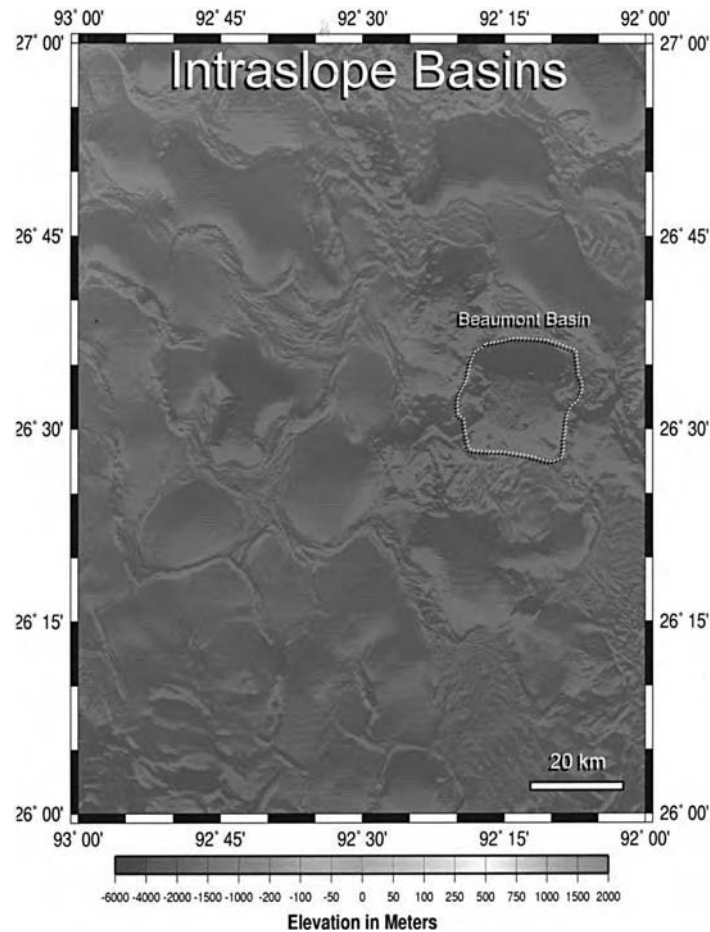
Fig. 6.11. High-resolution shaded relief image of bathymetry of the Beaumont Basin, located in the eastern part of Keathley Canyon block, Gulf of Mexico (see Tripsanas et al., 2004). Note highly irregular seafloor topography caused by salt tectonics. (Credit: NGDC (National Geophysical Data Center) Coastal Relief Model Vol. 04 Shaded Relief Images, NOAA Satellites and Information. Uniform Resource Locator (URL): http://www.ngdc.noaa.gov/mgg/coastal/grddas04/html/ gna27093.htm (accessed July 3, 2004).)

Although the 'S' Sand has been interpreted as deposits of turbidity currents, it shows planar clast fabric and rafted mudstone clasts (McGee et al., 1994, p. 247; Bilinski et al., 1995, their Figs. 9 and 10). This implies emplacement by laminar flows diagnostic of debris flows, not turbidity currents. As discussed earlier, study of piston cores from the Holocene–Pleistocene age in the Garden Banks Block suggests a dominance of slumps and debrites (see Table 6.2). These examples suggest that debris flows and slumps have been active in the Garden Banks area since the Miocene.

6.3.6 Agat region, Cretaceous, offshore Norway

A regional sedimentological study of Cretaceous sequences in the Mid-Norway region of the Norwegian Sea and in the Agat region (Gulbrandsen, 1987) of the northern North Sea was carried out (Shanmugam et al. 1994). In this section, results of the Agat study are summarized (Fig. 6.12). Cored intervals from the Agat region have been grouped into six lithofacies (Table 6.3):

(1) Facies 1: Contorted conglomerate and pebbly sandstone, amalgamated units, steep layers (Fig. 6.13), floating mudstone clasts, erosional bases, and fining-up trends (sandy slumps /debris flows, possibly in a channel setting).
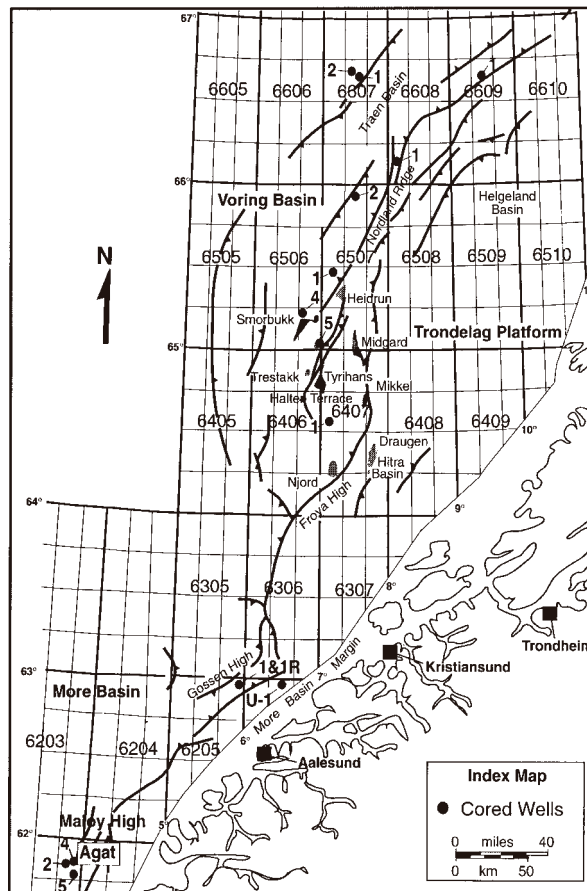

Fig. 6.12. Map showing the location of cored wells in the Mid-Norway (north of 62°) and Agat (south of 62°) regions, offshore Norway. (After Shanmugam et al. (1994). Reprinted by permission of the American Association of Petroleum Geologists whose permission is required for further use.)

Table 6.3 Distribution of lithofacies and other properties in the Agat Formation, Offshore Norway. (After Shanmugam et al. (1994))

Features	Saga 35/3–2		Saga 35/3–4		Saga 35/3–5	
Facies	m	%	m	%	m	%
1					0.30	0.46
2	26.90	46.00	49.40	53.60	48.20	74.38
3					1.90	2.93
4	1.70	2.90	1.10	1.20	3.90	6.01
5					0.80	1.23
6	0.10	0.20			0.40	0.61
1&2					1.70	2.62
3&6	29.80	50.90	39.40	42.78	6.50	10.03
4&2	0.10	0.20	2.00	2.20	1.10	1.70
4&3			0.20	0.20		
4&6					0.20	0.30
Total	58.60	100.20	92.10	99.98	64.80	100.27
Sandstone %	49		57		86	
Mudstone %	51		43		14	
Log motif	Blocky-serrated		Serrated-Blocky		Serrated	
Quartzite*	Absent		Absent		Present	
Thickest mudstone unit (m)	16		5		0.5	
Cyclicity	Poor		Good		Absent	

*Gravel sized.

(2) Facies 2: Contorted sandstone, fine- to medium-grained, steep layers, variable dips, shear zones, brecciated jumble of fragments, floating mudstone clasts and quartzite granules, planar clast fabric, water-escape structures, and sandstone dikes (sandy slump/debris flow in a non-channelized slope environment).
(3) Facies 3: Contorted mudstone, steep layers, slump folds, shear zones, floating clasts, planar fabric, and sandstone dikes and sills (muddy slumps/debris flows).
(4) Facies 4: Rippled sandstone/siltstone, horizontal lamination, and current ripple (bottom-current reworking).
(5) Facies 5: Normal size grading of fine-grained sandstone and siltstone (turbidity currents).
(6) Facies 6: Laminated mudstone (pelagic/hemipelagic settling).

   The Facies 2 with sandy slumps and sandy debrites is the most dominant type in the Agat region (Table 6.3). In general, slope facies are characterized by deposits of slumps, slides, and debris flows (Doyle and Pilkey, 1979). Such a slope system requires a sea-floor gradient of 1–2°. Arenaceous forms in interbedded shales also imply an upper slope to outer shelf environment. Thus a slope model,
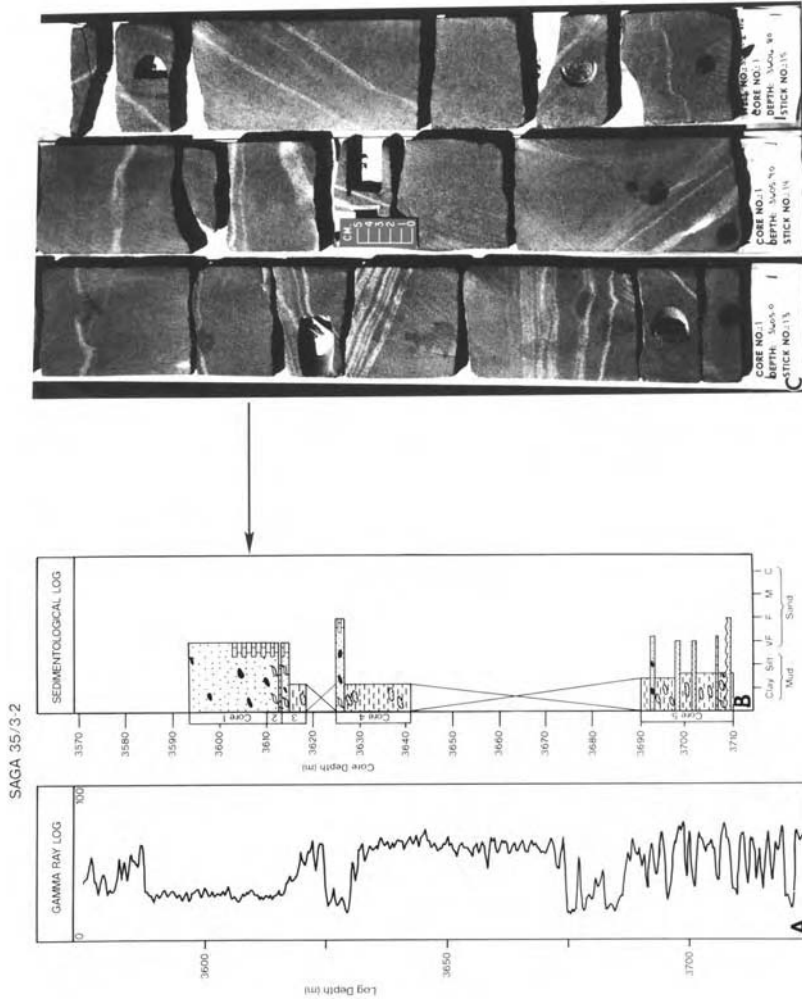
Fig. 6.13. (*A*) **Wireline log showing blocky log motif (near 3600 m) in the Agat Formation, Albian, Saga 35/3–2, offshore Norway. (*B*) Depth–tied sedimentological log. (*C*) Facies 2: Core photograph showing a variety of apparent dips of clay-filled layers (light color) in sandstone. Note steep layers adjacent to horizontal layers. Such variable dips may be explained by contortion caused by slumping. Agat Formation, Albian, Saga 35/3–2, 3604 m (upper left)–3606.8 m (lower right). Arrow shows stratigraphic position of core photograph. (After Shanmugam et al. (1994). Reprinted by permission of the American Association of Petroleum Geologists whose permission is required for further use.)**
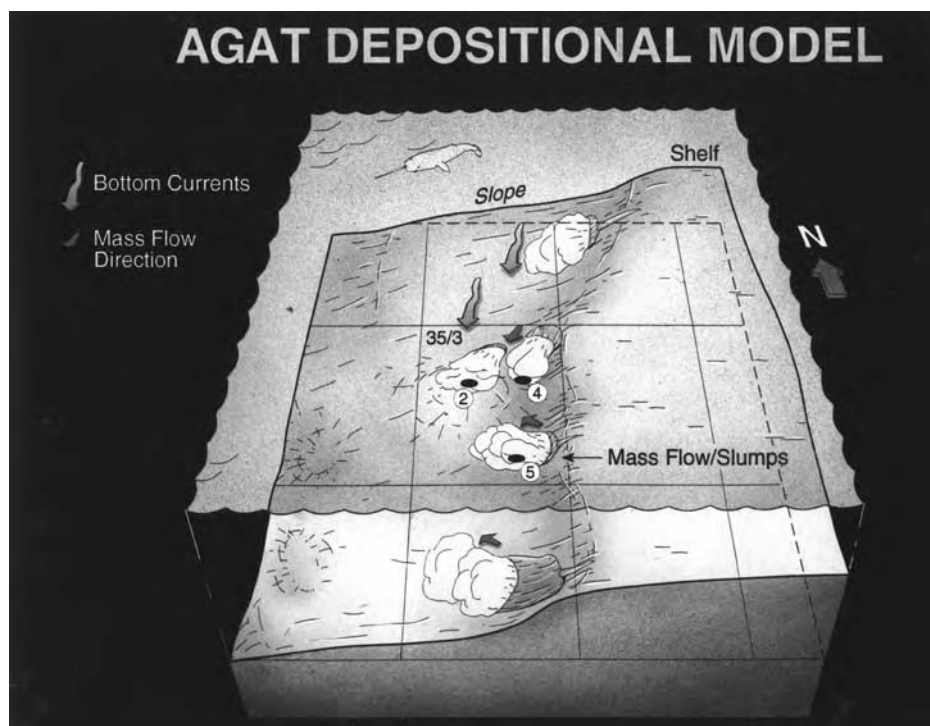
Fig. 6.14. Depositional model of the Agat Formation showing distribution of Facies 2 (sandy slump/mass flow or debris flow) on a slope environment in proximity to the shelf edge. Sea-floor topography is based on the Base-Cretaceous structure map. Note differences in sediment source for the 35/3–5 well (arrow from southeast) in comparison with 35/3–2 and 35/3–4 wells (arrow from northeast). (After Shanmugam et al. (1994). Reprinted by permission of the American Association of Petroleum Geologists whose permission is required for further use.)

dominated by deposits of slumps and debris flows, was proposed for the Agat cores (Fig. 6.14).

The proposed slope model has important implications for sand distribution: (1) this model provides an alternative to the conventional submarine-fan model previously applied to these sequences; (2) although slump/debris-flow emplaced sands are usually discontinuous and unpredictable, highly amalgamated slump/debrite sands may develop thick reservoirs; and (3) by using the Eocene Frigg Formation as an analog, externally mounded seismic facies in the Agat area has been predicted to be composed of sandy slumps and debrites in undrilled areas (Shanmugam et al. 1994).

6.4 Submarine canyon and gully environments

Submarine canyons have been discussed in detail by many researchers (Shepard and Dill, 1966; Shepard, 1973; Whitaker, 1976; Stanley and Kelling, 1978;

Shepard et al., 1979; Twichell and Roberts, 1982; Shanmugam, 2002d). Submarine canyons, which are steep-sided valleys that incise into the continental shelf and slope, serve as major conduits for sediment transport from land and the shelf to the deep-sea environment. Undersea canyons are prominent erosional features along both the U.S. Pacific (Fig. 6.3) and the Atlantic (Fig. 6.15)
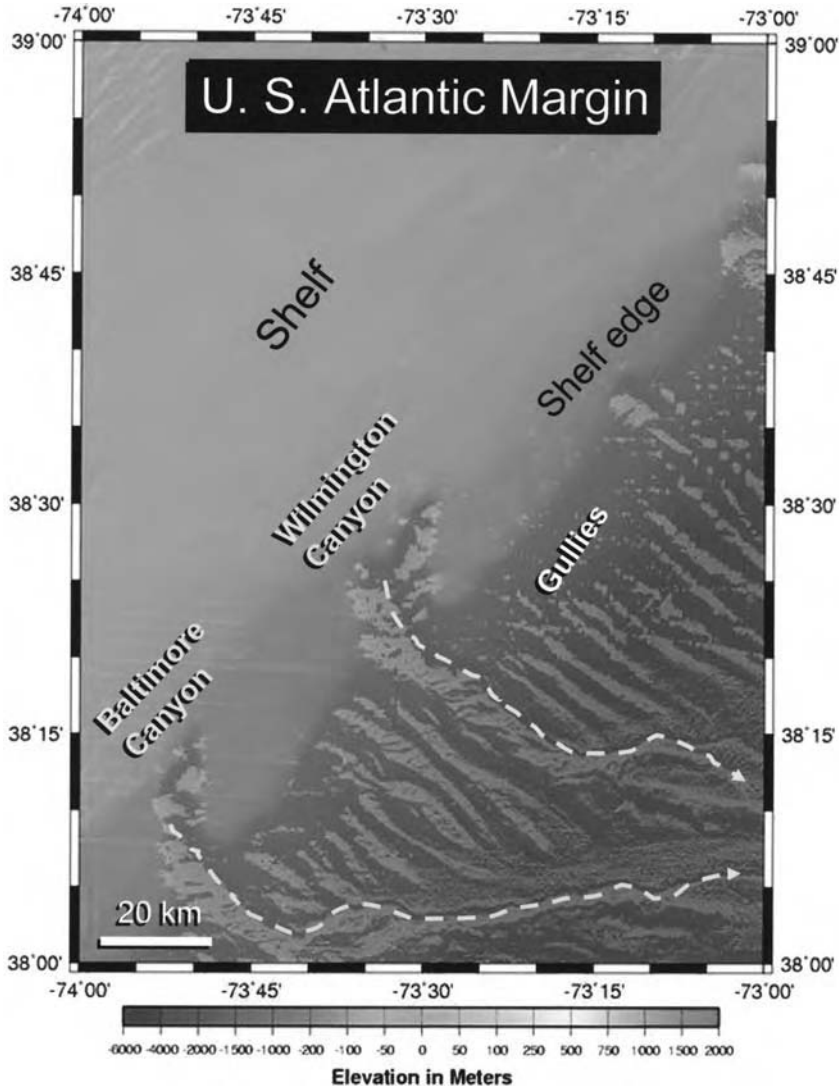

Fig. 6.15. High-resolution shaded relief image of bathymetry showing Wilmington and Baltimore Canyons. Note adjacent gullies originating near the shelf edge, U.S. Atlantic Margin. (Credit: NGDC (National Geophysical Data Center) Coastal Relief Model Vol. 02 Shaded Relief Images, NOAA Satellites and Information. Uniform Resource Locator (URL): http://www.ngdc.noaa.gov/ mgg/coastal/grddas02/html/gna38075.htm (accessed June 22, 2004).)

continental margins. Submarine canyons also develop along the slopes of many islands (e.g., Hawaii). Canyons are associated with deep siliciclastic margins (Fig. 6.15) as well as shallow-carbonate platforms (e.g., Great Bahama Canyon). Smaller erosional features on the continental slope are commonly termed gullies (Fig. 6.15); however, there are no standardized criteria to distinguish canyons from gullies. Similarly, the distinction between submarine canyons and submarine erosional channels is not straightforward. Thus alternative terms, such as gullies, channels, troughs, trenches, fault valleys, and sea valleys are in use for submarine canyons.

6.4.1 Modern canyons

Modern canyons are relatively narrow, deeply incised, steeply walled, and often sinuous valleys with predominantly V-shaped cross sections (Fig. 6.16C). U-shaped glacial troughs (e.g., the Gulf of St. Lawrence, Canada) on the shelf and upper slope may also develop into submarine canyons. Most canyons originate near the continental-shelf break (Fig. 6.17), and generally extend to the base of the continental slope. Canyons often occur off the mouths of large rivers, such as the Zaire (formerly the Congo), Amazon, Ganges, Mississippi, and Hudson. However, many other canyons, such as the Bering Canyon in the southern Bering Sea, are developed along structural trends.

Analogous to subaerial river valleys, submarine canyons are erosional features that carve into the seafloor and expose underlying strata. Like rivers, underwater canyons also develop sinuous (Fig. 6.16B) and braided patterns (Fig. 6.3). Unlike sinuous rivers that develop mainly on gentle gradients, sinuous submarine canyons can develop on steep gradients near the shelf edge, adjacent to braided canyons (Fig. 6.3).

Modern submarine canyons vary considerably in their dimensions (Table 6.4). The world's longest Bering Canyon is 1495 km long (Carlson and Karl, 1988). The average lengths of canyons have been estimated to be about 55 km. The shortest canyons are those off the Hawaiian Islands, and they average about 10 km in length.

Many submarine canyons in the U.S. Atlantic Margin commence at a depth of 200 m near the shelf edge (Fig. 6.17), however, heads of California canyons in the U.S. Pacific Margin begin at an average depth of about 35 m. The Redondo Canyon (Los Angeles Margin) commences at a depth of 10 m near the shoreline (Fig. 6.3). In general, the average depth of canyon termination has been estimated to be 2000 m.

The average relief of canyon walls is over 900 m. The Great Bahama Canyon, which lies northeast of the Great Bahama Bank, is the world's deepest canyon. The vertical rock walls of the Great Bahama Canyon rise 4285 m from the canyon floor. In comparison, the wall heights of the Grand Canyon of the Colorado River in the continental United States average 1680 m.
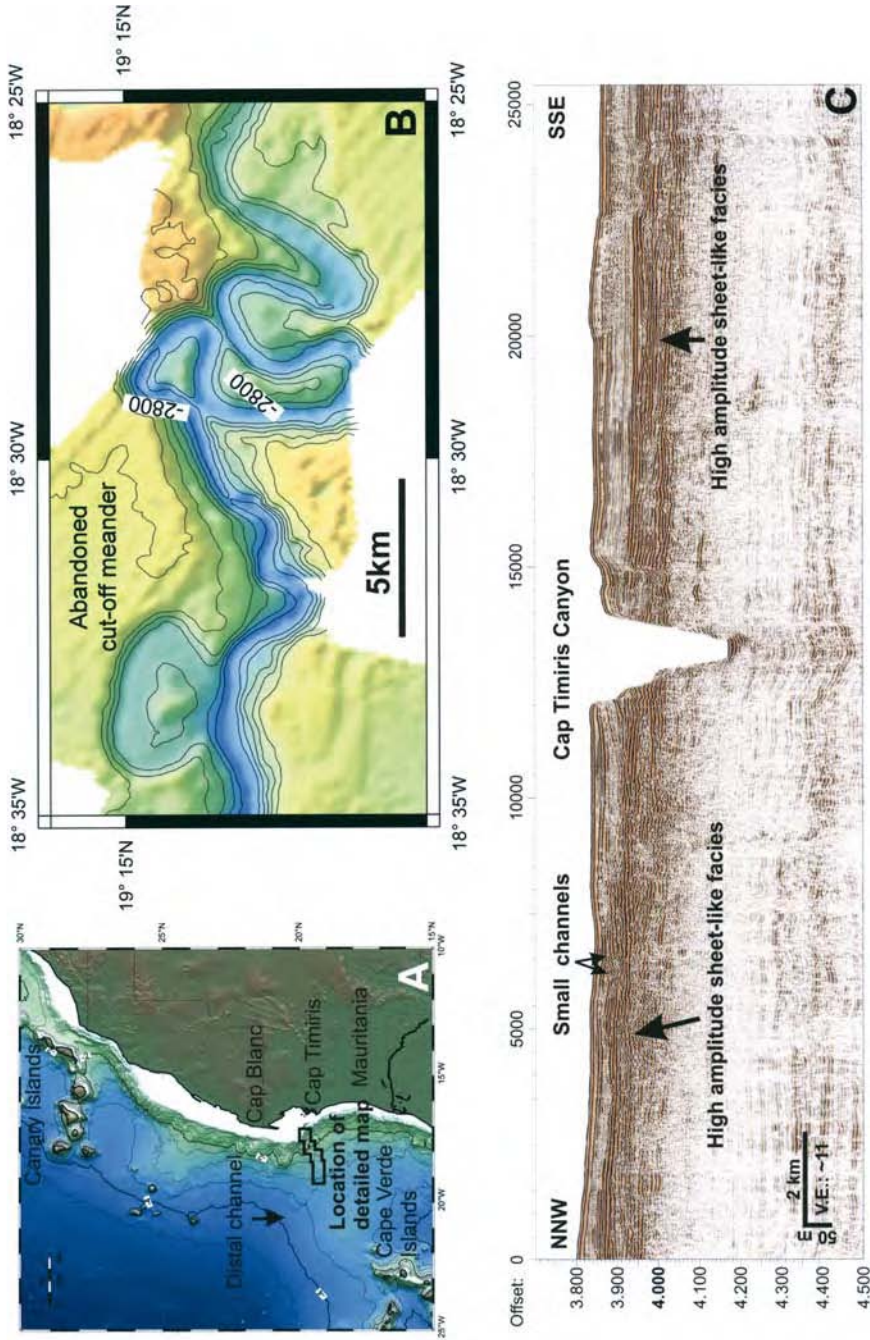
Fig. 6.16. Cap Timiris Canyon off Mauritania, northwestern Africa. (*A*) Location map. (*B*) Bathymetric map showing high sinuosity and an abandoned cut-off meander. (*C*) Seismic profile showing *V*-shaped cross section. Note steep erosional walls of the canyon. Simplified after Krastel et. al. (2004). (Images courtesy of Sebastian Krastel, Universität Bremen. Reprinted by Permission of the American Geophysical Union.)
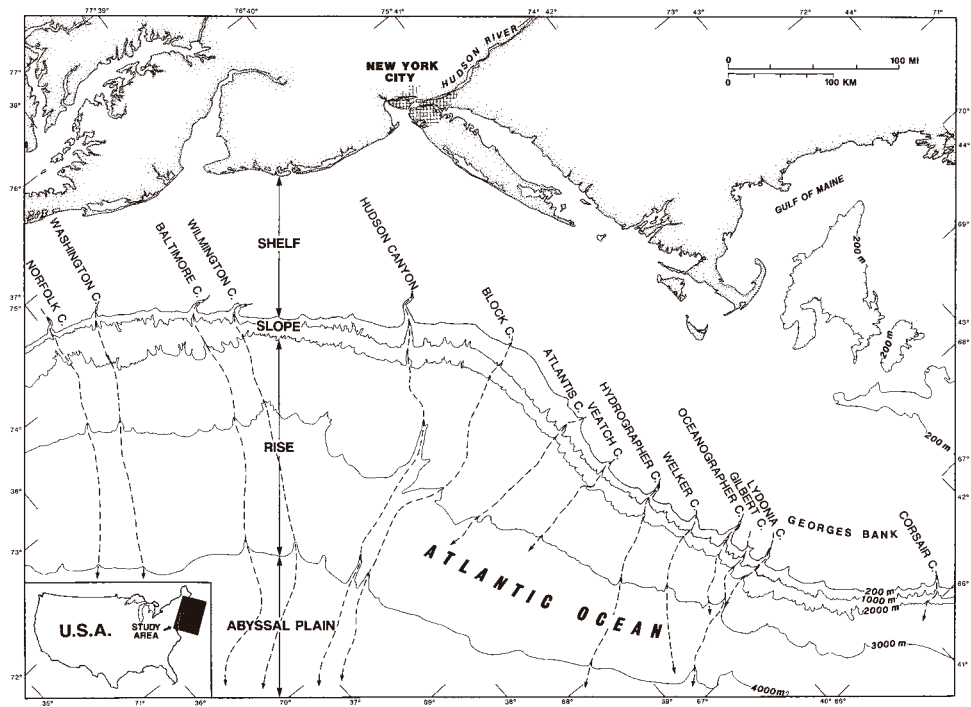
Fig. 6.17. Submarine canyons along modern continental margin off northeastern United States. Dashed lines with arrows show trends of submarine canyons and related deep-sea channels. Note most submarine canyons (dashed lines) commence in the vicinity of the shelf edge at a depth of 200 m. (Simplified from Uchupi (1965).)

Table 6.4 Dimensions of selected modern submarine canyons. (From Shepard and Dill (1966), Shepard (1973), Carlson and Karl (1988), and Uniform Resource Locator (URL): http://www.mbnms-simon.org/sections/submarineCanyons/overview.php?sec=sc (accessed November 23, 2004)

Modern canyon	Length (km)	Gradient (m/km)	Wall relief (m)
Bering, Bering Sea	1495	8	1840
Great Bahama, North Atlantic	225	60	4285
Zaire (Congo), Atlantic	222	10	1226
Pribilof, Bering Sea	159	20	2146
Monterey, Pacific	470	26	1839
Hudson, North Atlantic	93	22	1226
Hydrographer, North Atlantic	50	38	919
Rhone, Mediterranean	27	54	614
La Jolla, Pacific	14	38	307
Halawai, Pacific	11	90	307

Submarine canyons are characterized by relatively steep gradients. The average slope of canyon floors is 58 m/km. Shorter canyons tend to have steeper gradients. For example, shorter canyons of the Hawaiian group have an average gradient of 144 m/km, whereas the Bering Canyon has a slope of only 7.9 m/km.

A total of 115 incisions (canyons and gullies) on the continental margin off northwestern Africa were studied by Seibold and Hinz (1974). The average slope angle of the incisions is < 10° for 63% of the examples, 10–20° for 30%, 20–30° for 6%, and 30–40° for 1% of the cases studied. Many of these incisions are stepped. Evidence for slumping in these incisions is common. The incisions tend to widen through deepening of the sidewalls. The incisions deepen and spread landward and upward on the slope, and thus the entire continental margin recedes. Retrogressive slumping is a common cause of canyon formation.

On the upper U.S. Atlantic continental slope, canyon wall gradients vary from 6–30° with an average of 14° (Twichell and Roberts, 1982). On the middle slope, canyon wall gradients vary from 2–30° with an average of 10°. Gully distribution on the upper slope, where canyon wall gradients are higher, was considered to be evidence for their origin by mass wasting (Twichell and Roberts, 1982).

The world's largest submarine canyon is the Zhemchug Canyon in the southern Bering Sea. Its volume is approximately 8500 km^3. Zhemchug Canyon has an estimated length of 233 km, its width varies from 30–100 km, and its depth is about 8600 ft (2600 m). Most other submarine canyons have volumes less than 500 km^3.

The sinuous nature of the Wilmington Canyon is evident in high-resolution shaded relief imaging of the U.S. Atlantic Continental Slope (Fig. 6.15). The sinuous pattern has been referred to as a 'fluvial-like' meander system (Stubblefield et al., 1982; and McGregor et al., 1982). The absence of current ripples along the canyon axis was attributed to a lack of current activity within this canyon (Stubblefield et al., 1982, p. 32). A sample of 'gravel conglomerate' was collected at a depth of 2402 m in the South Wilmington Canyon (Stubblefield et al., 1982;

their Fig. 7C). The gravel grains are subrounded to rounded and well sorted, and the conglomerate sample did not contain any shell material. Based on this observation, Stubblefield et al. concluded that the gravel was transported down-slope *en masse* as part of a slump block.

A tight meander of the Monterey Canyon is evident in high-resolution shaded relief imaging of offshore central California (Fig. 6.18). This tight meander was
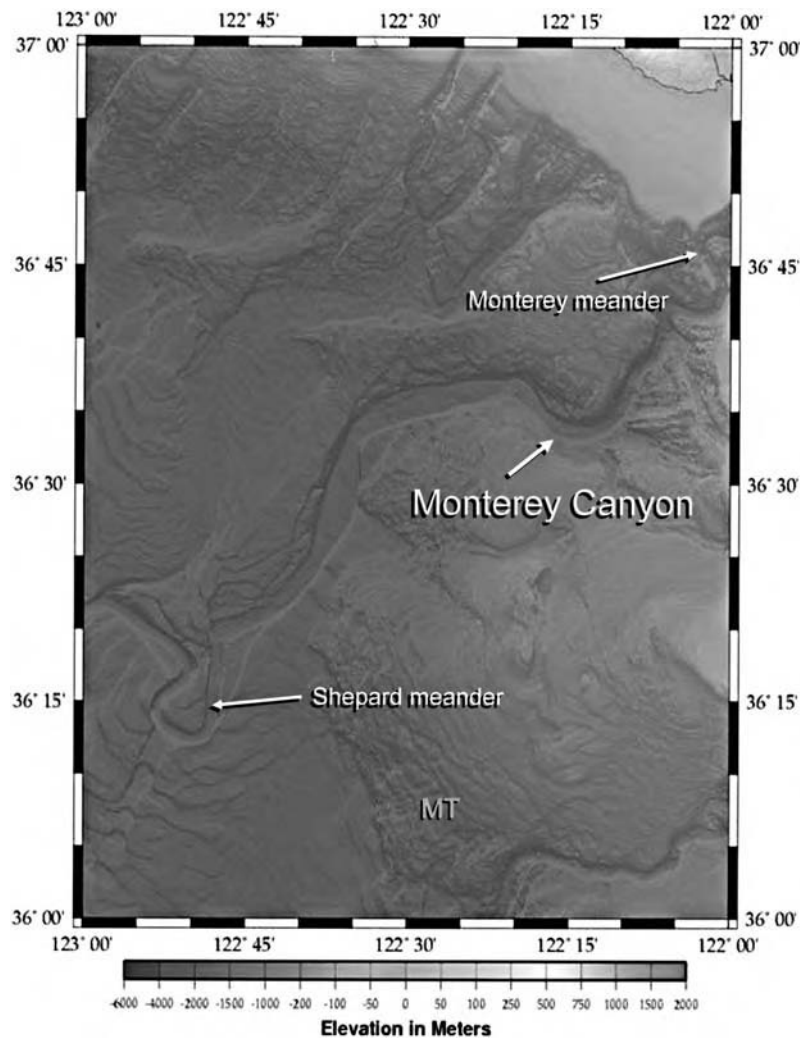

Fig. 6.18. High-resolution shaded relief image of the Monterey Canyon showing Monterey meander (Greene and Ward, 2003) and Shepard meander (Fildani and Normark, 2004), offshore California. MT = mass-transport deposit. (Credit: NGDC (National Geophysical Data Center) Coastal Relief Model Vol. 06 Shaded Relief Images, NOAA Satellites and Information. Uniform Resource Locator (URL): http://www.ngdc.noaa.gov/mgg/coastal/grddas06/html/gna37123.htm (accessed June 22, 2004).)

first reported by Shepard (1966). It has been named the 'Shepard meander' (Fildani and Normark, 2004). The meander in the Monterey Canyon is strongly controlled by the structural patterns of the area (Martin and Emery, 1967). The formation of the Monetery meander (Fig. 6.18), located near the Monterey Canyon Head Slump, has been attributed to three major throughgoing faults: (1) Navy; (2) Chupinas; and (3) Seaside (Greene and Ward, 2003, p. 345). Similarly, the origin of the Redondo Canyon of the Los Angeles Margin (Fig. 6.3) has been attributed to fault control (Yerkes et al., 1967).

The Cap Timiris Canyon was discovered in April–May 2003 off the arid north-western coast of Africa (Krastel et al., 2004) (Fig. 6.16A). It extends over a length of 215 km, from the shelf break to a depth of 3000 m. Its average depth is 250–300 m. Its sinuosity ranges from 1 to 4. It is qualified to be a meandering canyon in areas where its sinuosity is greater than 1.5. Furthermore, the canyon shows an abandoned cut-off meander (Fig. 6.16B). Such a feature, if it were formed by fluvial-like helical flows, should exhibit evidence for point-bar deposition. However, seismic profiles show that both sides of the canyon are steep erosional walls (Fig. 6.16C). There is no evidence of bar deposition on either side of the canyon. Clearly, this canyon was able to form high sinuosity (meandering) patterns by erosional processes without fluvial-like helical flows and related bar deposition (see Chapter 7). The exact process that created the meandering pattern of this erosional canyon is unclear.

6.4.2 Yoakum Canyon, Eocene, Texas

In comparison to modern submarine canyons, the dimensions of ancient canyons are considerably smaller (Table 6.5). One reason for this may be the limited size of the outcrops on land. Ancient submarine canyons observed in outcrops are characterized by major erosional surfaces. A large, mid-Eocene canyon near Yoakum,

Table 6.5 Dimensions of selected ancient submarine canyons. (From several sources (see Whitaker, 1976).)

Ancient canyon (age)	Length (km)	Width (km)	Depth (m)
Afam, W. Africa (Late Miocene)	100	30	300–790
Meganos, California (Late Paleocene)	80+	3–10	620
Yoakum, Texas (Middle Eocene)	80	15	920
Mississippi, Louisiana (Pleistocene)	80	3	610
Hackberry, Louisiana (Oligocene)	22	14	210
Gevaram, Israel (Early Cretaceous)	15+	15	940
Unnamed, Czechoslovakia (Late Eocene)	10+	6–8	150–200
Rosedale, California (Late Miocene)	10	2	370
Last Chance, Texas (Permian)	8	3	460
Cook, Texas (Early Permian)	5	2	30

Texas shows a well-developed erosional surface in a seismic profile (Shanmugam and Moiola, 1988, their Fig. 12). This canyon, which can be traced for more than 10 miles (16 km), is filled with as much as 1890 ft (576 m) of shale (Hoyt, 1959). Other case studies of ancient canyons have been discussed in Chapter 4.

6.4.3 Processes

Physical and biological processes that are common in submarine canyons are mass wasting, tidal bottom currents, and bioerosion. Major slumping events can lead to formation of submarine canyons. Active slumps, grain flows, and sandy debris flows in modern submarine canyons have been documented by direct observations and photographic documentations (see Chapter 3). In the world's largest Zhemchug Canyon, mass movement has been the most important process in shaping the canyon (Carlson et al. 1991).

The importance of tidal currents in submarine canyons has been discussed in Chapter 4. Although turbidity currents are frequently invoked as a major transport mechanism in submarine canyons, there are no direct observations or photographic documentations of turbidity currents in modern submarine canyons (see Chapter 3).

Bioerosion refers to destructive processes whereby invertebrates and fishes erode the terrigenous sedimentary rocks exposed along the walls and floors of submarine canyons (Warme et al., 1978). Boring by animals is perhaps the most common process of bioerosion.

In submarine canyons, sediment transport is considered to be ranging from episodic (e.g., mass wasting) to continuous (e.g., daily tidal currents). General triggering events of transport processes in canyons include sea level changes, earthquakes, storms, sea and surf conditions, tidal fluctuation, and flooding of rivers.

6.4.4 Deposits

Sand and mud deposited by large-scale slides, slumps, and debris flows are common in modern submarine canyons. In the La Jolla Canyon, offshore San Diego, rounded boulders were found at a depth of 585 m (Shepard and Dill, 1966, their Fig. 32). These boulders imply mass-transport deposition. A 6 m long piston core taken from a large submarine 'slide' on the eastern side of the Monterey Canyon is composed of mud clasts in mud matrix (Normark et al., 1985, their Fig. 7, Piston core: 1P). This core represents deposition from muddy debris flows. Sands deposited on canyon floors contain shallow-water organisms and pieces of land plants that have been transported by various gravity flows. Sediment cores taken from canyon floors reveal sand deposited from sandy debris flows, grain flows, and tidal currents (see Chapter 4). Studies of submarine canyons and their sediments from research submersibles have revealed that sediments on the canyon floors exhibit ripple marks at all depths, suggesting bottom-current reworking. The mud interval reflects pelagic and hemipelagic deposition from suspension settling.

At the mouths of major canyons (e.g., Mississippi Canyon in the Gulf of Mexico), land- and canyon-derived sediment often accumulates as submarine fans. Many large canyons continue as deep-sea channels on submarine fans (e.g., Amazon Fan).

6.4.5 Controlling factors

Tectonic setting plays an important role in the development of submarine canyons. In active-margin settings (e.g., U.S. Pacific Margin, Fig. 6.3), shelves are narrow and rivers discharge their sediment loads near the heads of canyons, where longshore currents carry the sediment directly into the canyon heads. As a consequence, canyons on the Pacific margin are undergoing some erosion by mass wasting at the present time, despite the current high stand of sea level. In contrast, canyons on mature passive-margin settings (e.g., U.S. Atlantic Margin, Fig. 6.15) are relatively inactive at present because the postglacial rise of sea level has drowned the heads of submarine canyons. Also, the rise in sea level has moved the shoreline far landward from the shelf edge, thereby cutting off the sediment source to the canyons. Therefore, canyons on the Pacific margin are active most of the time, whereas canyons on the Atlantic margin are active primarily during periods of low sea levels.

6.4.6 Origin

The origin of submarine canyons has been debated since the 1930s. Popular mechanisms for origin of canyons are:

(1) Heads of some present-day submarine canyons were originally cut by rivers during subaerial erosion when the continental margins were briefly uplifted and exposed during periods of low sea level. During subsequent rise in sea level, these subaerial river valleys were drowned to become submarine canyons. This hypothesis was based on the evidence that many submarine canyons closely resemble river-cut canyons, and on the juxtaposition of many land and sea canyons. Clearly, some canyons are of this origin.

(2) Submarine erosion by the mass movement of sediment down canyon by slides, slumps, debris flows, and sand falls can lead to formation of submarine canyons. Direct observational evidence for mass movements in modern canyons is substantial (Shepard and Dill, 1966). The Mississippi Canyon in the Gulf of Mexico is believed to have been formed by retrogressive slumping during the late Pleistocene fall in sea level and has been partially infilled during the Holocene rise in sea level.

(3) Daly's (1936) hypothesis for the origin of submarine canyons by density (turbidity) currents has been quite popular. However, on the basis of his study of Scripps Canyon, Dill (1964, p. 35) concluded, '*Very little erosion of*

bottom sediment or rock slopes is caused by sediment in suspension (turbidity currents) at the head of the canyon.' In a review article, Shepard (1981, p. 1062) concluded, '*Those advocating turbidity currents as the unique cause of canyons failed to appreciate that debris flows down the incipient valleys, as well as other types of landslides, could be an almost equally important factor in marine erosion*.' Although the mechanism of turbidity currents has been popular since the 1930s, there is no observational evidence for turbidity currents in modern canyons. Other possible mechanisms are bottom currents (e.g., deep tidal currents), glacial erosion, biologic activity, and faulting.

F. P. Shepard (1981), who devoted his professional life at the Scripps Institution of Oceanography in California to the study of submarine canyons, concluded that submarine canyons were formed not by a single mechanism, but by a combination of processes, such as subaerial erosion, submarine erosion (e.g., slides, slumps, debris flows, grain flows, tidal currents, turbidity currents, and biologic activity), and faulting, over a long period of time. Some canyons may be dated back to the Cretaceous period.

6.5 Submarine fan environments

6.5.1 Characteristics

Submarine fans are channel and lobe complexes in deep-marine environments (Shanmugam and Moiola, 1988). General characteristics of submarine fans and related problems are:

- The term submarine fans should be used only for deep-marine environments, (i.e., fan deltas are excluded).
- Submarine fans are fed by a point source (i.e., a canyon or a feeder channel).
- Submarine fans develop at the base-of-slope giving rise to numerous distributary channels that diverge seaward across the fan and terminate with lobes at channel mouths causing fan-shaped deposits.
- In theory, submarine fans represent fan-shaped deposits. In reality, however, many deep-water systems worldwide exhibit extreme variations in size and shape (Fig. 6.19). Irrespective of their complex outlines, all deep-water systems are commonly termed 'submarine fans' (Barnes and Normark, 1985).
- The outline of modern deep-water systems can be mapped reasonably using recent mapping techniques (e.g., hull-mounted multibeam mapping system). In contrast, the outlines of ancient deep-water systems in the subsurface are difficult to decipher because of post-depositional distortions by tectonic events.
- Not all submarine channels develop into depositional lobes forming divergent sediment-dispersal systems. The NAMOC channel system in the Labrador Sea,
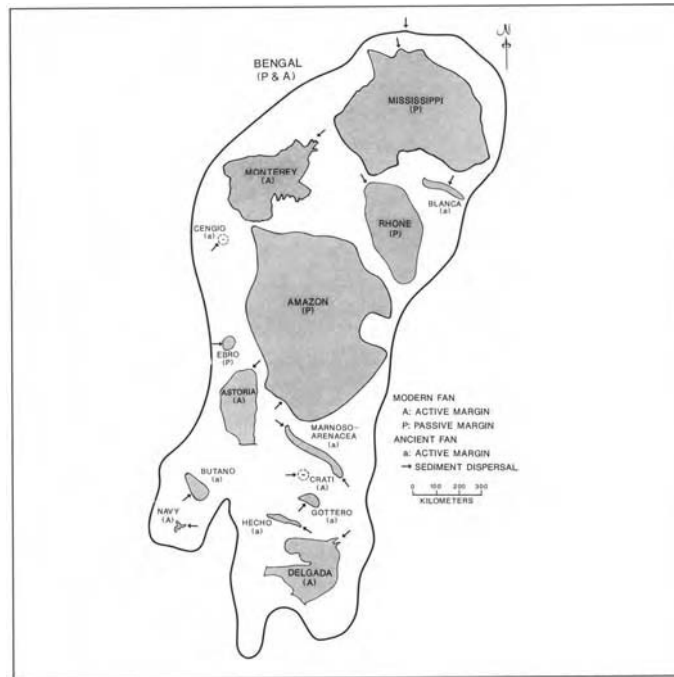
Fig. 6.19. Outlines of selected modern and ancient deep-water systems showing variability in size and shape. The popular tendency is to label them as submarine fans. (Compiled from Barnes and Normark (1985, wall chart). After Shanmugam and Moiola (1988). Reprinted by permission of Elsevier.)

for example, is a *convergent* sediment-dispersal system (Hesse, 1989). The term submarine fan is inappropriate for deep-water channel systems that do not develop into channel-mouth lobes.

- In addition to the concept of depositional lobes for ancient fans (Mutti, 1977), there are several other lobe concepts causing conceptual problems (see review by Shanmugam and Moiola, 1991).
- Lobes can be both sand-rich and mud-rich deposits.
- Division of submarine fans into upper, middle, and lower fans is not meaningful because each fan is sufficiently complex and unique.
- The term submarine fan is strictly a geomorphic term and it does not imply anything about depositional processes (e.g., turbidity currents). Elverhoi et al. (1997), for example, applied the term 'Bear Island Fan' for deposits of debris flows on the Norwegian-Barents Sea continental margin.

Aspects of sedimentologic and sequence-stratigraphic fan models are discussed in Chapters 9 and 10, respectively.

6.5.2 Submarine channels

According to Mutti and Normark (1987, p. 9), '*A channel is the expression of negative relief produced by confined turbidity current flow, and represents a major, long-term pathway for sediment transport.*' In other words, all submarine channels are of turbidity current origin, and they all must be long lived in order to be qualified as channels. There are practical problems in applying the above definition:

(1) It is not always possible to establish whether a channel in the rock record was cut by turbidity current or by some other process. This is because processes that cut channels are not necessarily the same processes that later fill those channels (see Chapter 7).
(2) Although many channels are filled with deposits of debris flows, debris flows are generally incapable of forming major erosional channels.
(3) Another problem is in determining whether an ancient channel acted as a pathway for a long period of time or a short period of time. This is because the terms 'long' and 'short' periods of time have not been defined.
(4) Finally, gravity-driven processes are instantaneous and episodic. Thus it is impossible to determine a long-term deposition in the rock record composed of deep-water gravity-flow deposits.

   Submarine channels can be erosional, aggradational, or both (Nelson and Kulm, 1973, their Fig. 3). Two major types of channels, braided and sinuous, are recognized in modern and ancient deep-water environments.

6.5.3 Modern and ancient braided channels

Submarine braided channels are characterized by low sinuosity and by many shallow channels. They generally develop in areas of high gradients. Selected modern examples are:

(1) The San Lucas Fan off Baja California (Normark, 1970)
(2) The Orinoco Fan in the western equatorial Atlantic (Belderson et al., 1984)
(3) The Northwest Atlantic Mid-Ocean Channel (NAMOC) in the Labrador Sea (Hesse, 1989)
(4) The Monterey Fan (Klaucke et al., 2004).

Selected ancient examples are:

(1) The Late Cretaceous sequences in southern Chile (Winn and Dott, 1979)
(2) The Cambro-Ordovician Cap Enrage Formation in Quebec, Canada (Hein and Walker, 1982)
(3) The Carboniferous Tesnus Formation in west Texas (Wuellner and James, 1989).

General characteristics of deposits of deep-water braided channels are (Shanmugam, 1990):

- Conglomerate and coarse-grained sandstone
- Erosional bases and multiple internal scours
- Vertical and lateral stacking of channelized packages (Fig. 6.20)
- General lack of interbedded mudstone
- Rip-up clasts
- Deposits of slides, slumps, debris flows, and turbidity currents
- Thick amalgamated units (10s to 100s of meters)
- Sheet-like sandbody geometry.

6.5.4 Modern Amazon Fan: sinuous channels

Submarine channels on mature passive-margin settings tend to be relatively long, bifurcating, of low gradient, and largely sinuous. The relatively fine-grained (mud-rich) character of the transported sediment associated with channels on mature passive-margin fans, such as the modern Amazon Fan (Damuth et al., 1988), gives rise to excellent bank stability and favors development of a single,

Fig. 6.20. Stacked channel-fill conglomerates and sandstones interpreted as deep-water braided channel facies deposited by sandy debris flows. Capistrano Formation, Upper Miocene, Dana Point, California.

largely sinuous, commonly meandering channel (Fig. 6.21). According to Pirmez and Flood (1995), sinuosity of the Amazon Fan channel is smaller than 1.5 over most of the upper half of the channel, but increases downdip to about 2.3 becoming a meandering channel (Fig. 6.22A). In cross-sectional view, these channel-levee complexes generate gull-wing geometry because of vertical levee build up (Fig. 6.23).

The Amazon Fan with 4 km of sediment core, taken from 17 drill sites during ODP Leg 155, has provided a great opportunity to understand the depositional origin of various fan elements (Normark, Damuth et al., 1997). The purpose of studying modern deep-water systems with abundant cores, such as the Amazon Fan, is to: (a) describe cores from known elements (i.e., channel, levee, HARP etc.), (b) interpret processes in each element, and, (c) most importantly, quantify the relative importance of depositional facies in each element. Such a quantitative data would help to establish a genetic link between a given element (e.g., channel-fill) and a process (e.g., turbidity currents). Then, sedimentologists could use this element-process linkage, derived from modern systems, for reconstructing ancient deep-water environments. Unfortunately, Normark, Damuth et al. (1997) did not quantify depositional facies in various elements of the Amazon Fan.

To establish a genetic link between processes and elements in the Amazon Fan, I have examined published graphic sedimentological columns (Shipboard Scientific Party, 1995a, their Fig. 4), grain-size variations, core description, and photographs (Shipboard Scientific Party, 1995a). Using this information, I have interpreted depositional processes and quantified the amount of various lithofacies from the Site 934. This quantification suggests that the principal sand unit is composed of fine- to-medium sand (i.e., Unit IV, Site 934, Shipboard Scientific Party, 1995a) in the Brown Channel. The cored interval is composed of sediments deposited by
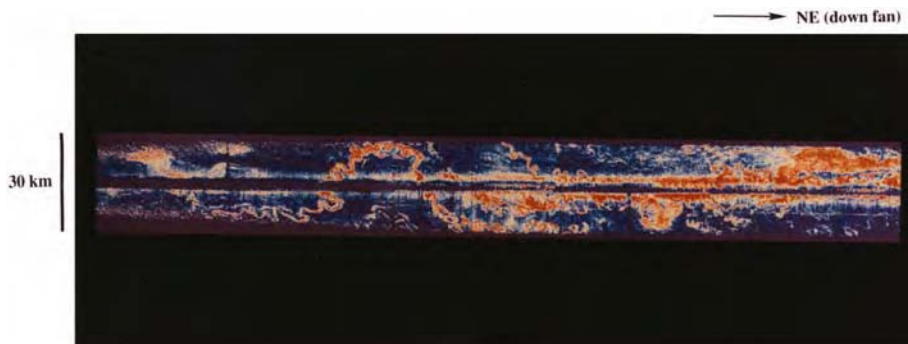
Fig. 6.21. Long-range sidescan-sonar (GLORIA) record showing sinuous channel pattern in the middle fan region of the Amazon Fan, western Equatorial Atlantic. Channel width ranges from one to two kilometers, Water depth: 2800–3500 m. (Image courtesy of J. E. Damuth.)
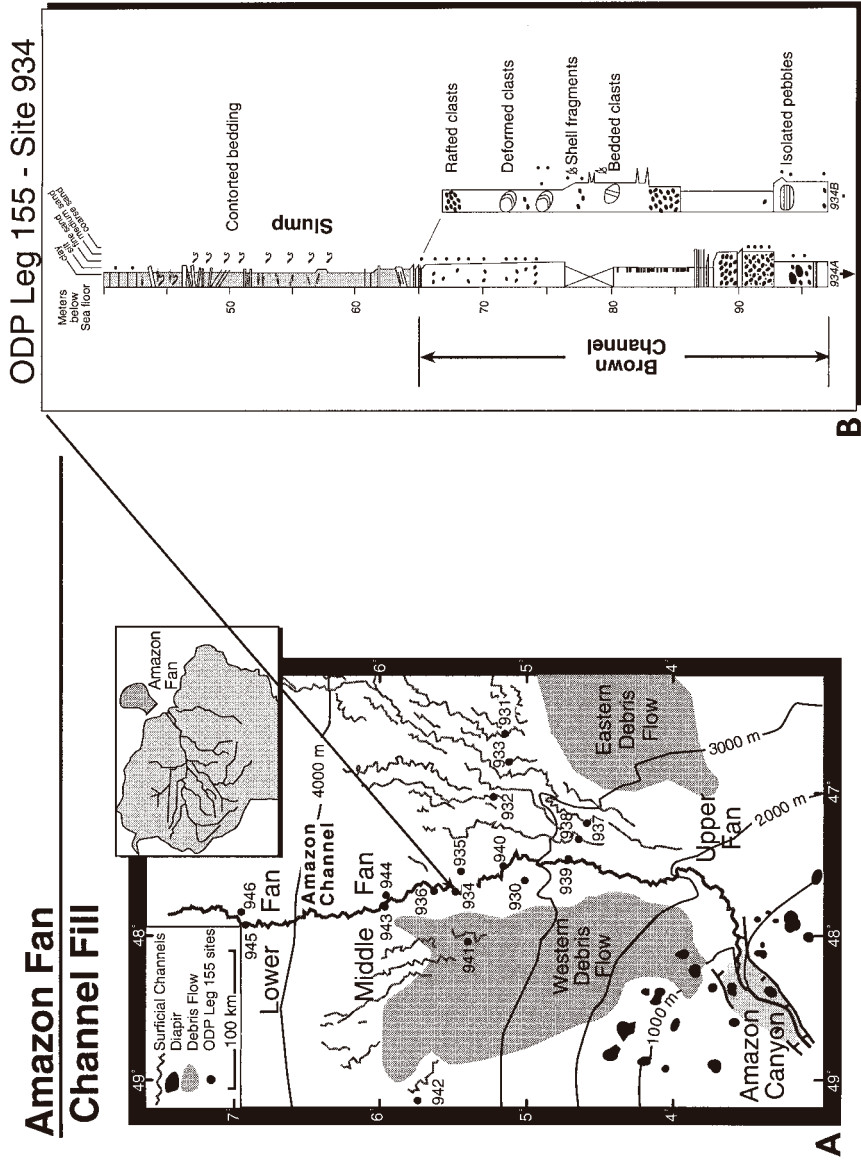
Fig. 6.22. (*A*) Ocean Drilling Program (ODP) Leg 155 Sites, Amazon Fan. (*B*) Sedimentological log of channel-fill element at Site 934. Note rafted clasts and deformed clasts in sandy matrix, suggesting deposition from sandy debris flow. (Location map after Normark, Damuth et al. (1997) and Site Log after Shipboard Scientific Party (1995a).)
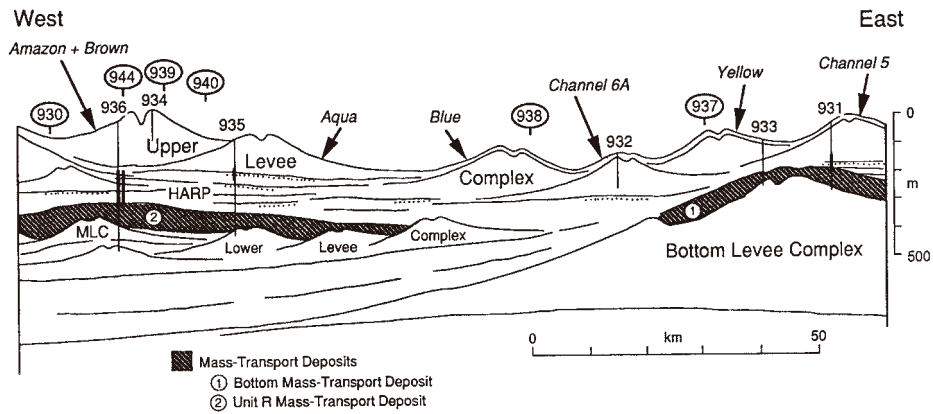
Fig. 6.23. Schematic cross section of channel and levee elements showing gull-wing geometry in the Amazon Fan. Note Site 934 near the west end of section. MLC = Middle Levee Complex. HARP = High Amplitude Reflection Packets. (After Pirmez et al. (1997).)

sandy debris flows (30%), muddy slumps (20%), and mixed sandy debris flows and bottom currents (11%). The remaining interval is composed of pelagic/hemipelagic mud (34%) and turbidites (5%) (Table 6.6).

My interpretations of Unit IV at Site 934 as deposits of sandy debris flows and Unit III as deposits of muddy slumps are consistent with the interpretation

Table 6.6 Quantification of channel-fill depositional facies in the cores at Site 934A & B, ODP Leg 55, Amazon Fan. (Core data from Shipboard Scientific Party (1995a).)

Unit (Shipboard Scientific Party, 1995a)	Interval (m) (mbsf)*	Thickness (m)	Depositional facies (Observation)	Depositional process (Interpretation by G. Shanmugam)	% (Cored interval)
IA, IIA, & IIB	0–23	23	Laminated mud	Pelagic/hemipelagic settling	21
IIB	23–28	5	Graded sand and mud	Turbidity currents	5
IIB & IIC	28–42.30	14.30	Laminated mud	Pelagic/hemipelagic settling	13
III	42.30–64.56	22.26	Contorted mud	Muddy slump	20
IV	64.56–97.30	32.74	Fine- to medium-sand with mud clasts	Sandy debris flow	30
V	97.30–108.88	11.58	Sand with mud clasts, rare ripples, and gas expanded silt	Mixed facies (Sandy debris flow and bottom current reworking)	11

*Meters below sea floor.

reached by the Shipboard Scientific Party (1995a). Also, Normark, Damuth et al. (1997, p. 632) described that '*The most prevalent facies is thick-bedded, disorganized structureless to chaotic sand…*' Their description suggests a dominance of deposition from debris flows and slumps in the Amazon channel-fill elements.

General characteristics of deposits of sinuous channels of the Amazon Fan are:

- Medium- to fine-grained sand
- Interbedded mudstone
- Erosional base
- Rip-up clasts
- Contorted mud layers (muddy slump) (Fig. 6.22B)
- Thick units of sand with rafted and deformed clasts (sandy debris flow) (Fig. 6.22B)
- Floating pebbles in sandy matrix (sandy debris flow) (Fig. 6.24)
- Thin units of normally graded sand and silt layers (turbidity currents) (Fig. 6.25)
- Several meters thick to thin units
- Lenticular sandbody geometry.
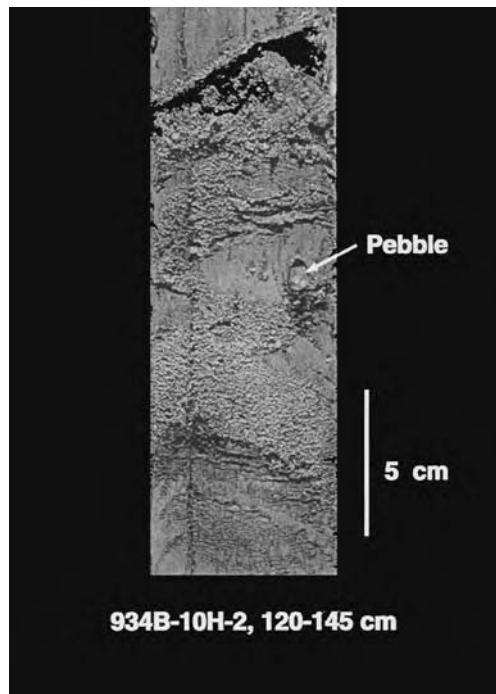
Fig. 6.24. Core photograph showing floating pebble in fine sandy matrix suggesting deposition from sandy debris flow. ODP Leg 155, Site 934B, channel fill, Amazon Fan. (Photo courtesy of J. E. Damuth.)

Amazon Fan
Channel Fill
ODP Leg 155, Hole 934A,
Core 10H, Section 6, 44-26 cm
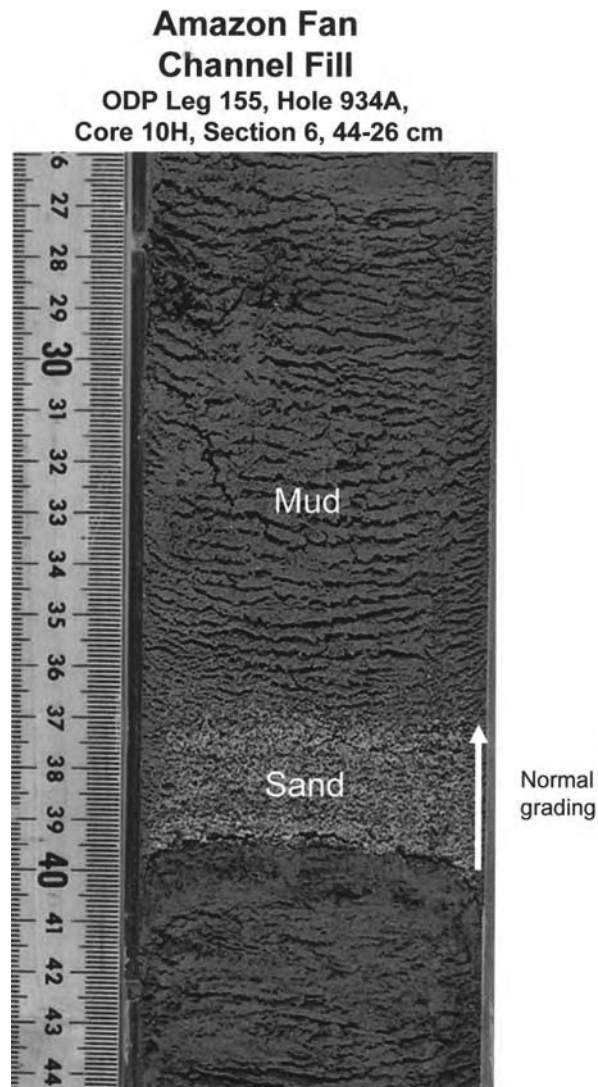
Fig. 6.25. Core photograph showing sharp-based and normally graded bed (arrow) with medium sand at the base (39.5 cm) and silt at top from channel-fill deposits. Normal grading is interpreted as evidence for deposition from turbidity currents. ODP Leg 155, Site 934A, 10H–6, 26–44 cm, Amazon Fan. (After Normark and Damuth et al., (1997). Photo courtesy of Ocean Drilling Program (ODP), College Station, Texas.)

Graphic sedimentological columns for cores from the Leg 155 Site 944 from a middle fan levee element of the Amazon Fan show a striking muddy facies in which contorted layers and mud clasts are common (Shipboard Scientific Party, 1995b, their Fig. 2). This muddy facies is interpreted to be deposits of muddy slumps and debris flows in a levee element. Core evidence is compelling that the

Amazon channels and levees were deposited by debris flows and slumps. This core-based interpretation, however, is not embraced by all researchers. Pirmez and Imran (2003), for example, concluded that the Amazon channels were originated by turbidity currents based mainly on seismic information.

6.5.5 Modern Amazon Fan: HARP units

In the Amazon Fan, channel bifurcation through avulsion is thought to lead initially to deposition of nonchannelized sandy flows in the interchannel area (Flood et al., 1991). Subsequent progradation of channels and levees over these sandy deposits has produced a sheet-like geometry at the base of the new channel-levee system. This sheet-like geometry returns High-Amplitude Reflection Packets (HARPs) on seismic data (Fig. 6.26). In a sequence-stratigraphic model, these sheet-like HARP Units overlain by a channel-levee system (gull-wing) are identical in appearance to a basin-floor fan overlain by a slope fan (Vail et al., 1991). However, there is a major difference between a basin-floor fan and a HARP unit. A basin-floor fan is formed by progradation primarily during lowstands of sea level (allocyclic process), whereas HARPs are formed by channel bifurcation (autocyclic process). More importantly, a basin-floor fan and a slope fan are not
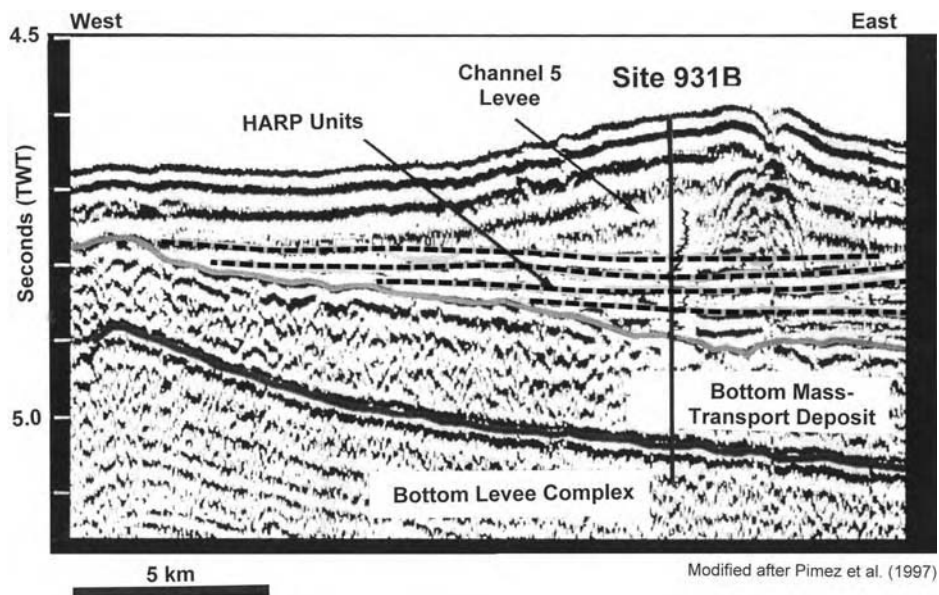
Fig. 6.26. Seismic profile showing HARP units (horizontal dashed lines) and overlying Channel 5 with levee units. Note position of Site 931B, Amazon Fan. Modified after Pirmez et al. (1997).
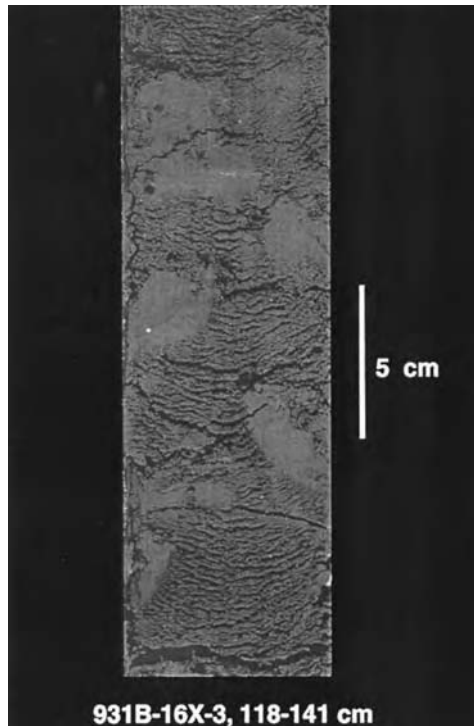
Fig. 6.27. Core photograph showing floating mud clasts in silty matrix. suggesting deposition from muddy debris flow. Site 931B, HARP unit, Leg 155, Site 931, Amazon Fan. See also Shipboard Scientific Party (1995c, their Fig. 7B). (Photo courtesy of J. E. Damuth.)

contemporaneous features (Vail et al., 1991); whereas a HARP unit and its overlying channel-levee system are contemporaneous elements. Thus caution must be exercised in interpreting seismic geometries in terms of depositional elements (see Chapter 10).

A HARP Unit at Site 931 was cored beneath Channel 5 (Fig. 6.26). Core shows floating mud clasts in muddy matrix at Site 931B (Fig. 6.27). Normark, Damuth et al. (1997) have summarized facies distribution in HARP units (Fig. 6.28). Without quantification of HARP facies, Normark, Damuth, et al. (1997, their Fig. 21, p. 651) stated the origin of HARP units as, '… *deposited by turbidity currents and related gravity-controlled flows*.' This statement implies a dominance of turbidity currents. However, evidence for a dominance of deposits of turbidity currents in the HARP Unit is lacking. Shipboard Scientific Party (1995c, their Fig. 7B) has published examples of floating mud clasts. These clasts are evidence for deposition from muddy debris flow. I have interpreted and quantified various depositional facies in this HARP Unit based on published ODP

Amazon Fan

Pelagic/Hemipelagic Drape
Facies:
13. Biogenic Mud
9. Color-Mottled Mud
14. Biogenic Sand
15. Chemogenic Sediment

HAR Units
Facies:
2. Disorganized Sand Beds
3. Organized Sand
12. Chaotic Mud

Levee Systems
Facies:
9. Color-Banded Clay
8. Color-Banded Silt
7. Irregular or Discontinuous Silt
6. Very Thin, Regular Silt & Mud
9. Organized Silt Beds
8. Disorganized Silt Beds
7. Organized Sand Beds & Laminae

MFS = Maximum Flooding Surface

Channel

Levee

Levee

Overbank Deposits

Overbank Deposits

HARs

HARP

Mass-Transport Deposits

Mass-Transport Deposits
Facies Present:
11. Disorganized Pebbly or Gravelly Mud & Sandy Mud
12. Chaotic Mud w/ Clasts
10. Homogeneous Mud
2. Disorganized, Chaotic Sand w/ Clasts

HARP Units (High Amplitude Reflection Packets)
Facies Present:
2. Disorganized Sand Beds
3. Organized Sand Beds
1. Disorganized Gravel & Sandy Gravel

(Normark, Damuth et al., 1997)

Fig. 6.28. Summary diagram showing depositional facies in various elements. Note similar facies association in both channel and HARP units, Amazon Fan. (Simplified after Normark, Damuth et al. (1997).)

Initial Reports for Site 931 (Shipboard Scientific Party, 1995c). The results are (Table 6.7):

(1)	Sandy and muddy debris flows and slumps:	29%
(2)	Muddy slumps:	36%
(3)	Pelagic and hemipelagic settling:	12%
(4)	Pelagic and hemipelagic settling, and bottom currents:	8%
(5)	Pelagic and hemipelagic settling, bottom currents, and turbidity currents:	14%

In this quantification, deposits of debris flows and slumps account for 65% of HARP facies and deposits of turbidity currents comprise less than 14%.

In the above HARP example, cored interval is composed mainly of mud (70%). Most sandy layers have been described as muddy sand. Mud-rich sands are characteristically low in porosity and permeability. Therefore, caution must be exercised in using HARP Units as modern analogs for predicting reservoir potential of petroleum sandstones in frontier areas.

Table 6.7 Quantification of HARP depositional facies in the cores at Site 931B co, ODP Leg 55, Amazon Fan. (Core data from Shipboard Scientific Party (1995c).)

Unit (Shipboard Scientific Party, 1995c)	Interval (m) (mbsf)*	Thickness (m)	Depositional facies (Observation)	Depositional process (Interpretation by G. Shanmugam)	% (Cored interval)
IIC	132.5–137.5	5.00	Muddy *vs.* fine sand with mud clasts up to 3 cm	Sandy and muddy debris flows	12%
IIC	162–167	5.00	Laminated mud	Pelagic/hemi-pelagic settling	12%
IIC	180.5–184	3.50	Laminated mud	Pelagic/hemi-pelagic settling bottom currents	8%
III	200–202.5	2.50	Muddy *vs.* fine sand with mud clasts	Sandy and muddy debris flows	6%
III	219–225	6.00	Laminated mud, rare sand with cross laminae, rare graded layers	Pelagic/hemi-pelagic settling, bottom currents, turbidity currents	14%
III	229–233.5	4.50	Muddy sand with mud clasts and contorted layers	Sandy and muddy debris flows and slumps	11%
III	239–254	15.00	Contorted mud	Muddy slumps	36%

*Meters below sea floor.

6.5.6 Modern Amazon Fan: lower-fan lobe units

Site 946 is located on a lower-fan lobe (Flood, Piper, Klaus et al., 1995, their Plate 1, inside pocket of back cover). Sedimentological description of cores from Site 946 (Flood, Piper, Klaus et al., 1995, Section 4: Cores, p. 1177–1197) shows:

- Banded and folded clasts in fine sand (23X)
- Rafted mud clasts in sand (14H and 11H)
- Chaotic sand beds with mud clasts (12H and 13H)
- Floating mud clast in mud (21X).

I have interpreted these features as deposits of slumps and debris flows. Cores taken from the Leg 155 Site 946, located in the lower-fan setting (Fig. 6.29), show floating siltstone pebbles in a muddy matrix (Fig. 6.30). These pebbles suggest deposition from muddy debris flows. At Site 946, normally graded turbidite sand layers have been recognized (Shipboard Scientific Party, 1995d; their Fig. 3), but they are rare in comparison to deposits of sandy slumps and debris flows.

HARP Units are also considered to be analogous to depositional lobes in the conventional submarine fan model (Normark, Damuth et al. 1997, their Fig. 4B caption, p. 617). They described deposits of depositional lobes as deposits with irregularly shaped mud clasts in poorly sorted, fine to coarse sand (their Facies 2).
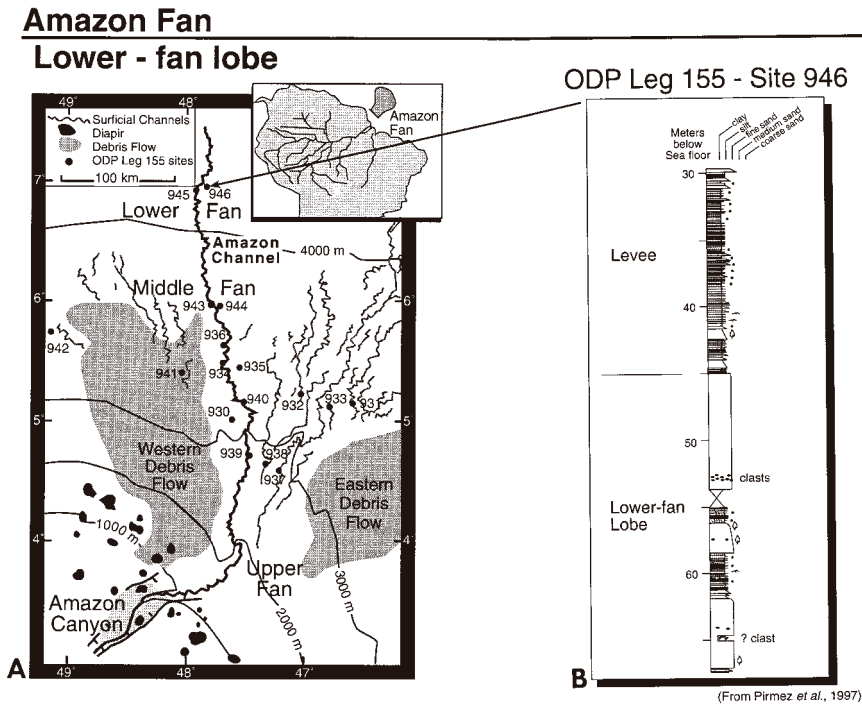
Fig. 6.29. (*A*) Ocean Drilling Program (ODP) Leg 155 Sites, Amazon Fan. (*B*) Sedimentological log of lower-fan lobe and levee facies at Site 946. Note rafted clasts in sandy matrix, suggesting deposition from sandy debris flow. (Location map after Normark, Damuth et al. (1997) and Site Log after Shipboard Scientific Party (1995d).)

This lobe facies is several meters in thickness. I have interpreted this lobe facies as debrites. A typical depositional lobe, however, should be composed of turbidites (Mutti, 1977). Normark, Damuth et al. (1997, p. 613) wrote, '… *it is difficult to explain why thick intervals with numerous mud clasts of variable size are randomly scattered into the sand matrix and are not also graded…*'' The reason is that these sandy intervals with mud clasts represent debrites, not turbidites.

Normark, Damuth et al. (1997, p. 642) concluded that

'*Insufficient sites were drilled in channel-fill and depositional lobe elements during Leg 155 to provide a clear insights regarding the models of asymmetric (thinning and fining upward and thickening and coarsening upward) cycles commonly used to identify channel-fill and lobe deposits, respectively, in outcrops and boreholes (Mutti and Ricci Lucchi, 1972; Mutti, 1979).*'

Quantification of facies, however, does suggest that the Amazon Fan channel and HARP elements (depositional lobes) are dominated by debrites and slumps, not turbidites. Thus the available core data from the Amazon Fan invalidates Mutti's conceptual models of ancient channels and lobes dominated by turbidites.
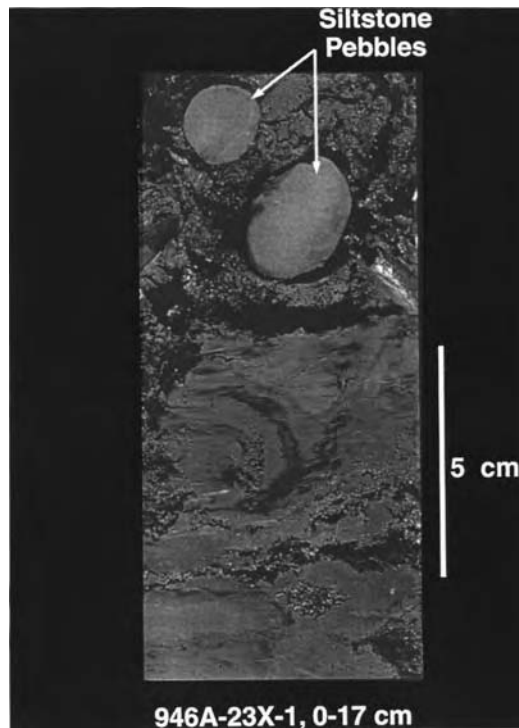
Fig. 6.30. Core photograph showing rafted siltstone pebbles in sandy (fine- to medium-grained) matrix, suggesting deposition from sandy debris flow in lower-fan lobe environments, Site 946A, Amazon Fan. (Photo courtesy of J. E. Damuth.)

More importantly, we should use modern systems as templates for reconstructing ancient environments (*Uniformitarianism*), not *vice versa*.

6.5.7 Modern Mississippi Fan: 'channelized lobes'

The Mississippi Fan in the Gulf of Mexico was the first modern deep-sea fan from which long DSDP cores were retrieved (Fig. 6.31). These cores were taken during the Leg 96 (Bouma et al., 1985; Bouma, Coleman et al., 1985). The cores from the Leg 96 suggest a variety of depositional facies (Fig. 6.32). Interpreted depositional processes of these facies are slumps, debris flows, turbidity currents, and bottom currents (Stow et al., 1985; Shanmugam et al., 1988a).

Conventionally, sheet-like geometries are associated with turbidites deposited at the terminus of a submarine fan. These sheet sands are also known as depositional lobes (Mutti, 1977). The outer fan areas of the Mississippi Fan were used as the modern analog for turbidite fans with sheet-like geometries (Shanmugam et al., 1988b). Such an analogy was based strictly on the parallel and continuous
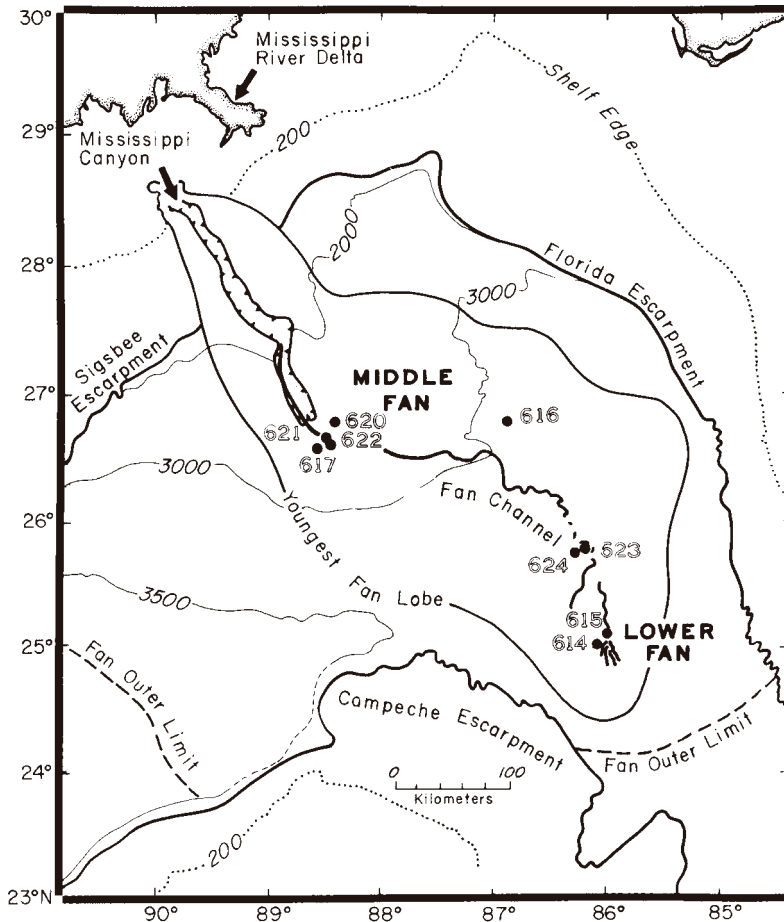
Fig. 6.31. Location map showing DSDP Leg 96 Sites, Mississippi Fan, Gulf of Mexico. (After Shanmugam et al. (1988a). Reprinted by permission of Elsevier.)

reflection patterns observed on seismic profiles (Fig. 6.33). However, subsequent SeaMARC 1A sidescan-sonar data (Twichell et al., 1992) as well as piston and gravity cores (Nelson et al., 1992; Schwab et al., 1996) taken from channels in the outer Mississippi Fan have revealed some important new information:

(1) The terminus of the Mississippi Fan is not sheet-like as previously thought.
(2) Piston and gravity cores taken from the terminus of the Mississippi Fan shows channels in the terminus of the Mississippi Fan (Fig. 6.34) are filled with debrites for the most part (Fig. 6.35).
(3) Contrary to popular belief, the terminus of the Mississippi Fan is channelized and dendriitic in nature (Twichell et al., 1995). SeaMARC 1A sidescan-sonar image mosaic of the distal Mississippi Fan shows dendritic pattern with abrupt
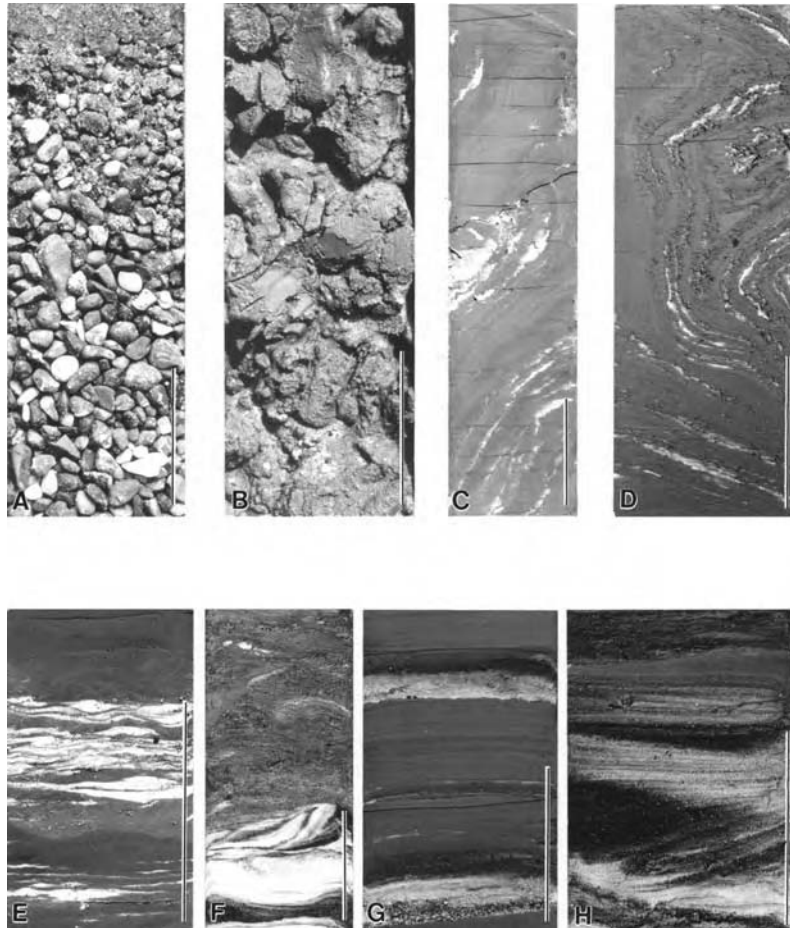
Fig. 6.32. Core photographs of DSDP Leg 96 cores, Mississippi Fan, Gulf of Mexico. (*A*) Gravelly unit with sand near the top of uncertain origin because of core disturbance, mid-fan channel, Site 621, 213.9 m. (*B*) Pebbly mud of debris flow origin, mid-fan channel, Site 621, 195.5 m. (*C*) Contorted mud of slump origin, mid-fan channel, Site 621, 202.3 m. (*D*) Contorted mud of slump origin, mid-fan channel, Site 617, 45.3 m. (*E*) Rippled silt of bottom-current reworking origin, mid-fan overbank, Site 617, 84.1 m. (*F*) Contorted sand of slump origin, lower fan, Site 614A, 129 m. (*G*) Normally graded fine sand layers of turbidity current origin, lower fan, Site 614A, 100.7 m. (*H*) Cross laminated fine sand of bottom current reworking origin, lower fan, Site 614A, 127.6 m. Scale bar = 5 cm. (After Shanmugam et al. (1988a). Reprinted by permission of Elsevier.)

edges (Fig. 6.36). Twichell et al. (1995, their Fig. 41.2 caption, p. 283) explained this pattern as '*The association of these high-backscatter deposits with channels and their abrupt edges suggest channelized transport of the sediments that compose these deposits and a sudden freezing of the flows at the site of deposition.*' Sudden freezing of flows is characteristic of plastic debris flows (see Chapter 3). Core 44 taken from these dendritic distal edges of the
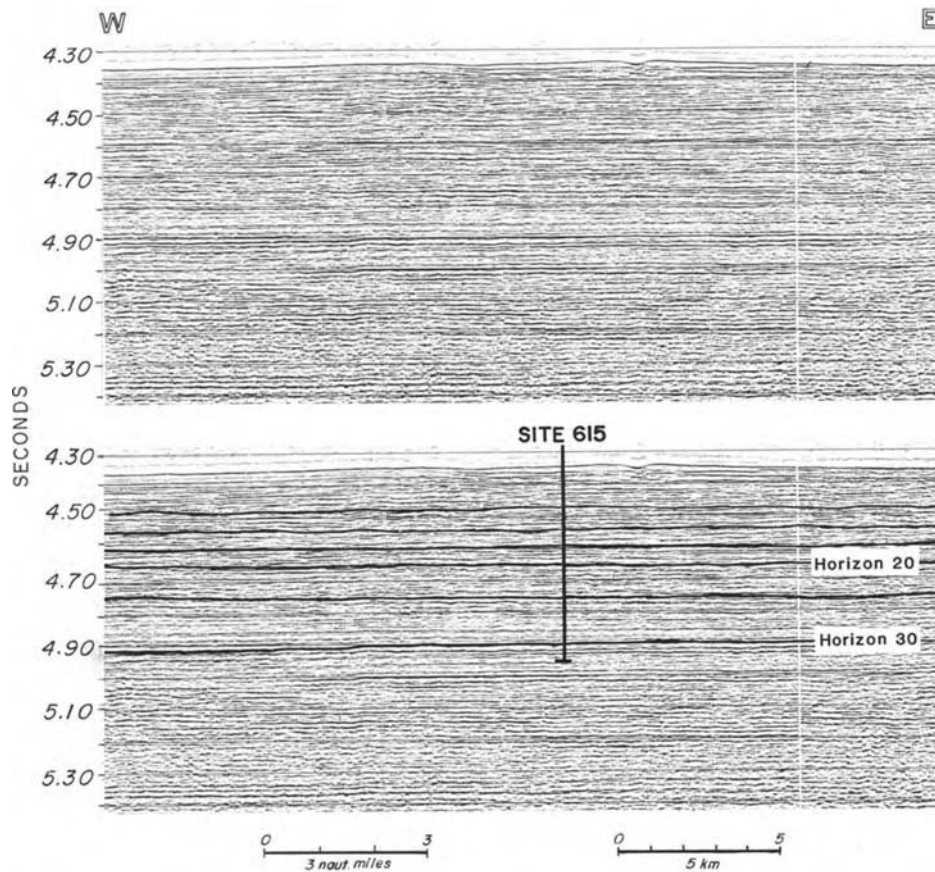
Fig. 6.33. Watergun seismic reflection profile (R/V 'Conrad') showing parallel and continuous reflection profiles of lower Mississippi Fan. See Fig. 6.31 for position of Site 615. (After Shanmugam et al. (1988a). Reprinted by permission of Elsevier.)

Mississippi Fan, composed of chaotic silt beds with floating clay clasts, has been interpreted to be composed of 100% debrites (Fig. 6.35). These dendritic features are called 'channelized lobes' in this book for distinguishing them from non-channeluzed depositional lobes. These 'channelized lobes' do not imply slope/upper fan environments as advocated by Nelson et al., (1985).

The application of the term depositional lobe, meant for turbidite-dominated fans (Mutti, 1977), to debrite-dominated terminus of the Mississippi Fan (Twichell et al., 1992; Nelson et al., 1992; Schwab et al., 1996) is inappropriate. Such a misapplication perpetuates the notion that turbidites are more common in modern fans than they actually are.
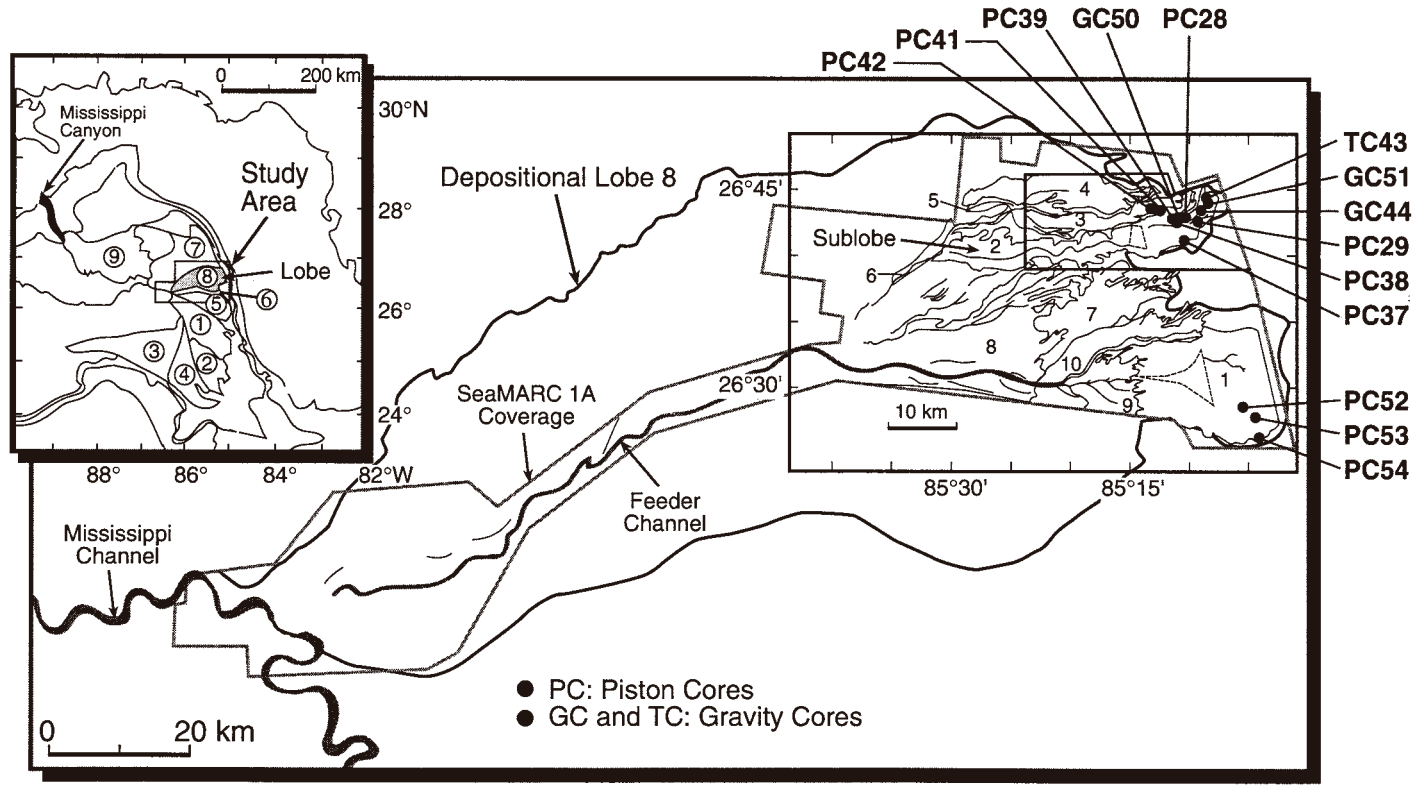
Fig. 6.34. Map showing location of piston and gravity cores taken from 'channelized lobes' in the outer Mississippi Fan, Gulf of Mexico. Compiled from Twichell et al. (1992) and Schwab et al. (1996). (After Shanmugam (1997a). Reprinted by permission of Elsevier.)
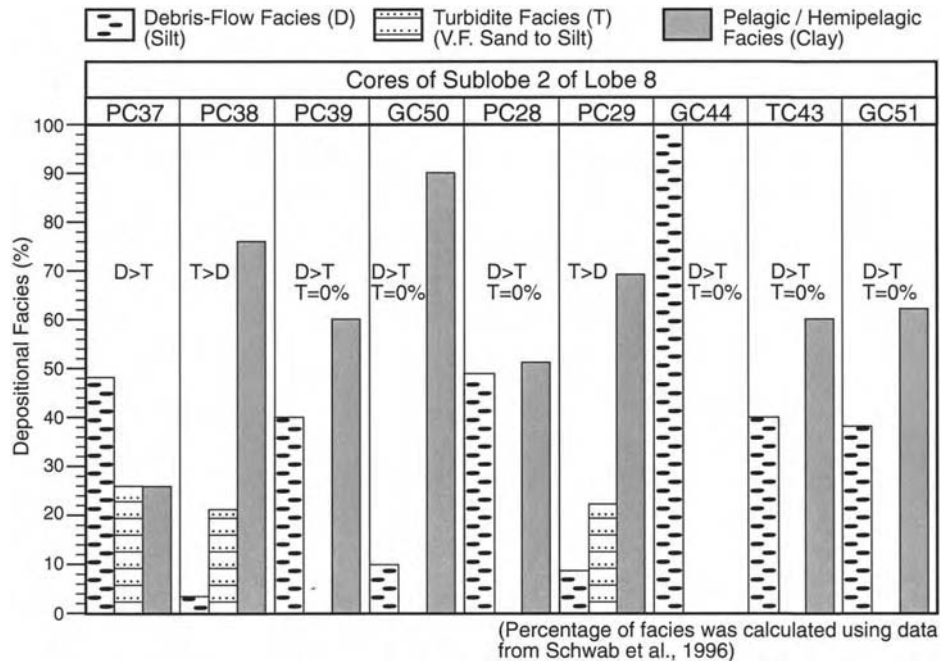
Fig. 6.35. **Histograms showing dominance of debris-flow facies in cores from 'channelized lobes' in the outer Mississippi Fan (see Fig. 6.34 for location of cores). Percentages of facies were calculated by the author using published data from Schwab et al. (1996). Note that all nine cores contain debris flows, whereas only three cores comprise turbidites. In seven out of nine cores, the amount of debris-flow facies far exceeds the amount of turbidite facies. In core GC 44, debris-flow facies comprises 100%. This facies distribution has important implications for submarine fan models. See text for details. (After Shanmugam (1997a). Reprinted by permission of Elsevier.)**

6.5.8 Modern Monterey Fan: depositional lobe

The Monterey Fan is located in offshore central California (Fig. 6. 37). Based on surface morphology, interpreted from geophysical data, the term 'depositional lobe' has been applied to this modern fan (Normark et al., 1985; Gardner et al., 1996). There are large boulders, which are 20 m or more in diameter, on the most recent depositional lobe of Monetery Fan (Fig. 6.38A). They occur both as isolated individual boulders and as fields of boulders (Gardner et al., 1996). 492 boulders were counted. The fields of boulders show a rough alignment with lineations in backscatter intensity that was interpreted as sediment-transport flow patterns (Fig. 6.38B). Gardner et al. interpreted these boulders as deposits of large mass-transport flows. Box cores taken from the Monterey Fan also show floating silt clasts in sand (Lee et al., 1996; their Fig. 13.11). This lithofacies may be interpreted as sandy debrites.
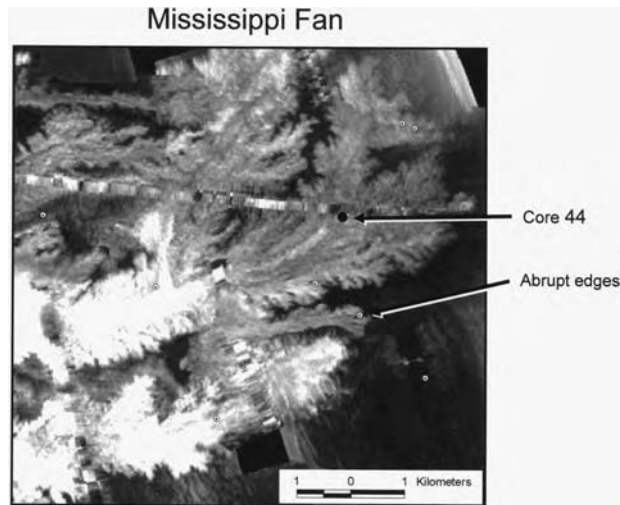
Fig. 6.36. SeaMARC 1A sidescan-sonar image mosaic of 'depositional lobes' of the distal Mississippi Fan showing dendritic pattern with abrupt edges. Strong acoustic returns (high backscatter) are white and light grey; weak acoustic returns (light backscatter) are black and dark grey. Note position of core 44, which contains chaotic silt beds and floating clay clasts (see Twichell et al., 1995, their Fig. 41.4, p. 286), suggesting deposition from slumps and debris flows. See Fig. 6.34 for location of core 44 that is composed of 100% debris flow (Fig. 6.35). (Modified after Lee et al. (1996). Image courtesy of D. C. Twichell.)
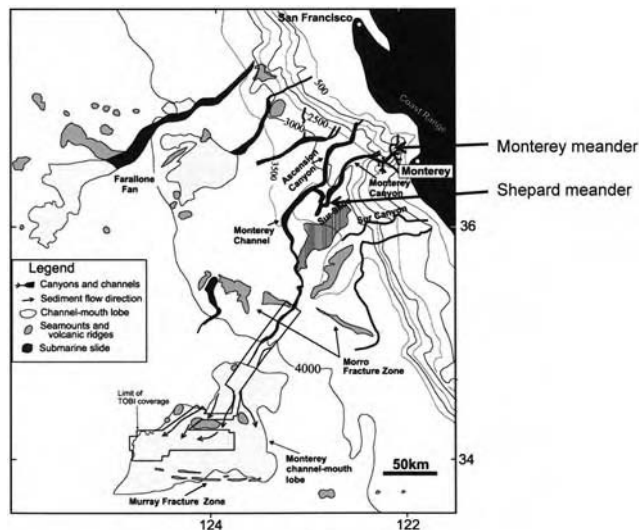
(Klaucke et al., 2004)

Fig. 6.37. Location map of Monterey Fan showing channel-mouth lobe, offshore California. Note locations of the Monterey meander (Greene and Ward, 2003) and the Shepard meander (Fildani and Normark, 2004). (Modified after Klaucke et al. (2004). Reproduced with permission from Elsevier.)
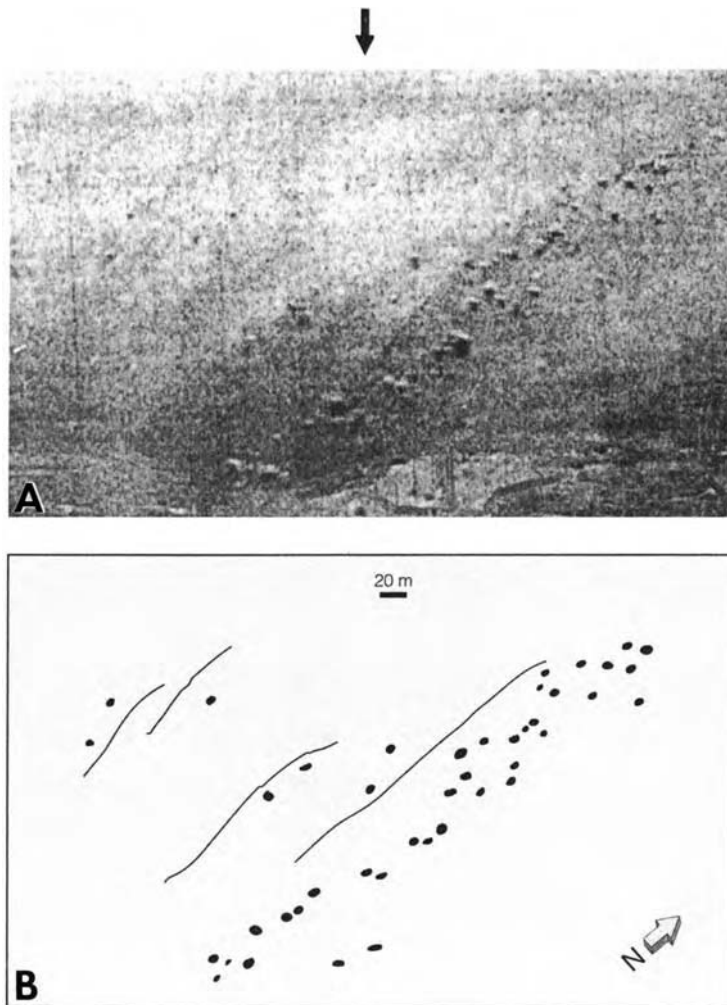
Fig. 6.38. (*A*) **TOBI (Towed Ocean Bottom Instrument) Sidescan-sonar image of boulders on surface of the most recent depositional lobe of the Monterey Fan.** (*B*) **Interpretation showing distribution of boulders. Lines represent sediment-transport flow patterns. Arrow on sonograph shows direction of insonification (i.e., sonar illumination). (After Gardner et al. (1996; their Fig. 12–17). Figure, published by Cambridge University Press, is not subject to U.S. copyright law. Reproduced with permission from J. V. Gardner.)**

In studying channel-mouth lobes of the Monterey Fan, Klaucke et al. (2004, p. 181) noted, '*Sand is particularly concentrated in finger-like areas of low backscatter intensity and is interpreted as the result of non-turbulent sediment-gravity flows depositing meters thick massive, fine sand.*' This interpretation clearly implies that finger-like deposits are products of laminar sandy debris flows (see Chapter 12).

Studies of the Monterey Fan, the Amazon Fan, and the Mississippi Fan clearly suggest that lobe-like features on modern deep-water systems are indeed dominated by debrite deposition.

6.5.9 Potter Sand, upper Miocene, California

The upper Miocene Potter Sand is the most prolific oil producing reservoir in the North Midway Sunset Field, Kern County, California (Fig. 6.39). Heavy oil is produced from this field by steamflooding (Schamel et al., 1998). Nearly 500 m of core from the upper Miocene Potter Sand were described by Shanmugam and Clayton (1989). Reservoir description of this sand-rich deep-water system revealed channel and lobe facies. In particular, the Potter Sand was interpreted to contain deposits of both braided channels and meandering channels.

Characteristics of braided channel deposits are:

• Coarse lithofacies composed of gravel and pebbly sand (Fig. 6.40)
• Erosional bases
• Amalgamated units
• Common occurrence in the upper part of the Potter Sand (Fig. 6.41)
• A general lack of interbedded mudstone facies
• Uniformly high permeability (e.g., 10000 mD) throughout the unit (Fig. 6.41)
• Sheet-like geometry.

The origin of braided channel facies in Potter Sand was originally attributed to density-modified grain flows (Shanmugam and Clayton, 1989, p. 411). A more appropriate interpretation of these sands would be sandy debris flows.

Characteristics of meandering channel deposits are:

• Coarse- to medium-grained sand (Fig. 6.41)
• Erosional bases
• Isolated sand units sandwiched between mudstone levee facies
• Occurrence below braided channel facies (Fig. 6.41)
• Rip-up clasts
• Fining-up trends
• Upward decrease in permeability mimicking grain-size trends (Fig. 6.41)
• Lenticular geometry.

Interpreted mechanisms for deposition of these sands are sandy debris flows, slumps, and turbidity currents.

6.6 Submarine non-fan environments

6.6.1 Modern examples

Not all deep-water systems make a submarine fan. Non-fan environments are common in the deep sea (Shanmugam and Moiola, 1988). Ancient examples of

Deep-water processes and facies models
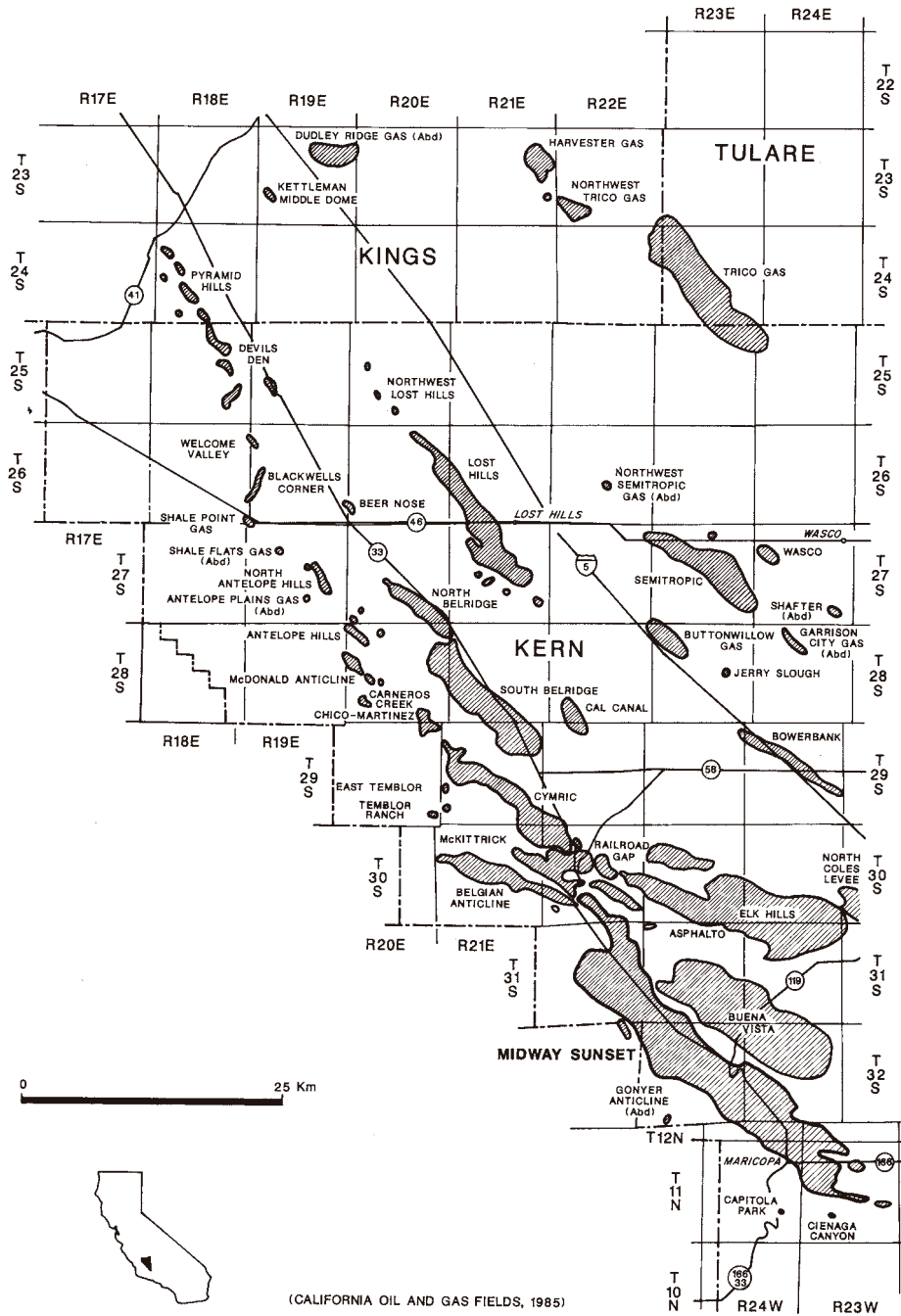
Fig. 6.39. Location map of Midway Sunset Field. After California Oil and Gas Fields (1985).
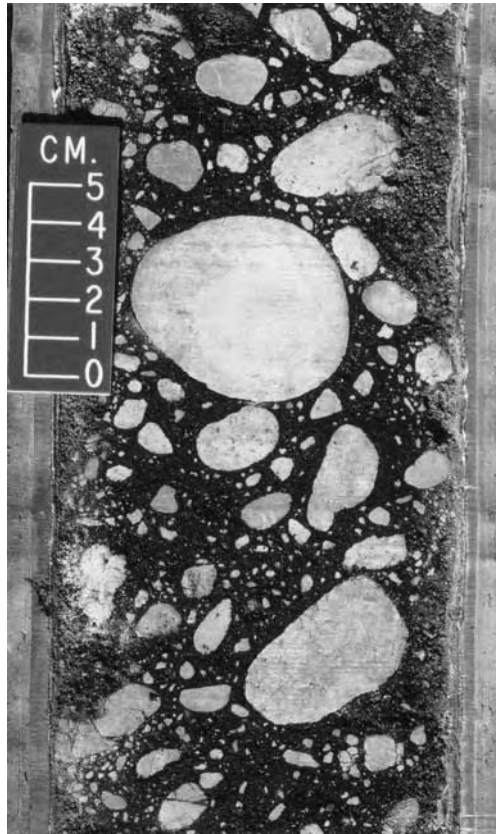
Fig. 6.40. Core photograph showing pebbly coarse sand interpreted as deposits of sandy debris flows in deep-water braided channel environments. Quartzite pebbles (white) are in coarse sandy matrix (oil stained). Upper Miocene Potter Sandstone, Midway Sunset Field, California.

non-fan systems were discussed by Chan and Dott (1983). Non-fan debris tongues occur in modern slope- to-basin environments in the northern Atlantic (Embley, 1980). Core sample taken from these tongues show floating mud clasts and planar fabric, indicating deposition from laminar debris flows. Multiple debris tongues have been mapped on the Norwegian-Barents Sea Continental Margin (Elverhoi et al. 1997). These tongues are part of the 'Bear Island Fan' (Fig. 6.42). These debris tongues have been ascribed to ice-stream processes on high-latitude continental margins (Dowdeswell et al., 2002). Other examples of non-fan debris tongues are the Saharan debris flow in offshore northwest Africa (Gee et al., 1999) and the 'East Breaks Slide' in the Gulf Mexico (Fig. 6.10).
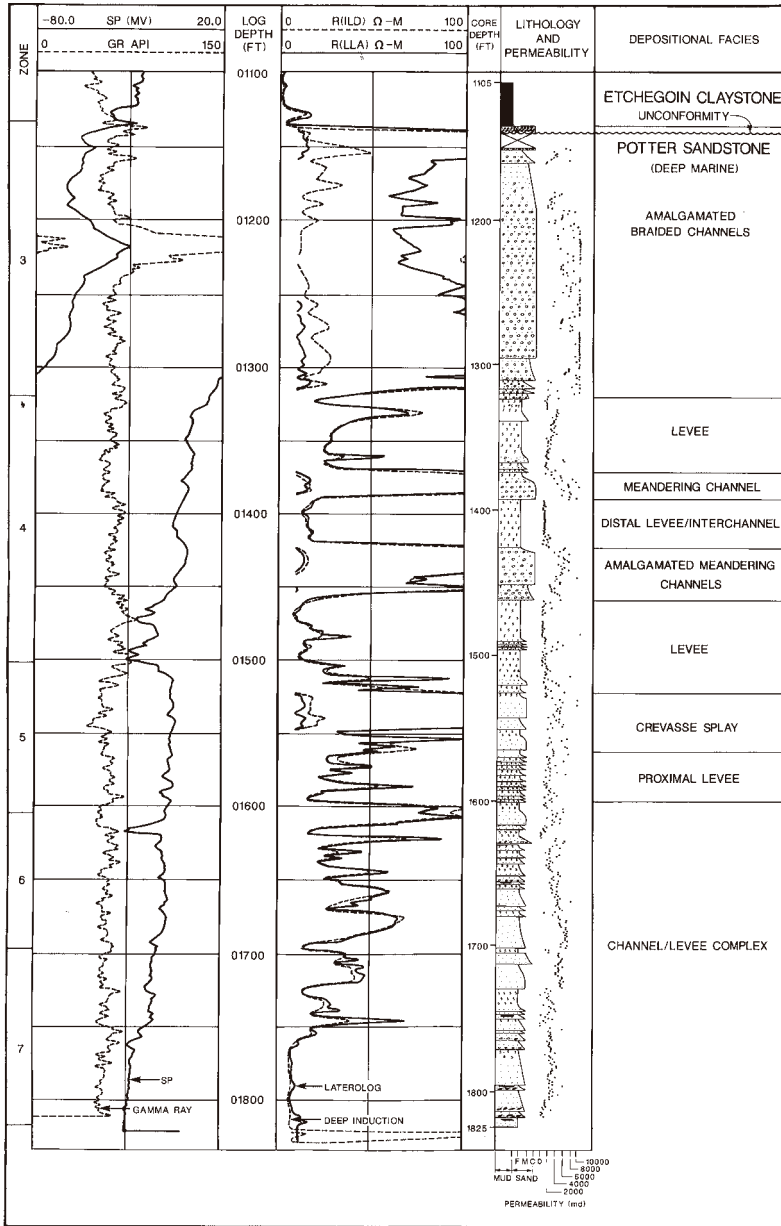
Fig. 6.41. Vertical distribution of depositional facies in the Upper Miocene Potter Sandstone, Midway Sunset Field, California. Note amalgamated braided channel facies and isolated meandering channel facies.
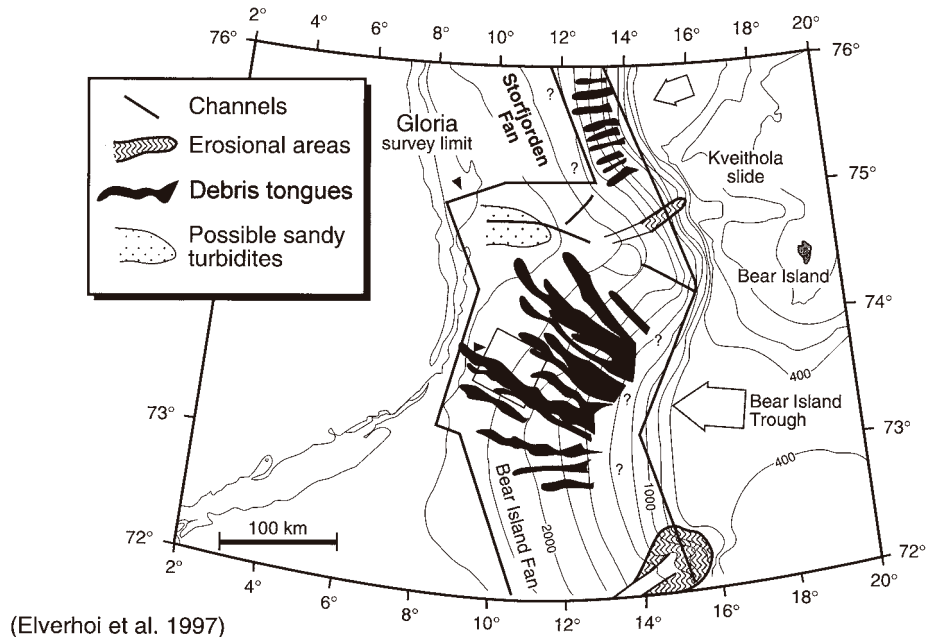
(Elverhoi et al. 1997)

Fig. 6.42. Map view of the 'Bear Island Fan' showing modern debris tongues on the Norwegian-Barents Sea Continental Margin. These features were originally described as 'debris lobes' by Elverhoi et al., (1997). In this book, these features are referred to as 'tongues' in order to distinguish them from 'lobes'. (Modified after Elverhoi et al. (1997). Reproduced with permission from Springer-Verlag.)

6.6.2 Zafiro field, Pliocene, Equatorial Guinea

The Zafiro Field (Fig. 6.43), discovered in March 1995 by Mobil and United Meridian Corporation (UMC), is the first oil field in Equatorial Guinea (Famakinwa et al., 1996; Monson and Pita, 1997; Shanmugam et al., 1997b; Williams et al., 1998). The Zafiro reservoirs are composed of the Pliocene Intra-Qua Iboe (IQI) member of the Agbada Formation. As discussed earlier, the IQI member is also the producing reservoir in the Edop Field, offshore Nigeria (see Chapter 4). Detailed sedimentological analysis of over 500 m of conventional cores from the Zafiro Field has established five major lithofacies:

(1) Lithofacies 1 is the principal reservoir facies. At the Zafiro 2 well, this lithofacies exhibits a fining-up trend in gamma-ray logs (Fig. 6.44A). The cored interval of this fining-up trend is composed of amalgamated, fine-grained, massive sand. The upper part of this sand is dominated by large mudstone clasts (Fig. 6.44C). These mudstone clasts show sharp edges and internal
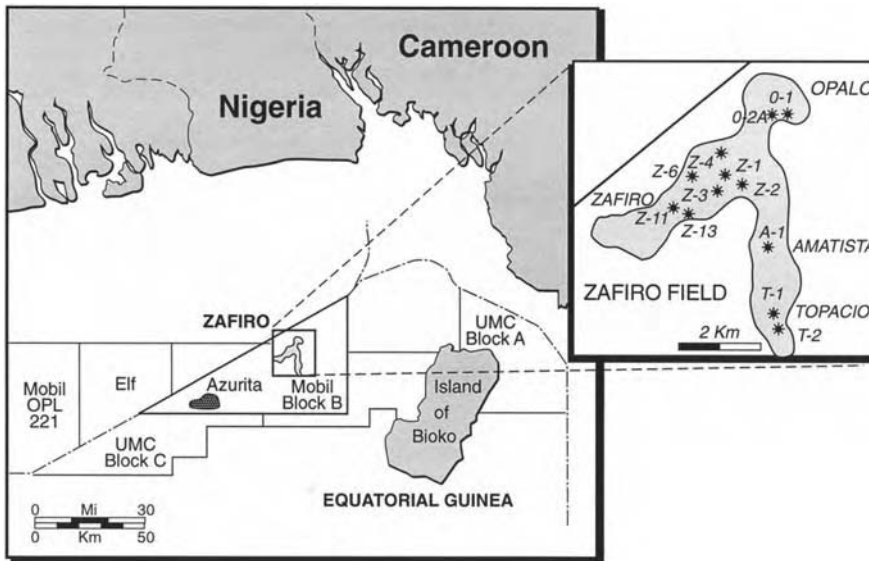
Fig. 6.43. Location map showing the Zafiro Field, Equatorial Guinea. Cored wells: Z–2 = Zafiro 2; Z–3 = Zafiro 3, Z–4 = Zafiro 4. (After Famakinwa et al. (1996).)

contortion (Fig. 6.45A). The 28-foot thick (9 m) sand interval has a sheared basal contact. Massive sand intervals with floating mudstone clasts and quartz granules are common in the Zafiro 3 well (Fig. 6.46). At the Zafiro 3 well, pockets of quartz pebbles are present in medium-grained massive sand (Fig. 6.45B). This facies has been interpreted to be deposits of sandy slumps and debris flows.

(2) Lithofacies 2 is a non-reservoir faces. It is composed of mudstone with slump folds, contorted bedding, floating mudstone clasts and quartz pebbles, and discordant dikes. It is interpreted as deposits of muddy slumps and debris flows.

(3) Lithofacies 3 is best developed in the Zafiro 3 well. There are two types: (a) amalgamated fine-grained sand layers; and (b) isolated fine-grained sand layers with interbedded mudstone layers. The isolated type is often rhythmic in nature (Fig. 6.45C). Current ripple laminae and parallel laminae are common in fine-grained sand. (Fig. 6.45C). This facies with traction structures has been interpreted as products of bottom-current reworking.

(4) Lithofacies 4 is composed of normally graded mudstone and fine-grained sand with sharp bases and gradational tops (Fig. 3.32). This facies, composed of thin layers, is interpreted as deposits of turbidity currents.

(5) Lithofacies 5, composed of laminated mudstone, is interpreted as deposits of pelagic and hemipelagic settling.
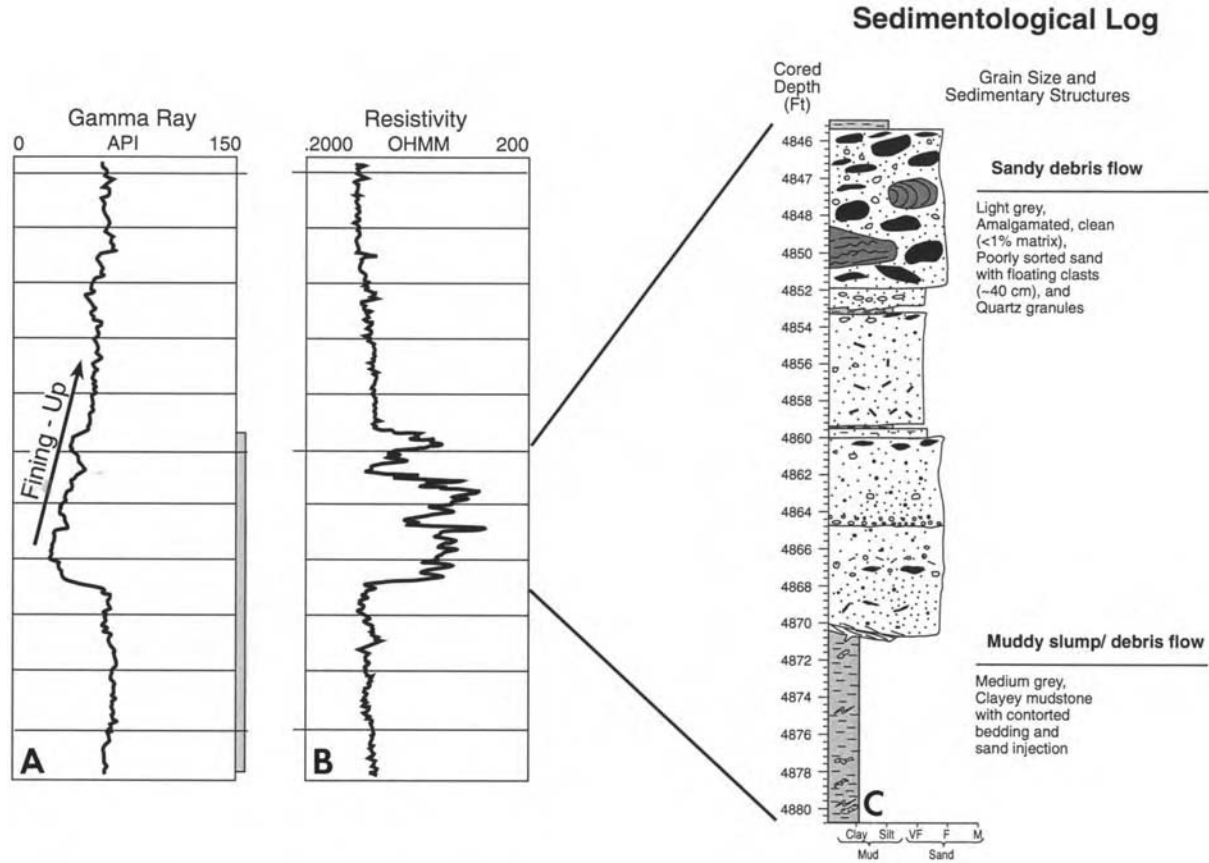
Fig. 6.44. (*A*) Gamma-ray log showing fining-up motif for a cored interval (shaded vertical bar). (*B*) Resistivity log. (*C*) Sedimentological log showing amalgamated massive sandy units with increasing amount of mudstone clasts near the top. Zafiro 2 well, Pliocene, Zafiro Field, offshore Equatorial Guinea. (From Famakinwa et al. (1996, 1997).)
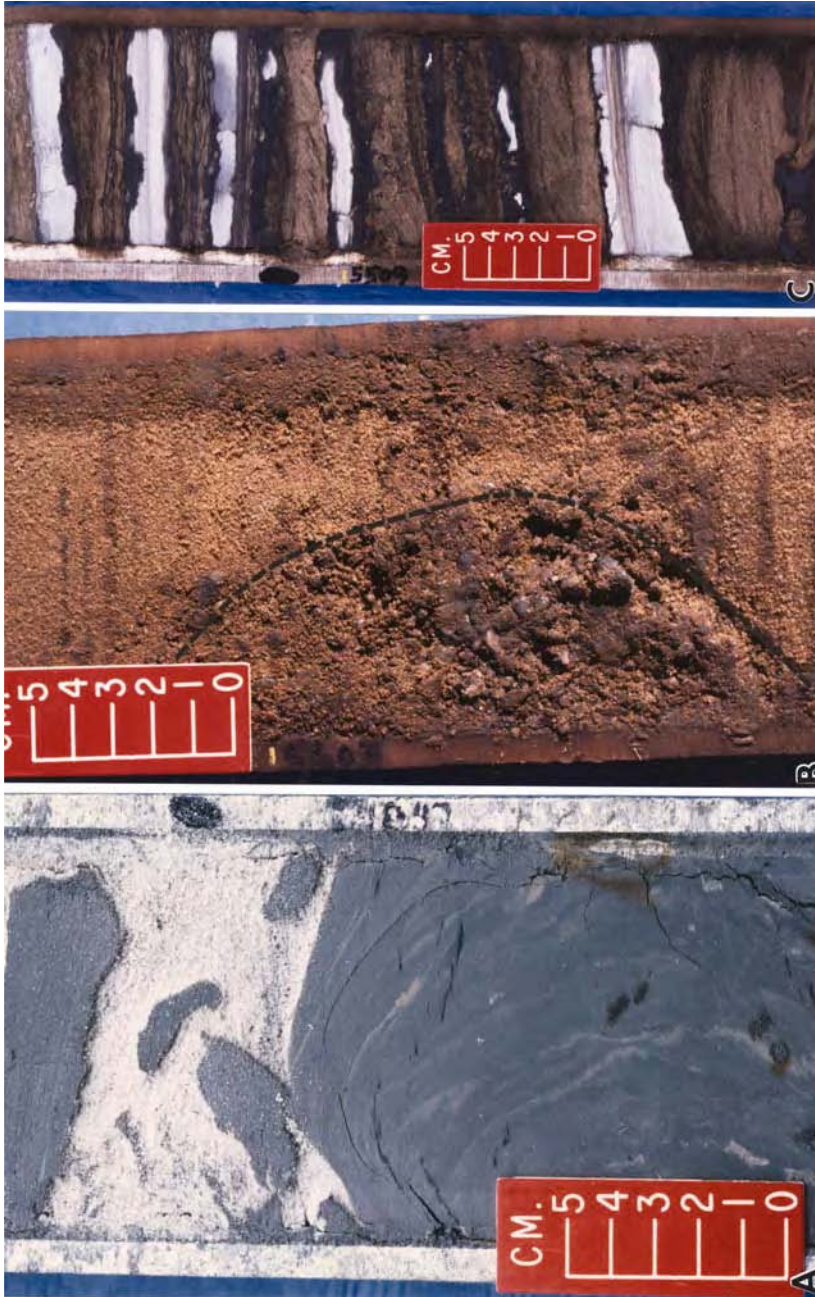
Fig. 6.45. (*A*) Facies 2: Core photograph showing floating mudstone clasts in fine-grained sand; 6847 ft (2087 m), Zafiro 2 well. (*B*) Facies 2: Pocket of quartz gravel (dashed line) in medium-grained sand; 5603 ft (1708 m), Zafiro 3 well. (*C*) Facies 3: Rhythmic occurrence of rippled sand and mudstone (white) layers; 5509 ft (1679 m), Zafiro 3 well. Pliocene, Zafiro Field, offshore Equatorial Guinea. (After Famakinwa et al. (1996) and Shanmugam et al. (1997b).)
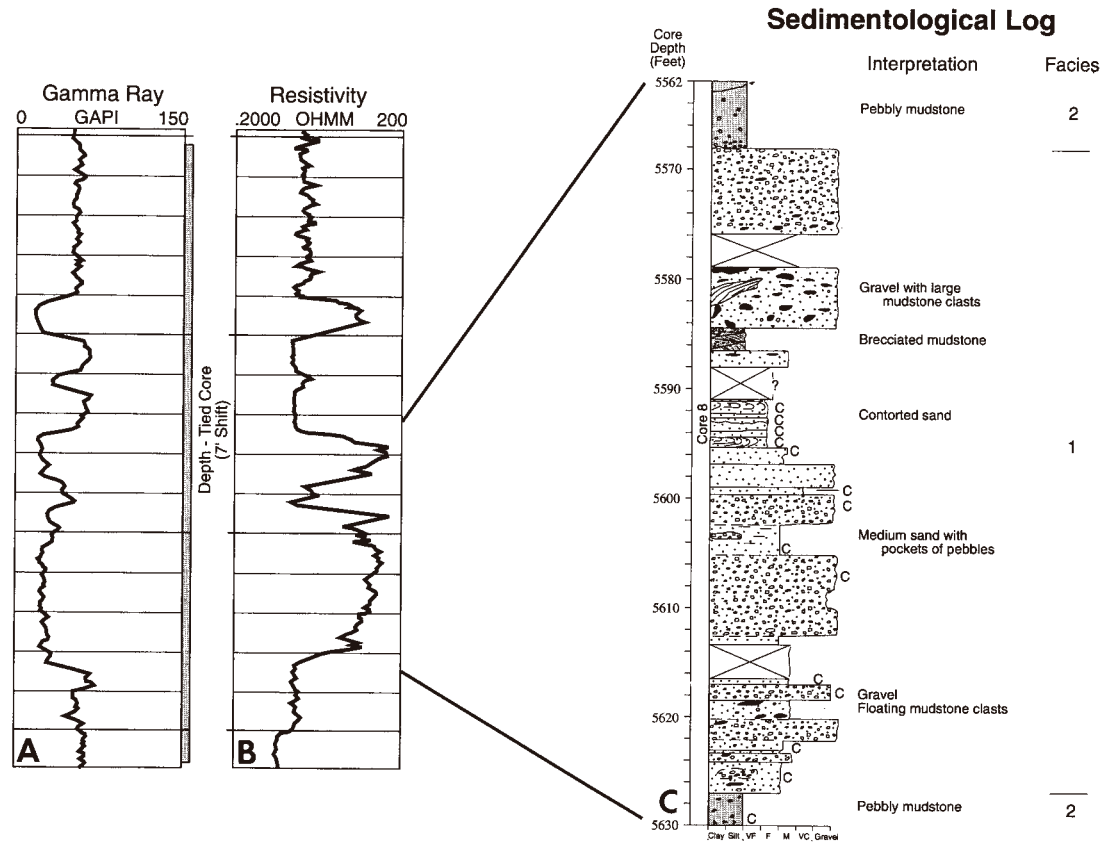
Fig. 6.46. (*A*) Gamma ray log showing blocky motif of a cored interval (shaded vertical bar). (*B*) Resistivity log. (*C*) Sedimentological log showing amalgamated massive gravelly and sandy units with mudstone clasts near the top. C = coaly fragments. Zafiro 3 well, Pliocene, Zafiro Field, offshore Equatorial Guinea. (After Famakinwa et al. (1996) and Shanmugam et al. (1997b).)
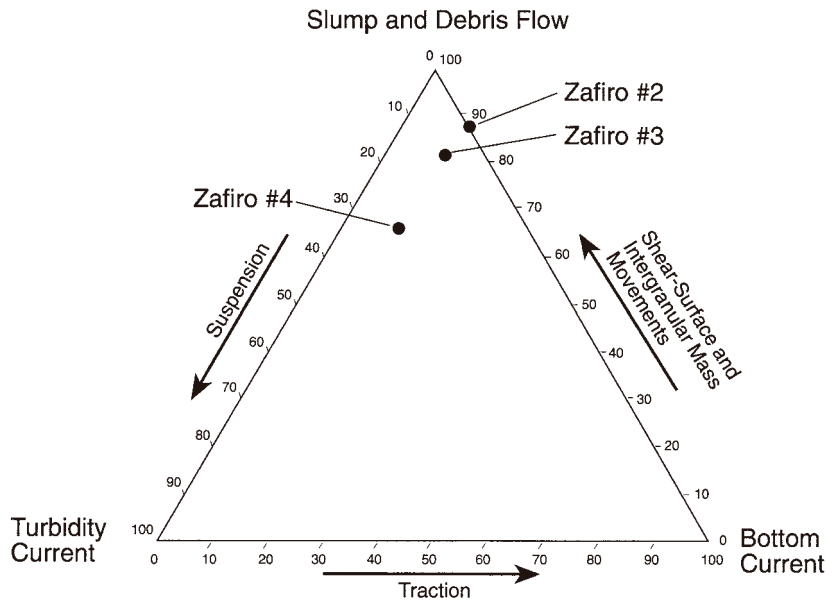
Fig. 6.47. Ternary diagram showing the volumetric abundance of slump and debrite facies in the Zafiro 2, 3, and 4 wells (Shanmugam et al., 1997b).

In the Zafiro area, cored interval is dominated by deposits of sandy slumps and sandy debris flows (Fig. 6.47). Famakinwa et al. (1996) proposed a base-of-slope setting, dominated by sandy slumps, sandy debris flows, and bottom current reworking with minor turbidity currents. This is a non-fan environment.

6.7 Submarine basin-plain environments

6.7.1 Modern and ancient examples

The flat region of the ocean floor, usually at the base of a continental rise, where the gradient is less than 1:1000 has been referred to as an 'abyssal plain' (Heezen et al., 1959). In referring to ancient abyssal plains, the geologic community commonly uses the more general term 'basin plain' (Fig. 1.2). Basin plains form in response to filling and leveling of sea-floor topography by various depositional processes. Because of their flat nature, basin plains are favorable sites for forming sheet-like geometries. Abyssal-plain deposits cover large areas. The modern Enderby abyssal plain (north of Antarctica) occupies a vast area covering nearly 3.7 million square kilometers (Weaver et al., 1987).

A well-known ancient example is the *Contessa* bed of the Miocene Marnoso-arenacea Formation in the northern Italian Apennines (Ricci Lucchi and

Valmori, 1980). The Contessa bed has been traced over one hundred kilometers. Basin-plain environments are ideal for forming sheet-like deposits from turbidity currents. Although basin-plain environments are dominated by muddy facies, basin plains are also areas in which large sandy slides and sandy debrites may accumulate.

6.8 Synopsis

Modern deep-water systems show a clear dominance of deposition by sandy debris flows and related mass-transport processes in slopes, canyons, channels, lobes, and basin-plain environments (Fig. 6.48). Conventionally, the two principal fan elements (i.e., channels and lobes) are considered to be dominated by turbidites. But modern
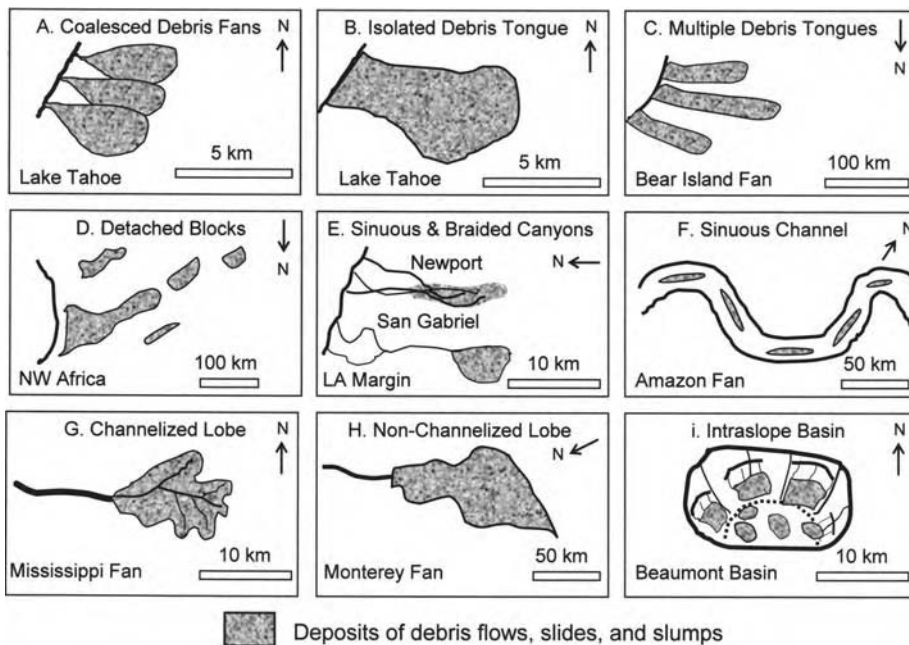
Fig. 6.48. Summary diagram showing types of modern environments in which deposits of debris flows, slides, and slumps have been documented. (*A*) Coalesced debris fans (subaqueous bajada) in Lake Tahoe (Gardner et al., 2000) (*B*) Isolated debris tongue in Lake Tahoe (Gardner et al., 2000). (*C*) Multiple debris tongues in the Bear Island Fan (Elverhoi et al., 1997). (*D*) Detached blocks in offshore northwestern Africa (Jacobi, 1976) (*E*) Los Angeles Margin with braided Newport Canyon (top) and sinuous San Gabriel Canyon (bottom). (*F*) Sinuous channel in the Amazon Fan (this book, and Normark, Damuth et al., 1997). (*G*) Channelized lobe in the Mississippi Fan (Twichell et al., 1995; Shanmugam, 1997a). (*H*) Non-channelized lobe in the Monterey Fan (Gardner et al. 1996; and Klaucke et al., 2004). (*I*) Intraslope Beaumont Basin (Tripsanas et al., 2004). Horizontal scale bar and north direction are approximate.

case studies demonstrate that channels and lobes are dominated by debrites. More importantly, these examples show that sands are distributed in a variety of manner in deep-water settings, not just as channels and lobes. This new information should help petroleum geoscientists to develop realistic depositional models in deep-water exploration (see Chapter 12).

Chapter 7

Process-related problems

7.1 Introduction

The objective of this chapter is to address important process-related problems. Most of these problems are the result of our skewed emphasis on turbidity currents and their deposits. These problems have manifested themselves into popular turbidite myths. Ten of these myths have been dispelled (Shanmugam, 2002a).

7.2 Conflicting definitions of turbidity currents

Kuenen (1951) used the term 'turbidity currents of high-density' for stratified flows with an upper turbulent layer and a lower non-turbulent (slide/debris flow) layer (Fig. 7.1A). In justifying his definition, Kuenen (see comment in Sanders, 1965, p. 217) explained that '*It is much simpler to leave out of the definition of turbidity current any reference to hydrodynamic mechanisms*.' However, one cannot practice process sedimentology without using basic principles of hydrodynamics. Because of this loophole in Kuenen's definition, later authors have misused the concept of turbidity currents. Examples are:

(1) McCave and Jones (1988, p. 250) advocated, '*… deposition of ungraded muds from high-density non-turbulent turbidity currents*.'
(2) Kneller and Buckee (2000) claimed that turbidity currents can be non turbulent (i.e., laminar) in state. Furthermore, they claimed that turbidity currents are natural phenomena whose exact hydrodynamic properties are unclear.
(3) Mutti et al. (2003b, p. 745) justified Kuenen's flawed definition for the sake of maintaining a stable terminology.

Sanders (1965) was the first process sedimentologist who made a clear distinction between laminar debris flows and turbulent turbidity currents. He clarified that turbidity currents are density currents caused by sediment in *turbulent* suspension. This clarity comes from experimental results of Bagnold (1954, 1956)
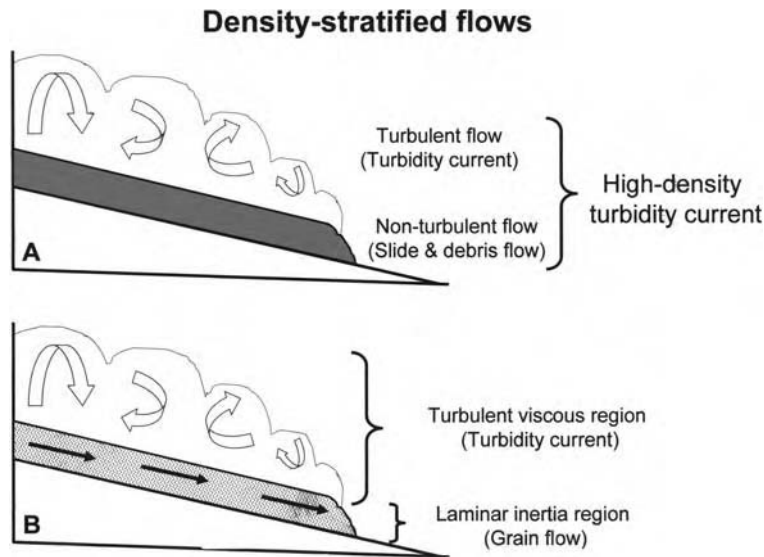
Fig. 7.1. (*A*) **Diagram showing Kuenen's (1950a, 1951) concept of 'high-density turbidity currents'
that includes both the basal non-turbulent (slide/debris flow) layer and the upper turbulent
(turbidity current) layer. (*B*) Diagram showing Bagnold's (1956) concept that distinguishes
basal laminar inertia region and upper turbulent viscous region as two different processes.**

who distinguished turbulent flows from laminar flows in density-stratified flows
(Fig. 7.1B). Middleton (1993, p. 93) clearly excluded laminar flows from turbid-
ity currents by stating, '… *if it is truly nonturbulent it can no longer be classified
as a turbidity current.*' Thus the characterization 'non-turbulent turbidity currents'
is an oxymoron from a hydrodynamic point of view.

7.3 Conflicting definitions of turbidites

The crux of the turbidite controversy can be attributed to conflicting definitions
of turbidity currents and turbidites. For example:

(1) Kuenen (see comment in Sanders, 1965, p. 218) defined, '*Deposits from all
     kinds and combinations of currents falling under the definition of turbidity
     currents are turbidites, whether there was bottom traction, laminar flow,
     non-turbulent flow etc., involved or not.*'
(2) Following the approach of Kuenen, Mutti (1992, p. 40), stated, '*Cohesive
     debris flows and turbidity currents should therefore be considered the two
     main mechanisms responsible for having transported and deposited the bulk
     of turbidite sediments.*'

(3) Furthermore, Mutti et al. (1999, p. 19) defined 'turbidites' as the deposits of all sediment-gravity flows, which include debris flows, grain flows, fluidized sediment flows, and turbidity currents (Fig. 7.2). This approach of Mutti et al., if applied, would undo the progress that have been made in process sedimentology during the past four decades in distinguishing deposits of debris flows, grain flows, fluidized/liquefied flows, and turbidity currents from one another.

(4) Sanders (1965) emphasized that the term turbidites should refer strictly to those deposits that formed from turbulent suspension of turbidity currents (Fig. 7.2). Middleton and Hampton (1973) also considered only those deposits of turbidity currents to be turbidites. In spite of this simple and straight forward concept, the term turbidite means different things to different researchers. To some, turbidite means any deep-water sand, to others, turbidite means a deep-water channel or lobe sand, but to process sedimentologists turbidite means deposit of a turbidity current solely.

(5) Kneller (1996, p. 76) claimed, '... *many features recently suggested as characteristic of debris flow (e.g. sharp upper grain-size breaks, floating or*

Sediment - Gravity Flows
(Middleton and Hampton, 1973)
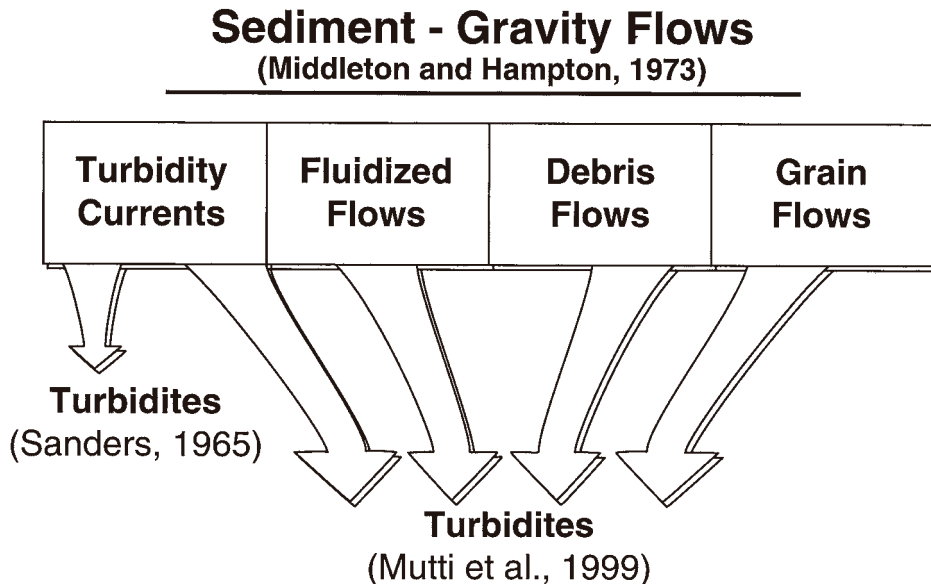
Fig. 7.2. Two differing definitions of the term 'turbidites.' According to Sanders (1965), turbidites are the exclusive deposits of turbidity currents. According to Mutti et al. (1999), deposits of all sediment-gravity flows, which include turbidity currents, fluidized flows, debris flows, and grain flows, are turbidites. In this book, Sanders' (1965) definition is followed. (After Shanmugam (2002a). Reproduced with permission from Elsevier.)

rafted mudstone clasts, inverse grading of clasts, moderate to high matrix content) or contourites (e.g. traction structures) are to be expected in turbidites.' In other words, Kneller would interpret features that are characteristic of debrites and contourites as that of turbidites.

Because of these conflicting definitions of turbidites, deposits of debris flows and avalanches have been classified as 'turbidites' using exotic nomenclature. Selected examples with my comments are (see Table 2.2):

(1) *Fluxoturbidites* (Dzulynski et al., 1959): deposits of sand avalanches.
(2) *Seismoturbidites* (Mutti et al., 1984): deposits of large-scale mass flows.
(3) *Megaturbidites* (Labaume et al., 1987): deposits of debris flows.
(4) *Atypical turbidites* and *problematica* (Stanley et al., 1978): deposits of slumps, debris flows, and sand flows.
(5) *High-concentration sandy turbidites* (Abreu et al., 2003): deposits of sandy debris flows.

In explaining the popularity of turbidites, Carter (1975, p. 147) wrote that '…*the temptation is always to tailor field observations to presently known processes of sediment deposition, rather than to tie them to speculative theoretical possibilities; it is therefore not surprising that many published studies of flysch sequences place great emphasis on features explicable by turbidity current hypothesis, and tend to be somewhat skeptical regarding deposition of individual beds by other mass-transport processes*.'

Lowe (1979, p. 81) observed that '*It is too often convenient to interpret deposits exhibiting textures and structures whose origins are problematic in terms of processes whose dynamics are equally poorly understood*.'

Fortunately, significant process sedimentological advances have been made during the past 50 years based on theoretical (Bagnold, 1954, Dott, 1963; Sanders, 1965, Middleton and Hampton, 1973; Enos, 1977; Allen, 1985a; Shanmugam, 1996a), experimental (Hampton, 1972; Marr et al., 2001), and observational (Hollister, 1967; Fisher, 1971; Shepard et al., 1979; Shanmugam et al., 1993a; Stow et al., 1998) basis. Thus we can now differentiate deposits of turbidity currents from those of other processes with confidence (see Chapters 3, 4, and 5).

7.4 Conflicting definitions of high-density turbidity currents

The concept of 'high-density turbidity currents' has been the center of controversy for more than 50 years. This is because the concept has been defined on the basis of four conflicting properties, namely, (1) flow density (Kuenen, 1950a) or grain concentration (Pickering et al., 2001); (2) driving force (Postma et al., 1988); (3) grain size (Lowe, 1982); and (4) flow velocity (Kneller, 1995). These definitions

are inconsistent with one another in terms of Newtonian rheology, turbulent state, and principal sediment-support mechanism of turbulence, the properties that define turbidity currents (Dott, 1963; Sanders, 1965; Middleton, 1993). As a consequence, virtually any process can be classified as a high-density turbidity current.

7.4.1 Flow density

Based on his experiments with subaqueous mud flows, Kuenen (1950a, p. 44) envisioned the concept of high-density turbidity currents. Kuenen conducted three series of experiments using an aquarium, a ditch, and a tank. In his experiments using an aquarium of 2 m in length and 50 cm in depth and breadth, he used slurries of clay, sand, and gravel with flow densities of up to 2 g/cm^3 on a slope of 8.5º. Unfortunately, Kuenen used the wrong term, 'turbidity currents of high density,' for density-stratified flows with densities of 2 g/cm^3. In terms of flow densities (e.g., Hampton, 1972), Kuenen's experimental flows are clearly debris flows. The clay content (23 to 33% of total solids by weight) in Kuenen's (1951) experiments was so high that his experimental flows were considered to be debris flows (Oakeshott, 1989). In Kuenen's (1951, p. 15) experiments, flows were observed to slide down a slope, move like a glacier, break up into slabs, crack on their surface, and come to rest on the slope (Fig. 7.3). These physical behaviors are typical of slides and debris flows rather than those of turbidity currents (see Chapter 3).
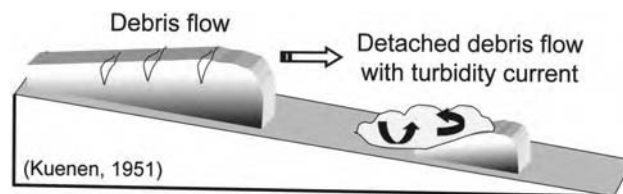
- Flow density: 1.57-1.59 g/cm³
- Clay content: 23-33% of solids
- Slides down the slope: Debris flow
- Moves like a glacier: Debris flow
- Breaks up into slabs: Debris flow
- Cracks on the surface: Debris flow
- Comes to rest: Freezing by debris flow
- Dilutes to turbidity current: Surface flow transformation

Fig. 7.3. Conceptual diagram illustrating properties of Kuenen's (1951) experimental 'Turbidity currents of High Density.' Note most properties are suggestive of deposition from debris flow, not turbidity currents.

In spite of its emphasis on flow density, the concept of high-density turbidity current has never been defined consistently on the basis of flow density (Shanmugam, 1996a). For example:

(1) The distinction between 'low' and 'high' density currents was set at a density value of 1.1 g/cm^3 (Kuenen, 1966).
(2) High-concentration flows (i.e., high-density turbidity currents) have a density range of 1.5 to 2.4 g/cm^3 (Middleton and Hampton, 1973).
(3) A debris flow has a density of 2.0 g/cm^3 (Hampton, 1972). Thus high-density turbidity currents and debris flows are one and the same from a density point of view (Fig. 7.4A).

Different researchers have used different sediment concentration values for high-density turbidity currents (Table 7.1 and Fig. 7.4B). For example:

(1) Kuenen's (1966) density value of 1.1 g/cm^3 converts into 6% concentration of solids by volume (Pickering et al., 1989, p. 17). This means that high-density behavior can begin at a low concentration value of 6% by volume.
(2) Middleton (1967) used a concentration value of 44% by volume in his experiments of high-density flows.
(3) Lowe (1982) considered that the sediment concentration must be greater than 20–30% by volume for the onset of high-density behavior.
(4) Postma et al. (1988) used a concentration value of 35–40% by volume in their experiments of high-density flows.
(5) Leclair and Arnott (2005) used concentration values of 20, 25, and 35% by volume in their experiments of high-density flows.
(6) Subaerial hyperconcentrated flows are often compared with subaqueous high-density turbidity currents. According to Pierson and Costa (1987), hyperconcentrated flow, which is intermediate between stream flow and debris flow (Beverage and Culbertson, 1964), has a sediment concentration of 20–60% by volume (Fig. 7.4B). Furthermore, Qian et al. (1980) considered a Bingham fluid (i.e., a debris flow) as a special homogeneous type of hyperconcentrated flow.

Because of these wide ranges of concentration values, a flow with 20% sediment concentration would be considered a low-density flow by Middleton, a high-density flow by Kuenen, a hyperconcentrated flow by Pierson and Costa, and a debris flow by Qian et al. In order to differentiate high-density turbidity currents from low-density turbidity currents, there must be a defining concentration or density value. But no such defining density value has been established.

A fundamental issue here is the upper limit of sediment concentration that controls fluid turbulence in Newtonian turbidity currents. Bagnold (1954, 1956) investigated aggregates of cohesionless grains in Newtonian fluid under shear
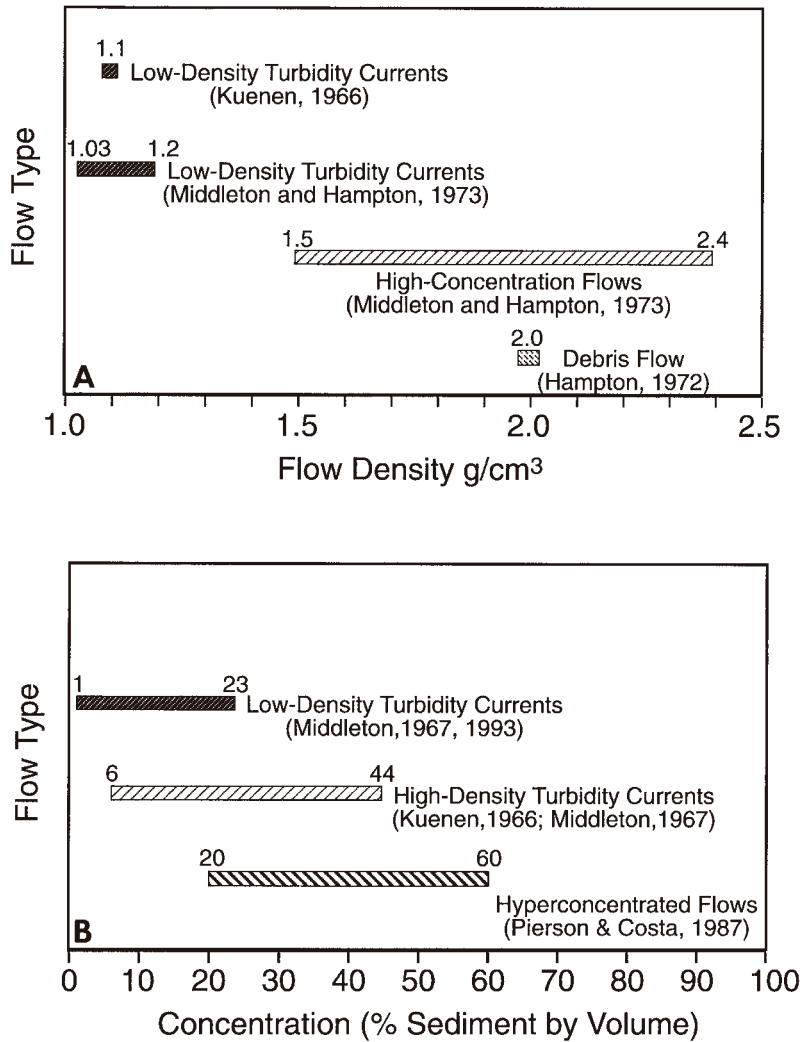
Fig. 7.4. (*A*) **Plot of flow density for different flow types. Note overlapping density values between high-concentration flows (i.e., high-density turbidity currents) and debris flows. (*B*) Range of sediment concentration for different flow types. Note a flow with 20% sediment concentration can be classified as any one of the three types. (After Shanmugam (1996a). Reproduced with permission from SEPM.)**

and introduced the concepts of 'inertia' and 'viscous' regions based on grain inertia and fluid viscosity, respectively (Fig. 7.1B). In a grain-inertia region the effects of grain concentration and related grain collision (i.e., dispersive pressure) dominate, whereas in a viscous region effects of fluid viscosity dominate. More importantly, in the grain-inertia region high grain concentration tends to suppress

Table 7.1 Variable concentration values of different flow types

Low-density turbidity current
- < 1% sediment by weight (Middleton, 1993)
- < 6% solids by volume (Pickering et al., 1989) or < 1.1 g/cm^3 (Kuenen, 1966)
- 23% solids by volume (Middleton, 1967)

High-density turbidity current
- > 6% solids by volume (Pickering et al., 1989) or > 1.1 g/cm^3 (Kuenen, 1966)
- > 10% sediment by weight (Middleton, 1970, 1993)
- > 20–30% solids by volume (Lowe, 1982)
- 20, 25, and 30% sediment by volume (Leclair and Arnott, 2005)
- 35–40% solids by volume (Postma et al., 1988)
- 44% solids by volume (Middleton, 1967)

Hyperconcentrated stream flow
- 20–60% sediment by volume or 40–80% by weight (Pierson and Costa, 1987)

fluid turbulence and promote laminar shear. In explaining suppression of turbulence by grain concentration I, Bagnold (1956, p. 288) stated,

'*At a certain stage the turbulence began to be suppressed, being damped out by the increasing overall shear resistance. And on a further increase in the grain population the turbulence vanished altogether … . When the turbulence finally ceased, C was apparently uniform from top to bottom, at about 0.3 … . Having attained uniformity in the now laminar fluid flow, C could be increased nearly to the mobile limit of about 0.53. Ultimately the whole flow 'froze' simultaneously at all depths.*'

Because a turbulent flow becomes laminar when its grain concentration reaches 30%, turbidity currents cannot theoretically exist at these high concentration values. Bagnold (1962) later demonstrated that gravity-driven turbulent currents could be maintained only in flows with low grain concentration of less than 9% by volume. To date, no one has ever demonstrated in flume experiments that fully turbulent flows (i.e., flows without basal high-concentration laminar layer) can be created and maintained using sediment concentration in excess of 9% by volume. Neither has any one documented such flows in the modern deep sea.

7.4.2 Driving force

Postma et al. (1988) used the concept of high-density turbidity current for density-stratified flows in which the basal high-concentration laminar layer is derived from and driven by over-riding turbidity currents (Fig. 7.5). However, the basal high-concentration layer (i.e., sandy debris flow) cannot be a turbidity current because of its pseudoplastic rheology and its laminar flow state (Fig. 7.5). The basal
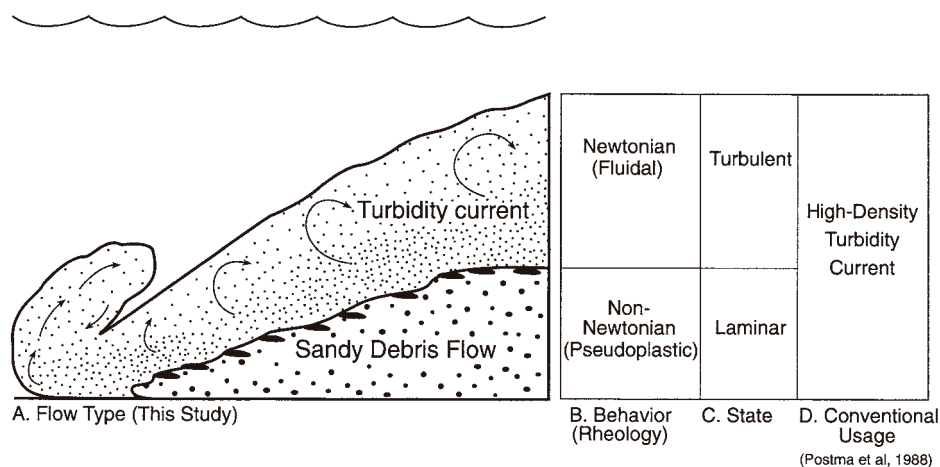
Fig. 7.5. (*A*) **Side view of experimental density-stratified flows. Postma et al. (1988) suggested that the basal high-concentration layer (labeled as sandy debris flow in this book) was driven by the upper low-concentration layer (labeled as turbidity current). Note mudstone clasts at the upper rheological boundary of sandy debris flow.** (*B*) **Lower (non-Newtonian) and upper (Newtonian) layers represent two separate rheologies.** (*C*) **Lower (laminar) and upper (turbulent) layers represent two different flow states.** (*D*) **Conventional usage has been to lump both lower and upper layers together under the term 'high-density turbidity currents.' (From Shanmugam (1997a). Reproduced with permission from Elsevier.)**

layer with high sediment concentration would severely hinder settling, and would freeze mudstone clasts in floating positions along a rheological boundary (Fig. 7.5). The basal laminar and upper turbulent layers in high-density turbidity currents are analogous to 'inertia' and 'viscous' regions of Bagnold (Fig. 7.1B).

In justifying their use of the concept of high-density turbidity currents, Mutti et al. (1999, p. 22) stated,

> '*The concept of basal granular layer coincides with that of 'high-density turbidity current' (cf. Lowe, 1982), the latter term being very popular among many sedimentologists and probably the easiest to use for general purposes of communication.*'

Such a practice is called popular sedimentology, not process sedimentology. We should use a concept because it is hydrodynamically sound, not because it is popular. Other authors have also expressed doubts about the concept of high-density turbidity currents.

(1) Hallworth and Huppert (1998, p. 1083), based on their experiments on high-concentration gravity flows with density stratification, stated that '… *we are still unsure of the physical causes behind the effects we present here* ….'

(2) Kneller and Buckee (2000, p. 87) emphasized that '... *existing theory seems inadequate to explain the behavior of some highly mobile dense dispersions, and arguments based solely on the geological interpretation of deposits may be inadequate to resolve issues of process.*'

(3) Pickering and Hilton (1998, p. 89) concluded that '... *the precise hydrodynamic conditions and sediment concentrations of high-concentration turbidity currents remains unresolved.*' Disappointingly, these authors went on to apply the concept of high-density turbidity currents in their subsequent studies (e.g., Pickering et al., 2001).

Fig. 7.6. An illustration of Lowe's (1982) classification of turbidity currents based on grain-size populations. Population 1 = low-density turbidity currents; population 2 = sandy high-density turbidity currents; population 3 = gravelly high-density turbidity currents. Rheology, depositional mechanism, and flow type are added for clarification. Because hindered settling, matrix buoyant lift and dispersive pressure are important sediment support mechanisms in 'high-density turbidity currents,' High-density turbidity currents, as defined by Lowe (1982), are considered to be more like plastic debris flows than Newtonian turbidity currents. (After Shanmugam and Moiola (1995). Reprinted by permission of the American Association of Petroleum Geologists whose permission is required for further use.)

7.4.3 Grain size

Lowe (1982) classified turbidity currents into two principal types, namely low-density flows and high-density flows. He based his classification on grain size populations, particle concentrations, and sediment support mechanisms (Fig. 7.6). Low-density turbidity currents are composed of population 1 grains (clay to medium-grained sand) in which the sediment-support mechanism (i.e., turbulence) is independent of particle concentration. As defined by Lowe (1982), these flows in terms of fluid rheology and sediment-support mechanism (i.e., flow turbulence) are true turbidity currents.

In high-density turbidity currents, sediment support is concentration dependent (above 20–30%). In sandy high-density flows composed of population 2 (coarse sand to small pebble), grains are supported by hindered settling and turbulence. In gravelly high-density flows containing population 3 (pebble and cobble), grains are supported mainly by matrix buoyant lift, and dispersive pressure (Lowe, 1982, p. 283). Because hindered settling, matrix buoyant lift, and dispersive pressure are the predominant sediment-support mechanisms in high-density turbidity currents (Lowe, 1982, p. 282), such high-density flows are more akin to plastic debris flows than they are to Newtonian turbidity currents. This conclusion validates Bagnold's (1962) original observation that true turbidity currents are low-density flows. And these low-density turbidity currents are incapable of carrying coarse sand and gravel in turbulence. Thus there is no need to classify turbidity currents into low- and high-density types.

7.4.4 Flow velocity

Kneller (1995) realized that simple normally graded beds are rare in deep-water sequences, and that most deep-water sequences with complications (e.g., massive sandstones, disordered sequences, abrupt grain-size breaks, large-scale bedforms, etc.) are difficult to interpret as turbidites. To alleviate this problem, Kneller has redefined turbidity currents using velocity (u), distance (x), and time (t). He classified turbidity currents into five types: (1) depletive waning flow; (2) uniform waning flow; (3) depletive steady flow; (4) depletive waxing flow; and (5) accumulative waning flow. This classification allows room for interpreting deep-water deposits with any kind of grading (i.e., normal or inverse) as turbidites (Fig. 7.7). Thus the very foundation of the turbidite paradigm, based on the relationship between turbidites and normal grading (Kuenen and Migliorini, 1950; Bouma, 1962), has been undermined by this redefinition.

Unlike the conventional definition of turbidity currents, which is based on fluid rheology and flow turbulence, and that take into consideration sediment concentration, velocity, thickness, and viscosity, Kneller's (1995) definition is primarily concerned with velocity. He considered waxing flows as analogous to medium- to high-density turbidity currents (his p. 37). Redefinition of turbidity
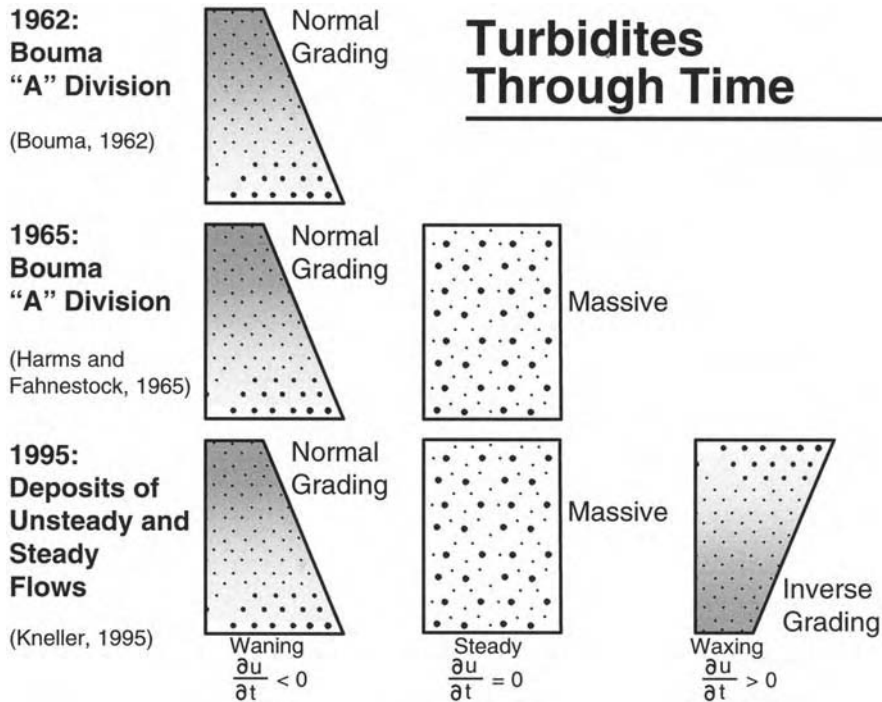
Fig. 7.7. Three publications showing how opinions on nature of grading in turbidites have changed through time. Top: Bouma (1962) suggested normal grading for turbidites. Middle: Harms and Fahnestock (1965) proposed normal grading and massive (i.e., no grading) types for turbidites. Bottom: Kneller (1995) advocated normal grading, massive (i.e., no grading), and inverse grading for turbidites. (After Shanmugam (2000a). Reproduced with permission from Elsevier.)

currents using velocity alone has opened up new avenues for interpreting virtually all deep-water sands as turbidites despite whether they were deposited by turbidity currents or not. Rarity of normally graded beds in the rock record simply means that turbidites are rare in nature. This does not warrant a redefinition of turbidity currents.

7.4.5 Synonyms

The untenable concept of high-density turbidity currents has resulted in a plethora of process terms for density-stratified flows. Gani (2004), for example, proposed the term *dense flow* for rheologically stratified flows that include both Newtonian (i.e., turbidity currents) and non-Newtonian fluids (i.e., debris flows). According to Gani (2004, his Fig. 3), the term dense flow is an alternative

for: (1) high-density turbidity currents (Lowe, 1982); (2) sandy debris flows (Shanmugam, 1996a); (3) slurry flows (Lowe and Guy, 2000); (4) concentrated density flows (Mulder and Alexander, 2001); and (5) liquefied flows/fluidized flows. When viewed in isolation, Gani's approach appears to be reasonable. However, when viewed in total from an historical perspective, a troubling trend emerges:

(1) The term *dense flow* was originally applied by Norem et al. (1990, Fig. 3 therein) strictly to the basal (debris flow) layer in density-stratified flows. This is meaningful because debris flows having higher densities than turbidity currents are bound to occur at the base. Gani (2004), however, applied the term dense flow for both basal (debris flows) and upper (turbidity currents) layers. Gani borrowed the concept of dense flow for a hybrid of turbidity current and non-cohesive debris flow from Allen (1997), who, in turn, borrowed it from Mulder and Cochonat (1996). Surprisingly, neither Mulder and Cochonat nor Gani acknowledged the conflict with the earlier use of the term by Norem et al.

(2) The term *gravitite* was originally introduced by Natland (1967) to represent deposits of primarily debris flow. Without acknowledging the contribution of Natland, Gani (2004) coined a slightly different term, *gravite*, for deposits of slide, slump, debris flow, dense flow, and turbidity current.

(3) The term *slurry flow* was previously applied by Carter (1975) to the basal (debris flow) layer in density-stratified flows. Later, Lowe and Guy (2000) applied the term for both basal and upper layers.

(4) The term inertia region, representing *grain flow*, was previously applied to the basal layer of density-stratified flows by Bagnold (1954, 1956). In contrast, Carter (1975) applied the term grain flow to the upper layer. According to Poliakov (2002), the term granular flow is an alternative for grain flow as well as for slumps, debris flows, high-density turbidity currents, and bottom avalanches.

Various factors, which include failure to acknowledge original contributions, have resulted in a proliferation of 34 published synonyms for high-density turbidity currents. In density-stratified flows, these names represent either the basal laminar layer alone or both the basal laminar and the upper turbulent layer together (Table 7.2). These synonyms, compiled from published sources (Kuenen, 1950a, 1951; Bagnold, 1954,1956; Dzulynski et al., 1959; Dzulynski and Sanders, 1962; Sanders, 1965, 1981; Middleton, 1967; Carter, 1975; Friedman and Sanders, 1978; Fisher and Schmincke, 1984; Valentine, 1987; Postma et al., 1988; Norem et al., 1990; Friedman et al., 1992; Fisher, 1995; Shanmugam, 1996a, 2002a; Sanders and Friedman, 1997; Vrolijk and Southard, 1997; Mutti et al., 1999;

Table 7.2 Synonyms for density-stratified flows (i.e., high-density turbidity currents). Modified after Shanmugam (2002a)

References	Upper layer (low-density)	Lower layer (high-density)
*Bagnold (1954, 1956)	Viscous region	Inertia region
Dzulynski and Sanders (1962)	Turbidity current	Traction carpet
Sanders (1965)	Turbidity current	Synonymous terms: Flowing-grain layer (p. 192) Inertia flow (p. 194) Fluidized flowing-grain layer (p. 210) Inertia-flow layer (p. 211) Avalanching flow (p. 213)
Friedman and Sanders (1978), Sanders (1981), Friedman, Sanders and Kopaska-Merkel (1992, p. 335)	Turbidity current (Suspended load)	Liquefied cohesionless-particle flow ('Bed load') Synonymous terms: Inertial flow Grain flow Mass flow Rheologic bed stage Fluidized cohesionless-particle flow
Sanders and Friedman (1997)	Turbidity current	Liquefied cohesionless coarse-particle flow
*Kuenen (1951)	Turbidity current	Slide
Dzulynski et al. (1959)	Turbidity current	Fluxoturbidity current
Carter (1975)	Grain flow	Slurry flow
*Postma et al. (1988)	Turbulent suspension	Laminar inertia-flow
Norem et al. (1990, their Fig. 2)	Suspension flow	Dense flow (i.e., debris flow)
Shanmugam (1996a)	Turbidity current	Sandy debris flow
*Marr et al. (2001)	Turbidity current	Sandy debris flow
*Vrolijk and Southard (1997)	Turbulent flow	Laminar sheared layer
*Kuenen (1950, 1951)	Turbidity currents of high density	
*Middleton (1967)	High-concentration turbidity current	
Lowe (1982)	High-density turbidity current	
*Postma et al. (1988)	High-density turbidity current	
Norem et al. (1990)	Flowslide	
Mutti et al. (1999)	High-density turbidity current	
Lowe and Guy (2000)	Slurry flow	
Mulder and Alexander (2001)	Concentrated density flow	
McCaffrey et al. (2001)	Particulate gravity currents	
*Poliakov (2002)	Granular flow	
Gani (2004)	Dense flow	

*Experimental studies.

Lowe and Guy, 2000; Marr et al., 2001; Mulder and Alexander, 2001; McCaffrey et al., 2001; Poliakov, 2002; Mulder et al., 2003; Gani, 2004), are:

(1) Inertia flow
(2) Inertia-flow layer
(3) Inertial flow

  (4) Laminar-inertia flow
  (5) Laminar sheared layer
  (6) Traction carpet
  (7) Flowing-grain layer
  (8) Fluidized flowing-grain layer
  (9) Fluidized cohesionless-particle flow
(10) Liquefied cohesionless-particle flow
(11) Liquefied cohesionless coarse-particle flow
(12) Avalanching flow
(13) Slide
(14) Slump
(15) Mass flow
(16) Grain flow
(17) Debris flow
(18) Sandy debris flow
(19) Fluxoturbidity current
(20) Pseudo-plastic quick bed
(21) Bed load
(22) Rheologic bed stage
(23) Bottom avalanches
(24) Stratified flow
(25) Density-stratified flow
(26) *Nuèe ardente* (i.e., applied for decoupling of pyroclastic flows)
(27) Slurry flow
(28) High-concentration turbidity current
(29) Flowslide
(30) Concentrated density flow
(31) Granular flow
(32) Particulate gravity currents
(33) Surge-type turbidity currents
(34) Dense flow.

This multiplicity of names may be a reflection of different researchers with different backgrounds (e.g., experimental *versus* outcrop) expressing their different perspectives. On the other hand, one might argue that inventing different names for density-stratified flows is a consequence (intended or unintended) of doing research on high-density turbidity currents repeatedly without addressing the fundamental problems. Such a practice might be construed as an act of insanity, as defined by Albert Einstein: '*Doing the same thing over and over again and expecting different results*' (Brainy Quote, 2005).

The solution to this chronic problem is to define a flow layer based on its fluid rheology and flow state, irrespective of whether a flow is stratified or unified. Otherwise, the current trend would result in nearly 100 synonyms for high-density

turbidity currents; a jungle of jargon that sedimentary geologists would dread by the end of the 21st century!

7.5 Unknowable flow transformations

The transformation of one type of flow (e.g., laminar debris flow) into another (e.g., turbulent turbidity current) during transport is probably the single most important and the least understood phenomenon in deep-water process sedimentology. Flow transformations can be observed in flume experiments, but they cannot be interpreted in the rock record. An understanding of flow transformation would be useful in petroleum geology because Newtonian turbidity currents are more likely to spread out laterally than plastic debris flows in channel-mouth environments (see Chapter 12).

Kuenen (1951) proposed downslope transformations of slumps to mud flows. Subsequently other researchers have proposed transformations of slumping and debris flows into turbidity currents (Dott, 1963; Hampton, 1972). Phillips and Davies (1991, p. 109) noted, '…*although a flow may start as a viscous plastic material it may subsequently develop grain-dispersive characteristics. Then, as shear rates are reduced, say, by a reduction in bed slope or by jamming of coarse grains in the channel, the flow may once again exhibit plastic-viscoplastic behavior*.' In other words, a debris flow may transform into a grain flow, and then revert back to a debris flow. Similarly, transformation of a grain flow into a turbidity current and back to a grain flow during last stages of deposition has been suggested by Middleton (1970).

Fisher (1983) proposed four types of transformations for sediment-gravity flows: (1) body transformation; (2) gravity transformation; (3) surface transformation; and (4) elutriation transformation. In experiments on stratified flows, the basal laminar flow was initially fully turbulent, but during the depositional stage the turbulent flow was transformed into a quasi-plastic laminar flow (Postma et al., 1988). This is called gravity-flow transformation. Experimental studies have also shown that plastic debris flows generated Newtonian turbidity currents *via* surface-flow transformation (Hampton, 1972). If a turbidity current were to generate a basal high-concentration laminar layer due to gravity-flow transformation (Fig. 7. 8), Postma et al. (1988) would classify this type a 'high-density turbidity current.' This is because the basal high-concentration layer is derived from and driven by over-riding turbidity currents. Similarly, if a laminar debris flow were to generate an upper turbulent cloud (i.e., turbidity current) due to surface-flow transformation (Fig. 7.8), one should classify this type a 'low-density debris flow,' following the logic of Postma et al. Such classifications of sediment-gravity flows based on flow transformation are not meaningful. This is because flow transformations cannot be established without knowing: (1) initial flow behavior; (2) transport mechanisms; and (3) final flow behavior. There are, however,
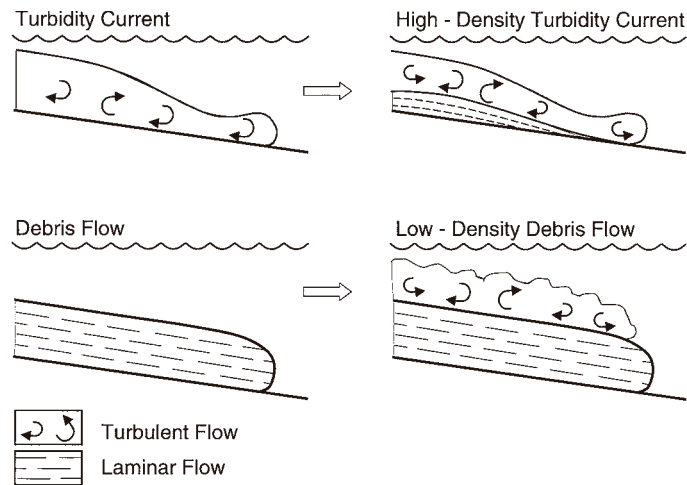
Fig. 7.8. Classification of flows based on flow transformations. Top: Gravity-flow transformation of a density-unified flow (turbidity current) into a density-stratified flow (high-density turbidity current). Open arrow shows direction of transport. Based on Postma et al. (1988). Bottom: Surface-flow transformation of a density-unified flow (debris flow) into a density-stratified flow (low-density debris flow). Open arrows show direction of transport. See text for details. (After Shanmugam (2000a). Reproduced with permission from Elsevier.)

no established criteria for recognizing initial flow behavior and transport mechanisms in the depositional record (Dott, 1963; Walton, 1967; Middleton and Hampton, 1973; Carter, 1975; Stanley et al., 1978; Lowe, 1982; Postma, 1986; Middleton, 1993; Shanmugam, 1996a).

Many of us use this universal constraint, which is the absence of evidence for transport mechanism in the deposit, as a license to assume that all deep-water sands must have been transported by turbidity currents but that they underwent late-stage plastic transformation so as to resemble debris-flow deposits. If we continue to follow such an assumption-based (i.e., model-driven) interpretation, then there is no need to examine deep-water sands to understand their depositional origin; we can simply assume that all deep-water sands are turbidites. Disappointingly, this is the approach that many pursue in the geologic community (e.g., Hiscott et al., 1997). As a result, the geologic literature is saturated with examples of 'turbidites,' irrespective of whether these sediments were transported and deposited by turbidity currents or by some other processes.

During surface-flow transformation, it is common for debris flows to become turbidity currents downslope (Fig. 7.9A). In this scenario, outrunning turbidity currents may initially cut channels that may be filled later by the following sandy debris flows in stratified flows. The upper muddy turbidity currents of stratified

Flow Transformation and Channel cutting
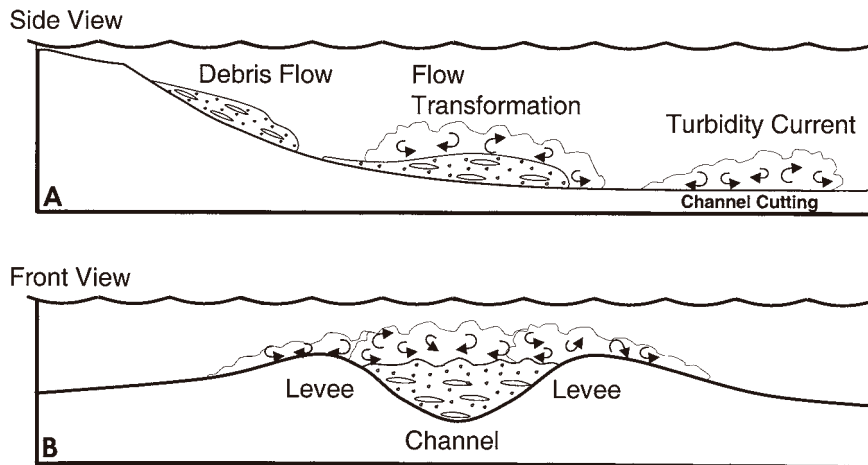
Fig. 7.9. (*A*) Side view showing downdip changes in sediment flows due to surface-flow transformation from a debris flow (left) through stratified flows with a lower debris flow and an upper turbidity current (center) to an outrunning turbidity current cutting channels (right). (*B*) Front view showing channel filling by lower sandy debris flows and deposition on the levee from upper muddy turbidity currents. In situations like this, the presence of turbidites on the levee does not imply that channels were also filled by turbidity currents.

flows may deposit turbidites on levees (Fig. 7.9B). As a result, the channel-fill deposits would be composed of sandy debrites, and the levee portion would be composed of muddy turbidites. Such a facies association has been observed in the Amazon Fan (see Chapter 6). The presence of turbidites on the levee does not automatically mean that associated channels were also filled by turbidity currents.

In discussing the physics of debris flows, Iverson (1997) stated, '*When mass movement occurs, the sediment–water mixtures transform to a flowing, liquid-like state, but eventually they transform back to nearly rigid deposits.*' Although such transformations occur during transport, evidence for flow transformations cannot be inferred from the final deposit. We may never resolve this issue of flow transformation because it would be like attempting to establish the previous life history of a human being after reincarnation!

7.6 Conflicting definitions of slurry flows

Conventionally, many researchers have considered *slurry flows* to be debris flows (e.g., Carter, 1975; Mutti et al., 1978; Stanley et al., 1978; Hiscott and Middleton,

1979; Pierson and Costa, 1987). Lowe and Guy (2000), however, equated slurry flows with high-density turbidity currents. Does this mean that slurry flows, debris flows, and high-density turbidity currents are one and the same process?

According to Lowe and Guy, deposits of slurry flows contain massive sandstone, sheared sandstone masses in a mud-rich sandstone matrix, subvertical fabric and restructuring by water escape, deformed blobs of sandstone in low-mud sandstone, and floating chunks of sandstone. These features are evidence for deposition from sandy slumps and debris flows (see Chapter 3).

In justifying that slurry flows are indeed high-density turbidity currents, Lowe and Guy (2000, p. 65) wrote, '*These cohesion dominated sublayers are analogous in many ways to friction-dominated traction carpets described previously from turbidity currents (Hiscott and Middleton, 1979; Lowe, 1982) and can be termed cohesive traction carpets*.' Traction carpets generally develop in mud-free or mud-poor basal granular layers in gravity currents due to dispersive pressure caused by grain collisions. In slurry flows, however, high mud content should greatly reduce the chances of collision between grains and diminish the development of traction carpets. Lowe and Guy did not explain this mechanical paradox. They claim that slurry flows had undergone a number of flow transformations; however, they did not present physical evidence of transformation. This is because all that can be inferred from the depositional record is what happened during the final moments of deposition.

Lowe and Guy proposed a sequence of structures for slurry-flow deposits (M_1, M_2, M_3, M_4, M_5, M_6, and M_7). More importantly, they suggested that these slurry-flow divisions are comparable to the vertical sequence of fine-grained turbidites (T_a, T_b, T_c, T_d, and T_e) proposed by Bouma (1962), and to the vertical sequence of coarse-grained turbidites or high-density turbidites (R_1, R_2, R_3, S_1, S_2, and S_3) proposed by Lowe (1982). A comparative analogy of these three facies models results in the following:

$$M_1 = S_1$$

$$M_2 \text{ and } M_3 = S_2$$

$$M_4 = S_3 = T_a$$

$$M_5 = T_b, T_c, T_d, \text{ and } T_e$$

M_6 and M_7 = Post-depositional structures that have no equivalents with structures in either the model of Bouma (1962) or that of Lowe (1982).

By comparing the vertical sequence of slurry-flow deposits with the Bouma Sequence, Lowe and Guy implied that the slurry-flow sequence represents a single depositional event. However, slurry-flow beds are amalgamated units that

represent multiple, random, depositional events (Lowe and Guy, 2000, see cap-
tion of their Fig. 24, p. 61). Thus the proposed vertical sequence of slurry-flow
deposits is an attempt to manufacture an artificial order from natural chaos.

7.7 Conflicting origins of flute structures

Flute structures that occur as sole marks of deep-water sands were interpreted as
turbidites (Hiscott and Middleton, 1979). The assumption being that the head of
a turbidity current was turbulent and that turbulence created the scour. Another
assumption is that the scour was subsequently filled by the body of the same
turbidity current. Care must be exercised in making these assumptions because
alternative explanations are possible.

   Flutes simply suggest that a turbulent state of flow was responsible for creat-
ing the scour. Flutes do not imply that the sand that fills a scour surface was
deposited by the same turbulent flow that created the scour surface (Sanders,
1965, p. 209). Scour surfaces or depressions on the sea floor, for example, can
be created initially by turbulent flows and filled later by laminar sandy debris
flows or by other processes (Fig. 7.10). Modern unfilled submarine channels and
canyons are a testimony to the fact that the processes that created these erosional
features in the past are probably not the same processes that may fill them in
the future. Furthermore, scour surfaces can also be created by processes other
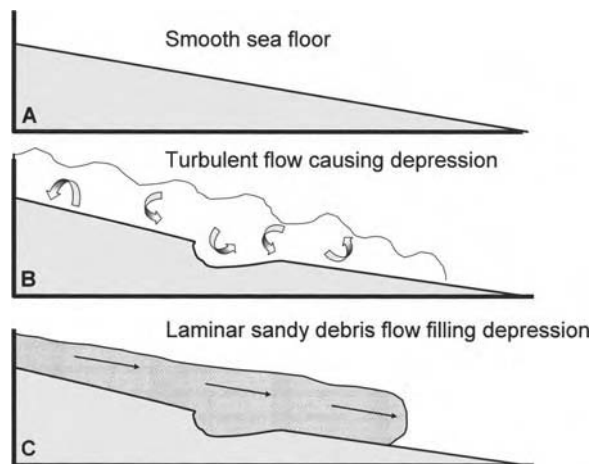
Fig. 7.10. Conceptual diagram showing the complex origin of flutes in deep-water sandstone.
(*A*) Smooth sea floor. (*B*) Formation of depression (flute) by erosion of the sea floor by turbu-
lent flows. (*C*) Subsequent filling of flute depression by laminar sandy debris flows. (Concept
is after Sanders (1965).)

than turbidity currents, such as bottom currents in deep-water environments (Klein, 1966). In a modern tidal flat at Abu Dhabi, Friedman and Sanders (1974) observed positive-relief 'bedforms' that resemble molds of flutes. These flutes were ascribed to sheet flow of an incoming tide. Because flutes can be formed by processes other than turbidity currents, the routine interpretation of flutes as evidence for turbidite deposition is incorrect. The origin of deep-water sands should be based on their internal depositional features, not on their erosional basal contacts or sole marks.

7.8 Conflicting definitions of normal grading

7.8.1 Single depositional event

The concept of normal grading for turbidites was first introduced by Kuenen and Migliorini (1950, p. 99; see also Kuenen, 1967, p. 212). According to this concept, a turbidite represents a single depositional event by a waning turbidity current. Many researchers have adopted this concept (e.g., Bouma, 1962; Harms and Fahnestock, 1965, p. 109; Sanders, 1965; Middleton, 1967). The link between normal grading and its deposition from a single turbidity current event is the single most important concept in process sedimentology of turbidites. However, Lowe and Guy (2000) applied the concept of normal grading to an amalgamated unit (i.e., their type II slurry) deposited by multiple depositional events of slurry flows. Such an application undermines the sedimentological meaning of normal grading.

   Mulder et al. (2001) also misused the term 'normal grading' for a unit composed of multiple sand and mud layers deposited from multiple events with alternating intervals of normal and inverse grading. Furthermore, Mulder et al. (2001) included four subintervals of inverse grading as part of normal grading. Clearly, the term normal grading has lost its original process-sedimentologic meaning for a single depositional event (Shanmugam, 2002b). As a result, one can manufacture a normal grading in any depositional package, composed of multiple depositional events, by selectively designating a coarse bottom unit and a fine top unit to achieve the desired outcome. This is one of the common underpinnings of the turbidite controversy.

7.8.2 Simple normal grading

Deposition from turbidity currents commonly occurs through sediment fallout from suspension (Kuenen and Migliorini, 1950; Dott, 1963). In truly turbulent Newtonian flows, coarse and fine-grained particles tend to settle separately during deposition depending on their fall velocities. This causes deposits of turbidity currents to be characterized by simple normal grading (i.e., upward decline in grain size) with gradational upper contacts.

Following Kuenen (1953), it is common practice to interpret an entire unit as a turbidite even if grading is restricted to the uppermost portion of the unit. For example, if a two meter thick massive sand has a two centimeter thick normally graded top, only the two centimeter graded top should be interpreted as a turbidite. The origin of the underlying sand requires independent evaluation using its own features. In other words, the two centimeter graded top does not reveal anything about the depositional origin of the underlying massive sand. There are examples in which thick massive sands with rafted ungraded clasts (i.e., a debris-flow origin) have thin graded tops (i.e., a turbidity current origin).

7.8.3 Description of normal grading

To interpret a normally graded unit as a turbidite, one must describe the graded unit with precision. One common pitfall involves description of a massive sand interval as a graded sand. This is achieved by simply connecting the base of a sand unit with the base of an overlying mud unit (Fig. 7.11). Such a practice invariably results in a normal grading.

In describing rocks, both megascopic and microscopic details should be documented. Some researchers tend to emphasize primarily microscopic variations
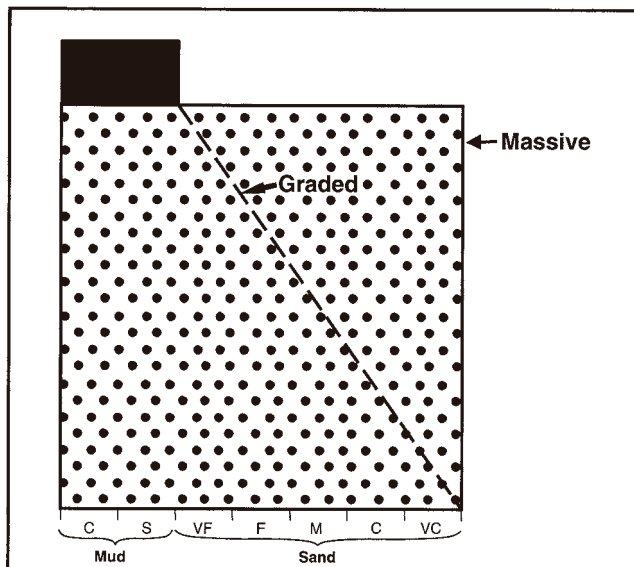
Fig. 7.11. Diagram showing how a massive sand unit, without grading, can be made into a normally graded unit simply by connecting the base of the sand unit with the base of the overlying mud unit.
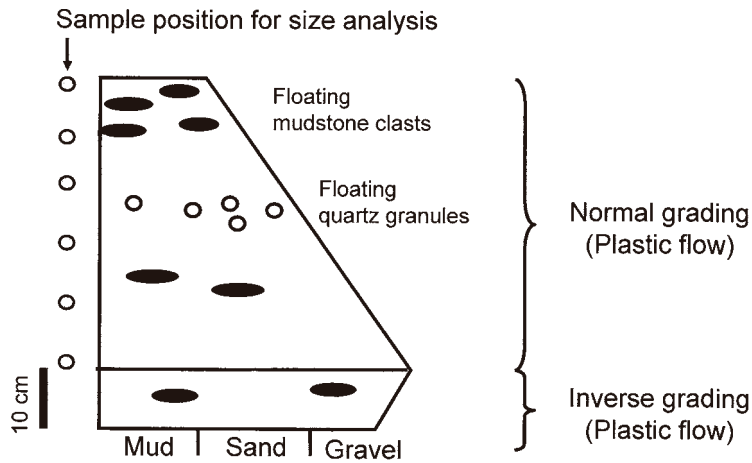
Fig. 7.12. Diagram showing inverse grading and normal grading of plastic debris flows. Note close sampling intervals for microscopic size analysis may not reveal megascopic features (floating granules and clasts) that are equally important for interpreting depositional processes.

in grain size. Depending on where samples for microscopic grain-size analysis are taken, one can easily overlook the importance of megascopic floating quartz granules and floating clasts (Fig. 7.12). Because both inverse and normal gradings are present in debrites (Fig. 7.12), all details are vital.

7.8.4 Grading in debrites

Although normal grading is the standard criterion for recognizing turbidites, plastic debris flows can also develop normal grading (Vallance and Scott, 1997). An example of a normally graded debrite in the northwestern continental slope of the Gulf of Mexico has been reported by Tripsanas et al. (2003). These normally graded debrite units are less than 1 m thick and consisted of mud matrix with mud clasts (1–5 mm in diameter). Because debrites can produce normal, massive, or inverse grading with or without clasts (Fig. 7.13), recognition of normally graded units without clasts as debrites will always be a challenge. In such cases, X-radiography may be useful for recognizing subtle amalgamation surfaces, buried clasts, and contorted layers.

7.9 Problematic origin of traction structures

Perhaps, the most problematic issue is the use of traction bed forms (i.e., plane bed, ripple, dune, upper flow regime plane bed, and antidune), observed in flume experiments (Simons et al., 1965; see also Southard, 1975), as analogs for the
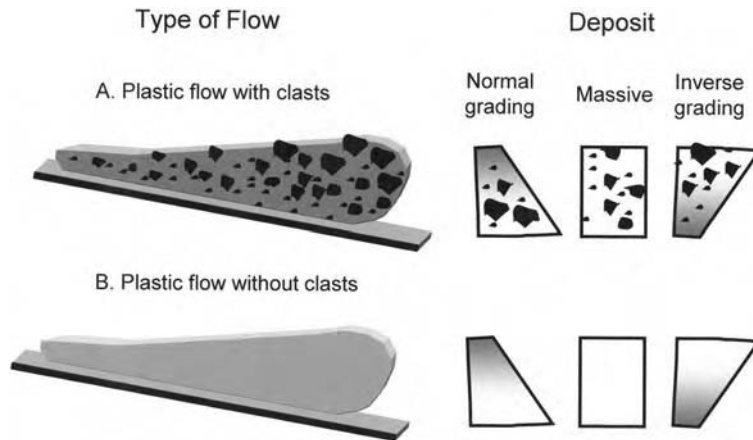
Fig. 7.13. (*A*) **Diagram showing a plastic debris flow with clasts can develop units of normal grading, massive (no grading), and inverse grading with clasts.** (*B*) **Diagram showing a plastic debris flow without clasts can also develop units of normal grading, massive (no grading), and inverse grading without clasts. A normally graded debrite unit without clasts may resemble a turbidite.**

five divisions of the Bouma Sequence deposited by turbidity currents (see Harms and Fahnestock, 1965; Walker, 1965). Although this analogy is deeply embedded in our psyche (Fig. 7.14), it is founded on unsound hydrodynamic principles.

Simons et al. (1965, p. 35) conducted flume experiments in unidirectional currents under equilibrium flow conditions that developed traction structures. Simons et al. (1965, p. 50) cautioned aptly that traction structures observed in their flume experiments are meaningful only for structures developed in subaerial alluvial channels. Walker (1965, p. 22–23) also cautioned that '... *the flume experiments were conducted under conditions of non-deposition, whereas many of the sedimentary structures of turbidites are formed under conditions of net deposition.*'

The time required to establish hydrodynamic equilibrium is greater than the time required for sedimentation (Allen, 1973). Natural turbidity currents are waning flows, and waning flows may never attain equilibrium (Allen, 1973). In most natural flows, changes in bed configurations tend to lag behind changes in flow conditions, and there have been almost no flume experiments on disequilibrium bed configurations (Southard, 1975, p. 33). Thus experimental traction structures are problematic analogs for natural turbidite deposits.

The interpretation of deep-water sands with thick divisions of 'parallel lamination' as upper flow regime flat beds of turbidity currents is problematic. This is because thick upper flat beds have never been generated by experimental
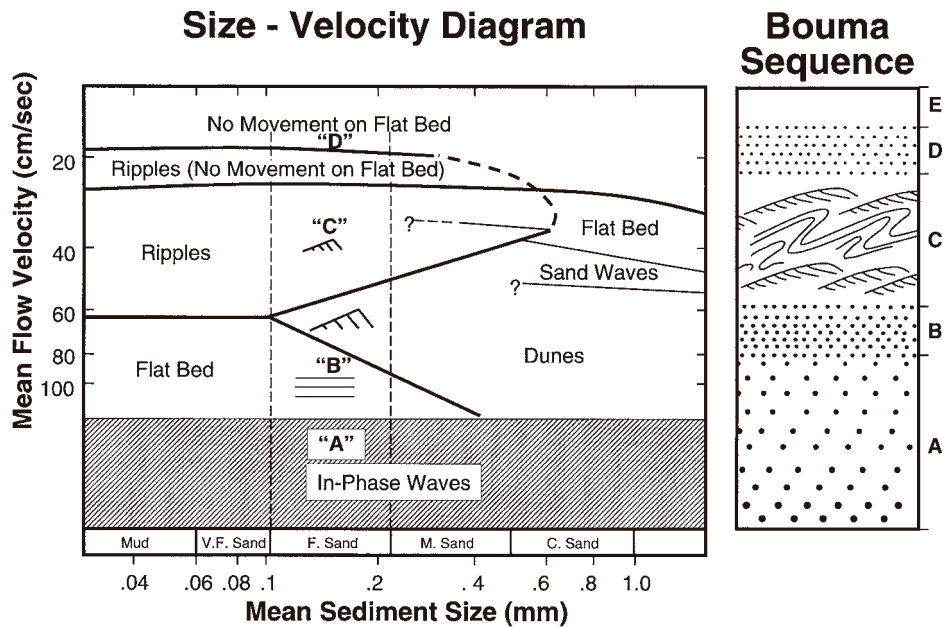
Fig. 7.14. Comparison of size-velocity diagram for bed forms developed in flume experiments at a flow depth of 20 cm (compiled from many sources, see Southard, 1975) with the five internal divisions (A, B, C, D, and E) of the Bouma Sequence (see Chapter 8). Bouma divisions A, B, C, and D are labeled in the size-velocity diagram for fine-grained sand for discussion purposes. Note that dunes and in-phase waves (antidunes) observed in flume experiments are absent in the Bouma Sequence. Also note that the basal normally graded division of the Bouma Sequence is absent in flume structures. Published size-velocity diagram of experimental structures by Southard (1975) is flipped vertically in order to make an easy comparison with the Bouma Sequence. (After Shanmugam (2000a). Reproduced with permission from Elsevier.)

turbidity currents. On the other hand, experimental studies of sandy debris flows have generated horizontal layers that mimic 'parallel lamination' (Fig. 3.24A). The development of pervasive lamination has also been ascribed to sediment shear during freezing of mass flows (Stauffer, 1967). Furthermore, deep bottom currents are traction currents and are quite capable of generating parallel lamination. There is no reason to assume that all laminated beds are turbidites (Murphy and Schlanger, 1962, p. 471). Based on their experimental studies, Leclair and Arnott (2005, p. 4) concluded that, '... *the debate on the upward change from massive (Ta) to parallel laminated (Tb) sand in a Bouma-type turbidite remains unresolved.*'

In bed forms produced in flume experiments of alluvial channels, dunes are an integral part (Simons et al., 1965), whereas cross beds (i.e., internal structures of dune bed forms) are absent in the Bouma Sequence (Fig. 7.14). In fact,

Kuenen (1964, p. 16) used the presence of dune structures in deep-water sandy sequences as evidence against turbidite deposition. Kuenen (1964, p. 25) stated, '*… a turbidity current must have carried its load of grains in suspension almost up to the point at which each particle comes to rest.*' For this reason, normal grading, which is typical of turbidite beds, is absent in experimental structures of alluvial channels (Fig. 7.14).

Large-scale cross bedding (dune bed forms) is generally absent in Bouma-type turbidites (Pickering et al., 1989). Their absence is ascribed to various causes, such as flows being too rapid (Walker, 1965), flows being too thin (Walker, 1965), flows being too fine-grained (Walton, 1967), or flows with Froude number greater than 0.35–0.40 (Hsü, 1989).

Although cross bedding has never been generated by turbidity currents in laboratory experiments, turbidity currents of varying densities have been proposed to explain the origin of cross beds. They are: (a) high-density turbidity currents (Lowe, 1982); (b) moderate- to low-density turbidity currents (Piper, 1970; Winn and Dott, 1979); and (c) low-density turbidity currents (Martinsen, 1994).

In attributing deep-water antidune 'cross bedding' to high-concentration turbidity currents (i.e., high-density turbidity currents), Pickering et al. (2001, p. 698) stated, '*The surface morphology and internal structure of the inclined sandy macroforms is inconsistent with well-constrained large-scale antidunes formed in fluvial environments. Although large-scale deep-water bedform fields interpreted as antidunes remain poorly studied, without clear contrary observations it seems reasonable to assume that their architecture would be similar to fluvial examples.*' The problems with high-density turbidity currents were discussed earlier.

Piper et al. (1988) suggested that deep-sea gravel waves in the Grand Banks area are products of bed load transport by turbidity currents, analogous to dune bed forms in subaerial rivers that involve traction processes. The implication is that these gravel waves are composed of cross bedding; however, no core information is available to prove the presence of cross bedding. Hsü (1989) proposed an alternative origin for gravel waves by debris avalanches. Until we establish a genetic link between turbidity currents and cross bedding either by direct observation in deep-water environments or by experimental studies in the laboratory, the origin of cross bedding by turbidity currents will remain controversial.

7.10 Problematic origin of mud waves

Large-scale features (10–80 m in height), such as 'migrating mud waves' or 'abyssal bedforms,' have been reported in the deep sea (Flood, 1988; Klaus and Ledbetter, 1988). However, these deep-water features should not be equated with dune bed forms in rivers that create cross bedding due to bed load transport of granular material, which must be larger than 125 microns in grain size (i.e., fine sand).

Deep-sea migrating waves are composed primarily of silt and clay, and therefore they do not have the necessary sand grade (i.e., granular material) to generate cross bedding. Mud waves are ascribed to sculpting of muddy sea floor by deep bottom currents, such as the Antarctic Bottom Water (AABW) in the Argentine Basin (Klaus and Ledbetter, 1988). The precise mechanism of mud wave origin is unclear.

Giant sediment waves (5 m in height) on the continental margin off Nice (southern France) that are composed of sand and boulders were ascribed to deposition by 'sediment flows' (Malinverno et al., 1988). These sediment flows have been considered to be a combination of both debris flow and turbidity current (Malinverno et al., 1988). However, it is unclear how these sediment waves were deposited by two rheologically different sediment flows composed of plastic debris flows and Newtonian turbidity currents.

7.11 Problematic subaerial analogs

A troubling practice is to compare *subaqueous* turbidity currents with *subaerial* river currents (Chikita, 1989). This comparison is incorrect for many reasons. River currents and turbidity currents are fundamentally different, although both are turbulent in state. River currents are generally low in suspended sediment (1–5% by volume; Galay, 1987), whereas turbidity currents are relatively high in suspended sediment (1–23% by volume; Middleton, 1967, 1993), although both currents are considered to be Newtonian in rheology. River currents are fluid-gravity flows, whereas turbidity currents are sediment-gravity flows.

A common perception is that high-density turbidity currents in subaqueous environments are analogous to hyperconcentrated flows in subaerial environments (Fig. 7.15). According to Pierson and Costa (1987), hyperconcentrated flows are plastic flows, and thus high-density turbidity currents cannot be true turbidity currents. In China (Qian et al., 1980), the term hyperconcentrated flow is used for two distinctly different types of flows: (1) Newtonian fluids characterized by a low sediment concentration and a turbulent state in which coarse and fine particles settle separately (i.e., settling); and (2) Bingham (i.e., non-Newtonian) fluids characterized by a high sediment concentration and a laminar state in which coarse and fine particles are deposited together (i.e., freezing).

Analogous to application of the term hyperconcentrated flow for both turbulent and laminar flows in subaerial environments (Qian et al., 1980), the term high-density turbidity current is applied to both turbulent and laminar flows in subaqueous environments (Postma et al., 1988). High-density turbidity currents are commonly perceived to occupy an intermediate position between low-density turbidity currents and debris flows (Fig. 7.15). The problem is that both hyperconcentrated flows and debris flows are considered to be non-Newtonian fluids that exhibit plastic behavior (Fig. 7.15). Thus the use of subaerial processes as analogs for subaqueous high-density turbidity currents is problematic.
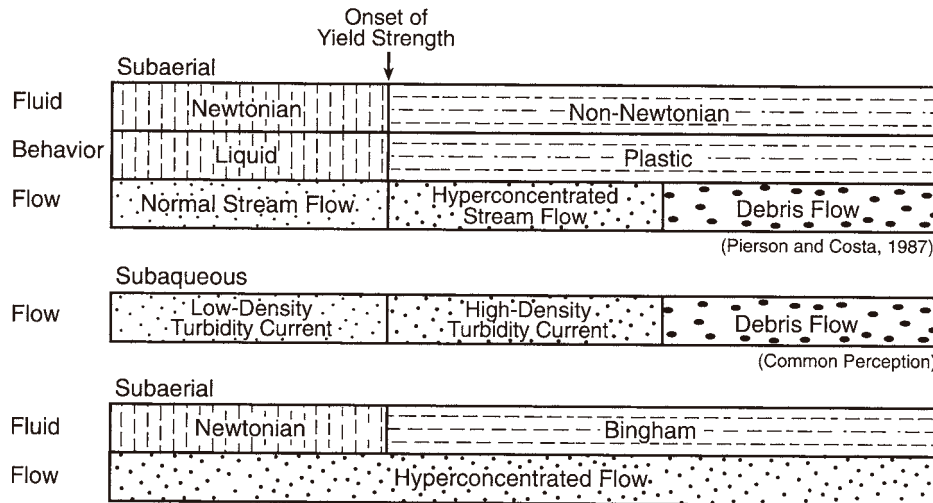
Fig. 7.15. Schematic diagram showing inconsistencies when comparing subaerial 'hypercon-centrated flow' with subaqueous 'high-density turbidity current.' (After Shanmugam (2000a). Reproduced with permission from Elsevier.)

7.12 Problematic origin of sinuous forms

Sinuous channel forms have been observed in both modern and ancient deep-water systems. Their origin in deep-water environments has not yet been resolved. This is because sinuous forms have been associated with seven contrasting processes: (1) fluvial helical flows; (2) turbidity currents; (3) debris flows; (4) volcanic lava flows; (5) glacial melting; (6) droplets on a glass plate; and (7) faulting.

7.12.1 Fluvial helical flows

In a fluvial channel, a meander (i.e., a stream with sinuosity >1.5) represents a curve or a bend. The outside portion of a meander, the concave feature known as a cut bank, is created by erosion. The inner portion of a meander, the convex feature known as a point bar, is created by deposition (i.e., lateral accretion). The point bar is formed when sediments drop from the bed load (traction) as the water velocity of helical flow at the meander slows upslope. In this setting, as the flow moves upslope over the inclined point-bar surface, bed shear stress decreases upward. As a consequence, larger bedforms with coarser grains are deposited near the bottom and finer grains with smaller bedforms are deposited near the top (Allen, 1964). Although the link between helical flows and point-bar deposition has been established, the precise mechanism by which a meandering channel develops in fluvial systems is still poorly understood.

There were attempts to explain deep-water meanders directly by fluvial mechanisms. This was accomplished by: (1) forming fluvial meanders in subaerial environments, and (2) later creating a deep-water environment at the site of fluvial meanders by a rapid rise in sea level. Such drastic changes in sea level are geologically unrealistic to explain deep-water meandering channels at a water depth of 3000 m (e.g., Amazon Fan, Atlantic Ocean).

7.12.2 Turbidity currents

The origin of sinuous channel forms in deep-water lower Miocene of offshore Angola has been explained by turbidity currents (Abreu et al., 2003). They called these turbidites as Lateral Accretion Packages (LAPs), and stated (p. 645),

'*The sinuous and erosionally confined Green Channel Complex, however, displays strong lateral and downdip migration of channels, accretion deposits at the inner portion of every channel bend (LAPs) and frequent cut-off meanders (about 20% of the meanders in the studied area). The apparent similarity of these deepwater deposits (LAPs) to fluvial point-bar deposits suggests that the controls on their formation may be similar. Therefore, the depositional model proposed for these deepwater LAPs is that the accretion surfaces would be formed by relatively continuous and gradual lateral sweep of channel bends by systematic erosion of the outer banks and deposition along inner banks …. This is similar to the classic fluvial point-bar model (Galloway and Hobday, 1983).*'

In this case, the implication is that deep-water turbidity currents behaved like fluvial helical flows and developed deep-water deposits of Angola. If true, then the Angolan deposits should exhibit the following depositional features that are characteristic of point bars: (1) lateral accretion package with a basal lag composed of bed load gravel; (2) imbrications of pebbles and cobbles; (3) large dune bedforms (cross bedding) at the lower part of the point bar; (4) ripples and plane beds at the upper part of the bar; and (5) mud drape by vertical accretion. However, none of these features has been documented by Abreu et al. in cores from Angola.

Interestingly, Abreu et al. (2003, their Fig. 23) used the Pennsylvanian Jackfork Group, which has served as the epicenter of turbidite controversy (see Chapter 9), as an outcrop analog for the Angolan sinuous channels. In this outcrop analogy, three lithofacies are used: (1) thick bedded Ta; (2) thin bedded Ta; and (3) mud-clast conglomerate. The origin of Ta division in the Bouma Sequence has been attributed to eight different processes (see Chapter 8). None of the eight processes can be related to helical flows in sinuous channels. More importantly, the Jackfork Group has been interpreted to be sandy debrites (see Chapter 9). Debris flows with plastic rheology cannot behave as helical flows in meander bends. Unlike prolonged fluvial currents that develop sinuous channel morphology on land, turbidity currents are episodic. Thus it is difficult to envision how such

episodic events could develop the highly meandering channel forms observed in the deep sea.

Abreu et al. used plan-view trends seen on seismic time slices and cross-sectional geometry seen on seismic profiles for developing their depositional models. These geometry-based models have to be ultimately validated by process-based models developed from cores. Unfortunately, no 'ground truth' has been presented from Angolan cores.

Our tendency to equate fluvial point-bar deposition by *traction* processes with turbidite deposition in deep-water sinuous channels by *suspension* processes is hydrodynamically not meaningful. Peakall et al. (2000) cautioned that the use of fluvial analogy for submarine channels is superficial. Importantly, experimental studies have failed to generate point bars in subaqueous meanders (Mètivier et al., 2005).

7.12.3 Debris flows

Sinuous channels of the Amazon Fan are dominated by deposits of sandy debris flows and slumps (see Chapter 6). The close association between sinuous canyons/channels and mass-transport deposits is also evident in modern slopes off the Los Angeles Margin, Lake Tahoe, the Monterey Fan, and the Mississippi Fan (see Chapter 6). The genetic link between sinuous channels and mass-flow deposits is unclear.

In subaerial channels with sharp bends, the cross-section of channels after debris flows had passed through showed occurrence of spill-over deposits on both sides of the channel (Johnson, 1984). Spill-over deposits have also been reported from submarine debris-flow chutes (Prior and Coleman, 1984). The geometry of the spill-over deposits of debris-flow chutes may mimic the popular gull-wing geometry of channel-levee complexes associated with sinuous channels (see Chapter 6). There are, however, no established criteria in seismic profiles to distinguish the origin of a 'gull-wing' geometry by turbidity current *versus* by debris flow. Future experimental research should focus on the development of sinuous channels and channel-levee complexes by debris flows.

7.12.4 Volcanic lava flows

Volcanic lava flows from Pu'u 'O' o cone in the Kilauea Volcano, Hawaii have generated channel forms ranging from braided to sinuous patterns (Fig. 7.16). In fact, the fluvial term levee has been applied to describe the behavior of lava flows (Sparks et al., 1976). There are clear plan-view patterns of lava flows that can be labeled as meandering channel, braided channel, levee, splay, and lobe. However, these terms do not reveal anything about depositional processes. Although lava flows represent a wide range of Reynolds Number, such flows are commonly plastic in rheology (Johnson, 1970; Griffiths, 2000). Similar to sinuous lava flows,

Fig. 7.16. Plastic lava flows showing sinuous and braided channel forms, Pu'u 'O' o cone, Kilauea Volcano, June 2, 1986. Credit: J. D. Griggs, USGS, Hawaiian Volcano Observatory. Uniform Resource Locator (URL): http://hvo.wr.usgs.gov/hazards/dds24167_photocaption. html (accessed February, 2005).

submarine debris flows with plastic rheology may also create sinuous patterns that may mimic *sinuous channel forms* in seismic amplitude slices.

7.12.5 Glacial melting

Melting glacier has developed meandering canyons in the Kennicott Glacier, Alaska (Mitchell, 2003, p. 75). Glacial meltwaters are hyperconcentrated flows and they often flow under pressure. The exact mechanism of these glacial meanders is unclear.

7.12.6 Droplets on a glass plate

Dewdrops from condensation of atmospheric moisture commonly develop meander patterns on a car windshield on a cold morning. Janosi and Horvath (1989) studied the phenomenon of meandering droplets on a glass plate. A water droplet begins to run down an inclined glass plate if the mass exceeds a static critical weight.

This depends mainly on interfacial tensions and on the slope of the glass. The route of the meandering droplet is determined by impurities on the surface as well as in the droplet itself. In spite of many theoretical and experimental studies, precise mechanism of this phenomenon is still poorly understood.

7.12.7 Faulting

A structural origin, controlled by fault motions, of tight meander in the Monterey Canyon was discussed earlier (see Chapter 6).

In summary, at the time of this writing (May 2005) there is no known mechanism that can explain the origin of sinuous channel forms in deep-water environments. Thus equating deep-water meanders seen on seismic amplitude slices with fluvial point bars is imprudent. The dangers of using seismic attributes in geologic interpretation have been known (Sheline, 2005). Since the recognition of a tight meander of the Monterey Canyon (Offshore California) by Shepard (1966), the number of papers published on deep-water meanders has been phenomenal, but the depth of our understanding of their origin has not been proportional. An unfortunate growing trend has been to reinvent concepts of the 1960s and to repackage them under erudite nomenclature.

7.13 Problematic hyperpycnal flows

The concept of hyperpycnal flows is popular because of the misperception that it can be used for explaining some complicated features of deep-water successions such as inverse grading (Mulder et al., 2002, 2003). Because inverse grading is an important feature of deep-water sands (see Chapter 8), the concept of hyperpycnal flows requires a critical evaluation.

In advocating a rational theory for delta formation, based on the concepts of Forel (1892), Bates (1953) suggested three major flow types: (1) *hypopycnal flow* for floating river water that has lower density than basin water (Fig. 7.17A); (2) *homopycnal flow* for mixing river water that has equal density as basin water (Fig. 7.17B); and (3) *hyperpycnal flow* for sinking river water that has higher density than basin water (Fig. 7.17C).

Although hyperpycnal flows were designed to describe river-dominated deltaic systems, they have been compared with turbidity currents. For example:

(1) In their study of the Huanghe (Yellow River) delta front, Wright et al. (1986, p. 99) stated, '... *high density hyperpycnal plume are most like the classical turbidity currents* ....'
(2) Wright et al. (1986, p. 98) suggested that '... *the hyperpycnal plumes are sustained (as opposed to episodic) turbulent suspension currents, or turbidity currents*.'
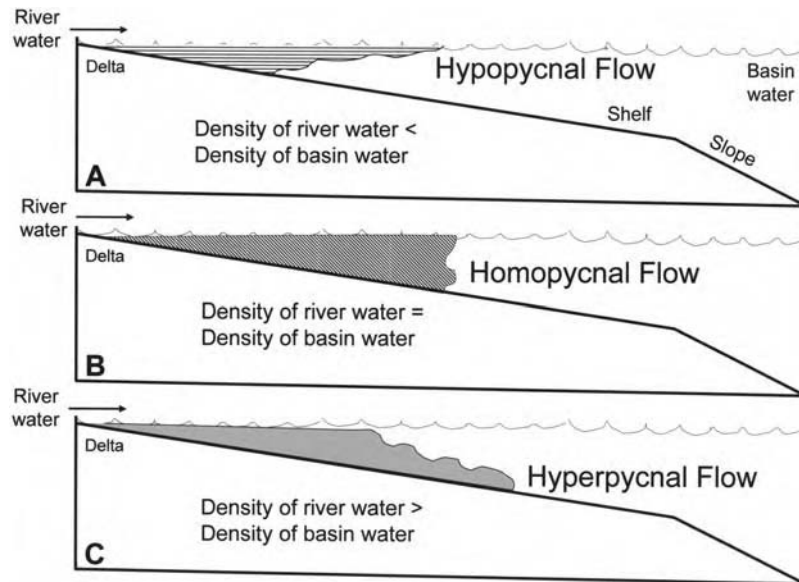
Fig. 7.17. Schematic diagrams showing three types of density variations in river water in deltaic environments. (*A*) *Hypopycnal flow* in which density of river water is less than density of basin water. (*B*) *Homopycnal flow* in which density of river water is equal to density of basin water. (*C*) *Hyperpycnal flow* in which density of river water is greater than density of basin water. (Based on concepts of Bates (1953).)

(3) Mulder et al. (2002, 2003) distinguished a slow-moving hyperpycnal turbidity current as a special type of *flood-generated* turbidity current that is different from *slide-generated surge-type* turbidity currents. More importantly, Mulder et al. (2003) equated hyperpycnal turbidity currents and surge-type turbidity currents with *low-density* and *high-density* turbidity currents of Lowe (1982), respectively.

Mulder et al. (2003) expanded the applicability of the concept of hyperpycnal turbidity currents from shallow-water (deltaic and continental shelf) to deep-water (continental slope and abyssal plain) environments. The application of the concept of hyperpycnal flows to deep-water systems is problematic for the following reasons:

(1) There is no documented evidence for the direct transportation of sediment from river mouths to abyssal plains by hyperpycnal flows in modern oceans. During periods of lowstands, hyperpycnal flows may play a role in shelf-edge deltaic settings that may promote sediment transport into deep-water environments. It is difficult to envision the long-distance travel of such

low-velocity hyperpycnal flows from river mouths to abyssal depths during periods of highstands on the Atlantic-type passive continental margins.

(2) Bates (1953) introduced the concept of hyperpycnal flow for river-dominated deltaic processes, whereas Bell (1942) introduced the concept of underflow for deep-water density currents. As a synonym for Bell's (1942) underflow, Mulder and Alexander (2001) used the term hyperpycnal turbidity current. Dasgupta (2003, p. 270) critiqued the hyperpycnal flow concept of Mulder and Alexander as follows: '*… use of the term hyperpycnal to qualify a type of turbidity current is not only superfluous, but to some extent, also creates ambiguity in understanding turbidity current*.'

(3) Prior and Bornhold (1990) proposed that Holocene fan deltas originated by a combination of processes, namely: (1) debris avalanching; (2) inertia flows (i.e., hyperpycnal flows); and (3) turbidity currents. In explaining inertia flows, Prior and Bornhold (1990, p. 80–81) stated, '*The near-bed or 'moving-bed' concentrations of sediment are largely unaffected by seawater density and thus begin moving across the subaqueous slope as hyperpycnal flow … . Gravel/coarse sand transport downslope over the fan appears to be achieved by high-density, pseudo-laminar 'inertia flows' described experimentally by Postma et al. (1988). These authors illustrated a mechanism by which coarse particles move over the bottom by a combination of dispersive pressure, hindered settling and enhanced buoyant lift.*' Clearly, these hyperpycnal flows are laminar flows, not turbulent turbidity currents.

(4) Mulder et al. (2003, their Table 1) classified certain major rivers such as the Mississippi, Amazon, and Zaire as *clean* rivers, rivers that cannot produce hyperpycnal flows. The problem with their classification is two fold: (a) Mulder and Syvitski (1995) originally classified the Zaire as a *clean* river that cannot produce hyperpycnal flows, but they now believe that the Zaire is a *dirty* river that *can* produce hyperpycnal flows (Mulder et al., 2003). If so, the classification of clean *versus* dirty rivers is not based on objective criteria. (b) The Mississippi and the Amazon Rivers have developed two of the largest submarine fans in the world. If these huge fans were not qualified to receive sediment from hyperpycnal flows, in the geologic record how would we know which deep-water fans received sediment from hyperpycnal turbidity currents and which ones received sediment from slide-generated surge-type turbidity currents?

(5) Mutti et al. (2003b) expressed doubts about sand deposition from hyperpycnal flows and stated, '*… even in the case of the Yellow river, the only modern large river that generates semi-permanent underflows at its mouth (Van Gelder et al., 1994), there is no evidence of substantial sand deposition in the delta front region.*'

(6) The synonymous use of deltaic hyperpycnal flows for deep-water underflows is problematic because underflows can be generated solely by differences in temperature and/or salinity (e.g., Gould, 1951). As a result, geostrophic

thermohaline currents, which are generated in the oceans solely by differences in temperature and salinity (see Chapter 4), could be considered to be underflows. Thermohaline currents, popularly known as contour currents, are density currents. As such these sediment-starved, bottom currents are neither sediment-gravity flows nor turbidity currents. Although all turbidity currents are density currents, but not all density currents are turbidity currents!

(7) Harms (1974) advocated a concept of deep-water density current, generated by increased salinity and lowered temperature, to explain traction structures in the Permian Brushy Canyon Formation, West Texas. Harms pointed out that these density currents were not turbulent turbidity currents.

The term hyperpycnal flow should be restricted to just deltaic processes. Otherwise, the danger exists for interpreting deep-water bottom-current deposits (e.g., contourites) as a special type of turbidites, known as *hyperpycnite* (e.g., Mulder et al., 2002, p. 119). For these reasons, Kuenen (see Sanders, 1965, p. 217) emphasized that any definition of turbidity currents should exclude muddy rivers (i.e., hyperpycnal flows) and normal marine currents (i.e., contour currents) from consideration. Or else, we might as well simply abolish specific process terms, such as turbidity currents and contour currents and revert back to the days of density currents of the 1930s.

7.14 Conflicting origins of massive sands

Deep-water massive sands have been defined as '… *very thick (>1 m) sand beds or units that are devoid of primary sedimentary structures and that occur in association with other deep-water sediments …*' (Stow and Johansson, 2000, p. 145). Other researchers consider deep-water massive sands as beds less than one meter in thickness (Rodriguez and Anderson, 2004). Although there is general consensus that massive sands are structureless, their origin is controversial (Parize et al., 1999; Stow et al., 1999).

A 400-ft (122 m) thick massive sand unit in the Gryphon Field (U.K. North Sea) contains floating mudstone clasts and internal shear plane (Fig. 7.18). This massive sand has been interpreted as deposits of sandy debris flows and slumps (Shanmugam et al., 1995a). The reservoir sand in the Gryphon Field has also been interpreted as sand injections (Purvis et al., 2002). The controversy over the origin of deep-water massive sands is of economic importance because many deep-water massive sands are major petroleum reservoirs.

Selected examples of deep-water massive sands associated with petroleum exploration, discovery, and production are (Stow and Johannson, 2000):

Paleogene fields in the North Sea:

(1) Alba* (*means that I have described cores from these examples)
(2) Gryphon*
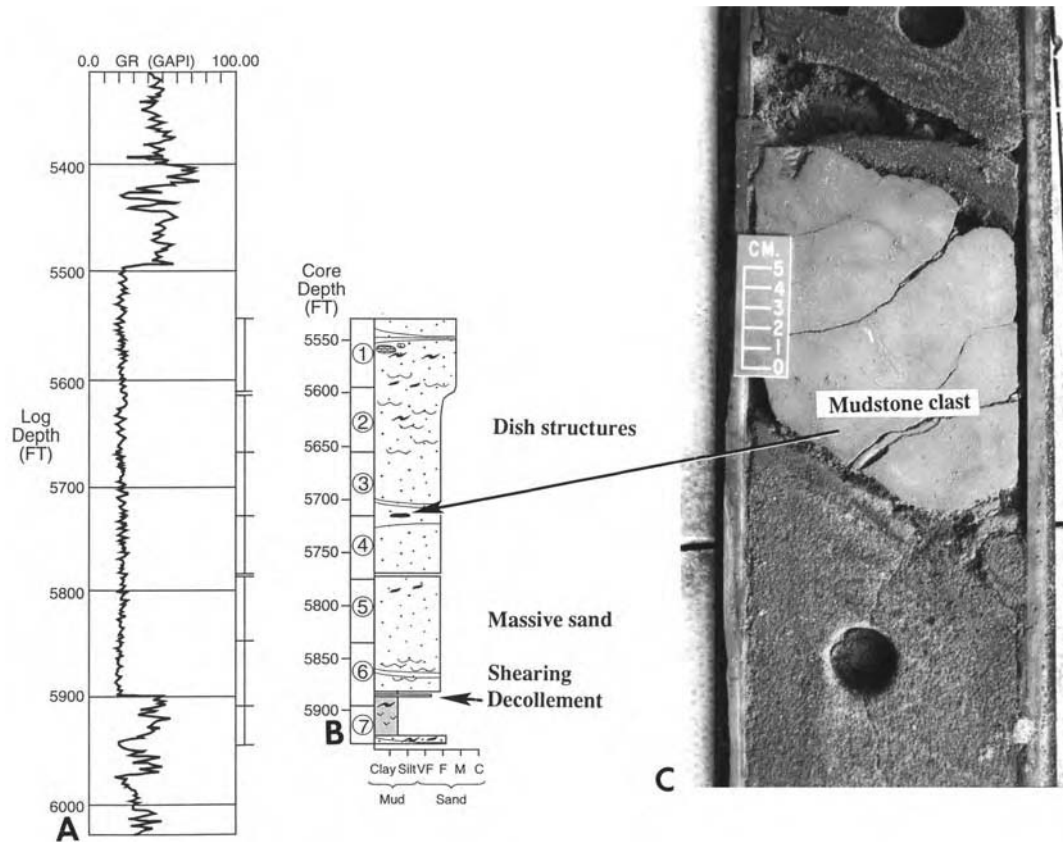
Fig. 7.18. An example of deep-water massive sand. (*A*) Well developed blocky wireline-log motif of a 400-ft (122 m) thick sand, Lower Eocene, Gryphon Field, North Sea. (*B*) Depth-tied sedimentological log showing massive sand with dish structures, floating mudstone clasts and a basal shearing plane. (*C*) Core photograph showing a floating mudstone clast in massive sand. Arrow shows stratigraphic position of clast. Well: Kerr-McGee 9/18b-7. See Chapter 10 for a case study of the Gryphon Field.

(3) Balder*
(4) Frigg*
(5) Heimdal
(6) Forties
(7) Montrose
(8) Arbroath
(9) Andrew*

Mesozoic Fields in the North Sea:

(1) Agat*
(2) Kopevic
(3) Galley
(4) Claymore
(5) Scapa
(6) Sonjefjord
(7) Brae-Miller complex

Offshore Brazil:

(1) Marlim*
(2) Carapeba
(3) Macae

West Africa:

(1) Baudroie
(2) Baliste
(3) Zafiro*
(4) Opalo*

West of Shetlands

(1) Foinaven*
(2) Schiehallion

Gulf of Mexico*

Seven processes have been proposed for the origin of deep-water massive sands:

(1) Low-density turbidity currents: Massive sands in the Annot Sandstone (SE
     France) were ascribed to the basal part of the turbidite facies model (Bouma,
     1962). These massive beds were interpreted as deposits of turbidity currents
     (i.e., classical, low-density, turbidity currents). The problems with the tur-
     bidite facies model and its controversial origin are discussed in Chapter 8.

(2) <u>High-density turbidity currents:</u> On the basis of experiments, Middleton (1967) proposed that massive parts of turbidite beds could result from high-concentration turbidity flows (i.e., high-density turbidity currents). However, Middleton's experimental high-concentration turbidity flows met all the criteria for mass flows (i.e., debris flows), as defined by Dott (1963): (a) these flows were flows of non-Newtonian fluids that exhibited plastic behavior; (b) these flows were high-concentration flows in which the sediment was supported by dispersive pressure; and (c) deposition from these flows occurred by 'freezing.' Therefore, the routine interpretation of deep-water massive sands as high-density turbidites is inappropriate.

(3) <u>Sandy debris flows</u>: The origin of massive sands has been attributed to deposition from sandy debris flows (Shanmugam, 1996a). Massive sands have been produced by experimental sandy debris flows (see Chapter 3).

(4) <u>Sandy debris flows and high-density turbidity currents</u>: The origin of massive sands has been attributed to both sandy debris flows and high-density turbidity currents (Stow and Johanssen, 2000). In an attempt to resolve the controversy over the origin of massive sandstones by high-density turbidity currents *versus* sandy debris flows, Baas (2004) presented a mathematical model (TDURE). In this model, deposits of high-density turbidity currents are presumed to develop traction structures in their upper parts. According to Baas, deep-water massive sands in which upper traction structures are absent must be due to post-depositional destruction of traction structures by liquefaction, bioturbation, and/or erosion. Baas (2004, p.309) concluded that '*The lack of stratification does not necessarily mean that massive sands are generated by 'en masse' freezing of a debris flow.*' The clear implication here is that all deep-water massive sands should be presumed to be deposits of high-density turbidity currents. Developing a mathematical model for a concept that is yet to be defined on flow density is of little value for solving the controversy. In an observational science like physical sedimentology (Allen, 1985a, p. ix), a mathematical model is not a substitute for observations of details from the rocks or for experimental observations.

(5) <u>Quasi-steady concentrated density currents</u>: The origin of massive sands has been attributed to quasi-steady concentrated density currents (Mulder and Alexander, 2001). However, Mulder and Alexander (2001, p. 288) acknowledged that '*There are no published records of such flows, and they are likely to be rare occurrences … .*' It is difficult to evaluate scientifically a flow that has been undocumented.

(6) <u>Sand injections</u>: Duranti and Hurst (2004) proposed fluidized sand injection as a mechanism for forming deep-water massive sands. This is a viable option, but distinguishing injected sands from debrite sands in cores is a challenge (see Chapter 5).

(7) <u>Contour currents:</u> A contourite origin for massive sands on shelf and upper slope, offshore Antarctica has been proposed by Rodriguez and Anderson (2004). These massive sands are attributed to deposition by Circumpolar Deep Water (CDW). This sandbody is composed of fine- to medium-grained massive sand. Its thickness ranges from 10–100 cm and it forms a large sheet (3200 km^2).

The most likely explanations for the origin of most deep-water massive sands are sandy debris flows and sand injections.

7.15 Conflicting definitions of turbidite systems

Different authors have defined the term 'turbidite systems' differently, but none of the definitions makes process sedimentological sense. For example:

(1) Mutti (1985, p. 70) defined a turbidite system as '… *a body of rocks where channel-fill deposits are replaced by nonchannelized sediments in a down-current direction*.' Mutti also proposed three types of ancient turbidite systems on the basis of where sand is deposited. In the Type I system, the bulk of the sandstone occurs in detached lobe deposits. In the Type II system, sandstone occurs in attached lobes and channel-lobe transition areas; and in the Type III system, sandstone occurs in channel-fill complexes.

(2) Mutti and Normark (1987) classified deep-water systems into five hierarchical orders: (a) A first order *Turbidite Complex* represents basin-fill scale. It is composed of multiple 'Turbidite Systems' deposited over several millions of years. (b) A second order *Turbidite System* represents an individual depositional system or a fan. It is deposited over hundreds of thousands of years. (c) A third order *Turbidite Stage* represents features within a 'Turbidite System'. It formed during tens of thousands of years. (d) Fourth order *Turbidite Elements* represents lobes and channels, and their facies associations. They are deposited during thousands of years. (e) Fifth order *Turbidite Beds* represents individual beds, and they are deposited essentially instantaneously. In this classification, all deep-water deposits (e.g., debrites, slumps, and slides) are labeled as *turbidites.*

(3) Bouma et al. (1985) used the term *submarine fans* for modern deep-water systems, and the term *turbidite systems* for ancient deep-water systems.

(4) Stelting et al. (2000, p. 2) defined the term *turbidite systems* as deposits of gravity flows. This is confusing because gravity flows (i.e., sediment-gravity flows) are composed of debris flows, grain flows, fluidized sediment flows, and turbidity currents. The term turbidite represents deposits of turbidity currents exclusively (Sanders, 1965). Therefore, to preserve the

original meaning of the term turbidite for deposits of tubidity currents, the term turbidite systems should also be used to represent deep-water systems that are dominated by turbidites (Shanmugam, 2001). Without such constraints, there is a danger of classifying deposits of debris flows and slumps under the catchall term turbidite systems.

7.16 Inadequate seismic resolution

Based on seismic facies and geometries, Vail et al. (1991) classified deep-water systems into basin-floor fans and slope fans in a sequence-stratigraphic framework. In turn, they used these fan models to predict specific depositional facies composed of turbidites (see Chapter 10). The practice of interpreting turbidite facies from seismic data can be misleading and even meaningless. This is because (1) interpretation of turbidite facies requires conventional core or outcrop (centimeter- to decimeter-thick turbidite units cannot be resolved in seismic data (Fig. 7.19); (2) seismically resolvable, thicker (>30 m), packages are composed commonly of more than one depositional facies; and (3) a single depositional facies can generate more than one seismic geometry (see Chapter 10). Until we systematically calibrate seismic facies with process sedimentology by use of long cores, process interpretation of seismic data using templates of seismic stratigraphy and seismic geomorphology is only an exercise of our imagination with little hydrodynamic basis.
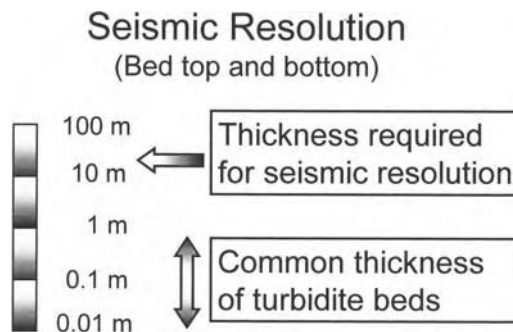
Fig. 7.19. Diagram showing that turbidite beds, commonly ranging in thickness from a few centimeter to a meter, cannot be resolved in standard seismic data.

7.17 Synopsis

In reviewing the literature for this book, it has become abundantly clear that fundamental concepts of turbidity currents were gradually reversed in the 1970s.

The Karma of Turbidity Currents and Their Deposits
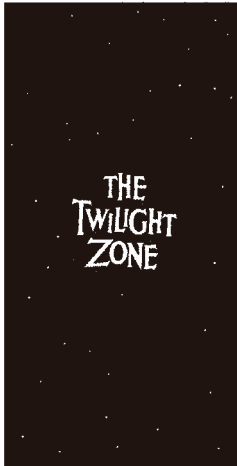
1950s and 1960s	1970s	1980s and 1990s
Subaqueous		Subaerial
Turbulent Flow		Laminar Flow
Waning Flow	THE TWILIGHT ZONE	Waxing Flow
Suspended Load		Bed Load
Newtonian Rheology		Plastic Rheology
Normal Grading		Inverse Grading
Dirty Sand		Clean sand

Fig. 7.20. Diagram illustrating that fundamental concepts of turbidity currents were gradually reversed in the 1970s without scientific basis.

There is no scientific basis for this reversal. It appears as if the turbidite paradigm had passed through a twilight zone (Fig. 7.20). The problem is that on the one extreme, turbidity currents are considered to be turbulent flows, and on the other extreme, they are laminar flows. Under these two extremes (Fig. 7.20), virtually any liquid that moves can be classified as a turbidity current! During the past 50 years, our purpose has shifted from one of describing and interpreting depositional origin of deep-water rocks to one of justifying their presumed turbidite origin. For no good scientific reason, we have elevated the concept of turbidity current from an ordinary process into an extraordinary phenomenon. That is the karma of turbidity currents!

This Page Intentionally Left Blank

Chapter 8

The turbidite facies model

8.1 Introduction
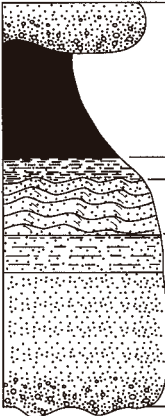
The objective of this chapter is to address the inadequacy of the turbidite facies model using sedimentological details of the Annot Sandstone, which served as the basis for the model, in the French Maritime Alps, SE France. A facies model, by definition, must act as a norm, a framework, a predictor, and a basis for interpretation (Walker, 1992b). The attraction of a facies model is that it serves as a short cut to complex geologic interpretations. Anderton (1985) cautioned that facies models are ephemeral, and that each facies model is unique to a certain environment. As a consequence, we are programmed to align our thinking and observation along a pre-destined path. To maintain the integrity of the model, we are often forced to de-emphasize features that are 'foreign' to the model (Kuhn, 1970). In criticizing the application of rigid fluvial facies schemes to the rock record, Leeder (1997, p. 374) cautioned, '*The main philosophical reason is that it, and other schemes like it, are lazy intellectually and deny the great potential richness of the sedimentary record, full of possible variation not adequately taped by rigid classification.*' In this chapter, we will explore the great potential richness of the Annot Sandstone without the rigid classification of the turbidite facies model.

8.2 The turbidite facies model

8.2.1 The Bouma Sequence

Since its introduction by Bouma (1962), the turbidite facies model has become known as the *Bouma Sequence*. The turbidite facies model is a fixed vertical sequence of structures with five internal divisions in ascending order: Ta = basal normally graded or massive, Tb = lower parallel laminated, Tc = current ripple and convolute laminated, Td = upper parallel laminated, and Te = uppermost pelitic (Fig. 8.1). Beds with all five divisions are also called classic turbidites.

The Bouma Sequence

	Grain Size		Bouma (1962) Divisions	Middleton and Hampton (1973)	Lowe (1982)	This study
	Mud	Te	Laminated to homogeneous	Pelagic and low - density turbidity current	Pelagic and hemipelagic	Pelagic and hemipelagic
	Sand–Silt	Td	Upper parallel laminae	Turbidity current	Low-density turbidity current	Bottom-current reworking
		Tc	Ripples, wavy or convoluted laminae			
		Tb	Plane parallel laminae			
	Sand (to granule at base)	Ta	Massive, graded		High-density turbidity current	Sandy debris flow

Fig. 8.1. The turbidite facies model (i.e., the Bouma Sequence) showing Ta, Tb, Tc, Td, and Te divisions. Conventional interpretation is that the entire sequence is a product of a turbidity current (Bouma, 1962; Walker, 1965; Middleton and Hampton, 1973). According to Lowe (1982), the Ta division is a product of a high-density turbidity current and Tb, Tc, and Td divisions are deposits of low-density turbidity currents. In this book, the Ta division is considered to be a product of a turbidity current only if it is normally graded, otherwise it is a product of a sandy debris flow; the Tb, Tc, and Td divisions are considered to be deposits of bottom-current reworking. (After Shanmugam (1997a). Reproduced with permission from Elsevier.)

Although earlier workers had recognized similar vertical sequences, Bouma was the first to make the link between the sequence of structures and its origin by turbidity currents (Table 8.1). Later workers explained the model with sophisticated hydrodynamic interpretations (Harms and Fahnestock, 1965; Walker, 1965; Middleton and Hampton, 1973).

This model has been the single most frequently used facies model for describing and interpreting deep-water deposits as turbidites (e.g., Harms and Fahnestock, 1965; Walker, 1984a; Ghibaudo, 1992; Lowe and Guy, 2000; Pickering et al., 2001). The Bouma Sequence has been discussed routinely in sedimentology textbooks as a template for interpreting deep-water deposits (e.g., Blatt et al., 1972; Pettijohn, 1975; Friedman and Sanders, 1978; Reineck and Singh, 1980; Leeder, 1982; Walker, 1984a; Allen, 1985a; Bjorlykke, 1989; Pickering et al., 1989; Reading, 1996; Boggs, 2001). Turbidite interpretation serves as the basis for developing submarine fan models (Mutti and Ricci Lucchi, 1972). Geoscientists in the petroleum industry commonly use fan models for predicting reservoir distribution in frontier exploration provinces.

Table 8.1 Summary of various turbidite facies models and turbidite facies association schemes

Reference	Turbidite facies models and facies associations
Sheldon (1928)	Description of the first vertical sequence in the U.S.
Signorini (1936)	Description of the first five-part vertical sequence (the pre-Bouma Sequence) in Italy.
Bailey (1936)	Introduction of 'graded facies' for deep-water sands.
Kuenen and Migliorini (1950)	Establishment of the link between graded beds and turbidity currents (i.e., the dawn of the turbidite paradigm).
Ten Haaf (1959a,b)	A basal normally graded part, a middle rippled and convoluted part, and an upper laminated mudstone part.
Basset and Walton (1960)	A basal normally graded part, a middle laminated part, and an upper mudstone part.
Bouma (1962)*	*Introduction of the first turbidite facies model with five divisions (Ta, Tb, Tc, Td, Te), known as the Bouma Sequence (Fig. 8.1), for a 'classic' or medium-grained turbidite deposited by a waning turbidity current.
Kuenen (1964)	Introduction of a turbidite facies model with six divisions (Ta, Tb, Tc, Td, Te, Tet, Tep). The last two divisions Tet and Tep represent turbiditic and pelagic (or hemipelagic) mud, respectively.
Rupke and Stanley (1974)	
Harms and Fahnestock (1965), Walker (1965), Middleton and Hampton (1973)	Application of flow-regime concepts to the Bouma Sequence. However, there is no experimental basis to link traction structures to deposition by turbidity currents (see Shanmugam, 2000a).
Van der Lingen (1969)	Introduction of a turbidite facies model with six divisions (Ta, Tb, Tc, Td, Te, Tf).
Hesse (1975)	
Piper (1978)	Introduction of a turbidite facies model with eight divisions (Ta, Tb, Tc, Td, Te1, Te2, Te3, Tf) for fine-grained turbidites.
Stow and Shanmugam (1980)	Introduction of a turbidite facies model with nine divisions (T0, T1, T2, T3, T4, T5, T6, T7, T8) for fine-grained turbidites.
Lowe (1982)	Introduction of a turbidite facies model with six divisions (R1, R2, R3, S1, S2, S3) for coarse-grained turbidites deposited by 'high-density turbidity currents'.
Walker (1984b)	Introduction of a turbidite facies model with six divisions (Ta, Tb, Tc, Td, Te Tet, Teh). The last two divisions Tet and Teh represent turbiditic and hemipelagic mud, respectively.
Hsu (1989)	Revision of the Bouma Sequence with three divisions (Tab, Tc, Te).
Mutti and Ricci Lucchi (1972)	Introduction of the first turbidite facies association scheme.
Walker and Mutti (1973)	Modified version of the turbidite facies association scheme.

*Focus of this chapter.
Note: A turbidite facies model represents a single depositional unit, whereas a turbidite facies association scheme represents groupings of multiple depositional units.

8.2.2 Critique of the model

Although the turbidite facies model is used widely in the petroleum industry and academia, aspects of this model and the explanations for the origin of the sequence have come under criticism for theoretical, experimental, and observational reasons (Sanders, 1965; Van der Lingen, 1969; Hsü, 1989; Shanmugam, 1997a).

In critiquing vertical facies models of turbidites, Middleton (1993, p. 90) wrote, '*It must first be emphasized that gravity flows are a very complex class of flows, more complex for example than open-channel flows such as rivers… No geologist would expect that rivers could deposit only a single type of sediment bed, characterized by a single suite of sedimentary structures and textures—yet many geologists have such a notion about turbidites.*'

The turbidite facies model suffers for the following reasons (Shanmugam, 1997a):

(1) Bouma divisions are used routinely for describing deep-water strata. In an observational science like physical sedimentology, one must always maintain a clear distinction between description and interpretation (see Chapter 1). This is particularly critical for deep-water sands whose depositional origins are much more complex than the published literature saturated with turbidite terminology would indicate. For example, if a bed is described in the field as Ta division (i.e., Bouma division A), the notation, Ta carries with it a powerful message and a built-in interpretation that the bed was deposited by a turbidity current. On the other hand, if the same bed were to be described without the Ta notation, simply as 'a structureless sand with a sharp upper contact and floating mudstone clasts near the top' then the description stands alone without any built-in interpretation. Thus the former description leaves one no choice but to interpret the bed as a turbidite, whereas the latter description allows room for alternative interpretations, such as a sandy debrite.

(2) The Bouma Sequence represents an interpretive depositional model for the deposit of a turbidity current (Fig. 8.1). Therefore, describing a deep-water sand unit as Ta is like describing a cross-bedded sand unit as a 'braided fluvial deposit.' Such a description with a built-in interpretation defeats the purpose of process sedimentology.

(3) Because the Bouma divisions are now so routinely applied during field descriptions, it is almost impossible to discern how many of the published examples of turbidites actually are deposits of true turbidity currents. This skepticism stems from the fact that the complete and partial Bouma Sequence can be explained by processes other than true turbidity currents.

In commenting on my paper (Shanmugam, 1997a), Miall (1999, p. 3) wrote that '… *it is precisely because we have in our minds a good concept of what a "true" Bouma turbidite should like, that we can readily appreciate how far off the track many sedimentological descriptions and interpretations have strayed, when someone like Shanmugam comes along and brings us up short with different observations. It turns out that many deep-marine sands may not be turbidites at all.*'

8.3 The Annot Sandstone

Bouma (1962) used the Annot Sandstone (Grès d' Annot Formation, Eocene–Oligocene) exposed in the Peira Cava area and vicinity of the French Maritime Alps for developing the first turbidite facies model. Later, he extended his study to Switzerland and other areas in Europe. Bouma documented his field observations in eight photographic plates, seven of which contain outcrop photographs from the Peira Cava type locality (Plates A, B, C, D, E, F, and H) and the eighth one contains outcrop photographs from Switzerland (Plate G).

The Annot Sandstone is a deep-marine deposit of a rectilinear foreland basin. The basin was created by lithospheric loading of both the Alpine thrust sheets to the east and the Sardinia-Corsica basement to the south in southeastern France (Pickering and Hilton, 1998). This large basin was bathymetrically complex (Ravenne et al., 1987). In discussing sedimentation and tectonic aspects of the Annot Sandstone, Ravenne et al. (1987, p. 530) stated, '*This formation, with a maximum observed thickness of 1200 m, is a fill-up sequence that overlaps the paleoslopes of the basin. The E-W extensional phase hardly continued during sandstone sedimentation, which is capped by an erosional surface with NE-SW submarine canyons.*'

Sediment was derived from the south (Pickering and Hilton, 1998). The Annot Sandstone occurs as a number of isolated remnants in SE France and NW Italy (Sinclair, 1997). The Annot outcrop described in this book represents a small part of one of the remnants of the original depositional system in the Peira Cava sub-basin (Fig. 4.37).

An important attribute of the Annot Sandstone is the suggestion that virtually every sandstone bed is normally graded (see Bouma, 1962, his measured sections K, ABC, and Q in Enclosures I, II, and III). Although the Annot Sandstone appears to show normal grading, detailed description offers a different story. To understand the nature of normal grading and related complexities, I examined in detail 12 sandstone units of the Annot Sandstone, exposed along a road section in the Peira Cava area of French Maritime Alps (Fig. 4.37). This is the same road section that Bouma (1962, p. 93, Fig. 23 therein) and Lanteaume et al. (1967) first used in their studies of the Annot Sandstone.

8.4 Basal sedimentary features

A summary of sedimentary features observed in the Annot Sandstone and their process interpretation is given in Table 8.2. In addition to systematically describing complex sedimentary features, two alternative interpretations are presented for each unit; one using the Bouma divisions (i.e., the conventional approach) and the other without using the Bouma divisions (i.e., unconventional approach).

Table 8.2. Summary of observed features and their process interpretations, Annot Sandstone. Most of these features are not part of the turbidite facies model (see Fig. 8.1)

Unit Number (This study)	Observation	Interpretation
Unit 2 (Fig. 8.14A) Unit 9 (Fig. 8.3A) Unit 12A (Fig. 8.4A)	Basal contorted layers	Shearing and slumping
Unit 5 (Fig. 8.8A) Unit 7 (Fig. 8.7B) Unit 8 (Fig. 8.11A) Unit 12B (Fig. 8.5A) Unit 12C (Fig. 8.6A)	Basal inverse grading	Sandy debris flow with flow strength
Unit 1 (Fig. 8.9A, 2–4.7 m)	Basal normal grading without complications	Newtonian flow (turbidity current) without flow strength
Unit 1 (Fig. 8.9B) Unit 5 (Fig. 8.8A) Unit 7 (Fig. 8.16A) Unit 8 (Fig. 8.11A) Unit 12B (Fig.8. 5A)	Lenticular layers	Sandy debris flow with flow strength and laminar state
Unit 8 (Fig. 8.11B)	Pockets of gravels	Sandy debris flow with flow strength
Unit 2 (Fig. 8.14B) Unit 8 (Fig. 8.11A) Unit 12C (Fig. 8.6A)	Armored mudstone balls	Sandy debris flow with flow strength and buoyancy
Unit 7 (Fig. 8.16B)	Floating mudstone clasts (random and planar)	Sandy debris flow with flow strength and buoyancy
Unit 7 (Fig. 8.16A, B)	Floating quartzose granules	Sandy debris flow with flow strength
Unit 12A (Fig. 8.4A)	Parallel laminae: 3 m thick interval	Bottom current reworking
Unit 2 (Fig. 8.14A)	Parallel- ripple- parallel- ripple alternation	Bottom current reworking (Tidal currents?)
Unit 2 (Fig. 8.14A, 8.4 m) Unit 12B (Fig. 8.5A, 5.3 m)	Sudden drop in grain size	Drop in flow velocity
Unit 2 (Fig. 8.14B)	Double mud layers	Deep-marine tidal currents
Unit 2 (Fig. 8.14A)	Mud-draped ripples	Deep-marine tidal currents
Unit 10 (Fig. 4.39B) Unit 11 (Fig. 4.40B)	Sigmoidal cross bedding (Full vortex)	Deep-marine tidal currents
Unit 2 (Fig. 8.14A) Unit 5 (Fig. 8.8A) Unit 7 (Fig. 8.16A) Unit 8 (Fig. 8.11A) Unit 12A (Fig. 8.4A) Unit 12B (Fig. 8.5A) Unit 12C (Fig. 8.6A)	Inverse to normal grading with complications (e.g. floating quartzose granules, mudstone clasts, armored mudstone balls, lenticular layers, and pockets of gravels)	Sandy debris flow with flow strength. Flow transformation from strongly coherent flow (i.e., basal inverse grading) to moderately and weakly coherent flows (i.e., upper normal grading).

Each Annot unit is composed of a basal and an upper part. The basal part of sandstone units is characterized by contorted layers, inverse grading, and normal grading without complications. Discrete contorted layers of slump origin also occur in association with the principal sandstone units (Fig. 8.2).
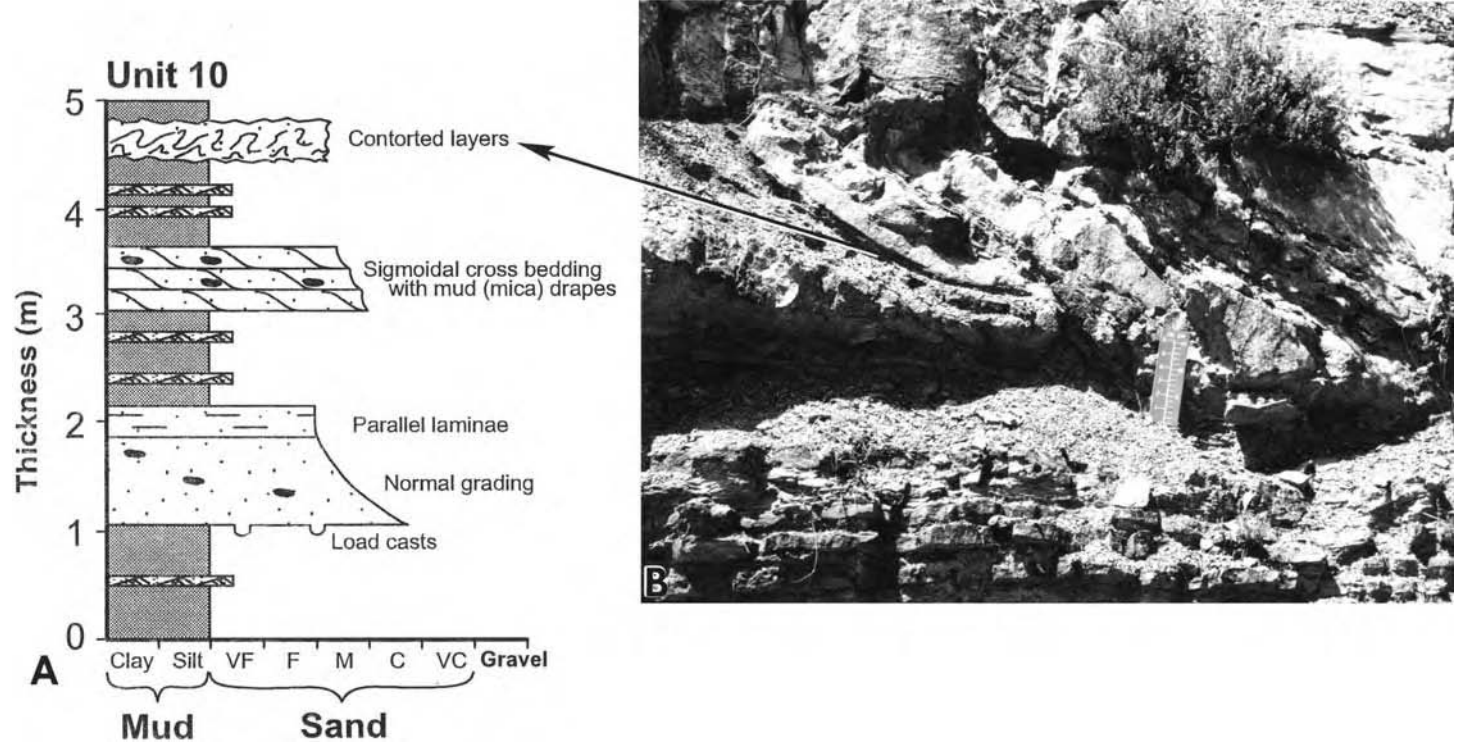
Fig. 8.2. (*A*) Sedimentological log of Unit 10 showing contorted layers in association with sigmoidal cross beds. (*B*) Outcrop photograph of contorted layers. Arrow shows stratigraphic position of contorted layers. Annot Sandstone (Eocene–Oligocene), Peira Cava area, French Maritime Alps. SE France.

8.4.1 Basal contorted layers

Unit 9 corresponds to Bouma's layer No. 1 in his measured section K (see Bouma, 1962, Enclosure I in inside pocket of back book cover). For this unit, Bouma assigned all five divisions of the model, but the unit is more complex with contorted layers at the base and deformed cross beds near the top (Fig. 8.3A). The basal contorted zones range in thickness from 1 to 3 m.
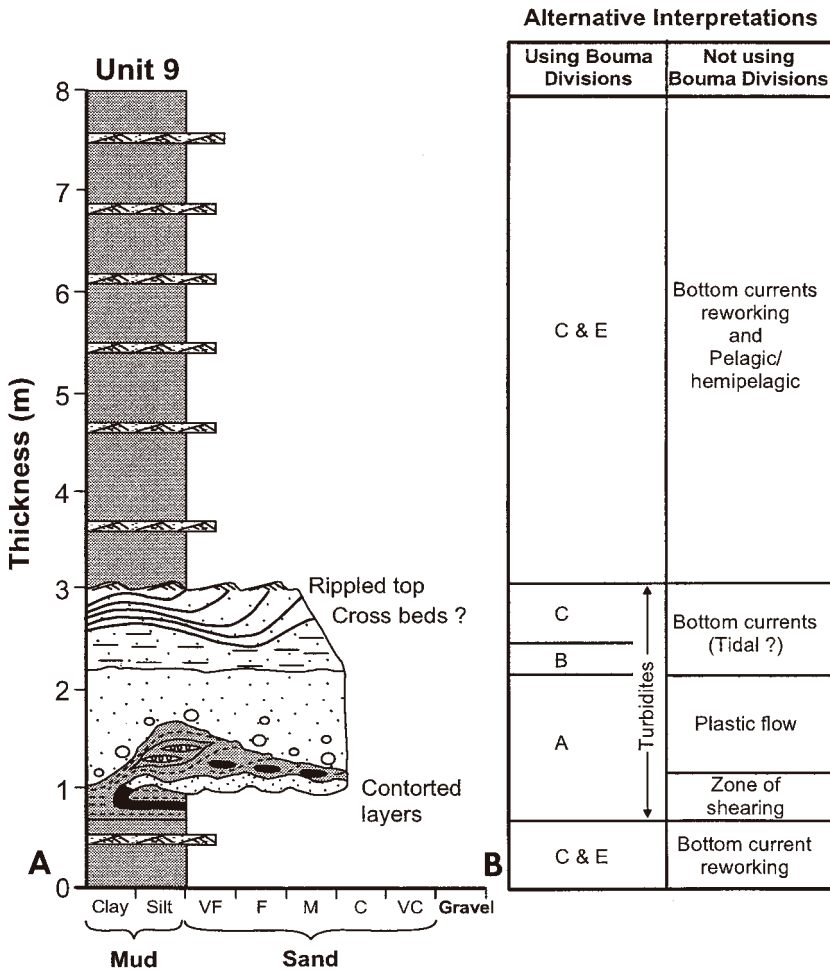
Fig. 8.3. (*A*) Sedimentological log of Unit 9 showing contorted layers, deformed cross beds, and rippled top. (*B*) Two alternative interpretations of field description. (1) By using Bouma divisions, the unit could be interpreted as a turbidite. (2) By not using Bouma divisions (this book), each layer of the unit is interpreted individually either as deposits of plastic flows or bottom current reworking or zone of shearing. Annot Sandstone (Eocene–Oligocene), Peira Cava area, French Maritime Alps. SE France.
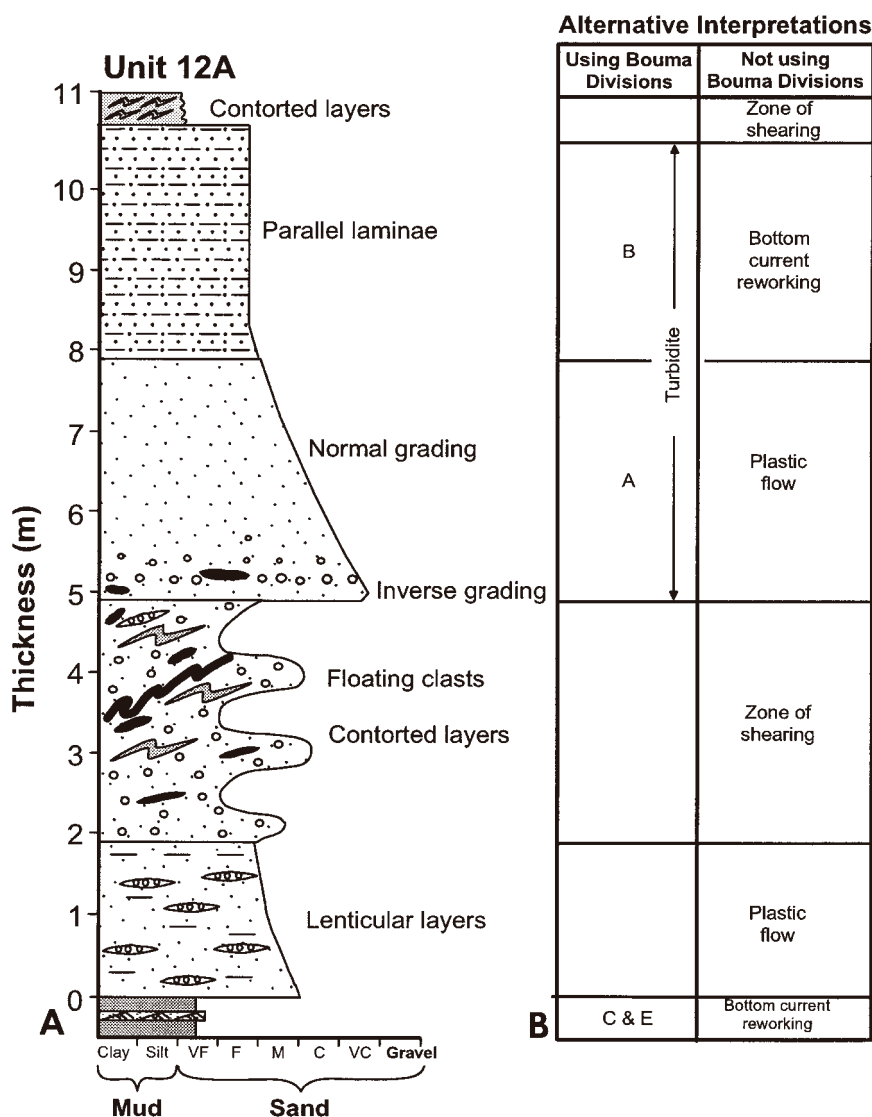
Fig. 8.4. (*A*) Field description of amalgamated Unit 12A showing basal inverse grading (at 5 m) with clasts and granules and upper intervals of normal grading and parallel laminae. Note underlying severely contorted layers. In cases like this, it is difficult to determine the true basal contact of the unit (i.e., at 0 m or at 5 m?). (*B*) Two alternative interpretations of field description. (1) By using Bouma divisions, the upper part (5–10.8 m) could be interpreted as a turbidite. (2) By not using Bouma divisions (this book), each layer of the unit is interpreted individually either as deposits of plastic flows or bottom current reworking. Plastic flows represent sandy debris flows. Unit 12A (see Fig. 4. 37 for location map in which Units 12A, 12B, and 12C are shown as a single dot). Annot Sandstone (Eocene–Oligocene), Peira Cava area, French Maritime Alps. SE France.

In addition to basal contorted layers, sandstone and mudstone beds are severely deformed below in Unit 2, Unit 12A (Fig. 8.4), Unit 12B (Fig. 8.5A), and Unit 12C (Fig. 8.6A). The underlying disturbed mudstone also shows sandstone injectites (Fig. 8.6A). Basal contorted layers are not part of the turbidite facies model (Fig. 8.1).

The contorted intervals beneath the sandstone are interpreted to be a product of shearing and slumping produced by stress exerted by overriding mass flows. Large-scale shear structures have been reported in the Annot Sandstone in other areas as well (Clark and Stanbrook, 2001).
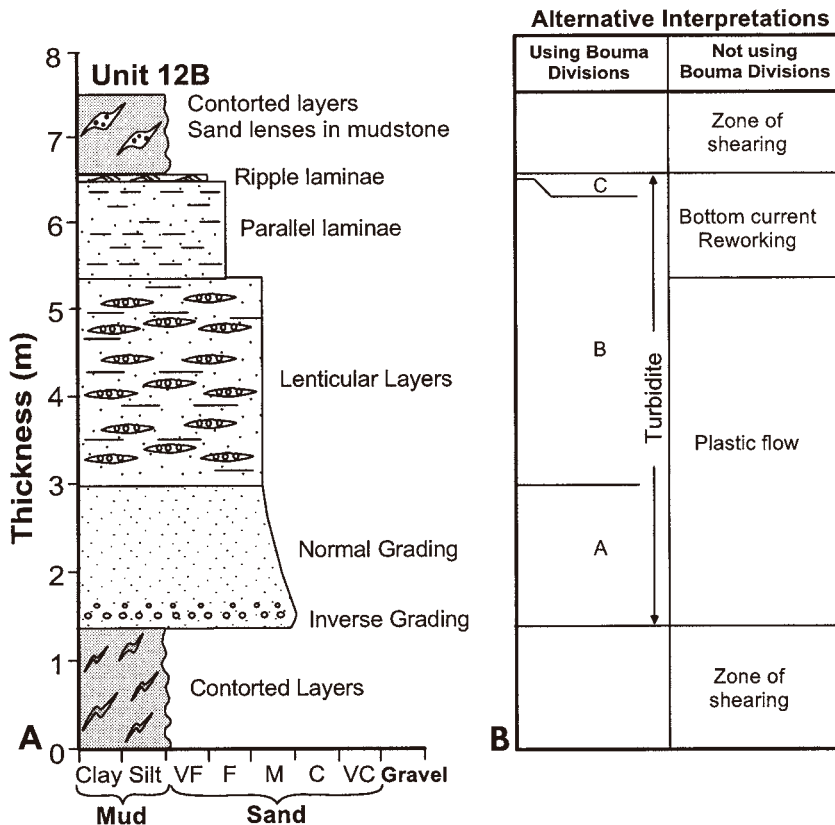
Fig. 8.5. (*A*) **Field description of amalgamated Unit 12B. Note underlying and overlying mudstone intervals with contorted layers (*B*) Two alternative interpretations of field description. (1) By using Bouma divisions, the unit could be interpreted as a turbidite. (2) By not using Bouma divisions (this book), each layer of the unit is interpreted individually either as deposits of plastic flows or bottom current reworking. Plastic flows represent sandy debris flows. Annot Sandstone (Eocene–Oligocene), Peira Cava area, French Maritime Alps. SE France.**
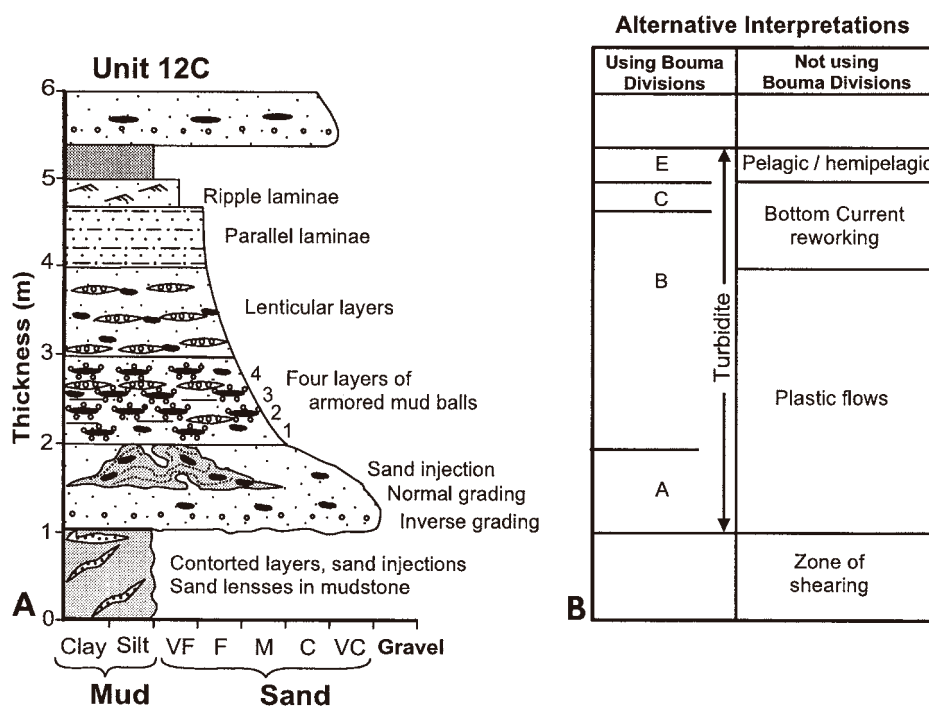
Fig. 8.6. (*A*) Field description of amalgamated Unit 12C showing basal inverse grading, four layers of armored mudstone balls, and lenticular layers. Note underlying mudstone with contorted layers and sandstone injectites. (*B*) Two alternative interpretations of field description. (1) By using Bouma divisions, the unit could be interpreted as a turbidite. (2) By not using Bouma divisions (this book), each layer of the unit is interpreted individually either as deposits of plastic flows or bottom current reworking. Plastic flows represent sandy debris flows. Annot Sandstone (Eocene–Oligocene), Peira Cava area, French Maritime Alps. SE France.

8.4.2 Basal inverse grading

Sandstone units are commonly amalgamated and have a thickness of up to 11 m. Sandstones are very coarse- to fine-grained in texture, and show inverse grading at their base. Commonly, pebbles and granules in sandstone constitute inverse grading (i.e., coarse-tail grading). Floating mudstone clasts also occur in basal inversely graded intervals. Inversely graded intervals are usually overlain by an interval of 'normal grading' with complications. Inverse grading is well developed in Unit 7 (Fig. 8.7A), Unit 5 (Fig. 8.8A), Unit 8, Unit 12A (Fig. 8.4A), Unit 12B (Fig. 8.5A), and Unit 12C (Fig. 8.6A). The lower contact of inversely graded unit is sharp. The upper contact is gradational. Inversely graded units vary in thickness from 1 cm to 2 m. Only a few researchers have discussed the occurrence of inverse grading in the Peira Cava area (e.g., Pickering and Hilton, 1998). Basal inverse grading is not part of the turbidite facies model (Fig. 8.1).
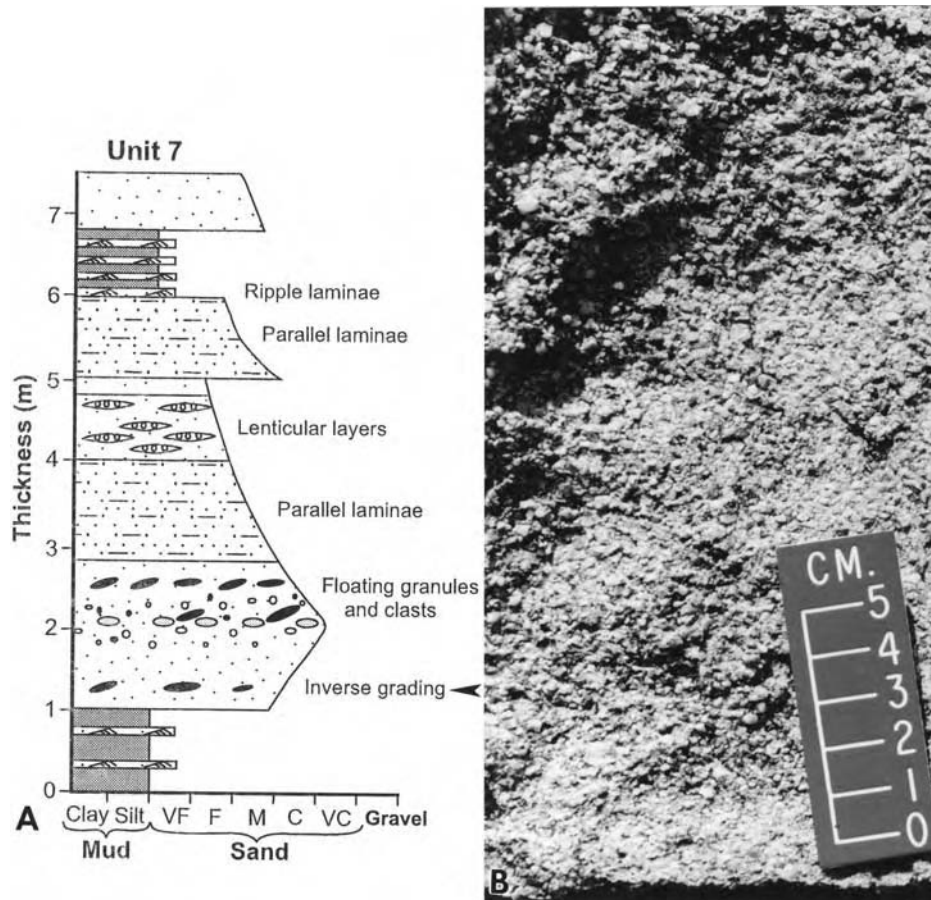
Fig. 8.7. (*A*) Sedimentological log of amalgamated sandstone Unit 7 showing basal inverse grading overlain by an interval of complex normal grading with floating granules and mudstone clasts, parallel laminae, and lenticular layers. Note sudden increase in grain size at 5 m. (*B*) Outcrop photograph of Unit 7 showing basal inversely graded interval in coarse- to granule-grade sandstone. Arrow shows stratigraphic position of photo. Annot Sandstone (Eocene–Oligocene), Peira Cava area, French Maritime Alps. SE France.

The origin of inverse grading by deep-water turbidity currents is problematic. This is because inverse grading cannot be explained by suspension settling from Newtonian-type turbidity currents. Thus other mechanisms have been proposed. Lowe (1982) explained inverse grading as traction carpets in high-density turbidity currents. The problem is that traction carpets are supposed to be less than 5 cm in thickness (Lowe, 1982), but the thickness of inverse grading in the Annot Sandstone is up to 2 m (Unit 5). Following the concept of Kneller (1995) and Kneller and Branney (1995), Mulder et al. (2002, p. 114) attributed the origin of inverse grading to waxing hyperpycnal turbidity currents, As pointed out
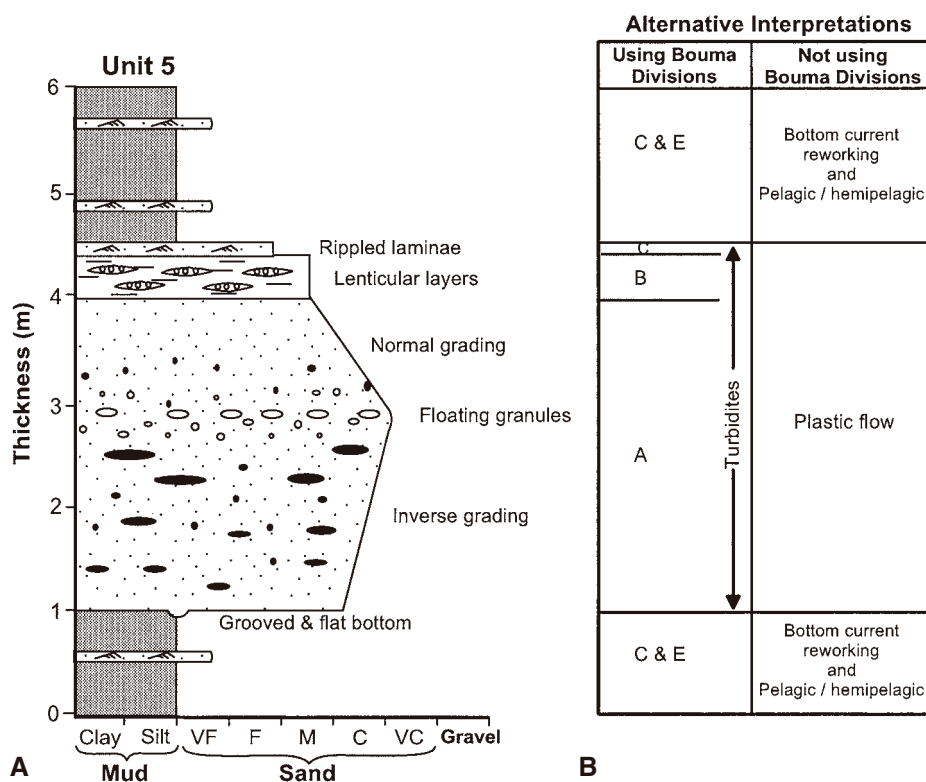
Fig. 8.8. (*A*) Sedimentological log of amalgamated sandstone Unit 5 showing a basal interval of inverse grading with floating quartzose granules and mudstone clasts, and an upper interval of complex normal grading with floating quartzose granules and lenticular layers. (*B*) Two alternative interpretations of field description of Unit 5. (1) By using Bouma divisions, the entire unit could be interpreted as turbidites. (2) By not using Bouma divisions (this book), each layer of the unit is interpreted individually either as deposits of plastic flows or bottom current reworking. Plastic flows represent sandy debris flows. Annot Sandstone (Eocene–Oligocene), Peira Cava area, French Maritime Alps. SE France.

earlier (Chapter 7), the concept of hyperpycnal flows was meant for deltaic environments.

Mechanisms that explain inverse grading are:

(1) Dispersive pressure, caused by grain-to-grain collision, tends to force larger particles toward the zone of least rate of shear (Bagnold, 1954).
(2) Kinetic sieving by which smaller particles tend to fall into gaps between larger particles (Middleton, 1970).
(3) The lift of individual grains toward the top of a flow with lower pressure (Fisher and Mattinson, 1968).
(4) Vibration mechanics (Poliakov, 2002).

Of these, the kinetic sieving mechanism may not be applicable here because many examples of inverse grading are composed mostly of pebbles and granules. A combined mechanism of dispersive pressure, matrix strength, hindered settling, and buoyant lift would explain the development of inverse grading. The inverse grading is attributed to a plastic debris-flow origin (Fig. 8.6B).

8.4.3 Basal normal grading

Simple normal grading represents sandy intervals showing upward-decrease in maximum and average grain size without any internal complications, such as amalgamation surfaces, floating quartz granules, floating mudstone clasts, heterolithic injections, and pockets of gravels. It occurs at the bases of sandstone units. The basal contacts of these normally graded units are invariably sharp or erosive. Although simple normal grading in the Peira Cava area is extremely rare (Fig. 8.9A, 2–4.7 m interval), it is the feature that Bouma emphasized the most in his turbidite facies model. In fact, Bouma (1962, p. 63) reported that all layers
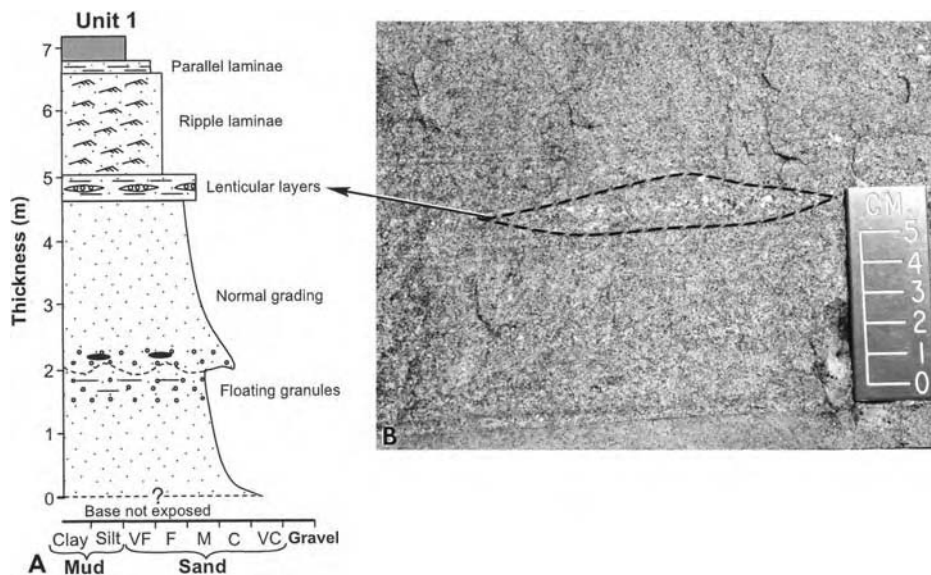
Fig. 8.9. (*A*) **Sedimentological log of amalgamated sandstone Unit 1 showing basal complex normal grading (0–2 m) with floating quartzose granules and a simple normal grading (2–4.7 m) without complications. Note a sudden increase in grain size with lenticular layers (4.7–5 m), and a sudden decrease in grain size (5 m) in the overlying division with ripple laminae. (*B*) Outcrop photograph of Unit 1 showing a lenticular layer, which is a lens (dashed line) of granule-sized particles of quartz, feldspar, and rock fragments in fine- to medium-grained sandstone. Long axes of lenticular layers are aligned parallel to bedding plane (i.e., planar fabric) indicating laminar state of flow. Arrow shows stratigraphic position of photo. Annot Sandstone (Eocene–Oligocene), Peira Cava area, French Maritime Alps. SE France.**
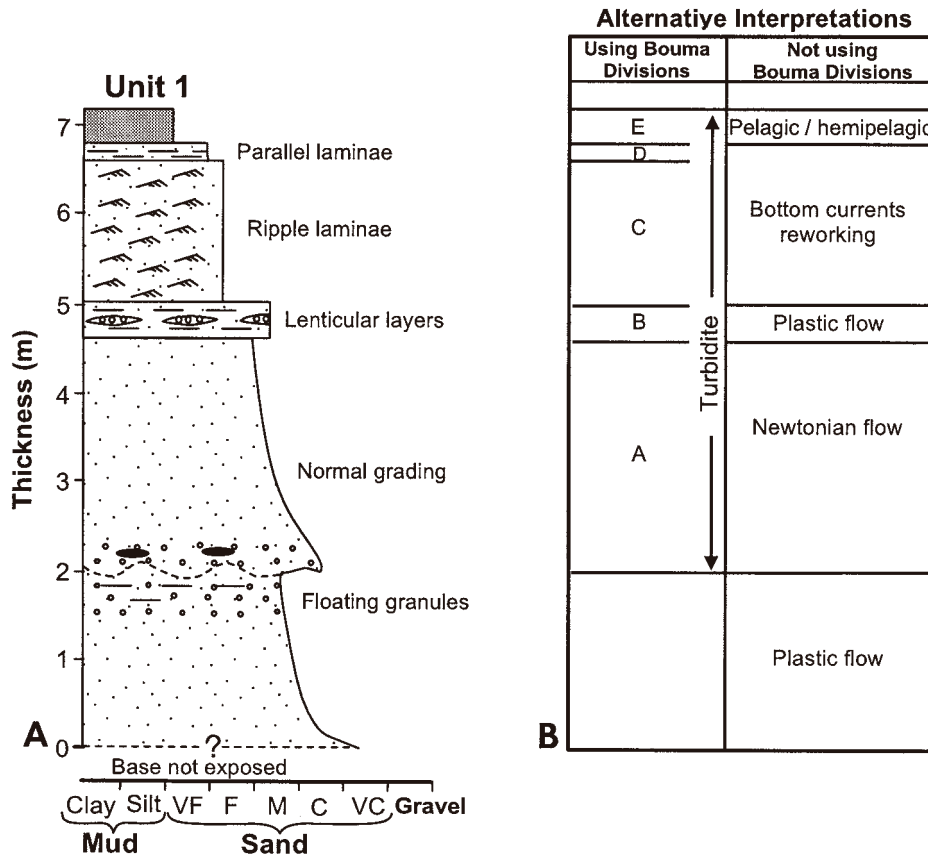
Fig. 8.10. (*A*) Sedimentological log of Unit 1 showing complex normal grading (0–2 m) simple normal grading (2–4.7 m), lenticular layers (4.7–5 m), and ripple laminae (5–6.7 m). Note a decrease in grain size at 5 m. (*B*) Two alternative interpretations of field description of Unit 1. (1) By using Bouma divisions, the upper part could be interpreted as turbidites. (2) By not using Bouma divisions (this book), each layer of the unit is interpreted individually either as deposits of Newtonian flow (turbidity currents), bottom current reworking or plastic flow. Plastic flows represent sandy debris flows. Annot Sandstone (Eocene-Oligocene), Peira Cava area, French Maritime Alps. SE France.

in the Peira Cava area show normal grading. Normally graded units reach a thickness of 4 m. Intervals of simple normal grading in the Annot Sandstone are interpreted as turbidites (Fig. 8.10B).

8.5 Upper 'normally graded' intervals

In addition to the true normal grading described above, there are intervals that resemble 'normal grading,' but that have complicated internal features.

These features are: (1) lenticular layers; (2) pockets of gravels; (3) floating armored mudstone balls; (4) floating mudstone clasts; (5) floating quartzose granules; (6) parallel laminae; (7) ripple laminae; (8) sudden decrease in grain size; (9) alternating mud-draped ripples and double mud layers; and (10) sigmoidal cross bedding. Because 'normally graded' intervals occur directly above intervals of inverse grading, most sandstone units exhibit an inverse to normally graded composite trend. The problem is that upper 'normally graded' intervals with complications cannot be interpreted as deposits of turbidity currents. This is because these sandstone intervals are not only amalgamated but composed of complex internal features.

8.5.1 Lenticular layers

Lenses of quartzose granules are present along faint layers in fine- to medium-grained sandstone. These lenticular layers are up to 15 cm long and 1 cm thick (Unit 1, Fig. 8.9A,B). Commonly, their long axes are aligned parallel to bedding, causing a planar fabric (Fig. 8.9A,B). The sandstone intervals with lenticular layers range in thickness from 40 cm (Fig. 8.9A) to 2.3 m (Fig. 8.5A). The lenticular layers commonly occur within intervals of parallel lamination (Fig. 8.5A). Lenticular layers occur as discrete divisions at the base of the 'normally graded' division in Unit 4, above the 'normally graded' division in Unit 5 (Fig. 8.8), above and below the parallel laminated divisions in Unit 7 (Fig. 8.7A), below the parallel laminated division in Unit 8, above sigmoidal cross bedding in Unit 11, and below the contorted sandstone division in Unit 12A (Fig. 8.4A). Lenticular layers are not part of the turbidite facies model (Fig. 8.1).

   Lenticular layers with quartzose granules in sandstone may be interpreted as deposits of non-Newtonian flows with strength. The presence of planar fabric supports the laminar state of flow (Fisher, 1971). By simply describing these sedimentary features without using the 'Bouma' divisions, lenticular layers would be interpreted to be deposits of plastic laminar flows (Fig. 8.5B).

8.5.2 Pockets of gravel

Unit 8 contains pockets of gravel in a 'normally graded' fine-grained sandstone interval (Fig. 8.11A,B). Gravelly material in the pocket consists of quartz, feldspar, rock fragments, and mudstone clasts. Unit 8 represents amalgamated sandstone deposited by multiple episodes. Pockets of gravel are not part of the turbidite facies model (Fig. 8.1).

   Unit 8 with pockets of gravel cannot be explained by a single waning turbidity current. The depositing flow must have had enough flow strength to support granules near its upper part. The pockets of gravels near the top of the bed reflect freezing of a plastic flow (Fig. 8.12B).
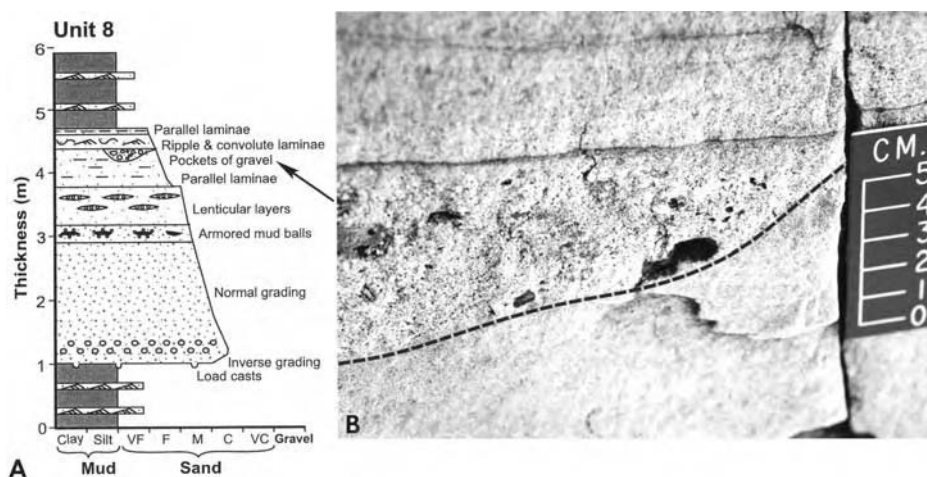
Fig. 8.11. (*A*) **Sedimentological log of amalgamated sandstone Unit 8 showing basal inverse grading, floating armored mudstone balls, lenticular layers, and pockets of gravel. (*B*) Outcrop photograph of Unit 8 showing a pocket of gravel (dashed line) with quartz, feldspar, rock fragments, and mudstone clasts in fine-grained sandstone. Arrow shows stratigraphic position of photo. Annot Sandstone (Eocene–Oligocene), Peira Cava area, French Maritime Alps. SE France.**

Depending on the degree of detail observed in the field, the same unit could be described and interpreted differently by different researchers. For example, with the least amount of detail Unit 8 could be described as a simple 'normally graded' bed (Level 1 description, Fig. 8.13), and with the most amount of detail the same unit would be described as 'amalgamated' (Level 3 description, Fig. 8.13). The significance of these differences in detail is that the level 1 description would ignore pockets of gravels and inverse grading, whereas the level 3 description would include pockets of gravels and inverse grading. A level 1 description would be interpreted as the unit a deposit of a single waning turbidity current, whereas a level 3 description would be interpreted as the unit deposits of multiple depositional events by sandy debris flows and bottom currents.

8.5.3 Floating armored mudstone balls

When mudstone balls, mudstone clasts, and quartzose granules are significantly larger in grain size than the matrix in which they occur, and they are at some distance above the basal depositional contact (i.e., in the middle and upper parts of a bed), the adjective 'floating' is used.

In the Annot Sandstone, sub-spherical to elongate floating mudstone clasts are armored (coated) with quartzose granules 3–4 mm in diameter (Fig. 8.14A,B).
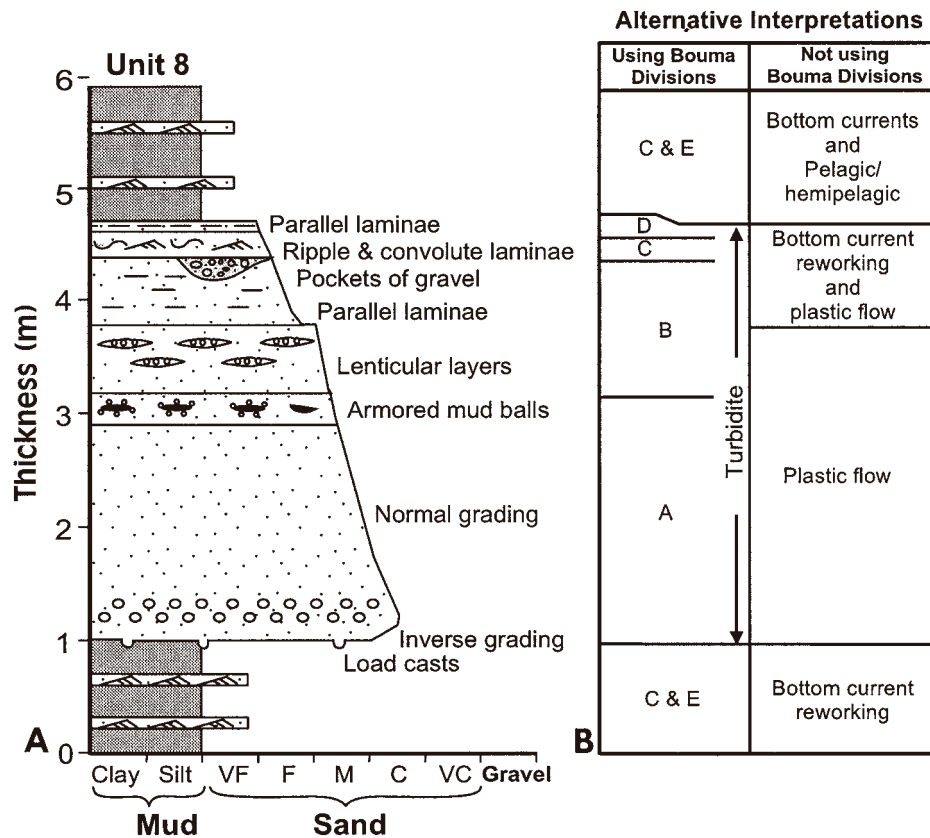
Fig. 8.12. (*A*) Sedimentological log of amalgamated Unit 8 showing complex internal features, such as basal inverse grading, armored mudstone balls, lenticular layers, and pockets of gravel. (*B*) Two alternative interpretations of field description of Unit 8. (1) By using Bouma divisions, the entire unit could be described as complete Bouma Sequence and could be interpreted as a turbidite. (2) By not using Bouma divisions (this book), each layer of the unit is interpreted individually either as deposits of plastic flows or bottom current reworking. Plastic flows represent sandy debris flows. Annot Sandstone (Eocene-Oligocene), Peira Cava area, French Maritime Alps. SE France.

In outcrop, floating armored mudstone balls create hollows during weathering away of the mudstone clasts encased in a medium- to coarse-grade sandstone matrix (Fig. 8.14B). Commonly, quartzose granules are preserved at the outer rim of the hollow. Within the hollows, remnants of mudstone clasts armored with quartzose granules also occur. These hollows with quartzose granules at their rims represent remnants of armored mudstone clasts (Fig. 8.14B). Some armored mudstone balls are up to 20 cm in length and up to 10 cm in width. They occur in the middle of 'normally graded' sandstone units (Units: 2, 6, 8, 12C); up to
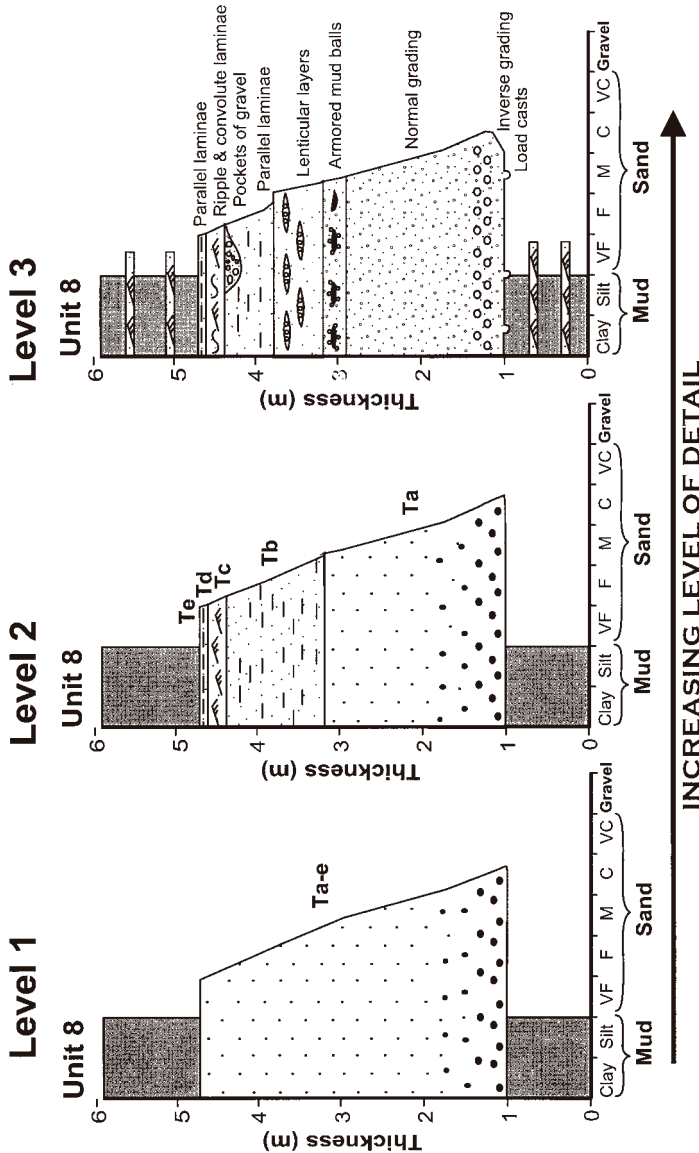
Fig. 8.13. Diagram showing three increasing levels of detail in field description of Unit 8. Level 1: Low degree of detail that shows a simple normally graded bed. Note absence of basal inverse grading and other complex features. This level of detail would result in interpretation of the sandstone unit as the deposit of a single turbidity current. Bouma's (1962) published graphic logs of 157 layers in measured sections of K (38 layers), ABC (28 layers), and Q (91 layers), which include Unit 8 of this study. They all show level 1 degree of detail (see Bouma, 1962, his Enclosures I, II, and III). Level 2: Moderate degree of detail shows a normally graded bed with Bouma divisions. This level of detail would also result in a turbidity current interpretation. Level 3: High degree of detail showing basal inverse grading, armored mudstone balls, lenticular layers, and pockets of gravels. This level of detail would result in interpretation of the unit as the deposit of multiple depositional events by plastic flows and bottom currents. Annot Sandstone (Eocene–Oligocene), Peira Cava area, French Maritime Alps. (After Shanmugam (2002a). Reproduced with permission from Elsevier.)
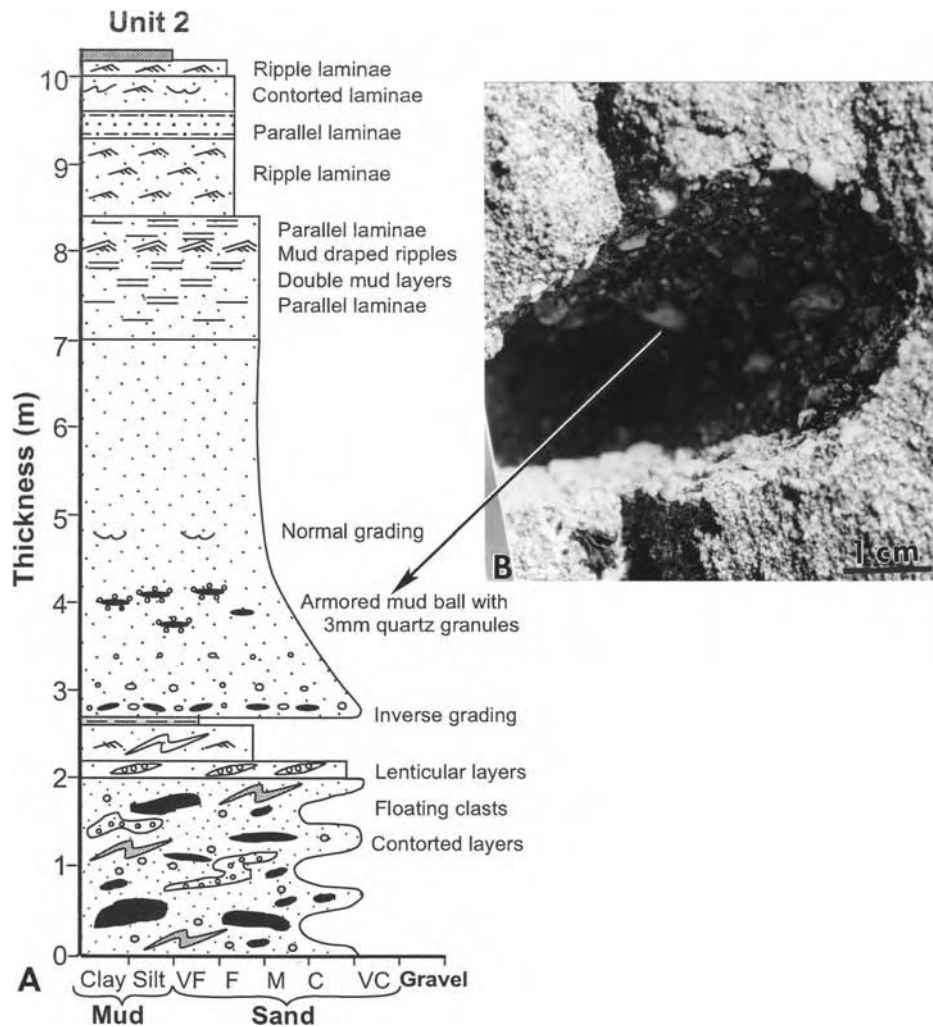
Fig. 8.14. (*A*) Sedimentological log of Annot Unit 2 in which the lower interval (0–2.75 m) is composed of contorted layers with pockets of gravel and floating mudstone clasts. The upper interval (2.75–10 m) is composed of a lower part (2.75–7 m) with basal inverse grading and armored mudstone balls with 3 mm quartz granules, and normal grading, and an upper part (7–10 m) with a complex alternation of parallel laminae, double mud layers, mud draped ripples, parallel laminae, ripple laminae, parallel laminae, contorted laminae, and ripple laminae. Note abrupt decrease in grain size at 2, 2.2, and 8.4 m, and change in sedimentary structures at 7 m. These planes represent amalgamation surfaces within the unit. (*B*) Outcrop photograph of Unit 2 showing a hollow created by weathering away of a mudstone clast in medium- to coarse- grade sandstone. Note quartzose granules at the outer rim of the hollow. Arrow shows stratigraphic position of photo. Annot Sandstone (Eocene-Oligocene), Peira Cava area, French Maritime Alps. SE France.

2 m above the base of a unit (Fig. 8.11). In Unit 12C, there are four distinct layers of armored mudstone balls (Fig. 8.6A), which represent amalgamation surfaces. Some armored mudstone-ball hollows are interbedded with lenticular layers. Pickering and Hilton (1998) reported armored mudstone balls in the Annot Sandstone, but did not discuss their origin. Armored mudstone balls are not part of the turbidite facies model (Fig. 8.1).

Bell (1940) discussed the origin of armored mudstone balls in fluvial deposits. Following a landslide and breakage into multiple mud blocks, individual mud blocks undergo quick rounding in the bed load, and absorb gravels during transport. In the deep-water Annot environments, however, fluvial processes are unrealistic. Also, in intervals with armored mudstone balls there is no evidence of bed-load transport. Conceivably, collapse of submarine canyon walls could have released large blocks of mud. These blocks could have been rapidly rounded and could have absorbed gravel while being transported. Mudstone balls 2 m above the base of the unit suggests that at the time of deposition the flow had strength, and that probably these mudstone balls were lifted buoyantly before the plastic flow froze (Fig. 8.15B). Stanley et al. (1978) interpreted armored mudstone balls in the Annot Sandstone to be associated with the filling of canyons by mass flows.

8.5.4 Floating mudstone clasts

In the Annot Sandstone, floating mudstone clasts are common (Fig. 8.16A). Large clasts occur that are up to 60 cm in length and up to 25 cm in width. Pockets of mudstone clasts occur at the base, in the middle, and at the top of 'normally graded' sandstone units. Most clasts, however, occur in the middle and the top of sandstone units. In Unit 7, a large pocket or lenticular nest of mudstone clasts occurs in the middle of the sandstone. This 'nest' is ~4 m long and ~1 m thick (see Chapter 12). Clasts are randomly distributed, imbricated, or show planar fabric in which long axes are aligned parallel to bedding. Floating mudstone clasts are not part of the turbidite facies model (Fig. 8.1).

Large pockets of mudstone clasts in the Annot may be attributed to rigid-plug deposition in debris flows (e.g., Johnson, 1970). Using fluvial point-bar analogy, Bouma and Coleman (1985) interpreted the deep-water Annot Sandstone, exposed in Peira Cava area (Unit 7), as lateral accretionary channel-fill turbidites. They used pebble nests, foreset bedding, and paleocurrent directions in support of their interpretations. This analogy is inappropriate for the following reasons:

(1) The Annot Sandstone does not show channel geometry (e.g., Bouma and Coleman, 1985, their Fig. 3), but does show a sheet-like geometry (see Chapter 12), which is an unlikely geometry of lateral-accretion deposits formed by a meandering channel.
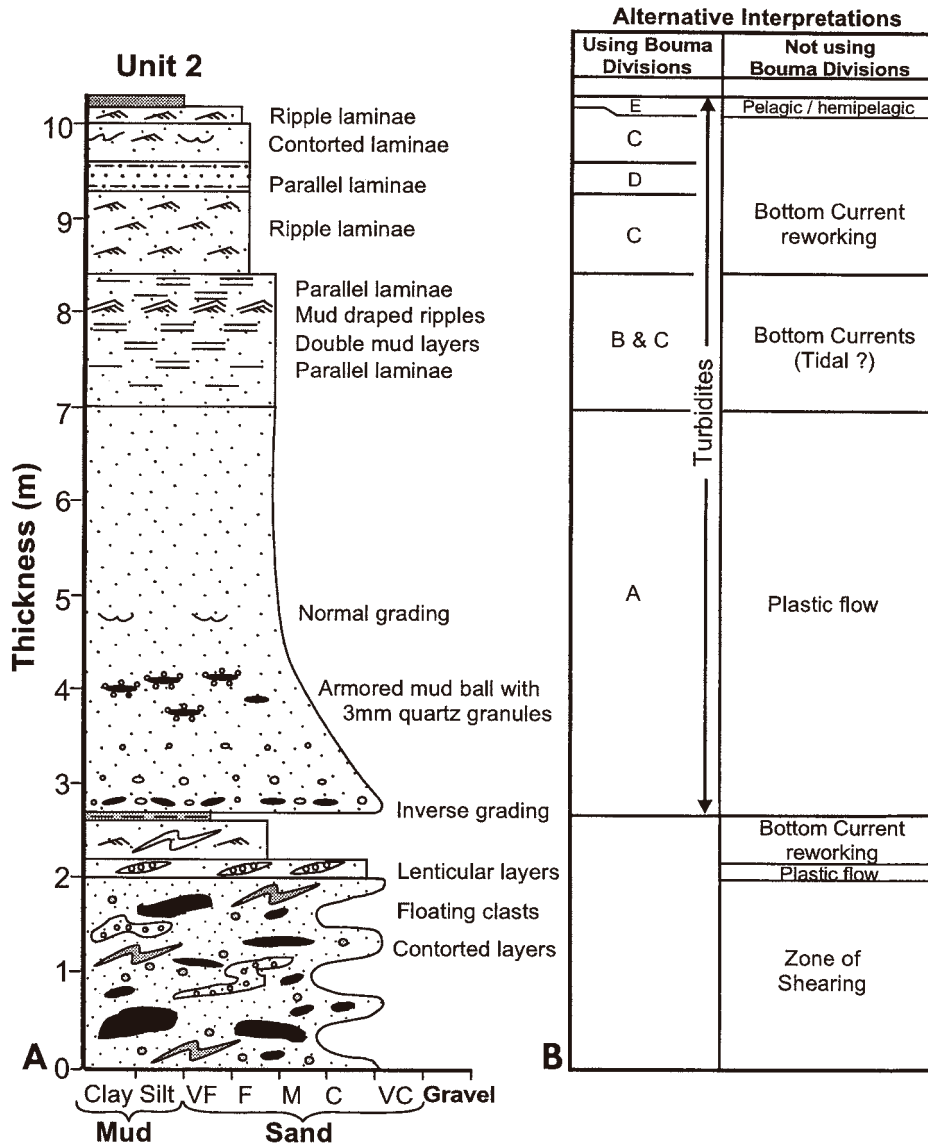
Fig. 8.15. (*A*) Sedimentological log of Annot Unit 2. (*B*) Two alternative interpretations of field description. (1) By using Bouma divisions, the upper part could be interpreted as turbidites. (2) By not using Bouma divisions (this book), each layer of the unit is interpreted individually either as deposits of plastic flows or bottom current reworking. Plastic flows represent sandy debris flows. Annot Sandstone (Eocene–Oligocene), Peira Cava area, French Maritime Alps. SE France.
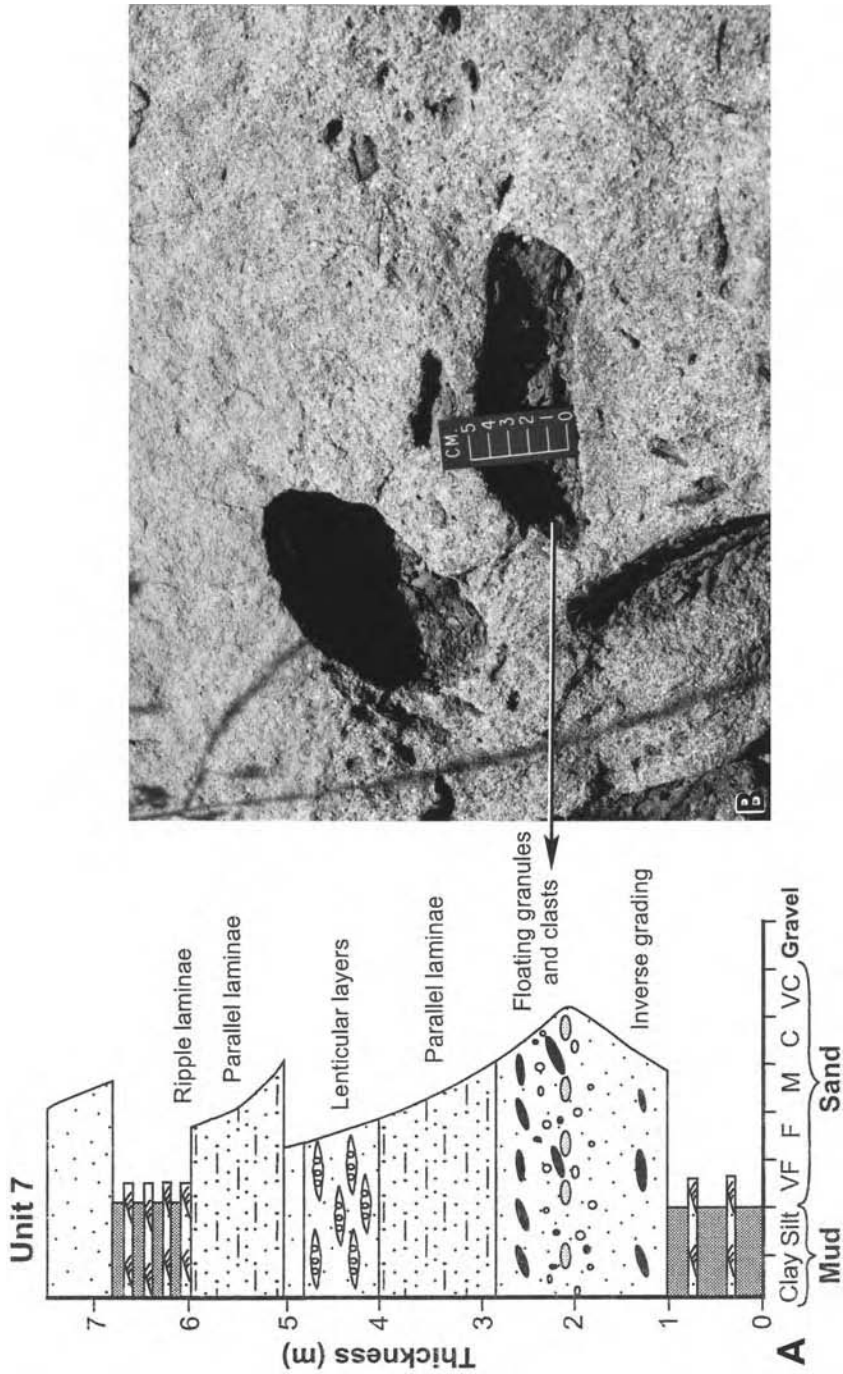
Fig. 8.16. (*A*) Sedimentological log of amalgamated sandstone Unit 7. (*B*) Outcrop photograph showing hollows created by weathering out of floating mudstone clasts. Note random orientation of mudstone clasts. Note floating quartzose granules in medium- to- coarse grade sandstone. Photo taken at about 2 m stratigraphic position in Unit 7 (arrow). Annot Sandstone (Eocene–Oligocene), Peira Cava area, French Maritime Alps. SE France.

(2) The logged sequences of the Annot Sandstone in Peira Cava do not contain sedimentary facies that would support the lateral accretion model (Oakeshott, 1989, p. 307).

(3) The pebble nests in the Annot Sandstone are analogous to slurried beds, which are deposits of debris flows (Mutti et al., 1978, p. 219).

(4) In addition to slurried beds, the Annot Sandstone exhibits inverse grading at its base and contains armored mud balls (see also Pickering and Hilton, 1998; Stanley et al., 1978). These features are probably products of debris flows. The problems concerned with the origin of sinuous channels in the deep sea have already been discussed (see Chapter 7).

Mutti and Nilsen (1981) explained floating mudstone clasts in Ta division of the Bouma Sequence by deposition *en masse* of the denser part of turbidity currents that is able to freeze rip up clasts. Because *en masse* deposition by freezing is characteristic of plastic flows rather than Newtonian flows (Fisher, 1971), these rafted clasts are attributed to a sandy debris flow. Also, planar clast fabric, attributed to the Ta division by Mutti and Nilsen (1981), is more indicative of laminar flow conditions in plastic debris flows than of turbulent flow conditions in turbidity currents (Johnson, 1970; Fisher, 1971; Shanmugam and Benedict, 1978).

By using the criteria of Postma et al. (1988), one could interpret these floating clasts as deposits of high-density turbidity currents. Postma et al., showed that outsized clasts can glide and subsequently rest at a rheological boundary (Fig. 7.5). Such an interpretation is not meaningful in the Annot Sandstone for three reasons. First, a high experimental slope of 25º was adopted to prevent or to delay 'freezing' of the inertia-flow layer (i.e., traction carpet). Such a slope is unrealistic for many deep-water environments that are less than one degree. Only steep submarine canyon walls, slump scars, and fault scarps exhibit such high slopes. Second, mudstone clasts in the experiments are confined to the rheological boundaries, but in the Annot Sandstone mudstone clasts are randomly distributed at the base, in the middle, and at the top of the sandstone units. Third, in the experimental deposit the basal inversely graded layer is overlain by a normally graded layer; however, in the Unit 11 of the Annot sandstone the basal inversely graded layer is overlain by sigmoidal cross bedding.

Using a fluvial analogy, imbricate clasts in deep-water sandstone beds have been ascribed to deposition from turbidity currents (Walker, 1984b). Major (1998), however, documented that debris flows can also develop a strongly imbricate clast orientation that mimics fabric developed during fluvial deposition. Caution must be exercised in discriminating between deposits of turbidity currents from those of debris flows using clast imbrications.

In Unit 7, intervals of floating mudstone clasts are interpreted as deposits of plastic debris flows (Fig. 8.17). A combination of dispersive pressure, matrix strength, hindered settling, and buoyant lift is proposed as the cause of floating clasts.
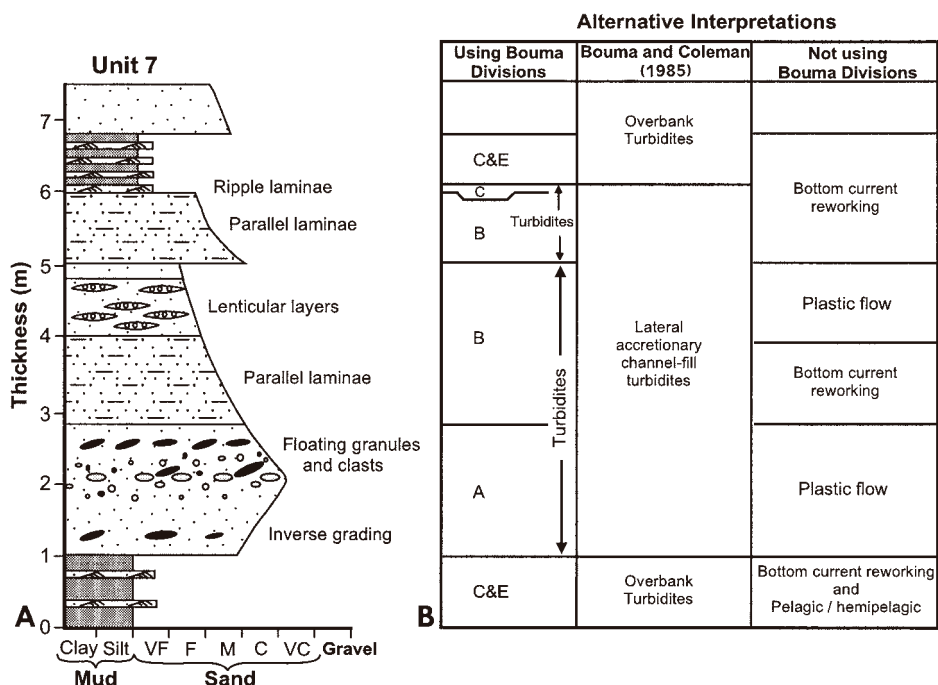
Fig. 8.17. (*A*) **Field description of amalgamated Unit 7.** (*B*) **Three alternative interpretations of field description. (1) By using Bouma (1962) divisions, the entire unit could be interpreted as turbidites. (2) Bouma and Coleman (1985) interpreted this unit as lateral accretionary channel-fill turbidites and associated overbank turbidites. See text for discussion on problems with this interpretation. (3) By not using Bouma divisions (this book), each layer of the unit is interpreted individually either as deposits of plastic flows or bottom currents. Plastic flows represent sandy debris flows in this case. Annot Sandstone (Eocene–Oligocene), Peira Cava area, French Maritime Alps. SE France.**

8.5.5 Floating quartzose granules

Granule-sized quartzose grains occur at the base, the middle, and the top of 'normally graded' sandstone intervals (e.g., Units: 2, 4, 5, 6, 7, 8, 9, and 12C). They occur either as individual granules (Fig. 8.16A) or as clusters in pockets near the top of units (Fig. 8.11). As mentioned earlier, quartzose granules also occur as lenticular layers and as part of inverse grading beneath 'normally graded' intervals. Floating quartzose granules are not part of the turbidite facies model (Fig. 8.1).

Even a single floating quartzose granule in a quartz-rich sandy matrix is of rheologic and hydrodynamic significance. In the Annot Sandstone, quartzose granules floating in a sandy matrix are evidence that the flow had strength and that settling of the grains is hindered. Because Unit 7 contains floating quartz

granules (Fig. 8.17A) and amalgamation surfaces, it has been interpreted to be deposits of multiple episodes of sandy debris flows and bottom currents (Fig. 8.17B).

8.5.6 Parallel laminae

In Unit 12A, a three-meter thick interval of parallel and horizontal laminae occurs as part of 'normally graded' interval (Fig. 8.4A). In Unit 12B, this interval is distinctly different (Fig. 8.5A). In Unit 8 (Fig. 8.11A), parallel laminae occur in close association with lenticular layers and with pockets of gravel. The thickness of this lithofacies varies from a few centimeters to 3 m (Fig. 8.4A). Intervals of parallel laminae have been considered to be the Tb division by Bouma (Fig. 8.4B). However, intervals of parallel laminae are interpreted to be products of reworking by bottom currents (see Chapter 4).

8.5.7 Ripple laminae

The ripple-laminated sandstone units are thinly bedded and often closely interbedded with dark grey mudstone. This lithofacies occurs both above and below the parallel-laminated division in Unit 2 (Fig. 8.14A), and therefore is not comparable to the Tc division of the Bouma Sequence. This lithofacies also occurs as discrete units, unassociated with parallel laminated divisions (e.g., Unit 3). Furthermore, this lithofacies occurs above lenticular layers in Unit 5, and above cross beds in Unit 9 (Fig. 8.3A). Ripple laminae also occur as lenticular bedding in interbedded mudstone in Unit 9 (Fig. 8.3A), Unit 7 (Fig. 8.7A), and Unit 8 (Fig. 8.11A). Bouma (1962, p. 49) observed that the ripple-laminated division is generally less than 5 cm thick. In Unit 1, however, the rippled interval is about 2 m thick (Fig. 8.9A).

Ripple-laminated sandstone and siltstone units represent traction deposits. Unusually thick rippled divisions are interpreted to be a product of long-lived traction processes. Such traction deposits in deep-water environments have been ascribed to bottom-current reworking (see Chapter 4).

Walker (1992a, p. 242) routinely classified rippled beds as thin-bedded turbidites without regard for their true origin. In the Gulf of Mexico, rippled sands have been interpreted to be channel-levee complexes deposited by overbank turbidity currents (e.g., Shew et al., 1994). Hsü (1989) suggested that rippled sands of the Tc division can be deposited by marine bottom currents unrelated to turbidity currents. The problematic origin of traction structures has been addressed in Chapter 7.

8.5.8 Sudden decrease in grain size

Bouma (1962, p. 98) reported a decrease in grain size between the underlying parallel laminated division (Tb) and the overlying ripple laminated division (Tc).

However, a sudden decrease in grain size has been observed at: (1) the base of parallel laminated division in Unit 12B (Fig. 8.5A, 5.3 m), and Unit 8 (Fig. 8.11A, 3.8 m); and (2) at the base of ripple laminated division in Unit 5, in Unit 1 (Fig. 8.9A, 5 m), and in Unit 2 (Fig. 8.14A, 8.4 m). This decrease in grain size also corresponds to a sudden increase in mica content from the underlying parallel laminated division to the overlying ripple laminated division. The ripple-laminated sandstone beds are interbedded with mudstone intervals. Some ripple-laminated divisions are much darker in outcrop than underlying parallel-laminated divisions.

Bouma speculated that the break in grain size reflected a break in turbidity currents. However, a break in turbidity currents is difficult to envision because primary function of turbulence is to mix and homogenize suspended sediment during transport. During deposition there would be a gradual grain-by-grain settling of sediment from turbulent suspension, resulting in normal grading. For these reasons, a sudden decrease in grain size is attributed to pulses of bottom current reworking with oscillating conditions of velocity (see Chapter 4).

8.5.9 Alternating mud-draped ripples and double mud layers

Ripple laminae are draped by mudstone or mica causing a dark coloration along laminae in fine-grained sandstone of Unit 2 (Fig. 8.14A). The upper part of the upper interval in Unit 2 (Fig. 8.14A, 7–10 m) is composed of a complex alternation of parallel laminae, double mud layers, mud draped ripples, parallel laminae, ripple laminae, parallel laminae, contorted laminae, and ripple laminae (Fig. 8.14A). Intervals containing these alternating features vary in thickness from a few centimeters to one m. In terms of the Bouma Sequence the above sequence should be precisely described as Tb, Tb, Tc, Td, Tc, Td, Tc, and Tc. This complex vertical succession suggests oscillating velocity conditions (accelerating and decelerating), which is inconsistent with the vertical sequence of structures of a typical turbidite bed (i.e., Ta, Tb, Tc, Td, and Te) deposited by a waning turbidity current (Bouma, 1962). Walker (1965, p. 26) stated, '*It is an important observational fact that the sequence ABCDE is never partly or completely reversed—that is, the turbidity current never speeds up again significantly during deposition*.' Therefore, these random positions of traction structures in Unit 2 are attributed to bottom-current reworking with varying energy conditions (Fig. 8.15B).

There are no analogous divisions for double mud layers in the Bouma Sequence. Double mud layers are unique to shallow-water tidal environments, and have been ascribed to alternating ebb and flood tidal currents with extreme time-velocity asymmetry in subtidal settings (Visser, 1980). In the Annot Sandstone (Fig. 8.15A), double mud layers have been interpreted to be deposits of deep-marine tidal currents (see Chapter 4).

8.5.10 Sigmoidal cross bedding

In Unit 10 (Fig. 4. 39) and Unit 11(Fig. 4. 40) in the Peira Cava area (see Chapter 4), the Annot Sandstone reveals cross beds that show sigmoidal cross bedding in fine- to coarse-grained sandstone. Sigmoidal cross bedding is not part of the turbidite facies model. Although Pickering and Hilton (1998, their Fig. 4K) recognized these cross beds, they did not classify them as the sigmoidal type. They interpreted these cross beds as deposits of high-concentration turbidity currents (i.e., high-density turbidity currents). Because the concept of high-density turbidity currents is flawed, an alternative origin for these sigmoidal cross beds is warranted. Tidal currents probably formed these cross beds in bathyal water depths, possibly in a canyon setting (see Chapter 4).

8.6 Origin of inverse to normally graded intervals

Annot units are characterized by inverse- to normal-grading trends (Table 8.2). In flume experiments, strong sandy debris flows have developed inverse grading. Weak flows have developed normal grading (see Chapter 3). Sandy debris flows commonly undergo surface flow transformation to turbidity currents (Shanmugam, 2000a; Marr et al., 2001; Mohrig and Marr, 2003). However, not all debris flows undergo complete transformation into turbidity currents; some debris flows undergo only partial transformation. In such cases, strongly coherent debris flows transform into moderately coherent and weakly coherent debris flows. This is accomplished by assimilation of ambient fluids (i.e., the dilution effect). The inverse to normal grading of the Annot Sandstone may be explained by partial flow transformation. The basal inverse grading in the Annot Sandstone is attributed to deposition from strongly coherent debris flows and the upper normal grading to deposition from weakly and moderately coherent debris flows (Fig. 8.18).

8.7 Inadequacy of the turbidite facies model

Rich and diverse sedimentary features of the Annot Sandstone indeed validate Leeder's (1997) cautionary remark on the limitations of facies models. These diverse features clearly show that there is a disconnect between the turbidite facies model and the reality (Table 8. 2). Some striking disparities are:

(1) The turbidite facies model represents an imaginary template with five internal divisions. The reality is that the complex features of the Annot Sandstone do not fit the template. These features are: (1) basal contorted layers; (2) basal inverse grading; and (3) upper 'normally graded' intervals with: (a) lenticular layers; (b) pockets of gravel; (c) floating armored
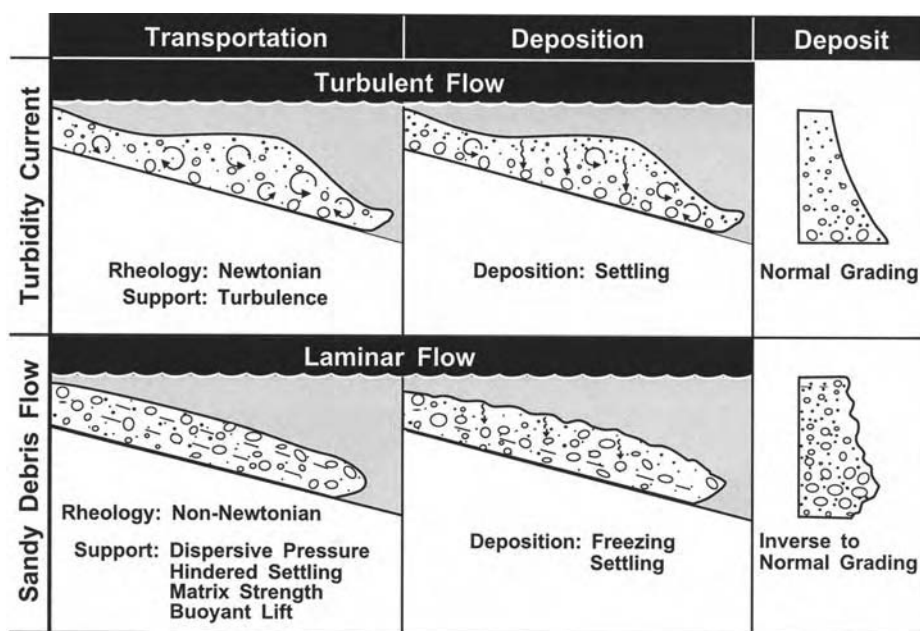
Fig. 8.18. *Top*: **Schematic diagram showing development of simple normal grading by suspension settling from a turbulent turbidity current.** *Bottom*: **Schematic diagram showing development of inverse- to-normal grading by partial flow transformation with freezing and late-stage hindered settling from a laminar debris flow. See text for details. (After Shanmugam (2000a). Reproduced with permission from Elsevier.)**

mudstone balls; (d) floating mudstone clasts; (e) floating quartzose granules; (f) alternating parallel-ripple-parallel-ripple laminae; (g) mud-draped ripples and double mud layers; and (h) sigmoidal cross bedding.

(2) The turbidite facies model advocates only normal grading, but field evidence shows common basal inverse grading. Most units show inverse- to normal-grading trends.

(3) The turbidite facies model advocates a single depositional event for each unit. Field data, however, shows that each individual unit in reality is composed of amalgamated intervals deposited by multiple depositional events.

(4) The turbidite facies model advocates a simple origin by turbidity currents. But the Annot Sandstone implies a complex origin by processes involving slumping, plastic debris flows, and tidal bottom currents. Deposits of true turbidity currents are extremely rare.

(5) Different researchers have proposed eight different processes for the origin of the Ta division. They are: (i) turbidity currents (Bouma, 1962); (ii) antidune phase of the upper flow regime (Harms and Fahnestock, 1965; Walker, 1967);
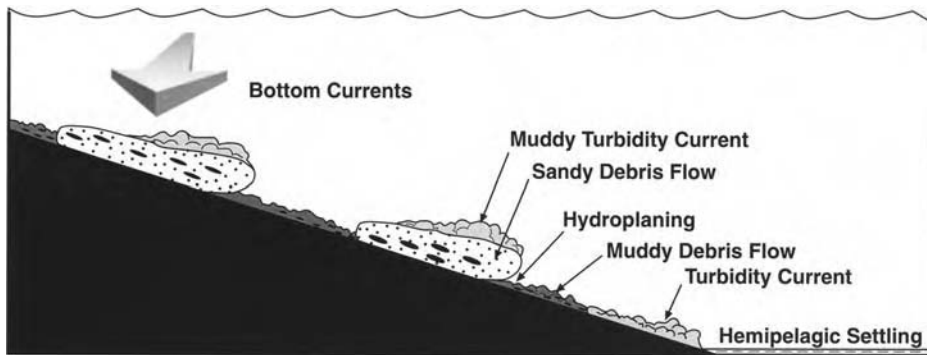
Fig. 8.19. Conceptual model showing reworking the tops of downslope sandy debris flows by along-slope bottom currents. Such complex deposits would generate a sandy unit with a basal massive division and upper reworked divisions with traction structures (ripple laminae), mimicking the 'Bouma Sequence'.

    (iii) grain flows (Stauffer, 1967); (iv) pseudoplastic quick bed (Middleton, 1967); (v) density-modified grain flows (Lowe, 1976); (vi) high-density turbidity currents (Lowe, 1982); (vii) upper-plane-bed conditions under high rates of sediment feed (Arnott and Hand, 1989); and (viii) sandy debris flow (Shanmugam, 1997a).

(6) According to the turbidite facies model, traction structures are originated by turbidity currents. In this re-evaluation, traction structures are attributed to reworking by deep-marine tidal currents.

The problem remains how we can explain deep-water units that show a partial Bouma Sequence composed of a basal massive division and an upper parallel-laminated division. In areas in which both downslope sandy debris flows and along-slope-bottom currents operate concurrently (Fig. 8.19), the reworking of the tops of sandy debris flows by bottom currents may be expected. Such a scenario could generate a basal massive sand division and an upper reworked division, mimicking a partial Bouma Sequence. The reworking of deep-water sands by bottom currents has been suggested by other researchers as well (e.g., Stanley, 1993; Ito, 2002).

8.8 Problems with other facies models

Since the introduction of the Bouma Sequence, other researchers have realized that the muddy division of the Bouma Sequence (Te) was inadequate to satisfactorily represent all of the divisions present in muddy turbidites (e.g., Piper, 1978). This realization led Stow and Shanmugam (1980) to propose a new vertical facies
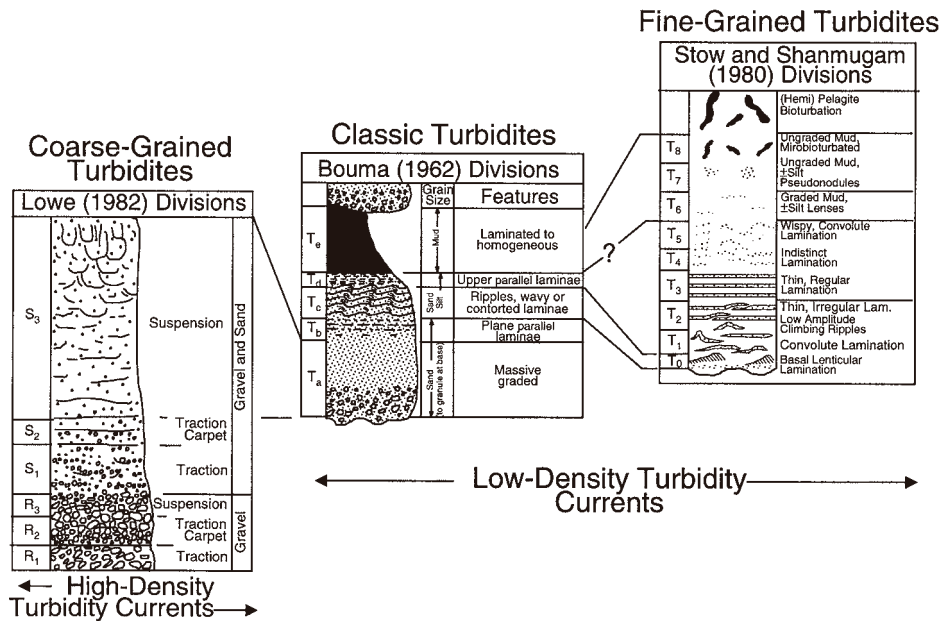
Fig. 8.20. Existing vertical facies models of (1) coarse-grained turbidites (Lowe, 1982), (2) classic turbidites (also known as the Bouma Sequence), and (3) fine-grained turbidites (Stow and Shanmugam, 1980). Correlation of the S3 division of coarse-grained turbidites with the Ta division of the Bouma Sequence is after Lowe (1982). Correlation of various divisions between classic turbidites and fine-grained turbidites is after Pickering et al. (1989). (After Shanmugam (2000a). Reprinted with permission from Elsevier.)

model with nine divisions (T0, T1, T2, T3, T4, T5, T6, T7, and T8) just for fine-grained turbidites. Similarly, Lowe (1982) introduced a new vertical facies model with six divisions (R1, R2, R3, S1, S2, and S3) exclusively for coarse-grained turbidites (i.e., deposits of high-density turbidity currents) (Fig. 8.20).

In natural environments there is only one type of turbidity current: a Newtonian flow in which sediment is suspended by fluid turbulence. Natural turbidity currents, no matter what grain size sediment they transport, will always behave the same hydrodynamically. Theoretically, an ideal turbidity current that carries gravel- to mud-size material should deposit a continuum of divisions representing coarse-grained turbidites at the bottom (R1, R2, R3, S1, S2, S3), classic turbidites in the middle (Ta, Tb, Tc, Td, Te), and fine-grained turbidites at the top (T0, T1, T2, T3, T4, T5, T6, T7, T8). There are no laws of physics that dictate that turbidity currents that carry coarse sediment must cease deposition at Lowe's S3 division, or that turbidity currents that carry fine sediment must commence deposition with Stow and Shanmugam's T0 division. The established

Stow and Shanmugam (1980)   Bouma (1962)   Lowe (1982)

T_8, T_7, T_6 T_5, T_4, T_3, T_2, T_1 T_0 T_e, T_d, T_c, T_b, T_a

Relative Thickness

$S_3 = T_a$

S_3

S_2 S_1

R_3 R_2 R_1

Flow Direction
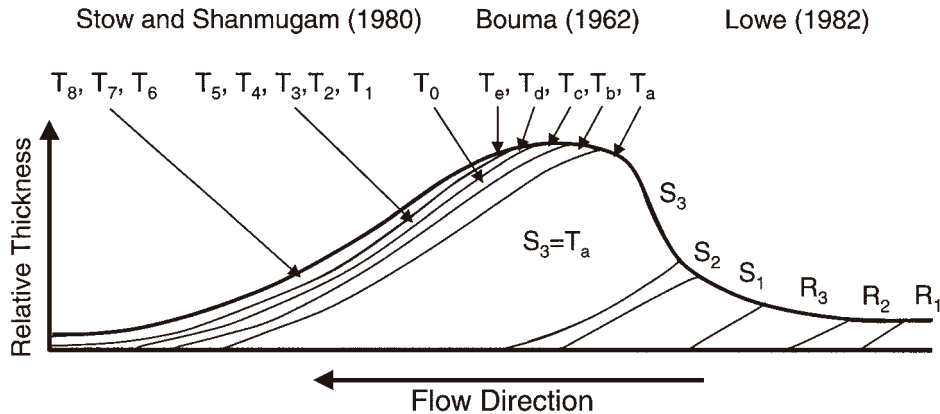
Fig. 8.21. **A schematic diagram showing downslope changes in turbidite divisions from coarse-grained turbidites (Lowe, 1982), through classic turbidites (Bouma, 1962), to fine-grained turbidites (Stow and Shanmugam, 1980). If existing turbidite facies models were realistic, then an ideal turbidite bed should develop 16 divisions. However, no one has ever documented such a turbidite bed with 16 divisions in the field or in flume experiments. (After Shanmugam (2000a). Reproduced with permission from Elsevier.)**

divisional boundaries between these three ideal facies models are artificial. If turbidite facies models were true, a turbidity current carrying a gravel- to- mud load should deposit all of its divisions from gravel (R1) to mud (T8). In fact, Lowe (1982) suggested a continuum of deposits from coarse-grained turbidites to classic turbidites (R1 to Te) totaling 11 divisions. If we were to add the nine divisions of fine-grained turbidites to this continuum (Fig. 8.21), an ideal turbidite bed should comprise a total of 16 divisions, eliminating four overlapping divisions. Such an expectation is realistic because many deep-water sequences contain lithologies ranging from gravel to mud. But no one has ever documented a complete turbidite sequence with all 16 divisions in either modern or in ancient deposits (Fig. 8.20). The absence of such a complete turbidite bed in the geologic record suggests that the ideal turbidite facies models may be incorrect.

   To date, no one has ever generated even the simple Bouma Sequence with five divisions by turbidity currents in flume experiments. There are no size-velocity type diagrams for turbidity currents. Therefore, the current hydrodynamic interpretation of the Bouma Sequence is tenuous. New experiments are needed to establish the true relationship between the sequence of structures, if any, in turbidites and their relationship to the hydrodynamic conditions of turbidity currents.

8.9 Synopsis

The turbidite facies model is a product of distillation of field details, whereas process sedimentology is a precise science that demands field details. Paradoxically, the turbidite facies model undermines the foundation of process sedimentology. Science is a journey toward the truth, but the turbidite facies model has terminated the journey and has become the final destination.

This Page Intentionally Left Blank

Chapter 9

Submarine fan models

9.1 Introduction

The objective of this chapter is to address problems with submarine fan models using sedimentologic details of the Jackfork Group in the Ouachita Mountains as a case study. A comprehensive review of submarine fans was provided by Shanmugam and Moiola (1988). Submarine fan models have been the most influential sedimentological tool in the petroleum industry for reconstructing deep-water environments (Weimer et al., 1994, 2000b).

9.2 Modern-fan model

Aspects of modern submarine fans have been discussed in Chapter 6. Normark (1970) presented the first widely used model for modern submarine fans based on studies of small, sand-rich, fans such as the San Lucas and Navy fans, offshore California. For the lobe-shaped bulge immediately downfan of the termination of the major feeder channel, he introduced the term 'suprafan.' Normark (1970, 1978) advocated that this morphologic feature was formed by rapid deposition of coarse sediment from turbidity currents. In high-resolution seismic data, the suprafan lobe was thought to exhibit an overall mounded, hummocky morphology. This was because the irregular surface of the suprafan produced multiple and overlapping hyperbolic reflections (Normark, 1991).

9.3 Ancient-fan model

Mutti and Ricci Lucchi (1972) proposed submarine fan models based on outcrop studies in Italy and Spain. They popularized the concept of submarine fans with channels in the middle-fan setting and depositional lobes in the lower-fan setting. Mutti and Ghibaudo (1972) were the first to apply the term 'depositional lobe' to ancient deep-sea fan sequences. General characteristics of the depositional lobes
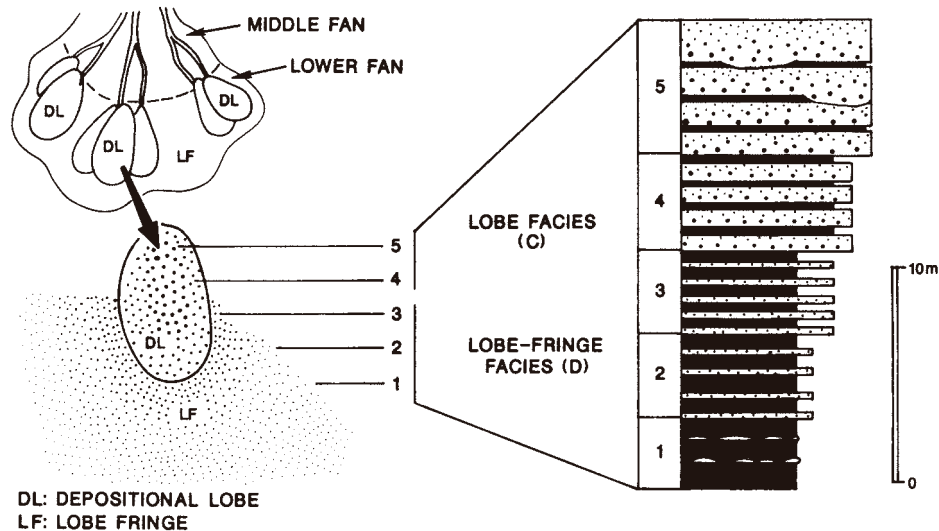
Fig. 9.1. Conventional submarine fan model showing middle-fan channels and lower-fan depositional lobes at channel-mouth environments. Note thickening-upward trends of depositional lobes. (Modified after Mutti (1977). Reproduced with permission from Blackwell.)

of ancient submarine fans (Mutti and Ghibaudo, 1972; Mutti and Ricci Lucchi, 1972; Mutti, 1977) are the following:

(1) Development near the mouths of submarine fan channels analogous to distributary mouth bars in deltaic systems.
(2) Absence of basal channeling.
(3) Thickening-upward depositional cycles composed of classic turbidites (Fig. 9.1).
(4) Common thickness in the range of 3–15 m.
(5) Sheet-like geometry.

9.3.1 Submarine lobe concepts

The term lobe has been applied to a wide range of deep-water environments, resulting in considerable confusion. Shanmugam and Moiola (1991) reviewed this problem at length. Selected example are: (1) suprafan lobe for middle-fan environments (Normark, 1978); (2) fanlobe for the entire fan (Bouma, Coleman, et al., 1985); (3) depositional lobe for lower-fan environments (Mutti and Ricci Lucchi, 1972); (4) erosional lobe for the entire fan (Thornburg and Kulm, 1987);

(5) channelized lobe for slope/upper-fan environments (Nelson et al., 1985); and (6) ponded lobe for slope/upper-fan environments (Nelson et al., 1985). The first five types represent turbidite-dominated systems, whereas the ponded lobe represents a slump-dominated system.

9.3.2 Attached *versus* detached lobes

Mutti and Ricci Lucchi (1972) originally proposed a submarine fan model in which depositional lobes were attached to feeder channels (Fig. 9.2). In a subsequent model, however, Mutti and Ricci Lucchi (1975) advocated detachment of lobes from their feeder channels as a result of sediment bypassing (Fig. 9.2). The detached lobe model is controversial because Mutti (1979) explained the sediment-bypass zone by 'hydrodynamic readjustment' of turbidity currents (Fig. 9.3B), whereas Shanmugam and Moiola (1985) attributed the bypass zone to a growing anticline (Fig. 9.3C). This controversy has implications for developing reservoir models. In a detached lobe, if it existed, a thick shale interval would separate a channel-mouth sandstone from a lobe sandstone (see Fig. 9.2). Such shale intervals would act as barriers between the channel-mouth sandstone and the lobe sandstone. These lobe models developed from the outcrop, without input from modern environments or without emphasis on process sedimentology, are of limited practical value for understanding reservoir geometry and quality.

9.4 General-fan model

Walker (1978) combined the major elements of Normark's (1970) model of modern fans with facies concepts of ancient submarine fans, and advocated a general-fan model with a single feeder channel in the upper-fan area and suprafan lobes in the middle- to lower-fan areas. Because of its predictive capabilities, this model became influential in hydrocarbon exploration and production. This general model was also meant for turbidite-dominated systems.

9.5 Turbidite facies association

The concept of turbidite facies was first introduced by Mutti and Ricci Lucchi (1972, p. 127–128). They defined facies as follows: '*Facies, or better, lithofacies, are used herein to indicate a group of strata, or less commonly a single stratum, with well-defined lithology, stratification, sedimentary structures, and texture*.' Subsequently, other researchers proposed similar facies schemes for deep-water deposits (Stow, 1985; Pickering et al., 1986; Ghibaudo, 1992). As the name implies, the *turbidite facies* scheme was developed for turbidite-dominated systems. Seven basic turbidite facies, namely A, B, C, D, E, F, and G, were proposed. These letters should not be confused with five divisions of the Bouma Sequence

ANCIENT SUBMARINE FAN MODEL WITH ATTACHED LOBES

ANCIENT SUBMARINE FAN MODEL WITH DETACHED LOBES

CMB: CHANNEL – MOUTH BAR
SBZ: SEDIMENT BYPASS ZONE
SL: SANDSTONE LOBE
LF: LOBE FRINGE
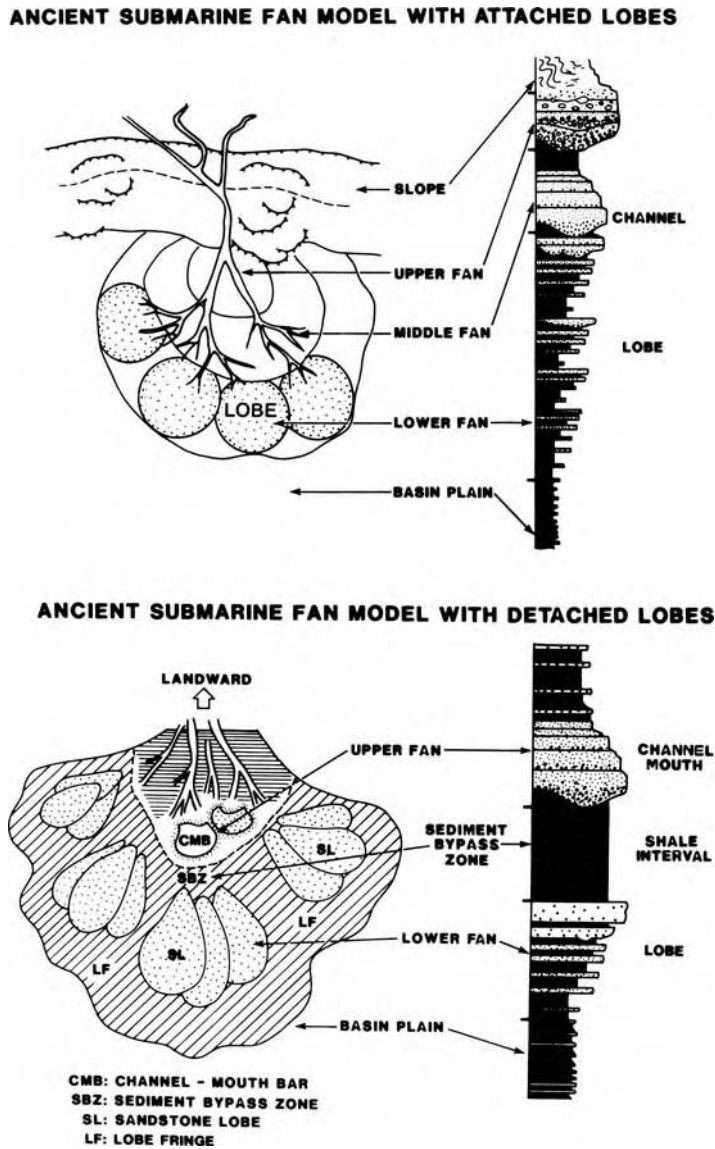
Fig. 9.2. Comparison of ancient submarine fan models with attached and detached lobes. See text for details. (After Shanmugam and Moiola (1988). Reproduced with permission from Elsevier.)

(i.e., Ta, Tb, Tc, Td, and Te; see Chapter 8). The attraction of this facies scheme to both the petroleum industry and academia was the belief that the facies association scheme could be used to interpret specific submarine-fan environments. Shanmugam et al. (1985a), however, questioned the turbidite facies associations for the following reasons:
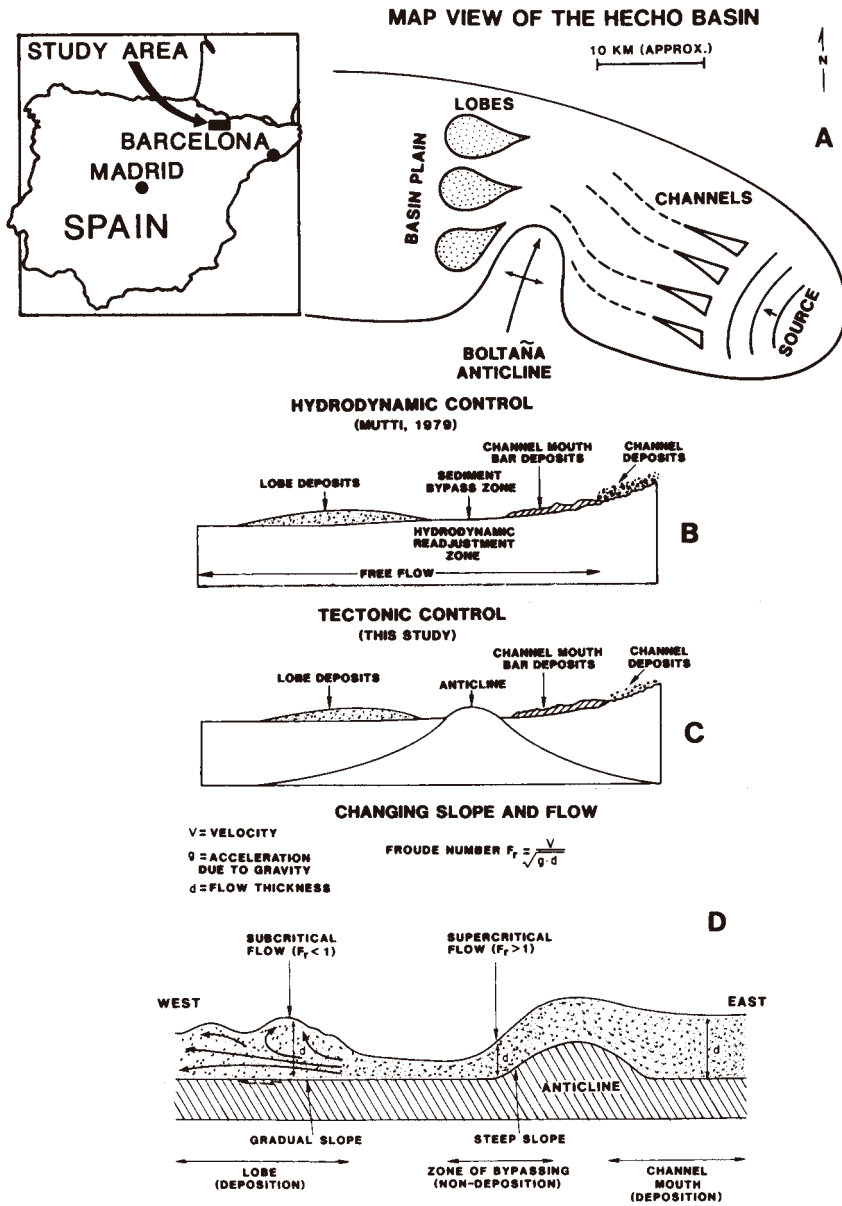
Fig. 9.3. Sedimentologic *versus* tectonic explanations for the detached lobe model of the Hecho Basin, Spain. See text for details. (After Shanmugam and Moiola (1985). Reproduced with permission from Springer-Verlag.)

(1) Mutti and Ricci Lucchi (1972) developed the facies scheme exclusively from outcrops such as those of the Eocene Hecho Group, Spain. However, the true relationship between turbidite facies and fan environments has not been confirmed from coring of modern fans. For example, cores from the modern Amazon and Mississippi Fans reveal that 'depositional lobes' in these fans are dominated by debrites, not by turbidites (see Chapter 6). Lobes are channelized in the Mississippi Fan. Also, cores taken from the Amazon Fan lobe do not validate the thickening-upward trend of depositional lobes (Normark, Damuth et al., 1997).

(2) The turbidite facies scheme does not account for scale problems that exist between modern and ancient systems. The canyon on the modern Bengal Fan, for example, is wide enough (15 km) to accommodate many individual ancient-fan systems.

(3) The turbidite facies scheme is meant for a canyon-fed submarine fan system with a point source; however, the scheme is not suitable for delta-fed systems with a line source (Heller and Dickinson, 1985).

(4) The turbidite facies scheme does not take into account bottom-current reworked sediments that are common in the deep sea (see Chapter 4).

The practice of using turbidite facies schemes as templates has waned in the 1990s. Popular submarine fan models were also abandoned by their proponents in the 1990s (see Chapter 10). The Jackfork Group of the Ouachita Mountains is a well known case study in which the conventional fan model was abandoned.

9.6 The Jackfork Group and the turbidite controversy

A field trip to examine the Pennsylvanian Jackfork Group in Arkansas (U.S.A.) was organized in conjunction with the 1997 AAPG/SEPM Annual Convention in Dallas, Texas (Bouma et al., 1997). The primary purpose was to debate its controversial reinterpretation of the Jackfork Group as deposits of sandy debris flows by Shanmugam and Moiola (1995). This paper, which debunked the *status quo* turbidite fan interpretation of the Jackfork Group, resulted in 42 printed pages of discussion and reply in the *AAPG Bulletin* (Bouma et al., 1997; Coleman, 1997; D'Agostino and Jordan, 1997; Lowe, 1997; Shanmugam and Moiola, 1997; Slatt et al., 1997). No other paper in the *Bulletin* has generated this much controversy. Thus the details that served as the basis for reinterpretation are presented here.

   The Pennsylvanian Jackfork Group in the Ouachita Mountains of Arkansas and Oklahoma has conventionally been interpreted as a classic flysch sequence composed of turbidites in a submarine fan setting (Cline, 1970; Morris, 1977; Moiola and Shanmugam, 1984; Shanmugam et al., 1988c; DeVries and Bouma, 1992; Mutti, 1992). These strata were deposited in a water depth of 1500–2000 m (Chamberlain, 1971). The Ouachita flysch was considered to be analogous to the modern Bengal Fan in a remnant ocean basin (Graham et al., 1975).

Moiola and Shanmugam (1984) originally advocated a turbidite-fan model for the Jackfork Group. Subsequently, Shanmugam and Moiola (1995) abandoned their turbidite-fan model and reinterpreted the Jackfork Group as deposits of sandy debris flows, slumps, and bottom currents in a slope setting. This change in their interpretation has been attributed to the following changes in methodology in Shanmugam and Moiola's later study:

(1) They recognized new sedimentary features in slabbed samples that appear massive in outcrop.
(2) They did not follow the conventional approach of assuming that massive sandstones are products of high-density turbidity currents.
(3) They avoided the use of 'Bouma' divisions in their field descriptions.
(4) They made bed-by-bed interpretation of depositional processes following the principles of process sedimentology.
(5) They used thin sections to gather data on vertical grain size variations and matrix content within individual units.

They measured the Pennsylvanian Jackfork Group exposed along the two spillway walls (east and west) of the DeGray Dam Spillway section; Arkansas and at the Kiamichi Mountain section, Oklahoma (Fig. 9.4). In addition, they
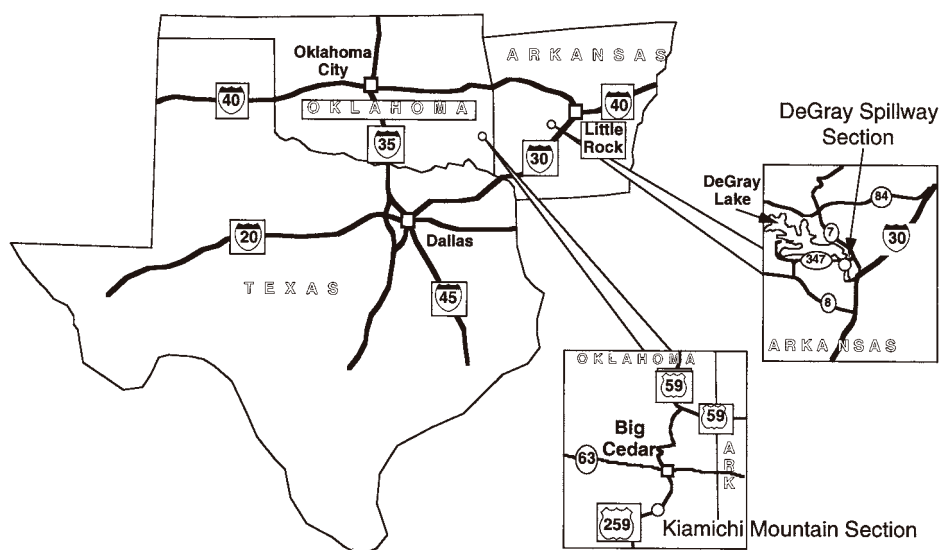
Fig. 9.4. Location map showing the DeGray Spillway section in Arkansas and the Kiamichi Mountain section in Oklahoma that were used in the study of the Jackfork Group. (After Shanmugam and Moiola (1995). Reprinted by permission of the American Association of Petroleum Geologists whose permission is required for further use.)

examined outcrops throughout Arkansas (e.g., Friendship section near DeGray Spillway; and Big Rocks Quarry) and Oklahoma (Moiola and Shanmugam, 1984; Moiola et al., 1988).

In the DeGray Spillway section the east and west walls are about 100 m apart and they exhibit similar lithofacies. They measured the entire east-wall section (Units 1–793, Fig. 9.5) and added the uppermost part (Unit 794) from the west-wall section to the top of the east-wall section to generate a composite sedimentological log (Fig. 9.6). In most cases, a unit represents a bed formed by a single depositional event, but many units are composed of amalgamated massive sandstone beds that represent multiple depositional events (e.g., Unit 794). Units thicker than 2 cm were measured and described. The measured thickness of the DeGray Dam Spillway section is 327 m (1072 ft) and the Kiamichi section is 42 m (138 ft). The total number of measured units at the DeGray Spillway section is 794 and at the Kiamichi Mountain section is 189 (Figs. 9.7, 9.8). At the DeGray Spillway section, the continuous exposure of 327 m of interbedded sandstone and mudstone presents an excellent opportunity to practice process sedimentology.

On the basis of both field and laboratory examination of these rocks, Shanmugam and Moiola recognized eight types of lithofacies: (1) massive sandstone; (2) sandstone with floating mudstone clasts; (3) pebbly sandstone; (4) contorted sandstone; (5) contorted shale; (6) mudstone/shale with floating clasts; (7) laminated and rippled sandstone and siltstone; and (8) laminated shale. Distribution of depositional facies in the DeGray Spillway and Kiamichi Mountain sections is given in Table 9.1. Each type of lithofacies has been interpreted in terms of specific depositional process (Table 9.2).

9.6.1 Massive sandstone (sandy debris flow)

The most common lithofacies in the DeGray Spillway section is massive sandstone that appears structureless in outcrop (Fig. 9.9B). When slabbed, however, it exhibits internal features. This lithofacies is composed predominantly of light- to medium-grey, fine- to medium-grained, moderately to poorly sorted sandstone. Basal contacts are sharp and planar or undulating. In thick units of massive sandstone, load casts are present, but directional sole marks (grooves and flutes) are rare to absent. Upper contacts are commonly sharp, but are undulating or irregular (Fig. 9.9D). Commonly, what appears to be a single bed in outcrop is composed of amalgamated units. Bed thickness generally ranges from 30 cm to 1 m. Beds pinch out laterally, some within a matter of a few meters (Fig. 9.10). Beds with pinch-out geometry do not show evidence of basal erosion.

Normal grading, typical of turbidites, is extremely rare, but in thin sections inverse grading is recognized. For example, Unit 741 at the DeGray section exhibits an average grain size of 0.19 mm at base and 0.26 mm near the top.

De Gray Spillway Section
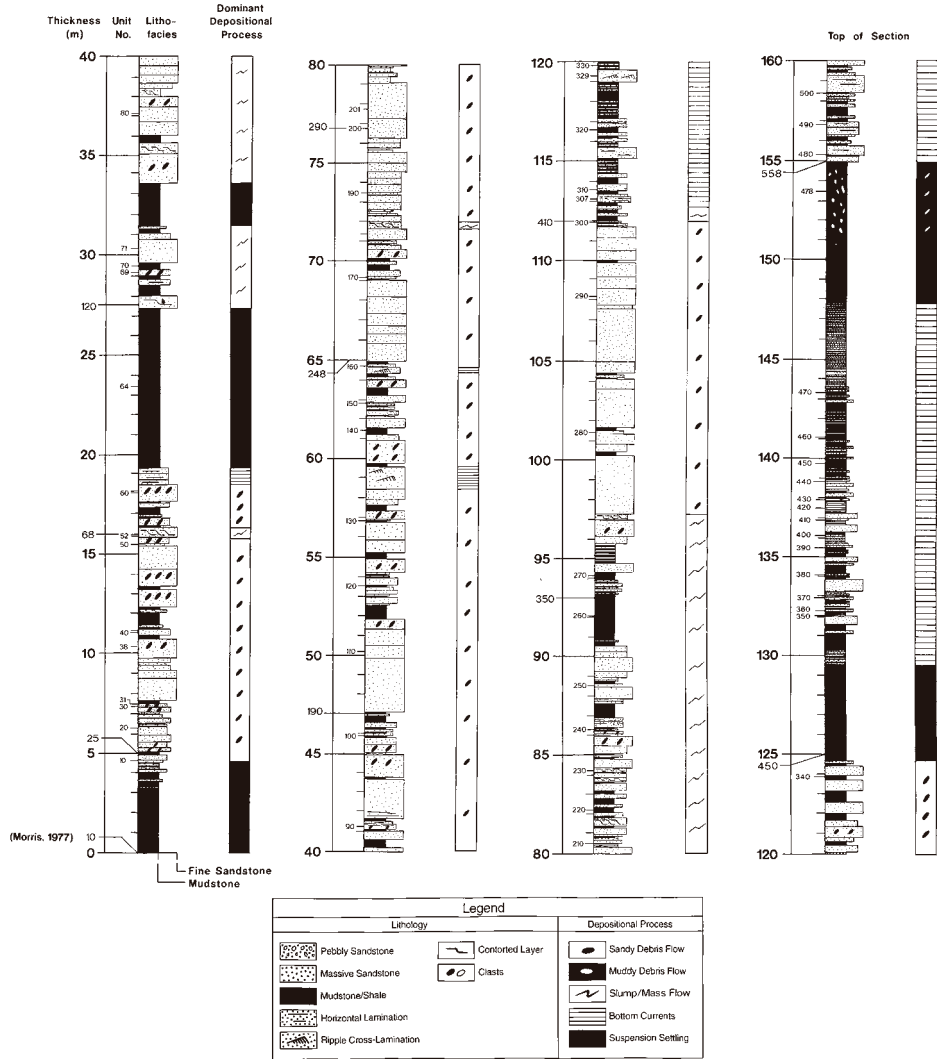
Fig. 9.5. Sedimentological log showing basal part (0–160 m) of the measured DeGray Spillway section. Each lithofacies column shows measured thickness in m (bold numbers on the left) and selected unit numbers. Morris (1977) measured thickness in ft (small numbers on the left) is shown for reference. Interpreted dominant depositional process is shown on the right-hand column corresponding to the lithofacies column. The upper part of this log is shown in Fig. 9.6. (After Shanmugam and Moiola (1995). Reprinted by permission of the American Association of Petroleum Geologists whose permission is required for further use.)

De Gray Spillway Section
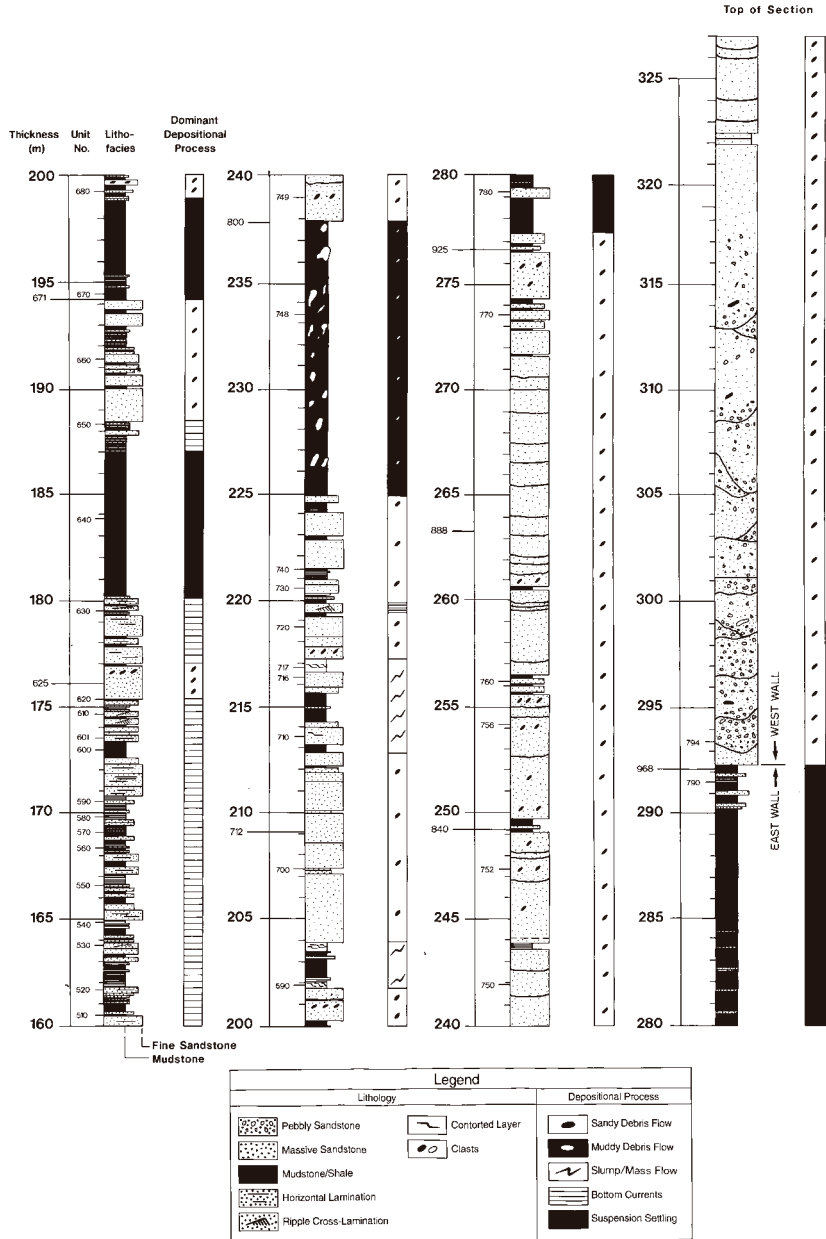
Fig. 9.6. Sedimentological log showing upper part (160–327 m) of the DeGray Spillway section. Note that Unit 794 and younger units from the west wall are combined with the east wall section at about 292 m. (After Shanmugam and Moiola (1995). Reprinted by permission of the American Association of Petroleum Geologists whose permission is required for further use.)

Kiamichi Mountain Section
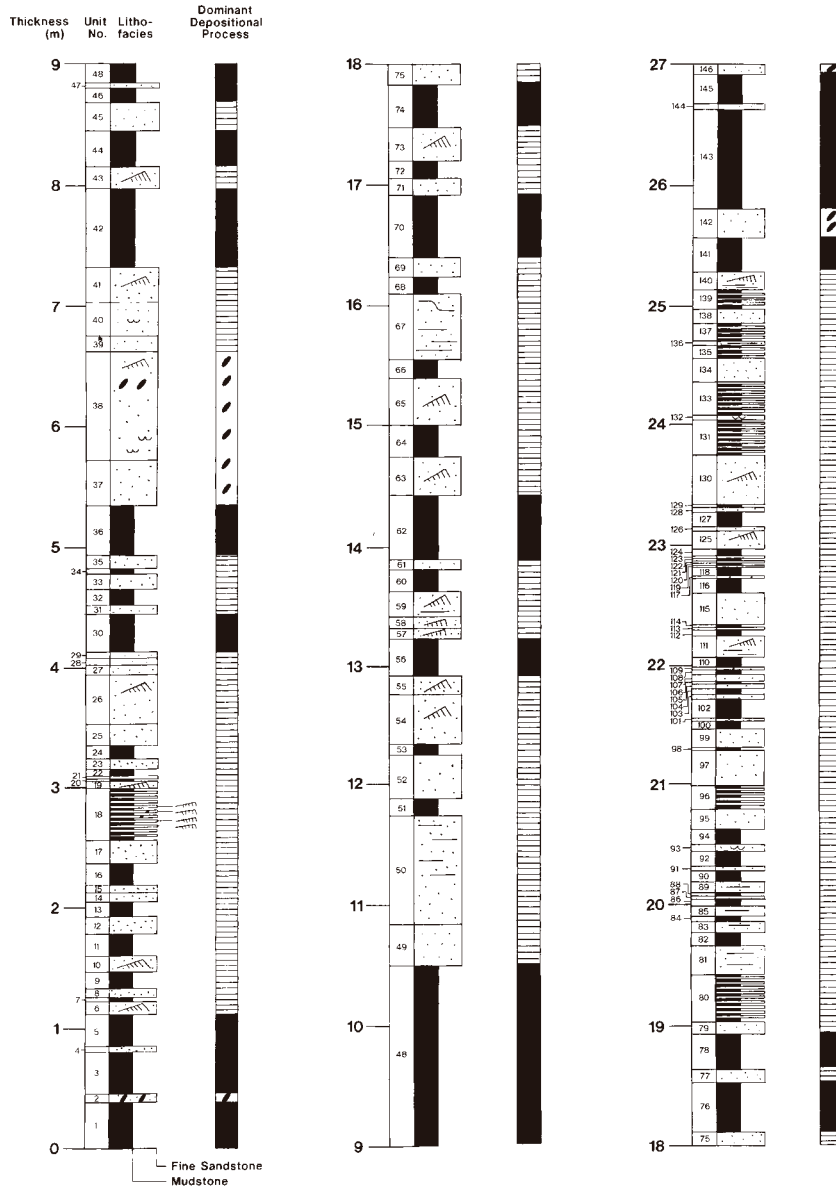
Fig. 9.7. Sedimentological log showing lower part (0–27 m) of the Kiamichi Mountain section. Each lithofacies column shows measured thickness in m (numbers on the left) and unit numbers. Interpreted dominant depositional process is shown on the right-hand column corresponding to lithofacies column. Upper part of this section (27–42 m) is shown in Fig. 9.8. For explanation of symbols see Fig. 9.8. (After Shanmugam and Moiola (1995). Reprinted by permission of the American Association of Petroleum Geologists whose permission is required for further use.)

Kiamichi Mountain Section
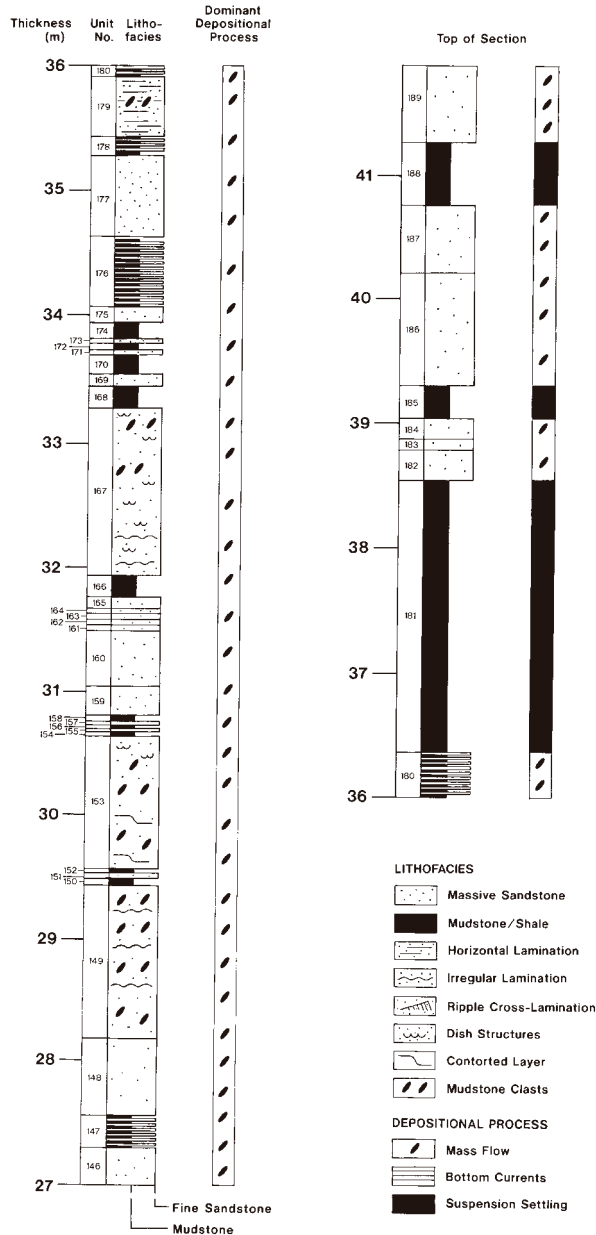
Fig. 9.8. Sedimentological log showing upper part (27–42 m) of the Kiamichi Mountain section. (After Shanmugam and Moiola (1995). Reprinted by permission of the American Association of Petroleum Geologists whose permission is required for further use.)

**Table 9.1 Lithofacies characteristics and interpreted depositional processes
of the Jackfork Group**

Lithofacies	Depositional process	DeGray section	Kiamichi section
Measured thickness		327 m (1072')	42 m (138')
Number of measured Units		794	189
Fine-grained 'massive' sandstone, pebbly sandstone, sharp top, inverse grading, floating mudstone clasts, floating quartzite pebbles, planar fabric, dish structures, high matrix content (up to 25%)	Sandy debris flow	53%	33%
Mudstone/shale, floating mudstone clasts, planar fabric	Muddy debris flow	5%	-
Sandstone/shale, sharp top, contorted bedding, sigmoidal imbricate slices, floating clasts, planar fabric	Mixed slump/debris flow	11%	-
Fine-grained sandstone and siltstone, current ripples, horizontal lamination, mud drapes on ripples	Bottom-current reworking	16%	40%
Shale, horizontal lamination, chert, *Nereites* trace fossils	Pelagic/hemipelagic (suspension settling)	15%	27%

Facies distribution was calculated as percent of number of measured units.

Table 9.2 Data, observed sedimentological features, and interpretation of the Jackfork Group

Data	Observed features	Interpretation
Shanmugam and Moiola (1995, their Figs. 12A, 16C)	High primary mud matrix (up to 25%) in sandstone	Flow strength (sandy debris flow)
Figure 9.11	Rafted (floating) mudstone chips (clasts) near tops of sandstone beds	Flow strength (sandy debris flow)
Figure 9.9 C	Floating boulder-size sandstone clasts in mudstone	Flow strength (cohesive muddy debris flow)
Figure 9.12	Poor sorting or variability in grain size	Flow strength
Figure 9.11	Inverse grading of clasts in sandstone	Flow strength/buoyant lift (sandy debris flow)
Figures 9.11, 9.12	Planar clast and/or pebble fabric in sandstone	Laminar flow (sandy debris flow)
Figure 9.9D	Lack of scour at base of sandstone	Laminar flow (sandy debris flow)
Figures 9.9B, 9.10	Sharp upper contacts of sandstone	Deposition by freezing (sandy debris flow)
Figure 9.9D	Irregular bed tops of sandstone	Freezing of primary relief (sandy debris flow)
Figure 9.10	Lateral pinch out geometry of sandstone	Possible snouts? (sandy debris flow)
Figure 9.14	Sigmoidal deformation structures (duplexes)	Slumping
Figure 9.13	Contorted bedding	Slumping
Shanmugam and Moiola (1995, their Fig. 14B)	Horizontal lamination	Traction (bottom currents)
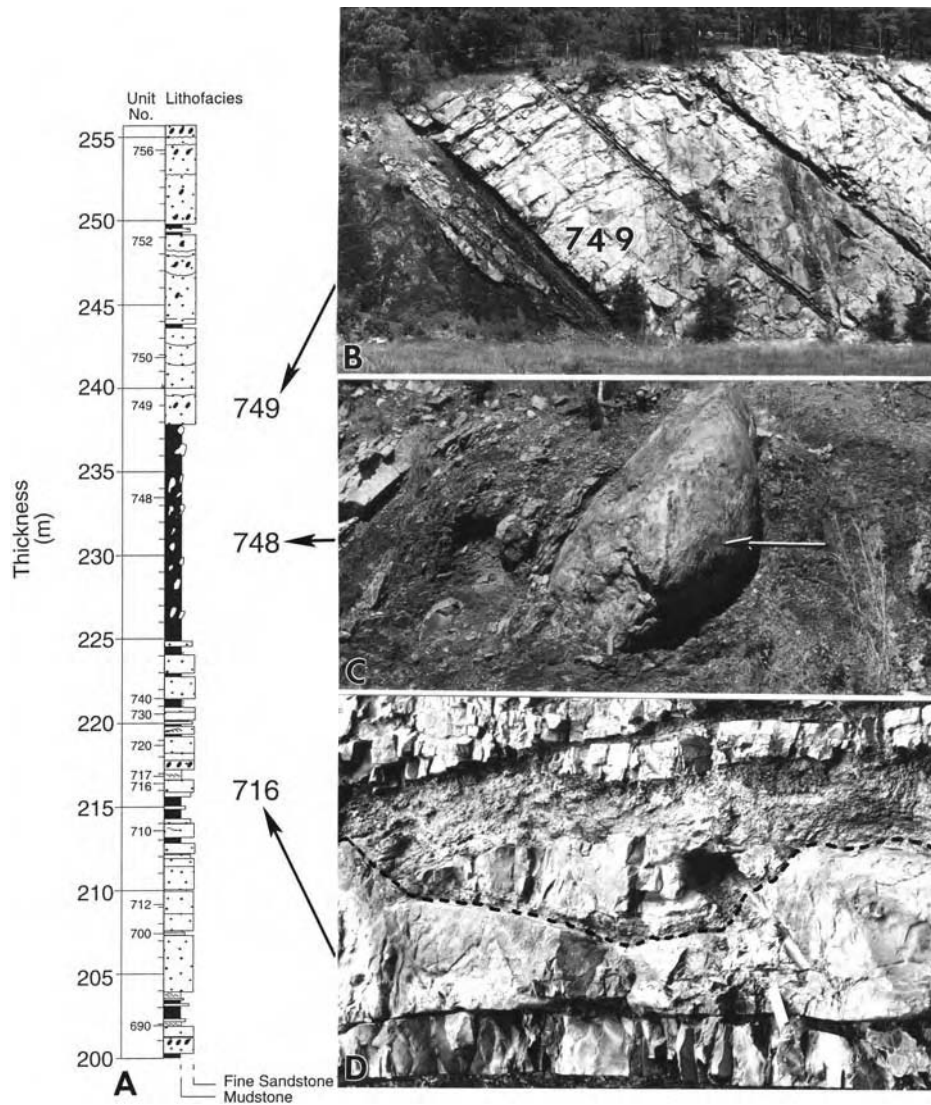
Fig. 9.9. (*A*) Sedimentological log of a portion of the DeGray Spillway east wall section. (*B*) Outcrop photograph showing massive sandstone beds of Unit 749 and overlying units to the right. (*C*) Outcrop photograph of an olistostrome showing a large sandstone intrabasinal clast (arrow) in mudstone (Unit 748). Note scale (15 cm) near the bottom of the clast. Photograph from the west wall. (*D*) Outcrop photograph showing a sandstone with irregular upper contact (dashed line), possibly representing primary relief (Unit 716). Note non-erosive basal contact (15-cm scale is at lower right).

Fig. 9.10. Outcrop photograph showing lateral pinch-out geometry of a massive sandstone unit (arrow) (Unit 602). Note the sharp lower and upper contacts of sandstone beds. Thin mudstone layers occur between sandstone and they do not show evidence of erosion. The lateral pinch out (arrow) may be interpreted as a possible snout of debris flow. DeGray Spillway east wall section.

At certain intervals, dish structures are present. Thin section study, based on 400 points per sample, showed that mud matrix in this facies ranged from 3 to 25% and that the bulk of the matrix is primary (i.e., depositional), not recrystallized (i.e., diagenetic).

At the DeGray Spillway section, Morris (1977) interpreted sandstone beds whose thickness exceeded 25 cm to be proximal turbidites and those averaging 2–15 cm to be distal turbidites. Jordan et al. (1991, p. 59) stated, *'... turbidity currents were responsible for deposition of virtually all the sandstone beds within the DeGray Lake Spillway section'*; And yet, no one has documented the virtual abundance of normal grading in the Jackfork Group at the DeGray Spillway section.

Fine-grained massive sandstones in the Jackfork had enough mud matrix (up to 25%) to provide strength to the flow. The presence of mud is an indication of laminar flow conditions associated with debris flows (Enos, 1977). Abrupt lateral pinch-out geometries (Fig. 9.10) of sandstones without basal erosion may be interpreted as snouts of sandy debrites formed by freezing of flows. Most sandstone units have sharp, but non-erosive bases. The underlying mudstone beds

are unaffected by scouring (Fig. 9.10), suggesting that the flow was not turbulent. Therefore, laminar flow conditions, typical of debris flows, may be inferred (Table 9. 2).

9.6.2 Sandstone with floating mudstone clasts (sandy debris flow)

This facies is composed of light- to-medium grey, lower fine- to medium-grained, moderately to poorly sorted massive sandstone with rafted mudstone clasts. The thickness of these sandstone units ranges from 5 cm to nearly 6 m. Their upper bedding contacts are sharp. Rounded to subrounded mudstone clasts, ranging in size from 2 mm to 20 cm in diameter are common (Fig. 9.11). Most clasts are composed of plates and chips. Floating clasts occur mainly near the tops of sandstone units. Some platy mudstone clasts are aligned parallel to bedding planes producing planar-clast fabric (Fig. 9.11). Some units (e.g., Unit 756, DeGray) exhibit inverse-size grading (i.e., mean grain size of 0.20 mm at base and 0.24 mm near the top). Unit 38 exhibits a subtle normal grading for sandy matrix (i.e., mean grain size of 0.13 mm at base and 0.09 mm near the top), but shows an inverse grading for mudstone clasts. Point-count data shows that the mud matrix varies from 10 to 19%. Unit 31 at DeGray is, for the most part, matrix-supported sandstone.

   The occurrence of mudstone clasts of various sizes (2 mm–20 cm in diameter) near the top of a sandstone bed suggests that the flow had strength to maintain

Fig. 9.11. Photograph of a massive sandstone slab with floating mudstone clasts of various sizes (Unit 38). Note the planar clast fabric near the top of the polished front surface. DeGray Spillway east wall section.

these clasts of different sizes, but of similar density. The presence floating clasts in matrix-supported sand is indicative of matrix strength. The failure of larger floating clasts to settle to the base is evidence for flow strength. Delicate mud clasts have also been cited as evidence of laminar flow in debrites (Johnson, 1970; Enos, 1977). Clast orientation (i.e., long axis of clasts aligned parallel to bedding surface) can be used to infer laminar flow conditions, a condition common to debris flow (Fisher, 1971; Enos, 1977; Shanmugam and Benedict, 1978).

9.6.3 Pebbly sandstone (sandy debris flow)

The pebbly sandstone facies occurs near the top of the measured DeGray section (Unit 794). Unusually large quartzite pebbles (20 mm in diameter) are admixed with smaller quartzite pebbles (3–4 mm in diameter) (Fig. 9.12). Both quartzite pebbles and shale clasts float in a 'matrix' composed of fine- to medium-grained sand. Quartz-rich sand and quartzite pebbles make it a poorly sorted lithofacies. Quartzite pebbles and mudstone clasts show planar fabrics. Inverse grading of pebbles has been observed. Small scour-like features, which are filled with
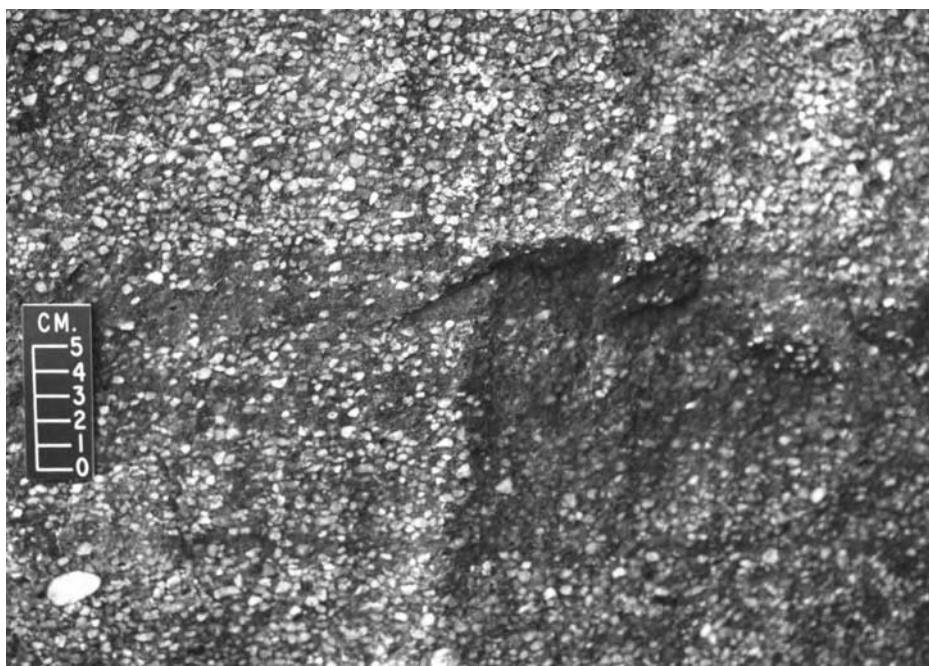
Fig. 9.12. Outcrop photograph of pebbly sandstone lithofacies. Note the side-by-side occurrence of large and small quartzite pebbles in a sandy matrix. Also note a faint alignment of long axes of pebbles parallel to bedding (planar pebble fabric). DeGray Spillway section.

quartzite pebbles, occur within the thick sandstone units. The small scours imply fluid turbulence; however, this is a minor component in this facies. On the basis of floating quartzite pebbles and clasts, planar fabric, and inverse grading, the pebbly sandstone beds were interpreted to be sandy debrites.

9.6.4 Contorted sandstone (sandy slump)

This facies is composed of light- to medium-grey, fine-grained, poorly sorted sandstone. The diagnostic feature of this facies is contorted bedding (Fig. 9.13). Sigmoidal imbricate slices or duplex structures occur (Fig. 9.14). The duplex structures at the DeGray Spillway section were described by Shanmugam et al. (1988c). Three types of duplexes (sigmoidal deformation structures) have been recognized in three different lithologies (Fig. 9.15). Units adjacent to these duplex units have opposing imbricate slices and they reach thicknesses of up to 75 cm. Dips of the imbricate slices vary from 25 to 40º. The units are bounded by undeformed planar beds, with sharp upper and lower contacts.

Conventionally, duplex features have been attributed to tectonic deformation of lithified units. However, a tectonic origin for the sigmoidal slices is considered
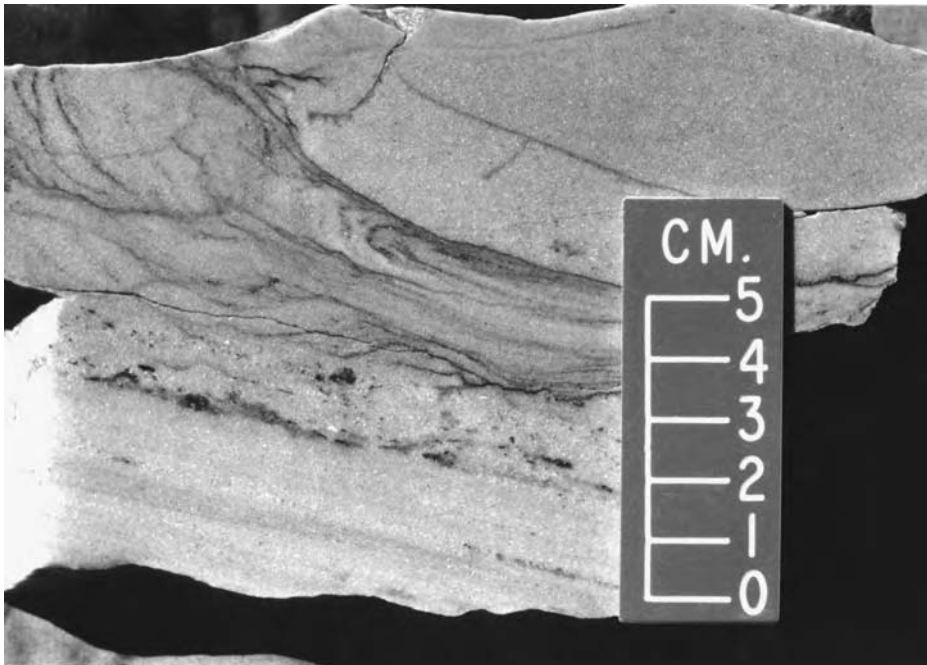
Fig. 9.13. Photograph of a polished sandstone slab showing contorted layers with floating mudstone clasts (Unit 153). Kiamichi Mountain section.

Fig. 9.14. Outcrop photograph showing two adjacent sigmoidal deformation structures (i.e., duplex-like structures) with opposing dips shown by arrows (Unit 52). Note a 15-cm scale is near upper right. DeGray Spillway east wall section.

unlikely because opposing directions of imbrication in stratigraphically adjacent units would require an unrealistic tectonic history. Therefore, the imbricate slices (i.e., duplexes) have been attributed to sedimentary slumping. This conclusion was based, in part, on an experimental model of a small-scale duplex structure generated in the laboratory in soft plaster (Shanmugam et al., 1988c, Fig. 3 therein). Contorted sandstones with floating mudstone clasts imply that these sandstones, originally emplaced by debris flows, were subsequently subjected to slumping.

9.6.5 Contorted shale (muddy slump)

This facies is composed of dark grey to black shale with stringers of siltstone or very fine sandstone. Contorted units of shale are sandwiched between uncontorted sandstone units. The thickness of these shale units varies from 10 to 20 cm. Analogous to the contorted sandstone facies, imbricate slices of shale are present (Unit 270, DeGray). Morris (1977) described these units as contorted, chaotic, and slurried beds. The origin of this facies, like that of the contorted sandstone facies, is sedimentary slumping.
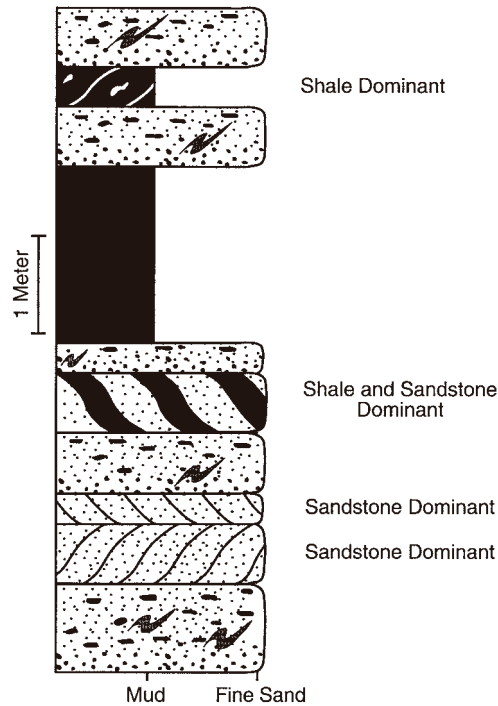
Fig. 9.15. Sketch illustrating three types of sigmoidal deformation structures (i.e., duplexes) observed in the Jackfork Group: (1) shale dominant, (2) shale and sandstone dominant, and (3) sandstone dominant lithologies. The presence of deformed units sandwiched between undeformed units suggests synsedimentary deformation. DeGray Spillway section. (After Shanmugam and Moiola (1995). Reprinted by permission of the American Association of Petroleum Geologists whose permission is required for further use.)

9.6.6 Mudstone/shale with floating clasts (muddy debris flow)

This facies is composed of dark grey to black mudstone/shale with floating clasts of sandstone, limestone, chert, and shale. Some floating clasts are nearly 3 m long (Fig. 9. 9C), but most are less than 30 cm. Clasts are angular to subrounded, and they exhibit both bedding-parallel and random orientations. An example of this facies is in Unit 748 (Fig. 9. 9C). It is 13 m thick and has sharp upper and lower contacts with adjacent sandstone units. Some clasts in these units are contorted suggesting synsedimentary deformation. This facies represents true debrites. Such debrites with large clasts are called 'olistostrome' (Fig. 9.9C).

9.6.7 Laminated and rippled sandstone, and siltstone (bottom currents)

This facies is composed of medium grey to reddish brown, very fine to fine-grained sandstone and siltstone. Parallel laminae are common and most laminae are less

than 5 mm in thickness. On the tops of beds, linguoid ripples are preserved (Unit 329, DeGray). Rippled beds commonly occur as discrete units with sharp tops and bottoms. Some ripples are draped with mud layers. Sole marks are common (e.g., Units 315, 370, 391, and 440, DeGray). Bed thickness ranges from 10 to 100 cm, but averages 20 cm.

Morris (1974, 1977) interpreted these beds as distal turbidites; however, these beds do not exhibit normal size grading. The presence of mud drapes in this lithofacies suggests fluctuating energy conditions, and therefore is difficult to explain them by a waning turbidity current. Discrete traction structures in deep-water sequences are indicative of bottom-current reworking (Hollister, 1967; Shanmugam et al., 1993a). Klein (1966) originally pointed out the importance of bottom currents in the Pennsylvanian strata of the Ouachitas. He argued that sole marks in these beds actually represented scouring by bottom currents rather than by turbidity currents. Influence of bottom-current reworking is evident in both sections studied (Fig. 9.16).
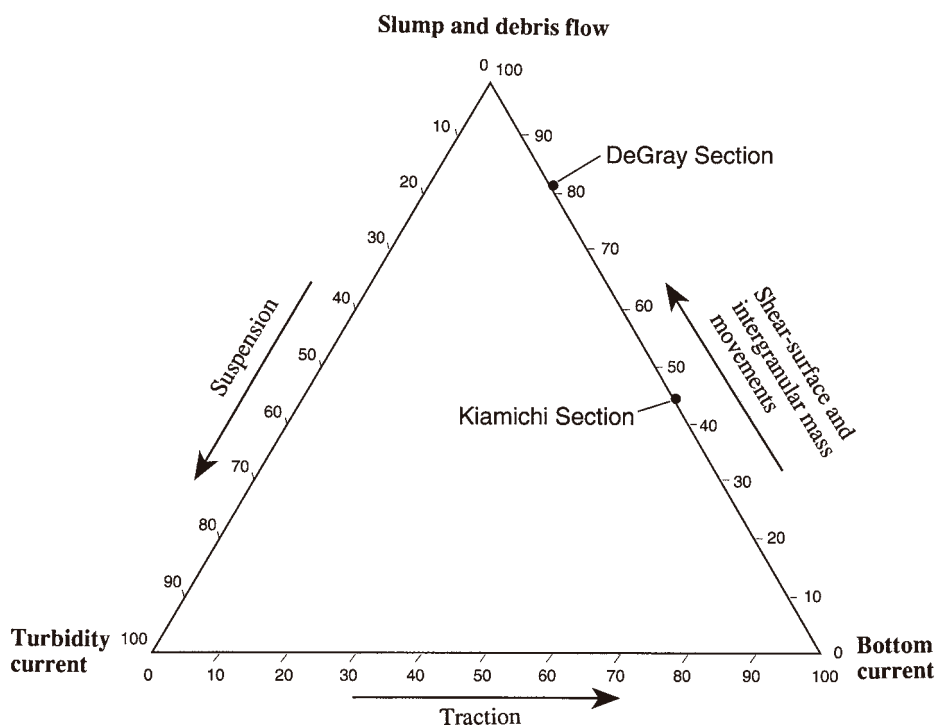
Fig. 9.16. **Ternary diagram showing the relative abundance of slump and debrite facies in comparison to turbidites and bottom-current deposits. Plots are based on normalized percentages of resedimented facies from Table 9. 1. Note the influence of bottom currents in the Kiamichi Mountain section. (After Shanmugam and Moiola (1995). Reprinted by permission of the American Association of Petroleum Geologists whose permission is required for further use.)**

9.6.8 Laminated shale (pelagic and hemipelagic settling)

This facies is composed of dark-grey to-black shale containing horizontal laminae of siltstone. Bedding contacts are sharp. Trace fossils of the *Nereites ichnofacies* are common and chert nodules are sparse. This lithofacies occurs throughout the section as thin intervals (a few cm thick) between sandstone beds, but its thickness can reach up to 8 m. This facies has been attributed to pelagic and hemipelagic settling of mud in a deep-water environment.

9.7 The impermanence of submarine fan models

White (1937) originally interpreted the Jackfork Group as deposits of slides and slumps in a deep-water setting. All later researchers have interpreted the Jackfork as being composed predominantly of turbidites in a submarine fan setting (e.g., Morris, 1974; Moiola and Shanmugam, 1984; Moiola et al., 1988; Shanmugam et al., 1988c; DeVries and Bouma, 1992; Mutti, 1992).

Moiola and Shanmugam (1984) proposed a conventional fan model for the Jackfork (Fig. 9. 17A). They advocated a middle-fan setting with channels ('thinning-upward' trends) for the DeGray section and an outer-fan setting with lobes ('thickening-upward' trends) for the Kiamichi section using the Mutti and Ricci Lucchi's (1972) depositional cycle concept. True turbidites are nearly absent in the Jackfork. The turbidite cycle concept, therefore, is not meaningful here because plastic debris flows and slumps that dominate these intervals do not emplace sediment in a predictable or organized (i.e., thinning- or thickening-upward) manner. The cycle concept was based on the assumption that individual outcrop units represent a single depositional event. Although individual units appear to be single beds in outcrop, when slabbed and examined in detail they are made up of multiple beds comprising multiple debrite and slump events.

Moiola and Shanmugam (1984) also applied the turbidite facies association scheme of Mutti and Ricci Lucchi (1972) to the Jackfork to establish middle fan (facies A, B, C, D, and G) and outer fan (facies D and G) settings. Soon afterwards, however, Shanmugam et al., (1985a) began to question the validity of this facies association scheme for interpreting submarine fan environments. Consequently, Shanmugam and Moiola (1988) avoided applying the facies association scheme as well as usage of middle fan and outer fan terminologies (Fig. 9.17B). Still, however, they believed that the Jackfork represented a longitudinal fan system in a remnant ocean basin setting (Fig. 9.17B).

Contrary to previous studies that advocated a dominance of turbidites, the DeGray Spillway section is dominated by debrite and slump deposits (69%). Associated bottom-current deposits (16%) and pelagic/hemipelagic deposits (15%) constituted the remainder of the section (Table 9.1). The Kiamichi Mountain section
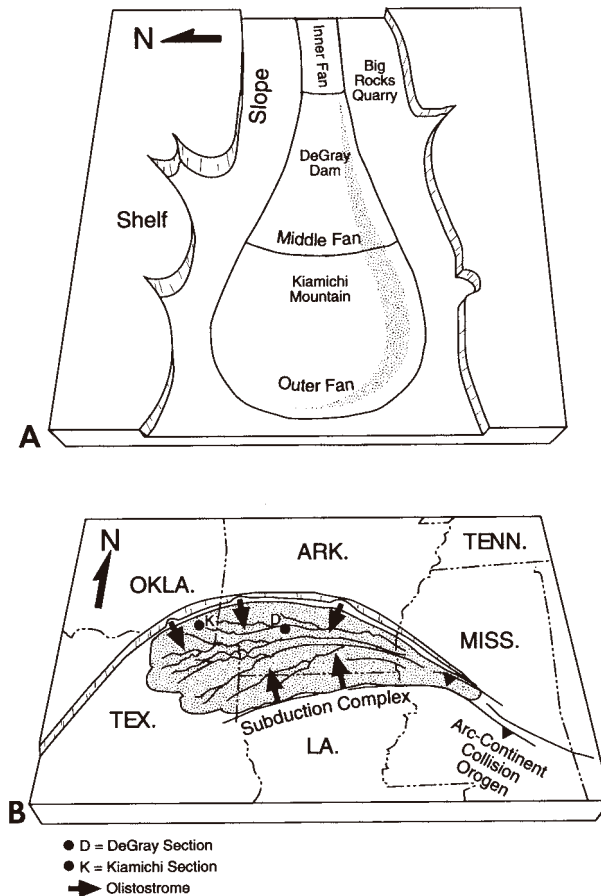
Fig. 9.17. (*A*) **Conventional fan model of Moiola and Shanmugam (1984) showing middle fan setting (channel dominated) for the DeGray section and outer fan setting (lobe dominated) for the Kiamichi section. (*B*) Fan model of Shanmugam and Moiola (1988) showing a longitudinal fan system in a regional tectonic framework. Note that the fan is not subdivided into inner, middle, and outer segments.**

showed more deposits of bottom-current reworking (40%), but debrite deposits (33%) still comprised a significant amount of the section. Pelagic/hemipelagic deposits (27%) made up the remainder of the Kiamichi Mountain section (Table 9.1). On the basis of sedimentological features (Table 9.2), and facies distribution (Table 9.1), Shanmugam and Moiola (1995) reinterpreted the Jackfork Group as deposits of slumps, debris flows, and bottom currents on a slope setting (Fig. 9. 18).
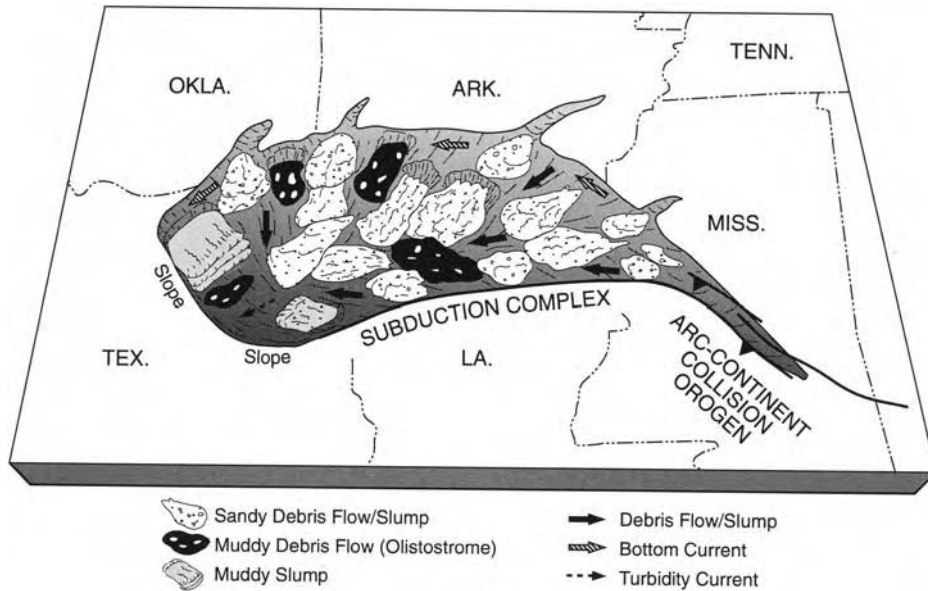
Fig. 9. 18. Revised model of the Jackfork Group showing the importance of debris flows and slumps on a slope setting. Tectonic framework is after Thomas (1985). Paleocurrent data of the Jackfork suggest a westward flow in southeastern Oklahoma (Briggs and Cline, 1967). (After Shanmugam and Moiola (1995). Reprinted by permission of the American Association of Petroleum Geologists whose permission is required for further use.)

9.8 Synopsis

In the 21st century, when all is said and done, data will dictate that many turbidite fans exist only in publications, not in the rock record. The reinterpretation of the Jackfork Group reflects a paradigm shift. Although the turbidite paradigm is still alive in some circles, turbidites themselves have become an endangered facies.

Chapter 10

Sequence-stratigraphic fan models

10.1 Introduction

The objective of this chapter is to address problems with sequence-stratigraphic fan models using sedimentologic details of petroleum-bearing reservoirs in the North Sea. In a deep-water sequence-stratigraphic framework (Fig. 10.1), basin-floor fans are considered to be attractive hydrocarbon reservoirs. This is because the sequence-stratigraphic model predicts that basin-floor fans are sand-rich reservoirs dominated by turbidites. According to Vail et al. (1991, p. 646), basin-floor fans are '*sheet mounds made up of massive sands deposited as lobes or sheets in a deep marine setting*.' This conceptual model is being used in the petroleum industry to predict reservoir facies in frontier and mature basins.

10.2 Basin-floor fans and slope fans

In seismic sequence stratigraphy, the concept of suprafan lobes with mounded seismic forms (Normark (1970) had a major influence. Sarg and Skjold (1982) applied the suprafan concept to Paleocene sands in the Balder area of the North Sea and mapped eight distinct suprafan lobes with mounded seismic geometries. Each individual mound was interpreted as a suprafan lobe containing an inner fan with fining-upward channelized deposits and an outer fan fringe with coarsening-upward sheet sands (Sarg and Skjold, 1982). Using Normark's model, Mitchum (1985) proposed a general seismic model for ancient fans that consist of an upper and a lower fan (Fig. 10.2). The upper fan consisted of leveed channels (i.e., channel-levee complex of Normark, 1970), and the lower fan consisted of lobate and mounded deposits (i.e., suprafan of Normark, 1970). Mitchum also equated mounded seismic facies with sheet-like turbidite sandstones of ancient depositional lobes. In Mitchum's model a lobe is considered to exhibit mounded external form and bidirectional downlap.

In a sequence-stratigraphic framework, the lowstand systems tract is composed of the basin-floor fan, the slope fan, and the prograding wedge (Vail, 1987;

A. Seismic Mounds

Canyon Fill
Mound

Slide Mound

Climbing
Toplap
Mound

Complex Mound
(Slope Fan)

Sheet Mound
(Basin-Floor Fan)
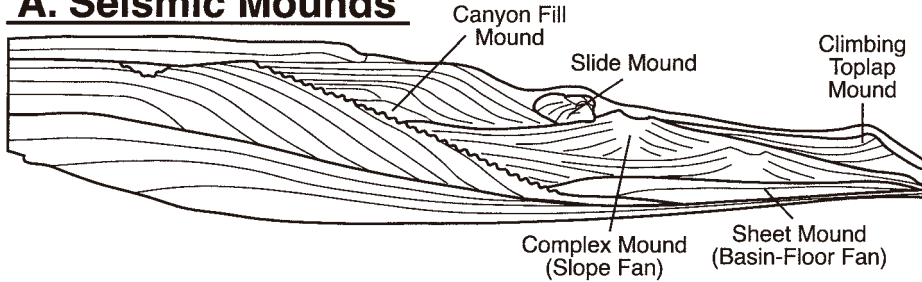
B. Wireline-Log Motifs

LST	Slope Fan	Mud Prone Channel/Levee Crescent Log Pattern Turbidites/Mass Flows
	Basin-Floor Fan	Sand Prone Lobe/Sheet/Mound Blocky Log Pattern Turbidites/Contourites
HST	Hemipelagic Mud	Mud Railroad Track Log Pattern

C. Slope-Fan Model

Type 1 Sequence
Boundary

Top Basin-Floor Fan
Downlap Surface

Top Slope Fan

D. Basin-Floor Fan Model

Type 1 Sequence
Boundary
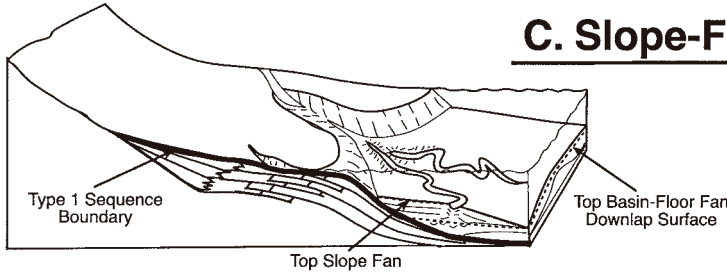
Top Basin-Floor
Fan

Fig. 10.1. Conceptual sequence-stratigraphic fan models. (*A*) Seismic geometries showing basin-floor fans (sheet mound) and slope fans (complex or gull-wing mound). (*B*) Wireline-log motifs showing blocky motif of basin-floor fans. (*C*) Slope-fan model. (*D*) Basin-floor fan model. Simplified from Vail et al. (1991). (After Shanmugam et al. (1995a). Reprinted by permission of the American Association of Petroleum Geologists whose permission is required for further use.)
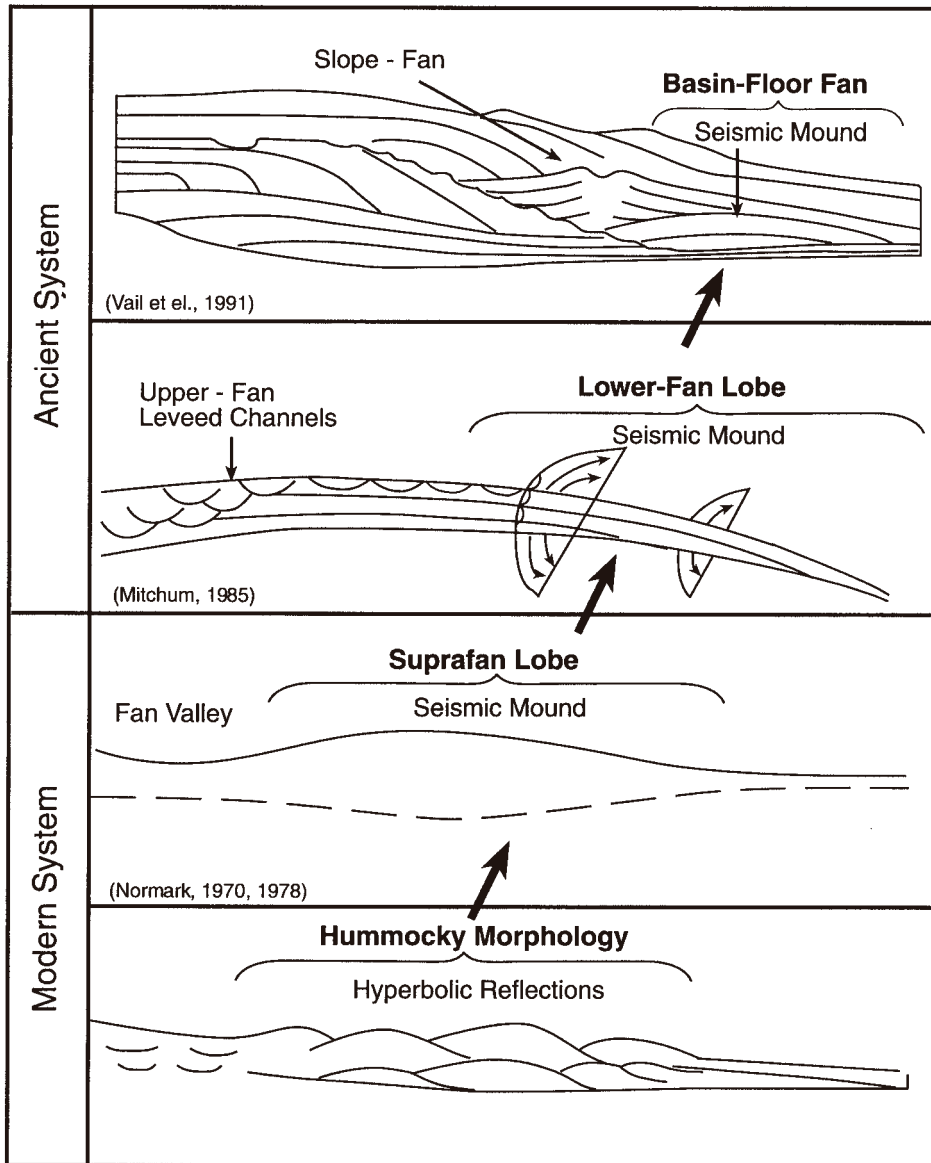
Fig. 10.2. Evolution of concepts on seismic mounds (bottom to top). Normark (1970) first proposed the seismic mound concept based on study of suprafan lobes of modern systems. Mitchum (1985) proposed a general seismic model for submarine fans, based on the seismic mound concept of Normark (1970), in which lobes exhibit an external mounded geometry with internal bidirectional downlaps. Vail et al. (1991) proposed a basin-floor fan model based on Mitchum's lobe concept. Thick upward arrows show the link between seismic mound concepts. See text for details. (After Shanmugam (2000a). Reproduced with permission from Elsevier.)

Vail et al., 1991). Vail's slope fans represent Mitchum's upper fan with leveed channels, and Vail's basin-floor fans represent Mitchum's lower fan with seismic mounds (Fig. 10.2). Thus the basin-floor fan concept is nothing but a combination of Normark's suprafan lobe concept (i.e., mounded seismic geometry) and Mutti and Ricci Lucchi's depositional lobe concept (i.e., sheet-like sandstone bodies). However, there is an important distinction between fan models of sedimentology and fan models of sequence stratigraphy. In sedimentologic fan models, channels and lobes are contemporaneous elements. In sequence-stratigraphic models, leveed fan channels are part of the younger slope fan, and they are not contemporaneous with the lobes that are part of the older underlying basin-floor fan.

Standard criteria have been proposed for recognizing basin-floor fans and slope fans in seismic profiles and wireline logs (Vail and Wornardt, 1990; Vail et al., 1991).

Basin-floor fans may exhibit the following characteristics:

(1) External mounded forms on seismic profiles that downlap or onlap onto Type 1 unconformities (sequence boundaries).
(2) Hummocky to chaotic internal reflections or seismic facies within mounds.
(3) High-amplitude reflections that show bi-directional downlap at the base of a mound or onlap onto bathymetric highs (Fig. 10.1A).
(4) Lateral punch-out seismic geometry.
(5) Blocky wireline-log motifs (Fig. 10.1B).
(6) Their position beneath slope fans (Fig. 10.1A).
(7) Basin-floor fans are predicted to be sand-rich turbidites with sheet-like geometries (Fig. 10.1D).

Slope fans may exhibit the following characteristics:

(1) Occurrence on a depositional slope and downlap onto basin-floor fans (Fig. 10.1A).
(2) Gull-wing mound or bow-tie reflections on seismic profiles (complex mound in Fig. 10.1A).
(3) Zones of chaotic internal reflections.
(4) They show crescent-shaped, wireline-log motifs (Fig. 10.1B).
(5) Slope fans are predicted to be predominantly mud-rich systems characterized by channel-levee complexes. Both turbidites and debrites are common in slope fans.

Although basin-floor fans have routinely thought to have been identified using seismic profiles (Jackson et al., 1992) and/or wireline logs (Mitchum et al., 1990), there have been very few attempts, using conventional core data, to systematically

document the actual depositional facies of these features. As a result, the validity of the conceptual model and its predictive capabilities remain questionable.

In testing the validity of the basin-floor fan concept, Shanmugam et al. (1995a, 1996) utilized conventional core data. To understand the relationship between process sedimentology (core-scale features) and seismic-sequence stratigraphy (seismic-scale features), long cores (up to 700′ or 213 m) were calibrated with seismic data. Shanmugam et al. utilized conventional cores from petroleum fields of the North Sea and from the continental margins of the United Kingdom and Norway. They used these settings because sequence-stratigraphic models were developed from such divergent continental margins (Vail et al., 1991). They examined approximately 12 000 ft (3658 m) of conventional core from 50 wells in 10 areas or fields. From this large data base, three areas are selected for discussion in this chapter using the following released wells: (1) Faeroe Basin area, west of the Shetland Islands, northern U.K. Atlantic Margin, (Esso 214/28-1 and Shell/Britoil 206/1-2); (2) Frigg area in the Norwegian North Sea (Elf 25/2-8); and (3) Gryphon–Harding (formerly Forth) area in the U.K. North Sea (Kerr–McGee 9/18b-7, Britoil 9/23b-7, and Conoco 9/18a-15). Six lithofacies have been recognized in the 3658 m of core examined on the basis of lithologic variations and physical sedimentary features. Each facies has been interpreted as a product of specific depositional process (Table 10.1): Distribution of depositional facies as a percentage of cored intervals is given in Tables 10.2 and 10.3.

Table 10.1 Types of lithofacies, their characteristics, and interpreted depositional processes in the Paleogene, North Sea. (After Shanmugam et al. (1995a))

Facies	Characteristics	Depositional process
1	Gravel and pebbly sand (coarse to medium grained), amalgamated units, contorted bedding, floating clasts	Gravelly slump, slide, debris flow
2	Fine- to medium-grained sand, amalgamated units, 'massive' appearing, sharp top, basal (primary) glide planes, internal (secondary) glide planes, slump folds, contorted bedding, steep layers, shear zones, floating clasts, planar clast fabric, inclined dish structures, brecciated zones, clastic injections, synsedimentary faulting	Sandy slump, slide, debris flow
3	Mudstone, sharp top, contorted bedding, steep layers, slump folds, shear zones, floating clasts, brecciated zones, planar clast fabric, clastic injections	Muddy slump, slide, debris flow
4	Fine-grained sand and silt, current ripples, horizontal lamination, mud offshoots	Bottom-current reworking
5	Fine-grained sand and silt, sharp base, gradational top, normal size grading	Turbidity currents
6	Mudstone, horizontal lamination, shell fragments, bioturbation, glauconite	Pelagic and hemipelagic (suspension settling)

Table 10.2 Distribution of lithofacies computed as percentage of cored interval in the Paleocene, Faeroe Basin. (After Shanmugam et al. (1995a))

Well		Esso 214/28-1 Sequence 70	Esso 214/28-1 Sequence 20	Shell/Britoil 206/1-2 Sequence 30
Core Thickness		115.5ft (35 m)	60.5 ft (18 m)	194 ft (59 m)
Mud		15%	31%	41%
Sand		85%	69%	59%
Fine sand		100%	100%	100%
	1	-	-	-
	2	69%	52%	58%
	3	15%	3%	6%
	4	4%	12%	1%
	5	-	-	1%
Facies	6	-	-	1%
	2&3	11%	-	-
	2&4	-	5%	-
	3&4	-	28%	-
	3&6	-	-	35%
	4&5	1%	-	-

Total core: 370′ (113 m).

Table 10.3 Distribution of lithofacies computed as percentage of cored interval in the Paleogene, Frigg and Gryphon–Forth (Harding) areas. (After Shanmugam et al. (1995a))

Well		Elf 25/2-8 (Frigg East)	Kerr–McGee 9/18b-7 (Gryphon)	Britoil 9/23b-7 (Forth) (Harding)	Conoco 9/18a-15
Core Thickness		218 ft (66 m)	398 ft (121 m)	714 ft (218 m)	296 ft (90 m)
Mud		19%	10%	28%	65%
Sand		81%*	90%	72%	35%
Fine sand		65%	-	40%	100%
Medium sand		30%	100%	60%	tr
Gravel		5%	-	-	-
	1	4%	-	-	-
	2	76%	90%	72%	35%
	3	6%	10%	16%	51%
	4	2%	-	-	-
	5	-	-	-	-
Facies	6	-	-	4%	-
	3/2	-	-	-	-
	3&6	-	-	8%	14%
	3&4	3%	-	-	-
	5&6	9%	-	-	-

Total core: 1626′ (496 m).
*Includes gravel.

10.2.1 Faeroe basin area, U.K. Atlantic Margin

Mitchell et al. (1993) described the Paleogene sequence-stratigraphic framework of the Faeroe basin, west of the Shetland Islands (Fig. 10.3), U.K. Atlantic Margin. They recognized eleven Paleocene and four Eocene sequences, each separated by Type 1 unconformities. Seismic facies units within the Paleocene sequences exhibit well developed external mounded forms with internal bi-directional downlap onto Type 1 unconformities (Fig.10.4). These mounded forms, interpreted to represent lowstand systems tract, were cored in the Esso 214/28-1 (Figs.10.5, 10.6, and 10.7) and Shell/Britoil 206/1-2 wells. Gamma-ray logs of the sandstone intervals show well-developed, blocky motifs (Fig. 10.5). On the basis of these seismic and wireline-log characteristics, and their occurrence in a basinal position, these mounded Paleocene units were interpreted to be basin-floor fans.

The seismic mound in Sequence 70 shows a high relief with an angle of approximately 9° on its flanks (Fig. 10.4). There is no evidence of erosion at its base. The mound has dimensions of approximately 10 by 7 km in size, and is about 810 ft (247 m) thick in the 214/28-1 well. The mound shows rapid lateral
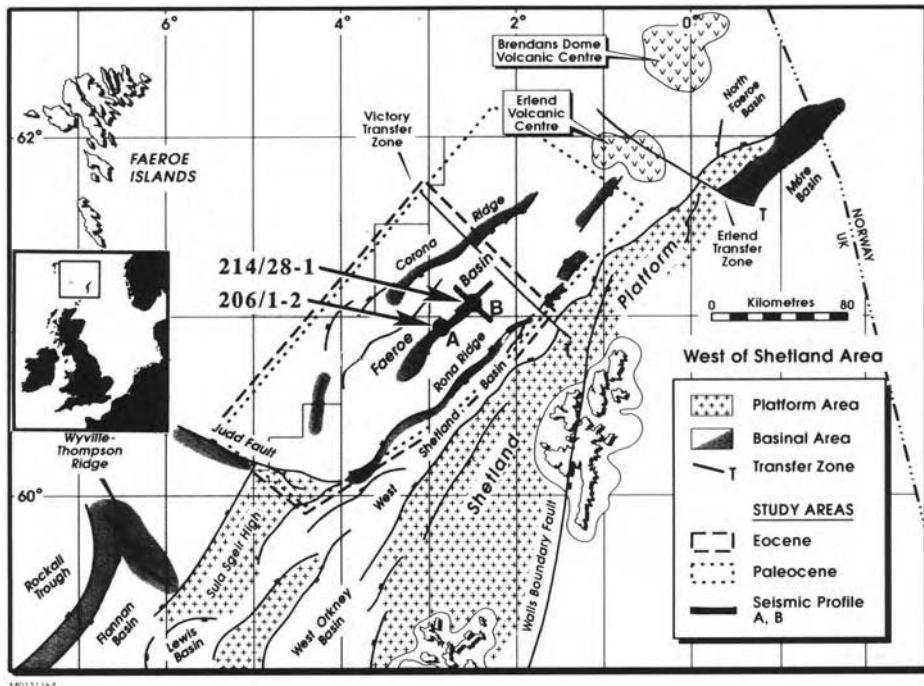
Fig. 10.3. Faeroe study area (outlined), west of the Shetland Islands, U.K. Atlantic Margin. The Esso 214/28-1 well (solid dot) is located at the intersection of seismic profiles A (see Fig. 10.4A) and B (see Fig. 10.4B).
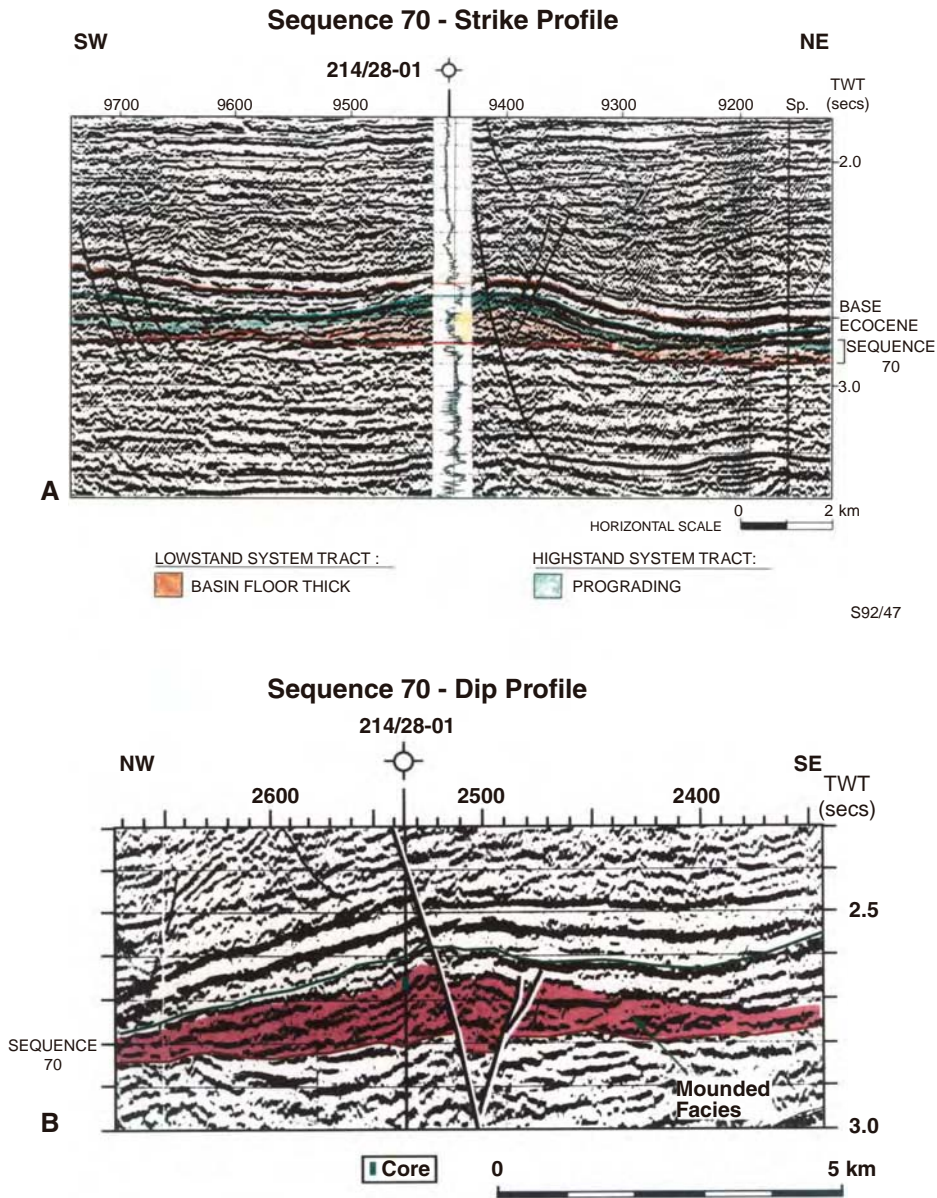
Fig. 10.4. (*A*) Strike section of a seismic profile showing external mounded form with bidirectional downlap in Sequence 70, Faeroe Basin. Note blocky log motif within sequence 70 at the Esso 214/28-1 well location. See Figure 10.3 (Profile A) for location of this section. (*B*) Dip section of a seismic profile showing external mounded form with internal bidirectional downlap, Sequence 70. Note lateral pinch-out geometries of seismic mounds. Note cored interval near the top of mound. See Figure 10.3 (Profile B) for location of this section. (After Shanmugam et al. (1995a). Reprinted by permission of the American Association of Petroleum Geologists whose permission is required for further use.)
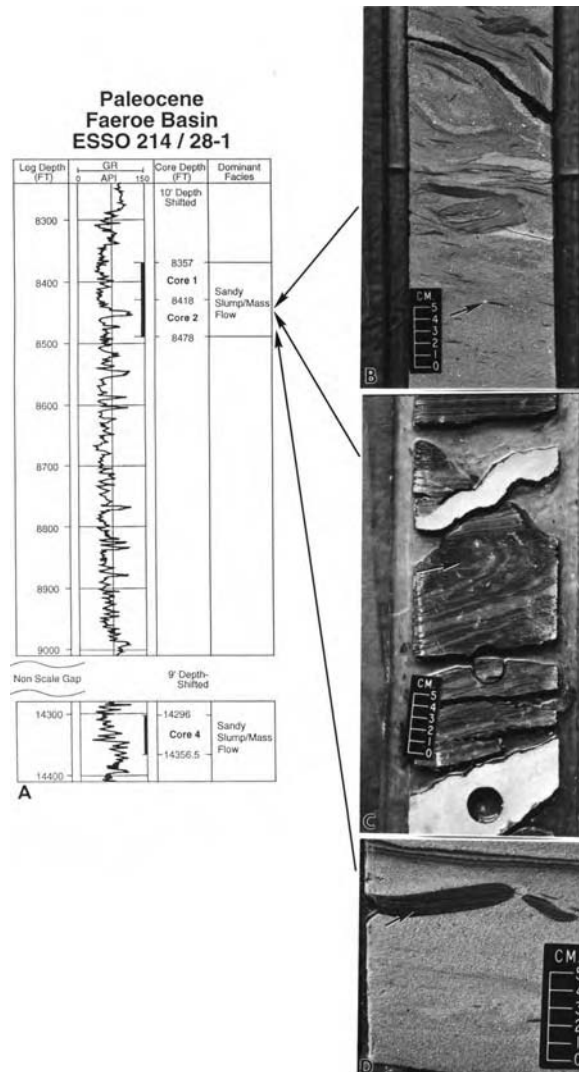
Fig. 10. 5. (*A*) **Blocky gamma-ray log motif of a 700-ft (213 m) thick sandstone unit with cored interval near the top of sandstone (cores 1 and 2, Sequence 70).** (*B*) **Facies 2: Core photograph showing fine-grained sandstone with contorted shale clasts and floating white quartzite pebbles (arrow), 8432′ (2570 m) core depth.** (*C*) **Facies 3: Core photograph showing slump folded mudstone (dark) with sandstone injectites (light), 8437′ (2572 m) core depth.** (*D*) **Facies 2: Core photograph showing floating elongate mudstone clasts near the top of a fine-grained sandstone unit with sharp upper contact, 8463′ (2580 m) core depth. Note planar clast fabric. See Table 10.1 for explanation of facies. See Figure 10.6 for a sketch of this photograph. (After Shanmugam et al. (1995a). Reprinted by permission of the American Association of Petroleum Geologists whose permission is required for further use.)**
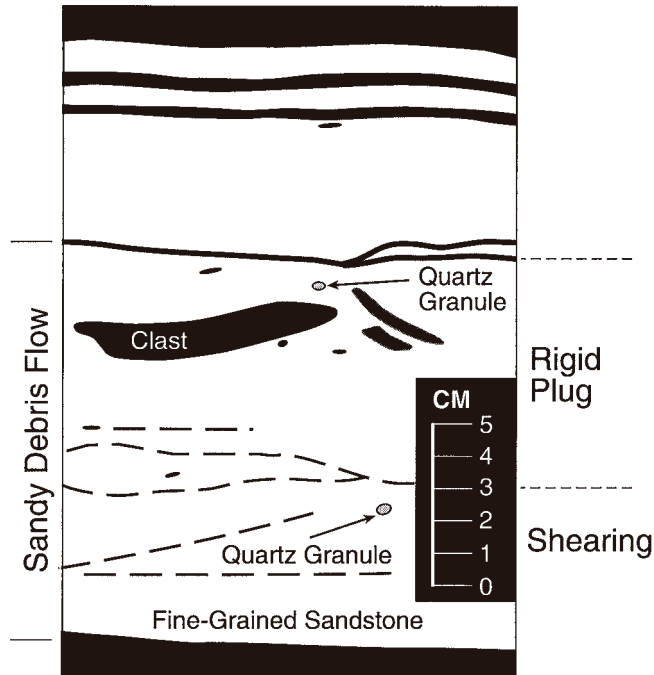
Fig. 10.6. Sketch of core photograph showing details of floating elongate mudstone clasts and quartz granule near 8463′ (2580 m) core depth in Esso 214/28-1 well, Faeroe Basin. The upper zone with rafted clasts and lower zone with quartz granules and shear planes are interpreted as rigid plug and shearing zone of a sandy debris flow.

pinch-out geometry is well developed (Fig. 10.4). The 214/28-1 well penetrated the thickest part of this mound, and the core was taken from the upper part of the mound (Fig. 10.4). The cored interval is composed of consolidated sandstone and mudstone. The sandstones show: (1) sharp upper contacts (Fig. 10.5D); (2) floating mudstone clasts (Fig. 10.5D); (3) a planar clast fabric (Fig. 10.6); (4) floating quartzite granules in fine-grained sandstone (Fig. 10.6); (5) sandstone units with inverse size grading; and (6) moderate (5–10%) to high (20–30%) matrix content. These features are interpreted to indicate deposition of the sand by debris flows.

Contorted bedding (Fig. 10.5C), slump folding (Figs. 10.7C) and associated clastic injection (Fig. 10.5C) are considered evidence for sandy slumps. In the Paleocene interval, slumping is prevalent. Calibration of the blocky log motif with the sedimentological log suggests that the sharp base of 'blocky' log interval results from the primary glide plane (decollement). In the Esso 214/28-1 well at 14 337.8 ft (4370 m), the primary glide plane is overlain by a 3-cm thick shear zone.
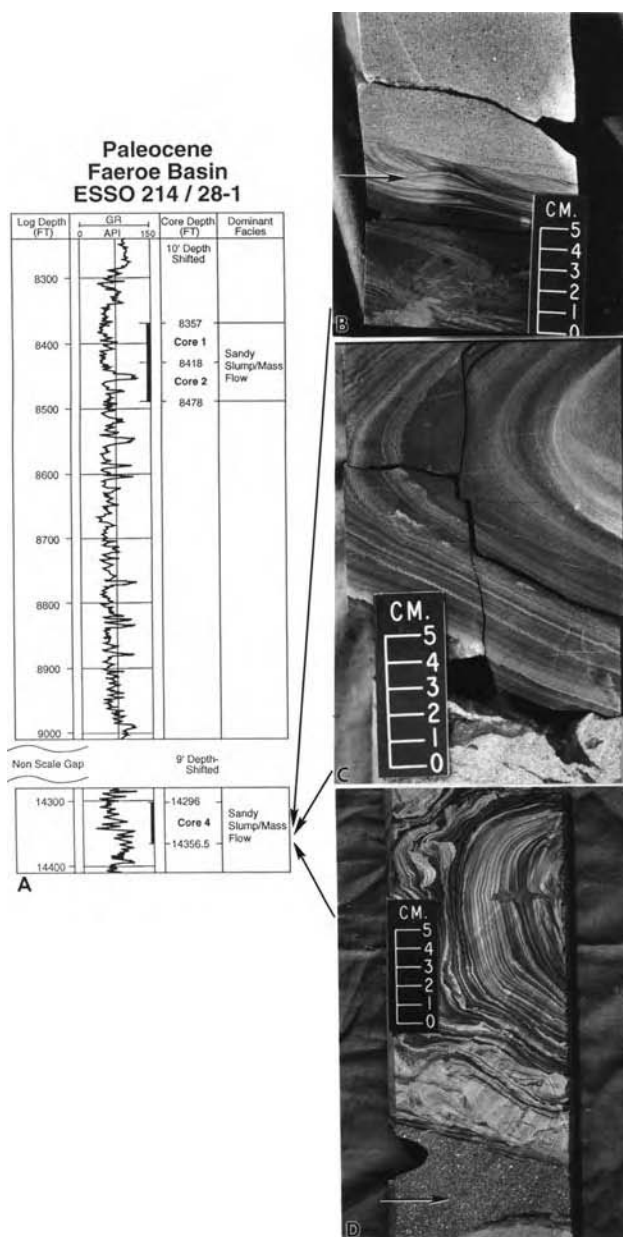
Fig. 10.7. (*A*) Crescent to serrated gamma-ray log motif of interbedded sandstone and mudstone unit (core 4, Sequence 20). (*B*) Facies 4: Core photograph showing the occurrence of a discrete ripple-laminated unit (near top of scale) between a contorted mudstone unit below and a massive sandstone unit with floating quartzite pebbles (white) above, 14 300′ (4359 m) core depth. (*C*) Facies 3: Core photograph showing a classic slump fold in mudstone, 14 339′ (4371 m) core depth. (*D*) Facies 2: Core photograph showing contorted slump fold in fine-grained sandstone, 14 354′ (4375 m) core depth. Note an injected sandstone (sill) near the bottom (arrow). See Table 10.1 for explanation of facies. Arrows show stratigraphic position of core photographs. (After Shanmugam et al. (1995a). Reprinted by permission of the American Association of Petroleum Geologists whose permission is required for further use.)

The bulk (nearly 95%) of the cored interval (175 ft or 53 m) in the 214/28-1 well is composed of deposits of slumps and debris flows (Table 10.2). Thin, graded beds (less than 5 cm thick) deposited from turbidity currents do occur, but they are extremely rare. Discrete ripple-laminated units above contorted mudstone units have been interpreted to represent reworking of slump sheets by bottom currents (Fig. 10.7B). In the 214/28-1 well, bottom-current reworked facies range from 4–12%. In this study area, bottom current velocities of up to 100 cm/sec have been estimated for the Norwegian Sea Deep Water (NSDW) in present-day water depths of 800–1200 m (Masson et al., 2004). In the Faeroe Basin, similar strong contour-current activity has been suggested for the Paleogene (Damuth and Olson, 1993).

Although the Paleocene mounds exhibit properties of basin-floor fans on seismic and log data, conventional core data do not support a basin-floor fan interpretation. This is because the cored interval is dominated by slumps and debrites, not turbidites. The other problem is that turbidites in an unconfined basinal environment commonly would form sheet-like geometries. Sheet turbidites cannot explain the observed seismic mounds with 9° of dip along their flanks. On the other hand, slumps and debrites can explain seismic mounds in the study area.

10.2.2 Gryphon area, U.K. North Sea

The Gryphon Field is located in U.K. Quadrant 9 of the North Sea (Fig. 10.8). Shanmugam et al. (1995a) described conventional core totaling 2700 ft (823 m) from 20 wells from this area. The following three wells with long cores are selected for discussion: (1) Kerr–McGee 9/18b-7 (Gryphon Field); (2) Britoil 9/23b-7 (Harding Field); and (3) Conoco 9/18a-15. The principal reservoirs are in the upper Paleocene/lower Eocene units (Balder/Frigg). A major source of sediment supply during the Paleogene was from the East Shetland Platform and the Scottish mainland (Stewart, 1987).

In the Gryphon Field, the lower Eocene reservoir exhibits well-developed 'blocky' log motifs (Fig. 10.9). The reservoir shows external mounded forms with lateral pinch-out geometries that rest upon on an unconformity surface (blue sequence boundary in Figs. 10.10 and 10.11). Based on sequence-stratigraphic concepts, Newman et al. (1993) interpreted the reservoir in the Gryphon Field as lowstand fans (i.e., basin-floor fans). In contrast, Timbrell (1993) interpreted the same reservoir as slope fans, and Reynolds and Mackay (1992) and Purvis et al. (2002) interpreted them to be a product of post-depositional sand injection.

Massive sand beds are common. The sands are poorly sorted with 5–15 % matrix, and show sharp upper contacts, floating mudstone clasts (up to 15 cm in diameter, Fig. 10.12C), primary (basal) glide planes, steep internal shear planes (Fig. 10.12D), and water-escape structures. These features suggest deposition from slumps and debris flows.
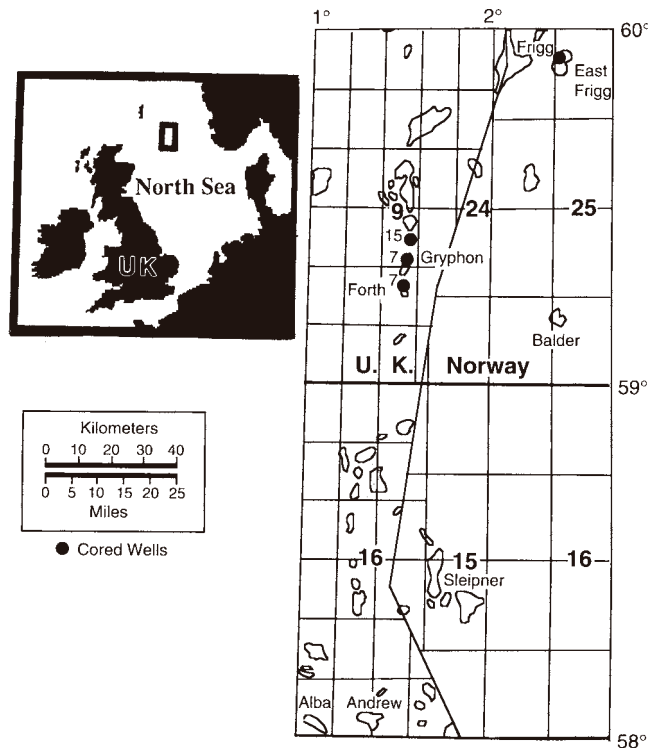
Fig. 10.8. Location map showing cored wells (solid dots) used in this study from Frigg (Elf 25/2-8) and Gryphon–Harding (formerly Forth) (Kerr–McGee 9/18b-7, Britoil 9/23b-7, Conoco 9/18a-15) areas, North Sea. (After Shanmugam et al. (1995a). Reprinted by permission of the American Association of Petroleum Geologists whose permission is required for further use.)

The nearly 400 ft (122 m) of continuous core in the 9/18b-7 well makes it possible to calibrate core-scale features with seismic-scale features using synthetic seismograms (Fig. 10.10 and 10.11). The cored interval penetrates most of the thickness of the pink and orange seismic mounds (Fig. 10.12E). Three distinct shear planes have been recognized in the core (see three arrows in Fig. 10.9B). A basal shear plane recognized in the core corresponds to the base of the blocky log motif and to the basal contact of the pink seismic mound (Fig. 10.10). The blue sequence boundary in the seismic profiles (Figs. 10.10 and 10.11) is coincident with the primary glide plane (or the decollement) of a slump sheet recognized in the core. The decollement is the basal contact of the 400-ft (122 m) thick sand with underlying Balder tuff. The chalk-like texture of the Balder tuff apparently provided a slippery shear surface for mass movements.

The middle shear plane (or secondary glide plane) and associated mudstone clasts recognized in the core (Fig. 10.12) coincides with the high-amplitude
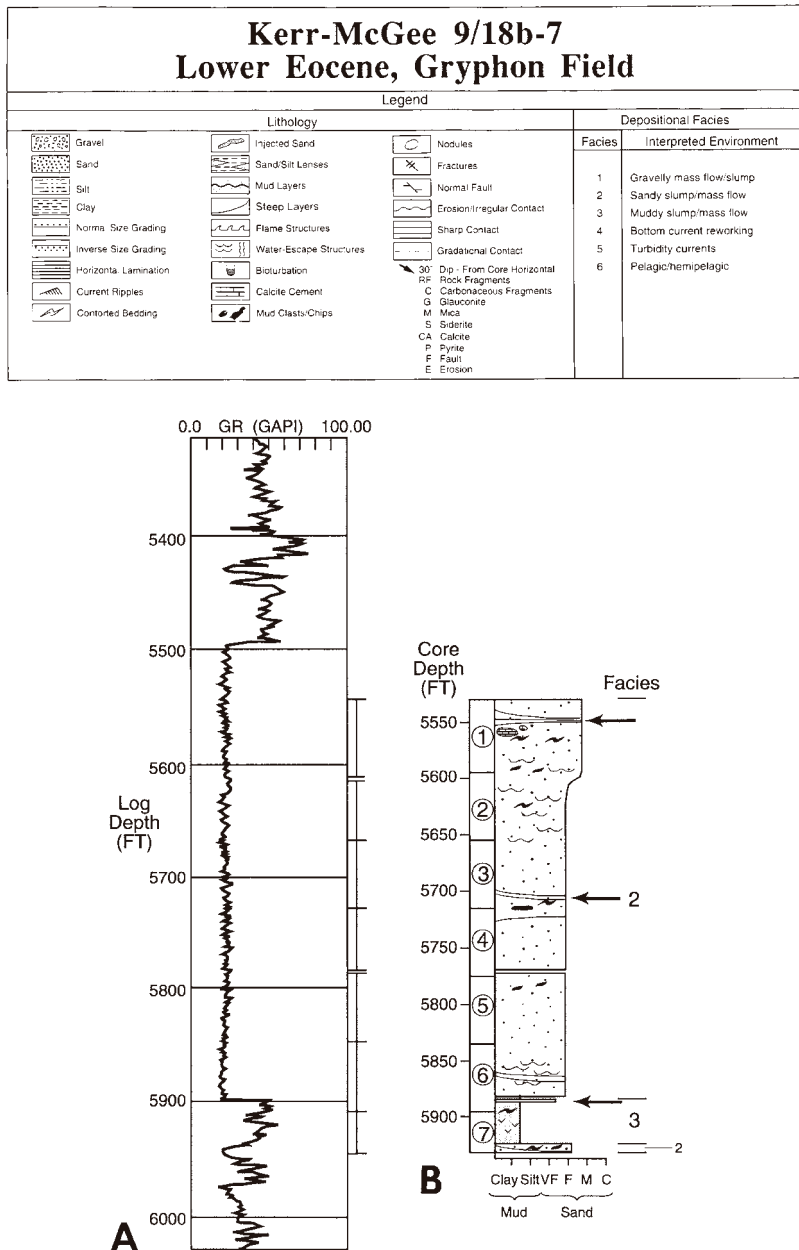
Fig. 10.9. (*A*) Well developed blocky wireline-log motif of a 400-ft (122 m) thick massive sand, Lower Eocene, Gryphon Field, Kerr–McGee 9/18b-7. (*B*) Depth-tied sedimentological log showing distribution of facies 2 and 3. Three arrows denote positions of shear planes (glide planes) observed in the core. Basal shear plane, which denotes decollement, also coincides with the sequence boundary. Note three shear planes in Figures 10.10 and 10.11. Core numbers are shown within circles. See Table 10.1 and 10.2 for explanation of facies and distribution. (After Shanmugam et al. (1995a). Reprinted by permission of the American Association of Petroleum Geologists whose permission is required for further use.)
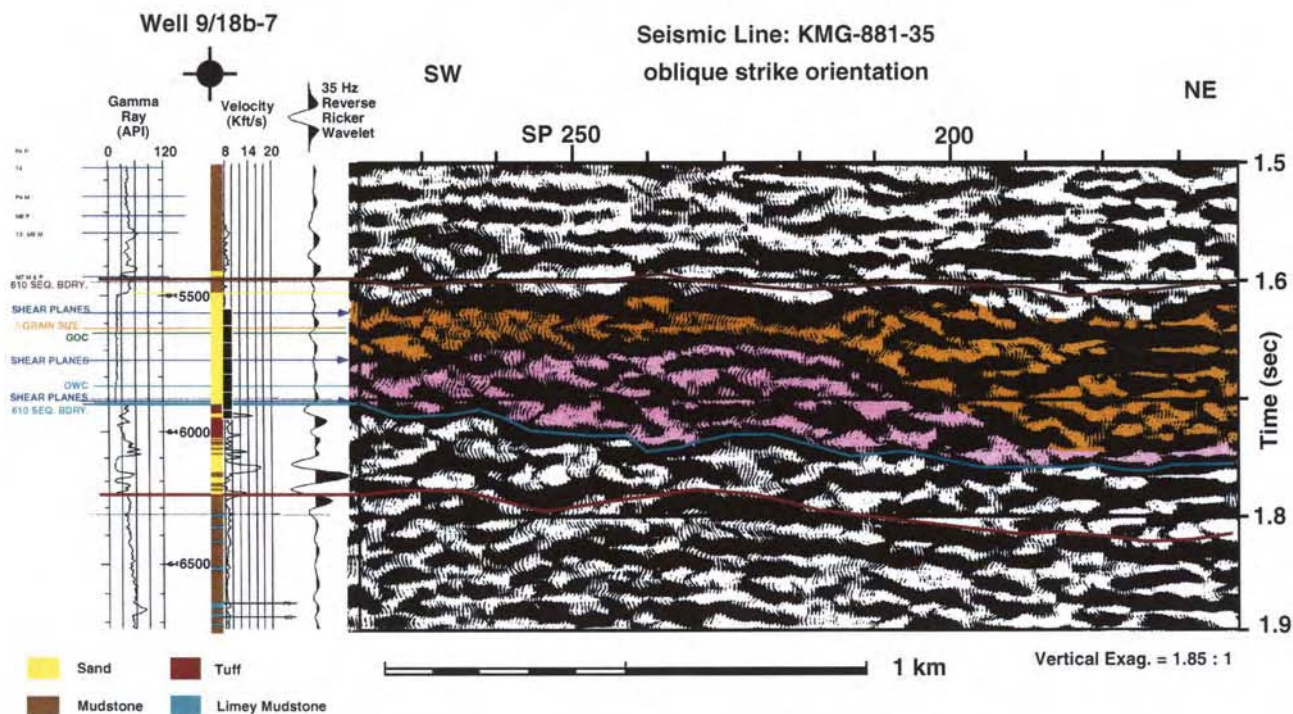
Fig. 10.10. Seismic line (KMG-881-35) showing mounded geometries of pink and orange packages with irregular upper surfaces and hummocky to chaotic internal reflections, Gryphon Field. Note lateral pinch-out geometry of the pink mound. Onlapping of reflections within the orange package occurs on the right-hand side of the pink mound. Calibration of well data with seismic data using synthetic seismogram shows that cored intervals (solid black bars) comprise the bulk of the mounded facies. Note basal shear plane coincides with the base of blocky log interval and the blue sequence boundary at the base of pink package. The middle shear plane corresponds to high amplitude reflection that separates pink and orange packages. (Shanmugam et al. (1995a). Reprinted by permission of the American Association of Petroleum Geologists whose permission is required for further use.)
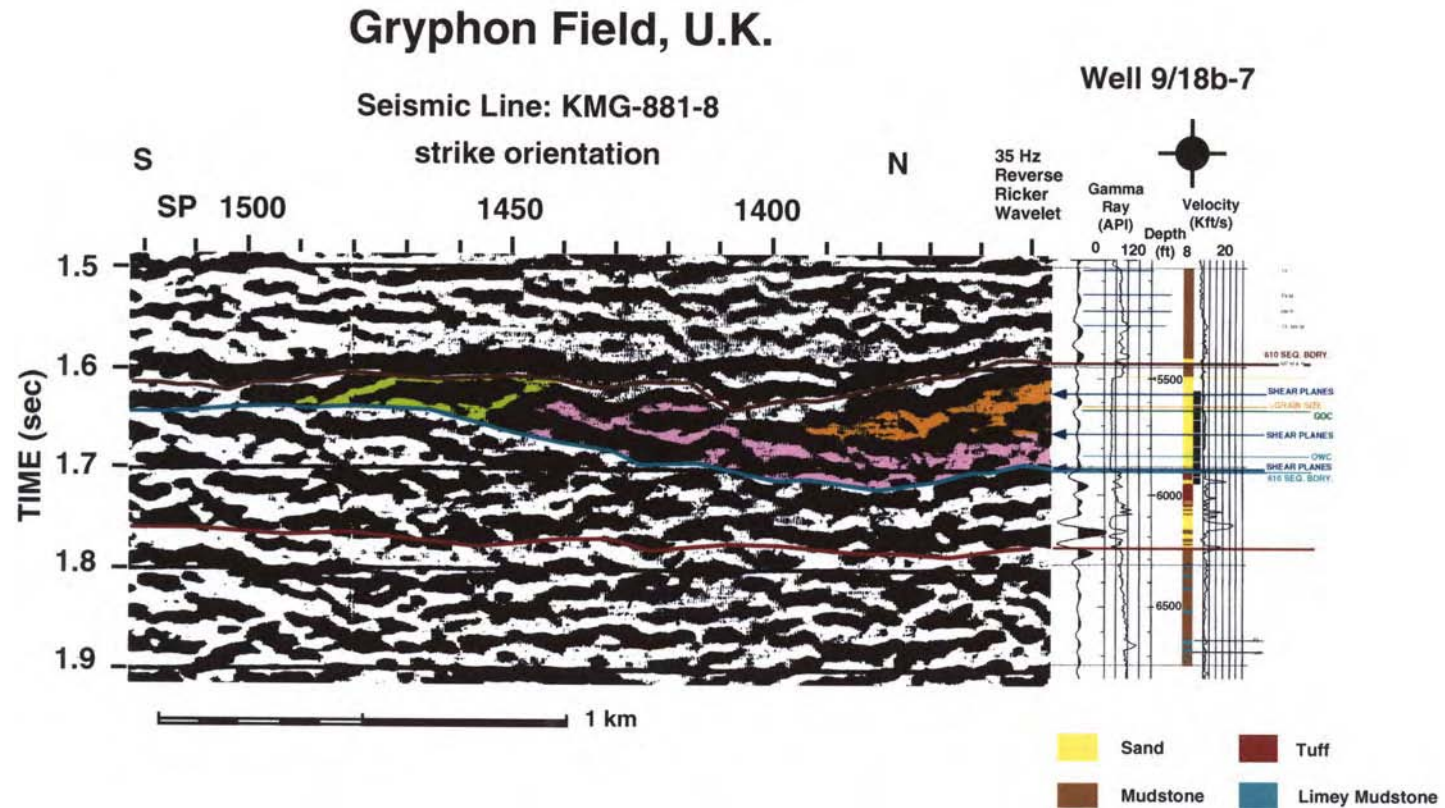
Fig. 10.11. Seismic line (KMG-881-8) showing stratigraphic relationships of three seismic mounds (pink, orange, and green) occurring on the blue sequence boundary, Gryphon Field. Note lateral pinch-out geometries of seismic mounds. See Figure 10.12E for sketches of seismic lines KMG-881-35 and KMG-881-8. (Shanmugam et al. (1995a). Reprinted by permission of the American Association of Petroleum Geologists whose permission is required for further use.)
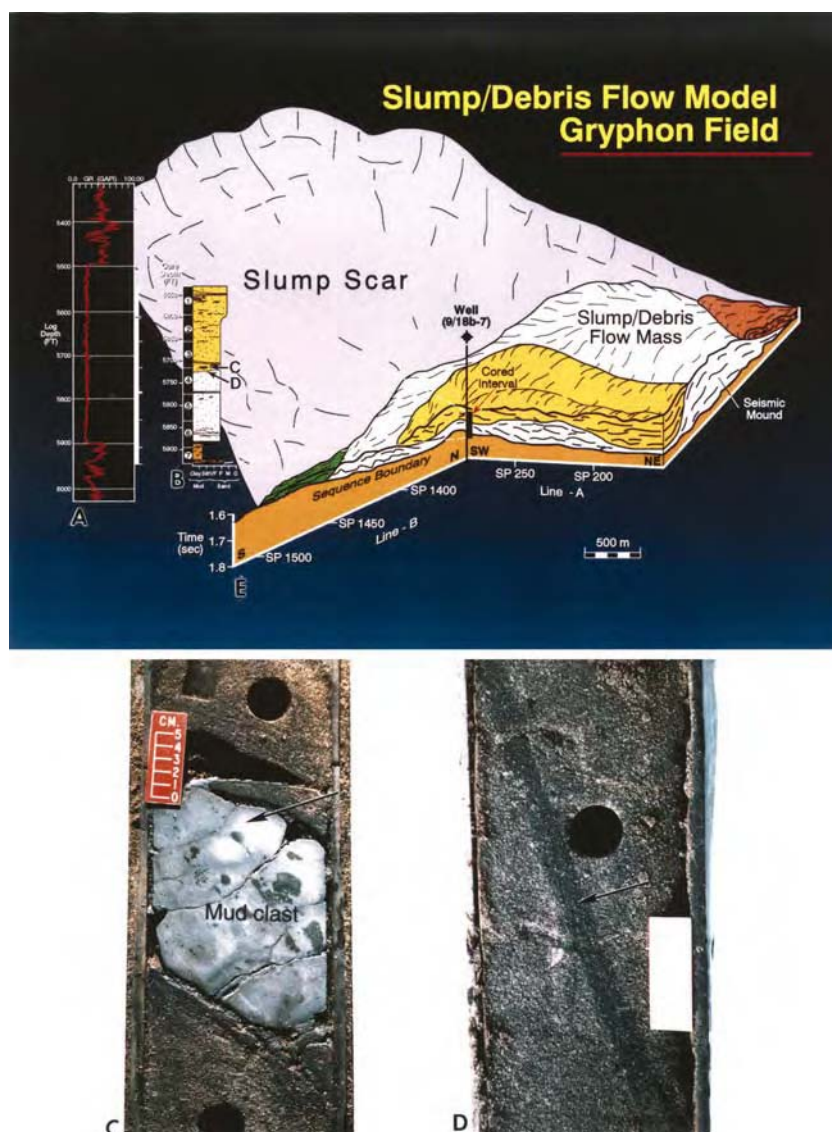
Fig. 10.12. Depositional model of Gryphon Field area. (*A*) Well-developed blocky log motif. Lower Eocene, Gryphon Field, Kerr-McGee 9/18b-7. (*B*) Depth-tied sedimentological log showing facies distribution. Stratigraphic positions of core features *C* and *D* are shown by arrows. (*C*) Facies 2: Core photograph showing a large mudstone clast (arrow) in fine-grained massive sand. Note irregular upper surface of mudstone clast. 5725 ft (1746 m). (*D*) Facies 2: Core photograph showing steeply dipping layer (arrow), interpreted as internal shear plane at 5726.7 ft (1746.6 m). See Table 10.1 for explanation of facies. The interval of shear plane and associated large mudstone clasts correlates with the high amplitude reflection that separates pink and orange packages (see Fig. 10.10). (*E*) Schematic depositional model, based on integration of core, log and seismic data, showing mounded seismic facies are a result of slumps and debris flows. Note that the 9/18b-7 well is located at the intersection of seismic lines KMG-881-35 and KMG-881-8 (shown by sketches) and that cored interval is shown by a solid black bar. Areal distribution of slump masses is speculative. (Shanmugam et al. (1995a). Reprinted by permission of the American Association of Petroleum Geologists whose permission is required for further use.)

reflection that separates the pink and orange mounds (Fig. 10.12E). The cored interval is probably composed of at least two slump sheets separated by an internal (middle) shear plane. Amalgamation of these two slump sheets (pink and orange) has created a 400-ft (122 m) thick sand unit with a prominent 'blocky' log motif. The seismic moundings observed in the Gryphon area apparently result from an accumulation of multiple packages of slumps and debris flows (Fig. 10.12E). Well-developed blocky log motifs, long cores, diagnostic core features of debris flows and slumps, and seismic mounding with pinch-out geometries allowed an integrated slump and debris-flow dominated model to be developed for the Gryphon area (Fig. 10.12). Slope angles of up to 15° on the flanks of seismic mounds further support a slump interpretation. The cored interval contains 0% turbidites (Table 10.3).

Seismic data show erosional features upslope from the seismic mounds that may represent slump scars (Fig. 10.12E), but distinguishing such slump scars from erosional channels using only seismic profiles is impossible. In the absence of cores, slump scars and associated slump mounds (Fig. 10.12E) may be misinterpreted in seismic profiles as channels and associated depositional lobes of submarine fans. Only through study of conventional cores, can we resolve these sedimentological issues.

Similar to the Gryphon Field area, seismic mounds and blocky to serrated log motifs are common in the adjacent Harding Field (Shanmugam et al., 1995a). Long continuous cores from the Harding Field is dominated by slump and debrite facies (Table 10.3), and by mudstone with sandstone dykes and sills. Although the reservoir sand in the Harding Field has been interpreted to represent a submarine channel system filled with stacked turbidites (Jager et al., 1993), core data suggest a dominance of slumps and debrites. The cored interval contains 0% turbidites in the Harding well (Table 10.3).

Regional mapping shows that the Gryphon–Harding area occurs about 15–20 km seaward of the paleo-shelf edge, a slope setting where major sediment failures are expected to generate slides, slumps, and debris flows. In the Conoco 9/18a-15 well, deep-water massive sands exhibit brecciated mud clasts in association with contorted layers (Fig. 10.13). Because both sandy debrites and sandy injectites can contain brecciated clasts, interpretation of these brecciated clasts (debrite versus injectite) is challenging.

10.2.3 Frigg area, Norwegian North Sea

The Frigg Field and its associated satellites form a giant complex of gas fields in the North Sea (Fig. 10.8). Based on regional sequence-stratigraphic analyses, the Lower Eocene Frigg Formation has been traditionally considered to be an example of a turbidite-rich submarine-fan system (Heritier et al., 1979; McGovney and Radovich, 1985). In the conceptual sequence-stratigraphic framework, 'sheet mounds' that characterize the Frigg Formation fit the seismic criteria of
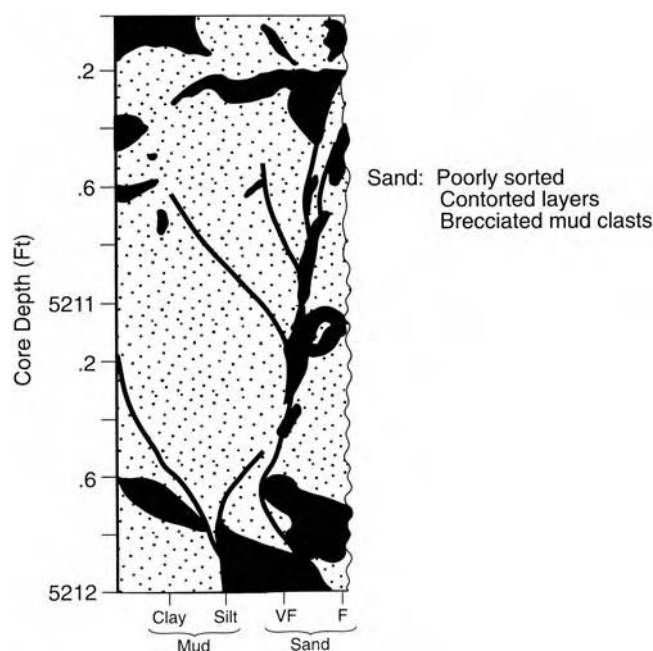
Fig. 10.13. Sedimentological log of core showing a massive sand unit with contorted layers and brecciated mudstone clasts (black). This could be interpreted as either sandy debrite or injectite. Conoco 9/18a-15; Lower Eocene, North Sea.

basin-floor fans (Shanmugam et al., 1995a). The upper part (1920–1980 m) of the cored interval in the 25/2-8 well, showing a 'blocky' log motif, is consistent with an interpretation as a basin-floor fan (Fig. 10.14).

Conventional cores from six wells in the main Frigg and Frigg East Alpha Fields were examined. The Elf 25/2-8 well in the Norwegian Sea was studied in detail owing to pristine preservation of sedimentary structures. The Frigg Formation is primarily comprised of unconsolidated sand. Although sand units of the Upper Frigg Formation were described as 'massive' (Brewster, 1991), they exhibit steeply dipping (up to 30°), discordant layers, slump folds, abrupt changes in fabric, inclined dish structures, and internal glide planes (Fig. 10.15A). These features are interpreted to be deposits of slumps (Facies 2).

Sand units of the Lower Frigg Formation are poorly sorted with 5–10 % matrix. They show sharp upper contacts, water-escape structures, and floating mudstone clasts. Both a planar fabric and a random fabric of mudstone clasts occur (Fig. 10.15B). These sands apparently represent sandy debrites. Slumps and debrites account for nearly 86% of the cored interval (Table 10.3). Classic turbidites are extremely rare and comprise less than 1% of the cored interval (Fig. 10.16). This rarity of turbidites is not unique to the Frigg area, but appears to be a global trend.
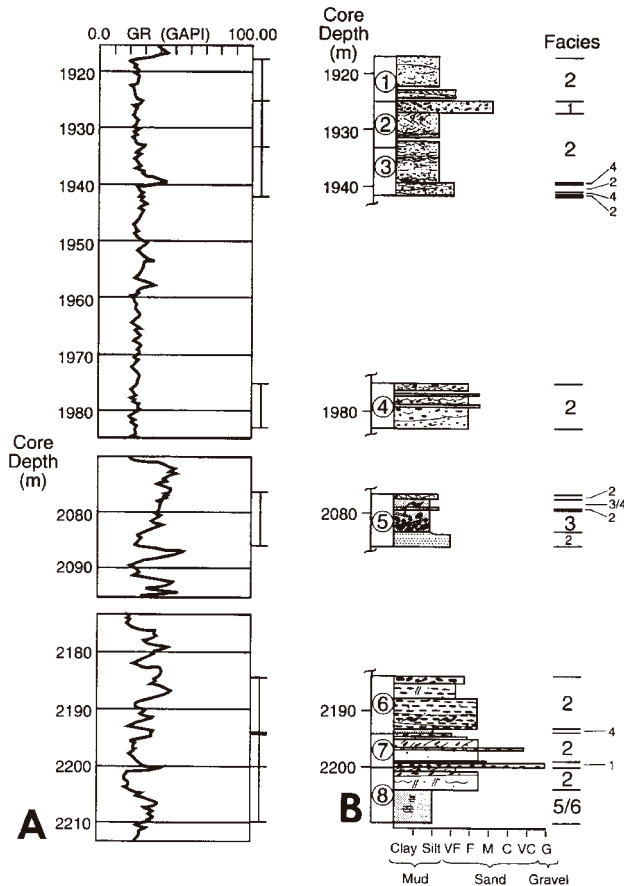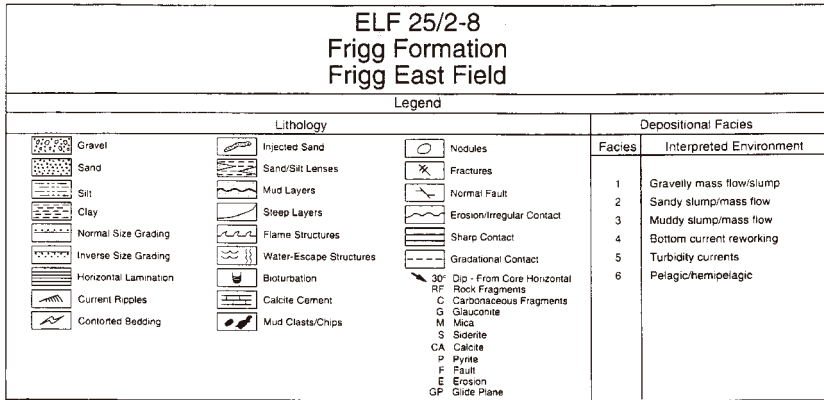
Fig. 10.14. (*A*) Upper 'blocky' log motif (1920–1980 m) and lower 'serrated' log motif (2070–2210 m) in the Lower Eocene Frigg Formation, Elf 25/2-8. (*B*) Depth-tied sedimentological log showing facies distribution. See Tables 10.1 and 10.3 for explanation of facies and distribution.
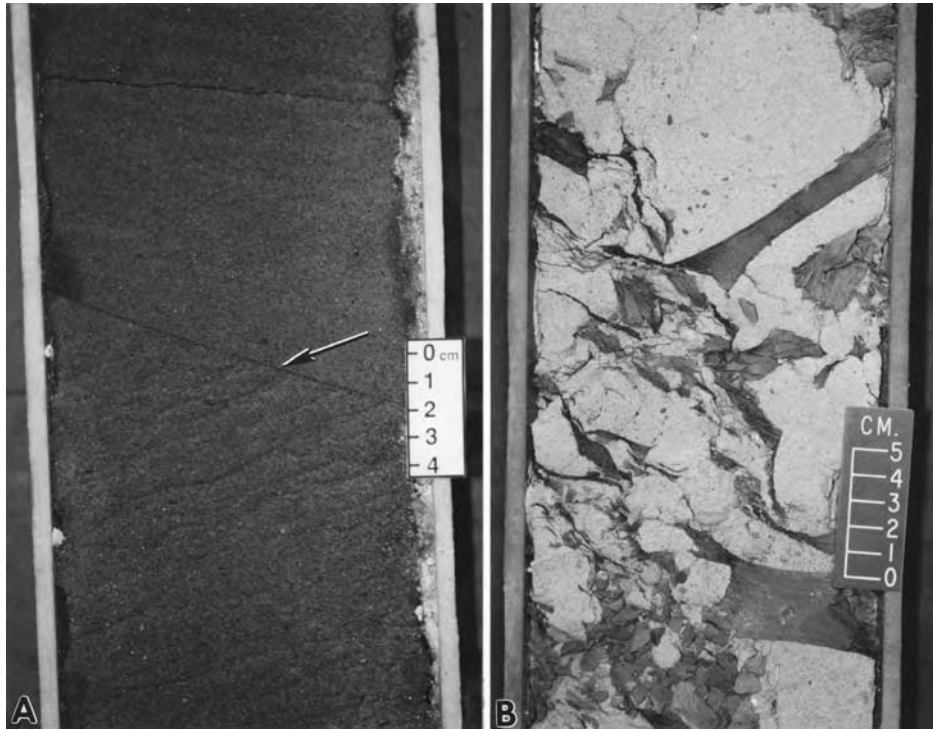
Fig. 10.15. (*A*) **Facies 2: Core photograph showing drastic changes in fabric in oil-stained sand. Note a secondary glide plane (arrow) and inclined dish structures beneath the glide plane; Lower Eocene Frigg Formation, Elf 25/2-8, 1978.8 m.** (*B*) **Facies 2: Core photograph showing random orientation of floating mudstone clasts in fine-grained sand. Lower Eocene Frigg Formation, Elf 25/2-8, 2185 m. See Table 10.1 for explanation of facies.**

10.2.4 Turbidite controversy

Conventionally, deep-water massive sands have been interpreted as deposits of high-density turbidity currents (e.g., Lowe, 1982). Shanmugam et al. (1995a), however, offered an alternative origin of massive sands by sandy debris flows. In line with Kuhn's (1996) concept (see Chapter 2), Hiscott et al. (1997, p. 665) were intolerant of an alternative interpretation and stated, '*We therefore reject the paradigm of Shanmugam et al. (1995a)… .*' Disappointingly, Hiscott et al. did not examine the cores used in my study. Other researchers, who did examine these cores, validated the importance of sandy debris flows for explaining the origin of deep-water massive sands (e.g., Stow and Johanssen, 2000; Purvis et al., 2002; Duranti and Hurst, 2004). This case study hammers the point that process sedimentology is based on looking at the rocks, not on theories or seismic geometries.
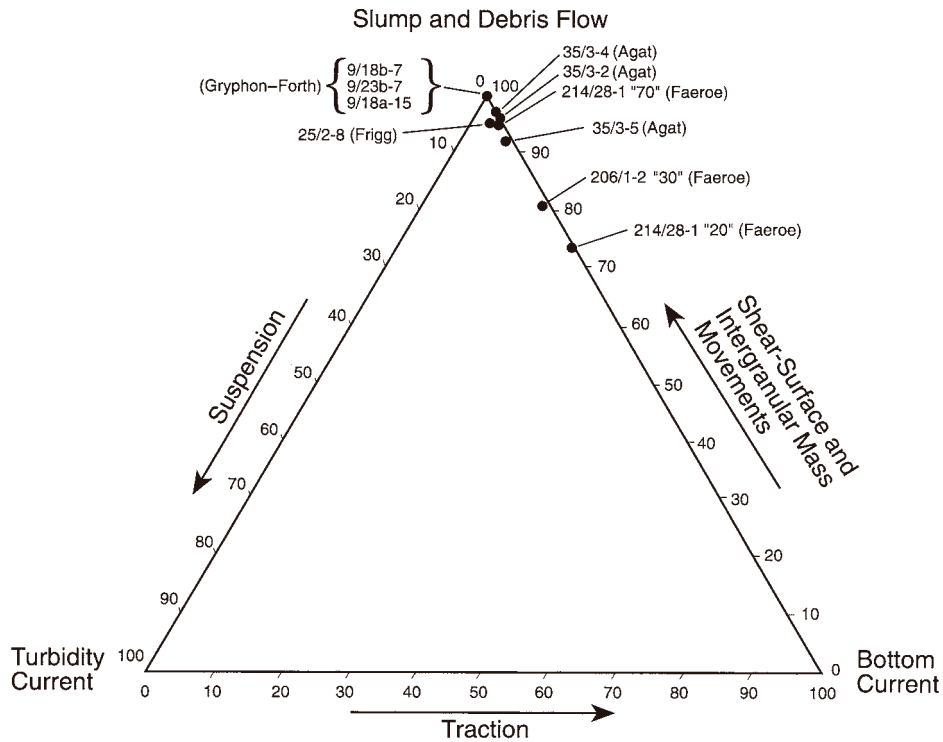
Fig. 10.16. Ternary diagram showing volumetric abundance of slump and debrite facies. Plots are based on normalized percentages of resedimented facies from Tables 6.3, 10.2, and 10.3. Note the influence of bottom currents in Sequences '20' and '30' in the Faeroe Basin. (Shanmugam et al. (1995a). Reprinted by permission of the American Association of Petroleum Geologists whose permission is required for further use.)

10.3 Seismic geometries

In a sequence-stratigraphic framework, seismic facies and geometries have been used to classify deep-water systems into basin-floor fans and slope fans (Vail et al., 1991). In turn, these models have been used to predict turbidite reservoirs. As discussed in Chapter 3, the term turbidite has a precise meaning in terms of its origin by a Newtonian turbidity current with a turbulent state. Evidence for Newtonian rheology and flow turbulence cannot be established directly from seismic-reflection profiles (see Chapter 7); rather, these properties can only be ascertained from actual sediment facies in cores.

Calibration of cored intervals with seismic reflection profiles (Shanmugam et al., 1995a, 1996; and Shanmugam and Zimbrick, 1996) suggests that seismic geometries are unreliable indicators of individual depositional facies in a systems
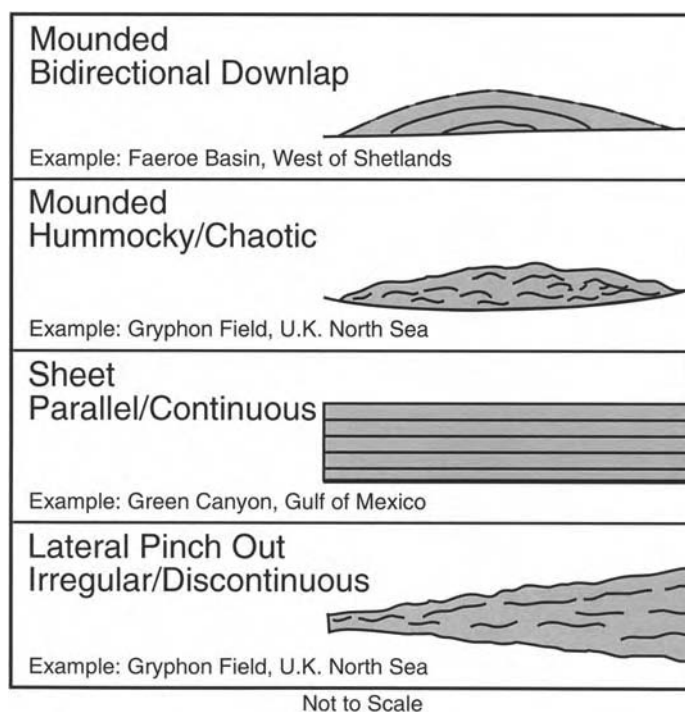
Fig. 10.17. Schematic diagram showing that a single depositional facies of sandy debrites can generate multiple seismic facies and geometries (e.g., mounded, sheet, and pinch out). See text for details. (After Shanmugam (2000a). Reprinted by permission of Elsevier.)

tract approach. The reason being that sandy slump/debris flow facies exhibit a variety of external (e.g., mounded, sheet, and lateral pinch out) and internal (e.g., bidirectional downlap, chaotic, parallel-continuous, and irregular-discontinuous) seismic facies (Fig. 10.17). Also, a single seismic facies can represent more than one depositional facies. Kilometer-scale seismic hummocks (i.e., mounds) have been interpreted as fluidization structures of a deep-water channel on the Niger Delta (Davies, 2003). At present, our understanding of the sedimentary facies that form different seismic facies is poor because of the insufficient core studies of these features. Also, in seismic profiles distinguishing autocyclic processes (e.g., slump scar) from allocyclic processes (e.g., sequence boundary) is difficult (Shanmugam et al., 1997c).

10.4 Wireline-log motifs

A common practice in the petroleum industry is to interpret deep-water depositional facies using wireline-log motifs. Wireline-log motifs for submarine channels and
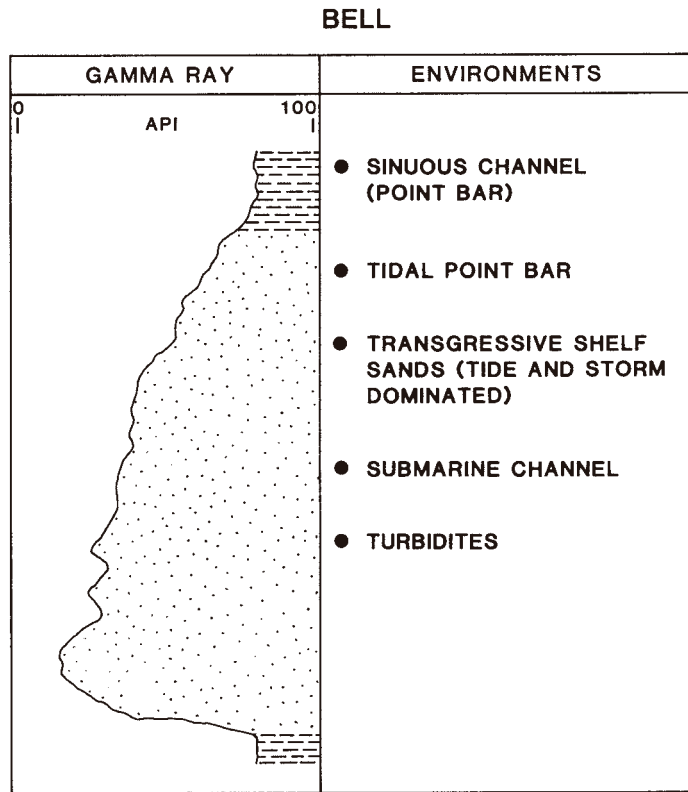
BELL

Fig. 10.18. Bell-shaped or 'fining-up' wireline-log motif and possible environmental interpretations.

lobes were first generalized by Selley (1979). In applying sequence-stratigraphic concepts, it is a common practice to interpret depositional facies using wireline-log motifs (Mitchum et al., 1993). However, wireline-log motifs reflect primarily the textural and mineralogical changes, not depositional facies. Depositional facies unrelated to deep-water deposition may produce log patterns mimicking deep-water facies. For example:

(1) Deposits of both a sinuous fluvial channel (point bar) and a submarine channel may generate a bell-shaped log motif (Fig. 10.18).
(2) Deposits of both a deltaic distributary mouth bar and a submarine-fan lobe may produce a funnel-shaped log motif (Fig. 10.19).
(3) Deposits of both a braided fluvial channel and a submarine canyon fill may generate a cylindrical or blocky log motif (Fig. 10.20).
(4) Deposits of both an alluvial plain and a deep-marine bottom current (e.g., contourites) may produce an irregular or serrated log motif (Fig. 10.21).

FUNNEL

GAMMA RAY	ENVIRONMENTS
0 100 API	• DELTA FRONT (DISTRIBUTARY MOUTH BAR) • CREVASSE SPLAY • BEACH AND BARRIER BEACH • PROGRADING SHELF SANDS • SUBMARINE FAN LOBE
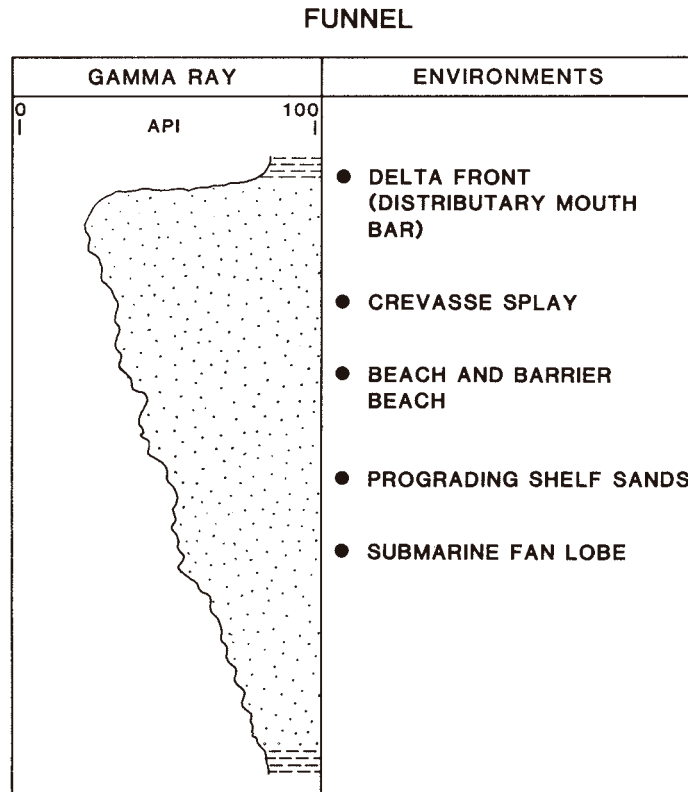
Fig. 10.19. Funnel-shaped wireline-log motif and possible environmental interpretations.

(5) Deposits of both a progradational delta and a submarine fan may generate an asymmetrical log motif (Fig. 10.22).

A single wireline-log motif (e.g., blocky) may be generated from more than one sandy depositional facies (e.g., slumps, debrites, turbidites) (Fig. 10.23). Plus, in wireline logs there are no established criteria for recognizing injected sands because both a sandy debrite and a sandy injectite can generate a blocky log motif (Fig. 10.23). Furthermore, a sand injectite in Norway shows a serrated log motif (Fig. 10.24). So a particular log motif is not unique to a particular depositional or post-depositional feature.

In sands deposited by slumps and debris flows, even in sands with uniform vertical grain-size distribution, a concentration of mudstone clasts at a particular horizon within the sand would generate different log motifs. For example:

(1) A 'blocky' log motif may be due to a uniform vertical distribution of mudstone clasts (Fig. 10.25A).
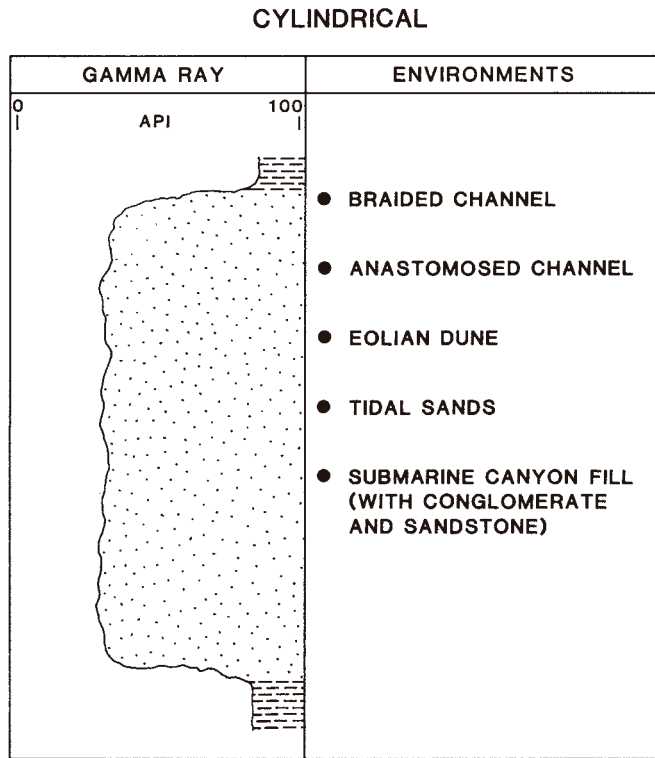
CYLINDRICAL

Fig. 10.20. Cylindrical or blocky wireline-log motif and possible environmental interpretations.

(2) A 'fining-up' log motif may be due to an upward increase in the amount of mudstone clasts (Fig. 10.25B). An example of this motif occurs in the Zafiro Field (Fig. 6.44).

(3) A 'coarsening-up' log motif may be due to an upward decrease in the amount of mudstone clasts (Fig. 10.25C).

   These log motifs, in the absence of cores, may be misinterpreted as 'coarsening-up' turbidite depositional lobes or 'fining-up' turbidite channels.

10.5 Parasequence concept

The application of sequence-stratigraphic concepts, intended for shallow-water systems (e.g., maximum flooding surface and parasequence), to deep-water systems has created confusion. Normark, Damuth et al. (1997), for example, applied the concept of '*maximum flooding surface*' to the modern Amazon Fan (Fig. 6.28). The term 'flood' literally means that a river or sea is flowing over its usual limits. At 3000 to 4000 m of water depths, where the Amazon Fan
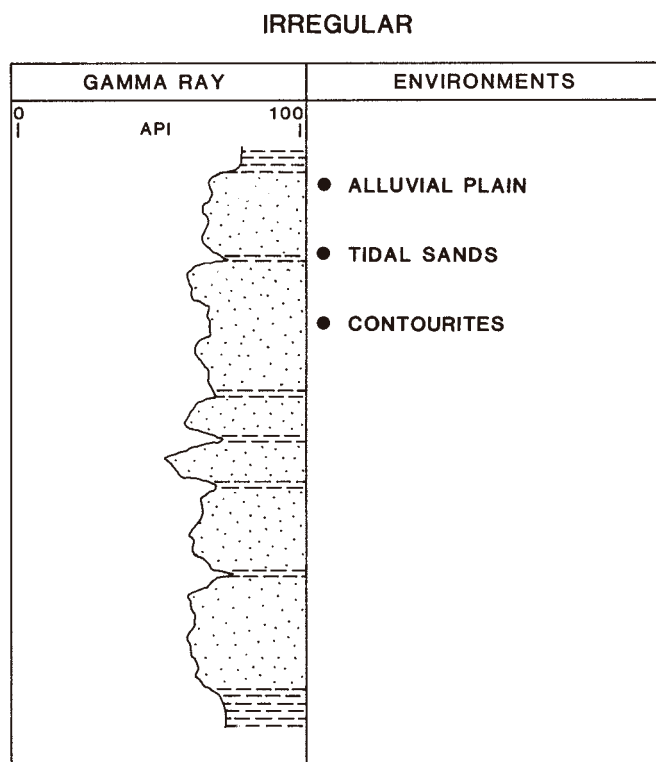
IRREGULAR

Fig. 10.21. Irregular or serrated wireline-log motif and possible environmental interpretations.

is located, irrespective of sea level changes, nothing is flowing over its usual limits. This is because bathyal environment is already flooded. This example exemplifies the ensuing confusion when a sequence-stratigraphic concept is applied to a modern deep-water system.

Another example is the application of the *parasequence* concept to deep-water (i.e., bathyal) turbidite sands of the Kakegawa Group, Japan (Sakai and Masuda, 1996). By definition, a parasequence is a deposit of a paracycle (Van Wagoner et al., 1988; Kamola and Van Wagoner, 1995). A parasequence is a relatively conformable succession of genetically related beds or bedsets bounded by flooding surfaces or their correlative surfaces (Van Wagoner et al., 1988). Because a parasequence is bounded by flooding surfaces, recognition of flooding surfaces is the key to establishing a parasequence. Van Wagoner, et al. (1988) defined a *flooding surface* as a surface that separates younger from older strata across which there is evidence of an abrupt increase in water depth. Sakai and Masuda (1996) interpreted parasequence boundaries in deep-water deposits. In shallow-water environments, of course, it is possible to recognize flooding surfaces because small changes in water depths (i.e., a few meters) are reflected in the deposits.
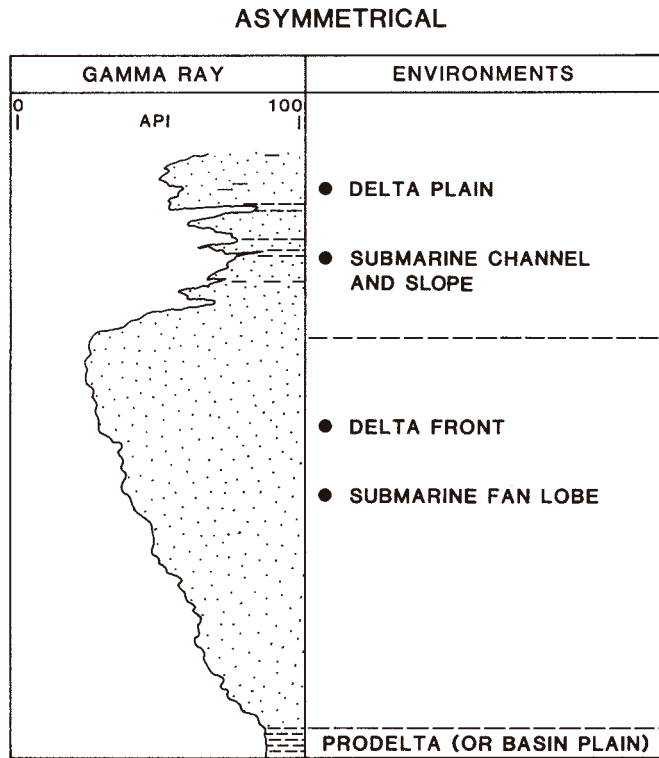
ASYMMETRICAL

Fig. 10.22. **Asymmetrical wireline-log motif and possible environmental interpretations.**

However, in bathyal water depths minor changes in water depths cannot be recognized. This is because deep-water environments are under flooded conditions all of the time. The common tendency to interpret a mudstone interval in deep-water sequences as evidence of increasing water depth is not meaningful. Although condensed sections are used commonly as evidence of a rise in sea level, mud intervals simply reflect low rates of deposition (Loutit et al., 1988), and cannot be routinely equated with a marine flooding surface or with a rise in sea level. Therefore, in terms of changing water depths it is unclear as to what the parasequence boundaries recognized by Sakai and Masuda (1996) really represent.

Within the interval bounded by flooding surfaces, a parasequence tends to show a gradual upward shallowing trend. Sakai and Masuda (1996) did not present evidence for upward shallowing trends within the parasequences of the Kakegawa Group. Considering that sands deposited in deep-water environments occur episodically often forming in a matter of hours or days (e.g., earth-quake induced mass flows), it is impractical to apply the parasequence concept to deep-water deposits in terms of changing water depths (Shanmugam, 1997b).
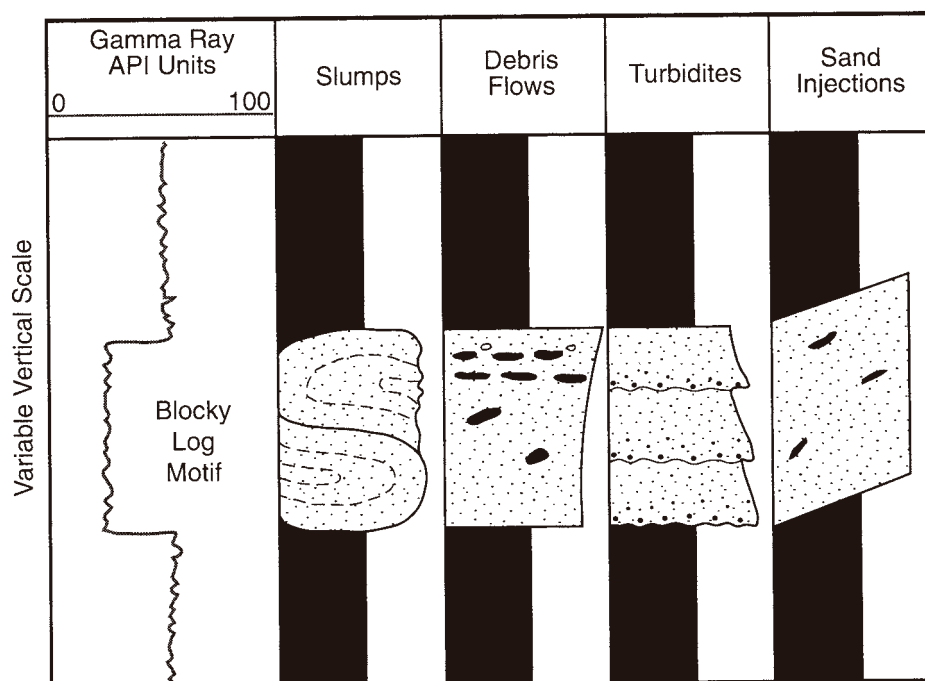
Fig. 10.23. Conceptual deep-water sequences showing that blocky log motifs can be caused by the occurrence of sandy (stippled) depositional facies of different origin (e.g., slumps, debris flows, and turbidites) and post-depositional (sand injectites) facies in association with mudstone (black). (After Shanmugam et al. (1995a). Reprinted by permission of the American Association of Petroleum Geologists whose permission is required for further use.)

10.6 Abandonment of submarine fan models

Although submarine fan models are still being applied, they were abandoned in the 1990s. For example:

(1) Data gathered from the modern Navy Fan since the publication of the suprafan lobe concept revealed that the suprafan area of modern fans is composed of a complex array of channel, lobe, and large-scale scour elements. This led Normark (1991, p. 9) to conclude that '... *the suprafan concept is no longer viable as a mappable, defining structure of turbidite systems*.' Because the morphologic characteristics of modern suprafan lobes are either not preserved in the rock record or because they cannot be planimetrically mapped in outcrops, Normark (1991) abandoned his suprafan-lobe concept altogether.
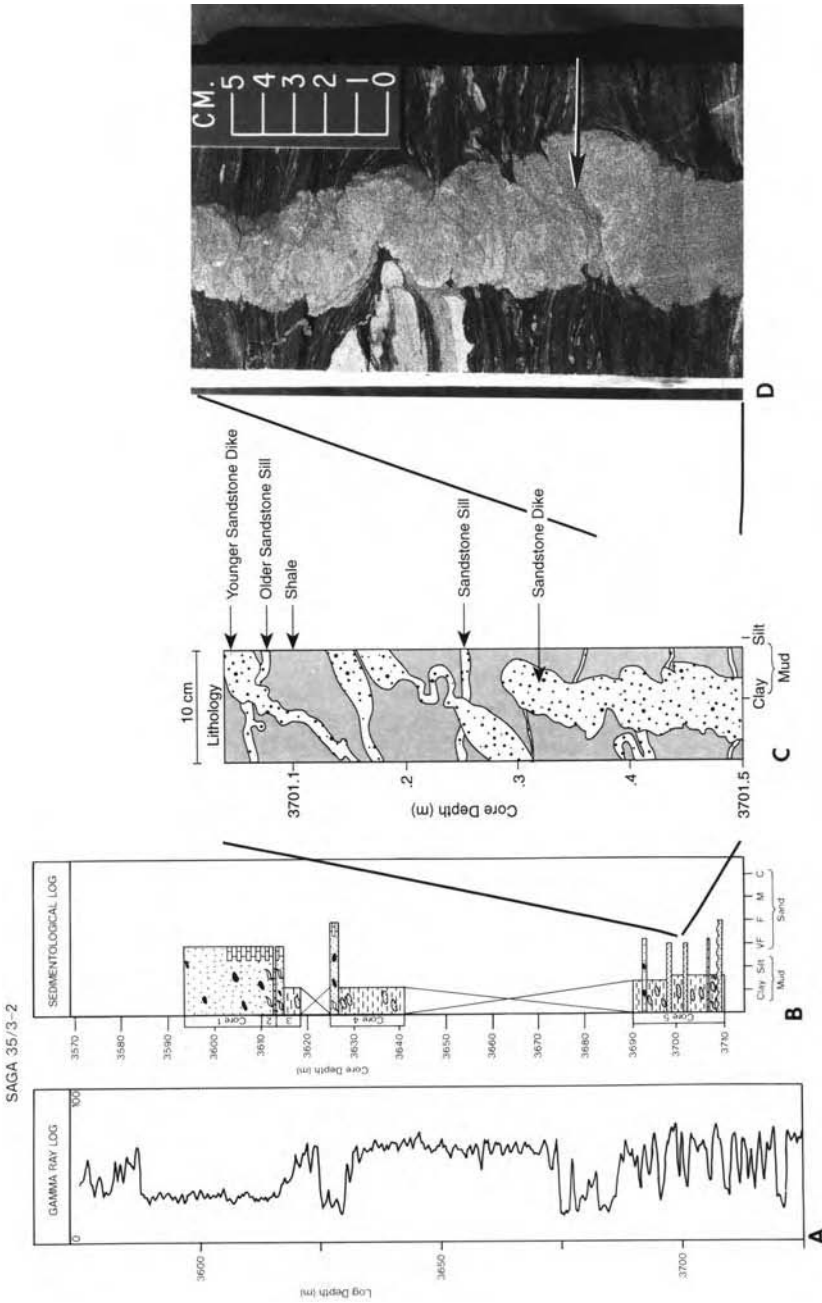
Fig. 10.24. **Wireline-log motif of clastic injections.** (*A*) Wireline-log motif showing serrated pattern for a cored interval near 3701 m. (*B*) Depth-tied sedimentological log. (*C*) Sketch of sandstone injectites at 3701.1–3701.5 m. (*D*) Core photograph showing ptygmatically folded sandstone dike (arrow) in mudstone. Agat Formation, Saga 35/3-2, offshore Norway (see Chapter 6). (From Shanmugam et al. (1994). Reprinted by permission of the American Association of Petroleum Geologists whose permission is required for further use.)
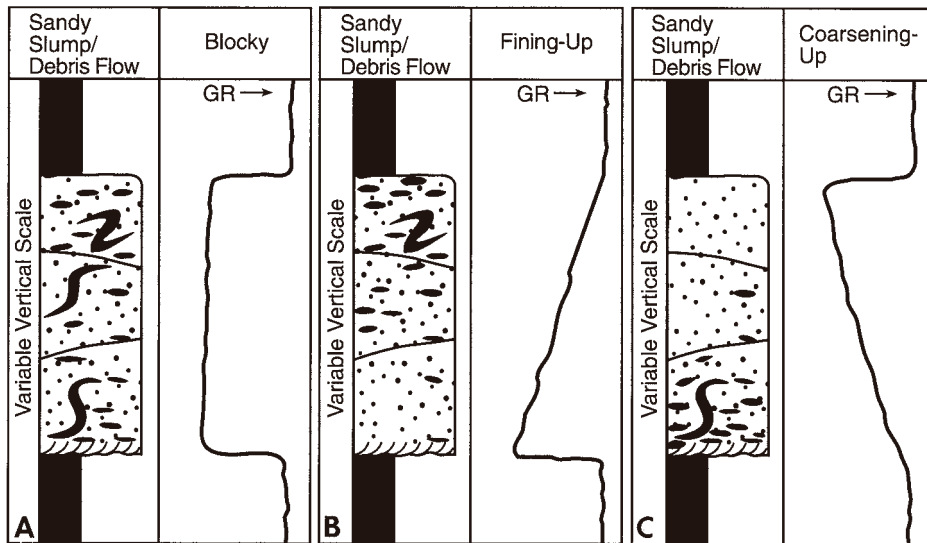
Fig. 10.25. Hypothetical wireline-log motifs caused by vertical changes in concentration of mudstone clasts in a sand unit with uniform grain size. (*A*) Blocky log motif may be caused by a uniform vertical distribution of mudstone clasts. (*B*) Bell-shaped or fining-up log motif may be caused by an upward increase in mudstone clasts (see Fig. 6.44). (*C*) Coarsening-up log motif may be caused an upward decrease in the amount of mudstone clasts.

(2) Walker (1992a, p. 263) also abandoned his general-fan model by stating, '*A submarine fan model of the channel-depositional lobe type, influential in its time, but now obsolete because it ignored external controls, especially sea level fluctuations*.'

(3) Mutti (1992, p. 10) also concluded that '*In reality, there are no general models available at present which can describe and interpret the variety of depositional systems observed in modern and ancient deep-water basins*.'

(4) The conceptual basin-floor fan model, characterized by mounded seismic facies, predicts sheet-like turbidite sands (Vail et al., 1991). However, Shanmugam et al. (1995a) documented that turbidites are extremely rare in these mounded features. Whereas features identified as basin-floor fans may occur at specific and predictable stratigraphic positions within a depositional package and produce characteristic seismic facies and reflection patterns on seismic data, core study indicates that basin-floor fans do not represent specific depositional facies (e.g., turbidites) and geometries (i.e., sheet-like) as the model predicts. Seismic mound models (e.g., basin-floor fan) are obsolete because they are based on the now defunct suprafan-lobe model.
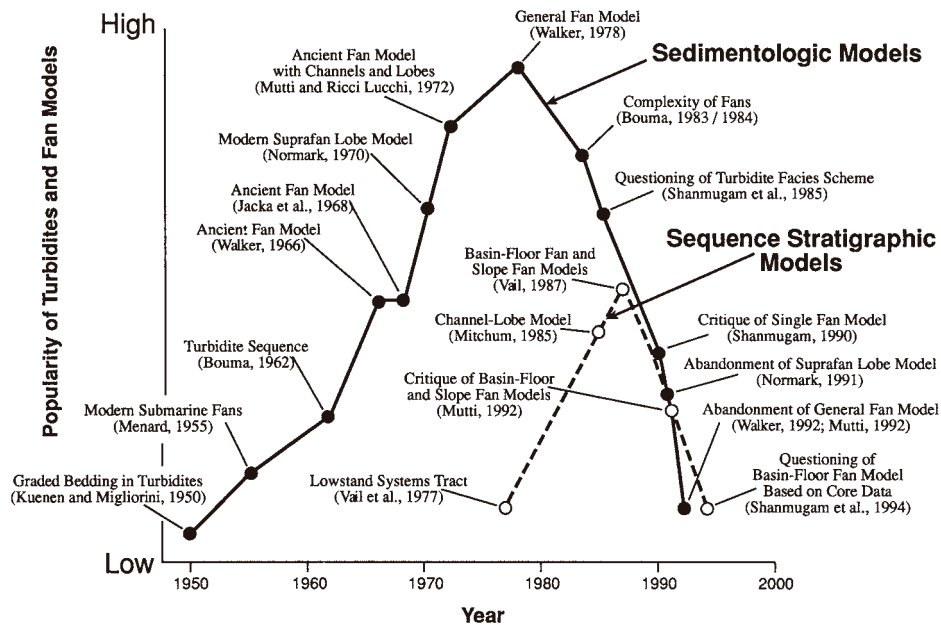
Fig. 10.26. Rise and fall of submarine fan models in sedimentology and sequence stratigraphy. (After Shanmugam (2000a). Reproduced with permission from Elsevier.)

10.7 Synopsis

Seismic profiles and wireline logs, the primary source of data in frontier areas of exploration, are unreliable for practicing process sedimentology. The popularity of sedimentologic and sequence-stratigraphic fan models escalated in the 1970s and 1980s, but declined to the point of abandonment in the 1990s (Fig. 10.26).

Chapter 11

Tectonic and eustatic controls

11.1 Introduction

The objective of this chapter is to review basin-scale tectonic and eustatic controls of deep-water sedimentation. This broader perspective is necessary for under-standing deep-water systems as a whole, even though this book is focused on small-scale depositional processes and products.

11.2 Tectonic control

Classifications of deep-water systems, based on tectonic settings, are the following:

(1) Barnes and Normark (1985) grouped modern and ancient deep-water systems under two broad tectonic categories, namely, active (accretionary, transform, and subduction) and passive margin settings.
(2) Pickering et al. (1989) discussed continental margins under: (a) evolving and mature passive margins; (b) active convergent margins; and (c) oblique slip margins.
(3) Shanmugam and Moiola (1988) classified deep-water systems into four basic types: (a) immature passive margin (North Sea type); (b) mature passive margin (Atlantic type); (c) active margin (Pacific type); and (d) mixed setting (Bay of Bengal type). The immature passive margin type (e.g., Balder Fan, North Sea), which represents an early stage of basin evolution on a divergent margin, is characterized by proximal source, narrow shelves, high gradients, high sand/mud ratios, and small basins (Fig. 11.1). Deep-water lakes have been associated with early rift phases of immature passive margins. The mature passive margin type is characterized by distal source, wide shelves, low gradients, low sand/mud ratios, and large basins (e.g., Amazon Fan, Atlantic Ocean). Characteristics of active margin type, such as the Hecho Group in Spain, are the same as immature passive margin type. The mixed type is necessary to classify deep-water systems that cannot be readily
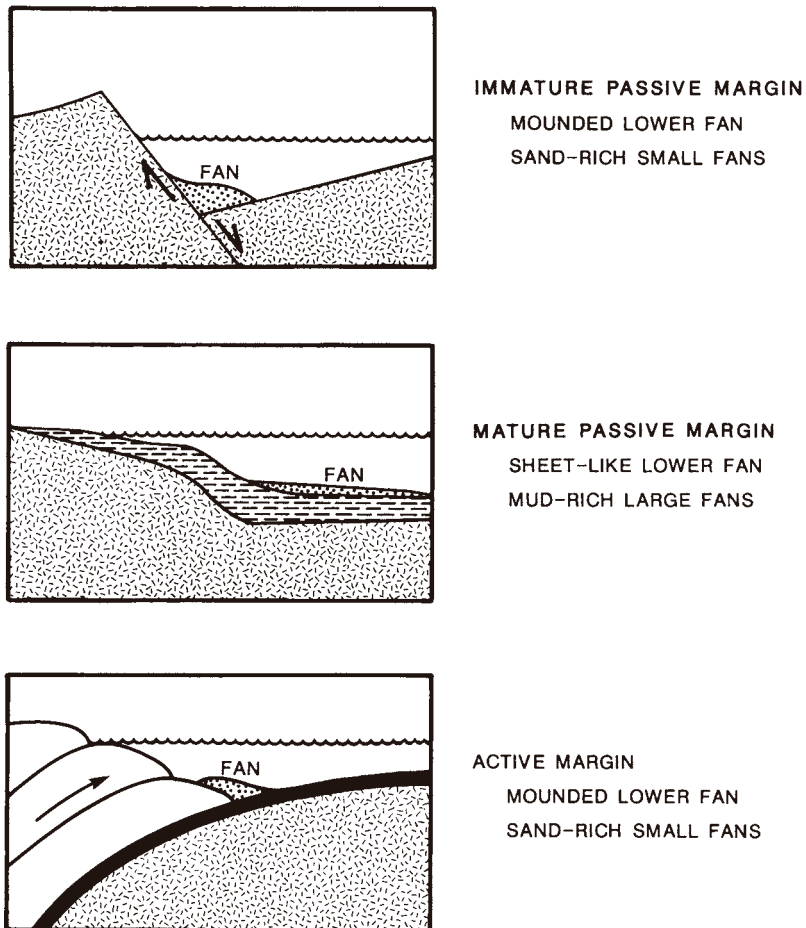
Fig. 11.1. Three common types of tectonic settings for deep-water systems. Sediment source from left. (After Shanmugam and Moiola (1988). Reproduced with permission from Elsevier.)

grouped into one of the above three types. An example is the Bengal Fan in the northeastern Indian Ocean. This fan is bounded by both active and passive margins.

11.2.1 Continental collision

The Bengal Fan, located in the Bay of Bengal, is the largest submarine fan in the world. This fan has a length of 3000 km (Fig. 11.2), a width of 1000 km, and a maximum thickness of 16.5 km (Curray et al., 2003). The Bengal Fan formed as a direct result of the India–Asia collision and uplift of the Himalayas and
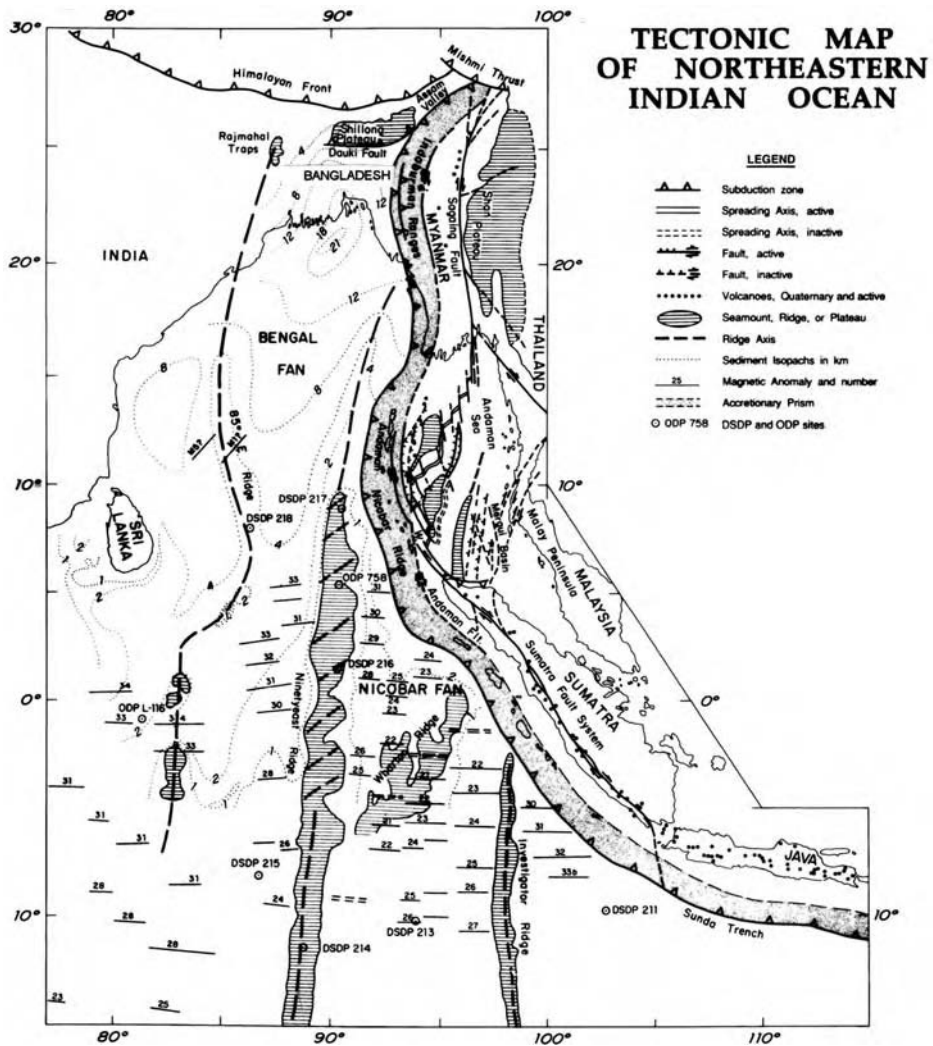
Fig. 11.2. Tectonic map showing the location of the Bengal Fan in the Bay of Bengal region, northeastern Indian Ocean. (From Curray et al. (2003). Reproduced with permission from Elsevier.)

the Tibetan Plateau. The fan is currently supplied mainly by the Ganges and Brahmaputra Rivers, with smaller contributions of sediment from several other large rivers in Bangladesh and India.

The Bay of Bengal was created by the initial Paleocene–Eocene collision of India with the subduction zone of the north side of the Tethys Ocean (Curray and Moore, 1971, 1974; Curray et al., 1982; Alam et al., 2003). Prior to collision, a thick, continental rise prism of sediment had formed off the eastern margin of India.

Rapid clastic sedimentation in the Bengal Basin, and fan formation on top of this continental rise began during continuing collision in the Eocene and prograded southward during the Tertiary. At the present time, there is only one active channel.

The western margin of the Bengal Fan is the continental slope of eastern India. The northern proximal fan lies off the Bangladesh continental slope. The eastern margin is the northern end of the Sunda trench. The accretionary prism of the Sunda Subduction Zone extends from Myanmar (Burma) through the Andaman–Nicobar Ridge into the Mentawai Islands off Sumatra (Fig. 11.2). Much of the Bengal Fan sediment has been subducted and/or uplifted into this accretionary prism.

The Zunda Subduction Zone is tectonically active. Its activity was exemplified by the Indian Ocean Earthquake, which occurred on December 26, 2004 at 00:58:53 UTC (Coordinated Universal Time) off the western coast of northern Sumatra, Indonesia. It had a magnitude of 9.0. The earthquake was unusually large in geographical extent. An estimated 1200 km of faultline slipped 20 m (60 ft) along the subduction zone where the India Plate dives under the Burma (Myanmar) Plate. The seabed of the Burma plate is estimated to have risen as much as five meters vertically up over the India plate, creating tsunami waves in the Indian Ocean that traveled at up to 800 km/h (see Chapter 5).

Using cores taken from the ODP Leg 116 on the distal Bengal Fan, Stow et al. (1990) discussed sediment facies and processes. The most dominant facies is muddy turbidites. Neither DSDP nor ODP cores recovered sandy intervals from the Bengal fan. This is puzzling because the Ganges and Brahmaputra Rivers, the two principal sources of sediment for the Bengal Fan, are sandy rivers (Coleman, 1969). Possible explanations for the enigma are: (1) the DSDP and ODP Sites are too distal to encounter sandy intervals, or (2) sands are restricted to isolated tongues of debris flows that have not yet been cored.

11.2.2 Folding and basin topography

In unconfined environments, turbidity currents generate radial or fan-shaped lobes. In tectonically active confined basins, however, regional basin topography controls spatial sand distribution. In the San Joaquin Basin, for example, Scott and Tillman (1981) suggested two models for the Miocene Stevens Sandstone, California: (1) the 'on-lap' model in which sandbodies lap on to a rising anticline (Fig. 11.3); and (2) the 'confinement' model in which sandbodies accumulate in a synclinal low between anticlinal highs (Fig. 11.4).

11.2.3 Salt tectonics and sea-floor topography

During the Tertiary in the northern Gulf of Mexico, principal factors that controlled sea-floor topography in intraslope minibasins were: (1) salt tectonics;

Stevens Sandstone (Miocene)
San Joaquin Basin, California

"On-Lap" Model
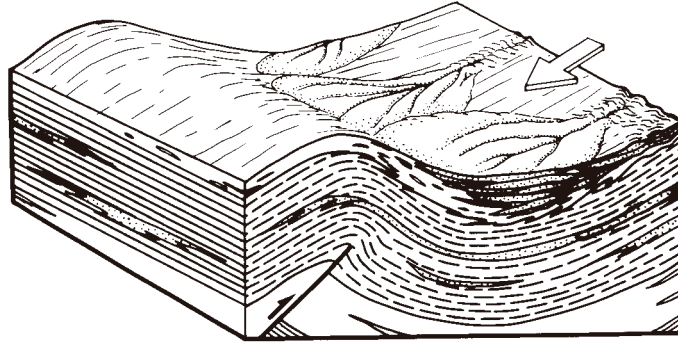
(Scott and Tillman, 1981)

Fig. 11.3. 'On-Lap' model showing sandbodies that lap onto structural highs. Note structural grain is perpendicular to sediment-transport direction and vertical stacking of sandbodies. Stevens Sandstone, Miocene, San Joaquin Basin, California. (After Scott and Tillman (1981). Reproduced with permission from SEPM.)

Stevens Sandstone (Miocene)
San Joaquin Basin, California

"Confinement" Model
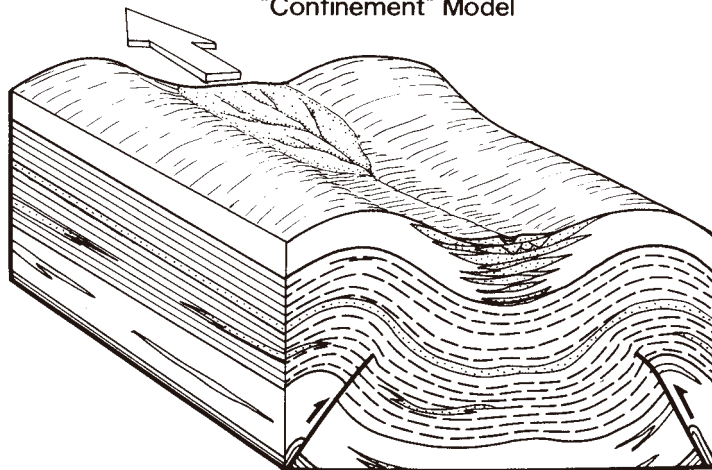
(Scott and Tillman, 1981)

Fig. 11.4. 'Confinement' model showing accumulation of sandbodies in a structural low. Note structural grain is parallel to sediment-transport direction. Stevens Sandstone, Miocene, San Joaquin Basin, California. (After Scott and Tillman (1981). Reproduced with permission from SEPM.)

(2) compression; and (3) strike slip along thin-skinned transfer zones (Apps et al., 1994). Among these, salt withdrawal and diapirism have been particularly important in controlling shape and relief of sea-floor topography of the modern continental slope of the Gulf of Mexico. The importance of slides, slumps, and debris flows caused by salt movements in the Beaumont Basin has been discussed earlier (see Chapter 6).

11.2.4 Fault-controlled sedimentation

The Yallahs Basin in southeastern Jamaica, at a depth of 1300 m, contains 500 m of sediments (Burke, 1967). This basin is structurally controlled and fault bounded. Near the eastern margin of the basin, the Yallahs submarine canyon appears to be controlled by a major fault (Fig. 11.5). Burke (1967, his Fig. 3) reported that the basin received its sediment from Yallahs fan deltas, which formed a major submarine fan on the outer edges of the narrow and steep slope. However, the Yallahs River that provides the sediment into this basin is braided (Wescott and Ethridge, 1980), and thus it actually represents a braid delta (McPherson et al., 1987), not fan delta.

Wescott and Ethridge (1980, p. 388) stated, '*Slumping occurs frequently in the heads of the submarine canyons and it is probably the principal process initiating the movement of sediment from the nearshore zone to the Yallahs Basin.*' They also pointed out that (p. 396), '*On the Yallahs-type deltas, coarse sands and gravels are introduced directly on the slope where gravity slides and slumps are the most important process.*'

Thus the Yallahs submarine slopes are considered to be dominated by deposits of slides, slumps, and debris flows in this book (Fig. 11. 5).

11.3 Eustatic control

Global changes in sea level are controlled primarily by tectonism and glaciation (Fig. 11.6) (Russell, 1968; Valentine and Moores, 1970; Vail et al., 1977; Pitman, 1979). Glaciation is considered to be the only mechanism capable of causing relatively rapid fluctuations (more than 1 cm/1000 years) in sea level (Vail and Hardenbol, 1979). Short-term rapid fluctuations in sea level appear to be related to glaciations and long-term gradual fluctuations in global sea level appear to be controlled by changes in mid-oceanic ridge volume (spreading rate) (Fig. 11.6), subsidence of the continental margin, and sediment compaction. Changes of intraplate stress-fields caused by changing plate movements have also been considered to be a cause for sea-level fluctuations (Cloetingh, 1986).

The primary factor in the development of submarine fans is global lowering of sea level (Damuth and Fairbridge, 1970; Shanmugam and Moiola, 1982, 1984; Shanmugam, et al., 1985b). The term 'fan' is used here to represent deep-water systems and it does not have any process connotation (i.e., turbidity current).
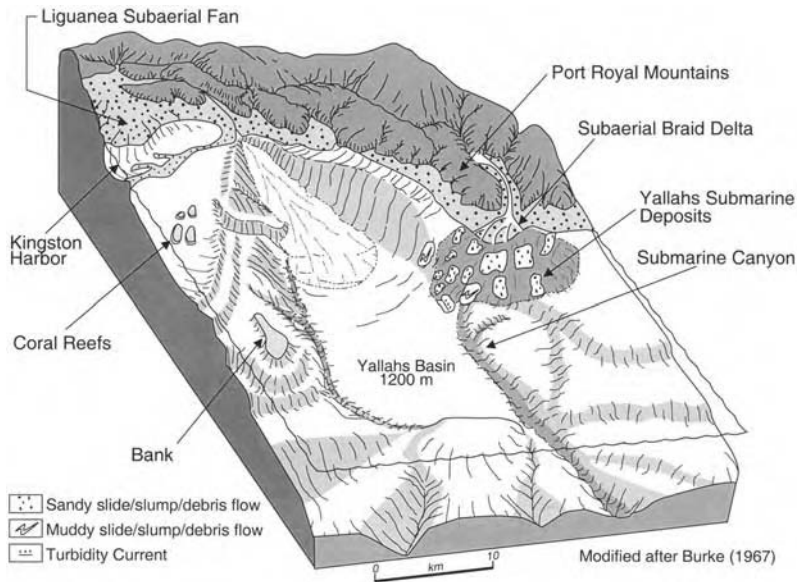
Fig. 11.5. A slope model of the Yallahs Basin, SE Jamaica showing subaerial braid delta and subaqueous dominance of slides and slumps on the Yallahs submarine slopes. The Yallahs deepwater system is unsuitable to be classified as a conventional submarine fan with turbidites. The Yallahs submarine canyon near the eastern basin margin appears to be controlled by a major fault. (Modified after Burke (1967). Reproduced with permission from Elsevier.)
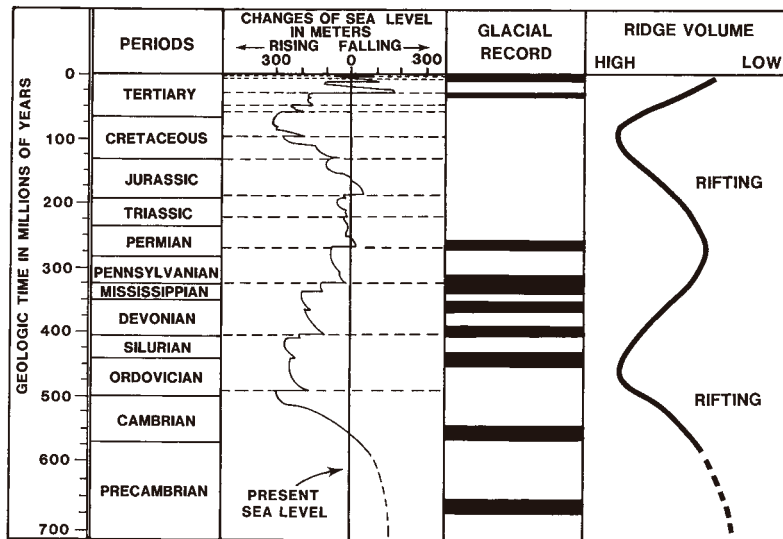
Fig. 11.6. Comparison of global changes in sea level, glacial record, and mid-oceanic ridge volume. (After Shanmugam and Moiola (1982). Reproduced with permission from Geological Society of America.)

The global sea-level curve of Vail et al. (1977), also referred to as the coastal onlap curve (Vail and Todd, 1981), is used here as a standard reference because of its coverage of the entire Phanerozoic. A refined sea-level curve for the Mesozoic and Cenozoic intervals has been presented by Haq et al. (1987).

During the last few million years, sedimentation and growth of most modern submarine fans have been controlled by Plio-Pleistocene glacioeustatic sea-level fluctuations. During the relatively short (5000–20000 years) interglacial phases such as the Holocene, recession of continental glaciers has caused sea level to rise above its present level. Highstands moved the locus of river sedimentation landward. The great width and low gradient of most shelves generally restricted river deposition to deltas on the innermost shelf, and the large volumes of terrigenous sediment needed to build submarine fans could not reach the continental slope or rise (Fig. 11.7). Hence, fan development was temporarily halted or diminished greatly during highstands of sea level. In contrast, during glacial phases such as the Wisconsin, sea level was lowered 40–150 m below the present level. Most continental shelves became emergent, and rivers discharged their sediment loads directly into the heads of submarine canyons at or near the shelf break (Damuth, 1977). Thus large quantities of terrigenous sediment were transported to the deep sea *via* gravity-driven processes, and submarine fan development was greatly accelerated (Fig. 11.7). This scenario is perhaps more representative of passive-margin settings where wide coastal plains and shelves are affected dramatically during low sea level. DSDP core data from the passive-margin Mississippi fan indeed demonstrate that the 'nondecompacted' rate of sedimentation was extremely high during low sea level (600–1100 cm/1000 years) but low (2–13 cm/1000 years) during high sea level (Fig. 11.8).

Exceptions to the above trend occur because in certain active-margin settings, tectonic uplift exerts a major control on sediment yield and on fan growth (Klein, 1984, 1985a). For example, in two submarine fans of the western Pacific (an unnamed fan at DSDP Site 210 and Toyama 'fan' at DSDP Site 299), turbidite deposition has been correlated with periods of tectonic uplift (Klein, 1985b). In island-arc settings, coastal plains and shelves are narrow, and sediment is transported directly into deep water. In certain arc systems (e.g., the northern Middle America Trench, DSDP Leg 66) where an abundant source of terrigenous detritus is available, large submarine canyons funnel coarse clastics directly to the trench floor, effectively bypassing depositional sites even along the lower slope (Underwood and Karig, 1980). In such cases, eustatic control of fan growth may be overshadowed by tectonic control.

In general, most modern fans of active margins (Astoria, Navy, Coronado, and Monterey), mature passive margins (Amazon and Mississippi), and mixed settings (Bengal and Indus) exhibit accelerated growth during periods of low sea level associated with Pleistocene glacials. These fans, however, were dormant during the Holocene and during previous interglacials (periods of high sea level).

HIGH SEA LEVEL
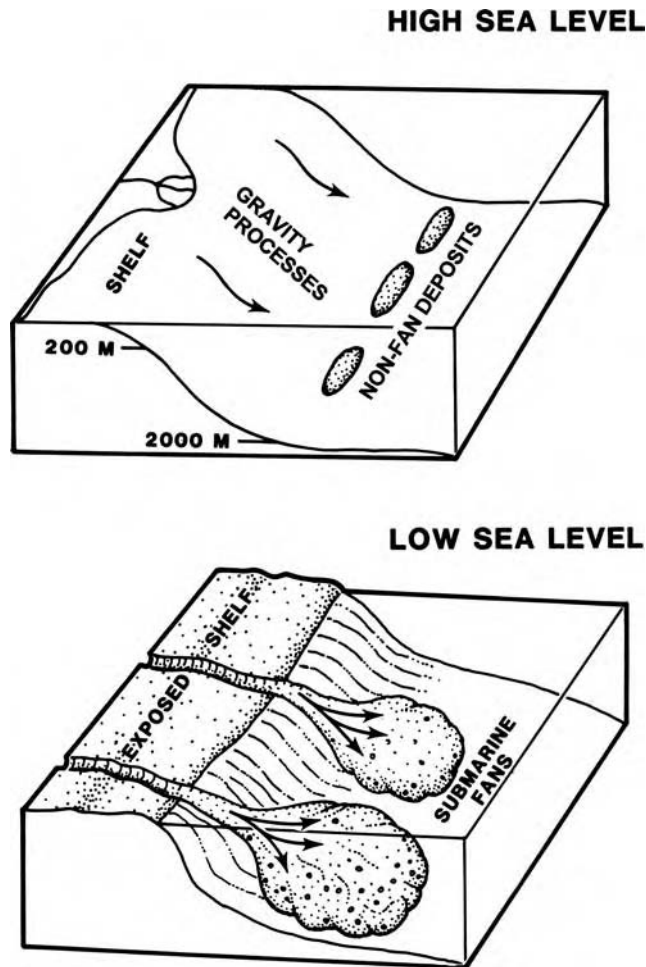
LOW SEA LEVEL

Fig. 11.7. Eustatic sea level models showing development of submarine fans during periods of low sea level and non-fan deposits during periods of high sea level.(After Shanmugam and Moiola (1988). Reproduced with permission from Elsevier.)

In most tectonic settings, therefore, the development of a submarine fan is influenced primarily by lowstands of sea level.

The following hydrocarbon-bearing submarine-canyon and fan deposits, which all correlate with periods of low sea level, occur on both active- and passive-margin settings: (1) the Pennsylvanian (Atokan) Red Oak Sandstone, Oklahoma; (2) the Lower Permian Cook Channel of the Jameson Field, Texas; (3) the Upper Cretaceous Woodbine-Eagle Ford Interval, Texas; (4) the Paleocene sequence of Forties and Montrose Fields, U.K. North Sea; (5) the Paleocene Balder Field,
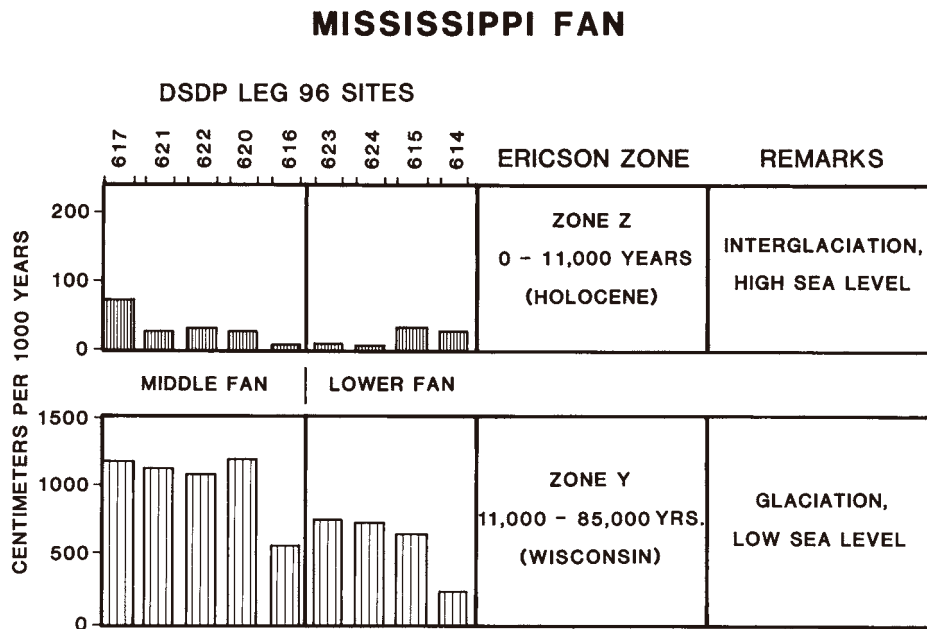
MISSISSIPPI FAN

Fig. 11.8. Histograms showing high sedimentation rates during periods of low sea level in the Mississippi Fan. (Compiled from Kohl et al. (1985), Shanmugam and Moiola (1988). Reproduced with permission from Springer-Verlag.)

Norwegian North Sea; (6) the Paleocene Cod Fan, Norwegian North Sea; (7) the Lower Eocene Yoakum Channel, Texas; (8) the Lower Eocene sequence of the Frigg Field in the North Sea; (9) the Upper Oligocene Lower Hackberry Sandstone in Texas; (10) the Upper Oligocene Puchkirchen Formation in Austria; (11) the Upper Miocene Stevens Sandstone of southeastern San Joaquin Valley, California; (12) the Upper Miocene Puente Formation of Wilmington Field, California; (13) the Lower Pliocene Repetto Formation of Ventura Field, California; and (14) the Pleistocene Mississippi Canyon, Louisiana (Fig. 11.9).

During highstands of sea level, major fans fail to grow significantly because of limited sediment yield into the deep sea caused by trapping of land-derived sediment on shelves. Only infrequent, generally minor gravity flows reach the deep sea where they mantle previously developed lowstand fans. These infrequent flows form a non-fan (starved) sequence (Fig. 11.10). A non-fan sequence is characteristically non-cyclic (Fig. 11.10). In the modern Atlantic, turbidite sand layers of non-fan affinity have been described by Pilkey et al. (1980). In the southwestern part of the Madeira Abyssal Plain, turbidites have been reported to have developed during periods of both regression and transgression (Weaver and Kuijpers, 1983).
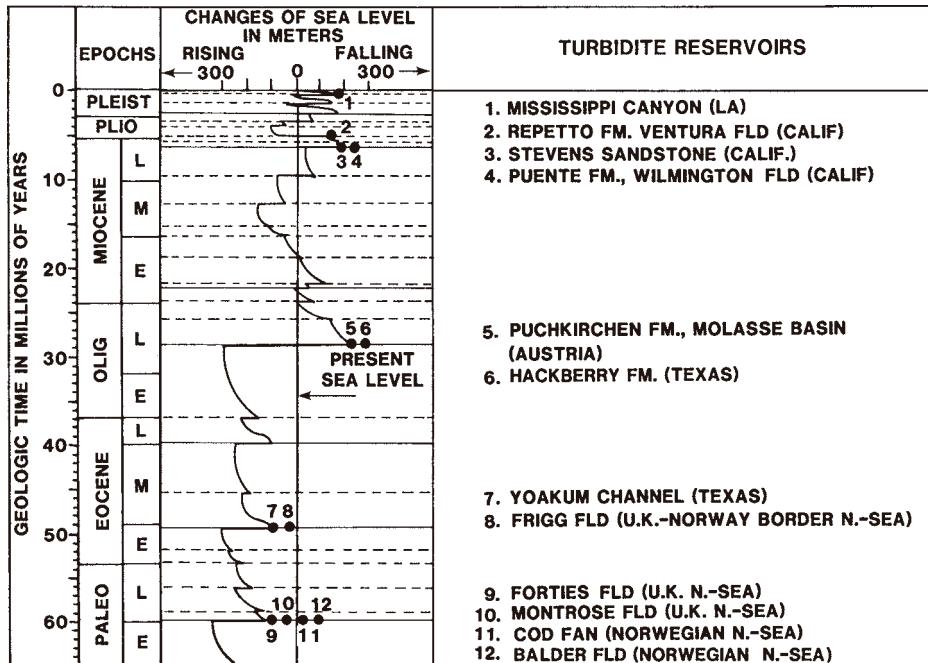
Fig. 11.9. Correlation of hydrocarbon-bearing submarine canyon and fan deposits with periods of low sea level. (After Shanmugam and Moiola (1988). Reproduced with permission from Elsevier.)
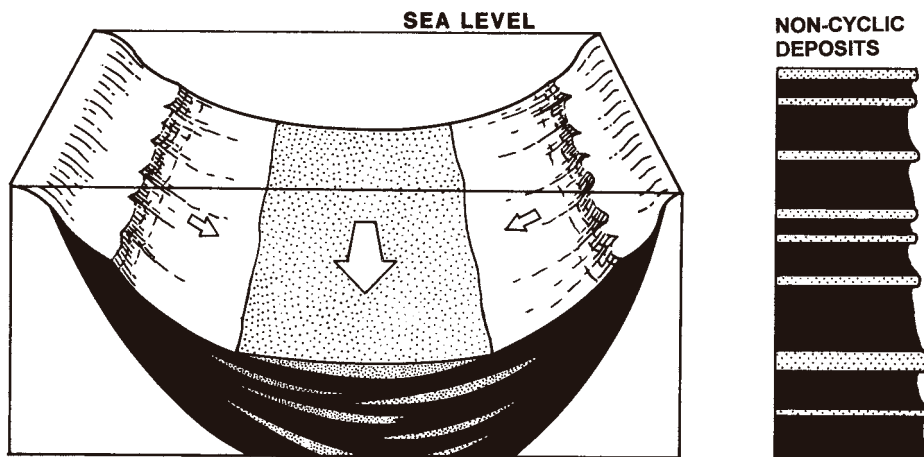
Fig. 11.10. Development of non-fan deposits during periods of high sea level. Note characteristic non-cyclic depositional patterns.

Although sandy fans tend to be dormant during highstands of sea level, hemipelagic sediments continue to be deposited. Thus hemipelagic sediments may drape the entire sandy fan forming an effective hydrocarbon seal. Such a seal appears to mantle the Balder field of the North Sea. Here shale occurs as a hemipelagic drape above the entire suprafan complex (Sarg and Skjold, 1982). Such mud drapes commonly form the seals associated with stratigraphic traps.

11.4 Synopsis

Active-margin settings and lowstands of sea level are conducive to deposition and preservation of deep-water fans. Highstands of sea level are periods of non-fan sequences and stratigraphic seals.

Chapter 12

Implications for sandstone petroleum reservoirs

12.1 Introduction

The objective of this chapter is to summarize the implications of deep-water processes and environments for sandstone reservoirs in terms of: (1) grain-size distribution; (2) spatial distribution of sand; (3) dimensions and geometries of sandbodies; (4) lateral changes in sediment thickness; (5) reservoir heterogeneity; (6) sand injection and reservoir communication; (7) correlation of sandbodies; (8) depositional mud matrix; (9) reservoir quality; and (10) depositional models.

12.2 Grain-size distribution

Grain-size data from modern and ancient deep-water systems show that depositional processes directly control grain-size distribution (Fig. 12.1). Slides, slumps, and debris flows have the strength to transport particles of any size for long distances. Turbidity currents, on the other hand, cannot transport large particles for long distances in suspension because they lack the strength. Experiments have shown that turbidity currents composed of pure sand (medium to coarse grained) without the fines tend to collapse soon after initiation (Shanmugam, 2000a). Turbidity currents are capable of transporting mainly mud and very fine-grained sand in suspensions. Thus, true turbidites are composed of fine-grained sandstone and mudstone, whereas sandy debrites are composed of pebbly sandstone and coarse- to medium-grained sandstone. Depositional processes directly influence reservoir quality. This is because grain size and sorting control porosity and permeability (Beard and Weyl, 1973).

12.3 Spatial distribution of sand

The spatial distribution of sandbodies in deep-water environments are controlled by depositional processes (e.g., slides, slumps, debris flows, turbidity currents,
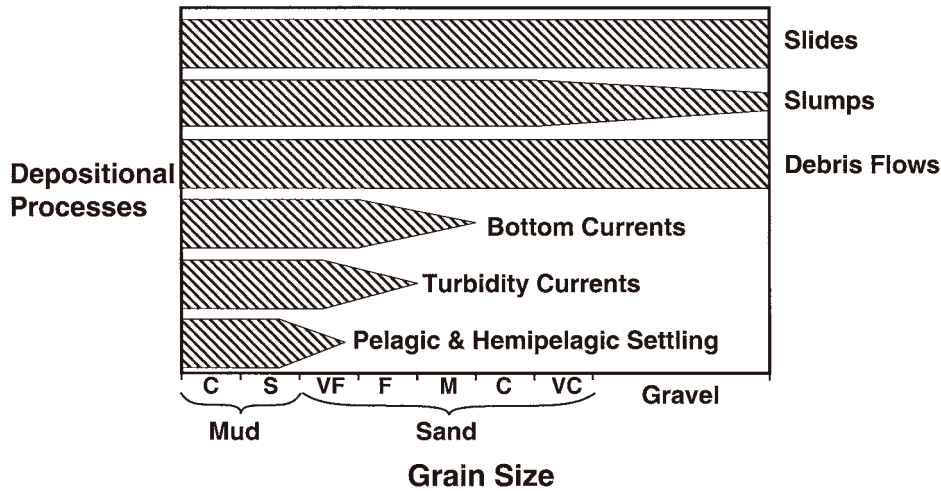
Fig. 12.1. Generalized grain-size distribution in deposits of different processes based on core and outcrop descriptions worldwide. Note slides, slumps, and debris flows have coarse-grained sediment because of their strength to carry large particles, whereas turbidity currents do not have coarse-grained sediment because of their lack of strength to transport coarse sediment in turbulent suspension.

bottom currents, etc.), depositional elements (e.g., channels, lobes, basin floor, etc.), and sea-floor topography (e.g., irregular, smooth, etc.). An evaluation of modern deep-water systems shows a dominance of deposition by *sandy debris flows* and related mass-transport processes in slopes, canyons, channels, lobes, and basin-plain environments (Fig. 6.48).

12.3.1 Turbidity currents *versus* debris flows

Flume experiments have shown a clear contrast between the distribution of turbidites and debrites in plan view. Because of their Newtonian rheology, turbidity currents flow freely as they exit a channel and spread out laterally. In channel-mouth environments, turbidity currents result in a fan-shaped sediment body called lobes (Fig. 12.2). Debris flows, on the other hand, when released from a flume channel formed tongue-like patterns (Fig. 12.3). Lobes show gradual increase in width downdip, whereas tongues maintain more or less the same width. Although some debris flows may develop small-scale lobate terminus (Allen, 1985a, his Fig. 9.28a), they are not comparable to large-scale turbidite lobes. Debris tongues are products of individual events. When multiple events coalesce, however, their geometry may be more complex than simple tongues.

The tongue-like patterns of debris flows are part of non-fan systems. Debris tongues have sharp and irregular fronts (i.e., snouts) due to freezing. Debris tongues have been mapped on the modern slopes of Gulf of Mexico (Fig. 6.10) and on the
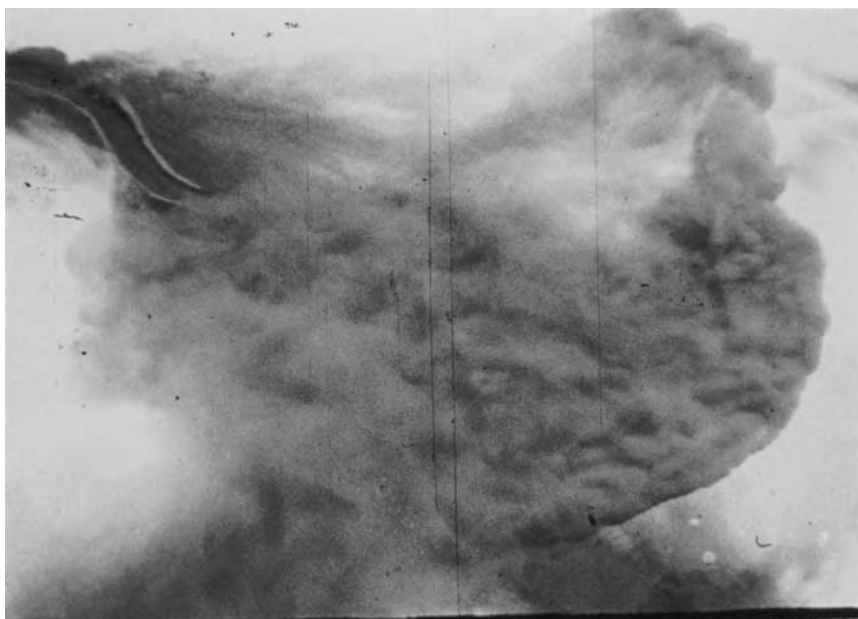
Fig. 12.2. Flume experiments of turbidity currents showing fan-shaped outline of the flow as it spreads out at the channel mouth. Flow from upper left to lower right. (Photo from experiments conducted by M. L. Natland, and courtesy of G. C. Brown.)

Fig. 12.3. Flume experiments of debris flows showing tongue-like sediment (arrows) in front of the channel mouth. Note sharp and irregular fronts (i.e., snouts). Flow from upper right to lower left. (Photo courtesy of J. Marr (St. Anthony Falls Laboratory, University of Minnesota).)
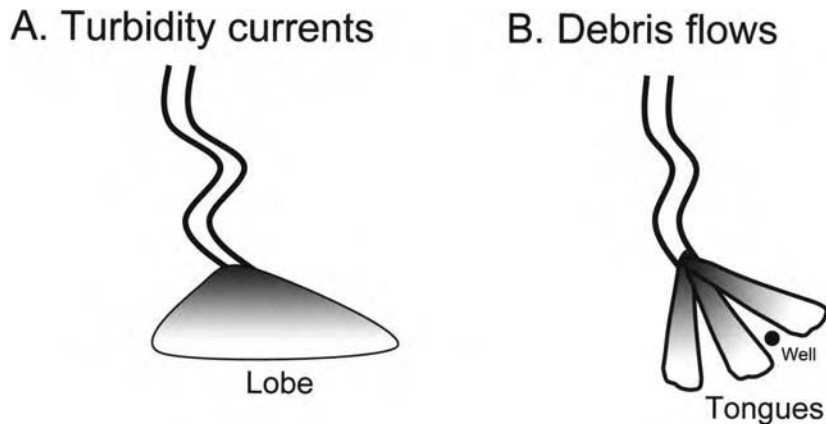
Fig. 12.4. Contrasting styles of deposition between turbidity currents and debris flows.
(*A*) Fan-shaped (i.e., lobe) distribution of fine-grained sand by turbidity currents in channel-mouth environments (see Fig. 12.2). (*B*) Tongue-like (non-fan) distribution of sediment by debris flows in channel-mouth environments (see Fig. 12.3). If the petroleum industry were to consider only the turbidite lobe model, there is a risk of drilling the mud-prone areas in between two sandy debrite tongues (solid dot).

Norwegian–Barents Sea Continental Margin (Fig. 6.42). The Saharan debris flow in the Atlantic Ocean, showing tongue-like distribution, has a thickness of 25 m. The basal 2.5 m is composed of a sandy debrite (Gee et al., 1999).

To predict reservoir-sand distribution in frontier areas of hydrocarbon exploration, the contrasting styles of sand distribution by turbidity currents (fan) *versus* debris flows (non-fan) must be considered (Fig. 12.4). If we were to apply the turbidite fan model invariably in frontier areas of exploration, we would predict widespread turbidite lobe sands in basinal areas (Fig. 12.4A). However, if debris flows were to control sand deposition in the area of interest then our prediction of lobe sand would be in error. This is because sand would be restricted to the tongues and the intervening areas would be composed of mud (Fig. 12.4B).

Sandy turbidity currents may also bypass channel areas and may deposit the entire sediment load as sandy lobes (Fig. 12.5A). In such cases, the channels may be filled with mud. The other possibility is surface flow transformation of sandy debris flows into muddy turbidity currents. In such cases, deposition of muddy turbidite lobes would occur in front of sandy debrite tongues (Fig. 12.5B). These possibilities are generally ignored by the petroleum industry.

12.3.2 Turbidity currents *versus* bottom currents

In the Ewing Bank area, Gulf of Mexico, most of the cored interval of nearly 180 ft (55 m) represents primarily deposits of bottom currents (see Chapter 4). Individual sand layers within the package are thin and discontinuous (Fig. 12.6), but this sediment package may be laterally continuous in the study area.
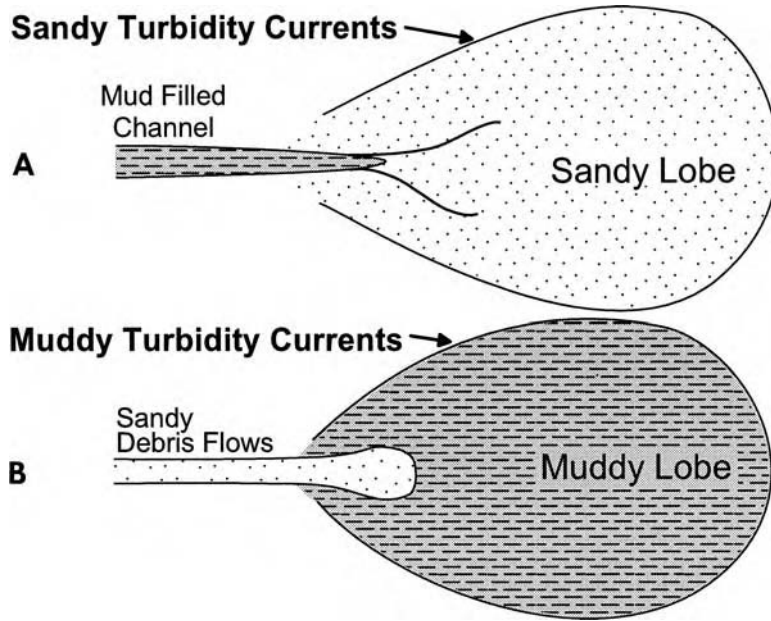
Fig. 12.5. Contrasting styles of deposition between turbidity currents and debris flows. (*A*) Fan-shaped (i.e., lobe) distribution of fine-grained sand in front of the channel mouth as sandy lobe by turbidity currents. Note channel is filled with mud because of sand bypassing of the channel. (*B*) Tongue-like pattern of sand deposited by debris flows with muddy turbidite lobe in front because of surface flow transformation of debris flows into turbidity currents.
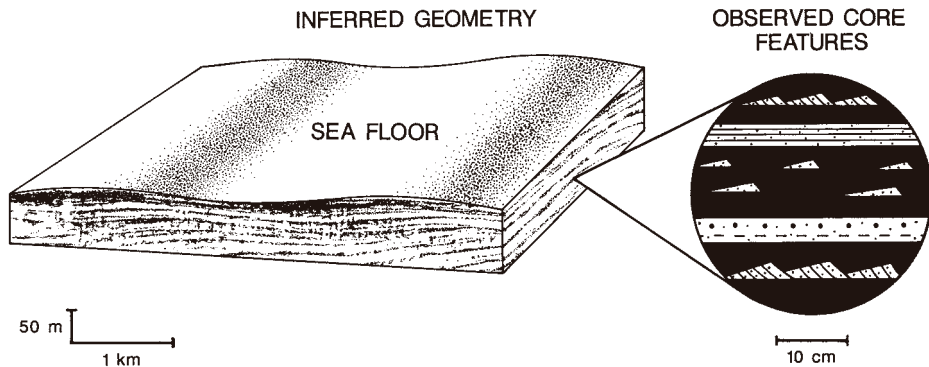
Fig. 12.6. Conceptual model of bottom-current reworked sediment showing laterally continuous large-scale sediment body (seismic scale) composed of small-scale discontinuous sand layers (core scale). (After Shanmugam et al. (1993a). Reprinted by permission of the American Association of Petroleum Geologists whose permission is required for further use.)
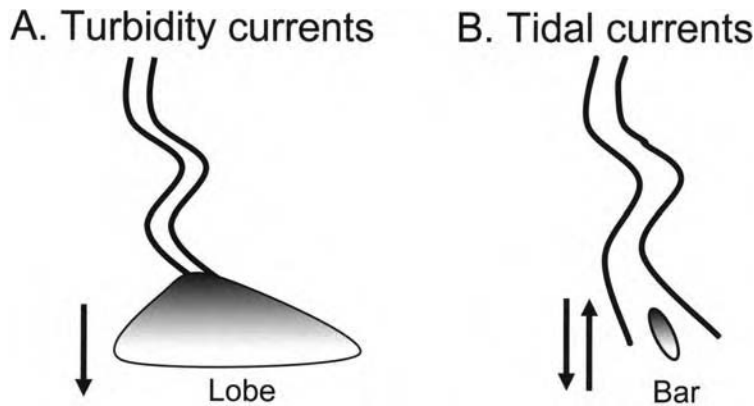
Fig. 12.7. Contrasting styles of deposition between turbidity currents and tidal currents in deep-water channel-mouth environments. (*A*) Turbidite lobes at the channel mouth are aligned perpendicular to channel axis. Lobes are larger than channel width. Sediment transport is unidirectional (arrow). (*B*) Deep-marine tidal deposits develop elongate bars within the channel. Bars are aligned parallel to channel axis. Tidal bars are smaller than channel width. Sediment transport is bidirectional (arrows). (After Shanmugam (2003). Reproduced with permission from Elsevier.)

Misinterpretation of deep-marine tidal deposits as 'turbidites' has important implications. For example, interpretation of climbing ripples as levee turbidites implies deposition outside submarine channels, whereas interpretation of the same climbing ripples as deep-marine tidal deposits implies deposition inside submarine canyons or channels.

In channel-mouth environments, downslope turbidity currents are likely to develop depositional lobes (Fig. 12.7A), whereas bi-directional tidal bottom currents are likely to develop elongate bars (Fig. 12.7B). Turbidite lobes are aligned perpendicular to channel axis, whereas tidal bars are aligned parallel to channel axis. Depositional lobes are likely to be much larger than channel width (Fig. 12.7A), whereas tidal sand bars are thought to be much smaller than channel width (Fig. 12.7B). Deep-water elongate tidal bars are speculated to be analogous to tidal bar sands that develop in shallow-water estuarine environments (see Shanmugam et al., 2000). In frontier exploration areas, an incorrect use of a turbidite-lobe model (with sheet geometry) instead of a tidal bar model (with bar geometry) will result in an unrealistic overestimation of sandstone reservoirs.

12.3.3 River-sourced fans *versus* ice-sheet sourced systems

In river-sourced systems, such as the Mississippi Fan in the Gulf of Mexico (Nelson et al., 1992), channel-mouth lobes are present (Fig. 12.8A). In ice-sheet sourced systems, such as the Wilkes Land 'Fan' in Antarctica (Escutia et al., 2000),
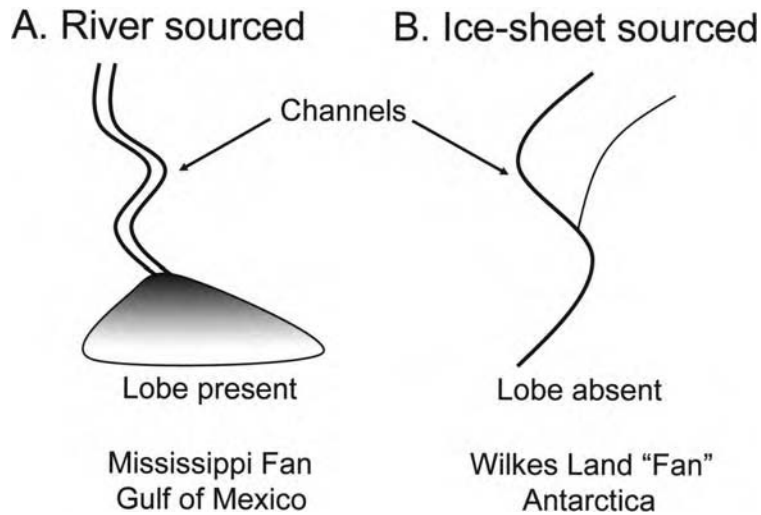
Fig. 12.8. Two contrasting models of deep-water systems. (*A*) River-sourced system with lobes, such as the Mississippi Fan in the Gulf of Mexico (Nelson et al., 1992). (*B*) Ice-sheet sourced system without lobes (non-fan), such as the Wilkes Land in Antarctica (Escutia et al., 2000).

channel-mouth lobes are absent (Fig. 12.8B). In the case of the Wilkes Land, although Escutia et al. (2000) used the term 'fan', this term is inappropriate because a typical fan shape is lacking due to the absence of channel-mouth lobes (Fig. 12.8B). The Wilkes Land system differs from the Mississippi Fan in the following respects:

(1) It is a non-fan system.
(2) It is located in a high-latitude region.
(3) It receives unusually large volume of coarse sediment from fast-moving ice streams.
(4) Its middle and lower fan areas have steeper gradients.
(5) It is subjected to bottom-current reworking.

Because some deep-water systems develop channel-mouth lobes and some do not, downdip prediction of reservoir facies is much more challenging than previously thought.

12.4 Dimensions and geometries

The dimension of a sandbody refers to measurement (e.g., length, width, thickness, etc.) in a single direction, and the geometry of a sandbody refers to three dimensional relationships in space. Data on vertical (thickness) and lateral (width/length/diameter) dimensions of deep-water facies have been compiled for both modern and ancient systems (Table 12.1).

Table 12.1 Dimensions of deep-water facies

Example	Width:Thickness Ratio (observed dimensions)
Slide, Lower Carboniferous, England (Gawthorpe and Clemmey, 1985)	**7:1** (100 m wide/long, 15m thick)
Slide, Cambrian–Ordovician, Nevada (Cook, 1979)	**30:1** (30 m wide/long, 1 m thick)
Slide, Jurassic, Antarctica (Macdonald et al., 1993)	**45:1** (20 km wide/long, 440 m thick)
Slide, Modern, U.S. Atlantic margin (Booth et al., 1993)	**40–80:1** (2–4 km wide/long, 50 m thick)
Slide, Modern, Gulf of Alaska (Carlson and Molina, 1977)	**130:1** (15 km wide/long, 115 m thick)
Slide, Middle Pliocene, Gulf of Mexico (Morton, 1993)	**250:1** (150 km wide/long, 600 m thick)
Slide/Slump/debris Flow/Turbidite 5000–8000 B. P., Norwegian continental margin (Jansen et al., 1987)	**675:1** (290 km wide/long, 430 m thick)
Slump (Cambrian–Ordovician, Nevada) (Cook, 1979)	**10:1** (100 m wide/long, 10 m thick)
Slump, Aptian–Albian, Antarctica (Macdonald et al., 1993)	**10:1** (3.5 km wide/long, 350m thick)
Slump/slide/debris flow, Lower Eocene, Gryphon Field, U.K., (Shanmugam et al., 1995a)	**21:1** (2.6 km wide/long, 120 m thick)
Slump/slide/debris flow, Paleocene, Faeroe Basin, west of Shetland Islands (Shanmugam et al., 1995a)	**28:1** (7 km wide/long, 245 m thick)
Slump, Modern, SE Africa (Dingle, 1977)	**171:1** (64 km wide/long, 374 m thick)
Slump, Carboniferous, England (Martinsen, 1989)	**500:1** (5 km wide/long, 10 m thick)
Slump, Lower Eocene, Spain (Mutti, 1992)	**900–3600:1** (18 km wide/long, 5–20 m thick)
Debrite, Modern, British Columbia (Prior et al., 1984)	**12:1** (50 m wide/long, 4 m thick)
Debrite, Cambrian–Ordovician, Nevada (Cook, 1979)	**30:1** (300 m wide/long, 10 m thick)
Debrite, Modern, U.S. Atlantic margin (Embley, 1980)	**500–5000:1** (10–100 km wide/long, 20 m thick)
Debrite, Quaternary, Baffin Bay (Hiscott and Aksu, 1994)	**1250:1** (75 km wide/long, 60 m thick)
Turbidite (depositional lobe) Cretaceous, California (Weagant, 1972)	**167:1** (10 km wide/long, 60 m thick)
Turbidite (depositional lobe) Lower Pliocene, Italy (Casnedi, 1983)	**1200:1** (30 km wide/long, 25 m thick)
Turbidite (basin plain) Miocene, Italy (Ricci Lucchi and Valmori, 1980)	**11 400:1** (57 km wide/long, 5 m thick)
Turbidite (basin plain) 16 000 B. P., Hatteras Abyssal Plain (Pilkey, 1988)	**125 000:1** (500 km wide/long, 4 m thick)

12.4.1 Slides and slumps

Examples of submarine slides and slumps reveal that modern slides are an order of magnitude larger than their ancient counterparts (Woodcock, 1979). The modern Storegga Slide on the Norwegian continental margin has a width of 290 km, a thickness of 430 m, and a width-to-thickness ratio of 675:1. From the Ablation Point Formation (Kimmeridgian), exposed in Alexander Island of Antarctica, Macdonald et al. (1993) described a seismic-scale slump sheet (6 km wide and 440 m thick) with a width-to-thickness ratio of 14:1. Individual sandy slide sheets reach a thickness of 50 m and a length of 1000 m (Fig. 12.9).

Thicknesses of slumps and slides vary from 1 to 600 m. Their lateral dimensions (width/length) reach up to 150 km. Width-to-thickness ratios vary from 7:1 to 500:1. Eocene slump deposits, which show sheet-like geometry, have been correlated for more than 18 km in Spain (Mutti, 1992). Not all slump deposits have a sheet-like geometry. Outcrop examples of slumped units usually pinch out within a few meters.

In the Cretaceous of the Norwegian North Sea, abrupt lateral changes in slump thickness have been observed between two adjacent wells separated by a distance

Fig. 12.9. Outcrop photograph showing sheet-like geometry of ancient sandy submarine slides. Ablation Point Formation, Kimmeridgian Alexander Island, Antarctica. Note the large sandstone sheet with rotated/slumped edge (left). Person (arrow) 1.8 m tall. (After Macdonald et al. (1993). Photo courtesy of D. J. M. Macdonald.)

of 29 m (Shanmugam et al., 1994). In outcrops of Antarctica, such abrupt termi-
nations for slide/slump deposits have been observed (Macdonald et al., 1993).
A positive aspect of slump facies is the potential for developing stratigraphic traps.
This occurs when isolated sand bodies deposited by slumps are subsequently
draped by hemipelagic mud, forming a seal (Shanmugam et al., 1994).

12.4.2 Debrites

Distribution of debrites is controlled primarily by depositional freezing. This is
commonly reflected in a lenticular geometry (Fig. 12.10). Using outcrop measure-
ments, Cook (1979) established that debrites are likely to have a width-to-thickness
ratio of 30–50:1. Debrite facies can have width-to-thickness ratios of 500:1 or
more (Table 12.1), generally due to amalgamation of depositional units. The dis-
tribution of debrites within channel environments, however, is controlled by the
configuration of the channel. The thicknesses of debrites commonly range from
1 to 60 m, but unusually thick deposits may occur.

In the Cretaceous Agat Formation in the Saga 35/3-2 well, offshore Norway (see
Chapter 6), the lateral distribution of sandy facies has been inferred using a thickness-
to-width ratio of 1:30–50 for mass-flow deposits. In this model (Fig. 12.11A),
sandstones are clearly disconnected from each other by thick intervening mud-
stones that might act as permeability barriers. In contrast to the 35/3-2 well, the
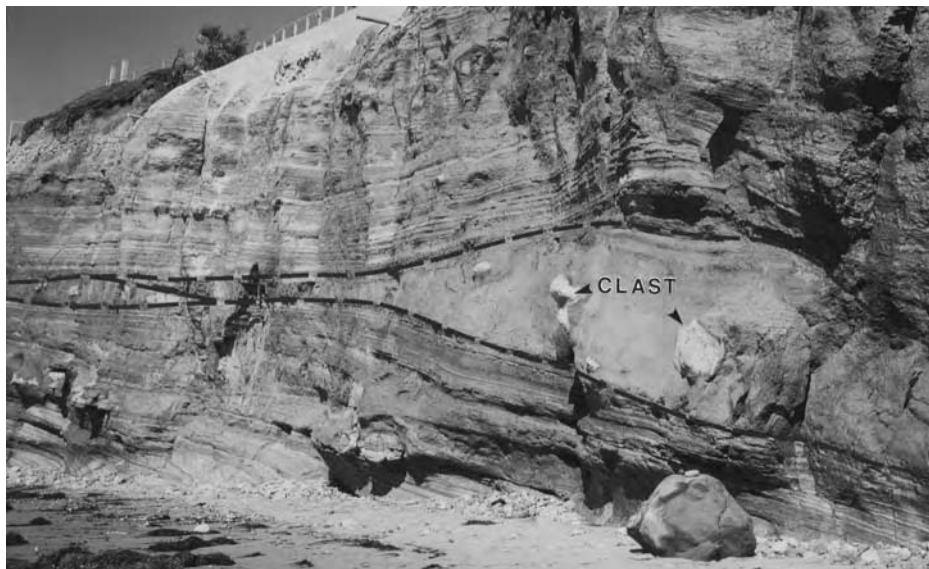
**Fig. 12.10. Outcrop photograph showing lenticular geometry of debrite with floating clasts
(arrowheads). Cretaceous, Tourmaline Beach, California.**
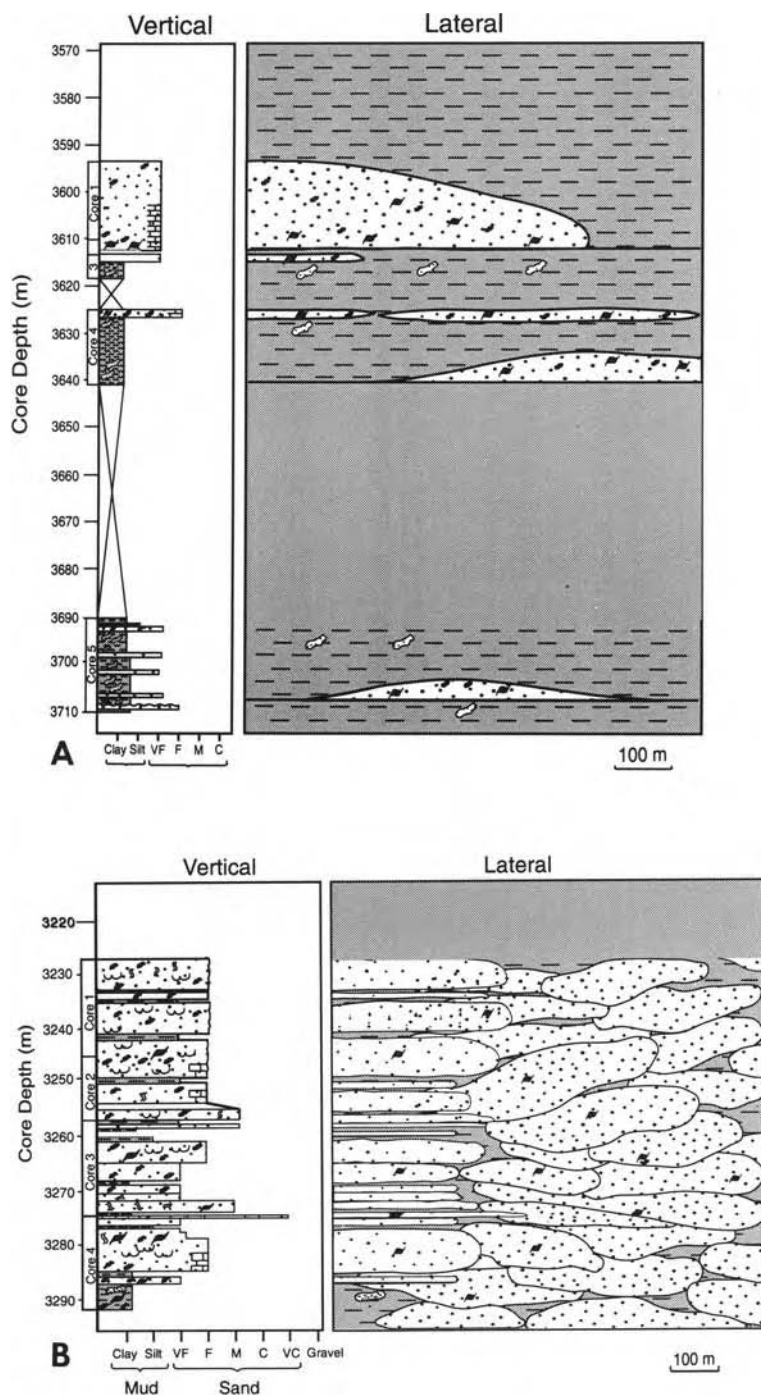
Fig. 12.11. (*A*) Isolated sandstone unit encased in mudstone, Saga 35/3-2 well. (*B*) Amalgamated sandstone package with good lateral and vertical communication, Saga 35/3-5 well. Agat Formation, offshore Norway (see Chapter 6). (From Shanmugam et al. (1994). Reprinted by permission of the American Association of Petroleum Geologists whose permission is required for further use.)

35/3-5 well shows an amalgamation of sandstone units and a lack of interbedded mudstone units (Fig. 12.11B). For example, in the 35/3-2 well the thickest mudstone interval observed in the core is 16 m as opposed to only 0.5 m in the 35/3-5 well (Table 6.3). The amalgamated sandstone units suggest an abundant sand supply and a high frequency of slump/debris flow events. Although slump/debris-flow emplaced sands are generally discontinuous and unpredictable, highly amalgamated slump/debrite sands develop thick reservoirs. Furthermore, sandstone injectites tend to increase connectivity between isolated sand bodies (Shanmugam et al., 1994).

12.4.3 Turbidites

Turbidite lobes show width-to-thickness ratios of about 167:1 to 1200:1 (Shanmugam, 1998). Lateral dimensions of turbidites deposited on modern abyssal plains have been unusually large. The 'Black Shell turbidite' on the Hatteras Abyssal Plain in the western North Atlantic Ocean, for example, is 4 m thick and extends for 500 km (Pilkey, 1988). It has a width-to-thickness ratio of 125 000:1 (Table 12.1) and covers an area of 44 000 km². Classic examples of ancient basin-plain turbidites, exposed along the foreshore at Zumaya, Spain are usually in the range of 10 cm to a meter in thickness, but can be traced for several kilometers (Fig. 12.12). In basin-plain environments, sheet-like geometries of thin-bedded muddy turbidites and pelagites/hemipelagites are the norm.

In the Miocene Marnoso-arenacea Formation, which is interpreted to consist of basin-plain turbidites, a 7-m thick sandstone unit has been traced for over 120 km in the northern Italian Apennines (Ricci Lucchi and Valmori, 1980). Although interpreted as turbidites by Ricci Lucchi and Valmori (1980), this unit has a complex origin judging from large floating mudstone clasts in some sections. Extensive sheet-like turbidites deposited in the open oceans of Atlantic-type margins, however, are seldom preserved in the geologic record.

12.5 Lateral changes in sediment thickness

Westcott and Ethridge (1983, their Fig. 11) proposed a submarine fan model for the Eocene Wagwater Group of Jamaica. In their model, the thick proximal (channelized) fan deposits tend to become thin distal (non-channelized sheet) fan deposits. This lateral thinning of fan deposits was originally proposed for turbidite fan deposits (Bouma, 1962; Mutti, 1977). However, care must be exercised in such generalizations because differences in depositional processes and settings can create wide variations in lateral thickness of individual beds.

In unconfined environments, deposits of slides, slumps, and debris flows show significant variations in lateral thickness. For sands deposited inside canyons or channels, however, the channel boundaries would be the primary controlling factor of lateral sand distribution. Channel-fill deposits may be composed of

Fig. 12.12. Sheet-like geometry of basin-plain turbidite sandstone with interbedded hemipelagite mudstone, Eocene, Zumaya, northern Spain.

sandy debrites (Fig. 12.13A), muddy debrites (Fig. 12.13B), heterolithic slumps (Fig. 12.13C), combination of sandy debrites and deep tidal sands (Fig. 12.13D), and muddy hemipelagites (Fig. 12.13E). From a reservoir standpoint, the critical factor is the lateral thickness variation of a single depositional unit and its inherent reservoir quality.
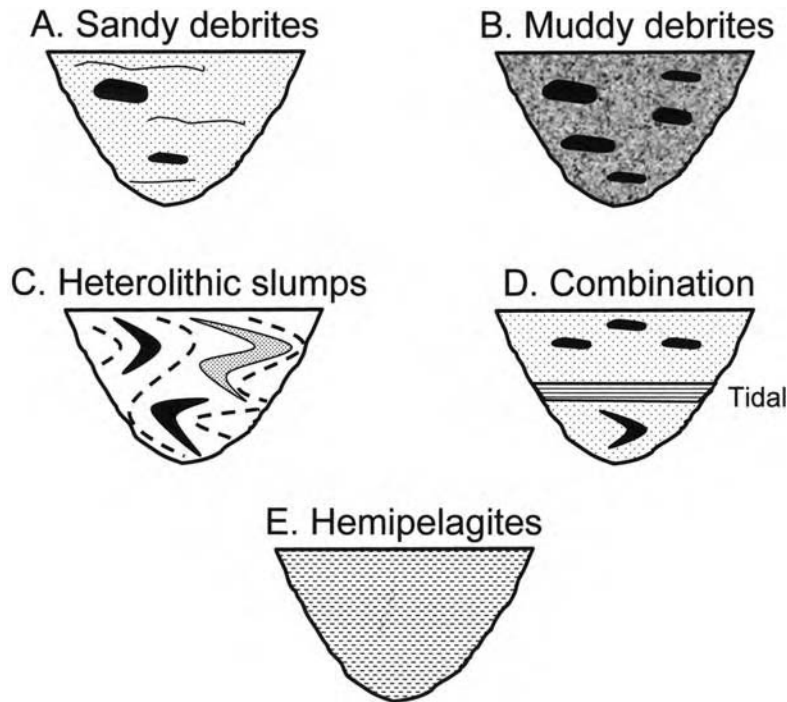
Fig. 12.13. Conceptual cross sections of canyons or channels filled with different types of lithofacies. (*A*) Sandy debrites composed of massive sand. (*B*) Muddy debrites composed of mud. (*C*) Heterolithic slumps composed of sand and mud. (*D*) Combination of sandy debrites and deep-marine tidal sand. (*E*) Hemipelagites composed of mud.

12.6 Reservoir heterogeneity

To understand reservoir heterogeneity, Unit 7 has been selected from the Annot Sandstone in SE France (see Chapter 8). Unit 7 exhibits a sheet-like geometry (Fig. 12.14B). Such sandbody geometry is attractive to the petroleum industry because of its lateral predictability and ease of reserve calculations. Unit 7 was interpreted originally as a turbidite bed (Bouma, 1962). However, basal inverse grading and floating mudstone clasts with planar fabric in Unit 7 have been used as evidence for deposition from sandy debris flows, not turbidity currents (Fig. 8.17). More importantly, Unit 7 contains large pockets of mudstone clasts along an internal amalgamation surface (Fig. 12.14B). The pocket investigated is about 420 cm long and 90 cm thick (Fig. 12.15). Amalgamation surfaces with pockets of mudstone clasts are evidence of reservoir heterogeneity. Although Unit 7 appears to be a single depositional bed, it is composed of three depositional layers with internal amalgamation surfaces (Fig. 12.16). In developing reservoir simulation
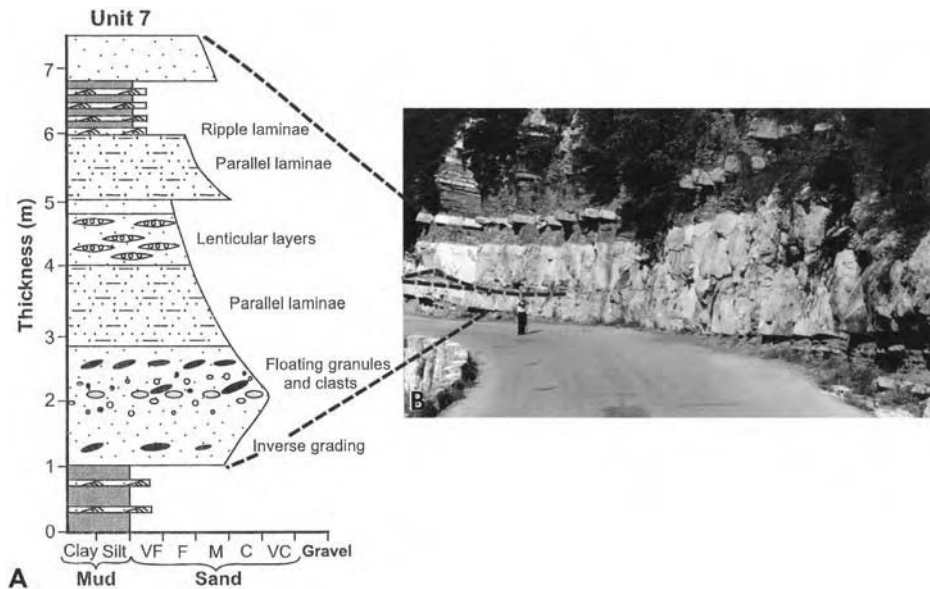
Fig. 12.14. (*A*) Sedimentological log of an amalgamated sandstone unit showing basal inverse grading overlain by an interval with floating granules and mudstone clasts with planar fabric, parallel laminae, and lenticular layers. (*B*) Outcrop photograph showing sheet-like geometry of the unit. Sedimentological log of this unit laterally varies in space because of amalgamation. For example, at extreme left of outcrop, the unit is composed of a basal sandstone, a middle pebble nest (pyramid shape shown by dashed line, see Fig. 12.15 for a close-up photograph), and an upper sandstone, but as we move to the right of outcrop, the middle pebble nest gradually thins out. Two dashed lines shows stratigraphic position of the unit. Unit 7 of the Annot Sandstone (Eocene–Oligocene), Peira Cava area, French Maritime Alps. SE France. (After Shanmugam (2002a). Reproduced with permission from Elsevier.)

models, such units with lateral and vertical heterogeneity should be evaluated carefully.

12.7 Sand injection and reservoir communication

In the Edop Field, offshore Nigeria (see Chapter 4), sand injectites occur both as sills and as dikes. Sand injectites cutting through mudstone permeability barriers can increase the connectivity between sand bodies thereby creating an ineffective permeability barrier (Fig. 12.17).

   In the Edop Field area, the vertical connectivity of sand bodies also depends on the amount of sand available in the source area and on the frequency of debris flows that pass through the site of deposition. Amalgamated sandstone units in the IQI-3 sequence in the Edop Field suggest an abundance of sand supply and a

Fig. 12.15. Outcrop photograph showing pebble nest (shown by dashed line) or pocket of mudstone clasts in mud matrix in Unit 7 (see 12.14B for overall photo). The nest is about 420 cm long and 90 cm thick. Annot Sandstone (Eocene–Oligocene), Peira Cava area, French Maritime Alps. SE France.
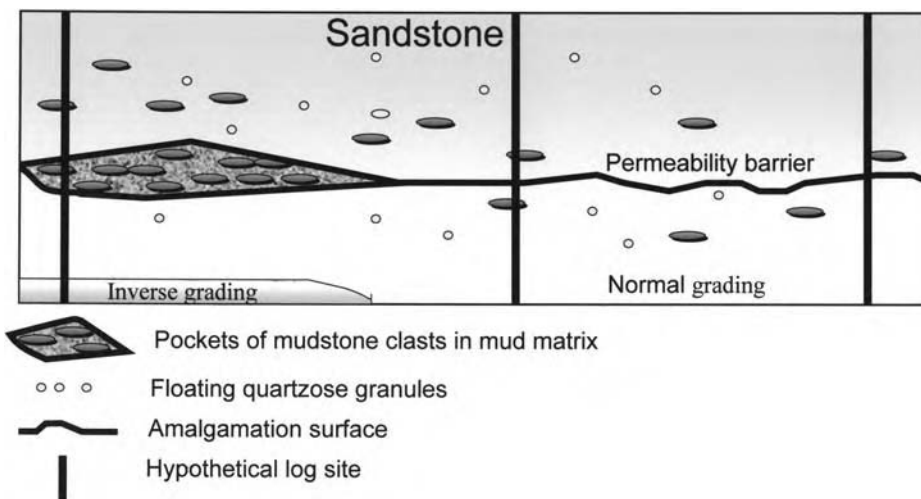
Fig. 12.16. Schematic diagram of Unit 7 of the Annot Sandstone showing pockets of mudstone clasts along an amalgamation surface enriched in mudstone (see Figs. 12.14, 12.15). Such internal mud-rich amalgamation surfaces could act as permeability barriers. Diagram not to scale.
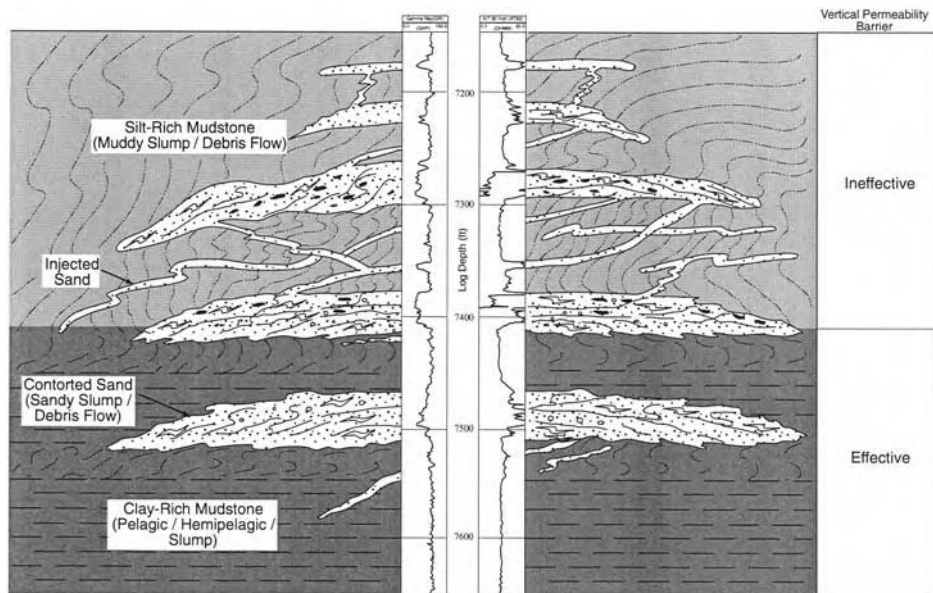
Fig. 12.17. Conceptual model showing the influence of sandstone injectites on permeability barriers. Thick interbedded mudstone intervals tend to serve as permeability barriers. However, sandstone injectites through these mudstone permeability barriers can increase the connectivity between sandbodies and thereby creating ineffective permeability barriers (upper part). Based on core observation from Edop 21D well, offshore Nigeria (see Chapter 4).

high frequency of slump/debris flow events within a 'fairway' or a 'canyon' (Fig. 4.29). In such confined environments, sands are likely to be in communication both due to amalgamations of sand beds and to sand injectites between sand beds (Fig. 12.17). In fact, production data from the Edop Field suggest that IQI-3 sands are in pressure communication with one another (Shanmugam, 1997c).

In their core study of Gryphon–Harding areas on the U.K. Continental Shelf (UKCS), Shanmugam et al. (1995a) reported sandstone sills and dikes. Purvis et al. (2002) reported a range of injection structures in the Gryphon Field from thin, centimeter-scale dikes to meter-scale injectites. They observed the cross-cutting nature of the injection structures in both core and seismic sections. In modelling the Gryphon reservoir, Purvis et al. (2002, p. 172) stated,

> '*The presence of injected sands within the reservoir interval of the Gryphon Field has major implications for the correlation and subsequent 3D reservoir modelling. The large-scale cross-cutting nature of the injection structures probably accounts for the high degree of vertical and lateral connectivity observed in the field. All sand units where data have been acquired are in pressure communication and production data supports excellent connectivity throughout the reservoir. An injected origin for*

the sand units would account for the fact that the thinner sand units above the main sand bodies are poorly correlatable, i.e., they appear not to be laterally extensive. The injection of sand from lower sand bodies into higher stratigraphic units (or vice versa) suggests that the shale stratigraphy as determined by tuff markers and biostratigraphy (Hatton et al., 1992) has some limitations on dating and hence correlating the sand units.'

In cases where vertical sand injectites connect two sand units (S1 and S2) separated by an intervening muddy stratigraphic marker, it is invalid from a reservoir standpoint to separate these two sands vertically using conventional layer-cake stratigraphy (Fig. 12.18).

In summary, clastic injections occur in all sizes and shapes and allow both vertical and lateral fluid communication between sandstone bodies. These sandstone injectites are commonly oil stained (Fig. 5.8), suggesting that these clastic injectites have served as conduits for fluid migration. Therefore, for developing realistic geological models and for dynamic reservoir simulation of deep-water sequences, aspects of post-depositional clastic injectites are as important as depositional geometries.
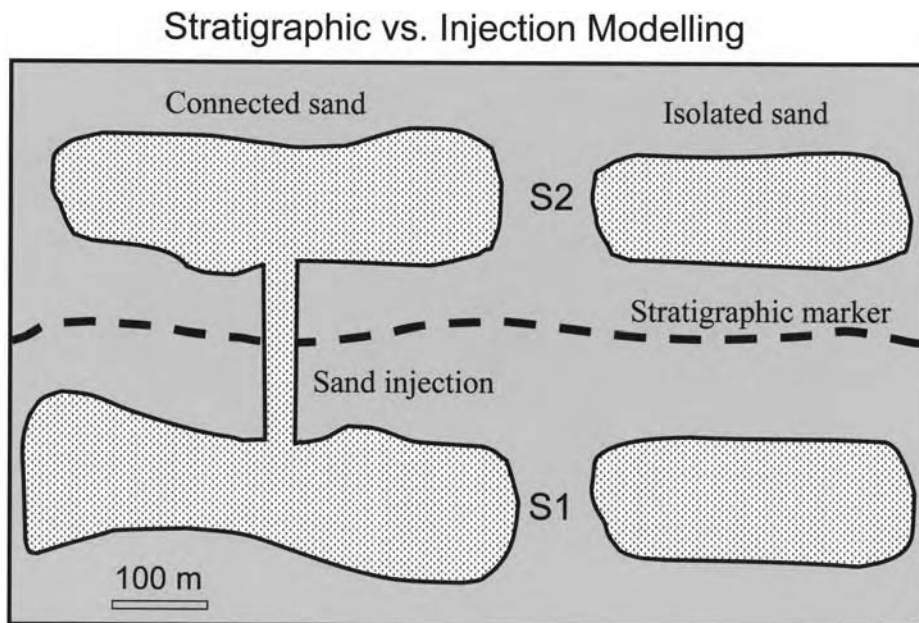
Fig. 12.18. Cross section showing two stratigraphically different sands (older S1 and younger S2) connected by a vertical sand injectite. Note a vertical sand injection is cutting across the stratigraphic marker. In cases like this, stratigraphic correlation of sand units is not meaningful for understanding reservoir communication. (See text for details. Diagram is simplified after Purvis et al. (2002, their Fig. 12B).)

12.8 Correlation of sandbodies

A major problem in slump-dominated systems is correlation of sandbodies using wireline logs because there are no reliable log motifs for slump and debrite deposits. Examples are:

(1) In the Edop Field, offshore Nigeria, it is difficult to correlate sand beds of slump origin in two closely spaced wells that are only 12 m apart (Fig. 12.19).
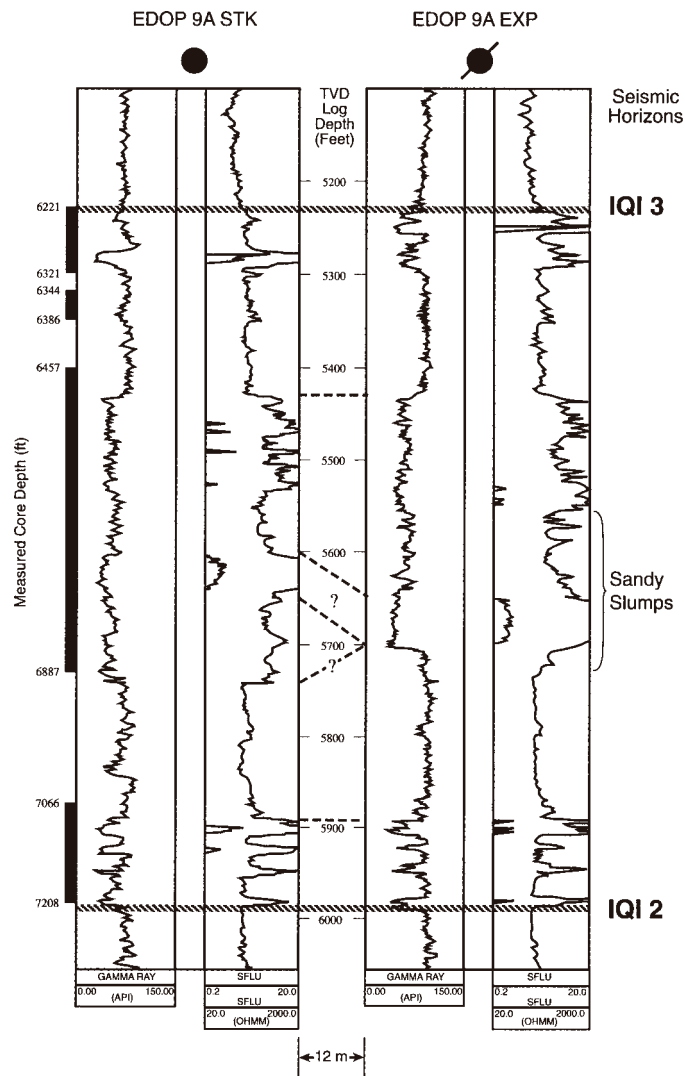
Fig. 12.19. Uncertainties in correlating sandy slump facies (IQI-3) in two closely spaced wells that are only 12 m apart, Edop Field, offshore Nigeria. (After Shanmugam (1997c).)

(2) In the Mid Norway region, deep-water sandstone units of slump and debris-flow origin show drastic lateral variations in thicknesses between two adjacent wells that are only 29 m apart (Shanmugam et al., 1994, their Fig. 23).

(3) In the Cretaceous Agat Formation, offshore Norway, difficulties exist in correlating deep-water sandstones of because of their slump and debris-flow origin (Fig. 12.20).

(4) In the lower Eocene Frigg Formation in Frigg Field, North Sea, deep-water sandstone is laterally discontinuous because of their debris-flow origin (Fig. 12.21).

Thus correlation of deep-water sandbodies using wireline logs is neither helpful in interpreting their depositional origin nor reliable in establishing their
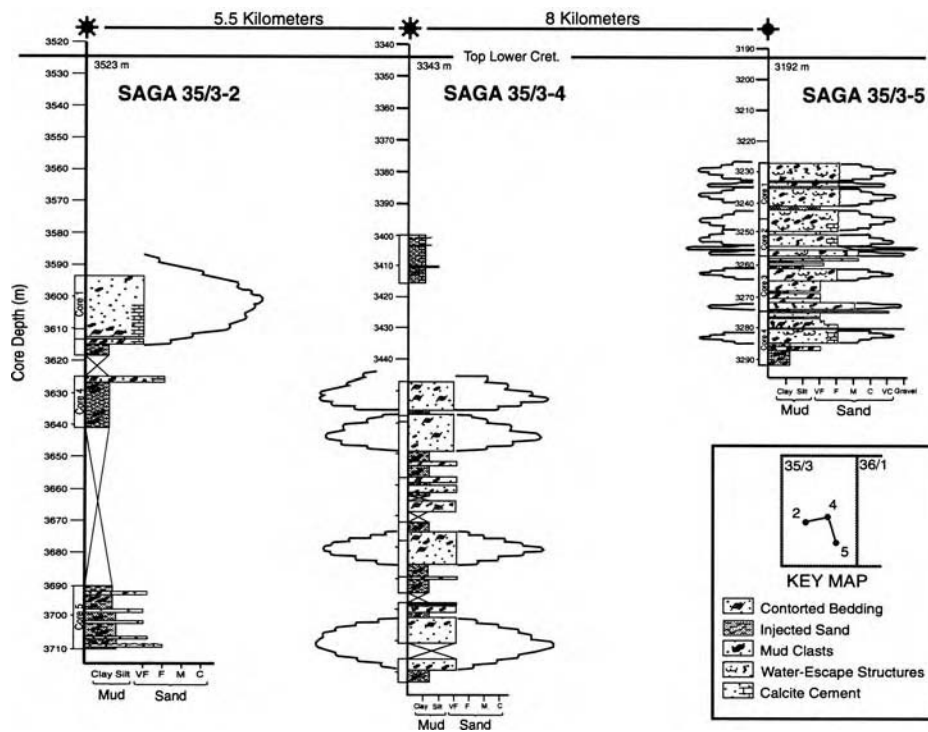
Fig. 12.20. Cross section showing difficulties in correlating Agat sandstone units between three wells. Datum: Top Lower Cretaceous. Note differences in relative stratigraphic position, thickness, and frequency of units among three wells. Also note, interbedded mudstone is well developed in the 3-2 and 3-4 wells, but not in the 3-5 well. See Figure 6.12 for regional map. Agat area, offshore Norway. (After Shanmugam et al. (1994). Reprinted by permission of the American Association of Petroleum Geologists whose permission is required for further use.)
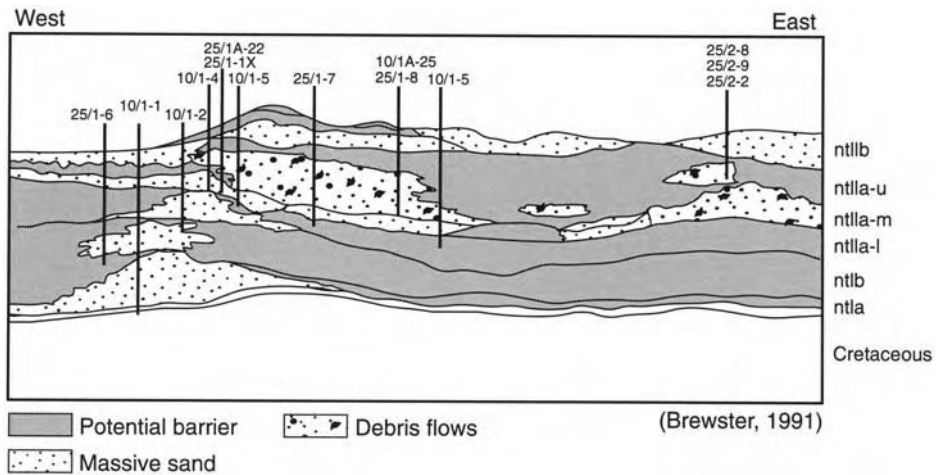
Fig. 12.21. An east-west cross section across the Frigg Field in the North Sea showing laterally discontinuous debrite sands and intervening fine-grained barrier units. Core photos of sandy debrites from Elf 25/2-8 well are shown in Figure 10.15. Simplified after Brewster (1991). (Reprinted by permission of the Geological Society of London.)

areal distribution. Furthermore, the layer-cake stratigraphy, which is the result of wireline-log correlations, can be misleading for developing realistic geocellular models for reservoir simulation purposes.

12.9 Depositional mud matrix

Depositional (primary) mud matrix, which occludes porosity and reduces permeability, is of importance in evaluating the reservoir potential of deep-water sands. In the 1950s and 1960s, 'turbidites' were considered to be poor reservoirs because of their high mud content. The 'turbidite-graywacke-flysch-dirty sand' linkage and its negative influence on the petroleum industry have been eloquently summarized by Sanders and Friedman (1997). Pettijohn (1957, p. 288) championed the link between the high detrital matrix of deep-water sandstones (greywackes) and their turbidity current origin. In referring to turbidite sandstones, Pettijohn (1957, p. 288) stated, '*The second group, therefore, probably owes its detrital matrix or "paste" to deposition from fluids with higher sediment/fluid ratios. Such media are the subaqueous turbidity flows found in some lakes and in many marine environments…*'

Sullwold (1960, p. 438) reported the high mud content (13.5–34.5%) from sieve analysis of upper Miocene sandstone beds that were interpreted to be turbidites. The following comments of Sullwold (1961, p. 64–66) reflect the views that

existed in the early 1960s concerning the muddy nature of turbidity currents and their deposits:

(1) '*A turbidity current is opaque and muddy (by definition)…*'
(2) '*Poor sorting is an expected feature in turbidites.*'
(3) '*The large percentage of silt and clay in these sands has caused them to be termed wackes and graywackes by most workers.*'
(4) '*Sorting is directly related to porosity, and turbidites must therefore have less original porosity than shallow-water sands…*'

Although the term 'graywacke' is no longer used synonymously with turbidites, the above comments are still valid. That turbidity currents would deposit mud-rich sediment makes sense because it is easier to transport mud in turbulent suspension than it is sand or gravel.

Since the 1990s, however, there has been a tendency to perpetuate the opposite notion: i.e., turbidites are clean (i.e., mud poor) sands (Fig. 7.20). Mitchum et al. (1993, p. 167), for example, considered the turbidites of basin-floor fans to be '*… clean, well sorted sandstone with good reservoir quality.*' This popular notion is apparently based on misinterpretation of clean, deep-water, massive sands as 'turbidites' using the concept of 'high-density turbidity currents' with traction carpets (see Chapter 7). Under the false notion that all sandy debrites are mud-rich facies, the low mud content of certain deep-water sands has been misinterpreted as turbidites. When compared to turbidity currents, sandy debris flows have a better chance of depositing mud-poor, clean, sands for the following reasons:

(1) Experiments have shown that sandy debris flows can deposit sands with only a minute amount of clay (less than 0.5% by weight) (see Chapter 3). Low mud matrix can be explained by elutriation of mud during flow transformation (Fisher, 1983). Flow transformation not only depletes underlying debris flows of mud but also enriches overlying turbidity currents with mud (Fig. 3.23). Consequently, sandy debris flows are able to emplace clean sands with low mud content (Fig. 12.22).
(2) Experiments have also shown that because of the upward mobility of fines the basal parts of sandy debrites are cleaner (see Fig. 3.23). In amalgamated sandy debrite packages, the mud-rich upper portion is eroded and the mud-poor basal portion is preserved, resulting in overall clean, amalgamated sandy debrites (Fig. 12.22).
(3) Mud is an integral component of turbidity currents. Sanders and Friedman (1997, p. 82) emphasized, *'From the point of view of petroleum geology, sands deposited from turbulent suspension are poorly sorted and includes large amounts of silt and clay.'* Sanders and Friedman maintained simply that 'dirty' (i.e., mud rich) sands are turbidites, and 'clean' (i.e., mud free) sands are non-turbidites.
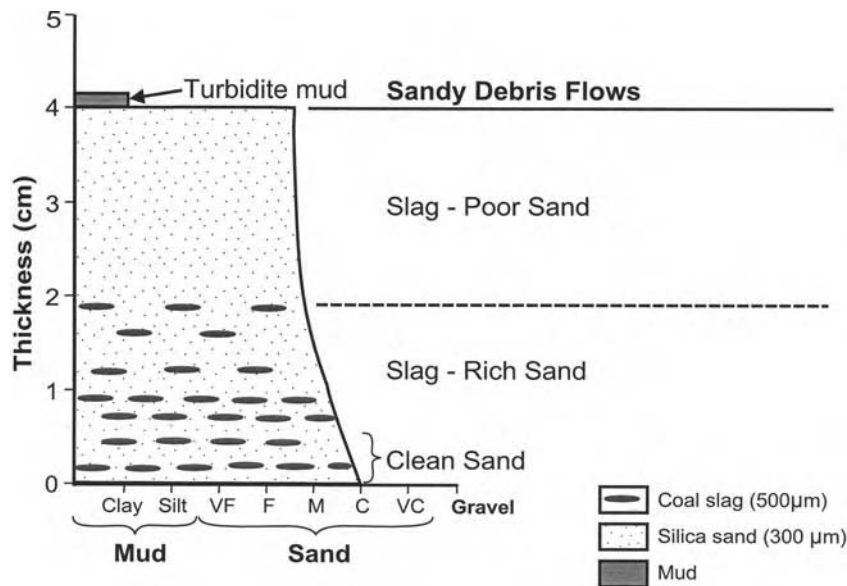
Fig. 12.22. A sketch of normal grading observed in experimental sandy debris flows with concentration of coarse-grained coal slag at the bottom and medium-grained silica sand near the top. The development of a basal clean sand interval is caused by upward migration of fines (i.e., elutriation) (see Fig. 3.23). Amalgamation of such clean intervals may develop thick zones of clean reservoir sand by sandy debris flows. Such normally graded deposits are prone to be misinterpreted as 'turbidites.' However, associated features, such as sharp upper contacts, floating clasts, and planar fabric, would help distinguish debrites.

(4) Experiments have shown that pure sandy turbidity currents, without mud, support sand and gravel in turbulent suspension for only short distances during transport, and they invariably collapse.

(5) Subaqueous debris flows are prone to develop hydroplaning (Mohrig et al., 1998). Furthermore, debris flows are laminar in state. As a result, subaqueous debris flows with hydroplaning are unlikely to erode the sea-floor and to incorporate eroded mud into the flow. In contrast, turbidity currents are perpetually turbulent in state. Turbulence tends to cause erosion of the muddy sea floor, and eroded mud gets incorporated into the turbulent turbidity current. Thus turbidites are rich in mud.

12.10 Reservoir quality

12.10.1 Nigeria

In the Edop Field, offshore Nigeria, the reservoir is composed of slump, debrite, and turbidite facies (see Chapter 4). Thickness of individual units varies from
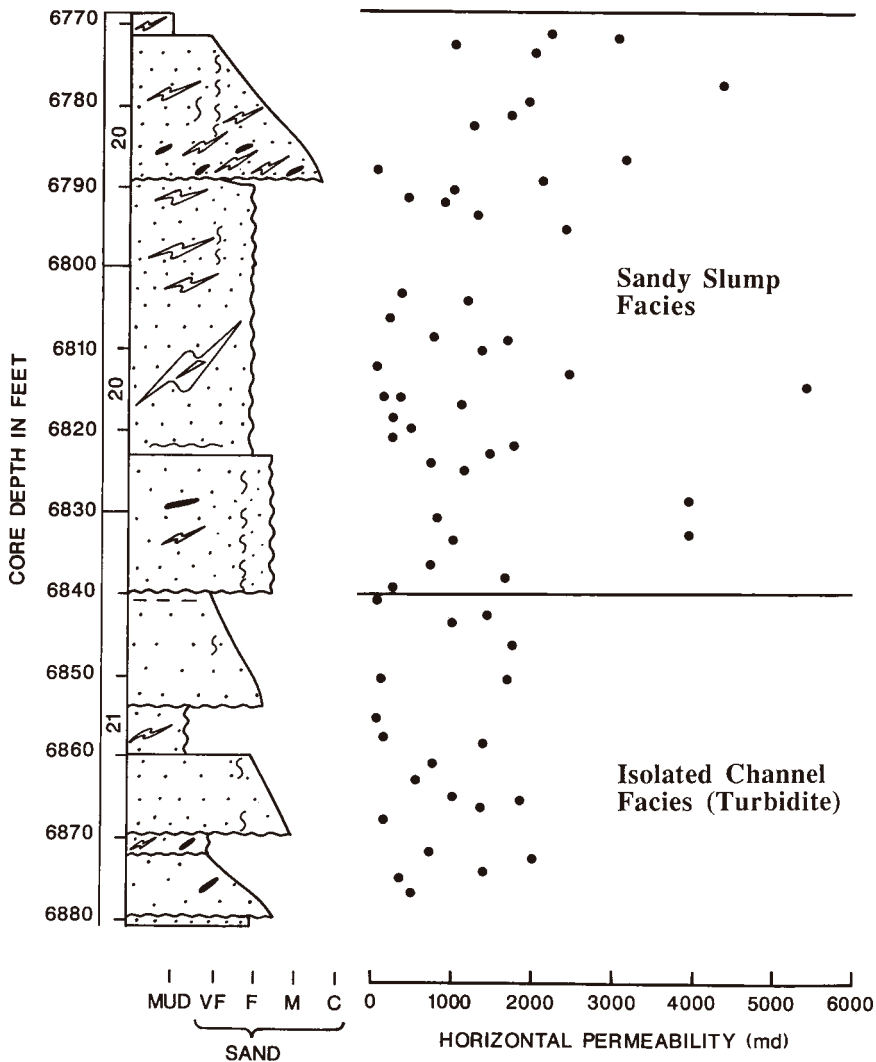
Fig. 12.23. Distribution of horizontal permeability in sandy slump facies and isolated turbidite channel facies. Note higher permeability values in slump facies. Well 9 Sidetrack. Edop Field, offshore Nigeria. (After Shanmugam et al. (1997c).)

1 to 34 ft (0.3–10 m). Amalgamated intervals reach a thickness of up to 70 ft (21 m). Porosity commonly ranges from 20 to 35%, and horizontal permeability commonly ranges from 1000–3000 mD. Depending on the grain size, on the depositional process, and on the environment, reservoir quality varies. Distribution of horizontal permeability in sandy slump facies is much higher (5500 mD) than that of the turbidite channel facies (2000 mD) (Fig. 12.23).

According to Houghton (1997), sands deposited by sandy slumps and debris flows are interconnected in the Edop Field. In these sands, baffles and barriers are sparse between individual depositional events. In the deep-water sands of the Edop Field, depositional matrix and authigenic cement are generally low. Pores in these sands are dominantly depositional in origin (i.e., primary porosity) and are well connected.

12.10.2 Equatorial guinea

In the Zafiro Field, Equatorial Guinea, the Pliocene reservoir was deposited by sandy slumps and debris flows (see Chapter 6). The reservoir has porosities in the range of 20–35% and permeabilities generally between 1000–3000 mD. DST flow rates were more than 10 000 BOPD on a 2 3/8″ choke (Famakinwa et al., 1996, 1997). The IQI reservoir sands in the Edop Field (Offshore Nigeria) that occur updip from the Zafiro Field also exhibit the same depositional facies and about the same reservoir properties. The Edop–Zafiro trend provides a test case for non-fan reservoirs that are dominated by deposits of sandy slumps and debris flows having excellent reservoir quality.

12.10.3 Gabon

Teisserenc and Villemin (1990) described the geology of sedimentary basins and oil systems of Gabon, West Africa. In the Anguille Field, located offshore 25 km southwest of Port Gentil, Gabon, Anguille and Pointe Clairette Sandstones (Upper Cretaceous) contain four deep-marine sedimentary units. These units consist of: (1) alternating fine-grained sandstone and shale; (2) shale; (3) interbedded sandstone and shale; and (4) contorted shale. The best reservoir is in fine-grained massive sandstone interpreted as deposits of grain flows and sandy debris flows. In describing the reservoir quality, Teisserenc and Villemin (1990, p. 172) stated, '*The best reservoirs are found in the first and third units in the grain-flow/debris-flow sandstones, porosity is as much as 24% and permeability is as high as 700 mD. In laminated sandstones, maximum permeability decreases to 300 to 400 mD. Net sandstone thickness ranges from 10–100 m.*'

In the M'Bya field, offshore Gabon, the Lucina Sandstone (Lower Cretaceous) is composed of fine-grained argillaceous and micaceous sandstone. It has been interpreted to consist of deep-lacustrine turbidites (Teisserenc and Villemin, 1990). Porosities range from 15–25%, and permeabilities are as high as 100 mD.

In the Lucina West Marine Field, South Gabon, Early Cretaceous reservoir sandstones were interpreted to be deposits of deep-lacustrine 'turbidites' (Smith, 1995). But sedimentological evidence suggests a debrite origin (see Chapter 6 for facies description). These reservoirs are composed of moderately sorted, fine-grained sandstones with mean porosities of 22–24%. Their geometric mean permeabilities range from 45–145 mD.

12.10.4 North Sea

The lower Eocene sands of the Frigg Field in the North Sea contain, thick, amalgamated units. They were interpreted as deposits of sandy slumps and debris flows (Shanmugam et al., 1995a). They exhibit high porosity (27–32%) and permeability (900–4000 mD) values (Brewster, 1991).

In the Gryphon Field, U.K. North Sea, the Balder formation (upper Paleocene-lower Eocene) was interpreted as deposits of sandy slumps and debris flows (Shanmugam et al., 1995a). In the Gryphon Field, the reservoir has 400–650 ft (122–198 m) gross thickness, 35% Net/Gross ratio, 32% porosity, and 3D permeability (Purvis et al., 2002). The Balder sands show a maximum permeability of up to 10D (Newman et al., 1993).

In Gannet Fields, U.K. North Sea, Eocene Tay sands were interpreted as submarine fan lobes deposited by turbidity currents (Armstrong et al., 1987). However, a reexamination of cores of these same sands suggests deposition by sandy debris flows, slumps, and slides (Shanmugam, 1992a). In the northern area, these sands show a highly amalgamated distribution, whereas in the southern area these sands are isolated by thick interbedded shale layers (Fig. 12.24). The Tay sands in the northern area exhibit high permeability (1000–6000 mD) comparison to the Tay sands in the southern area (100s mD) (Fig. 12.24).

In the North Sea Palaeogene, at least 2.4×10^9 BOE reserves are associated with injectite fields, or fields modified by sand injection (Hurst et al., 2005). In the Eocene Alba Formation, U.K. North Sea, porosity measured on core plugs averages 33.8% in the injected sands and 36.5% in the depositional sands (Fig. 12.25). This difference in reservoir quality may probably be attributed to a relative increase in the clay fraction in the injected sand (Duranti and Hurst, 2004).

12.10.5 Gulf of Mexico

Aspects of bottom-current reworked sands in the Ewing Bank Block 826 Field are discussed in Chapter 4. Both the L-1 and N-1 sands in the No. 3 well show porosity values in a range of 25–40%. In the No. 3 well, the horizontal air permeability, measured at 200 psi, commonly ranges from 100 to 1000 mD (Fig. 12.26). Although the cored intervals of both the L-1 and N-1 sands in the No. 3 well are products of bottom-current reworking, the L-1 reservoir with 80% sand exhibits higher permeability values (100–1800 mD) than the N-1 reservoir with 26% sand (50–800 mD). Microfractures, although seen in both L-1 and N-1 sands, enhance vertical permeability only in the L-1 sand because of higher sand content (80%). This allows greater juxtaposition of sand layer against sand layer across fractures. Vertical permeability values of N-1 sand are expected to be poor because of the ubiquitous interbedded mud layers throughout the sequence.

In the No. 3 Sidetrack well, sedimentary structures in cores reveal that the reservoir is composed of a lower unit with a turbidite channel sand, and an upper
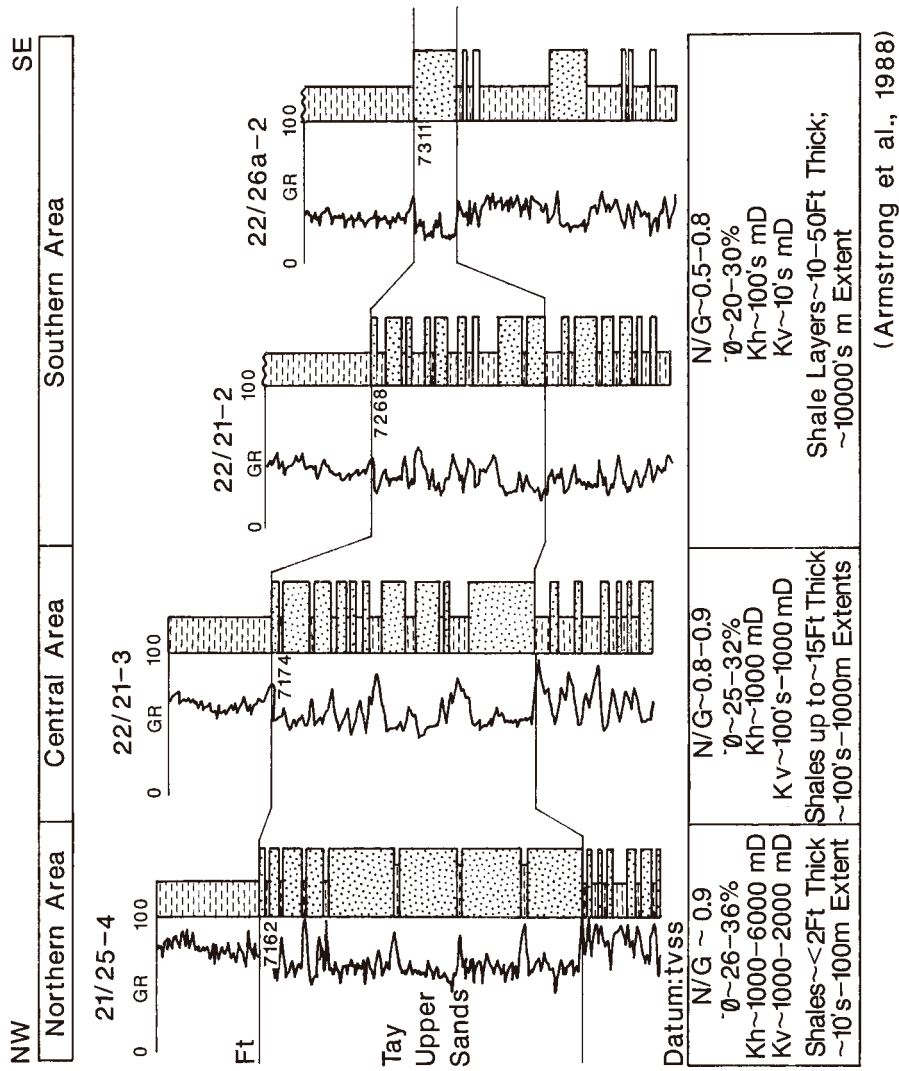
Fig. 12.24. Reservoir facies showing differences in N/G (Net to Gross), stacking pattern, interbedded shale layers, porosity, and permeability. Gannet Field, central North Sea. (After Armstrong et al. (1988). Reproduced with permission from Springer-Verlag.)
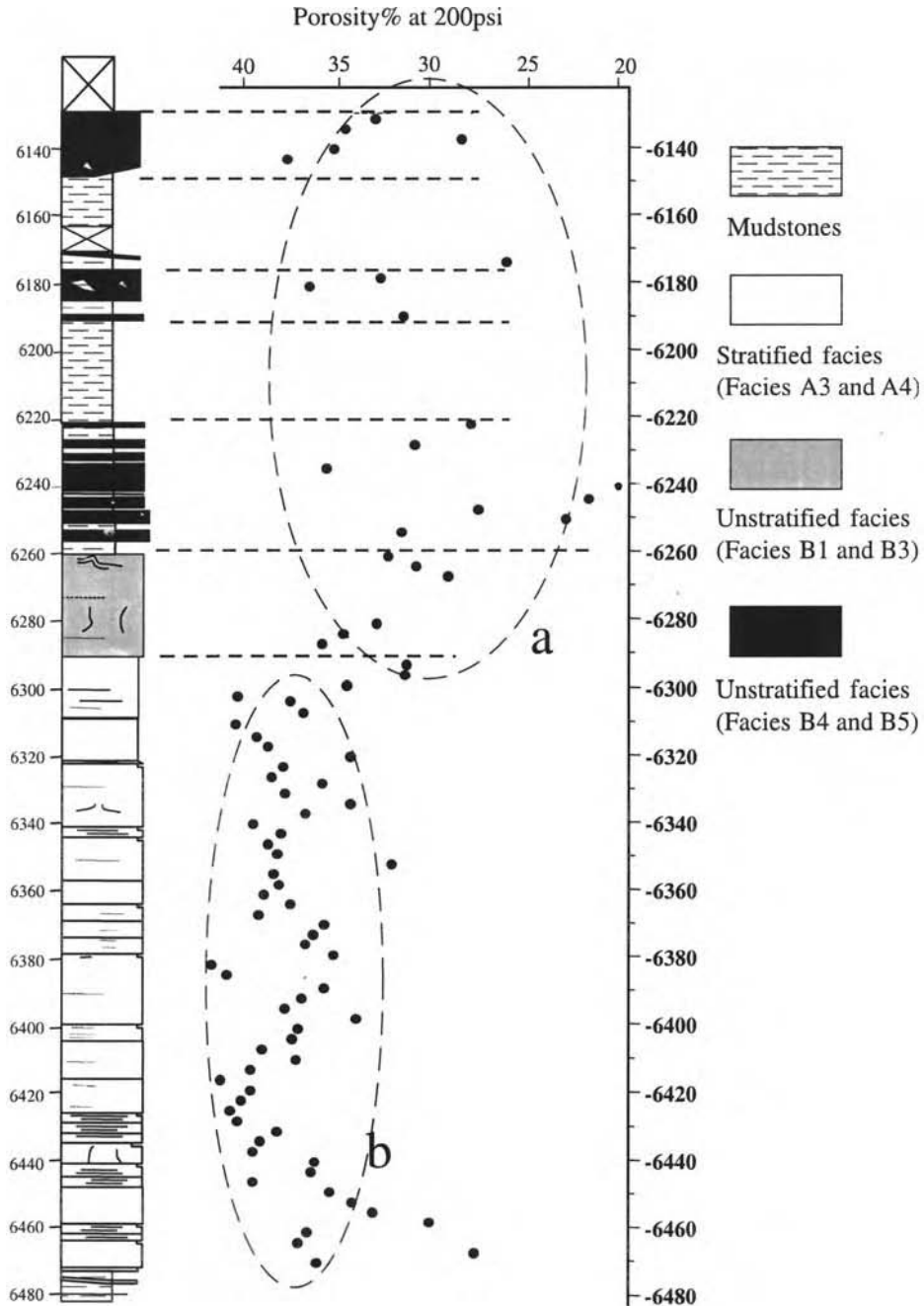
Fig. 12.25. Porosity distribution in injected (cluster a) and depositional (cluster b) sands in the Eocene Alba Formation. Note higher porosity values in the depositional sands. Data from vertical well 16/26-6. (After Duranti and Hurst (2004). Reproduced with permission from Blackwell.)
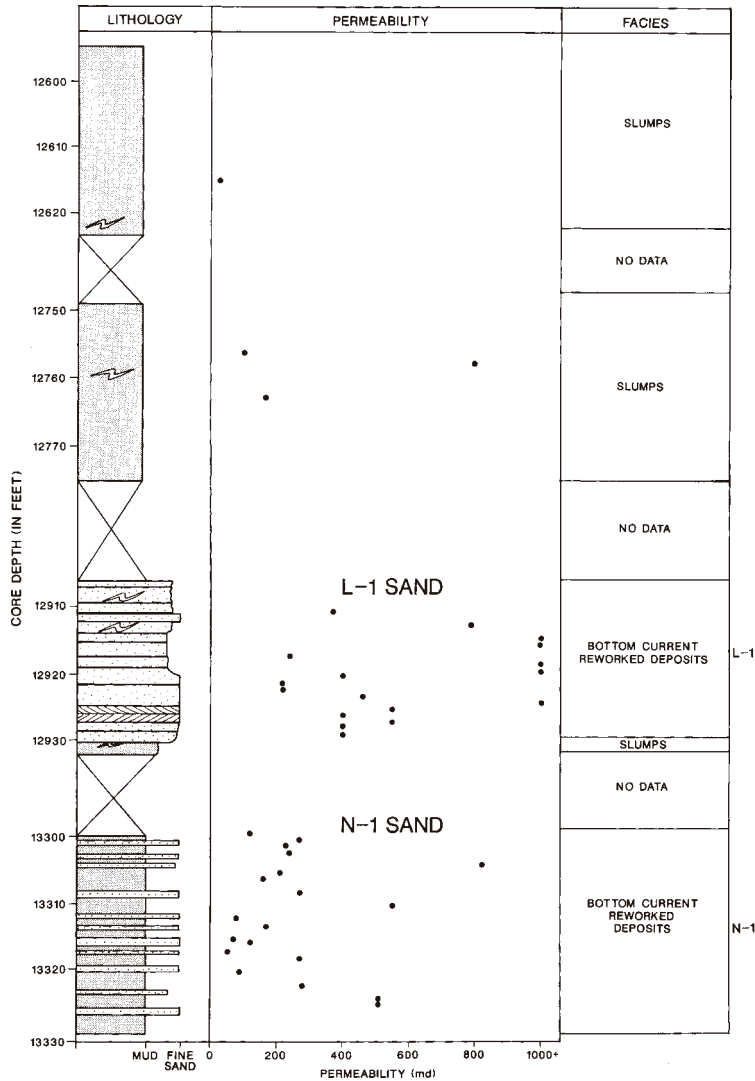
Fig. 12.26. Permeability distribution in the L-1 and N-1 Sands. Note amalgamated L-1 Sand shows higher permeability values than the isolated N-1 Sand. Lower permeability values in N-1 Sand may be attributed to interbedded mud layers. Well No. 3, Ewing Bank Block 826, Gulf of Mexico.

unit with a bottom-current reworked sand (Fig. 12.27). Although both the turbidite and the reworked sands show porosity values in a range of 35–42%, their permeability values are strikingly different. The basal turbidite channel sand unit shows a distinct upward decrease in permeability with maximum values (5000 mD) at its base (Fig. 12.27). This permeability trend probably mimics a subtle upward
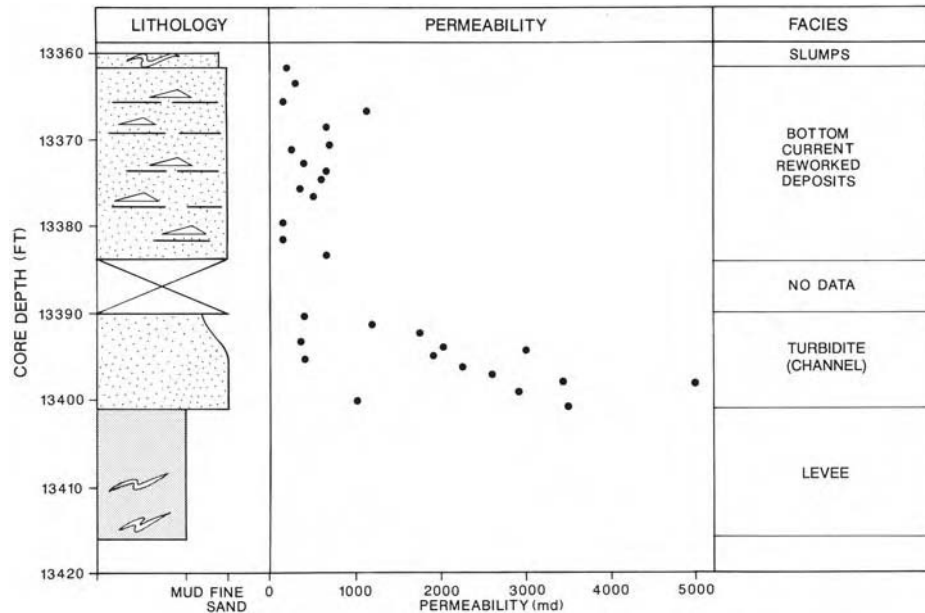
Fig. 12.27. Permeability distribution in the L-1 Sand. Note upward decrease in permeability within the turbidite channel unit reflecting upward decrease in grain size. In comparison, permeability within bottom-current reworked facies is much less variable because of uniform grain size. Lower permeability values of bottom-current reworked facies may be attributed to interbedded mud layers. Well No. 3 Sidetrack 1, Ewing Bank Block 826, Gulf of Mexico. (After Shanmugam et al., (1993a). Reprinted by permission of the American Association of Petroleum Geologists whose permission is required for further use.)

decrease in grain size within the channel package. The upper unit having bottom-current-reworked deposits exhibits near uniform vertical distribution of permeability values of about 500 mD (Fig. 12.27), reflecting uniform vertical grain size distribution.

On the basis of reservoir quality, sands in the Ewing Bank area may be classified into two types (Fig. 12.28). Type 1 exhibits a greater number of sand layers per unit area than Type 2. The permeability of Type 1 (e.g., L-1) is much higher (up to 1800 mD) than that of Type 2 (e.g., N-1) (up to 800 mD). Porosity values, however, remain about the same in both types (Fig. 12.28). Shanmugam et al. (1993a) attributed the higher permeability in the Type 1 to: (1) increased overall sand content; (2) vigorous bottom-current reworking; and (3) microfractures.

The Type 1 sands are clean, porous, and well sorted. A lack of interbedded mud layers facilitates good communication between sand layers. Communication between sand layers is further enhanced by fractures. For these reasons, Type 1
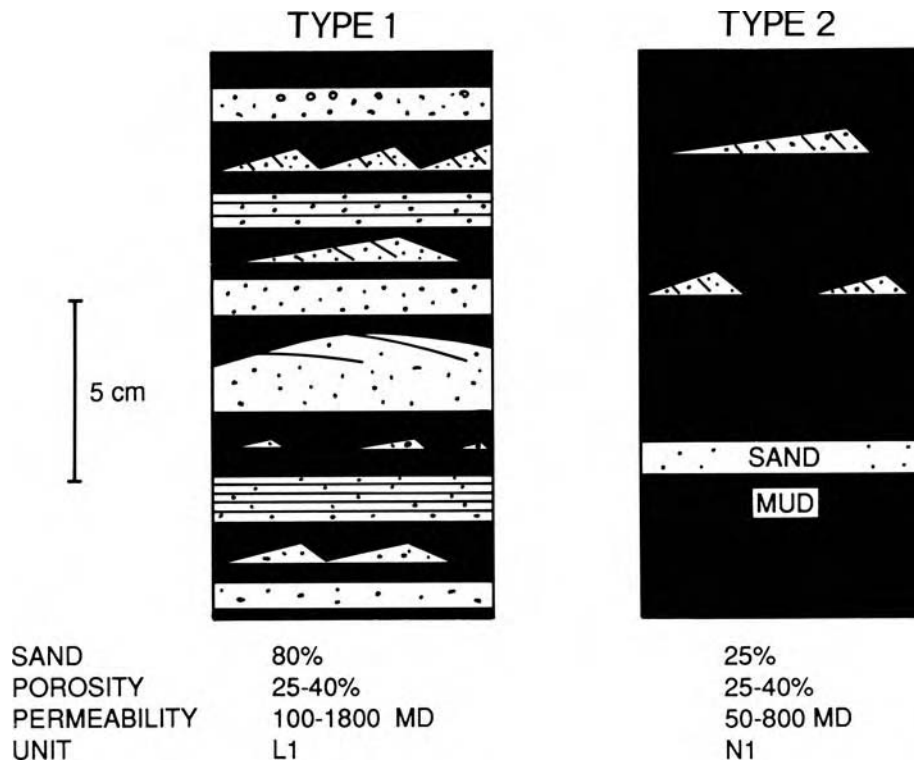
Fig. 12.28. **Two types of reservoir facies showing differences in sand content and permeability. Type 1 with higher sand content exhibits higher permeability than sand-poor Type 2. Note both types show similar values of porosity from core plugs taken from the sand layers. (After Shanmugam et al. (1993a). Reprinted by permission of the American Association of Petroleum Geologists whose permission is required for further use.)**

sands are produced at good rates. In contrast, Type 2 sands contain numerous interbedded mud layers, which greatly reduce communication between sand layers. Therefore, they are produced at poor rates.

Studies of Miocene–Pliocene reservoirs in the Auger Field concluded that the 'S' Sand in the Garden Banks 426, 427, 470, and 471 blocks of Gulf of Mexico is a turbidite sheet sand (McGee et al., 1994). Production began in 1994 from a Tension Leg Platform (TLP) at a water depth of 2862 ft (872 m). These sands have produced at an average rate of 10 MBOPD. The 'S' Sand has a thickness of 200 ft (61 m) and is correlatable over a distance of 4.4 km. The 'S' Sand has an average porosity of 24% and permeability of 150 mD. Published sedimentary features of the 'S' Sand suggest that it was probably emplaced by laminar flows diagnostic of debris flows (see Chapter 6).

12.10.6 California

The prolific oil producing clastic reservoir in the North Midway Sunset Field, Kern County, California, is the upper Miocene Potter Sand (see Chapter 6). The reservoir quality of this unit is controlled by grain size, depositional processes, and environments. The amalgamated, braided channel facies with gravel and coarse sand exhibits high permeability values (10 000+ mD) (see Fig. 6.41).The isolated meandering channel facies with medium-grained sand shows an upward decrease in permeability, mimicking fining-up trends (9000 to 500 mD). The levee facies with bioturbated fine-grained sand shows low permeability values (100 mD).

12.10.7 Brazil

The reservoir quality of deep-water petroleum reservoirs in the Campos basin (Namorado, Enchova and Bonito, and Marlim fields), offshore Brazil, has been discussed by Guardado et al. (1990). The producing reservoir in the Namorado field is Cenomanian/Turonian 'turbidite' sandstone. These sandstone units are medium grained, massive, and locally conglomeratic.

In the Enchova and Bonito fields, located close to the present-day shelf edge, the Eocene 'turbidite' reservoirs are composed of medium-to coarse-grained friable sandstones with 26–30% porosity and with 1 D permeability.

The Marlim field is located in the central part of the Campos Basin about 110 km offshore Brazil (Guardado et al., 1990). The producing reservoirs are late Oligocene in age. In these fine-to medium-grained massive sandstones, average porosities range from 25–30% and the permeabilities are between 2 and 3 D.

In the Lagoa Parda oil field, siliciclastic deep-water reservoirs deposited in the early Eocene Regencia Canyon of the Espirito Santo Basin, Brazil, are composed of unstratified conglomerate and sandstone with interbedded bioturbated mudstone and thick-bedded sandstone (Bruhn and Walker, 1997). These sandstones were interpreted as deposits of 'high-density turbidity currents' by Bruhn and Walker (1997). In the Well: 7-LP-33-ES of this field, sandstone shows average porosities of 25% and permeabilities of 427 mD.

12.10.8 India

Operator Reliance Industries and Niko Resources discovered an estimated 14 Tcf of gas in the deep-water tertiary siliciclastic reservoirs of the Krishna–Godavari basin off India's southeastern coast in 2002. Geologic studies based on 3D seismic data have shown sinuous deep-water channel forms for the Pliocene reservoir (Bastia, 2004). Conventional core taken from the Pliocene interval is composed of unconsolidated and amalgamated sand with floating mudstone clasts, planar clast fabric, inverse grading of clasts, and floating quartz granules.

These sands have been interpreted to be deposits of sandy debris flows. In addition, these cores show evidence for reworking by deep-marine tidal bottom currents (e.g., double mud layers) and post-depositional sand injections (e.g., razor-sharp margins and roof pendants). Clean debrite sands exhibit high porosities (35–43%) and permeabilities (2000–6000 md) at 300 psi.

12.11 Depositional models

There are no general facies models for deep-water systems because each deep-water system is unique. Any depostional model should reflect basic depositional processes, depositional setting, sediment supply, sediment types, and basin architecture. In developing depositional models, the use of modern systems is critical (see Chapter 6). Mass transport processes (slides, slumps, sand flows, and debris flows) have been observed in modern oceans (e.g., Shepard, 1951; Dill, 1964, Shepard and Dill,1966); however, convincing direct observations of turbidity currents in modern oceans are lacking. It is ironic that there are numerous deep-water facies models for deposits of turbidity currents that have not been observed, but there are no facies models for deposits of mass flows that have been photographed. This is perhaps because of the simplicity of both turbidity current concepts and submarine-fan models, and the historical association between turbidites and sheet geometries. Basinal turbidites are indeed sheet-like in geometry, however, such turbidite sands are commonly thin bedded, fine grained, and contain large amounts of mud. Therefore, basinal turbidites are of poor quality. In contrast, slope sands of debris-flow origin are thicker bedded, coarser grained, and contain lower amounts of mud in comparison to turbidites. Therefore, slope sandy debrites are of good quality. The current trend in the petroleum industry is to routinely apply submarine fan models that have been developed for base-of-slope settings with smooth sea floors to intraslope settings with highly irregular sea floors, such as that of the Gulf of Mexico. We need to develop separate models for slopes emphasizing slope processes and products. The conventional wisdom that slopes are areas of 'bypassing' of sand is invalid. Slopes are important areas of sand deposition (see Chapter 6).

As a counterpart to turbidite-dominated fan models suited for base-of-slope settings, an alternative model, representative of debris-flow dominated slope systems, is proposed (Fig. 12.29). Unlike submarine fans with organized turbidite packages in channels and lobes, the proposed slope model advocates a complexity of deposits consisting of debris flows and other processes. Debris-flow dominated systems can be broadly classified into: (1) non-channelized (non-fan); and (2) channelized types (Fig. 12.29). In this model, nature of shelf (sand rich *vs.* mud rich), sea-floor topography (smooth *vs.* irregular) and depositional process (settling *vs.* freezing) tend to control sand distribution and geometry. Contrary to popular belief, sandy debris flows can be thick, spatially extensive, and highly
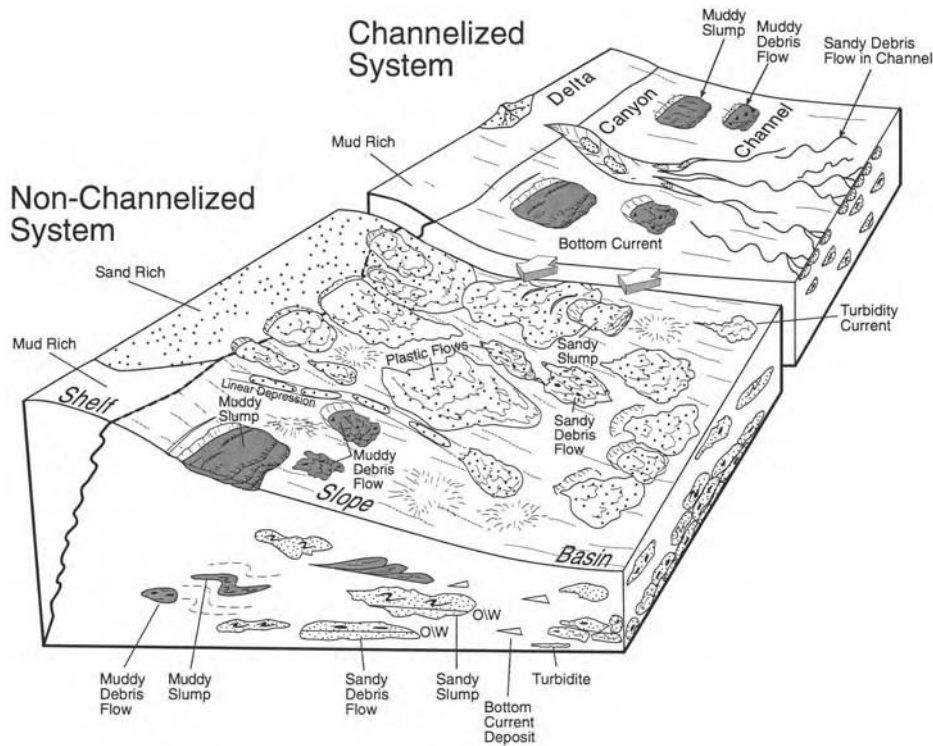
Fig. 12.29. Depositional model for non-channelized and channelized debris-flow dominated systems in slope and base-of-slope settings. In non-channelized systems (non-fan), sandy debris flows are expected to occur downdip from sand-rich shelf. In channelized systems, sandy debris flows are expected to occur mainly within channels and at their terminus. Debris flows generate tongue-like sand bodies and they are not analogous to typical depositional lobes formed by classical turbidity currents in submarine fans (e.g., Mutti and Ricci Lucchi, 1972). Different oil–water contacts (O/W) may be encountered in debrite reservoirs because of their lateral discontinuity. However, debrite reservoirs are also sheet-like with good vertical and lateral connectivity caused by amalgamation of sand units. (After Shanmugam (2000a). Reproduced with permission from Elsevier.)

permeable reservoirs. High frequency flows tend to develop amalgamated debrites with lateral connectivity and sheet-like geometry. In addition, we need to develop models for deposits of bottom currents.

12.12 Epilogue

Distribution, geometry, and quality of deep-water sandstones are controlled primarily by depositional processes. Interpretation of depositional processes in the geologic record requires the rigor of process sedimentology. Which means back to basics—the rocks!

References

Abegg, R., 2004. Sedimentology in deepwater exploration. The Sedimentary Record, 2, 9.

Abreu, V., Sullivan, M., Pirmez, C., Mohrig, D., 2003. Lateral accretion packages (LAPs): an important reservoir element in deep water sinuous channels. Marine and Petroleum Geology, 20, 631–648.

Ager, D.V., 1974. Storm deposits in the Jurassic of the Moroccan High Atlas. Paleogeogr. Paleoclimatol. Paleoecol., 15, 83–93.

Akhurst, M.A., 1991. Aspects of late Quaternary sedimentation in the Faeroe-Shetland Channel, north-west U.K. continental margin. British Geological Survey Technical Report. WB/91/2.

Alam, M.M., Curray, J.R., Chowdhury, M.L.R., Gani, M.R., 2003. An overview of the sedimentary geology of the Bengal Basin in relation to the regional tectonic framework and basin-fill history. Sedimentary Geology, 155, 179–208.

Alexander, C.R., Davis, R.A., Henry, V.J., 1998. Tidalites: Processes and Products. SEPM Special Publication, 61, p. 171.

Allen, J.R.L., 1964. Studies in fluviatile sedimentation. Six cyclothems from the Lower Old Red Sandstone, Anglo-Welsh Basin. Sedimentology, 3, 163–198.

Allen, J.R.L., 1965. Late Quaternary Niger Delta, and adjacent areas: sedimentary environments and lithofacies. AAPG Bulletin, 49, 547–600.

Allen, J.R.L., 1970. Physical Processes of Sedimentation. American Elsevier Publishing Company, Inc., New York, p. 239.

Allen, J.R.L., 1973. Phase differences between bed configuration and flow in natural environments, and their geological relevance. Sedimentology, 20, 323–329.

Allen, J.R.L., 1982. Mud drapes in sand-wave deposits: a physical model with application to the Folkstone Beds (early Cretaceous, Southeast England). Proceedings of the Royal Society of London, Series A 306, 291–345.

Allen, J.R.L., 1984. Sedimentary Structures, their Character and Physical Basis, Unabridged one-volume. Elsevier, Amsterdam, I, p. 593, and II, p. 663.

Allen, J.R.L., 1985a. Principles of Physical Sedimentology. George Allen & Unwin, London, p. 272.

Allen, J.R.L., 1985b. Loose-boundary hydraulics and fluid mechanics: selected advances since 1961. In: Brenchley, P.J., Williams, P.J. (Eds.), Sedimentology: Recent Developments and Applied Aspects, published for the Geological Society by Blackwell Scientific Publications, Oxford, pp. 7–28.

Allen, P.A., 1997. Earth Surface Processes. Blackwell Science, London, p. 404.

American Institute of Physics, 2004. Gallery of fluid motion. Uniform Resource Locator (URL): http://pof.aip.org/pof/gallery/archives.jsp (accessed April 28, 2005).

Amos, A.F., Gordon, A.L., Schneider, E.D., 1971. Water masses and circulation patterns in the region of the Blake-Bahama Outer Ridge. Deep-Sea Research, 18, 145–165.

Andersen, J.C.Ø., Rasmussen, H., Nielsen, T.F.D., Rønsbo, J.G., 1998. The Triple Group and the Platinova gold and palladium reefs in the Skaergaard intrusion: stratigraphic and petrographic relations. Economic Geology, 93, 488–509.

Anderton, R., 1985. Clastic facies models and facies analysis. In: Brenchley, P.J., Williams, P.J. (Eds.), Sedimentology: Recent Developments and Applied Aspects, published for the Geological Society by Blackwell Scientific Publications, Oxford, pp. 31–47.

Anspach, D.H., Tripp, S.E., Berlitz, R.E., Gilreath, J.A., 1989. Study of shelf-slope environments of deposition, High Island A-474/A-499 Area. AAPG Bulletin, 73, 328–329.

Apel, J.R., 1987. Principles of Ocean Physics, Academic Press, New York, p. 631.

Apps, G.M., Peel, F.J., Travis, C .J., Yeilding, C.A., 1994. Structural controls on Tertiary deep water deposition in the northern Gulf of Mexico. In: Weimer, P., Bouma, A.H., Perkins, R.F. (Eds.), Submarine Fans and Turbidite Systems, Gulf Coast Section of SEPM 15th Annual Research Conference, pp. 1–7.

Archer, A.W., 1998. Hierarchy of controls on cyclic rhythmite deposition: carboniferous basins of eastern and mid-continental U.S.A. In: Alexander, C.R., Davis, R.A., Henry, V.J. (Eds.), Tidalites: Processes and Products, SEPM Special Publication 61, pp. 59–68.

Armstrong, L.A., Ten Have, A., Johnson, H.D., 1987. The geology of the Gannet Fields, Central North Sea, UK sector. In: Brooks, J., Glennie, K. (Eds.), Petroleum Geology of North-West Europe, Graham & Trotman, London, vol. 1, pp. 533–549.

Arnott, R.W.C., Hand, B.M., 1989. Bedforms, primary structures and grain fabric in the presence of suspended sediment rain. Journal of Sedimentary Petrology, 59, 1062–1069.

Arrhenius, G., 1952. Sediment cores from the east Pacific: Reports of the Swedish Deep-Sea Expedition 1947–1948, (1), p. 89.

Arrhenius, G., 1963. Pelagic sediments. In: Hill, M.N. (Ed.), The Sea, New York, Wiley, vol 3, pp. 655–727.

Arthur, M.A., Dean, W.E., Stow, D.A.V., 1984. Models for the deposition of Mesozoic-Cenozoic fine-grained organic-carbon-rich sediment in the deep sea. In: Stow, D.A.V., Piper, D.J.W. (Eds.), Fine-Grained Sediments: Deep-Water Processes and Facies, Geological Society of London Special Publication, 15, 527–560.

Aschoff, J.L., Giles, K.A., Lawton, T.F., 2001. Origin of Upper Cretaceous (Latest Maastrichtian) massive, boulder-cobble conglomerates, Porterillos Formation, La Popa Basin, northeastern Mexico: incised valley-fill or mega-tsunamite? Geological Society of America Annual Meeting, Session No. 84, Booth # 139.

Baas, J.H., 2004. Conditions for formation of massive turbiditic sandstones by primary depositional processes. Sedimentary Geology, 166, 293–310.

Babonneau, N., Savoye, B., Cremer, M., Klein, B., 2002. Morphology and architecture of the present canyon and channel system of the Zaire deep-sea fan. Marine and Petroleum Geology, 19, 445–467.

Bagnold, R.A., 1954. Experiments on a gravity free dispersion of large solid spheres in a Newtonian fluid under shear. Proceedings of the Royal Society of London (A), 225, 49–63.

Bagnold, R.A., 1956. The flow of cohesionless grains in fluids. Phil. Trans. Royal Society of London, Series A. Mathematical and Physical Sciences, 249, 235–297.

Bagnold, R.A., 1962. Auto-suspension of transported sediment; turbidity currents. Royal Society of London Proceedings, Series A, 265, 315–319.

Bailey, E.B., 1936. Sedimentation in relation to tectonics. GSA Bulletin, 47, 1713–1726.

Bailey, E.B., 1940. Submarine canyons. Nature, 146, 493.

Bakun, A., 1978. Guinea Current Upwelling. Nature, 271, 147–150.

Ballance, P.F., Gregory, M.R., Gibson, G.W., 1981. Coconuts in Miocene turbidites in New Zealand; possible evidence for tsunami origin of some turbidity currents. Geology, 9, 592–595.

Banerjee, I., 1989. Tidal sand sheet origin of the transgressive Basal Colorado Sandstone (Albian): a subsurface study of the Cessford Field, Southern Alberta. Bulletin of Canadian Petroleum Geology, 37, 1–17.

Barnes, N.E., Normark, W.R., 1985. Diagnostic parameters for comparing modern submarine fans and ancient turbidite systems. In: Bouma, A.H., Normark, W.R., Barnes, N.E. (Eds.), Submarine Fans and Related Turbidite systems, Springer-Verlag, New York, pp. 13–14 and wall chart.

Barnett, S.F., Ettensohn, F.R., 2003. A possible Middle Devonian tsunamite: Duffin Bed, New Albany Shale of south-central Kentucky. Geological Society of America Abstracts with Programs, 35, 602.

Barrett, J.R., 1965. Subsurface currents off Cape Hatteras. Deep-Sea Research, 12, 173–184.

Basset, D.A., Walton, E.K., 1960. The Hell's Mouth Grits: Cambrian greywackes in St. Tudwal's Peninsula, North Wales. Quarterly Journal of Geological Society of London, 116, 85–110.

Bastia, R., 2004. Depositional model and reservoir architecture of Tertiary deep-water sedimentation, Krishna–Godawari offshore basin, India. Journal of Geological Society of India, 64, 11–20.

Bates, C.C., 1953. Rational theory of delta formation. AAPG Bulletin, 37, 2119–2162.

Bates, R.L., Jackson, J.A., 1980. Glossary of Geology, 2nd Edition. American Geological Institute, Falls Church, Virginia, p. 751.

Beard, D.C., Weyl, P.K., 1973. Influence of texture on porosity and permeability of unconsolidated sand. AAPG Bulletin, 57, 349–369.

Beaulieu, S., Baldwin, R., 1998. Temporal variability in currents and the benthic boundary layer at an abyssal station off central California. Deep-Sea Research Part II, 45, 587–615.

Bein, A., Weiler, Y., 1976. The Cretaceous Talme Yafe Formation: a contour current shaped sedimentary prism of calcareous detritus at the continental margin of the Arabian craton. Sedimentology, 23, 511–532.

Belderson, R.H., Kenyon, N.H., 1976. Long-range sonar views of submarine canyons. Marine Geology, 22, M69–M74.

Belderson, R.H., Kenyon, N.H., Stride, A.H., 1984. A 'braided' distributary system on the Orinoco deep-sea fan. Marine Geology, 56, 195–206.

Bell, H.S., 1940. Armored mud balls - their origin, properties and role in sedimentation: Journal of Geology, 48, 1–31.

Bell, H.S., 1942. Density currents as agents for transporting sediments. Journal of Geology, 50, 512–547.

Berggren, W.A., Hollister, C.D., 1977. Plate tectonics and paleocirculation – Commotion in the ocean. Tectonophysics, 38, 11–48.

Beverage, J.P., Culbertson, J.K., 1964. Hyperconcentration of suspended sediment. American Society of Civil Engineers, Proceedings Journal of the Hydraulics Division, 90, HY 6, November, 117–128.

Bilinski, P.W., McGee, D.T., Pfeiffer, D.S., Shew, R.D., 1995. Reservoir characterization of the 'S' Sand, Auger Field, Garden Banks 426, 427, 470, and 471. In: Winn, R.D., Armentrout, J.M. (Eds.), Turbidites and Associted Deep-Water Facies, SEPM Core Workshop No. 20, pp. 75–93.

Bjørlykke, K., 1989. Sedimentology and Petroleum Geology. Berlin: Springer-Verlag, p. 363.

Blatt, H., Middleton, G., Murray, R., 1972. Origin of Sedimentary Rocks. Englewood Cliffs, New Jersey: Prentice-Hall, Inc., p. 634.

Blumberg, R., 1964. Hurricane waves, winds, and currents test marine pipeline design: Pipeline Industry, 20, pp. 43–72.

Boggs Jr., S., 2001. Principles of Sedimentology and Stratigraphy, 3rd Edition. New Jersey: Prentice Hall, p. 726.

Bondevik, S., Svendsen, J-.I., Mangerud, J., 1997. Tsunami sedimentary facies deposited by the Storegga tsunami in shallow marine basins and coastal lakes, Western Norway. Sedimentology, 44, 1115–1131.

Booth, J.S., O'Leary, D.W., Popenoe, P., Danforth, W.W., 1993. U.S. Atlantic continental slope landslides: Their distribution, general attributes, and implications. In: Schwab, W.C., Lee, H.J., Twichell, D.C. (Eds.), Submarine Landslides: Selected Studies in the U.S. Exclusive Economic Zone, U.S. Geological Survey Bulletin 2002, pp. 14–22.

Bouma, A.H., 1962. Sedimentology of Some Flysch Deposits: A graphic approach to facies interpretation. Amsterdam: Elsevier, p. 168.

Bouma, A.H., (Ed.), 1983/1984. COMFAN. Geo-Marine letters 3, Nos. 2, 312/13/2005, 4, 53–224.

Bouma, A.H., Brouwer, A. (Eds.), 1964. Turbidites: Developments in Sedimentology 3, Elsevier, Amsterdam, p. 264.

Bouma, A.H., Coleman, J.M., l985. Peira Cava turbidite system, France. In: Bouma, A.H., Normark, W.R., Barnes, N.E. (Eds.), Submarine Fans and Related Turbidite Systems, Springer-Verlag, New York, pp. 217–222.

Bouma, A.H., Coleman, J.M., DSDP Leg 96 Shipboard Scientists, l985. Mississippi Fan: Leg 96 program and principal results. In: Bouma, A.H., Normark, W.R., Barnes, N.E. (Eds.), Submarine Fans and Related Turbidite Systems, Springer-Verlag, New York, pp. 247–252.

Bouma, A.H., Hollister, C.D., 1973. Deep ocean basin sedimentation. In: Middleton, G.V., Bouma, A.H. (Eds.), Turbidites and Deep-Water Sedimentation, Anaheim, SEPM Pacific section Short Course. California, pp. 79–118.

Bouma, A.H., Normark, W.R., Barnes, N.E. (Eds.) l985. Submarine Fans and Related Turbidite Systems, Springer-Verlag, New York, p. 351.

Bouma, A.H., DeVries, M.B., Stone, C.G., 1997. Reinterpretation of depositional processes in a classic flysch sequence (Pennsylvanian Jackfork Group), Ouachita Mountains, Arkansas and Oklahoma: Discussion. AAPG Bulletin, 81, 470–472.

Bouma, A.H., Stelting, C.E., Stone, C.G. (Leaders), 1997. Fine-grained submarine fan architecture and turbidite nomenclature, Jackfork Group, Arkansas. Trip # 14. Official Program–1997 AAPG Annual Convention, Dallas, Texas, 22.

Bouma, A.H., Stone, C.G. (Eds.), 2000. Fine-grained turbidite systems. AAPG Memoir 72 and SEPM Special Publication 68, p. 342.

Bourgeois, J., Hansen, T.A., Wiberg, P.L., Kauffman, E.G., 1988. A tsunami deposit at the Cretaceous-Tertiary boundary in Texas. Science, 241, 567–570.

Brainy Quote, 2005. Albert Einstein Quotes. Uniform Resource Locator (URL): http://www.brainyquote.com/quotes/quotes/a/alberteins133991.html (accessed February 4, 2005).

Bramlette, M.N., Bradley, W.H., 1940. Geology and Biology of North Atlantic deep-sea cores. U.S. Geological Survey, Professional paper 196-A, 1–34.

Bramlette, M.N., 1946. The Monterey Formation of California and the origin of its siliceous rocks. U.S. Geological Survey, Professional Paper 212, p.57.

Brenchley, P.J., 1985. Storm influenced sandstone beds. Modern Geology, 9, 369–396.

Brennecke, W., 1921. Die oceanographis-chen Arbeiten derdeutschen antarktisschen Expedition 1911–1912 Arch dt. Seewarte 39 (1), 1–216.

Brewster, J., 1991. The Frigg field, Block 10/1 UK North Sea and 25/1, Norwegian North Sea. In: Abbotts, I.L. (Ed.), United Kingdom Oil and Gas Fields, 25 Years Commemorative vol. Geological Society Memoir No. 14, 117–126.

Briggs, G., Cline, L.M., 1967. Paleocurrents and source areas of Late Paleozoic sediments of the Ouachita Mountains, Southeastern Oklahoma. Journal of Sedimentary Petrology, 37, 985–1000.

Brooke, C.M., Trimble, T.J., Mackay, T.A., 1995. Mounded shallow gas sands from the Quaternary of the North Sea: analogues for the formation of sand mounds in deep water Tertiary sediments? In: Hartley, A.J., Prosser, D.J. (Eds.), Characterisation of Deep Marine Clastic Systems, Geological Society, Special Publications, London, 94, pp. 95–101.

Brown, G.C., 1990. Historical perspectives and evolution in the studies of deep marine deposition. In: Brown, G.C., Gorsline, D.S., Schweller, W.J. (Eds.), Deep-Marine Sedimentation: Depositional Models and Case Histories in Hydrocarbon Exploration & Development, San Francisco: SEPM Pacific Section Short Course vol. 66, pp. 1–22.

Brown, G.C., Gorsline, D.S., Schweller, W.J. (Eds.), 1990. Deep-Marine Sedimentation: Depositional models and case histories in hydrocarbon exploration & development. San Francisco: SEPM Pacific Section Short Course vol. 66, p. 326.

Bruhn, C.H.L., Walker, R.G., 1997. Internal architecture and sedimentary evolution of coarse grained, turbidite channel-levee complexes, Early Eocene Regencia Canyon, Espirito Santo basin, Brazil. Sedimentology, 44, 17–46.

Brush Jr., L.M., 1965. Experimental work on primary sedimentary structures. In: Middleton, G.V. (Ed.), Primary Sedimentary Structures and their Hydrodynamic Interpretation, SEPM Special Publication 12, pp. 17–24.

Bryant, E., 2001. Tsunami: The Underrated Hazard. Cambridge, New York, Melbourne, Cambridge University Press, p. 320.

Bucher, W.H., 1940. Submarine valleys and related geologic problems of the North Atlanitic. GSA Bulletin, 51, 489–451.

Bugge, T., 1983. Submarine slides on the Norwegian continental margin, with special emphasis on the Storegga area. IKU Continental Shelf Institute Publication 110, Norway, p. 152.

Bullard, E., 1975. The emergence of plate tectonics: A personal view. Annual Review of Earth and Planetary Sciences, 3, 1–30.

Burke, K., 1967. The Yallahs Basin: A sedimentary basin southeast of Kingston, Jamaica. Marine Geology, 5, 45–60.

Buss, E., Heim, A., 1881. Der Bergsturz von Elm: Zurich, Worster. p. 133.

Bussert, R., Aberhan, M., 2004. Storms and tsunamis: evidence of event sedimentation in the Late Jurassic Tendaguru Beds of Southeastern Tanzania. Journal of African Earth Sciences, 39, 549–555.

Butman, B., Noble, M., Folger, D.W., 1979. Long-term observations of bottom current and bottom sediment movement on the mid-Atlantic continental shelf. Journal of Geophysical Research, 84, 1167–1205.

California Oil and Gas Fields, 1985. Central California. The California Department of Conservation, Division of Oil and Gas, Sacramento, vol. 1.

Campbell, C.S., 1989. Self-lubrication for long runout landslides. Journal of Geology, 97, 653–665.

Campbell, C.S., 1990. Rapid granular flows. Annual Review of Fluid Mechanics, 22, 57–91.

Carlson, P.R., Karl, H.A., 1988. Development of large submarine canyons in the Bering Sea indicated by morphologic, seismic, and sedimentologic characteristics. GSA Bulletin, 100, 1594–1615.

Carlson, P.R., Molnia, B.F., 1977. Submarine faults and slides on the continental shelf, northern Gulf of Alaska. Marine Geotechnology, 2, 275–290.

Carlson, P.R., Karl, H.A., Edwards, B.D., 1991. Mass sediment failure and transport features revealed by acoustic techniques, Beringian margin, Bering Sea, AK. Marine Geotechniques, 10, 33–51.

Carter, R.M., 1975. A discussion and classification of subaqueous mass-transport with particular application to grain flow, slurry flow, and fluxoturbidites. Earth-Science Reviews, 11, 145–177.

Carver, R.E., 1971. Procedures in Sedimentary Petrology. Wiley-Interscience, New York, p. 653.

Casnedi, R., 1983. Hydrocarbon-bearing submarine fan system of Cellino Formation, central Italy: AAPG Bulletin, 67, 359–370.

Chamberlain, C.K., 1971. Bathymetry and paleoecology of Ouachita geosyncline of southeastern Oklahoma as determined from trace fossils. AAPG Bulletin, 55, 34–50.

Chan, M.A., Dott, R.H., 1983. Shelf and deep-sea sedimentation in Eocene forearc basin, western Oregon-fan or non-fan? AAPG Bulletin, 67, 2100–2116.

Cheel, R.J., Leckie, D.A., 1993. Hummocky cross-stratification. In: Wright, P.V. (Ed.), Sedimentology Review 1, Blaclwell Scientific Publications, Oxford, pp. 103–122.

Cheel, R.J., Leckie, D.A., 1997. From sandstone to chaos: a symposium in honor of Gerard V. Middleton on his retirement, 1996. Geoscience Canada, 24, 2.

Chikita, K., 1989. A field study on turbidity currents initiated from spring runoffs. Water Resources Research, 25, 257–271.

Chough, S.K., Hesse, R., 1985. Contourites from the Eirik Ridge, South of Greenland. Sedimentary Geology, 41, 185–199.

Cita, M.B., Aloisi, G., 2000. Deep-sea tsunami deposits triggered by the explosion of Santorini (3500 y BP), eastern Mediterranean. Sedimentary Geology, 135, 181–203.

Cita, M.B., Camerlenghi, A., Rimoldi, B., 1996. Deep-sea tsunami deposits in the eastern Mediterranean: new evidence and depositional models. Sedimentary Geology, 104, 155–173.

Cita, M.B., Maccagni, A., Pirovano, G., 1982. Tsunami as triggering mechanism of homogenites recorded in areas of the eastern Mediterranean characterized by the 'Cobblestone Topography'. In: Saxov, S., Neuwenhuis, J.K. (Eds.), Marine Slides and Other Mass Movements, Plenum Press, London, pp. 233–261.

Clark, J.D., Pickering, K.T., 1996. Submarine Channels: Processes and architecture. Vallis Press, London, p. 231.

Clark, J.D., Stanbrook, D.A., 2001. Formation of large-scale shear structures during the deposition of high-density turbidity currents, Grès d'Annot Formation, SE France, In: McCaffrey, W.D., Kneller, B.C., Peakall, J. (Eds.), Particulate Gravity Currents, IAS Special Publication 31, pp. 219–232.

Cline, L.M., 1970. Sedimentary features of Late Paleozoic flysch, Ouachita Mountains, Oklahoma. In: Lajoie, J. (Ed.), Flysch Sedimentology in North America, The Geological Association of Canada Special Paper 7, pp. 85–101.

Cloetingh, S., 1986. Intraplate stresses: A new mechanism for fluctuations of relative sea level. Geology, 14, 617–620.

Coleman Jr., J.L., 1997. Reinterpretation of depositional processes in a classic flysch sequence (Pennsylvanian Jackfork Group), Ouachita Mountains, Arkansas and Oklahoma: Discussion. AAPG Bulletin, 81, 466–469.

Coleman, J.M., 1969. Brahmaputra River: Channel processes and sedimentation. Sedimentary Geology, 3, 129–239.

Coleman, J.M., Garrison, L.E., 1977. Geological aspects of marine slope stability, northwestern Gulf of Mexico. In: Richards, A.F.(Ed.), Marine Geotechnology, Marine Slope Stability, vol. 2. Crane, Russak & Company, Inc., pp. 9–44.

Coleman, J.M., Prior, D.B., 1982. Deltaic environments. In: Scholle, P.A., Spearing, D. (Eds.), Sandstone Depositional Environments, AAPG Memoir 31, 139–178.

Coleman, P.J., 1968. Tsunamis as geological agents. Geological Society of Australia, 15, 267–273.

Collinson, J.D., 1994. Sedimentary deformational structures. In: Maltman, A., (Ed.) The geological Deformation of Sediments, Chapman & Hall, London, pp. 95–125.

Collinson, J.D., Thompson, D.B., 1982. Sedimentary Structures, George Allen & Unwin, London, p. 194.

Cook, H.E., 1979. Ancient continental slope sequences and their value in understanding modern slope development. In: Doyle, L.J., Pilkey, O.H. (Eds.), Geology of Continental Slopes, SEPM Special Publication 27, pp. 287–305.

Cook, H.E., Enos, P. (Eds.), 1977. Deep-water carbonate environments. SEPM Special Publication 25, p. 335.

Cooper, C., Forristall, G.Z., Joyce, T.M., 1990. Velocity and hydrographic structure of two Gulf of Mexico warm-core rings. Journal of Geophysical Research, 95, No. C2, 1663–1679.

Cooperman, A.I., Rosendal, H.E., 1962. Great Atlantic Storm, 1962. Mariners Weather Log, 6, 79–85.

Costa, J.E., Williams, G.P., 1984. Debris-flow Dynamics (videotape). U.S. Geological Survey Open File Report OF 84-0606.

Coussot, P., Meunier, M., 1996. Recognition, classification and mechanical description of debris flows. Earth-Science Reviews, 40, 209–227.

Cowan, E.A., Cai, J., Powell, R.D., Seramur, K.C., Spurgeon, V.L., 1998. Modern tidal rhythmites deposited in a deep-water estuary. Geo-Marine Letters, 18, 40–48.

Crease, J., 1965. The flow of Norwegian Sea Water through the Faeroe Bank Channel. Deep-Sea Research, 12,. 143–150.

Crowell, J.C., 1957. Origin of pebbly mudstones. GSA Bulletin, 68, 993–1009.

Crowell, J.C., 1961. Depositional structures from Jurassic Boulder Beds, East Sutherland. Transactions of the Edinburgh Geological Society, 18, 202–220.

Crowell, J.C., 1964. Deep-water sedimentary structures Pliocene Pico Formation, Santa Paula Creek, Ventura Basin, California. California Division of Mines and Geology Special Report H89.

Cummins, W.A., 1962. The greywacke problem. Liverpool and Manchester Geology Journal, 3, 51–72.

Curray, J.R., Emmel, F.J., Moore, D.G., 2003. The Bengal Fan: morphology, geometry, stratigraphy, history and processes. Marine and Petroleum Geology, 19, 1191–1223

Curray, J.R., Moore, D.G., 1971. Growth of the Bengal deep-sea fan and denudation in the Himalayas. GSA Bulletin, 82, 563–572.

Curray, J.R., Moore, D.G., 1974. Sedimentary and tectonic processes in the Bengal Deep-sea Fan and Geosyncline. In: Burk, C.A., Drake, C.L. (Eds.,), Continental Margins, Springer, New York, pp. 617–627.

Curray, J.R., Emmel, F.J., Moore, D.G., Raitt, R.W., 1982. Structure, tectonics, and geological history of the northeastern Indian Ocean. In: Nairn, A.E.M., Stehli, F.G. (Eds.), Ocean Basins and Margins, Plenum Press, New York, vol. 6, pp. 399–450.

D'Agostino, A.E., Jordan, D.W., 1997. Reinterpretation of depositional processes in a classic flysch sequence (Pennsylvanian Jackfork Group), Ouachita Mountains, Arkansas and Oklahoma: Discussion. AAPG Bulletin, 81, pp. 473–475.

Dalrymple, R.W., 1992.Tidal depositional systems. In: Walker, R.G., James, N.P. (Eds.), Facies Models: Response to Sea Level Change, GEOtext 1. Geological Association of Canada, pp. 195–218.

Dalrymple, R.W., Narbonne, G.M., 1996. Continental slope sedimentation in the Sheepbed Formation (Neoproterozoic, Windermere Supergroup), Mackenzie Mountains, N.W.T. Canadian Journal of Earth Science, 33, 848–862.

Daly, R.A., 1936 Origin of submarine canyons. American Journal of Science, 31, 410–420.

Damuth, J.E., 1977. Late Quaternary sedimentation in the western equatorial Atlantic. GSA Bulletin, 88, 695–710.

Damuth, J.E., Embley, R.W., 1981. Mass-transport processes on Amazon Cone: Western Equatorial Atlantic. AAPG Bulletin, 65, 629–643.

Damuth, J.E., Fairbridge, R.W., 1970. Equatorial Atlantic deep-sea sands and ice age aridity in tropical South America. GSA Bulletin, 81, 585–601.

Damuth, J.E., Flood, R.D., Kowsmann, R.O., Gorini, M.A., Belderson, R.H., 1988. Anatomy and growth-pattern of Amazon deep-sea fan revealed by long-range side-scan sonar (GLORIA) and high-resolution seismic studies. AAPG Bulletin, 72, 885–911.

Darwin, C., 1846. The geology of the voyage of the Beagle, part 3: Geological Observations on South America. London: Smith, Elder and Company, p. 279.

Dasgupta, P., 2003. Sediment-gravity flow–the conceptual problems. Earth-Science Reviews, 62, 265–281.

Davies, G. R., 1997. Interpretites: the new universal, non-genetic, non-descriptive classification of sedimentary products and environments. Canadian Society Petroleum Geologists, Reservoir, 24, 22–23.

Davies, R.J., 2003. Kilometer-scale fluidization structures formed during early burial of a deep-water slope channel on the Niger Delta. Geology, 31, 949–952.

Dawson, A.G., Shi, S., 2000. Tsunami deposits. Pure and Applied Geophysics, 157, 875–897.

de Boer, P.L., Oost, A.P., Visser, M.J., 1989. The diurnal inequality of the tide as a parameter for recognizing tidal influences. Journal of Sedimentary Petrology, 59, 912–921.

DeVries, M.B., Bouma, A.H., 1992. Lateral correlation trends in bedded and massive turbidites, with an example from DeGray Lake, Arkansas. Gulf Coast Association of Geological Societies Transactions, 42, 789–791.

Dewey, J.F., Bird, J.M., 1970. Mountain belts and the new global tectonics. Journal of Geophysical Research, 75, 2625–2647.

Dill, R.F.,1964. Sedimentation and erosion in Scripps submarine canyon head. In: Miller, R.L. (Ed.), Marine Geology, Macmillan, London, pp. 23–41.

Dill, R.F., Marshall, N.F., Reimnitz, E., 1975. In situ submersible observations of sediment transport and erosive features in Rio Balsas Submarine Canyon, Mexico (Abs). Geological Society of America, 7, 1052–1053.

Diller, G.S., 1890. Sandstone dykes. GSA Bulletin, 1, 411–442.

Dingle, R.V., 1977. The anatomy of a large submarine slump on a sheared continental margin (SE Africa). Journal of Geological Society of London, 134, 293–310.

Dixon, R.J., Schofield, K., Anderton, R., Reynolds, A.D., Alexander, R.W.S., Williams, M.C., Davies, K.G., 1995. Sandstone diapirism and clastic intrusion in the Tertiary sub-marine fans of the Bruce–Beryl Embayment, Quadrant 9, UKCS. In: Hartley, A.J., Prosser, D.J. (Eds.), Characterization of Deep Marine Clastic Systems, Geological Society, London, Special Publications, 94, pp. 77–94.

Doreen Jr., J.M., 1951. Rubble bedding and graded bedding in Talara Formation of northwestern Peru. AAPG Bulletin, 35, 1829–1849.

Dott Jr., R.H., 1963. Dynamics of subaqueous gravity depositional processes. AAPG Bulletin, 47, 104–128.

Dowdeswell, J.A., Ó Cofaigh, C., Taylor, J., Kenyon, N.H., Mienert, J., Wilken, M., 2002. On the architecture of high-latitude continental margins: the influence of ice-sheet and sea-ice processes in the Polar North Atlantic. In: Dowdeswell, J.A., Ó Cofaigh, C. (Eds.), Glacier-Influenced Sedimentation on High-Latitude Continental Margins, Geological Society. London. Special Publication 203, pp. 33–54.

Doyle, L.J., Pilkey, O.H. (Eds.) 1979. Geology of Continental Slopes. SEPM Special Publication 27, p. 374.

Drake, C.L., Ewing, M., Sutton, G.H., 1959. Continental margins and geosynclines: the east coast of North America, north of Cape Hatteras. In: Ahrens, L.H., et al. (Eds.), Physics and Chemistry of the Earth, vol. 3, Pergamon Press, Oxford, pp. 110–198.

Droz, L., Rigaut, F., Cochonat, P., Tofani, R., 1996. Morphology and recent evolution of the Zaire turbidite system (Gulf of Guinea). GSA Bulletin, 108, 253–269.

Dunnavan, G.M., Diercks, J.W., 1980. Supertyphoon Tip. Monthly Weather Review, 108, 1915–1923.

Duranti, D, Hurst, A., 2004. Fluidization and injection in the deep-water sandstones of the Eocene Alba Formation (U.K. North Sea). Sedimentology, 51, 503–529.

Dzulynski, S., Sanders, J.E., 1962 Current marks on firm mud bottoms. Connecticut Academy of Arts and Science, transactions, 42, 57–96.

Dzulynski, S., Walton, E.K., 1965. Sedimentary features of flysch and greywackes, Elsevier, Amsterdam, p. 274.

Dzulynski, S., Ksiazkiewicz, M., Kuenen, Ph. H., 1959. Turbidites in flysch of the Polish Carpathian Mountains. GSA Bulletin, 70, 1089–1118.

Egbert, G.D., Ray, R.D., 2000. Significant dissipation of tidal energy in the deep ocean inferred from satellite altimeter data. Nature, 405, June 15, pp. 775–778.

Einsele, G., Chough, S.K., Shiki, T., 1996. Depositional events and their records—an introduction. Sedimentary Geology, 104, 1–9.

Elverhoi, A., Norem, H., Anderson, E.S., Dowdeswell, J.A., Fossen, I., Haflidason, H., Kenyon, N.H., Laberg, J.S., King, E.L., Sejrup, H.P., Solheim, A., Vorren, T., 1997. On the origin and flow behavior of submarine slides on deep-sea fans along the Norwegian-Barents Sea continental margin. Geo-Marine Letters, 17, pp. 119–125.

Embley, R.W., 1976. New evidence for occurrences of debris flow deposits in the deep sea. Geology, 4, 371–374.

Embley, R.W., 1980. The role of mass transport in the distribution and character of deep-ocean sediments with special reference to the North Atlantic. Marine Geology, 38, 23–50.

Embley, R.W., Jacobi, R.D., 1977. Distributions and morphology of large sediment slides and slumps on Atlantic continental margins. Marine Geotechnology, 2, 205–228.

Embley, R.W., Jacobi, R.D., 1986. Mass wasting in the western North Atlantic. In: Vogt, P.R., Tucholke, B.E. (Eds.), The geology of North America, Geological Society of America Volume M, 479–490.

Enos, P., 1969. Anatomy of a flysch. Journal of Sedimentary Petrology, 39, 680–723.

Enos, P., 1977. Flow regimes in debris flow. Sedimentology, 24, 133–142.

Ericson, D.B., Ewing, W.M., Heezen, B.C., 1952. Turbidity currents and sediments in North Atlantic. AAPG Bulletin, 56, 489–511.

Escutia, C., Eitreimm, S.L., Cooper, A.K., Nelson, C. H., 2000. Morphology and acoustic character of the Antarctic Wilkes Land turbidite systems: Ice-sheet sourced versus river-sourced fans. Journal of Sedimentary Research, 70, 84–93.

Ewing, M., Thorndike, E.M., 1965. Suspended matter in deep ocean water. Science, 147, 1291–1294.

Ewing, M., Ettrium, S.L., Ewing, J.L., Le Pichon, X., 1971. Sediment transport and distribution in the Argentine Basin: Part 3, Nepheloid layer and process of sedimentation. In: Ahrens, L.A., Press, F., Runcorn, S.K., Urey, H.C. (Eds.), Physics and Chemistry of the Earth, Pergamon Press, London, pp. 55–77.

Famakinwa, S.B., Shanmugam, G., Hodgkinson, R.J., Blundell, L.C., 1996. Deep-water slump and debris flow dominated reservoirs of the Zafiro Field area, offshore Equatorial Guinea. Offshore West Africa Conference and Exhibition, November 5–7, Libreville, Gabon, pp. 1–14.

Famakinwa, S.B., Shanmugam, G., Hodgkinson, R.J., Blundell, L.C., 1997. Deep-water slump and debris flow dominated reservoirs of the Zafiro Field area, offshore Equatorial Guinea. Official Program-1997 AAPG Annual Convention, Dallas, Texas, A 34.

Faugères, J.C., Gonthier, E., Stow, D.A.V., 1984. Contourite drift molded by deep Mediterranean outflow. Geology, 12, 296–300.

Feldhausen, P.H., Stanley, D.J., Knight, R.J., Maldonado, A., 1981. Homogenization of gravity-emplaced muds and unifites: models from the Hellenic Trench. In: Wezel, F.C. (Ed.), Sedimentary Basins of Mediterranean margins. Tecnoprint, Bologna, pp. 203–226.

Fildani, A., Normark, W.R., 2004. Late Quaternary evolution of channel and lobe complexes of Monterey Fan. Marine Geology, 206, 199–223.

Filkin, D., 1997. Stephen Hawking's Universe: The Cosmos Explained. Basic Books, New York, p. 288.

Fisher, R.V., 1971. Features of coarse-grained, high-concentration fluids and their deposits. Journal of Sedimentary Petrology, 41, 916–927.

Fisher, R.V., 1983. Flow transformations in sediment gravity flows. Geology, 11, 273–274.

Fisher, R.V., 1995. Decoupling of pyroclastic currents and hazards assessments. Special Issue, Glicken Volume, Jour. Volcanol. Geotherm. Res., 66, 257–263.

Fisher, R.V., Mattinson, J.M., 1968. Wheeler Gorge turbidite-conglomerate series, California, Inverse Grading: Journal of Sedimentary Petrology, 38, 1013–1023.

Fisher, R.V., Schmincke, H.U., 1984. Pyroclastic Rocks. Springer-Verlag, Berlin, p. 472.

Flint, R.F., Sanders, J. E., Rodges, J., 1960. Diamictite: a substitute term for symmictite. Geological Society of America Bulletin, 71, 1809–1810.

Flood, R.D., 1988. A lee-wave model for deep-sea mudwave activity. Deep-Sea Research, 35, 973–983.

Flood, R.D., Manley, P., Kowsmann, R.O., Appi, C.J., Pirmez, C., 1991. Seismic facies and Late Quaternary growth of Amazon submarine fan. In: Weimer, P., Link, M.H. (Eds.), Seismic Facies and Sedimentary Processes of Submarine Fans and Turbidite Systems, Springer-Verlag, New York, pp. 415–433.

Flood, R.D., Piper, D.J.W., Klaus, A., Burns, S.J., Busch, W.H., Cisowski, S.M., Cramp, A., Damuth, J.E., Goñi, M.A., Haberle, S.G., Hall, F.R., Hinrichs, K-U., Hiscott, R.N., Kowsmann, R.O., Kronen,

Jr., J.D., Long, D., Lopez, M., McDaniel, D.K., Manley, P.L., Maslin, M.A., Mikkelsen, N., Nanayama, F., Normak, W.R., Pirmez, C., dos Santos, J.R., Schneider, R.R., Showers, W.J., Soh, W., Thibal, J., 1995. Proceedings of the Ocean Drilling Program, Initial Reports 155, College Station, Texas (Ocean Drilling Program), p. 1233.

Flores, G., 1955. Discussion of a paper by F. Beneo: Les resultants des etudes pour la recherché pétrolifêre en Sicilie. Proce. 4th World Petroleum Congress, Sec. 1, 121–122.

Folk, R.L., 1968. Petrology of Sedimentary Rocks. Austin, Texas, Hemphill's, p. 170.

Forel, F.A., 1885. Le ravin sous-lacustre des fleuves glaciaires. C. r. hebd. Seanc. Acad. Sci. Paris 191, 725–728.

Forel, F.A., 1887. Le ravin sous-lacustre de Rhone dans le lac Leman. Bulletin de la Societe Vaudoise Science Naturelle, 23, 85–107.

Forel, F.A., 1892. Le Feman, Monographie Limnologique, vol. 1, Geographie, Hydrographie, Geologie, Climatologie, Hydrologie. F. Rouge, Lasusanne, p. 543.

Forristall, G.Z., Hamilton, R.C., Vardone, V.J., 1977. Continental shelf currents in Tropical Storm Delta: observations and theory. Journal of Physical Oceanography, 87, 532–546.

Friedman, G.M., 1998. Sedimentology and stratigraphy in the 1950s to mid-1980s: The story of a personal perspective. Episodes, 21, 172–177.

Friedman, G.M., 2000. My friend and colleague John Essington Sanders (1926–1999), a personal perspective and history. In: Friedman, G.M. (Ed.), Conference on the History of Geologic Pioneers, Troy, Rensselaer Center of Applied Geology, New York, pp. 7–8.

Friedman, G.M., Sanders, J.E., 1974. Positive-relief bedforms on modern tidal flat that resemble molds of flutes and grooves; implications for geopetal criteria and for origin and classification of bedforms. Journal of Sedimentary Petrology, 44, 181–189.

Friedman, G.M., Sanders, J.E., 1978. Principles of Sedimentology, John Wiley & Sons, New York, p. 792.

Friedman, G.M., Sanders, J.E., 1997. Dispelling the myth of sea-floor tranquility. Geotimes, 42, 24–27.

Friedman, G.M., Sanders, J.E., Kopaska-Merkel, D.C., 1992. Principles of Sedimentary deposits: Stratigraphy and Sedimentology. McMillan Publishing Company, New York, p. 717.

Fuglister, F.G., 1951. Multiple currents in the Gulf Stream System. Tellus, 3, 230–233.

Galay, V., 1987. Erosion and sedimentation in the Nepal Himalaya. Singapore: Kefford Press Pvt. Ltd., p. 10, 11.

Galaziy, G.I. (Ed.), 1993. Baikal Atlas. Federal Agency for Geodesy and Cartography, Moscow.

Galloway, W.E., 1998. Siliciclastic slope and base-of-slope depositional systems: Component facies, stratigraphic architecture, and classification. AAPG Bulletin, 82, 569–595.

Galloway, W.E., Hobday, D.K., 1983. Terrigenous clastic depositional systems: applications to petroleum, coal, and uranium exploration, Springer-Verlag, New York, pp. 423.

Gani, R., 2004. From turbid to lucid: A straightforward approach to sediment gravity flows and their deposits. The Sedimentary Record, 3, pp. 4–8.

Gardner, J.V., Bohannon, R.G., Field, M.E., Masson, D.G., 1996. The morphology, processes, and evolution of Monterey Fan: A revisit. In: Gardner, J.V., Field, M.E., Twichell, D.C. (Eds.), Geology of the United States' Sea Floor: The View from GLORIA, Cambridge University Press, New York, pp. 193–220.

Gardner, J.V., Dartnell, P., Christopher Stone, J., Mayer, L.A., Hughes Clark, J.E., 2002. Bathymetry and selected perspective views Offshore Greater Los Angeles, California. U.S. Geological Survey, Water-Resources Investigations Report 02–4126.

Gardner, J.V., Mayer, L.A., Hughes Clarke, J.E., 2000. Morphology and processes in Lake Tahoe (California–Nevada). GSA Bulletin, 112, 736–746.

Gardner, M.H., Borer, J.M., Melick, J.J., Mavilla, N., Dechesne, M., Wagerle, R.N., 2003. Stratigraphic process-response model for submarine channels and related features from studies of Permian Brushy Canyon outcrops, West Texas. Marine and Petroleum Geology, 20, pp 757–787.

Gawthorpe, R.L., Clemmey, H., 1985. Geometry of submarine slides in the Bowland Basin (Dinantian) and their relation to debris flows. Journal of Geological Society of London, 142, 555–565.

Gee, M.J.R., Masson, D.G., Watts, A.B., Allen, P.A., 1999. The Saharan debris flow: an insight into the mechanics of long-runout submarine debris flows. Sedimentology, 46, 317–335.

Ghibaudo, G., 1992. Subaqueous sediment gravity flow deposits: practical criteria for their field description and classification. Sedimentology, 39, 423–454.

Ginsburg, R.N. (Ed.), 1973. Evolving concepts in sedimentology. Baltimore and London: The Johns Hopkins University Press, p. 191.

Gong-Yiming 1988. Tempestite, seismite, and tsunamite: a discussion of seceral sedimentological terms. Geological Review, 34, 481–482.

Gonthier, E.G., Faugeres, J.-C., Stow, D.A.V., 1984. Contourite facies of the Faro Drift, Gulf of Cadiz. In: Stow, D.A.V., Piper, D.J.W. (Eds.), Fine-Grained Sediments: Deep-Water Processes and Facies, Geological Society of London Special Publication, 15, pp. 275–292.

Gorsline, D.S., 1980. Deep-water sedimentologic conditions and models. Marine Geology, 38, 1–21.

Gorsline, D.S., Emery, K.O., 1959. Turbidity current deposits in Sand Pedro and Santa Monica basins off southern California. GSA Bulletin, 70, 279–290.

Gould, H.R., 1951. Some quantitative aspects of Lake Mead turbidity currents. In: Hough, J.L. (Ed.), Turbidity Currents and the Transportation of Coarse Sediments to Deep Water, a Symposium, SEPM Special Publication, 2, pp. 34–52.

Graham, S.A., Dickinson, W.R., Ingersoll, R.V., 1975. Himalayan-Bengal model for flysch dispersal in the Appalachian-Ouachita System. GSA Bulletin, 86, 273–286.

Gray, W.M., 1968. Global view of the origin of tropical disturbances and storms. Monthly Weather Review, 96, 669–700.

Greene, H.G., Ward, S.N., 2003. Mass movement features along the central California margin and their modeled consequences for tsunami generation. In: Locat, J., Mienert, J. (Eds.), Submarine Mass Movements and their Consequences, Kluwer Academic Publishers, Dordrecht, pp. 343–356.

Greenly, E., 1919. The Geology of Anglesey. Great Britain Geological Survey Memoir, p. 980.

Griffiths, J.C., 1960. Aspects of measurement in the geosciences. Mineral Industries. College of Mineral Industries, The Pennsylvania State University, 29, No. 4, 4–8.

Griffiths, R.W., 2000. The dynamics of lava flows. Annual Review of Fluid Mechanics, 32, 477–518.

Grover, N.C., Howard, C.S., 1938. The passage of turbid water through Lake Mead. American Society of Civil Engineers Transactions, 103, 720–790.

Guardado, L.R., Gamboa, L.A.P., Lucchesi, C.F., 1990. Petroleum geology of the Campos basin, A model for a producing Atlantic type basin. In: Edwards, J.D., Santogrossi, P.A. (Eds.), Divergent/Passive margin basins, AAPG Memoir, 48, pp. 3–79.

Gulbrandsen, A., 1987. Agat. In: Spencer, A.M. et al. (Eds.), Geology of the Norwegian Oil and Gas Fields. Graham & Trotman, London, pp. 363–370.

Gusiakov, V.K., 2005. Tsunami generation potential of different tsunamigenic regions in the Pacific. Marine Geology, 215, 3–9.

Gutenberg, B.A., 1939. Tsunamis and earthquakes. Sismological Society of America Bulletin, 29, 517–526.

Hallworth, M.A., Huppert, H.E., 1998. Abrupt transitions in high-concentration, particle-driven gravity currents. Physics of Fluids, 10, 1083–1087.

Hampton, M.A., 1972. The role of subaqueous debris flows in generating turbidity currents. Journal of Sedimentary Petrology, 42, 775–793.

Hampton, M.A., 1975. Competence of fine-grained debris flows. Journal of Sedimentary Petrology, 45, 834–844.

Hampton, M.A., Lee, H.J., Locat, J., 1996. Submarine landslides. Reviews of Geophysics, 34, 33–59.

Haner, B.E., 1971. Morphology and sediments of Redondo submarine fan, Southern California. GSA Bulletin, 82, 2413–2432.

Hansen, S.M., Fett, T., 2000. Identification and evaluation of turbidite and other deepwater sands using Open Hole Logs and Borehole Images. In: Bouma, A.H., Stone, C.G. (Eds.), Fine-Grained Turbidite Systems, AAPG Memoir 72 and SEPM Special Publication, 68, pp. 317–337.

Haq, B.U., Hardenbol., J., Vail, P.R., 1987. Chronology of fluctuating sea levels since the Triassic. Science, 235, 1156–1167.

Harland, W. B, Herod, K. N., Krinsley, D.H., 1966. The definition and identification of tills and tillites. Earth-Science Reviews, 2, 225–256.

Harms, J.C., 1974. Brushy Canyon Formation, Texas: A deep-water density current deposit. GSA Bulletin, 85, 1763–1784.

Harms, J.C., Fahnestock, R.K., 1965. Stratification, bed forms, and flow phenomena (with an example from the Rio Grande). In: Middleton, G.V. (Ed.), Primary Sedimentary Structures and their Hydrodynamic Interpretation, SEPM Special Publication 12, pp. 84–115.

Harms, J.C., Southard, J.B., Spearing, D.R., Walker, R.G., 1975. Depositional environments as interpreted from primary sedimentary structures and stratification sequences. SEPM Short Course No. 2, Dallas, Texas, p. 161.

Harms, J.C., Southard, J.B., Walker, R.G., 1982. Structures and Sequences in Castic Rocks. SEPM Short Course No. 9, Calgary, Canada, p. 8–51.

Hartley, A.J., Prosser, D.J. (Eds.), 1995. Reservoir Characterization of Deep-water Clastic Systems. Geological Society of London Special Publication, 94, p. 256.

Harvey, J.G., 1976. Atmosphere and Ocean: Our Fluid Environments. Artemis Press, Sussex, p. 143.

Hatton, I.R., Reeder, M., Newman, M.S.T.J., Roberts, D., 1992. Techniques and applications of petrophysical correlation in submarine fan environments, early Tertiary sequence, North Sea. In: Hurst, A, Griffiths, C.M., Worthington, P.F., (Eds.), Geological Applications of Wireline Logs II. Geological Society, London, Special Publication, 65, pp. 21–30.

Hay, A., Burling, R.W., Murray, J.W., 1982. Remote acoustic detection of a turbidity current surge. Science, 217, 833–835.

Heezen, B.C., 1956. Corrientes de turbidez del Rio Magdalena. Sociedad Geografica de Columbia Bulletin, 51–52, 135–143.

Heezen, B.C., Drake, C.L., 1964. Grand Banks slump. AAPG Bulletin, 48, 221–225.

Heezen, B.C., Ewing, M., 1952. Turbidity currents and submarine slumps, and the 1929 Grand Banks earthquake. American Journal of Science, 250, 849–873.

Heezen, B.C., Hollister, C.D., 1971. The Face of the Deep, Oxford University Press, New York, p. 659.

Heezen, B.C., Hollister, C.D., Ruddiman, W.F., 1966. Shaping of the continental rise by deep geostrophic contour currents. Science, 152, 502–508.

Heezen, B.C., Tharp, M., Ewing, M., 1959. The floors of the oceans: I. The North Atlantic. Geological Society of America Special Paper 65, p. 122.

Heezen, B.C., Menzies, R.J., Schneider, E.D., Ewing, W.M., Granelli, N.C., 1964. Congo submarine canyon. AAPG Bulletin, 48, 1126–1149.

Hein, F.J., Walker, R.G., 1982. The Cambto-Ordovician Cap Enrage Formation, Quebec, Canada: Conglomeratic deposits of braided submarine channel with terraces. Sedimentology, 29, 309–329.

Heller, P., Dickinson, W.R., 1985. Submarine ramp facies model for delta-fed, sand-rich turbidite systems. AAPG Bulletin, 69, 960–976.

Hendry, H.E., 1973. Sedimentation of deep water conglomerates in Lower Ordovician rocks of Quebec–Composite bedding produced by liquefaction of sediment?. Journal of Sedimentary Research, 43, 125–136.

Henkel, D.J., 1970. The role of waves in causing submarine landslides. Geotechnique, 20, 75–80.

Herbich, J.B., 1977. Wave-induced scour around offshore pipelines. Offshore Technology Conference, 4, 79–90.

Herdendorf, C.E., 1990. Distribution of the world's large lakes. In: Tilzer, M.M., Serruya, C. (Eds.), Large Lakes: Ecological Structure and Function, Springer-Verlag, New York, pp. 3–38.

Heritier, F.E., Lossel, P., Wathne, E., 1979. Frigg field-large submarine-fan trap in lower Eocene rocks of North Sea. AAPG Bulletin, 63, 1999–2020.

Hess, H.H., 1955. Serpentines, progeny and epeirogeny. In: Poldervaart, A. (Ed.), The Crust of the Earth. Geological Society of America Special Paper 62, pp. 391–408.

Hesse, R., 1975. Turbiditic and non-turbiditic mudstone of Cretaceous flysch sections of the East Alps and other basins. Sedimentology, 22, 387–416.

Hesse, R., 1989. 'Drainage systems' associated with mid-ocean channels and submarine yazoos: Alternative to submarine fan depositional systems. Geology, 17, 1148–1151.

Hesse, R., Klaucke, I., Khodabakhsh, S., Piper, D.J.W., Ryan, W.B.F., NAMOC Study Group 2001. Sandy submarine braidplains: Potential deep-water reservoirs. AAPG Bulletin, 85, 1499–1522.

Hiscott, R.N., 1979. Clastic sills and dikes associated with deep-water sandstones, Tourelle Formation, Ordovician, Quebec. Journal of Sedimentary Petrology, 49, 1–10.

Hiscott, R.N., Aksu, A.E., 1994. Submarine debris flows and continental slope evolution in front of quaternary ice sheets, Baffin Bay, Canadian Arctic. AAPG Bulletin, vol. 78, p. 445–460.

Hiscott, R.N., Middleton, G.V., 1979. Depositional mechanics of thick-bedded sandstones at the base of a submarine slope, Tourelle Formation (Lower Ordovician), Quebec, Canada. In: Doyle, L.J., Pilkey, O.H. (Eds.), Geology of Continental Slopes, SEPM Special Publication 27, pp. 307–326.

Hiscott, R.N., Pickering, K.T., Bouma, A.H., Hand, B.M., Kneller, B.C., Postma, G., Soh, W., 1997. Basin-floor fans in the North Sea: Sequence stratigraphic models *vs.* sedimentary facies: Discussion. AAPG Bulletin, 81, 662–665.

Hollister, C.D., 1967. Sediment distribution and deep circulation in the western North Atlantic. Unpublished Ph.D. dissertation. Columbia University, New York, p. 467.

Hollister, C.D., 1993. The concept of deep-sea contourites. Sedimentary Geology, 82, 1–7.

Hollister, C.D., Heezen, B.C., 1972. Geologic effects of ocean bottom currents: western north Atlantic. In: Gordon, A.L. (Ed.), Studies in Physical Oceanography. vol. 2, Gordon and Breach Science Publishers, New York, pp. 37–66.

Hollister, C.D., McCave, I.N., 1984. Sedimentation under deep-sea storms. Nature, 309, 220–225.

Hollister, C.D., Nowell, A.R.M., 1991. HEBBLE epilogue. Marine Geology, 99, 445–460.

Hollister, C.D., Johnson, D.A., Lonsdale, P.F., 1974. Current-controlled abyssal sedimentation: Samoan Passage, equatorial west Pacific. Journal of Geology, 82, 275–300.

Holman, W., Robertson, S.S., 1994. Field development and depositional model, and production performance of the turbiditic "J" Sands at prospect Bullwinkle, Green Canyon 65 Field, outer shelf Gulf of Mexico. In: Weimer, P. Bouma, A.H., Perkins, R.F. (Eds.), Submarine Fans and Turbidite Systems, Gulf Coast Section of SEPM 15th Annual Research Conference, pp. 139–150.

Houghton, N.M., 1997. Sedimentology, Diagenesis, and Reservoir Quality of Deepwater Clastics, Pliocene Intra Qua Iboe 3 and 4 intervals, Agbada Formation, Offshore Nigeria, Unpublished M.S. Thesis. Dallas, Southern Methodist University, Dedman College, Texas, p. 115.

Howe, J.A., Humphrey, J.D., 1995. Photographic Evidence for Slope Current Activity on the Hebrides slope, North-East Atlantic Ocean. Scott. Journal of Geology, 30, 107–115.

Howell, D.G., Normark, W.R., 1982. Sedimentology of submarine fans. AAPG Memoir, 31, 365–404.

Hoyt, W.V., 1959. Erosional Channel in the Middle Wilcox near Yoakum, Lavaca County, Texas. Transactions-Gulf Coast Association of Geological Societies, IX, 41–50.

Hsü, K.J., 1959. Flute- and groove-casts in the Prealpine Flysch, Switzerland. American Journal of Science, 257, 529–536.

Hsü, K.J., 1970. The meaning of the word Flysch—a short historical search. In: Lajoie, J. (Ed.), Flysch Sedimentology in North America, Geological Association of Canada Special Paper No. 7, pp. 1–11.

Hsü, K.J., 1974. Mélanges and their distinction from olistostromes. In: Dott Jr., R.H., Shaver, R.H., (Eds.), Modern and Ancient Geosynclinal Sedimentation, Soc. Econ. Paleont. and Mineral. Special Publ. 19.

Hsü, K.J., 1975. Catastrophic debris streams (sturzstroms) generated by rock falls. GSA Bulletin, 86, 129–140.

Hsü, K.J., 1977. Studies of Ventura Field, California I: Facies geometry and genesis of lower Pliocene turbidites. AAPG Bulletin, 61, 137–168.

Hsü, K.J., 1989. Physical principles of sedimentology. Springer-Verlag, New York, p. 233.

Hsü, K.J., 2004. Physics of sedimentology. 2nd Edition. Springer, Berlin, p. 240.

Hubbard, D.K., 1992. Hurricane-induced sediment transport in open shelf tropical systems–An example from St. Croix, U.S. Virgin Islands. Journal of Sedimentary Petrology, 62, 946–960.

Hubert, J.F., 1964. Textural evidence for deposition of many western North Atlantic deep-sea sands by ocean-bottom currents rather than turbidity currents. Journal of Geology, 72, 757–785.

Hungr, O., Evans, S.G., 2004. Entrainment of debris in rock avalanches: An analysis of a long run-out mechanism. GSA Bulletin, 116, 1240–1252.

Hurst, A., Cartwright, J.A., Duranti, D., Huuse, M., Nelson, M., 2005. Sand injectites: an emerging global play in deep-water clastic environments. In: Doré, A.G., Vining, B.A. (Eds.), Petroleum Geology: North-West Europe and Global Perspectives–Proceedings of the 6th Petroleum Geology Conference, Petroleum Geology Conferences Ltd. Published by the Geological Society, London, pp. 133–144.

Hutton, J., 1788. Theory of the earth. Royal Society of Edinburgh Transactions, 1, 209–304.

Hyne, N.J., Goldman, C.R., and Court, J.E., 1973. Mounds in Lake Tahoe, California-Nevada: A model for landslide topography in the subaqueous environment. Journal of Geology, 81, 176–188.

Ingersoll, R.V., Suczek, C.A., 1979. Petrology and provenance of Neogene sand from Nicobar and Bengal fans, DSDP Sites 211 and 218. Journal of Sedimentary Petrology, 49, 1217–1228.

Inman, D.L., Nordstrom, C.E., Flick, R.E., 1976. Currents in submarine canyons: an air-sea-land interaction. Annual Review of Fluid Mechanics, 8, 275–310.

Iqbaluddin, G. 1978. Occurrence of seismite in the Precambrian rocks of Rajasthan, India. Current Science, 47, 230–231.

Ito, M., 2002. Kuroshio current-influenced sandy contourites from the Plio-Pleistocene Kazusa forearc basin, Boso Peninsula, Japan. In: Stow, D.A.V., Pudsey, C.J., Howe, J.A., Faugères, J.-C., Viana, A.R. (Eds.), Deep-water contourite systems: Modern Drifts and Ancient Series, Seismic and Sedimentary Characteristics, Geological Society Memoirs 22, London, pp. 421–432.

Iverson, R.M., 1997. The physics of debris flows. Reviews of Geophysics 35, 245–296.

Jacka, A.D., Beck, R.H., St. Germain, L.C., Harrison, S.C., 1968. Permian deep-sea fans of the Delaware Mountain Group (Guadalupian), Delaware basin, SEPM Permian Basin Section Publication 68–11, 49–90.

Jackson, M.J., Diekman, L.J., Kennard, J.M., Southgate, P.N., O'Brien, P.E., Sexton, M.J., 1992. Sequence stratigraphy, basin-floor fans and petroleum plays in the Devonian- Carboniferous of the northern Canning Basin. The APEA Journal, 32, 214–230.

Jacobi, R.D., 1976. Sediment slides on the northwestern continental margin of Africa. Marine Geology, 22, 157–173.

Jaffe, B., 2005. Preliminary analysis of sedimentary deposits from the 1998 Papua New Guinea (PNG) Tsunami. Uniform Resource Locator (URL): http://walrus.wr.usgs.gov/tsunami/itst.html (accessed June 9, 2005).

Jager, D.D., Giles, M.R., Griffiths, G.R., 1993. Evolution of Paleogene fans of the North Sea in space and time. In: Parker, J.R. (Ed.), Petroleum Geology of Northwest Europe, Proceedings of the 4th Conference, the Geological Society, London, pp. 59–71.

Janosi, I.M., Horvath, V.K., 1989. Dynamics of Water Droplets on a Window Pane. Physical Review, 40, 5232–5237.

Jansen, E. Befring, S. Bugge, T. Eidvin, T. Holtedahl, H., Petter Sejrup, H., 1987. Large submarine slides on the Norwegian continental margin: Sediments, transport and timing. Marine Geology, 78, 77–107.

Johnson, A.M., 1970. Physical processes in geology. San Francisco: Freeman, Cooper and Co., p. 577.

Johnson, A.M., 1984. Debris flow. In: Brunsden, D., Prior, D. B. (Eds.), Slope Instability, John Wiley & Sons Ltd, Chichester, pp. 257–361.

Johnson, D., 1938. The origin of submarine canyons. Journal of Geomorphology, 1, 111–340.

Johnson, D., 1939. The origin of submarine canyons, a critical review of hypotheses, Columbia University Press, New York, p. 126.

Johnson, D.A., Damuth, J.E., 1979. Deep thermohaline flow and current controlled sedimentation in the Amirante Passage: western Indian Ocean. Marine Geology, 33, 1–44.

Johnson, D.W., 1919. Shore Processes and Shoreline Development. Wiley, New York, p. 584.

Johnson, H.D., Baldwin, C.T., 1996. Shallow clastic sea. In: Reading, H.G. (Ed.), Sedimentary Environments: processes, Facies, and Stratigraphy, Blackwell Science, Oxford, pp. 232–280.

Jolly, R.J.H., Lonergan, L., 2002. Mechanisms and control on the formation of sand intrusions. Journal of the Geological Society of London, 159, 605–617.

Jordan, D.W., Lowe, D.R., Slatt, R.M., Stone, C.G., D'Agostino, A., Scheihing, M.H.,. Gillespie, R. H 1991. Scales of geological heterogeneity of Pennsylvanian Jackfork Group, Ouachita Mountains, Arkansas: Applications to field development and exploration for deep-water sandstones. Dallas Geological Society Field Trip # 3, 4–7 April, 1991, p. 142.

Kamola, D.L., Van Wagoner, J.C., 1995. Stratigraphy and facies architecture of parasequences with examples from the Spring canyon Member, Blackhawk Formation, Utah. In: Van Wagoner, J.C., Bertram, G.T. (Eds.), Sequence stratigraphy of foreland basin deposits – Outcrop and subsurface examples from the Cretaceous of North America (pp. 27–54). AAPG Memoir 64.

Karcz, I., Shanmugam, G., 1974. Decrease in scour rate of fresh deposited muds. Proc. American Society of Civil Engineers, Jour. of the Hydraulics Division, 100, No. HY 11, 1735–1738.

Karl, H.A., Carlson, P.R., Cacchione, D.A., 1983. Factors that influence sediment transport at the shelf break. In: Stanley, D.J., Moore, G.T. (Eds.), The shelfbreak: critical interface on continental margins. SEPM Special Publication No. 33, pp. 219–231.

Karl, H.A., Cacchione, D.A., Carlson, P.R., 1986. Internal-wave currents as a mechanism to account for large sand waves in Navarinsky Canyon Head, Bering Sea. Journal of Sedimentary Petrology, 56, 706–714.

Kastens, K.A., Cita, M.B., 1981. Tsunami induced sediment transport in the Abyssal Mediterranean Sea. GSA Bulletin, 89, 591–604.

Kawakami, G., Kawamura, M., 2002. Sediment flow and deformation (SFD) layers: evidence for intrastratal flow in laminated muddy sediments of the Triassic Osawa Formation, Northeast Japan. Journal of Sedimentary Research, 72, 171–181.

Keller, G.H., Shepard, F.P., 1978. Currents and sedimentary processes in submarine canyons off the northeast United States. In: Stanley, D.J., Kelling, G.K. (Eds.), Sedimentation in Submarine Canyons, fans, and Trenches, Dowden, Hutchinson & Ross, Inc., Stroudsburg, Pennsylvania, pp. 15–32.

Kelts, K., Arthur, M.A., 1981. Turbidites after ten years of deep-sea drilling – wringing out the mop? In: Warme, J.E., Douglas, R.G., Winterer, E.L. (Eds.), The Deep Sea Drilling Project: A Decade of Progress, SEPM Special Publication 32, pp. 91–127.

Kenyon, N.H., 1987. Mass-wasting features on the continental slope of northwest Europe. Marine Geology, 74, 57–77.

Khripounoff, A., Vangriesheim, A., Babonneau, N., Crassous, P., Dennielou, B., Savoye, B., 2003. Direct observation of intense turbidity current activity in the Zaire submarine valley at 4000 m water depth. Marine Geology, 194, 151–158.

Khvorova, I.V., 1978. Terrigenous clastic formations of oceans and certain seas. Lithologiya i Polenzye Iskopaemye, 3, 3–24.

Kimura, G., Koga, K., Fujioka, K., 1989. Deformed soft-sediments at the junction between the Mariana and Yap trenches. Journal of Structural Geology, 11, 463–472.

Klaucke, I., Masson, D.G., Kenyon, N.H., Gardner, J.V., 2004. Sedimentary processes of the lower Monterey Fan channel and channel-mouth lobe. Marine Geology, 206, 181–198.

Klaus, A., Ledbetter, M.T., 1988 Deep-sea sedimentary processes in the Argentine Basin revealed by high-resolution seismic records (3.5 kHz echograms). Deep-Sea Research, 35, 899–917.

Klein, G.D., 1966. Dispersal and petrology of sandstones of Stanley-Jackfork boundary, Ouachita fold belt, Arkansas and Oklahoma. AAPG Bulletin, 50, 308–326.

Klein, G.D., 1970. Depositional and dispersal dynamics of intertidal sand bars. Journal of Sedimentary Petrology, 40, 1095–1127.

Klein, G. D., 1971. A sedimentary model for determining paleotidal range. Geological Society of America Bulletin, 82, 2585–2592.

Klein, G.D., 1975. Resedimented pelagic carbonate and volcaniclastic sediments and sedimentary structures in Leg 30 DSDP cores from the western equatorial Pacific. Geology, 3, 39–42.

Klein, G.D., 1984. Relative rates of tectonic uplift as determined from episodic turbidite deposition in marine basins. Geology, 12, 48–50.

Klein, G.D., 1985a. The control of depositional depth, tectonic uplift, and volcanism on sedimentation processes in the back-arc basins of the western Pacific Ocean. Journal of Geology, 93, 1–25.

Klein, G.D., 1985b. The frequency and periodicity of preserved turbidites in submarine fans as a quantitative record of tectonic uplift in collision zones. Tectonophysics, 119, 181–193.

Klein, G.D., 1998. Clastic tidalites–a partial retrospective view. In: Alexander, C.R., Davis, R.A., Henry, V.J. (Eds.), Tidalites: Processes and Products, SEPM Special Publication 61, pp. 5–14.

Knauss, J., 1965. A technique for measuring deep ocean currents close to the bottom with an unattached current meter and some preliminary results. Journal of Marine Research, 23, 237–245.

Kneller, B., 1995. Beyond the turbidite paradigm: physical models for deposition of turbidites and their implications for reservoir prediction. In: Hartley, A.J., Prosser, D.J. (Eds.), Characterization of Deep-Marine Clastic Systems, Geological Society Special Publication No. 94, pp. 31–49.

Kneller, B., 1996. When is a turbidity current not a turbidity current? A question of mobility. AAPG 1996 Annual Meeting Abstracts, 76.

Kneller, B., Branney, M.J., 1995. Sustained high-density turbidity currents and the deposition of thick massive beds: Sedimentology, vol. 42, p. 607–616.

Kneller, B., Buckee, C., 2000. The structure and fluid mechanics of turbidity currents: a review of some recent studies and their geologic implications. Sedimentology, 47 (Suppl. 1), 62–94.

Koch, S.P., Barker, J.W., Vermersch, J.A., 1991. The Gulf of Mexico Loop Current and deepwater drilling. Journal of Petroleum Technology, 43, 1046–1050 and 1118–1119.

Kohl, B., DSDP Leg 96 Shipboard Scientists. 1985. Biostratigraphy and sedimentation rates of the Mississippi Fan. In: Bouma, A.H., Normark, W.R., Barnes, N.E. (Eds.), Submarine Fans and Related Turbidite Systems, Springer-Verlag, New York, pp. 267–273.

Komar, P.D., 1971. Hydraulic jumps in turbidity currents. GSA Bulletin, 82, 1477–1481.

Komar, P.D., 1976. Beach Processes and Sedimentation. Englewood Cliffs, Prentice-Hall, Inc., New Jersey, p. 429.

Komar, P.D., Neudeck, R.H., Kulm, L.D., 1972. Origin and significance of deep-water oscillatory ripple marks on the Oregon continental shelf. In: Swift, D.J.P., Duane, D.B., Pilkey, O.H. (Eds.), Shelf Sediment Transport Processes and Pattern, Dowden, Hutchinson, and Ross, Stroudsburg, pp. 601–619.

Krastel, S., Hanebuth, T.J.J., Antobreh, A.A., Henrich, R., Holz, C., Kolling, M., Schulz, H.D., Wien, K., Wynn. R.B., 2004. Cap Timiris Canyon: A newly discovered channel system offshore of Mauritania. EOS, 85, 417–423.

Krumbein, W.C., Sloss, L.L., 1963. Stratigraphy and Sedimentation, 2nd Edition, W.H. Freeman and Company, San Francisco, p. 660.

Kudrass, H.R., Michels, K.H., Wiedicke, M., 1998. Cyclones and tides as feeders of a submarine canyon off Bangladesh. Geology, 26, 715–718.

Kuecher, G.J., Woodland, B.G., Broadhurst, F.M., 1990. Evidence of deposition from individual tides and of tidal cycles from the Francis Creek Shale (host rock to the Mazon Creek Biota), Westphalian D (Pennsylvanian), northeastern Illinois. Sedimentary Geology, 68, 211–221.

Kuenen, Ph. H., 1937. Experiments in connection with Daly's hypoThesis on the formation of submarine canyons. Leidse Geol. Meded. 8, 327–335.

Kuenen, Ph. H., 1950a. Turbidity currents of high density. 18th International Geological Congress 1948, London, Reports, pt.8, 44–52.

Kuenen, Ph. H., 1950b. Marine Geology, John Wiley & Sons, New York, p. 568.

Kuenen, Ph. H., 1951. Properties of turbidity currents of high density. In: Hough, J.L. (Ed.), Turbidity currents and the transportation of coarse sediments to deep water. A Symposium, SEPM Special Publication 2, pp. 14–33.

Kuenen, Ph. H., 1953. Significant features of graded bedding. AAPG Bulletin, 37, 1044–1066.

Kuenen, Ph. H., 1957. Sole markings of graded greywacke beds. Journal of Geology, 65, 231–258.

Kuenen, Ph. H., 1958. Problems concerning source and transportation of flysch sediments. Geologie en Mijnbouw. 20, 329–339.

Kuenen, Ph. H., 1964. Deep-sea sands and ancient turbidites. In: Bouma, A.H., Brouwer, A. (Eds.), Turbidites, Developments in Sedimentology 3, Elsevier, Amsterdam, pp. 3–33.

Kuenen, Ph. H., 1966. Experimental turbidite lamination in a circular flume. Journal of Geology, 74, 523–545.

Kuenen, Ph. H., 1967. Emplacement of flysch-type sand beds. Sedimentology, 9, 203–243.

Kuenen, Ph. H., Migliorini, C.I., 1950. Turbidity currents as a cause of graded bedding. Journal of Geology, 58, 91–127.

Kuhn, T.S., 1970. The structure of scientific revolutions. University of Chicago Press, Chicago, p. 172.

Kuhn, T.S., 1996. The structure of scientific revolutions. 3rd Edition. The University of Chicago Press, Chicago, p. 212.

Kumar, N., Sanders, J.E., 1976. Characteristics of shoreface storm deposits: modern and ancient examples. Journal of Sedimentary Petrology, 46, 145–162.

Kundu, P.K., Cohen, I.M. (2002). Fluid Mechanics. 2nd Edition. Academic Press, San Diego, p. 730.

Kvenvolden, K.A., 1981. Organic geochemistry in the deep sea drilling project. In: Warme, J.E., Douglas, R.G., Winterer, E.L. (Eds.), The Deep Sea Drilling Project: A Decade of Progress, SEPM Special Publication 32, pp. 227–249.

Labaume, P., Mutti, E., Seguret, M., 1987. Megaturbidites: a depositional model from the Eocene of the SW-Pyrenean foreland basin, Spain. Geo-Marine Letters, 7, 91–101.

Lahee, F.H., 1923. Field Geology. McGraw-Hill Book Company, Inc., New York, p. 651.

Laird, M.G., 1972. Sedimentology of the Greenland group of the Paparoa Range, west coast, South Island, New Zealand. New Zealand Journal of Geology and Geophysics, 15, 372–393.

Lamb, M.P., Hickson, T., Marr, J.G., Sheets, B., Paola, C., Parker, G., 2004. Surging versus continuous turbidity currents: flow dynamics and deposits in an experimental intraslope minibasin. Journal of Sedimentary Research, 74, 148–155.

Lambiase, J.J., 1990. A model for tectonic control of lacustrine stratigraphic sequences in continental rift basins. In: Katz, B.J. (Ed.), Lacustrine Basin Exploration—Case Studies and Modern Analogs, AAPG Memoir 50, pp. 265–286.

Lanteaume, M. Beaudoin, B., Campredon, R., 1967. Figures sedimentaires du flysch 'gres d' Annot' du synclinal de Peira-Cava. Centre National de la Recherche Scientifique, Paris, p. 97.

Laughton, A.S., 1981. The first decade of GLORIA. Journal of Geophysical Research, 86, 11511–11534.

Lawson, D.E., 1981. Mobilization, movement and deposition of active subaerial sediment flows, Matanuska Glacier, Alaska. Journal of Geology, 90, 279–300.

Lawton, T.F., Shipley, K.W., Aschoff, J.L., Giles, K.A., Vega, F.J., 2005. Basinward transport of Chicxulub ejecta by tsunami-induced backflow, La Popa basin, northeastern Mexico, and its implications for distribution of impact-related deposits flanking the Gulf of Mexico. Geology, 33, 81–84.

Le Heron, D.P., Etiene, J.L., 2005. A complex subglacial clastic dyke swarm, Sólheimajökull, Southern Iceland. Sedimentary Geology, 181, 25–37.

Le Heron, D.P., Sutcliffe, O.E., Whittington, R.J., Craig, J., 2005. The origins of glacially related soft-sediment deformation structures in Upper Ordovician glaciogenic rocks: implication for ice-sheet dynamics. Palaeogeography, Palaeoclimatology, Palaeoecology, 218, 75–103.

Leatherman, S.P., Williams, A.T., 1977. Lateral textural grading in overwash sediments. Earth Surface Processes, 2, 333–341.

Leclair, S., Arnott, R.W.C., 2005. Parallel lamination formed by high-density turbidity currents. Journal of Sedimentary Research, 75, 1–5.

Lee, H.J., Schwab, W.C., Booth, J.S., 1993. Submarine landslides: an introduction. In: Schwab, W.C., Lee, H.J., Twichell, D.C. (Eds.), Submarine Landslides: Selected Studies in the U.S. Exclusive Economic Zone, U.S. Geological Survey Bulletin 2002, pp. 1–13.

Lee, H.J., Kayen, R.E., Edwards, B.D., Field, M.E., Gardner, J.V., Schwab, W.C., Twichell, D.C., 1996. Ground-truth studies of west coast and Gulf of Mexico submarine fans. In: Gardner, J.V., Field, M.E., Twichell, D.C. (Eds.), Geology of the United States' Sea Floor: The View from GLORIA, Cambridge University Press, New York, pp. 221–233.

Lee, H.J., Syvitski, J.P.M., Parker, G., Orange, D., Locat, J., Hutton, E.W.H., Imran, J., 2002. Distinguishing sediment waves from slope failure deposits: field examples, including the 'Humboldt slide', and modeling results. Marine Geology, 192, 79–104.

Lee, H.J., Kayen, R.E., Gardner, G.V., Locat, J., 2003. Characteristics of several tsunamigenic submarine landslides. In: Locat, J., Mienert, J. (Eds.), Submarine Mass Movements and their Consequences, Kluwer Academic Publishers, Dordrecht, pp. 357–366.

Leeder, M.R., 1982. Sedimentology. George Allen & Unwin, London, p. 344.

Leeder, M.R., 1997. Book reviews, 'The geology of fluvial deposits – sedimentary facies, basin analysis, and petroleum geology' by A.D. Miall. Journal of Sedimentary Research, 67, 374–375.

Lesieur, M., 1987. Turbulence in Fluids: Stochastic and Numerical Modeling. M. Nijhoff, Dordrecht, p. 286.

Lewis, K.B., 1971. Slumping on a continental slope inclined at 1–4. Sedimentology, 16, 97–110.

Lisitsyn, A.P., 1986. Avalanche sedimentation in seas and oceans. Part V: Special mechanisms of transport of sedimentary matter and formation of sedimentary bodies of the second global level. Gravitites, their classes and series. Lithologiya i Polenzye Iskopaemye, 4, 3–28.

Locat, J., Mienert, J. (Eds.), 2003. Submarine Mass Movements and their Conseqenecs. Kluwer Academic Publishers, Dordrecht, p. 540.

Loizou, N., 2004. Exploration along the UK Atlantic Margin – The Story So Far. In DTI Oil & Gas–Maximising Recovery Programme (formerly SHARP) IOR views. Uniform Resource Locator (URL): http://ior.rml.co.uk/issue8/articles/dti_atlantic/ (accessed February 9, 2005).

Lonsdale, P., Malfait, B., 1974. Abyssal dunes of foraminiferal sand on the Carnegie Ridge. GSA Bulletin, 85, 1697–1712.

Lonsdale, P., Spiess, F.N., 1977. Abyssal bedforms explored with a deeply towed instrument package. Marine Geology, 28, 57–75.

Loutit, T.S., Hardenbol, J., Vail, P.R., 1988. Condensed sections: the key to age determination and correlation of continental margin sequences. In: Wilgus, C.K., Hastings, B.S., Kendall, C.G.St.C., Posamentier, H.W.,

Ross, C.A., Van Wagoner, J.C. (Eds.), Sea-level Changes: An Integrated Approach, SEPM Special Publication No. 42, pp. 183–213.

Lovell, J.P.B., Stow, D.A.V., 1981. Identification of ancient sandy contourites. Geology, 9, p. 347–349.

Lowe, D.R., 1975. Water escape structures in coarse grained sediments. Sedimentology, 22, 157–204.

Lowe, D.R., 1976. Subaqueous liquefied and fluidized sediment flows and their deposits. Sedimentology, 23, 285–308.

Lowe, D.R., 1979. Sediment gravity flows: their classification, and some problems of application to natural flows and deposits. In: Doyle, L.J., Pilkey, O.H. (Eds.), Geology of Continental Slopes, SEPM Special Publication 27, pp. 75–82.

Lowe, D.R., 1982. Sediment gravity flows: II. depositional models with special reference to the deposits of high-density turbidity currents. Journal of Sedimentary Petrology, 52, 279–297.

Lowe, D.R., 1997. Reinterpretation of depositional processes in a classic flysch sequence (Pennsylvanian Jackfork Group), Ouachita Mountains, Arkansas and Oklahoma: discussion. AAPG Bulletin, 81, 460–465.

Lowe, D.R., Guy, M., 2000. Slurry-flow deposits in the Britannia formation (Lower Cretaceous), North Sea: a new perspective on the turbidity current and debris flow problem. Sedimentology, 47, 31–70.

Lowe, D.R., Lopiccolo, R.D., 1974. The characteristics and origins of dish and pillar structures. Journal of Sedimentary Research, 44, 484–501.

Macdonald, D.I.M., Moncrieff, A.C.M., Butterworth, P.J., 1993. Giant slide deposits from a Mesozoic fore-arc basin, Alexander Island, Antarctica. Geology, 21, 1047–1050.

Macsotay, O., Vivas, V., Peraza, T., 1997. Injectites as indicators of syn-tectonic activity in the Cretaceous-Paleogene sediments of Venezuela. In: 8th Venezuelan Geological Congress, Porlamar, Venezuela, 2, 25–32.

Macsotay, O., Erlich, R.N., Peraza, T., 2003. Sedimentary structures of the La Luna, Navay and Querecual Formations, Upper Cretaceous of Venezuela. Palaios, 18, 334–348.

Major, J.J., 1998. Pebble orientation on large, experimental debris-flow deposits: Sedimentary Geology, 117, 151–164.

Malinverno, A., Ryan, W.B.F., Auffret, G., Pautot, G., 1988. Sonar images of the path of recent failure events on the continental margin off Nice, France. In: Clifton, H.E. (Ed.), Sedimentologic Consequences of Convulsive Geologic Events, Geological Society of America Special Paper 229, pp. 59–75.

Maltman, A., (Ed.), 1994. The Geological Deformation of Sediments. Chapman & Hall, London, p. 382.

Marr, J.G., Harff, P., Shanmugam, G., Parker, G., 1997. Experiments on subaqueous sandy debris flows. In: Supplement to EOS Transactions, AGU Fall Meeting, San Francisco, 78, Number 46, F347.

Marr, J.G., Harff, P.A., Shanmugam, G., Parker, G., 2001. Experiments on subaqueous sandy gravity flows: the role of clay and water content in flow dynamics and depositional structures. GSA Bulletin, 113, 1377–1386.

Marshall, N.F., 1978. Large storm-induced sediment slump reopens an unknown Scripps submarine canyon tributary. In: Stanley, D.J., Kelling, G. (Ed.), Sedimentation in Submarine Canyons, Fans, and Trenches, Hutchinson and Ross, Stroudsburg, Pennsylvania, pp. 73–84.

Martin, B.D., Emery, K.O., 1967. Geology of Monterey Canyon, California. AAPG Bulletin, 51, p. 2281–2304.

Martinsen, O.J., 1989. Styles of soft-sediment deformation on a Namurian (Carboniferous) delta slope, Western Irish Namurian Basin, Ireland. In: Whateley, K.G., Pickering, K.T. (Eds.), Deltas: Sites and Traps for Fossil Fuels, Geological Society Special Publication No. 41, pp. 167–177.

Martinsen, O.J., 1994. Mass movements. In: Maltman, A. (Ed.), The Geological Deformation of Sediments, Chapman & Hall, London, pp. 127–165.

Masson, D.G., van Niel, B., Weaver, P.P.E., 1997. Flow processes and sediment deformation in the Canary Debris flow on the NW African continental rise. Sedimentary Geology, 110, 163–179.

Masson, D.G., Wynn, R.B., Bett, B.J., 2004. Sedimentary environment of the Faroe-Shetland and Faroe Bank Channels, north-east Atlantic, and the use of bedforms as indicators of bottom current velocity in the deep ocean. Sedimentology, 51, 1207–1241.

Mattern, F., 2005. Ancient sand-rich submarine fans: depositional systems, models, identification, and analysis. Earth-Science Reviews, 70, 167–202.

May, J.A., Warme, J.E., Slater, R.A., 1983. Role of submarine canyons on shelfbreak erosion and sedimentation: modern and ancient examples. In: Stanley, D.J., Moore, G.T., (Eds.), The Shelfbreak: Critical Interface on Continental Margins, SEPM Special Publication No. 33, pp. 315–332.

McBride, E.F., 1962a. Flysch and associated beds of the Martinsburg formation (Ordovician), central Appalachians. Journal of Sedimentary Petrology, 32, 39–91.

McBride, E.F., 1962b. The term greywacke. Journal of Sedimentary Petrology, 32, 614–615.

McCaffrey, W.D., Kneller, B.C., Peakall, J. (Eds.), 2001. Particulate Gravity Currents. IAS Special Publication 31, Blackwell, p. 320.

McCave, I.N., 2002. Charles Davis Hollister, 1936–1999: a personal scientific appreciation of the father of 'contourites.' In: Stow, D.A.V., Pudsey, C.J., Howe, J.A., Faugères, J.-C., Viana, A.R. (Eds.), Deep-Water Contourite Systems: Modern Drifts and Ancient Series, Seismic and Sedimentary Characteristics, Geological Society Memoirs 22, London, pp. 1–5.

McCave, I.N., Jones, P.N., 1988. Deposition of ungraded muds from high-density non-turbulent turbidity currents. Nature, 333, 250–252.

McGee, D.T., Bilinski, P.W., Gary, P.S., Pfeiffer, D.S., Sheimanan, J.L., 1994. Geologic models and reservoir geometries of Auger Field, Deepwater Gulf of Mexico. In: Weimer, P., Bouma, A.H., Perkins, R.F. (Eds.), Submarine Fans and Turbidite Systems, Gulf Coast Section of SEPM 15th Annual Research Conference, pp. 245–256.

McGovney, J.E., Radovich, B.J., 1985. Seismic stratigraphy and facies of the Frigg fan complex. In: Berg, O.R., Woolverton, D.G. (Eds.), Seismic Stratigraphy II, AAPG Memoir 39, pp. 139–154.

McGregor, B.A., Stubblefield, W.L., Ryan, W., B., F., Twichell, D.C., 1982. Wilmington submarine canyon: a marine fluvial like system. Geology, 10, 21–30.

McGregor, B.A., Rothwell, R.G., Kenyon, N.H., Twichell, D.C., 1993. Salt tectonics and slope failure in an area of salt domes in the northwestern Gulf of Mexico. In: Schwab, W.C., Lee, H.J., Twichell, D.C. (Eds.), Submarine Landslides: Selected Studies in the U.S. Exclusive Economic Zone, U.S. Geological Survey Bulletin 2002, pp. 92–96.

McPherson, J.G., Shanmugam, G., Moiola, R.J., 1987. Fan-deltas and braid deltas: varieties of coarse-grained deltas. Geological Society of America Bulletin, 99, 331–340.

Melosh, H.J., 1979. Acoustic fluidization: a new geologic process? Journal of Geophysical Research, 84, 7513–7520.

Menard, H.W., 1955. Deep-sea channels, topography, and sedimentation. AAPG Bulletin, 39, 236–255.

Mètivier, F., Lajeunesse, E., Cacas, M-C., 2005. Submarine canyons in the bathtub. Journal of Sedimentary Research, 75, 6–11.

Miall, A.D., 1996. The Geology of Fluvial Deposits. Springer, Berlin, p. 582.

Miall, A.D., 1999. In defense of facies classifications and facies models. Journal of Sedimentary Research, 69, 2–5.

Michalik, J., 1997. Tsunamites in a storm-dominated Anisian carbonate ramp (Vysoka Formation, Male Karpaty Mts., Western Carpathians). Geological Carpathica, 48, 221–229.

Middleton, G.V. (Ed.), 1965. Primary Sedimentary Structures and their Hydrodynamic Interpretation. SEPM Special Publication 12, p. 265.

Middleton, G.V., 1966. Experiments on density and turbidity currents. I. Motion of the head. Canadian Journal of the Earth Science, 3, 523–546.

Middleton, G.V., 1967. Experiments on density and turbidity currents: III. deposition of sediment. Canadian Journal of Earth Sciences, 4, 475–505.

Middleton, G.V., 1970. Experimental studies related to problems of flysch sedimentation. In: Lajoie, J. (Ed.), Flysch Sedimentology in North America, Geological Association of Canada Special Paper No. 7, pp. 253–272.

Middleton, G.V., 1993. Sediment deposition from turbidity currents. Annual Review Earth Planetary Sciences, 21, 89–114.

Middleton, G.V., Bouma, A.H. (Eds.), 1973. Turbidites and Deep-water Sedimentation. SEPM Pacific section Short Course, Anaheim, California, p. 157.

Middleton, G.V., Hampton, M.A., 1973. Sediment gravity flows: mechanics of flow and deposition. In: Middleton, G.V., Bouma, A.H. (Eds.), Turbidites and Deep-water Sedimentation, SEPM Pacific section Short Course, Anaheim, California, pp. 1–38.

Middleton, G.V., Southard, J.B., 1977. Mechanics of Sediment Movement. Short Course No. 3, Eastern section of SEPM, Binghamton, New York, p. 10.2.

Middleton, G.V., Wilcock, P.R., 1994. Mechanics in the Earth and Environmental Sciences. Cambridge University Press, Cambridge, p. 459.

Mienert, J., 2004. COSTA–continental slope stability: major aims and topics. Marine Geology, 213, 1–7.

Miller, D.J., 1960. The Alaska earthquake of 10 July, 1958: giant wave in Lituya Bay. Bulletin of the Seismological Society of America, 50, 253–266.

Milne, J., 1897. Suboceanic changes. Geographical Journal, 10, 129–146, 259–289.

Mitchell, J.G., 2003. Alaska's giant of ice and stone: Wrangell-St. Elias National Park. National Geographic, 203(3), p. 56–83.

Mitchell, S.M., Beamish, G.W.J., Wood, M.V., Malecek, S.J., Armentrout, J., Damuth, J.E., Olson, H.C., 1993. Paleogene sequence stratigraphic framework of the Faeroe Basin. In: Parker, J.R. (Ed.), Petroleum geology of Northwest Europe, Proceedings of the 4th Conference of the Geological Society, London, pp. 1011–1023.

Mitchum Jr., R.M., 1985. Seismic stratigraphic expression of submarine fans. AAPG Memoir 39, 117–136.

Mitchum Jr., R.M., Sangree, J.B., Vail, P.R., Wornardt, W.W., 1990. Sequence stratigraphy in Late Cenozoic expanded sections, Gulf of Mexico. In: Proceedings of 11th Annual Research Conference, Gulf Coast SEPM Foundation, 237–256.

Mitchum Jr., R.M., Sangree, J.B., Vail, P.R., Wornardt, W.W., 1993. Recognizing sequences and systems tracts from well logs, seismic data, and biostratigraphy: examples from Late Cenozoic of the Gulf of Mexico. In: Weimer, P. Posamentier, H. (Eds.), Siliciclastic Sequence Stratigraphy: Recent Developments and Applications, AAPG Memoir 58, pp. 163–197.

Mohrig, D., Marr, J.G., 2003. Constraining the efficiency of turbidity current generation from submarine debris flows and slides using laboratory experiments. Marine and Petroleum Geology, 20, 883–899.

Mohrig, D., Whipple, K.X., Hondzo, M., Ellis, C., Parker, G., 1998. Hydroplaning of subaqueous debris flows. GSA Bulletin, 110, 387–394.

Moiola, R.J., Shanmugam, G., 1984. Submarine fan sedimentation, Ouachita Mountains, Arkansas and Oklahoma. Transactions-Gulf Coast Association of Geologists Societies, 34, 175–182.

Moiola, R.J., Briggs, G., Shanmugam, G., 1988. Carboniferous flysch, Ouachita Mountains, Southeastern Oklahoma; Big Cedar-Kiamichi Mountain section. Geological Society of America Centennial Field Guide-South-Central Section, 149–152.

Monson, G., Pita, J., 1997. Neural network prediction of pseudo-logs for net pay and reservoir property interpretation: Greater Zafiro field area, Equatorial Guinea, 67th Ann. Internat. Mtg: Soc. of Expl. Geophys., 627.

Moore, G.W., Moore, J.G., 1988. Large-scale bedforms in boulder gravel produced by giant waves in Hawaii. In: Clifton, H.E. (Ed.), Sedimentologic Consequences of Convulsive Geologic Events, Geological Society of America Special Paper 229, pp. 101–110.

Moore, G.T., Starke, G.W., Bonham, L.C., Woodbury, H.O., 1978. Mississippi Fan, Gulf of Mexico – Physiography, stratigraphy, and sedimentological patterns. In: Bouma, A.H., Moore, G.T., Coleman, J.M. (Eds.), Framework, Facies, and Oil-trapping Characteristics of the Upper Continental Margin. AAPG Studies in Geology 7, p. 326.

Moore, J.G., Clague, D.A., 2002. Mapping the Nuuanu and Wailau landslides in Hawaii. In: Takahashi, E., Lipman, P.W., Garcia, M.O., Naka, J., Aramaki, S. (Eds.), Hawaiian Volcanoes: Deep Underwater Perspectives, Geophysical Monograph 128, American Geophysical Union, Washington, D.C., pp. 223–244.

Morris, R.C., 1974. Carboniferous rocks of the Ouachita Mountains, Arkansas: a study of facies patterns along the unstable slope and axis of a flysch trough. In: Briggs, G. (Ed.), Carboniferous of the Southeastern United States, Geological Society of America Special Paper 148, pp. 241–279.

Morris, R.C., 1977. Flysch facies of the Ouachita trough- with examples from the Spillway at the DeGray Dam, Arkansas. In: Symposium on the Geology of the Ouachita Mountains, Arkansas Geological Commission, v. 1, pp. 158–169.

Morton, R.A., 1988. Nearshore responses to great storms. In: Clifton, H.E. (Eds.), Sedimentologic Consequences of Convulsive Geologic Events, Geological Society of America Special Paper 229, pp. 7–22.

Morton, R.A., 1993. Attributes and origins of ancient submarine slides and filled embayments: examples from the Gulf Coast Basin. AAPG Bulletin, 77, pp. 1064–1081.

Mosher, D.C., Piper, D.J.W., Campbell, D.C., Jenner, K.A., 2004. Near-surface geology and sediment-failure geohazards of the central Scotian slope. AAPG Bulletin, 88, 703–723.

Mulder, T., Alexander, J., 2001. The physical character of subaqueous sedimentary density flows and their deposits. Sedimentology, 48, pp. 269–299.

Mulder, T., Cochonat, P., 1996. Classification of offshore mass movements. Journal of Sedimentary Research, 66, 43–57.

Mulder, T., Syvitski, J.P.M., 1995. Turbidity currents generated at river mouths during exceptional discharges to the world oceans. Journal of Geology, 103, 285–299.

Mulder, T., Migeon, S., Savoye, B., Faugeres, J-C., 2001. Inversely graded turbidite sequences in the deep Mediterranean. A record of deposits from flood-generated turbidity currents? Geo-Marine Letters, 21, 86–93.

Mulder, T., Migeon, S., Savoye, B., Faugeres, J.-C., 2002. Reply to discussion by Shanmugam on Mulder et al. (2001, Geo-Marine Letters, 21, 86–93) Inversely graded turbidite sequences in the deep Mediterranean. A record of deposits from flood-generated turbidity currents? Geo-Marine Letters, 22, 112–120.

Mulder, T., Syvitski, J.P.M., Migeon, S., Faugeres, J.-C., Savoye, B., 2003. Marine hyperpycnal flows: initiation, behavior and related deposits. A review. Marine and Petroleum Geology, 20, 861–882.

Mulder, T., Weber, O., Anschutz, P., Jorissen, F., Jouanneau, J.M., 2001. A few months-old storm-generated turbidite deposited in the Capbreton Canyon (Bay of Biscay, SW France). Geo-Marine Letters, 21, 149–156.

Mullins, H.T., Gardulski, A.F., Wise Jr., S.W., Applegate, J., 1987. Implications for seismic stratigraphic succession and Loop Current/Gulf Stream circulation. GSA Bulletin, 98, 702–713.

Murchison, R.I., 1827. Supplementary remarks on the Oolitic Series in the Counties of Sutherland and Ross, and in the Hebrides. Transactions of the Geological Society, 2, p. 353.

Murphy, M.A., Schlanger, S.O., 1962. Sedimentary structures in llhas sao Sebastiao Formations (Cretaceous), Reconcavo Basin, Brazil. AAPG Bulletin, 46, 457–477.

Murray, J., Renard, A.F., 1891. Report on deep-sea deposits based on specimens collected during the voyage of H.M.S. Challenger in the years 1872–1876. Government Printer, Challenger Reports, London, p. 525.

Murray, S.P., 1970. Bottom currents near the coast during Hurricane Camille. Journal of Geophysical Research, 75, 4579–4582.

Mutti, E., 1977. Distinctive thin-bedded turbidite facies and related depositional environments in the Eocene Hecho Group (southcentral Pyrenees, Spain). Sedimentology, 24, 107–131.

Mutti, E., 1979. Turbidites et cones sous-marins profonds. In: Homewood, P. (Ed.), Sedimentation Detrique (Fluviatile, Littorale et Marine). Institut de Geologie, Universite de Fribourg, Suise, pp. 353–415.

Mutti, E., 1985. Turbidite systems and their relations to depositional sequences. In: Zuffa, G.G. (Ed.), Provenance of Arenites, D. Reidel Publishing Company, Dordrecht, pp. 65–93.

Mutti, E., 1992. Turbidite sandstones. Agip Special publication, Milan, Italy, p. 275.

Mutti, E., Ghibaudo, G., 1972. Un esempio di torbiditi di coniode sottomarina esterina: le Arenarie di San Salvatore (Formatione di Bobbio, Miocene) nell 'Appennino di Piacenza. Memorie dell' Academia delle Scienze di Torino, Classe di Scienze Fisiche, Mathematiche e Naturali, Serie 4, no.16, p. 40.

Mutti, E., Nilsen, T., 1981. Significance of intraformational rip-up clasts in deep-sea fan deposits. International Association of Sedimentologists 2nd European Regional Meeting Abstracts, Bologna, Italy, p. 117–119.

Mutti, E., Normark, W.R., 1987. Comparing examples of modern and ancient turbidite systems: problems and concepts. In: Leggett, J.R., Zuffa, G.G. (Eds.), Marine Clastic Sedimentology: Concepts and Case Studies, Graham and Trotman, London, pp.1–37.

Mutti, E., Ricci Lucchi, F., 1972. Turbidites of the northern Apennines: introduction to facies analysis (English translation by Nilsen, T.H., 1978). International Geology Review, 20, 125–166.

Mutti, E., Ricci Lucchi, F., 1975. Turbidite facies and facies associations. In examples of turbidite facies and facies associations from selected formations of the northern Apennines. In: Field Trip Guidebook A-11, International Sedimentologic Congress IX, Nice, 21–36.

Mutti, E., Nilsen, T.H., Ricci Lucchi, F., 1978. Outer fan depositional lobes of the Laga Formation (Upper Miocene and Lower Pliocene), east-central Italy. In: Stanley, D.J., Kelling, G. (Eds.), Sedimentation in Submarine Fans, Canyons, and Trenches, Hutchinson and Ross, Stroudsburg, Pennsylvania, pp. 210–223.

Mutti, E., Ricci Lucchi, F., Seguret, M., Zanzucchi, G., 1984. Seismoturbidites: a new group of resedimented deposits. In: Cita, M.B., Ricci Lucchi, F. (Eds.), Seismicity and Sedimentation, Elsevier Scientific Publication, Amsterdam, pp. 103–116.

Mutti, E., Steffans, G.S., Pirmez, C., Orlando, M., 2003a. Proceedings from Parma, Italy Workshop, 21–25 May 2002 ('Turbidites: models and problems'). Marine and Petroleum Geology, 20, 523–526.

Mutti, E., Tinterri, R., Benvelli, G., di Biase, D., Gavanna, G., 2003b. Deltaic, mixed and turbidite sedimentation of ancient foreland basins. Marine and Petroleum Geology, 20, 733–755.

Mutti. E., Tinterri, R., Remacha, E., Mavilla, N., Angella, S., Fava, L., 1999. An introduction to the analysis of ancient turbidite basins from an outcrop perspective. AAPG Continuing Education Course Note Series # 39, Tulsa, Oklahoma, p. 61.

Nakajima, T., Kanai, Y., 2000. Sedimentary features of seismoturbidites triggered by the 1983 and older historical earthquakes in the eastern margin of the Japan Sea. Sedimentary Geology, 135, 1–19.

Nardin, T.R., Hein, F.J., Gorsline, D.S., Edwards, B.D., 1979. A review of mass movement processes, sediment and acoustic characteristics, and contrasts in slope and base-of-slope systems versus canyon-fan-basin floor systems. In: Doyle, L.J., Pilkey, O.H. (Eds.), Geology of Continental Slopes, SEPM Special Publication 27, pp. 61–73.

Natland, M.L., 1967. New classification of water-laid clastic sediments. AAPG Bulletin, 51, 476.

Natland, M.L., Kuenen, Ph. H., 1951. Sedimentary history of the Ventura Basin, California, and the action of turbidity currents. In: Hough, J.L. (Ed.), Turbidity Currents and the Transportation of Coarse Sediments to Deep-Water, SEPM Special Publication 2, pp. 76–107.

Naylor, M.A., 1980. The origin of inverse grading in muddy debris flow deposits – a review. Journal of Sedimentary Petrology, 50, 1111–1116.

Nelson, C.H., 1968. Marine geology of Astoria deep-sea fan, Unpublished Ph.D. Dissertation, Corvallis, Oregon: Oregon State University, p. 287.

Nelson, C.H., Karabanov, E.B., Colman, S.M., Escutia, C., 1998. Tectonic and sediment supply control of deep rift lake turbidite systems: Lake Baikal, Russia. Geology, 27, 163–166.

Nelson, C.H., Kulm, L.D., 1973. Submarine fans and deep-sea channels. In: Middleton, G.V., Bouma, A.H. (Eds.), Turbidites and Deep-Water Sedimentation, SEPM Pacific section Short Course, Anaheim, California, pp. 39–78.

Nelson, C.H., Nilsen, T.H., 1984. Modern and ancient deep-sea fan sedimentation. SEPM Short Course 14, p. 404.

Nelson, C.H., Maldonado, A., Coumes, F., Got, H., Monaco, A., 1985. Ebro Fan, Mediterranean. In: Bouma, A.H., Normark, W.R., Barnes, N.E. (Eds.), Submarine Fans and Related Turbidite Systems, Springer-Verlag, New York, pp. 121–127.

Nelson, C.H., Twichell, D.C., Schwab, W.C., Lee, H.J., Kenyon, N.H., 1992. Upper Pleistocene turbidite sand beds and chaotic silt beds in the channelized, distal, outer-fan lobes of the Mississippi fan. Geology, 20, 693–696.

Nemec, W., 1990. Aspects of sediment movement on steep delta slopes. In: Colella, A., Prior, D.B. (Eds.), Coarse-Grained Deltas, International Association of Sedimentologists Special Publication No. 10, pp. 29–73.

Neumann, G., Pierson Jr., W.J., 1966. Principles of Physical Oceanography. Englewood Cliffs, New Jersey: Prentice-Hall, p. 545.

Newman, M. St., Leeder, M.L., Woodruff, A.H.W., Hatton, I.R., 1993. The geology of the Gryphon Field. In: Parker, J.D. (Ed.), Petroleum Geology of Northwest Europe, Proceedings of the 4th Conference of the Geological Society, London, pp. 123–133.

Nichols, R.J., 1995. The liquefaction and remobilization of sandy sediments. In: Hartley, A.J., Prosser, D.J., (Eds.), Characterisation of Deep Marine Clastic Systems, Geol. Soc. London Spec. Publ., 94, pp. 63–76.

Nilsen, T.H., 1979. AAPG Deep-water Clastic Reservoir School. Field trip guidebook, Ventura, California.

Nilsen, T.H., 1980. Modern and ancient submarine fans: discussion of papers by. Walker R.G., Normark W.R., AAPG Bulletin, 64, 1094–1112.

Nio, S-D., Yang, C-S., 1991. Diagnostic attributes of clastic tidal deposits: a review. In: Smith, D.G., Zaitlin, B.A., Reinson, G.E., Rahmani, R.A. (Eds.), Clastic Tidal Sedimentology, Canadian Society of Petroleum Geologists, Calgary, pp. 3–27.

NOAA (National Ooceanic and Atmospheric Admininistratin), 2005a. International Tsunami Information Center. Uniform Resource Locator (URL): http://www.prh.noaa.gov/itic/library/about_tsu/faqs.html (accessed January 15, 2005).

NOAA (National Oceanic and Atmospheric Admininistration), 2005b. Pacific Marine Environmental Laboratory, Tsunami Research Program. Uniform Resource Locator (URL): http://www.pmel.noaa.gov/tsunami/indo_1204.html (accessed June 15, 2005).

NOAA (National Oceanic and Atmospheric Administration), 2005c, NOAA News Online, Story 2365. Uniform Resource Locator (URL): http://www.noaanews.noaa.gov/stories2005/s2365.htm (accessed June 15, 2005).

Noji, M., Imamura, F., Shuto, N., 1993. Numerical simulation of movement of large rocks transported by tsunamis. In: Tsuchiya, Y., Shuto, N. (Eds.), Tsunami '93 Proceedings of the IUGG: IOC International Tsunami Symposium, Wakayama, Japan, 23–27 August, 1993, pp. 189–198.

Norem, H., Locat, J., Schieldrop, B., 1990. An approach to the physics and the modeling of submarine flowslides. Marine Geotechnology, 9, 93–111.

Normark, W.R., 1970. Growth patterns of deep sea fans. AAPG Bulletin, 54, 2170–2195.

Normark, W.R., 1978. Fan valleys, channels, and depositional lobes on modern submarine fans: characters for recognition of sandy turbidite environments. AAPG Bulletin, 62, 912–931.

Normark, W.R., 1991. Turbidite elements and the obsolescence of the suprafan concept. Giornale di Geologia, ser 3a, 53/2, 1–10.

Normark, W.R., Gutmacher, C.E., Chase, T.E., Wilde, P., 1985. Monterey Fan, Pacific Ocean. In: Bouma, A.H., Normark, W.R., Barnes, N.E. (Eds.), Submarine Fans and Related Turbidite Systems, Springer-Verlag, New York, pp. 79–86.

Normark, W.R., Moore, J.G., Torresan, M.E., 1993. Giant volcano-related landslides and the development of the Hawaiian Islands. In: Schwab, W.C., Lee, H.J., Twichell, D.C. (Eds.), Submarine Landslides: Selected Studies in the U.S. Exclusive Economic Zone, U.S. Geological Survey Bulletin 2002, pp. 184–196.

Normark, W.R., Damuth, J.E., The Leg 155 Sedimentology Group, 1997. Sedimentary facies and associated depositional elements of the Amazon Fan. In: Flood, R.D., Piper, D.J.W., Klaus, A., Peterson, L.C. (Eds.), Proceedings of the Ocean Drilling Program, Scientific Results, 155. College Station, Texas (Ocean Drilling Program), pp. 611–651.

Normark, W.R., Piper, D.J.W., 1972. Sediment and growth pattern of Navy deep-sea fan, San Clemente Basin, California borderland. Journal of Geology, 80, 198–223.

Nowlin Jr., W.D., 1972. Winter circulation patterns and property distributions. In: Capurro, L.R.A., Reid, J.L., (Eds.), Contributions on the Physical Oceanography of the Gulf of Mexico, Texas A&M University Oceanographic Studies, vol. 2, Gulf Publishing Co, Houston, pp 3–51.

Nowlin Jr., W.D., Hubert, J.M., 1972. Contrasting summer circulation patterns for the eastern Gulf. In: Capurro, L.R.A., Reid, J.L. (Eds.), Contributions on the Physical Oceanography of the Gulf of Mexico, Texas A&M University Oceanographic Studies, vol. 2. Gulf Publishing Co, Houston, pp. 119–137.

Oakeshott, J.M. D'Ivry, 1989. Aspects of depositional mechanisms of high concentration sediment gravity flows, Unpublished Ph.D. Thesis, University of Keele, Keele, p. 502.

Oakman, Martin, C.D., J.H., Corbett, P.W.M. (Eds.), 1997. Cores from the Northwest European Hydrocarbon Province. The Geological Society, London, p. 232.

Obermeier, S.F., 1989. The New Madrid Earthquakes: An Engineering-Geologic Interpretation of Relict Liquefaction Features. U.S. Geological Survey Professional Paper, 1336-B.

Obermeier, S.F., 1998. Seismic liquefaction features: examples from paleoseismic investigations in the continental United States. USGS Open-file Report 98–488. Available only on the world wide web. Uniform Resource Locator (URL): http://pubs.usgs.gov/openfile/of98–488/index.html (accessed February 24, 2005).

Osborne, R.H. (Ed.), 1991. From Shoreline to Abyss: Contributions in Marine Geology in Honor of Francis Parker Shepard. SEPM Special Publication 46, p. 320.

Oswatitsch, K., Wieyhardt, K., 1987. Ludwig Prandtl and his Kaiser-Wilhelm-Institut. Annual Reviews of Fluid Mechanics, 19, 1–25.

Papadopoulos, G.A., Kortekaas, S., 2003. Characteristics of landslide generated tsunamis from observational data. In: Locat J., Mienert, J. (Eds.), Submarine Mass Movements and their Consequences, Kluwer Academic Publishers, Dordrecht, pp. 367–374.

Parize, O., Beaudoin, B., Friès, G., 1999. Deep-water massive sands: facies, processes and channel geometry in the Numidian Flysch, Sicily — comment. Sedimentary Geology, 127, 111–118.

Parsons, J.D., Schweller, W.J., Stelting, C.W., Southard, J.B., Lyons, W.J., Grotzinger, J.P., 2003. A preliminary experimental study of turbidite fan deposits—reply. Journal of Sedimentary Research, 73, 839–841.

Peakall, J., McCaffrey, W.D., Kneller, B.C., Stelting, C.E., McHargue, T.R., Schweller, W.J., 2000. A process model for the evolution of submarine fan channels: implications for sedimentary architecture. In: Bouma, A.H., Stone, C.G. (Eds.), Fine-Grained Turbidite Systems, AAPG Memoir 72/SEPM Special Publication No. 68, pp. 73–88.

Pelinovsky, E., Tinti, S., 2005. Editorial. Marine Geology, 215, 1–2.

Pequegnat, W.E., 1972. A deep bottom current on the Mississippi Cone. In: Capurro, L.R.A., Reid, J.L., (Eds.), Contributions on the Physical Oceanography of the Gulf of Mexico, Texas A&M University Oceanographic Studies, vol.2. Gulf Publishing Co, Houston, pp. 65–87.

Peterson, G.L., 1966. Structural interpretation of Sandstone dikes, Northwest Sacramento Valley, California. GSA Bulletin, 77, 833–842.

Petruncio, E.T., Rosenfeld, L.K., Paduan, J.D., 1998. Observations of the internal tide in Monterey Canyon. Journal of Physical Oceanography, 28, 1873–1903.

Petters, S.W., 1984. An ancient submarine canyon in the Oligocene-Miocene of the western Niger Delta. Sedimentology, 31, 805–810.

Pettijohn, F.J., 1957. Sedimentary Rocks, 2nd Edition. Harper, New York, p. 718.

Pettijohn, F.J., 1975. Sedimentary Rocks, 3rd Edition. Harper & Row, Publishers, New York, p. 628.

Pettijohn, F.J., Potter, P.E., 1964. Atlas and Glossary of Primary Sedimentary Structures. Springer, Berlin, p. 770.

Pettingill, H.S., 1998.Turbidite giants—lessons from the world's 40 largest turbidite discoveries. EAGE/AAPG 3rd Research Symposium on Developing and Managing Turbidite Reservoirs, 3–9 October 1998, Almeria, Spain, A027.

Phillips, C.J., Davies, T.R.H., 1991 Determining rheological parameters of debris flow material. Geomorphology, 4, 101–110.

Pickering, K.T., Hilton, V., 1998. Turbidite Systems of Southeast France. Vallis Press, London, p. 229.

Pickering, K.T., Stow, D.A.V., Watson, M., Hiscott, R., 1986. Deep-water facies, processes and models: a review and classification scheme for modern and ancient sediments. Earth-Science Reviews, 23, 75–174.

Pickering, K.T., Hiscott, R.N., Hein, F.J., 1989. Deep-Marine Environments. Unwin Hyman, London, p. 416.

Pickering, K.T., Soh, W., Taira, A., 1991. Scale of tsunami-generated sedimentary structures in deep water. Journal of the Geological Society, London, 148, 211–214.

Pickering, K.T., Hiscott, R.N., Kenyon, N.H., Ricci Lucchi, F., Smith, R.D.A. (Eds.), 1995. Atlas of Deep Water Environments: Architectural Style in Turbidite Systems. Chapman and Hall, London, p. 333.

Pickering, K.T., Hodgson, D.M., Platzman, E., Clark, J.D., Stephens, C., 2001. A new type of bedform produced by backfilling processes in a submarine channel, late Miocene, Tabernas-Sorbas basin, SE Spain. Journal of Sedimentary Research, 71, 692–704.

Pierce, J.W., 1976. Suspended sediment transport at the shelf break and over the outer margin. In: Stanley, D.J., Swift, D.J.P. (Eds.), Marine Sediment Transport and Environmental Management, John Wiley, New York, pp. 437–448.

Pierson, T.C., Costa, J.E., 1987. A rheologic classification of subaerial sediment-water flows. In: Costa, J.E., Wieczorek, G.F. (Eds.), Debris Flows/Avalanches: Process, Recognition, and Mitigation, Geological Society of America Reviews in Engineering Geology, VII, pp. 1–12.

Pilkey, O.H., 1988. Basin plains: giant sedimentation events. In: Clifton, H.E. (Ed.), Sedimentologic Consequences of Convulsive Geologic Events, Geological Society of America Special Paper 229, pp. 93–99.

Pilkey, O.H., Locker, S.D., Cleary, W.J., 1980. Comparison of sand-layer geometry on flat floors of 10 modern depositional basins. AAPG Bulletin, 64, 841–856.

Piper, D.J.W., 1970. A Silurian deep sea fan deposit in western Ireland and its bearing on the nature of turbidity current. Journal of Geology, 78, 509–522.

Piper, D.J.W., 1972. Turbidite origin of some laminated mudstones. Geological Magazine, 108, 115–126.

Piper, D.J.W., 1978. Turbidite muds and silts in deep-sea fans and abyssal plains. In: Stanley, D.J., Kelling, G. (Eds.), Sedimentation in Submarine Fans, Canyons, and Trenches, Hutchinson and Ross, Stroudsburg, Pennsylvania, pp. 163–176.

Piper, D.J.W., Brisco, C.D., 1975. Deep-water continental-margin sedimentation, DSDP Leg 28, Anterctica. In: Hayes, D.E. et al. (Eds), Initial Reports of the Deep Sea Drilling Project, U.S. Govt. Printing Office, Washington, D.C., pp. 727–755.

Piper, D.J.W., Normark, W.R., 1983. Turbidite depositional patterns and flow characteristics, Navy submarine fan, California Borderland. Sedimentology, 30, 681–694.

Piper, D.J.W., Normark, W.R., 2001. Sandy fans—from Amazon to Hueneme and beyond. AAPG Bulletin, 85, 1407–1438.

Piper, D.J.W., Shor, A.N., Hughes Clarke, J.E., 1988. The 1929 'Grand Banks' earthquake, slump, and turbidity current. In: Clifton, H.E. (Ed.), Sedimentologic Consequences of Convulsive Geologic Events, Geological Society of America Special Paper 229, p. 77–92.

Pirmez, C., Flood, C., 1995. Morphology and structure of Amazon Channel. In: Flood, R.D., Piper, D.J.W., Klaus, A. et al. (Eds.), Proceedings of the Ocean Drilling Program, Initial Reports 155, College Station, Texas (Ocean Drilling Program), pp. 23–45.

Pirmez, C., Imran. J., 2003. Reconstruction of turbidity currents in Amazon Channel. Marine and Petroleum Geology, 20, 823–849.

Pirmez, C., Hiscott, R.N., Kronen Jr., J.D., 1997. Sandy turbidite successions at the base of channel-levee systems of the Amazon Fan revealed by FMS logs and cores: unraveling the facies architecture of large submarine fans. In: Flood, R.D., Piper, D.J.W., Klaus, A., Peterson, J.C. (Eds.), Proceedings of the Ocean Drilling Program Scientific Results, 155, pp. 7–33.

Pitman III, W.C., 1979. The effect of eustatic sea level changes on startigraphic sequences at Atlantic margins. AAPG Memoir 29, 453–460.

Pluenneke, J.L., 1976. Comparative analysis of debrites, turbidites, and contourites, Unpublished M.S. Thesis. College Station, Texas A&M University, Texas, p. 93.

Poliakov, A.S., 2002. Properties of granular media and transportation mechanism of subaqueous debris flows. Lithology and Mineral Resources, 37, 25–38.

Postma, G., 1986. Classification of sediment gravity-flow deposits based on flow conditions during sedimentation. Geology, 14, 291–294.

Postma, G., Nemec, W., Kleinspehn, K.L., 1988. Large floating clasts in turbidites: a mechanism for their emplacement. Sedimentary Geology, 58, 47–61.

Prandtl, L., 1904. Uber Flfissigkeitsbewegung bei sehr kleiner Reibung. Int. Math.-Kongr., Heidelberg, 3rd, 1904, Teubner, Leipzig, 1905, pp. 484–491.

Prandtl, L., 1925. Bericht fiber Untersuchungen zur ausgebildeten Turbulenz. ZAMM, 5, 136–139.

Prandtl, L., 1926. Bericht fiber neuere Turbulenzforschung. In: Hydraulische Probleme, VDI-Verlag, Berlin, pp. 1–13.

Prandtl, L., 1952. Essentials of Fluid Dynamics. Hafner Publishing Co., New York, p. 452.

Pratson, L.F., Haxby, W.F., 1996. What is the slope of the U.S. continental slope? Geology, 24, 3–6.

Pratt, B.R., 2002. Storms *versus* tsunamis: dynamic interplay of sedimentary, diagenetic, and tectonic processes in the Cambrian of Montana. Geology, 30, 423–426.

Prior, D.B., Bornhold, B.D., 1990. The underwater development of Holocene fan deltas. In: Colella, A., Prior, D.B. (Eds.), Coarse-grained Deltas, International association of Sedimentologists Special Publication 10, Blackwell Scientific Publications, Oxford, pp. 75–90.

Prior, D.B., Coleman, J.M., 1984. Submarine slope instability. In: Brunsden, D., Prior, D.B. (Eds.), Slope Instability, John Wiley & Sons Ltd, Chichester, pp. 419–455.

Prior, D.B., Bornhold, B.D., Coleman, J.M., Bryant, W.R., 1982. The morphology of a submarine slide, Kitimat Arm, British Columbia. Geology, 10, 588–592.

Prior, D.B., Bornhold, B.D., Johns, M.W., 1984. Depositional characteristics of a submarine debris flow. Journal of Geology, 92, 707–727.

Puig, P., Ogston, A.S., Mullenbach, B.L., Nittrouer, C.A., Sternberg, R.W., 2003. Shelf-to-canyon sediment-transport processes on the Eel continental margin (northern California). Marine Geology, 193, 129–149.

Purvis, K., Kao, J., Flanagan, K., Henderson, J., Duranti, D., 2002. Complex reservoir geometries in a deep water clastic sequence, Gryphon Field, UKCS: injection structures, geological modeling and reservoir simulation. Marine and Petroleum Geology, 19, 161–179.

Qian, Y., Yang, W., Zhao, W., Cheng, X., Zhang, L., Xu, W., 1980. Basic characteristics of flow with hyperconcentrations of sediment. In: Proceedings of the International Symposium on River Sedimentation, Chinese Society of Hydraulic Engineering, Beijing, pp. 175–184.

Racki., G., 2002. What is hot in sedimentary research over the millennium crossroad? Acta Geologica Polonica, 52, 577–584.

Racki, G., 2003. 'HOT' Articles in modern sedimentary research: The updated list. International Association of Sedimentologists Newsletter, August. Issue 187, 1–4. Uniform Resource Locator (URL): http://www.blackwellpublishing.com/uk/society/ias/news1187.htm (accessed February 24, 2005).

Ravenne, C., Vally, R., Riche, P., Tremolieres, P., 1987. Sedimentation et tectonique dans le basin marin Eocene superieur-Oligocene des Alpes du sud. Revue de I'Institut de Ftancais du Petrole, 42, 529–553.

Raymond, L.A., 1975. Tectonite and mélange—a distinction. Geology, 3, 7–9.

Reading, H.G., 1986a. Introduction. In: Reading, H.G. (Ed.), Sedimentary Environmentsand Facies, 2nd Edition, Blackwell Scientific Publications, Oxford, pp. 1–3.

Reading, H.G., 1986b. Facies. In: Reading, H.G. (Ed.), Sedimentary Environments and Facies, 2nd Edition, Blackwell Scientific Publications, Oxford, pp. 4–19.

Reading, H.G. (Ed.), 1996. Sedimentary Environments: Processes, Facies and Stratigraphy. Blackwell Science, Oxford, p. 688.

Reading, H.G., Collinson, J.D., 1996. Clastic coasts. In: Reading, H.G. (Ed.), Sedimentary Environments: Processes, Facies, and Stratigraphy, Blackwell Science, Oxford, pp. 154–231.

Reading, H.G., Richards, M., 1994. Turbidite systems in deep-water basin margins classified by grain size and feeder system. AAPG Bulletin, 78, 792–822.

Rebesco, M., Pudsey, C.J., Canals, M., Camerlenghi, A., Barker, P.F., Estrada, F., Giorgetti, A., 2002. Sediment drifts and deep-sea channel systems, Antarctic Peninsula Pacific Margin. In: Stow, D.A.V., Pudsey, C.J., Howe, J.A., Faugères J.-C., Viana A.R. (Eds.), Deep-Water Contourite Systems: Modern Drifts and Ancient Series, Seismic and Sedimentary Characteristics, Geological Society Memoirs 22, London, pp 353–372.

Reid, J.L., 1969. Preliminary results of measurements of deep currents in the Pacific Ocean. Nature, 221, 848.

Reineck, H.E., Singh, I.B., 1980. Depositional Sedimentary Environments, 2nd Edition, Springer-Verlag, Berlin, p. 549.

Reineck, H.E., Wunderlich, F., 1968. Classification and origin of flaser and lenticular bedding. Sedimentology, 11, 99–104.

Reynolds, J., Mackay, T., 1992. Post depositional modification of deep water sandstones-reservoir geometry of the Gryphon sand, Gryphon Field, U.K. Sector 9/18b. In: D. Stow, A.V. (Convenor), Deep Water Massive Sands: Arthur Holmes European Research Conferences Programme, 19.

Ricci Lucchi, F., 1975. Depositional cycles in two turbidite formations of northern Apennines (Italy). Journal of Sedimentary Petrology, 45, 3–43.

Ricci Lucchi, F., 1981. Excursion guidebook with contributions on sedimentology of some Italian Basins. In: 2nd IAS European Regional Meeting, Bologna, Italy, p. 342.

Ricci Lucchi, F., Valmori, E., 1980. Basin-wide turbidites in a Miocene, over-supplied deep-sea plain: a geometrical analysis. Sedimentology, 27, 241–270.

Rich, J.L., 1950. Flow markings, groovings, and intrastratal crumplings as criteria for recognition of slope deposits with illustrations from Silurian rocks of Wales. AAPG Bulletin, 34, 717–741.

Richardson, G.E., French, L.S., Baud, R.D., Peterson, R.H., Roark, C.D., Montgomery, T.M., Kazanis, E.G., Conner, G.M., Gravois. M.P., 2004. Deepwater Gulf of Mexico 2004: America's Expanding Frontier.

U.S. Department of the Interior, Minerals Management Service, Gulf of Mexico OCS Region, OCS Report MMS 2004–021, p. 166. Uniform Resource Locator (URL): http://www.gomr.mms.gov/homepg/offshore/deepwtr.html (accessed September 5, 2004).

Richardson, M.J., Wimbush, L., Mayer, M. 1981. Exceptionally strong near-bottom flows on the continental rise of Nova Scotia. Science, 213, 887–888.

Rizzini, A., Passega, R., 1964. Évolution de la sédimentation et orogenèse, Vallée du Santerno, Apennin Septentrional. In: Bouma, A.H., Brouwer, A. (Eds.), Turbidites, Developments in Sedimentology 3, Elsevier, Amsterdam, pp. 65–74.

Rodine, J.D., Johnson, A.M., 1976. The ability of debris, heavily freighted with coarse clastic material to flow on gentle slopes. Sedimentology, 23, 213–234.

Rodolfo, K.S., 2003. Tsunamites and Seismites. McGraw-Hill Encyclopedia of Science & Technology, AccessScience, Uniform Rresource Locator (URL): http://www.accessscience.com/ResUpdates/2003/YB_030915_frameset.html?qq=&q=tsunamite|tsunamites (accessed January 21, 2005).

Rodriguez, A.B., Anderson, J.B., 2004. Contourite origin for shelf and upper slope sand sheet, offshore Antarctica. Sedimetology, 51, 699–711.

Rossetti, D. de F., Góes, A.M., Truckenbrodt, W., Anaisse Jr., J., 2000. Tsunami-induced large-scale scour-and-fill structures in Late Albian to Cenomanian deposits of the Grajaü Basin, northern Brazil. Sedimetology, 47, 309–323.

Rothwell, R.G., Kenyon, N.H., McGregor, B.A., 1991. Sedimentary features of the south Texas continental slope as revealed by side-scan sonar and high-resolution seismic data. AAPG Bulletin, 75, 298–312.

Rouse, C., 1984. Flowslides. In: Brunsden, D., Prior, D.B. (Eds.), Slope Insatbility, John Wiley & Sons Ltd, Chichester, pp. 491–522.

Rowe, G.T., 1971. Observations on bottom currents and epibenthonic populations in Hatteras submarine canyon. Deep-Sea Research, 18, 569–581.

Rowe, G.T., Menzies, R.T., 1968. Deep bottom currents off the coast of North Carolina. Deep-Sea Research, 15, 711–720.

Runcorn, S.K., 1962. Paleomagnetic studies for continental drift and its geophysical cause. In: Runcorn, S.K. (Ed.), Continental Drift, Academic, New York, pp. 1–40.

Rupke, N.A., Stanley, D.J., 1974. Distinctive properties of turbiditic and hemipelagic mud layers in the Algero-Baleric Basin, Western Mediterranean Sea. Smithsonian Contributions to the Earth Science, No. 13, p. 40.

Rusnak, G.A., 1991. Afoot to afloat along the edge: adventures of an ingenuous beachcomber—a tribute to Francis Parker Shepard (1897–1985). In: Osborne, R.H. (Ed.), From Shoreline to Abyss: Contributions in Marine Geology in Honor of Francis Parker Shepard, SEPM Special Publication 46, pp. 1–7.

Russell, K.L., 1968. Oceanic ridges and eustatic changes in sea level. Nature, 218, 861–862.

Sakai, T., Masuda, F., 1996. Slope turbidite packets in a fore-arc basin fill sequence of the Plio-Pleistocene Kakegawa Group, Japan: their formation and sea-level changes. Sedimentary Geology, 104, 89–98.

Sanders, J.E., 1963. Concepts of fluid mechanics provided by primary sedimentary structures. Journal of Sedimentary Petrology, 33, 173–179.

Sanders, J.E., 1965. Primary sedimentary structures formed by turbidity currents and related resedimentation mechanisms. In: Middleton, G.V. (Ed.), Primary Sedimentary Structures and their Hydrodynamic Interpretation, SEPM Special Publication 12, pp. 192–219.

Sanders, J.E., 1973. Map of parts of floor of Santa Barbara Channel, California, compiled from side-scanning sonar records. AAPG Bulletin, 57, 802–803.

Sanders, J.E., 1981. Principles of Physical Geology. John Wiley & Sons, New York, p. 624.

Sanders, J.E., Friedman, G.M., 1997. History of petroleum exploration in turbidites and related deep-water deposits. Northeastern Geology and Environmental Sciences 19(1/2), 67–102.

Sarg, J.F., Skjold, L.J., 1982. Stratigraphic traps in Paleocene sands in the Balder area, North Sea. AAPG Memoir, 32, p. 197–206.

Savage, S.B., 1984. The mechanics of rapid granular flows. Advances in Applied Mechanics, 24, 289–366.

Sayles, R. W., 1931. Bermuda during the Ice Age. Proceedings of the American Academy of Arts & Sciences, 66, 382–467.

Schamel, S., Forster, C., Deo, M., Sprinkel, D., Olson, K., Simmons, M., Jenkins, C., 1998. Optimization of heavy-oil production by steam flood from a shallow sandstone reservoir, Midway-Sunset Field, southern San Joaquin Basin, California (abs). AAPG Annual Convention Extended Abstracts, A576.

Scheffers A., Kelletat, D. 2003. Sedimentologic and geomorphologic tsunami imprints worldwide—a review. Earth-Science Reviews, 63, 83–92.

Scheidegger, A.E., 1975. Physical aspects of natural catastrophes. Elsevier Science Publishing Co., New York, p. 289.

Scholle, P.A., 1971. Sedimentology of fine-grained deep-water carbonate turbidites, Monte Antola Flysch (Upper Cretaceous), Northern Apennines, Italy. GSA Bulletin, 82, 629–658.

Schwab, W.C., Lee, H.J., Twichell, D.C., Locat, J., Hans Nelson, C., McArthur, W.C., Kenyon, N.H., 1996. Sediment mass-flow processes on a depositional lobe, outer Mississippi Fan. Journal of Sedimentary Research, 66, 916–927.

Scott, R.M., Tillman, R.W., 1981. Stevens Sandstone (Miocene), San Joaquin Basin, California. In: Siemers, C.T., Tillman, R.W., Williamson, C.R. (Eds.), Deep-Water Clastic Sediments: A Core Workshop, SEPM Core Workshop 2, pp. 116–248.

Seibold, E., Hinz, K., 1974. Continental slope construction and destruction, West Africa. In: Burk, C.A., Drake, C.L. (Eds.), The Geology of Continental Margins, Springer-Verlag, New York, pp. 179–196.

Seilacher, A., 1967. Bathymetry of trace fossils. Marine Geology, 5, 413–428.

Seilacher, A., 1984. Sedimentary structures tentatively attributed to seismic events. Marine Geology, 55, 1–12.

Selley, R.C., 1979. Dipmeter and log motifs in North Sea submarine-fan sands. AAPG Bulletin, 63, 905–917.

Shanmugam, G., 1978. The stratigraphy, sedimentology, and tectonics of the Middle Ordovician Sevier Shale Basin in East Tennessee. Unpublished Ph.D. dissertation, The University of Tennessee, Knoxville, Tennessee, p. 222.

Shanmugam, G., 1980. Rhythms in deep sea, fine-grained turbidite and debris-flow sequences, Middle Ordovician, eastern Tennessee. Sedimentology, 27, 419–432.

Shanmugam, G., 1984. Rock names challenged. Geotimes, 29, 6.

Shanmugam, G., 1985. Types of porosity in sandstones and their significance in interpreting provenance. In: Zuffa, G.G. (Ed.), Provenance of Arenites, D. Reidel Publishing Company, Holland, pp. 115–137.

Shanmugam, G., 1986. Conventional wisdom and scientific progress. Geology, 14, 718.

Shanmugam, G., 1988. Origin, recognition and importance of erosional unconformities in sedimentary basins. In: Kleinspehn, K.L., Paola, C. (Eds.), New Perspectives in Basin Analysis, Springer-Verlag, New York, pp. 83–108.

Shanmugam, G., 1990. Deep-marine facies models and the interrelationship of depositional components in time and space. In: Brown, G.C., Gorsline, D.S., Schweller, W.J. (Eds.), Deep-Marine Sedimentation: Depositional Models and Case Histories in Hydrocarbon Exploration & Development, San Francisco, SEPM Pacific Section Short Course, vol. 66, pp. 199–246.

Shanmugam, G., 1992a. Origin and implications of massive sands in the North Sea. In: Stow, D.A.V. (Convener), Deep-water Massive Sands, Arthur Holmes European Research Conferences, Cefalu, Sicily, 23–28 September, 1992, sponsored by the Geological Society of London, Programme and Abstracts, pp. 20.

Shanmugam, G., 1992b. Submarine canyons. 7th Edition of Encyclopedia of Science and Technology, McGraw-Hill Book Company, New York, pp. 548–552.

Shanmugam, G., 1996a High-density turbidity currents: are they sandy debris flows? Journal of Sedimentary Research, 66, 2–10.

Shanmugam, G., 1996b. Perception *vs*. reality in deep-water exploration. World Oil, 217, 37–41.

Shanmugam, G., 1997a. The Bouma Sequence and the turbidite mind set. Earth-Science Reviews, 42, 201–229.

Shanmugam, G., 1997b. Slope turbidite packets in a fore-arc basin fill sequence of the Plio–Pleistocene Kakegawa Group: their formation and sea-level changes – discussion. Sedimentary Geology, 112, 297–300.

Shanmugam, G., 1997c. Deep-water exploration: conceptual models and their uncertainties: NAPE (Nigerian Association of Petroleum Explorationists) Bulletin, 12/01, 11–28.

Shanmugam, G., 1998. Dimensions and geometries of the components of deep-water systems. Mobil Technology Company Special Publication, Dallas, Texas, p. 110.

Shanmugam, G., 2000a. 50 years of the turbidite paradigm (1950s–1990s): deep-water processes and facies models—a critical perspective. Marine and Petroleum Geology, 17, 285–342.

Shanmugam, G., 2000b. John E. Sanders and the turbidite controversy. In: Friedman, G.M. (Ed.), Conference on the History of Geologic Pioneers, Rensselaer Center of Applied Geology, Troy, New York, pp. 19–20.

Shanmugam, G., 2001. Book Review of 'Fine-grained turbidite systems' (Bouma, A.H., Stone, C.G. (Eds.) 2000, AAPG Memoir 72 and SEPM Special Pub. 68. Episodes, 24, 284.

Shanmugam, G., 2002a. Ten turbidite myths. Earth-Science Reviews, 58, 311–341.

Shanmugam, G., 2002b. Discussion on Mulder et al. 2001, Geo-Marine Letters, 21, 86–93. Inversely graded turbidite sequences in the deep Mediterranean. A record of deposits from flood-generated turbidity currents? Geo-Marine Letters, 22, 108–111.

Shanmugam, G., 2002c. Deep-marine sediments. AccessScience McGraw-Hill Encyclopedia of Science & Technology. Uniform Resource Locator (URL): http://www.accessscience.com/Encyclopedia/7/75/Est_757553_frameset.html?doi (accessed February 21, 2005).

Shanmugam, G., 2002d. Submarine Canyon. AccessScience McGraw-Hill Encyclopedia of Science & Technology. Uniform Resource Locator (URL): http://www.accessscience.com/Encyclopedia/6/66/Est_664300_frameset.html?doi (accessed February 21, 2005).

Shanmugam, G., 2002e. Deep-water processes and turbidite facies models: a paradigm shift. In: Swamy, S.N., Kapoor, P.N. (Eds.), Stratigraphic Challenges and Paradigm Shift in Hydrocarbon Exploration with Special References to Frontier Basins, Mussoorie, India, Proceedings of the 1st APG (Association of Petroleum Geologists) Conference and Exhibition, vol. 1, pp. 155–162.

Shanmugam, G., 2003. Deep-marine tidal bottom currents and their reworked sands in modern and ancient submarine canyons. Marine and Petroleum Geology, 20, 471–491.

Shanmugam, G., 2004. Modern deep-water environments: implications for sandstone petroleum reservoirs. In Promoting xcellence in exploration for more oil and gas, Technical Session: Sedimentology and depositional modeling with special reference to deep-water basins. Khajuraho, India: Proceedings of the 2nd APG (Association of Petroleum Geologists) Conference and Exhibition, 14 pp (CD-ROM).

Shanmugam, G., 2006. The tsunamite problem. Journal of Sedimentary Research, 76 (in press).

Shanmugam, G., Benedict, G.L., 1978. Fine-grained carbonate debris flow, Ordovician basin margin, Southern Appalachians. Journal of Sedimentary Petrology, 48, 1233–1240.

Shanmugam, G., Clayton, C.A., 1989. Reservoir description of a sand rich submarine fan complex for a steamflood project: Upper Miocene Potter Sandstone, North Midway Sunset Field, California. AAPG Bulletin, 73, 411.

Shanmugam, G., Lash, G.G., 1982. Analogous tectonic evolution of the Ordovician foredeeps, southern and central Appalachians. Geology, 10, 562–566.

Shanmugam, G., Moiola, R.J., 1982. Eustatic control of turbidites and winnowed turbidites. Geology, 10, 231–235.

Shanmugam, G., Moiola, R.J., 1984. Eustatic control of calciclastic turbidites. Marine Geology, 56, 273–278.

Shanmugam, G., Moiola, R.J., 1985. Submarine fan models: problems and solutions. In: Bouma, A.H., Normark, W.R., Barnes, N.E. (Eds.), Submarine Fans and Related Turbidite Systems, Springer-Verlag, New York, pp. 29–34.

Shanmugam, G., Moiola, R.J., 1988. Submarine fans: characteristics, models, classification, and reservoir potential. Earth-Science Reviews, 24, 383–428.

Shanmugam, G., Moiola, R.J., 1991. Types of submarine fan lobes: models and implications. AAPG Bulletin, 75, 156–179.

Shanmugam, G., Moiola, R.J., 1994. An unconventional model for the deep-water sandstones of the Jackfork Group (Pennsylvanian), Ouachita Mountains, Arkansas and Oklahoma. In: Weimer, P., Bouma, A.H., Perkins, R.F. (Eds.), Submarine Fans and Turbidite Systems, Houston, Gulf Coast Section SEPM Foundation 15th Annual Research Conference, pp. 311–326.

Shanmugam, G., Moiola, R.J., 1995. Reinterpretation of depositional processes in a classic flysch sequence (Pennsylvanian Jackfork Group), Ouachita Mountains, Arkansas and Oklahoma. AAPG Bulletin, 79, 672–695.

Shanmugam, G., Moiola, R.J., 1997. Reinterpretation of depositional processes in a classic flysch sequence (Pennsylvanian Jackfork Group), Ouachita Mountains, Arkansas and Oklahoma: reply. AAPG Bulletin, 81, 476–491.

Shanmugam, G., Walker, K.R., 1978. Tectonic significance of distal turbidites in the Middle Ordovician Blockhouse and lower Sevier formations in east Tennessee. American Journal of Science, 278, 551–578.

Shanmugam, G., Zimbrick, G., 1996. Sandy slump and sandy debris flow facies in the Pliocene and Pleistocene of the Gulf of Mexico: implications for submarine fan models. In: AAPG International Congress and Exhibition, Caracas, Venezuela, Official Program, A45.

Shanmugam, G., Damuth, J.E., Moiola, R.J., 1985a. Is the turbidite facies association scheme valid for interpreting ancient submarine fan environments? Geology, 13, 234–237.

Shanmugam, G., Moiola, R.J., Damuth, J.E., 1985b. Eustatic control of submarine fan development. In: Bouma, A.H., Normark, W.R., Barnes, N.E. (Eds.), Submarine Fans and Related Turbidite Systems, Springer-Verlag, New York, pp. 23–28.

Shanmugam, G., Moiola, R.J., McPherson, J.G., O'Connell, S., 1988a. Comparison of turbidite facies associations in modern passive-margin Mississippi Fan with ancient active-margin fans. Sedimentary Geology, 58, 63–77.

Shanmugam, G., Moiola, R.J., McPherson, J.G., O'Connell, S., 1988b. Comparison of modern Mississippi Fan with selected ancient active-margin fans. Gulf Coast Association of Geological Societies Transactions, 38, 157–165.

Shanmugam, G., Moiola, R.J., Sales, J.K., 1988c. Duplex-like structures in submarine fan channels, Ouachita Mountains, Arkansas. Geology, 16, 229–232.

Shanmugam, G., Spalding, T.D., Rofheart, D.H., 1993a. Process sedimentology and reservoir quality of deep-marine bottom-current reworked sands (sandy contourites): an example from the Gulf of Mexico. AAPG Bulletin, 77, 1241–1259.

Shanmugam, G., Spalding, T.D., Rofheart, D.H., 1993b. Traction structures in deep-marine bottom-current reworked sands in the Pliocene and Pleistocene, Gulf of Mexico. Geology, 21, 929–932.

Shanmugam, G., Lehtonen, L.R., Straume, T., Syversten, S.E., Hodgkinson, R.J., Skibeli, M., 1994. Slump and debris flow dominated upper slope facies in the Cretaceous of the Norwegian and Northern North Seas (61–67 N): implications for sand distribution. AAPG Bulletin, 78, 910–937.

Shanmugam, G., Bloch, R.B., Mitchell, S.M., Beamish, G.W.J., Hodgkinson, R.J., Damuth, J.E., Straume, T., Syvertsen, S.E., Shields, K.E., 1995a. Basin-floor fans in the North Sea: Sequence stratigraphic models *vs*. sedimentary facies. AAPG Bulletin, 79, 477–512.

Shanmugam, G., Hermance, Olaifa, W.E., J.O., Odior, E.G., 1995b. Slump dominated upper slope reservoir facies, Intra Qua Iboe (Pliocene), Edop Field, Offshore Nigeria (abs.). AAPG Annual Convention, Official Program, 88A.

Shanmugam, G., Spalding, T.D., Rofheart, D.H., 1995c. Deep-marine bottom-current reworked sand (Pliocene and Pleistocene), Ewing Bank 826 Field, Gulf of Mexico. In: Winn, R.D., Armentrout, J.M. (Eds.), Turbidites and Associted Deep-Water Facies, SEPM Core Workshop No. 20, pp. 25–54.

Shanmugam, G., Bloch, R.B., Mitchell, S.M., Damuth, J.E., Beamish, G.W.J., Hodgkinson, R.J., Straume, T., Syvertsen, S.E., Shields, K.E., 1996. Slump and debris-flow dominated basin-floor fans in the North Sea: an evaluation of conceptual sequence-stratigraphical models based on conventional core data. In: Hesselbo, S.P., Parkinson, D.N. (Eds.), Sequence Stratigraphy in British Geology, Geological Society Special Publication No. 103, pp. 145–175.

Shanmugam, G., Bloch, R.B., Damuth, Hodgkinson, R.J., 1997a. Basin-floor fans in the North Sea: Sequence stratigraphic models *vs*. sedimentary facies: Reply. AAPG Bulletin, 81, 666–672.

Shanmugam, G., Famakinwa, S.B., Hodgkinson, R.J., Blundell, L.C., 1997b. Deep-marine slump and debris flow dominated reservoirs of the Zafiro Field, offshore Equatorial Guinea, 1997. In: AAPG International Conference and Exhibition, Vienna, Austria, 6.

Shanmugam, G., Moiola, R. J, Wagner, J.B. 1997c. Turbidite paradigm and sequence stratigraphy: a critical perspective. In: Official Program-1997 AAPG Annual Convention, Dallas, Texas, A106.

Shanmugam, G., Poffenberger, M., Toro Alava, J., 2000. Tide-dominated estuarine facies in the Hollin and Napo ('T' and 'U') formations (Cretaceous), Sacha Field, Oriente Basin, Ecuador. AAPG Bulletin, 84, 652–682.

Shapiro, A.H., 1961. Shape and Flow: The Fluid Dynamics of Drag. Anchor Books, Doubleday & Company, Inc., Garden City, New York, p. 186.

Sheldon, P.G., 1928. Some sedimentation conditions in Middle Portage rocks. American Journal of Science, 15, 243–252.

Sheline, H.E., 2005. Don't abuse seismic attributes. AAPG Explorer, 26, 22–23.

Shepard, F.P., 1951. Mass movements in submarine canyon heads. Trans. Am. Geophys. Union, 32, 405–418.

Shepard, F.P., 1966. Meander in valley crossing a deep-ocean fan. Science, 154, 386–386.

Shepard, F.P., 1973. Submarine geology, 3rd Edition. Harper & Row Publishers, New York, p. 517.

Shepard, F.P., 1976. Tidal components of currents in submarine canyons. Journal of Geology, 84, 343–350

Shepard, F.P., 1979. Currents in submarine canyons and other sea valleys. In: Doyle, L.J., Pilkey, O.H. (Eds.), Geology of Continental Slopes, SEPM Special Publications 27, pp. 85–94.

Shepard, F.P., 1981. Submarine canyons: multiple causes and long-time persistence. AAPG Bulletin, 65, 1062–1077.

Shepard, F.P., Dill, R.F., 1966. Submarine canyons and other sea valleys. Rand McNally & Co., Chicago, p. 381.

Shepard, F.P., Emery, K.O., 1973. Congo submarine canyon and fan valley. AAPG Bulletin, 57, 1679–1691.

Shepard, F.P., Marshall, N.F., 1978. Currents in submarine canyons and other sea valleys. In: Stanley, D.J., Kelling, G. (Eds.), Sedimentation in Submarine Fans, Canyons, and Trenches, Hutchinson and Ross, Stroudsburg, Pennsylvania, pp. 3–14.

Shepard, F.P., Revelle, R.R., Dietz, R.S., 1939 Ocean-bottom currents off the California coast. Science, 89, 488–489.

Shepard, F.P., Dill, R.F., Von Rad, U., 1969. Physiography and sedimentary processes of La Jolla Submarine Fan and Fan-Valley, California. AAPG Bulletin, 53, 39–420.

Shepard, F.P., Marshall, N.F., McLoughlin, P.A., Sullivan, G.G., 1979. Currents in submarine canyons and other sea valleys. AAPG Studies in Geology No. 8, p. 173.

Shew, R.D., Rollins, D.R., Tiller, G.M., Hackbarth, C.J., White, C.D., 1994. Characterization and modeling of thin-bedded turbidite deposits from the Gulf of Mexico using detailed subsurface and analog data. In: Weimer, P., Bouma, A.H., Perkins, R.F. (Eds.), Submarine Fans and Turbidite Systems, Gulf Coast Section SEPM Foundation 15th Annual Research Conference, pp. 327–334.

Shiki, T., Yamazaki, T., 1996. Tsunami-induced conglomerates in Miocene upper bathyal deposits, Chita Peninsula, central Japan. Sedimentary Geology, 104, 175–188.

Shiki, T., Cita, M.B., Gorsline, D.S., 2000. Sedimentary features of seismites, seismo- turbidites, and tsunamites—an introduction. Sedimentary Geology, 135, vii–ix.

Shipboard Scientific Party, 1995a. Site 934. In: Flood, R.D., Piper, D.J.W., Klaus, A. et al., Proceedings of the ODP Initial Reports 155, College Station, Texas (Ocean Drilling Program), pp. 241–271.

Shipboard Scientific Party, 1995b. Site 944. In: Flood, R.D., Piper, D.J.W., Klaus, A. et al., Proceedings of the ODP Initial Reports 155, College Station, Texas (Ocean Drilling Program), pp. 591–633.

Shipboard Scientific Party, 1995c. Site 931. In: Flood, R.D., Piper, D.J.W., Klaus, A. et al., Proceedings of the ODP Initial Reports 155, College Station, Texas (Ocean Drilling Program), pp. 123–174.

Shipboard Scientific Party, 1995d. Site 946, In: Flood, R.D., Piper, D.J.W., and Klaus, A. et al., Proceedings of the ODP Initial Reports 155, College Station, Texas (Ocean Drilling Program), pp. 657–688.

Shreve, R.L., 1968. The Blackhawk Landslide. Geological Society of America Special Paper 108, p. 47.

Shultz, A.W., 1984. Subaerial debris-flow deposition in the upper Paleozoic Cutler Formation, Western Colorado. Journal of Sedimentary Petrology, 54, 759–772.

Signorini, R., 1936. Determinazione del senso di sedimentazione degli strati nelle formazione arenacea dell' Appennino settentrionale. Boll. Soc.Geol. Ital., 55, 259–267.

Simms, M.J., 2003. Uniquely extensive seismite from the latest Triassic of the United Kingdom: evidence for bolide impact? Geology, 31, 557–560.

Simons, D.B., Richardson, E.V., Nordin Jr., C.F., 1965. Sedimentary structures generated by flow in alluvial channels. In: Middleton, G.V. (Ed.), Primary Sedimentary Structures and their Hydrodynamic Interpretation, SEPM Special Publication 12, pp. 34–52.

Simpson, J.E., 1982. Gravity currents in the laboratory, atmosphere, and ocean. Ann. Rev. Fluid Mechanics, 14, 213–234.

Simpson, R.H., Lawrence, M.B., 1971. Atlantic hurricane frequencies along the U.S. coastline. NOAA Memorandum NWS SR-58, p. 14.

Sinclair, H.D., 1997. Tectonostratigraphic model for underfilled peripheral foreland basins, an Alpine perspective. GSA Bulletin, 109, 324–346.

Skempton, A.W., 1953. Soil mechanics in relation to geology. Proceedings of the Yorkshire Geological Society, 29, 33–62.

Skilbeck, C.G., 1982. Carboniferous depositional systems of the Myall lakes, northern New South Wales. In: Flood, P.G., Runnegar, B. (Eds.), New England Geology, University of New England, pp. 121–132.

Slatt, R.M., Weimer, P., Stone, C.G., 1997. Reinterpretation of depositional processes in a classic flysch sequence (Pennsylvanian Jackfork Group), Ouachita Mountains, Arkansas and Oklahoma: discussion. AAPG Bulletin, 81, 449–459.

Smith, R.D.A., 1995. Reservoir architecture of syn-rift lacustrine turbidite systems, early Cretaceous, offshore South Gabon. In: Lambiase, J.J. (Ed.), Hydrocarbon Habitat in Rift Basins, Geological Society Special Publication, 80, pp. 197–210.

Snedden, J.W., Nummedal, D., Amos, A.F., 1988. Storm- and fair-weather combined flow on the Central Texas continental shelf. Journal Sedimentary Petrology, 58, 580–595.

Sohn, Y.K., Choe, M.Y., Jo, H.R., 2002. Transition from debris flow to hyperconcentrated flow in a submarine channel (the Cretaceous Cero Toro Formation, southern Chile). Terra Nova, 14, 405–415.

Solheim, A., Bryn, P., Sejrup, H.P., Mienert, J., Berg, K., 2005. Ormen Lange—an integrated study for the safe development of a deep-water gas field within the Storegga Slide Complex, NE Atlantic continental margin; executive summary. Marine and Petroleum Geology, 22, 1–9.

Sorby, H.C., 1908. On the application of quantitative methods to the study of rocks. Quarterly Journal of the Geological Society, 64, 171–233.

Southard, J.B., 1975. Bed Configutations. In: Harms, J.C., Southard, J.B., Spearing, D.R., Walker, R.G. (Eds.), Depositional Environments as Interpreted from Primary Sedimentary Structures and Stratification Sequences, Dallas, Texas, Lecture Notes for SEPM Short Course No. 2, pp. 5–43.

Southard, J.B., Stanley, D.J., 1976. Shelf-break processes and sedimentation. In: Stanley, D.J., Swift, D.J.P. (Eds.), Marine Sediment Transport and Environmental Management. John Wiley & Sons, New York, pp. 351–377.

Sparks, R.S.J., Pinkerton, H., Hulme, G., 1976. Classification and formation of lava levees on Mount Etna, Sicily. Geology, 4, 269–271.

Srurkel, B.F.F., Ormö, J., 1997. Impact-related clastic injections in the marine Ordovician Lockne impact structure, Central Sweden. Sedimentology, 44, 793–804.

Stanley, D.J., 1963. Vertical petrographic variability in Annot Sandstone turbidites. Journal of Sedimentray Petrology, 33, 783–788.

Stanley, D.J., 1975. Submarine canyon and slope sedimentation (Gres D'Annot) in the French Maritime Alps. In: IXth Congress International de Sedimentologie, Nice, France, Field Guide, p. 129.

Stanley, D.J., 1981. Unifites: structureless muds of gravity flow origin in Mediterranean basins. Geo-Marine Letters, 1, 77–83.

Stanley, D.J., 1993. Model for turbidite-to-contourite continuum and multiple process transport in deep marine settings: example in the rock record. Sedimentary Geology, 82, 241–255.

Stanley, D.J., Kelling, G. (Eds), 1978. Sedimentation in Submarine Canyons, Fans, and Trenches. Dowden, Hutchinson and Ross, Inc., Stroudsburg, Pennsylvania, p. 395.

Stanley, D.J., Moore, G.T., (Eds.), 1983. The Selfbreak: Critical Interface on Continental Margins. SEPM Special Publication No. 33, p. 467.

Stanley, D.J., Palmer, H.D., Dill, R.F., 1978. Coarse sediment transport by mass flow and turbidity current processes and downslope transformations in Annot Sandstone canyon-fan valley systems. In: Stanley, D.J., Kelling, G. (Eds.), Sedimentation in Submarine Canyons, Fans, and Trenches, Hutchinson and Ross, Stroudsburg, Pennsylvania, pp. 85–115.

Stauffer, P.H., 1967. Grain flow deposits and their implications, Santa Ynez Mountains, California. Journal of Sedimentary Petrology, 37, 487–508.

Steele, T.H., Barrett, T R., Worthington, L.V., 1962. Deep currents south of Iceland. Deep-Sea Research, 9, 465–474.

Steinmann, G., 1905. Geologische Beobachtungen in den Alpen. Naturf. Gesell. Freiberg, Ber., 16, 18–67.

Stelting, C.E., Bouma, A.H., Stone, C.G., 2000. Fine-grained turbidite systems: overview. In: Bouma, A.H., Stone, C.G. (Eds.), Fine-Grained Turbidite Systems, AAPG Memoir 72 and SEPM Special Publication No. 68, Tulsa, Oklahoma, pp. 1–7.

Stetson, H.C., 1936. Geology and paleontology of the Georges Bank canyons, I. geology. GSA Bulletin, 47, 339–366.

Stewart, I.J., 1987. A revised stratigraphic interpretation of the Early Palaeogene of the Central North Sea. In: J. Brooks, Glennie, K.W. (Eds.), Petroleum Geology of North West Europe, vol. 1, pp. 555–576.

Stickel, J.J., Powell, R.L., 2005. Fluid mechanics and rheology of dense suspensions. Annual Review of Fluid Mechanics, 37, 129–149.

Stöffler, D., Grieve, R.A.F., 2003. Towards a unified nomenclature of metamorphic petrology. 11. Impactites. A proposal on behalf of the IUGS Subcommission on the Systematics of Metamorphic Rocks. Web version of April 30, 2003. Uniform Resource Locator (URL): http://www.bgs.ac.uk/scmr/docs/paper_12/scmr_paper_12_1.pdf, (accessed February 22, 2005).

Stommel, H., 1958. The abyssal circulation. Deep-Sea Research, 5, 80–82.

Stow, D.A.V., 1979. Distinguishing between fine-grained turbidites and contourites off Nova Scotia. Sedimentology, 26, 371–387.

Stow, D.A.V., 1984. Anatomy of debris-flow deposits. In: Hay, W.W., Sibuet, J.C. et al., Initial Reports, Deep Sea Drilling Project 75, Washington D.C., U.S. Government Printing Office, pp. 801–807.

Stow, D.A.V., 1985. Deep-sea clastics: where are we and where are we going? In: Brenchly, P.J., Williams, P.J. (Eds.), Sedimentology: Recent Developments and Applied Aspects, published for the Geological Society by Blackwell Scientific Publications, Oxford, pp. 67–94.

Stow, D.A.V., (Convenor) 1992. Deep-water massive sands. Arthur Holmes European Research Conferences, Cefalu, Sicily, 23–28 September, 1992, sponsored by the Geological Society of London, Programme and Abstracts, p. 28.

Stow, D.A.V., Faugères, J.C. (Ed.) 1998. Contourites, turbidites and process interaction. Sedimentary Geology, 115, 1–381.

Stow, D.A.V., Johansson, M., 2000. Deep-water massive sands: nature, origin and hydrocarbon implications. Marine and Petroleum Geology, 17, 145–174.

Stow, D.A.V., Lovell, J.P.B., 1979. Contourites: their recognition in modern and ancient sediments. Earth-Science Reviews, 14, 251–291.

Stow, D.A.V., Mayall, M., 2000. Deep-water sedimentary systems: new models for the 21st century. Marine and Petroleum Geology, 17, 125–135.

Stow, D.A.V., Piper, D.J.W. (Eds.), 1984. Fine-Grained Sediments: Deep-water Processes and Facies. Geological Society Special Publication No. 15, p. 659.

Stow, D.A.V., Shanmugam, G., 1980. Sequence of structures in fine-grained turbidites: comparison of recent deep-sea and ancient flysch sediments. Sedimentary Geology, 25, 23–42.

Stow, D.A.V., Cremer, M., Droz, L., Normark, W.R., O'Connell, S., Pickering, K.T., Stelting, C.E., Meyer-Wright, A.A., DSDP Leg 96 Shipboard Scientists, 1985. Mississippi fan sedimentary facies, composition, and texture. In: Bouma, A.H., Normark, W.R., Barnes, N.E. (Eds.), Submarine Fans and Related Turbidite Systems, Springer-Verlag, New York, pp. 259–266.

Stow, D.A.V., Amano, K., Batson, B.S., Brass, G.W., Corrigan, J., Raman, C.V., Tiercelin, J-J., Townsend, M., Wijayananda, N.P., 1990. 31. Sediment facies and processes on the distal Bengal Fan, Leg 116. In: Cochran, J.R., Stow, D.A.V. et al., Proceedings of the Ocean Drilling Project, Leg 116, Scientific Results, College Station, Texas, Ocean Drilling Program, pp. 377–396.

Stow, D.A.V., Reading, H.G., Collinson, J.D., 1996. Deep seas. In: Reading, H.G. (Ed.), Sedimentary Environments: Processes, Facies and Stratigraphy, Blackwell Science, Oxford, pp. 395–453.

Stow, D.A.V., Faugères, J.C., Viana, A., Gonthier, E., 1998. Fossil contourites: a critical review. Sedimentary Geology, 115, 3–31.

Stow, D.A.V., Johansson, M., Braakenburg, N.E., Faugeres, J.C., 1999. Deep-water massive sands: facies, processes and channel geometry in the Numidian Flysch, Sicily: reply. Sedimentary Geology, 127, 119–123.

Stow, D.A.V., Pudsey, C.J., Howe, J.A., Faugères, J.C., Viana, A.R. (Eds.), 2002. Deep-water Contourite Systems: Modern Drifts and Ancient Series, Seismic and Sedimentary Characteristics, Geological Society Memoirs 22, London, p. 464.

Strahler, A.N., Strahler, A.H., 1974. Introduction to Environmental Science. Hamilton Publishing Company, Santa Barbara, California, p. 633.

Strangways, W.T.H.F., 1821. Description of strata in the Brook Pulcova, near the village of Great Pulcova in the neigbourhood of St. Petersburg. Transactions of the Geological Society, First Series 5, 382–458.

Strickland, H.E., 1840. On some remarkable dykes of Calcareous Grit, at Ethie in Ross-shire. Transactions of the Geological Society, Second Series 5, 599–600.

Stubblefield, W.L., McGregor, B.A., Forde, E.B., Lambert, D.N., Merrill, G.F., 1982. Reconnaissance in DSRV Alvin of a 'fluvial-like' meander system in Wilmington Canyon and slump features in South Wilmington Canyon. Geology, 10, 31–36.

Studer, B., 1827. Remarques géognostiques sur quelques parties de la chaîne Septentrionale des Alpe. Ann. Sci. nat. Paris, 11, 1–47.

Sullwold Jr., H.H., 1960. Tarzana fan, deep submarine fan of Late Miocene age, Los Angeles County, California. AAPG Bulletin, 44, 433–457.

Sullwold Jr., H.H., 1961. Turbidites in oil exploration. In: Peterson, J.A., Osmond, J.C. (Eds.), Geometry of Sandstone Bodies, American Association of Petroleum Geologists, Tulsa, Oklahoma, pp. 63–81.

Surlyk, F., 1987. Slope and deep shelf gully sandstones, Upper Jurassic, East Greenland. AAPG Bulletin, 71, 464–475.

Swallow, J.C., Worthington, L.V., 1961. An observation of a deep counter current in the western North Atlantic. Deep-Sea Research, 8, 1–9.

Swanson, R.G., 1981. Sample examination manual. AAPG Methods in Exploration Series IV, p. 45.

Swift, D.J.P., Han, G., Vincent, C.E., 1986. Fluid processes and sea floor response on a modern storm-dominated shelf; middle Atlantic shelf of North America. Part 1: the storm-current regime. In: Knight, R.J., McLean, J.R. (Eds.), Shelf Sands and Sandstones, Canadian Society of Petroleum Geologists, Memoir 11, pp. 99–119.

Syvitski, J.P.M., 1985. Subaqueous slope failures within seismically active fjords. In: Vilks, G., Syvitski, J.P.M. (Eds.), Arctic Land-Sea Interactions, Geological Survey of Canada, Open File 1223, pp. 60–63.

Syvitski, J.P.M., Farrow, G.E., 1989. Fjord sedimentation as an analogue for small hydrocarbon-bearing fan deltas. In: Whateley, M.K.G., Pickering, K.T. (Eds.), Deltas: Sites and Traps for Fossil Fuels, The Geological Society, London, pp. 21–44.

Taira, K., Teramoto, T., 1985. Bottom currents in Nankai Trough and Sagami Trough. Journal of Oceanographical Society of Japan, 41, 388–398.

Takahashi, T., 1981. Debris flow. Ann. Rev. Fluid Mechanics, 13, 57–77.

Takahasi, R., Hatori, T., 1961. A summary report of the Chilean tsunami of 1960. In: Takahasi, R. (Ed.), Report on the Chilean Tsunami of 24 May, 1960, as Observed along the Coast of Japan. Committee for field investigation of the Chilean tsunami of 1960, Maruzen Co., Tokyo, p. 23–34.

Tappin, D.R., 2004. Submarine slump-generated tsunamis. Marine Geology, 203, 199–200.

Tappin, D.R. Watts, P., McMurthy, G.M., Lafoy, Y. Matsumoto, T., 2001. The Sissano, Papua New Guinea tsunami of July 1998 – offshore evidence on the source mechanism. Marine Geology, 175, 1–23.

Taylor, B., Huchon, P., Klaus, A. et al., 2000. Proc. ODP, Init. Repts., 180 (Online). Uniform Resource Locator (URL):http://www-odp.tamu.edu/publications/180_IR/VOLUME/CORES/COR_1108.PDF (accessed July 22, 2004).

Teisserenc, P., Villemin, J., 1990. Sedimentary basin of Gabon—Geology and oil systems. In: Edwards, J.D., Santogrossi, P.A. (Eds.), Divergent/Passive Margin Basins, AAPG Memoir, 48, pp. 117–199.

Ten Haaf, E., 1959a Properties and occurrence of turbidites. Geologie en Mijnbouw, 21, 217–222.

Ten Haaf, E., 1959b. Graded beds of the Northern Apennines, Thesis. University of Groningen, Groningen.

Terwindt, J.H.J., 1981. Origin and sequences of sedimentary structures in inshore mesotidal deposits of the North Sea. In: Nio, S-D., Shuttenhelm, R.T.E., Van Weering, Tj.C.E. (Eds.), Holocene Marine Sedimentation in the North Sea Basin, International Association of Sedimentologists Special Publication No. 5, pp. 4–26.

The Learning Channel, 1997. Landslides (videotape). Produced for the Learning Channel (a cable television channel in the U.S.) by the BBC Television, London, England.

Thomas, W.A., 1985. The Appalachian-Ouachita Connection: Paleozoic orogenic belt in the southern margin of North America. Annual Review of Earth and Planetary Sciences, 13, 175–199.

Thomsen, L., van Weering, T., Gust, G., 2002. Processes in the benthic boundary layer at the Iberian continental margin and their implication for carbon mineralization. Progress in Oceanography, 52, 315–329.

Thornburg, T.M., Kulm, I.D., 1987. Sedimentation in the Chile Trench: depositional morphologies, lithofacies and stratigraphy. GSA Bulletin, 98, 33–52.

Tillman, R.W., Ali, S.A. (Compilers), 1982. Deep water canyons, fans, and facies: models for stratigraphic trap exploration. AAPG Reprint Series No. 26, p. 596.

Timbrell, G., 1993. Sandstone architecture of Balder Formation depositional system U.K. Quad 9 and adjacent areas. In: Parker, J.R. (Ed.), Petroleum Geology of Northwest Europe, Proceedings of the 4th Conference: Geological Society, London, pp. 107–121.

Tripsanas, E.K., Bryant, W.R., Prior, D.B., 2003. Structural characteristics of cohesive gravity-flow deposits, and a sedimentological approach on their flow mechanisms. In: Locat, J., Mienert, J. (Eds.), Submarine Mass Movements and their Consequences, Kluwer Academic Publishers, Dordrecht, pp. 129–136.

Tripsanas, E.K., Bryant, W.R., Phaneuf, B.A., 2004. Slope-instability processes caused by salt movements in a complex deep-water environment, Bryant Canyon area, northwest Gulf of Mexico. AAPG Bulletin, 88, 801–823.

Truswell, J.F., 1972. Sandstone sheets and related intrusions from Coffee Bay, South Africa. Journal of Sedimentary Petrology, 42, 578–583.

Tsuji, Y., 1993. Tide influenced high energy environments and rhodolith-associated carbonate deposition on the outer shelf and slope off the Miyako Islands, southern Ryukyu Island Arc, Japan. Marine Geology, 113, 255–271.

Tucholke, B.E., Embley, R.W., 1984. Cenozoic regional erosion of the abyssal sea floor off South Africa. In: Schlee, J.S. (Ed.), Interregional Unconformities and Hydrocarbon Accumulation, AAPG Memoir, 36, pp. 145–164.

Tuholke, B.E., Wright, W.R., Hollister, C.D., 1973. Abyssal circulation over the greater Antilles Outer Ridge. Deep-Sea Research, 20, 973–995.

Tucholke, B.E., Hollister, C.D., Biscaye, P.E., Gardner, W.D., 1985. Abyssal current character determined from sediment bedforms on the Nova Scotian continental rise. Marine Geology, 66, 43–57.

Turner, F.J., Weiss, L.E., 1963. Structural Analysis of Metamorphic Tectonites. McGraw-Hill, New York, p. 545.

Twenhofel, W.H., 1932. Treatise on Sedimentation, 2nd Edition, Completely Revised. The Williamas & Wilkins Company, Baltimore, p. 926.

Twichell, D.C., Roberts, D.G., 1982. Morphology, distribution, and development of submarine canyons in the United States Atlantic continental slope between Hudson and Baltimore Canyons. Geology, 10, 408–412.

Twichell, D.C., Schwab, W.C., Nelson, C.H., Kenyon, N.H., Lee, H.J., 1992. Characteristics of a sandy depositional lobe on the outer Mississippi Fan from Sea MARC 1A sidescan sonar images. Geology, 20, 689–692.

Twichell, D.C., Schwab, W.C., Kenyon, N.H., 1995. Geometry of sandy deposits at the distal edge of the Mississippi Fan, Gulf of Mexico. In: Pickering, K.T., Hiscott, R.N., Kenyon, N.H., Ricci Lucchi, F., Smith, R.D.A. (Eds.), Atlas of Deep Water Environments: Architectural Style in Turbidite Systems, Chapman & Hall, London, pp. 282–286.

Uchupi, E., 1965. Map showing relation of land and submarine topography, Nova Scotia to Florida. Department of the Interior, U.S. Geological Survey, Miscellaneous Investigations, Map 1–141.

Underwood, M.B., Bachman, S.G., 1982. Sedimentary facies associations within subduction complexes. In: Leggett, J.K., (Ed.), Trench-forearc Geology: Sedimentation and Tectonics on Modern and Ancient Active Plate Margins, Geol. Soc. London Spec. Publ., 10, pp. 537–550.

Underwood, M.B., Karig, D.E., 1980. Role of submarine canyons in trench and trench-slope sedimentation. Geology, 8, 432–436.

Union College Geology Department, 2005. Field trip to the Skaergaard intrusion, east Greenland. Uniform Resource Locator (URL): http://www.union.edu/PUBLIC/GEODEPT/hollocher/skaergaard/ (accessed February 15, 2005).

University of Washington, 2005. Tsunami, Uniform Resource Locator (URL): http://www.geophys.washington.edu/tsunami/general/physics/meaning.html (accessed January 4, 2005).

Unrug, R., 1977. Ancient deep-sea traction currents deposits in the Lgota Beds (Albian) of the Carpathian flysch. Rocznik Polskiego Towarzystwa Geologicznego Annales de la Societe Geologique de Pologne, 47, 355–370.

USGS (U.S. Geological Survey), 2005. Magnitude 9.0 – Sumatra–Andaman Island earthquake: Uniform Resource Locator (URL): http://earthquake.usgs.gov/eqinthenews/2004/usslav/ (accessed January 15, 2005).

Vail, P.R., 1987. Seismic-stratigraphy interpretation using sequence stratigraphy. Pt. 1: seismic stratigraphy interpretation procedures. In: Bally, A.W. (Ed.), Atlas of Seismic Stratigraphy, AAPG Studies in Geology 27, vol. 1, pp. 1–10.

Vail, P.R., Hardenbol, J., 1979. Sea-level changes during the Tertiary. Oceanus, 22, 71–79.

Vail, P.R., Todd, R.G., 1981. Northern North Sea Jurassic unconformities, chronostratigraphy and sea-level changes from seismic stratigraphy. In: Illing, L.V., Hobson, G.D. (Eds.), Petroleum Geology of the Continental Shelf of Northwest Europe, Heydon and Son, Ltd, London, pp. 216–235.

Vail, P.R., Wornardt, W.W., 1990. Well log-seismic sequence stratigraphy: an integrated tool for the 90's. In: Sequence Stratigraphy as an Exploration Tool, Concepts and Practices in the Gulf Coast, 11th Annual Research Conference, Gulf Coast SEPM Foundation, pp. 379–388.

Vail, P.R., Mitchum Jr., R.M., Thompson III, S., 1977. Seismic stratigraphy and global changes of sea level, part 4: global cycles of relative changes of sea level. In: Payton, C.E. (Ed.), Seismic Stratigraphy – Applications to Hydrocarbon Exploration, AAPG Memoir 26, pp. 83–97.

Vail, P.R., Audemard, F., Bowman, S.A., Eisner, P.N., Perez-Cruz, C., 1991. The stratigraphic signatures of tectonics, eustacy and sedimentology – an overview. In: Einsele, G., Ricken, W., Seilacher, A. (Eds.), Cycles and Events in Stratigraphy, Springer-Verlag, Berlin, pp. 618–659.

Valentine, G.A., 1987. Stratified flow in pyroclastic surges. Bull. Volcanology, 49, 616–630.

Valentine, J.W., Moores, E.M., 1970. Plate-tectonic regulation of faunal diversity and sea level: a model. Nature, 228, 657–659.

Vallance, J.W., Scott, K.M., 1997. The Oseola mudflow from Mount Rainier: sedimentology and hazard implications of a huge clay-rich debris flow. GSA Bulletin, 109,143–163.

Valloni, R., 1985. Reading provenance from modern marine sands. In: Zuffa, G.G. (Ed.), Provenance of Arenites, D. Reidel Publishing Company, Dordrecht, pp. 309–332.

Van den Bergh, G.D., Boer, W., de Haas, H., van Weering, Tj. C.E., van Wijhe, R., 2003. Shallow marine tsunami deposits in Teluk Banten (NW Java, Indonesia), generated by the 1883 Krakatau eruption. Marine Geology, 197, 13–34.

Van der Lingen, G.J., 1969. The turbidite problem. New Zealand Journal of Geology and Geophysics, 12, 7–50.

Van Gelder, A., Van der Berg, J.H., Cheng, G., Xue, C., 1994. Overbank and channelfill deposits of the modern Yellow River delta. Sedimentary Geology, 90, 293–305.

Van Wagoner, J.C., Posamentier, H.W., Mitchum, R.M., Vail., P.R., Sarg, J.F., Loutit, T.S., Hardenbol, J., 1988. An overview of the fundamentals of sequence stratigraphy and key definitions. In: Wilgus, C.K., Hastings, B.S., C.G. St. C. Kendall, Posamentier, H.W., Ross, C.A., Van Wagoner, J.C. (Eds.), Sea-Level Changes: An Integrated Approach, SEPM Special Publication No. 42, pp.39–45.

Van Wazer, J.R., Lyons, J.W., Kim, K.Y., Colwell, R.E., 1963. Viscosity and Flow Measurement. Interscience, New York, p. 405.

Vanneste, M., De Batist, M., Golmshtok, A., Kremlev, A., Versteeg, W., 2001. Multi-frequency seismic study of gas hydrate-bearing sediments in Lake Baikal, Siberia. Marine Geology, 172, 1–21.

Vanney, J.R., Stanley, D.J., 1983. Shelfbreak physiography: an overview. In: Stanley, D.J., Moore, G.T. (Eds.), The Shelfbreak: Critical Interface on Continental Margins, SEPM Special Publication No. 33, pp. 1–24.

Varnes, D.J., 1958. Landslide types and processes. In: Eckel, E.D. (Ed.), Landslide and Engineering Practice, Highway Research Board Special Report 29, pp. 20–47.

Varnes, D.J., 1978. Slope movement types and processes. In: Schuster, R.L., Krizek, R.J. (Eds.), Landslides: Analysis and Control, National Academy of Science, Special Report 176, Washington, D.C., pp. 11–33.

Viana, A.R., Faugeres, J.C., Kowsmann, R.O., Lima, J.A.M., Caddah, L.F.G., Rizzo, J.G., 1998. Hydrology, morphology, and sedimentology of the Campos continental margin, offshore Brazil. Sedimentary Geology, 115, 133–157.

Vine, F.J., Mathews, D.H., 1963. Magnetic anomalies over ocean ridges. Nature, 199, 947–949.

Visher, G.S., 1965. Use of vertical profile in environmental recognition. AAPG Bulletin, 49, 41–61.

Visser, M.J., 1980. Neap-spring cycles reflected in Holocene subtidal large-scale bedform deposits: a preliminary note. Geology, 8, 543–546.

Vivas, V., Macsotay, O., Furrer, M., Alvarez, E., 1988. Injectitas clásticas asociadas a desplomes en sedimentitas batiales del Cretáceo Superior de Venezuela nor-oriental. Boletín de la Sociedad Venezolana de Geología, 34, 3–33.

Volkman, C., 1962. Deep current observations in the western North Atlantic. Deep-Sea Research, 9, 493–500.

Vrolijk, P.J., Southard, J.B., 1997. Experiments on rapid deposition of sand from high-velocity flows. Geoscience Canada, 24, 45–54.

Walker, J.R., Massingill, J.V., 1970. Slump features on the Mississippi Fan, northeastern Gulf of Mexico. GSA Bulletin, 81, 3101–3108.

Walker, N.D., 1986. Satellite observations of the Agulhas Current and episodic upwelling south of Africa. Deep-Sea Research, 33, 1083–1106.

Walker, R.G., 1965. The origin and significance of the internal sedimentary structures of turbidites. Proceedings of the Yorkshire Geological Society, 35, 1–32.

Walker, R.G., 1966. Shale grit and grindslow shales: transition from turbidite to shallow water sediments in the Upper Carboniferous of northern England. Journal of Sedimentary Petrology, 36, 90–114.

Walker, R.G., 1967. Turbidite sedimentary structures and their relationships to proximal and distal environments. Journal of Sedimentary Petrology, 37, 25–43.

Walker, R.G., 1973. Mopping up the turbidite mess. In: Ginsburg, R.N. (Ed.), Evolving Concepts in Sedimentology, The Johns Hopkins University Press, Baltimore, pp. 1–37.

Walker, R.G., 1978. Deep-water sandstone facies and ancient submarine fans: models for exploration for stratigraphic traps. AAPG Bulletin, 62, 932–966.

Walker, R.G., 1984a. General introduction: facies, facies sequences and facies models. In: Walker, R.G. (Ed.), Facies Models, 2nd Edition, Geoscience Canada, Reprint Series 1, pp. 1–9.

Walker, R.G., 1984b. Turbidites and associated coarse clastic deposits. In: Walker, R.G. (Ed.), Facies Models, 2nd Edition, Geoscience Canada, Reprint Series 1, pp. 171–188.

Walker, R.G., 1992a. Turbidites and submarine fans. In: Walker, R.G., James, N.P. (Eds.), Facies Models: Response to Sea Level Change, GEOtext 1, Geological Association of Canada, pp. 239–263.

Walker, R.G., 1992b. Facies, facies models, and modern stratigraphic concepts. In: Walker, R.G., James, N.P. (Eds.), Facies Models: Response to Sea Level Change, GEOtext 1. Geological Association of Canada, pp. 1–14.

Walker, R.G., 2004. Facies models revisited. AAPG 2004 Annual Convention Abstracts Volume. Dallas, Texas, A144.

Walker, R.G., Mutti, E., 1973. Turbidite facies and facies associations. In: Middleton, G.V., Bouma, A.H. (Eds.), Turbidites and Deep-water Sedimentation, SEPM Pacific section Short Course, Anaheim, California, pp. 119–157.

Wallis, G.B., 1969. One-dimensional Two-phase Flow. McGraw-Hill, New York, p. 408.

Waltham, D., 2004. Flow transformations in particulate gravity currents. Journal of Sedimentary Research, 74, 129–134.

Walther, J., 1894. Einleitungin die Geologieals HistorischeWissenschaft, Bd. 3. Lithogenesis der Gegenwart. Fischer Verlag, Jena, 535–1055.

Walton, E.K., 1967. The sequence of internal structures in turbidites. Scottish Journal of Geology, 3, 306–317.

Ward, W.H., 1945. The stability of natural slopes. The Geographical Journal, 105, 170–191.

Warme, J.E., Slater, R.A., Cooper, R.A., 1978. Bioerosion in submarine canyons. In: Stanley, D.J., Kelling, G.K. (Eds.), Sedimentation in Submarine Canyons, Fans, and Trenches, Dowden, Hutchinson & Ross, Inc., Stroudsburg, Pennsylvania, pp. 65–70.

Warme, J.E., Douglas, R.G., Winterer, E.L. (Eds.), 1981. The Deep Sea Drilling Project: A Decade of Progress. SEPM Special Publication 32, p. 564.

Weagant, F.E., 1972. Grimes gas field. In King, R.E. (Ed.), Stratigraphic Oil and Gas Fields. AAPG Memoir 16, pp. 428–439.

Weaver, P.P.E., Kuijpers, A., 1983. Climatic control of turbidite deposition on the Madeira Abyssal Plain. Nature, 306, 360–363.

Weaver, P.P.E., Thomson, J., Hunter, P.M., 1987. Introduction. In: Weaver, P.P.E., Thomson, J. (Eds.), Geology and Geochemistry of Abyssal Plains, Geological Soc. London Special Publication 31, pp. vii–xii.

Weimer, P., 1990. Sequence stratigraphy, facies geometries, and depositional history of the Mississippi Fan, Gulf of Mexico. AAPG Bulletin, 74, 425–453.

Weimer. P., Link, M.H. (Eds.), 1991. Seismic facies and sedimentary processes of submarine fans and turbidite systems. Springer-Verlag, New York, p. 447.

Weimer, P., Bouma, A.H., Perkins, R.F. (Eds.), 1994. Submarine Fans and Turbidite Systems. Gulf Coast Section SEPM 15th Annual Research Conference, Houston, p. 440.

Weimer, P., Slatt, R.M., Dromgoole, P., Bowman, M., Leonard, A., 2000a. Developing and managing turbidite reservoirs: case histories and experiences: results of the 1998 EAGE/AAPG Research Conference. AAPG Bulletin, 84, 453–465.

Weimer, P., Slatt, R.M., Coleman, J., Rosen, N.C., Nelson, H., Bouma, A.H., Styzen, M.J., Lawrence, D.T. (Eds.), 2000b. Deep-water reservoirs of the World. In: GCSSEPM Foundation 20th Annual Bob F. Perkins Research Conference, p. 1105.

Wentworth, C.M., 1967. Dish structure, a primary sedimentary structure in coarse turbidites (abstract). AAPG Bulletin, 51, 485.

Wescott, W.A., Ethridge, F.G., 1980. Fan-delta sedimentology and tectonic setting–Yallahs fan delta. AAPG Bulletin, 64, 374–399.

Wescott, W.A., Ethridge, F.G., 1983. Eocene fan delta-submarine fan deposition in the Wagwater trough, east-central Jamaica. Sedimentology, 30, 235–247.

Whelan, F., Keating, B., 2004. Tsunami deposits on the Island of Oahu, Hawaii. Coastline Reports, 1, 77–82.

Whitaker, McD., J.H. 1974. Ancient submarine canyons and fan valleys. In: Dott Jr., R.H., Shaver, R.H. (Eds.), Modern and Ancient Geosynclinal Sedimentation, SEPM Special Publication 19, pp. 106–125.

Whitaker, McD., J.H. (Ed.), 1976. Submarine Canyons and Deep-sea Fans. Dowden, Hutchinson and Ross, Inc., Stroudsburg, Pennsylvania, pp. 460.

White, D., 1937. Fossil plants from the Stanley Shale and Jackfork Sandstone in southern Oklahoma and western Arkansas. U.S. Geological Survey Professional Paper 186-C, p. 66.

Wikipedia, the free Encyclopedia, 2005. 2004 Indian Ocean earthquake. Uniform Resource Locator (URL): http://en.wikipedia.org/wiki/2004_Indian_Ocean_earthquake#Countries_affected (accessed January 28, 2005).

Williams, T.A., Humphreys, N.V., Monson, G.D., Blundell, L.C., 1998. Technology application as an enabler for rapid development of the Zafiro complex, Equatorial Guinea. In: EAGE/AAPG Research Conference, Almeria, Spain.

Winn Jr., R.D., Dott Jr., R.H., 1979. Deep-water fan-channel conglomerates of Late Cretaceous age, southern Chile. Sedimentology, 26, 203–228.

Wood, D.S., 1974. Ophiolites, mélanges, blueschists, and ignimbrites: Early Caledonian subduction in Wales. In: Dott Jr., R.H., Shaver, R.H. (Eds.), Modern and Ancient Geosynclinal Sedimentation, Soc. Econ. Paleont. and Mineral., Special Publ. 19, pp. 334–344.

Woodbury, H.O., Spotts, J.H., Akers, W.H., 1978. Gulf of Mexico continental slope sediments and sedimentation. In: Bouma, A.H., Moore, G.T., Coleman, J.M. (Eds.), Framework, Facies, and Oikl-Trapping Characteristics of the Upper Continental Margin, AAPG Studies in Geology 7, pp. 117–137.

Woodcock, N.H., 1979. Sizes of submarine slides and their significance. Journal of Structural Geology 1, 137–142.

Woodgate, R.A., Fahrbach, E., 1999. Benthic storms in the Greenland Sea. Deep-Sea Research Part I, 46, 2109–2127.

Worthington, L.V., 1976. On the North Atlantic Circulation, Oceanographic Studies. The John Hopkins University, Baltimore, MD, 6, 1–110.

Worthington, L.V., Volkman, G.H., 1965. The volume transport of the Norwegian Sea overflow in the North Atlantic. Deep-Sea Research, 12, 667–676.

Wright, L.D., Yang, Z.-S., Bornhold, B.D., Keller, G.H., Prior, D.B., Wiseman Jr., W.J., 1986. Hyperpycnal plumes and plume fronts over the Huanghe (yellow River) delta front. Geo-Marine Letters, 6, 97–105.

Wuellner, D.E., James, W.C., 1989. Braided and meandering submarine fan channel deposits, Tesnus Formation, Marathon Basin, Texas. Sedimentary Geology, 62, 27–45.

Wust, G., 1936. Schichtung und Zikulation des Atlantischen Ozeans. Das Bodenwasser und die Stratosphare: Duetschen Atlantischen Expedition. Tiefsee.Geologische Rundschhau, 47, 187–195.

Wust, G., 1950. Block diagramme der Atlantischhen Zirkulation auf Grand der Meteor Ergibribe. Kider Meeresforsch, 7, 24–34.

Wust, G., 1963. On the stratification and circulation in the cold water sphere of the Antillean-Caribbean basins. Deep-Sea Research, 10, 165–167.

Xu, J.P., Noble, M., Eittreim, S.L., Rosenfeld, L.K., Schwing, F.B., Pilskaln, C.H., 2002. Distribution and transport of suspended particulate matter in Monterey Canyon, California. Marine Geology, 181, 215–234.

Yamazaki, T., Yamaoka, M., Shiki, T., 1989. Miocene offshore tractive current-worked conglomerates - Tsubutegaura, Chita Peninsula, central Japan. In: Taira, A., Masuda, F. (Eds.), Sedimentary Features in the Active Plate Margin, Terra Scientific Publishing Company, pp. 483–494.

Yerkes, R.F., Gorsline, D.S., Rusnak, G.A., 1967. Origin of Redondo submarine canyon, southern California. U.S. Geological Survey Research Professional Paper 575-C, 97–105.

Young, R.W., Bryant, E.A., 1998. Morphology and process on the lateritic coastline near Darwin, Northern Australia. Zeitschrift für Geomorphologie, 42, 97–107.

Zenk, W.O., 1981. Detection of overflow events in the Shag Rocks Passage, Scotia Ridge. Science, 213, 1113–1114.

Zimmerman, H.B., 1971. Bottom currents on the New England continental rise. Journal of Geophysical Research, 76, 5865–5876.

Index

This Page Intentionally Left Blank

About the Author

G. (Shan) Shanmugam is an adjunct professor of sedimentology at the University of Texas at Arlington, USA. He was born in India in 1944, emigrated to the U.S. in 1970, and became a naturalized U.S. citizen in 1990. He holds degrees from Annamalai University in southern India (B.Sc., 1965, Geology and Chemistry), Indian Institute of Technology in Bombay (M.Sc., 1968, Applied Geology), Ohio University in Athens (M.S., 1972, Geology), and the University of Tennessee in Knoxville (Ph.D., 1978, Geology). He joined Mobil Research and Development Corporation in Dallas, Texas as a Research Geologist in 1978 and retired from Mobil (now ExxonMobil) as a Geological Scientist in 2000.

He conducted outcrop studies of deep-water deposits in the Southern Appalachians (Tennessee, USA), Ouachita Mountains (Arkansas and Oklahoma, USA), and Peira Cava area (SE France). He described conventional cores (1:20 to 1:50 scale) from 32 deep-water sandstone petroleum reservoirs worldwide

during a span of 30 years. He organized deep-water sandstone workshops for: (1) the UK Department of Trade and Industry (DTI) in Scotland (1995 and 1997), (2) Petrobras, Mobil, and Unocal in Brazil (1998 and 1999), (3) Oil and Natural Gas Corporation (ONGC) in India (2002 and 2004), and (4) Reliance Industries Ltd. in India (2006). He also studied coal deposits in Victoria (Australia), coniferous rain forests in the North Island (New Zealand), limestone karst in Guilin (China), fluvial deposits in Gujarat (India), tsunami-related coastal deposits in Tamil Nadu (India), shallow-marine deposits in Qassim area (Saudi Arabia), and estuarine deposits in the Oriente Basin (Ecuador).

His 325 publications since 1970, which include 2 books, 120 peer-reviewed articles, 3 online Encyclopedia articles, and 65 abstracts, cover a wide range of topics (e.g., deep-water process sedimentology, sequence stratigraphy, phenomena of tsunamis, sandstone diagenesis, organic geochemistry, and tectonics). He received the 1995 best paper award from NAPE (Nigerian Association of Petroleum Explorationists) for his paper 'Deepwater Exploration: Conceptual Models and their Uncertainties.' His paper 'High-density turbidity currents: are they sandy debris flows?' published in the Journal of Sedimentary Research in 1996, has achieved the status of the single most cited paper in sedimentological research published in three world-renowned periodicals - Journal of Sedimentary Research, Sedimentology, and Sedimentary Geology - during the survey period of 1996-2003 (Source: International Association of Sedimentologists Newsletter, August 2003). He has been a member of SEPM (Society for Sedimentary Geology) since 1970.

He and his wife (Jean) have been involved in the feeding and clothing of poor children of his hometown (Sirkali) in southern India.